

**Beteiligung purinerger Rezeptoren am Schmerzgeschehen und an
der neuronalen Entwicklung**

**Der Medizinischen Fakultät
der Universität Leipzig
eingereichte**

HABILITATIONSSCHRIFT

zur Erlangung des akademischen Grades

Doctor habilitatus

Dr. rer. med. habil.

vorgelegt

**von Dr. rer. med. Patrizia Rubini Illes
geboren am 28. März 1956 in Milano (It.)**

Eingereicht: 23. Juni 2016

Verleihungsbeschluss der Medizinischen Fakultät: 28.02.2017

Bibliographische Beschreibung

Rubini, Patrizia

Beteiligung purinergere Rezeptoren am Schmerzgeschehen und an der neuronalen Entwicklung

Universität Leipzig, Habilitation

Die Arbeit umfasst 42 Seiten, 90 Literaturzitate, 3 Abbildungen, 9 eigene Publikationen im Anhang

Referat: Diese kumulative Arbeit umfasst neun Publikationen, welche die Beteiligung purinergere P2-Rezeptoren (P2R) am Schmerzgeschehen sowie der neuronalen Entwicklung belegen. Im Fokus stehen zwei ATP-aktivierte Rezeptor-Kanäle (P2X3R, P2X7R) und ein G-Protein-gekoppelter, ATP-empfindlicher Rezeptor (P2Y1R). (1) Da sich humane P2X3R an peripheren und zentralen Endigungen primärer-sensorischer Afferenzen befinden, ist die Entschlüsselung der Agonisten-Bindungsstelle für die Entwicklung potenziell analgetisch wirkender, kompetitiver Antagonisten von großer Bedeutung. Wir identifizierten Gruppen konservierter und nicht-konservierter Aminosäure-Reste, die an der Schnittstelle zweier benachbarter Untereinheiten, die Agonisten-Bindungstasche auskleiden. Abhängig vom Mengenverhältnis der zur Transfektion verwendeten cDNA, bilden P2X2-, P2X3- und P2X6-Untereinheiten heteromere Rezeptoren (P2X2/3R, P2X2/6R) in einer variablen Stöchiometrie. (2) Adulte neurale Progenitorzellen (NPZ) der Subventrikulärzone der Maus besitzen Apoptose- bzw. Nekrose-vermittelnde P2X7R. Diese kommen in Assoziation mit P2X4R vor, bilden jedoch wahrscheinlich keinen heteromeren P2X4/7R. P2X7R könnten zum Absterben der, nach metabolischen Schäden im Überschuss gebildeten, NPZ beitragen. Im Laufe der neuronalen Entwicklung verlieren die NPZ ihre P2X7R. Im Gegensatz hierzu bleiben diese bei ihren astrozytären Nachkommen erhalten. (3) Humane mesencephale embryonale NPZ sind mit P2Y1R ausgestattet, die über eine Ca^{2+} -Wellenaktivität die Proliferation der NPZ beschleunigen und in Differenzierungsvorgänge eingreifen. De-differenzierte, kultivierte Neurone des Ratten-Striatum enthalten ebenfalls P2Y1R. Diese setzen Ca^{2+} aus seinen intrazellulären Speichern frei und öffnen somit Ca^{2+} -selektive „store-operated channels“ in der Zellmembran. Wir konnten zeigen, dass der P2Y1R-stimulierte Anstieg der intrazellulären Ca^{2+} -Konzentration in den striatalen Neuronen durch die Aktivierung von Dopamin D1- und D2R inhibiert wurde. Die vorliegende Arbeit belegt die Bedeutung einiger P2R für zahlreiche, auch potentiell therapeutisch bedeutsame Funktionen des menschlichen und tierischen Organismus.

Inhaltsverzeichnis

Kapitel	Seite
Abkürzungen.....	5
1. Einführung in die Thematik.....	7
1.1. Freisetzung von Nukleotiden und ihre Metabolisierung im Extrazellulärraum.....	7
1.2. P2X-Rezeptoren.....	9
1.3. P2Y-Rezeptoren.....	12
1.4. P2-Rezeptoren und Schmerz.....	14
1.5. P2-Rezeptoren und neuronale Entwicklung; embryonale und adulte neurale Vorläuferzellen.....	17
1.6. Referenzen.....	19
2. Wissenschaftliche Ergebnisse.....	23
2.1. Komplex I. Struktur-Wirkungs-Zusammenhänge bei rekombinanten, humanen P2X3- und P2X2/3-Rezeptoren in Expressionssystemen.....	24
2.1.1. <i>Amino acid residues constituting the agonist binding site of the human P2X3 receptor.....</i>	<i>24</i>
2.1.2. <i>ATP binding site mutagenesis reveals different subunit stoichiometry of functional P2X2/3 and P2X2/6 receptors.....</i>	<i>26</i>
2.1.3. <i>Flexible subunit stoichiometry of functional human P2X2/3 heteromeric receptors.....</i>	<i>28</i>
2.2. Komplex II. Vorhandensein und Wirkung von P2X7-Rezeptoren an kultivierten adulten, neuronalen Vorläuferzellen und Astrozyten.....	29
2.2.1. <i>P2X7 receptors at adult neural progenitor cells of the mouse subventricular zone.....</i>	<i>29</i>
2.2.2. <i>Co-expression of functional P2X4 and P2X7 receptors at adult neural precursor cells of the mouse subventricular zone.....</i>	<i>32</i>
2.2.3. <i>Functional P2X7 receptors at cultured hippocampal astrocytes but not neurons.....</i>	<i>32</i>

2.3. Komplex III. Vorhandensein und Wirkung von P2Y-Rezeptoren an embryonalen neuronalen Vorläuferzellen und dedifferenzierten kultivierten striatalen Neuronen.....	33
2.3.1. <i>Increase of intracellular Ca²⁺ by adenine and uracil nucleotides in human midbrain-derived neuronal precursor cells.....</i>	33
2.3.2. <i>Regulation of intracellular Ca²⁺ by P2Y1 receptors may depend on the developmental stage of cultured rat striatal neurons.....</i>	35
2.3.3. <i>Modulation by D1 and D2 dopamine receptors of ATP-induced release of intracellular Ca²⁺ in cultured rat striatal neurons.....</i>	36
3. Zusammenfassung und Ausblick.....	37
4. Erklärungen, Lebenslauf, Danksagung.....	38
Erklärung über die eigenständige Anfertigung der Arbeit.....	38
Erklärung über den eigenen Anteil an den einzelnen Arbeiten.....	39
Lebenslauf.....	40
Danksagung.....	42

Abkürzungen

[Ca ²⁺] _i	freie intrazelluläre Ca ²⁺ -Konzentration
[K ⁺] _o	extrazelluläre K ⁺ -Konzentration
2-MeSATP	2-Methylthio ATP
ADP	Adenosin-5'-diphosphat
AMP	Adenosin-5'-monophosphat
AS	Aminosäure
ATP	Adenosin-5'-triphosphat
α,β-meATP	α,β-Methylen-ATP
BDNF	“brain-derived neurotrophic factor”
Bz-ATP	Dibenzoyl-ATP
cDNA	komplementäre DNA, “complementary DNA”
CXCR4	CXC-Motiv-Chemokinrezeptor 4
DMEM	Dulbecco's Modified Eagles Medium
DRG	Hinterwurzelganglion, “dorsal root ganglion”
EC ₅₀	50%-igen Effekt auslösende Konzentration
GDNF	“glial cell-derived neurotrophic factor”
GFAP	gliales fibrilläres saure Protein, “glial fibrillary acidic protein”
G _i , G _s , G _q	GTP-bindende Proteine
GPCR	G Protein-gekoppelter Rezeptor; “G protein-coupled receptor”
h	human
IP ₃	Inositol 1,4,5-Trisphosphat
K.O.	“knockout”
MAP2	“microtubule-associated protein 2”
Mut	Mutante
NBM	Neurobasalmedium
NBS	Nukleotid-bindendes Segment
NGF	Nervenwachstumsfaktor, “nerve growth factor”
NPP	Nukleotid-Pyrophosphatase
NPTDase	Nucleosid-Triphosphat-Diphosphohydrolase
NPZ	neurale Vorläuferzelle, “neural progenitor cell”
PAGE	Polyacrylamid-Gel-Elektrophorese

SGZ	Subgranulärzone
siRNA	“small interference RNA”
SNAP	„soluble N-ethylmaleimide-sensitive factor attachment protein“
SOC	“store operated channel”
SVZ	Subventrikulärzone
TM	Transmembranregion
TrkA	Rezeptor-Tyrosinkinase
TRPV1	“transient receptor vanilloid-1”
UTP	Uridin 5'-Triphosphat
VNUT	vesikulärer Nukleotidtransporter
WT	Wildtyp
zf	Zebrafisch

1. Einführung in die Thematik

Das Konzept der purinergen synaptischen Übertragung wurde eingeführt, nachdem diverse Experimente belegten, dass ATP ein Transmitter der nicht-adrenergen, nicht-cholinergen Neurone im peripheren vegetativen Nervensystem ist (Burnstock, 1972). Kurz danach wurde gezeigt, dass ATP nicht nur eigenständiger Transmitter sondern auch Ko-Transmitter klassischer erregungsübertragender Stoffe, wie Noradrenalin und Acetylcholin, in den entsprechenden Nervenendigungen ist (Burnstock, 1976). Heute wissen wir, dass ATP als ein weit verbreitetes Signalmolekül im peripheren (PNS) und zentralen Nervensystem (ZNS) fungiert (Burnstock, 2007; Abbraccio et al., 2008; Khakh and North, 2012). Allerdings üben nicht nur Adenosin- sondern auch Uridin-Nukleotide eine ähnliche Signalfunktion im Nervensystem aus.

1.1. Freisetzung von Nukleotiden und ihre Metabolisierung im Extrazellulärraum

ATP und weitere Nukleotide werden in sekretorischen/synaptischen Vesikeln gespeichert. Die Aufnahme dieser Substanzen geschieht mittels eines Cl⁻-abhängigen vesikulären Nukleotidtransporters (VNUT), der eine vergleichbare Struktur besitzt wie der vesikuläre Glutamattransporter (Sawada et al., 2008). Allerdings wird ATP nicht nur in Vesikeln gespeichert sondern kommt auch im Zytosol der unterschiedlichsten Zellen des ZNS vor, woher es auf Einwirkung (patho)-physiologischer Stimuli ausgeschüttet werden kann (Lazarowski et al., 2003; Illes und Ribeiro, 2004). Eine regulierte Exocytose ist bei der Freisetzung von ATP aus Neuronen und Astrozyten von Bedeutung; beide Zelltypen nutzen dafür das SNARE-Protein („soluble N-ethylmaleimide-sensitive factor attachment protein“, SNAP). In einer späten Phase der Neuro(Glio)transmitter-Freisetzung binden Syntaxin/SNAP-25 an das vesikuläre Protein Synaptotagmin, das ein Ca²⁺-Sensor ist und die Verschmelzung der synaptischen Vesikel mit der Plasmamembran einleitet (Rettig und Neher, 2002; Zorec et al., 2012). Kürzlich wurde über eine lysosomale Exocytose von ATP aus Astrozyten ebenfalls berichtet (Zhang et al., 2007).

Aus nicht-neuronalen Zellen des ZNS (Astrozyten, Oligodendrozyten, Mikroglia, Endothelzellen) wird ATP auch nicht-exozytotisch ausgeschüttet. Die beteiligten Mechanismen sind die Folgenden: (1) ATP-bindende Kassettenproteine; (2) osmolytische Transporter; (3) Connexin- und Pannexin-Hemikanäle; (4) ein Subtyp der ATP-aktivierten Kationenkanäle (P2X7R) und (5) passives Ausströmen über die

geschädigte Zellmembran bei mechanischen oder hypoxischen Noxen (Illes und Ribeiro, 2004; Abbracchio et al., 2008). Die extrazelluläre Konzentration von ATP kann (1) mithilfe von „sniffer“-Zellen, die rekombinante P2X2R enthalten, biotitriert, (2) mit enzymatisch beschichteten Biosensoren gemessen, oder (3) mit der Luziferin/Luziferase-Methode bestimmt werden (Lazarowski et al., 2003; Wall et al., 2010). Keine dieser Messmethoden ist optimal, da entweder die ATP-Empfindlichkeit oder die zeitliche Auflösung zu wünschen übrig lässt.

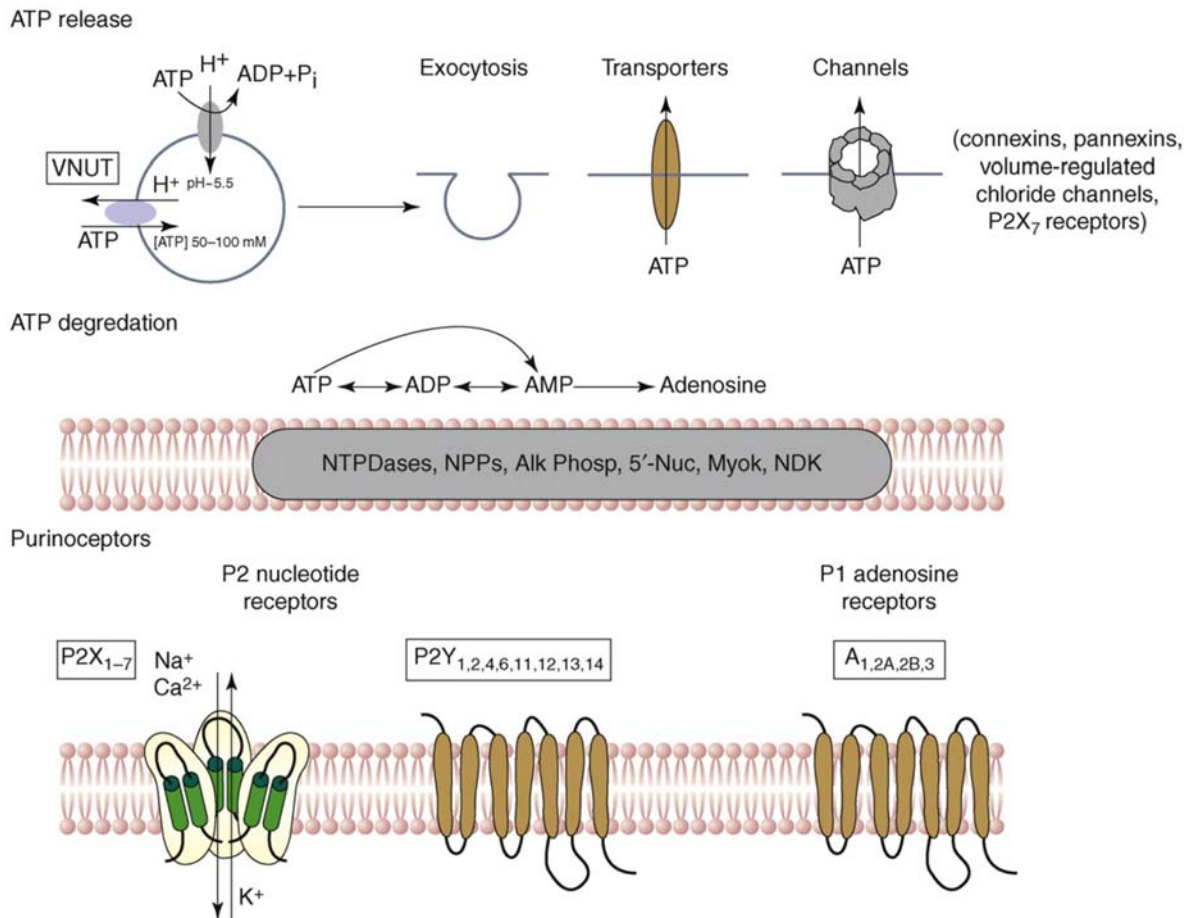


Abb. 1. Mechanismen der Freisetzung und des enzymatischen Abbaus von ATP sowie seine Wirkung an P2-Rezeptoren. Abkürzungen: Alk Phosp, alkalische Phosphatase; Myok, Myokinase (Adenylkinase); NDK, Nukleosid-Diphosphat-Kinase; NPPs, Nukleotid-Pyrophosphatase und/oder -Phosphodiesterasen; 5'-Nuc, 5'-Nukleotidase; VNUT, vesikulärer Nukleotid-Transporter. Für weitere Erläuterungen s. den Text. Abbracchio et al. (2009).

ATP und andere Nucleotide wirken nach ihrer Freisetzung an Membranlokalisierten Rezeptoren (s. unten). Dieser Effekt wird durch schnellen enzymatischen Abbau mittels Ekto-Nucleotidasen beendet (Abbracchio et al., 2008). Die gebildeten ATP-Metaboliten (ADP, P2YR; Adenosin, P1R) sind physiologische

Liganden für purinerge Rezeptoren, die anderen Gruppen zugehören als die ursprünglich aktivierten. Somit bestimmen die Ekto-Nukleotidasen nicht nur die Lebensdauer der Nukleotide, indem sie die Wirkung der freigesetzten Substanzen an ihrem eigenständigen Rezeptor beenden, sondern bilden außerdem Agonisten für zusätzliche P2- oder P1-Rezeptoren (Zimmermann und Braun, 1999; Zimmermann, 2000). Die Familie der Ekto-Nukleotidasen besteht aus den Enzymen Nukleosid-Triphosphat-Diphosphohydrolase (NTPDase), Nukleotid-Pyrophosphatase (NPP), alkalische Phosphatase und 5'-Nukleotidase. Die einzelnen Enzyme unterscheiden sich in ihrer Substratspezifität. Die NTPDasen und NPP hydrolysieren ATP und ADP zu AMP, das wiederum durch die 5'-Nukleotidase zu Adenosin umgebaut wird. Die alkalische Phosphatase hydrolysiert die Nukleosid-Tri-, Di- und Monophosphate gleichermaßen.

1.2. P2X-Rezeptoren

Nach ihrem Erscheinen im Extrazellulärraum wirken ATP und weitere Nukleotide an membranständigen ionotropen (P2X) oder metabotropen (P2Y) Rezeptoren (Abbraccio und Burnstock, 1994; von Kügelgen, 2011; Khakh und North, 2012). Aus Geweben von Säugetieren wurden sieben ATP-empfindliche P2XR-Subtypen kloniert (P2XR1-7), die sich in ihren strukturellen, pharmakologischen und biophysikalischen Eigenschaften voneinander unterscheiden (North, 2002). Sie bestehen aus jeweils drei identischen oder unterschiedlichen Untereinheiten, die sich zu homomeren oder heteromeren Rezeptoren zusammenschließen. Die Untereinheiten sind unterschiedlich lang und enthalten 379 (P2X6) bis 595 (P2X7) Aminosäuren. Sie besitzen eine glycosylierte, cysteinreiche extrazelluläre Schleife, zwei Transmembranregionen (TM1, TM2) und intrazelluläre N- und C-terminale Endigungen (Köles et al., 2007, 2008). Der P2X7R enthält ein C-terminales Ende, das länger ist als das der anderen P2XR. Es reguliert Funktionen wie die sog. Porendilatation, zelluläre Lokalisation, Protein-Protein-Interaktion und post-translationale Modifikation des Rezeptors (Costa-Junio et al., 2011).

Die trimere Struktur der P2XR wurde mit biochemischen Methoden belegt. Blau-nativ Polyacrylamid-Gel-Electrophorese (PAGE) zeigte, dass das Molekulargewicht der homomeren P2X1- und P2X3R fast ausschließlich dieser Zusammensetzung entspricht (Nicke et al., 1998). Ko-Immünpräzipitation der Epitop-markierten Untereinheiten belegte, dass alle rekombinanten Rezeptoren, mit Ausnahme von

P2X7, bei Überexpression in Oozyten, Hetero-Oligomere bilden (Torres et al., 1999; Saul et al., 2013).

P2X7R können nach langdauernder oder repetitiver Agonisten-Applikation Membranporen generieren, die den Durchtritt großer organischer Kationen und zahlreicher Farbstoffe (600-800 Da) aus dem Extrazellulärraum in die Zelle oder in umgekehrte Richtung zulassen. Das Entstehen einer solchen Pore wird über zwei alternative Mechanismen erklärt. Einerseits könnte ihr eine Konformationsänderung des Rezeptor-Proteins zugrunde liegen, wie für andere P2XR (P2X2 und P2X4) bereits nachgewiesen (Chaumont and Khakh, 2008). Andererseits besteht die Möglichkeit, dass ein akzessorisches Protein miteinbezogen wird und Pannexin-1 Kanäle für die Porenbildung verantwortlich sind (Pelegri, 2011). Die beiden Mechanismen werden intensiv diskutiert und z.Z. gibt es noch keine abschließende Beurteilung.

P2X1- und P2X3R reagieren auf ATP bereits im hohen nanomolaren Bereich, während die Empfindlichkeit der P2X7R im mikromolaren Bereich liegt; dazwischen einzuordnen ist die ATP-Sensitivität der P2X2,4,5R (North, 2002; Jarvis and Khakh, 2008). Falls strukturelle Modifikationen im ATP-Molekül durchgeführt werden, kann sich die Rezeptor-Selektivität ändern. α,β -Methylen ATP (α,β -meATP) aktiviert ausschließlich P2X1,3R; Dibenzoyl-ATP (Bz-ATP) wirkt stärker am P2X7R als ATP selbst. Allosterische Modulatoren, wie Protonen und Schwermetall-Ionen beeinflussen die einzelnen P2XR entweder potenzierend oder inhibitorisch (Coddou et al., 2011). Es wurden zahlreiche subtyp-selektive und kompetitive Antagonisten synthetisiert, unter denen A-317491 (P2X3R) und A-438079 (P2X7R) besonders häufig experimentell genutzt werden.

Die P2XR können in schnell (P2X1,3R) und langsam desensibilisierende (P2X2,4,5R) Klassen unterteilt werden. Zwei P2X2R Splice-Varianten, die mit unterschiedlich langen C-Termini bestückt sind [P2X2(a), lang; P2X2(b), kurz], desensibilisieren dementsprechend langsam bzw. schnell (Brändle et al., 1997). An dieser Stelle sei erwähnt, dass der homomere P2X6R wegen eines Trafficking-Defekts nicht in die Zellmembran eingebaut wird (Ormond et al., 2006). Ein solcher Defekt besteht beim heteromeren P2X2/6R nicht. Am Beispiel des heteromeren P2X2/3R kann demonstriert werden, dass die Agonisten-Selektivität von der P2X3-Untereinheit bestimmt wird, während die Desensibilisierungskinetik von der P2X2-Untereinheit bestimmt wird. Durch Hetero-Oligomerisierung entsteht ein Rezeptor,

der α,β -meATP-empfindlich ist und dennoch langsam desensibilisiert (Nörenbert und Illes, 2000).

Bevor die Kristallstruktur der P2XR entschlüsselt wurde, wurden Mutagenese-Studien benutzt, um Aminosäuren zu identifizieren, die an der Agonisten/Antagonisten-Bindung, allosterischen Modulation, Desensibilisierung und Kanal-Öffnung beteiligt sind (Egan et al., 2004; Roberts et al., 2006). Es wurden zahlreiche Aminosäuren in der extrazellulären Schleife durch andere ersetzt, um nachzuweisen, dass drei konservierte und in jeweils vier Bindungssegmente (NBS1-4; Mager et al., 2004) organisierte Gruppen von Aminosäuren für die Bindung des ATP-Moleküls an den Rezeptor verantwortlich sind (Zemkova et al., 2007). Ursprünglich wurde angenommen, dass die drei in einen Rezeptor assoziierten Untereinheiten jeweils eine komplette Agonisten-Bindungsstelle enthalten (Vial et al., 2004). Es wurde aber bald geklärt, dass die hypothetische Bindungstasche am Schnittpunkt von zwei benachbarten Untereinheiten untergebracht ist und sich somit NBS1-2 auf der einen und NBS3-4 auf der anderen Untereinheit befinden (Wilkinson et al., 2006; Marquez-Klaka et al., 2009).

Weitere Experimente belegten, dass für die Aktivierung des Rezeptors die Besetzung von 2-3 Bindungsstellen notwendig ist: (1) Einzelkanalanalysen der P2X2R-Ströme zeigten 2-3 aufeinander folgende Bindungsschritte (Ding und Sachs, 1999); (2) das kinetische Verhalten des makroskopischen P2X3R-Stromes konnte mit einem allosterischen Modell simuliert werden, das die Kanalöffnung sowohl nach der Anheftung von zwei als auch von drei Agonisten Molekülen voraussetzte (Karoly et al., 2008); (3) mit einander stabil verlinkte P2X2R-Untereinheiten (konkatalmerische Rezeptoren) reagierten auf den Agonisten ATP bereits im Fall, wenn sie nur zwei freie Bindungsstellen enthielten (Stelmashenko et al., 2012). Die Besetzung einer einzigen Bindungsstelle durch niedrige Agonisten-Konzentrationen führte zur Desensibilisierung des P2X3R bei fehlender Kanal-Öffnung (Sokolova et al., 2006).

Die Kristallstruktur des C-terminal trunkierten Zebrafish-(zf)P2X4R (bestehend aus TM1-2 und extrazellulärer Schleife) wurde erst vor relativ kurzer Zeit entschlüsselt, erst in der geschlossenen und dann in der ATP-bindenden offenen Konformation (Kawate et al., 2009; Young, 2010; Hattori und Gouaux, 2012; Habermacher et al., 2016). Basierend auf dieser Struktur wurden Homologiemodelle für alle weiteren P2XR-Subtypen erstellt. Der zfP2X4R besitzt eine Kelch-ähnliche Struktur, die sich um etwa 70 Å über die Oberfläche der Membran erhebt. Die Form

der Transmembran-Regionen ähnelt einer Sanduhr und wird durch sechs Transmembran-Helices gebildet. Die Form des gesamten Rezeptors erinnert an einen Delphin; an den Körper des Delphins schließen sich die Kopf-Domäne und drei strukturell unterschiedliche Elemente (Rückenflosse sowie die beiden Vorderflossen) an. Die ATP-Bindungstasche befindet sich zwischen zwei benachbarten Untereinheiten und sieht wie ein offener Kiefer aus. Er wird ausgestaltet von der Kopfdomäne (A-Untereinheit), dem Oberkörper (A-Untereinheit), dem Unterkörper (B-Untereinheit) und den Rückenflossen (B-Untereinheit). ATP bindet mit seinen negativ geladenen Phosphatgruppen über Salz- und Wasserstoffbrücken an hochkonservierte basische und polare Aminosäure-Reste. Nach der Agonisten-Bindung und Übergang von dem geschlossenen in den offenen Zustand, ordnen sich die Transmembran-Helices neu, und geben den Ionen-Permeationsweg frei. In geladener Form passieren die Kationen den Rezeptor-Kanal nicht über die zentrale Pore, sondern über eine laterale Fenestration.

1.3. P2Y-Rezeptoren

Die P2YR haben weniger Aufmerksamkeit erfahren als die P2XR, da sie einen eher konventionellen Rezeptortyp darstellen (G-Protein-gekoppelter Rezeptor; GPCR). Die funktionelle Bedeutung der P2YR ist jedoch keinesfalls geringer, da sie nicht nur in erregbaren sondern auch in nicht-erregbaren Geweben weit verbreitet sind. Im peripheren (PNS) und zentralen Nervensystem (ZNS) vermitteln P2YR langsame Reaktionen, die durch Nukleotide ausgelöst werden, die vom Freisetzung- zum Wirkort über relativ lange Strecken diffundieren können.

Alle P2YR besitzen die typischen strukturellen Merkmale der GPCR mit sieben hydrophoben Transmembranregionen, die durch drei extrazelluläre und drei intrazelluläre Schleifen miteinander verbunden sind; der N-Terminus liegt auf der extrazellulären Seite der Membran, der C-Terminus auf der intrazellulären Seite (von Kügelgen, 2006, 2011; Jacobson et al., 2012). Die humanen Orthologe bestehen aus 328 (P2Y6R) bis 377 (P2Y4R) Aminosäuren. Ihre biochemische Analyse zeigt, dass P2YR glykolytisch sind und ihre extrazellulären Domänen vier Cystein-Reste enthalten, die miteinander Disulfid-Brücken bilden. Sie können zwei Gruppen zugeordnet werden, der P2Y1R-Subfamilie, zu der die P2Y1,2,4,6- und 11R gehören sowie der P2Y12R-Subfamilie, zur der die P2Y12,13- und 14R gehören.

Die P2Y1-Typ Rezeptoren sind an G_q-Proteine gekoppelt, die P2Y12-Typ-Rezeptoren an G_i-Proteine; PY11R koppeln a G_q und G_s. Die räumliche Struktur der P2YR war bis Anfang 2014 nicht geklärt, da keine Kristallstruktur vorlag. Allerdings konnten anhand der Struktur des Rhodopsins bzw. des CXC-Motiv-Chemokinrezeptor 4 (CXCR4) Peptid-Rezeptors Homologie-Modelle erstellt werden (Jacobson et al., 2012; Boeynaems et al., 2012). Es stehen außerdem ausführliche Ergebnisse aus Mutagenese-Studien zur Verfügung. Für die Bindungsstelle vom P2Y1R gilt, dass die supponierte Agonisten-Bindungstasche innerhalb des oberen Drittel der TM-3,6,7 liegt. Die positiv geladenen Aminosäure-Reste dieser TM-Domänen gruppieren sich um die negativ geladenen Phosphat-Gruppen von ADP. Kürzlich gelang es jedoch die Kristallstruktur des P2Y12R in der Antagonisten- und Agonisten-bindenden Konformationen zu entschlüsseln (Zhang et al., 2014a, b). Dadurch wurde das Vorhandensein zweier Bindungstaschen nachgewiesen; offenbar sind beide dieser Taschen für die Nukleotid-Bindung unerlässlich.

P2Y1,11,12,13R reagieren nur auf Adenin-Nukleotide, P2Y6 ist ein Uridin-Nukleotid-Rezeptor (Illes und Ribeiro, 2004; von Kügelgen und Harden, 2011). P2Y2- und P2Y4R der Ratte und Maus besitzen eine gemischte Adenin/Uridin-Nukleotid Sensitivität. Hingegen sind humane P2Y4R ausschließlich gegenüber UTP und seine Strukturanaloga empfindlich. P2YR sind insofern einzigartig, als dass sie nur durch UDP-Zucker, wie UDP-Glukose und -Galaktose, aktivierbar sind. Mittlerweile besitzen wir, dank der Bemühungen von Ken Jacobson und seiner Arbeitsgruppe, für die Mehrzahl der P2YR selektive Antagonisten. Vor allem P2Y1R (MRS2179; MRS2279) und P2Y12R (AR-C69931MX, Cangrelol; AZD6140, Ticagrelol) werden experimentell häufig verwendet (Jacobson und Boeynaems, 2010; Jacobson et al., 2011). An dieser Stelle sei erwähnt, dass P2Y12R-Antagonisten Thrombozyten-Aggregationshemmer sind, die zur Thromboseprophylaxe als alternative Medikation zu einer Azetylsalicylsäure-Behandlung von großer Bedeutung sind (Walsh and Price, 2014). Clopidogrel oder Prasugrel wurden für dieselbe Indikation entwickelt; diese Medikamente wirken jedoch nicht selbst sondern über ihre aktiven, P2Y12R-antagonistischen Metabolite (Cattaneo, 2011).

1.4. P2-Rezeptoren und Schmerz

In sensorischen Ganglien wurden alle sieben klonierten P2XR nachgewiesen (Chizh und Illes, 2001; Wirkner et al., 2007). In den Zellkörpern der Hinterwurzel-Ganglien-Neuronen („dorsal root ganglion“; DRG) sind die Rezeptor-mRNA und das -Protein für P2X2- und P2X3R vorhanden.

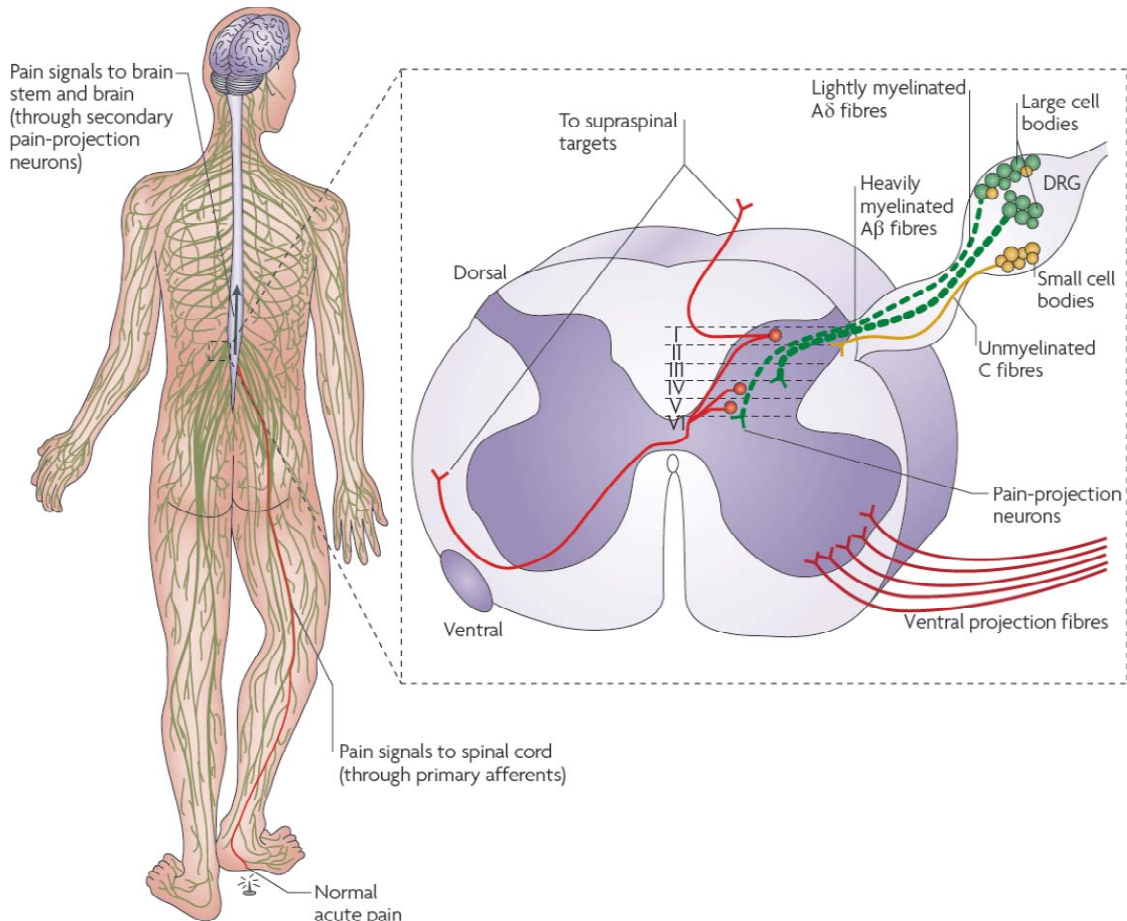


Abb. 2. Neuronale Bahnen des Schmerzempfindens. Verletzung an der Ferse durch einen spitzen Gegenstand aktiviert die peripheren Endigungen der Hinterwurzelganglienzellen. In den Hinterwurzelganglien befinden sich die Zellkörper der primär-afferenten Nervenfasern; sie projizieren sowohl in periphere Gewebe als auch in das Hinterhorn des Rückenmarks. Diese sensorischen Fasern sind stark myelinisiert und leiten schmerzhafte Stimuli (A_{β} ; große Zellkörper; schnelle Reizleitung), sind schwach myelinisiert (A_{δ} ; große Zellkörper; langsamere Reizleitung) oder unmyelinisiert (C; kleine Zellkörper; langsame Reizleitung). Sie enden in unterschiedlichen Schichten des Rückenmark-Hinterhorns, wo sie auf Projektionsneurone synaptisch umgeschaltet werden. Aus der Schicht I steigen unilaterale Nervenfasern in höhere Areale des Gehirns auf; aus den Schichten IV und V steigen die Faserbündel auf der kontralateralen Seite ebenfalls zu supraspinalen Targets hoch (Hirnstamm und thalamische Kerne). Nach synaptischer Umschaltung im Thalamus gibt es weitere Projektionen zum somatosensorischen und frontalen Cortex. Für detaillierte Erläuterungen s. den Text. Milligan and Watkins (2009)

Die nozizeptiven C-Faser-Neurone sind entweder peptiderg (sie enthalten die Rezeptor-Tyrosinkinase [TrkA] für den Nerven-Wachstumsfaktor [„nerve growth factor“; NGF]), oder nicht-peptiderg. Eine Subpopulation der nicht-peptidergen C-Faser-Neuronen exprimieren den Rezeptor-Komplex für den „glial cell-derived neurotrophic factor“ (GDNF), welcher durch Isolectin B4 markiert werden kann (Molliver et al., 1997). Die Mehrzahl der P2X3-positiven Neurone gehören zur GDNF-sensitiven Population und exprimieren Capsaicin-empfindliche TRPV1-Rezeptor-Kanäle.

ATP und ihre Strukturanaloga induzieren schnell desensitisierende Einwärtsströme an akut dissoziierten, P2X3R-enthaltenden, DRG-Neuronen (Chen et al., 1995). α,β -meATP aktiviert diese Rezeptoren mit einer hohen Selektivität; ähnliche Konzentrationen des Agonisten stimulieren außer P2X3R- nur noch P2X1- und P2X2/3R. An Neuronen des Ganglion nodosum befinden sich vorwiegend P2X2/3R, die auf α,β -meATP mit langsam desensitisierenden Strömen reagieren (Lewis et al., 1995). Es wird angenommen, dass sowohl die homomeren als auch die heteromeren Rezeptortypen an peripheren Endigungen der sensorischen Neurone lokalisiert sind und auf, nach chronisch schmerzhaften Stimuli freigesetztes ATP antworten. Exogen appliziertes ATP löst bei humanen Probanden und Labortieren akuten, durch P2R-Antagonisten aufhebbarer Schmerz aus. Endogenes ATP scheint jedoch an der Vermittlung von akuten thermischen und mechanischen Schmerzen nicht beteiligt zu sein, da diese Sinnesqualitäten bei P2X3R-defizienten Mäusen unverändert bleiben (Cockayne et al., 2000). Neuere Ergebnisse sind im Einklang mit der Rolle von P2X3R bei solchen Schmerz-zuständen, die mit chronischer Entzündung oder neuronalem Schaden assoziiert sind (Donnelly-Roberts et al., 2008). Knockout-Methoden, Antisens-Nukleotid-Technologien und kurze interferierende RNA („small interference“ [si]RNA)-Technologien sowie selektive P2X3R-Antagonisten stützen durchweg diese Annahme. Folglich sind, im Gegensatz zum akuten Schmerz, ATP-aktivierte Kationenkanäle der P2X3- und P2X2/3-Typen an Entzündungs-/Neuropathie-bedingten Schmerzen sowie viszerale Schmerzen und Migräne beteiligt (Wirkner et al., 2007).

Zusätzlich zu ihrer Lokalisation an den peripheren Endigungen und Zellkörpern der sensorischen Neurone befinden sich P2X3R auch an den zentralen Terminalen derselben Neurone im Hinterhorn des Rückenmarks. ATP steigert die elektro-physiologisch gemessene Freisetzung von Glutamat aus den DRG-Nerven-

endigungen in der Schicht II des Rückenmarks (Nakatsuka et al., 2003). Die Hemmung der Glutamatfreisetzung durch P2XR-Antagonisten belegte die Beteiligung von P2X3R. Im Projektionsgebiet der A δ -Fasern in der Schicht V induzierten ATP und α,β -meATP eine langanhaltende Glutamatfreisetzung, die wahrscheinlich durch andere P2XR-Subtypen als P2X3R vermittelt wurde (Nakatsuka und Gu, 2001).

Während P2XR sich vorwiegend an kleinen DRG-Neuronen befinden, erscheinen P2YR an kleinen, mittleren und großen sensorischen Neuronen gleichermaßen (Gerevich und Illes, 2004). Der immunhistochemische Nachweis der Rezeptorproteine zeigte, dass P2X3-, TRPV1- und P2Y1R an kleinen DRG-Neuronen der Ratte ko-lokalisiert sind (Gerevich et al., 2004). Die Aktivierung von P2Y1R durch ADP oder sein Strukturanalogon ADP- β -S hemmte N-Typ Ca²⁺-Kanäle und ließ andere Ca²⁺-Kanaltypen unbeeinflusst. Die Wirkung von ADP- β -S wurde durch P2Y1R-selektive Antagonisten aufgehoben. Schließlich erhöhte intrathekal appliziertes ADP- β -S die Schmerzschwelle im Analgesie-Modell des Tail-Flick-Tests. Diese Ergebnisse weisen darauf hin, dass spinale P2X3R die Glutamatfreisetzung auf Schicht II-Neurone fördern, während P2Y1R einen gegenteiligen Effekt ausüben und analgetisch wirken.

Wir begannen die Rolle von ATP beim neuropathischen Schmerzen zu verstehen, als entdeckt wurde, dass P2X4R an den Begleitsymptomen der taktilen Allodynie und Hyperalgesie beteiligt sind (Burnstock, 2011). P2X4R steigern die Ausschüttung von „brain-derived neurotrophic factor“ (BDNF) aus Mikrogliazellen des Rückenmarks und lösen eine Verschiebung des anionischen Umkehrpotentials der spinalen Schicht I-Neuronen in die depolarisierende Richtung aus (Coull et al., 2005). Dies hat zur Folge, dass die Polarität des vorher inhibitorischen (auswärtsgerichteten) GABA_A-R-Stromes sich in exzitatorisch (einwärtsgerichtet) ändert. Demzufolge wird die Aktivität der Schicht I-Neurone, die die Information „Schmerz“ an höhere Areale des Gehirns weiterleiten, gesteigert.

P2X7R nutzen einen anderen Transduktionsweg, um Schmerzen auszulösen (Burnstock, 2011). Sie fördern die Freisetzung inflammatorischer Zytokine und Arachidonsäure-Metaboliten, wie Interleukin-1 β und PGE₂ aus Makrophagen und Mikroglia und sensibilisieren somit Nozizeptoren (Endigungen der C- und A δ -Faser Neurone) in peripheren Geweben oder Schmerz-übermittelnden Neuronen im ZNS (Clark, 2010). Astrozyten sind ebenfalls bedeutsam für die Entwicklung chronischer

Schmerzen, indem sie die klassischen immunologischen Signalmoleküle, Zytokine und Chemokine sekretieren (Milligan und Watkins, 2009).

1.5. P2-Rezeptoren und neuronale Entwicklung; embryonale und adulte neurale Vorläuferzellen

P2XR erschienen recht früh im Laufe der Phylogenese. Besonders ausführliche Untersuchungen wurden an der Amöbe *Dictyostelium discoideum* durchgeführt, deren kontraktile Vakuolen in ihrer intrazellulären Membran fünf Subtypen eines P2XR enthalten (DdP2X_{A-E}R; Burnstock und Verkhratsky, 2009; Fountain, 2013). Die Transfektion der DdP2X_{A,B,E}R in HEK293 Zellen ergab Liganden-aktivierte Ionenkanäle, die durch ATP und einige seiner Strukturanaloga stimuliert werden konnten. Diese Ionenkanäle sind nicht nur für Kationen sondern auch für Cl⁻ permeabel. Ähnlicherweise wurden P2XR an Algen (*Ostreococcus tauri*) und Saugwürmern (*Schistosoma mansoni*) nachgewiesen. G-Protein-gekoppelte P2YR sind evolutionär gesehen entweder gleich alt oder etwas jünger als die P2XR (Burnstock und Verkhratsky, 2009).

Neuroepitheliale Stammzellen der embryonalen ventrikulären Zone bilden Neurone und Gliazellen des sich entwickelnden Gehirns aus (Doetsch, 2003). Zu Beginn der Neurogenese entstehen aus neuroepithelialen Stammzellen Radialgliazellen, die zwar das astrozytenspezifische gliale fibrilläre saure Protein („glial fibrillary acidic protein“; GFAP) exprimieren, aber gleichzeitig gemeinsame Vorläufer von Neuronen, Astrozyten und Oligodendrozyten sind (Morest and Silver, 2003). Sie senden ihre radialen Zellausläufer zu der subpialen Oberfläche der Gehirnrinde und bilden Endfüsse in deren marginale Zone aus (Dale, 2008). Nach asymmetrischer Zellteilung der Radialglia wandern ihre Tochterzellen entlang der Radialglia-Zellausläufer und differenzieren in Neurone der verschiedenen Schichten der Gehirnrinden. Daher sind Radialglia einerseits neurale Vorläuferzellen (neurale Progenitorzellen; NPZ) und andererseits sind sie am Entstehen komplexer kortikaler Strukturen beteiligt.

Es wurde nachgewiesen, dass Radialgliazellen im Erwachsenenalter in den sog. Stammzellnischen des Gehirns persistieren und ihre Kapazität zur Neubildung von neuronalen Zellen erhalten (Buffo et al., 2005). Diese Stammzellnischen befinden sich in der Subventrikulärzone (SVZ) des Seitenventrikels und in der Subgranulärzone (SGZ) des hippocampalen Gyrus dentatus. In der SVZ des Seitenventrikels und im SGZ des

Hippocampus bilden Radialglia-artige NPZ über mehrere Zwischenstufen hinweg Neuroblasten, die in ihre Zielregionen im Bulbus olfactorius und Gyrus dentatus migrieren und in die dort vorhandenen, neuronalen Netzwerke als reife Körnerzellen integriert werden (Lledo et al., 2006; Platel and Bordey, 2016).

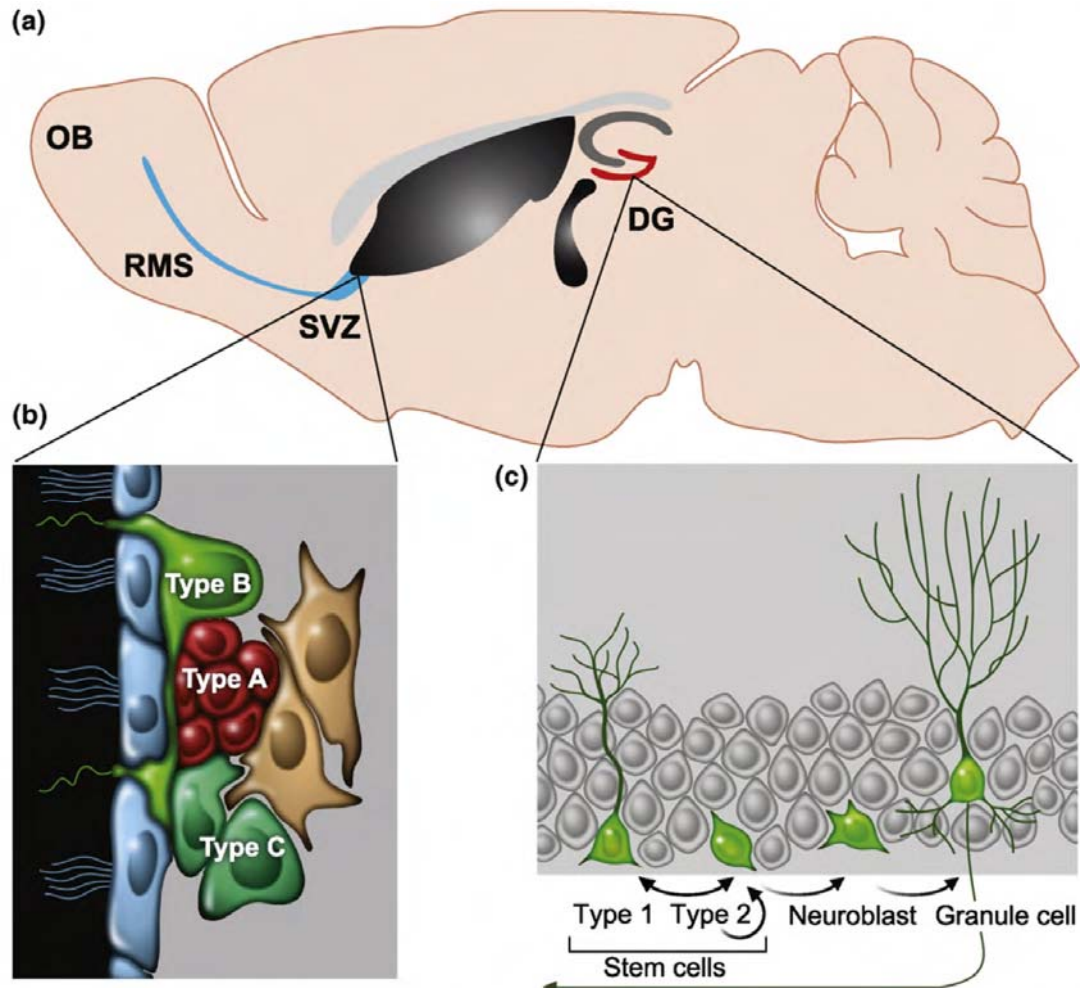


Abb. 3. Neurogenese im erwachsenen Gehirn. A, B, Die adulten, neuralen Progenitorzellen (NPZ) befinden sich in zwei Stammzellnischen: in der Subventrikulärzone (SVZ) des Seitenventrikels und der Subgranulärzone (SGZ) des hippocampalen Gyrus dentatus (DG). Radialgliazellen (Typ-A) des SVZ generieren sich schnell teilende, nicht-radiale Zellen (Typ-C), aus denen Neuroblasten (Typ-A) entstehen. Die Neuroblasten wandern in den Bulbus olfactorius (OB) über den rostralen migratorischen Strom („rostral migratory stream“, RMS) und werden in die dortigen Körnerzellen integriert. C, Eine ähnliche neurale Entwicklung findet im Hippocampus statt. Für weitere Erläuterungen s. den Text. Mu et al. (2010).

Extrazelluläre Nukleotide können die Proliferation und Differenzierung der NPZ während der embryonalen Entwicklung und im adulten Gehirn beeinflussen (Neary and Zimmermann, 2009; Illes et al., 2013). P2Y1R regeln besonders viele Funktionen

embryonaler und adulter NPZ. Ca^{2+} -Oszillationen in einzelnen Astrozyten und fortgeleitete Ca^{2+} -Wellen im glialen Synzytium dienen der Kommunikation zwischen Astrozyten (Kuga et al., 2011). Diese Form der interzellulären Kommunikation wird durch die Diffusion von Inositol 1,4,5-Trisphosphat (IP_3) in benachbarte Astrozyten und gleichzeitig durch die Ausschüttung von ATP auf dieselben Astrozyten vermittelt. ATP aktiviert danach P2Y1R und setzt ebenfalls intrazelluläres IP_3 frei (Rubini et al., 2009). Im Neokortex breiten sich die Ca^{2+} -Wellen über die Radialgliazellen in die ventrikuläre Zone aus und fördern die Proliferation von NPZ im Laufe der embryonalen Neurogenese (Weissman et al., 2004). Falls die Ca^{2+} -Wellenaktivität blockiert wird, nimmt die Vermehrung der NPZ ab. Dieser Effekt von NPZ wurde mehrfach in Zellkulturen durch Messung der Zellzahl (Mishra et al., 2006) oder Bestimmung des Einbaus von Bromodeoxyuridin in die DNA (Pearson et al., 2005) nachgewiesen.

P2Y1R regulieren die Migration der embryonalen NPZ aus der SVZ in den Bulbus olfactorius (Scemes et al., 2003). Die NPZ zeigten spontane Ca^{2+} -Oszillationen, die durch das P2Y1R-antagonistische MRS2179 aufgehoben werden konnten. Darüber hinaus blockierte MRS2179 das Migrationsverhalten der SVZ-NPZ. Schließlich wurde ATP als negativer Regulator der terminalen Ausdifferenzierung embryonaler NPZ der Maus beschrieben (Lin et al., 2007).

An adulten NPZ des Hippocampus und der SVZ von Ratte und Maus wurden Bz-ATP-induzierte Ströme nachgewiesen, die möglicherweise über P2X7R vermittelt werden (Hogg et al., 2004; Shukla et al., 2005; Delarasse et al., 2009). P2X7R verursachen Apoptose/Nekrose verschiedener Zellen (Sperlagh et al., 2006), inklusive Stammzellen, obwohl relativ niedrige Konzentrationen von ATP an gewissen Splice-Varianten von P2X7R Wachstum und Proliferation auslösen können (Adinolfi et al., 2012).

1.6. Referenzen

- Abbracchio MP, Burnstock G (1994) Purinoceptors: are there families of P2X and P2Y purinoceptors? *Pharmacol Ther* 64:445-475.
- Abbracchio MP, Burnstock G, Verkhratsky A, Zimmermann H (2009) Purinergic signalling in the nervous system: an overview. *Trends Neurosci* 32:19-29.
- Adinolfi E, Raffaghello L, Giuliani AL, Cavazzini L, Capece M, Chiozzi P, Bianchi G, Kroemer G, Pistoia V, Di Virgilio F (2012) Expression of P2X7 receptor increases in vivo tumor growth. *Cancer Res* 72:2957-2969.
- Boeynaems JM, Communi D, Robbaya B (2012) Overview of the pharmacology and physiological roles of P2X receptors. *WIREs Membr Transp Sign* 1:581-588.
- Brändle U, Spielmanns P, Osteroth R, Sim J, Surprenant A, Buell G, Ruppersberg JP, Plinkert PK, Zenner HP, Glowatzki E (1997) Desensitization of the P2X2 receptor controlled by alternative splicing. *FEBS Lett* 404:294-298.

- Buffo A, Vosko MR, Erturk D, Hamann GF, Jucker M, Rowitch D, Götz M (2005) Expression pattern of the transcription factor Olig2 in response to brain injuries: implications for neuronal repair. *Proc Natl Acad Sci U S A* 102:18183-18188.
- Burnstock G (1972) Purinergic nerves. *Pharmacol Rev* 24:509-581.
- Burnstock G (1976) Do some nerve cells release more than one transmitter? *Neuroscience* 1:239-248.
- Burnstock G (2007) Physiology and pathophysiology of purinergic neurotransmission. *Physiol Rev* 87:659-797.
- Burnstock G, Krügel U, Abbracchio MP, Illes P (2011) Purinergic signalling: from normal behaviour to pathological brain function. *Prog Neurobiol* 95:229-274.
- Burnstock G, Verkhratsky A (2009) Evolutionary origins of the purinergic signalling system. *Acta Physiol (Oxf)* 195:415-447.
- Cattaneo M (2011) The platelet P2Y₁₂ receptor for adenosine diphosphate: congenital and drug-induced defects. *Blood* 117:2102-2112.
- Chaumont S, Khakh BS (2008) Patch-clamp coordinated spectroscopy shows P2X₂ receptor permeability dynamics require cytosolic domain rearrangements but not Panx-1 channels. *Proc Natl Acad Sci U S A* 105:12063-12068.
- Chen CC, Akopian AN, Sivilotti L, Colquhoun D, Burnstock G, Wood JN (1995) A P2X purinoceptor expressed by a subset of sensory neurons. *Nature* 377:428-431.
- Chizh BA, Illes P (2001) P2X receptors and nociception. *Pharmacol Rev* 53:553-568.
- Clark AK, Staniland AA, Marchand F, Kaan TK, McMahon SB, Malcangio M (2010) P2X₇-dependent release of interleukin-1 β and nociception in the spinal cord following lipopolysaccharide. *J Neurosci* 30:573-582.
- Cockayne DA, Hamilton SG, Zhu QM, Dunn PM, Zhong Y, Novakovic S, Malmberg AB, Cain G, Berson A, Kassotakis L, Hedley L, Lachnit WG, Burnstock G, McMahon SB, Ford AP (2000) Urinary bladder hyporeflexia and reduced pain-related behaviour in P2X₃-deficient mice. *Nature* 407:1011-1015.
- Coddou C, Stojilkovic SS, Huidobro-Toro JP (2011) Allosteric modulation of ATP-gated P2X receptor channels. *Rev Neurosci* 22:335-354.
- Costa-Junior HM, Sarmiento VF, Coutinho-Silva R (2011) C terminus of the P2X₇ receptor: treasure hunting. *Purinergic Signal* 7:7-19.
- Coull JA, Beggs S, Boudreau D, Boivin D, Tsuda M, Inoue K, Gravel C, Salter MW, De Koninck Y (2005) BDNF from microglia causes the shift in neuronal anion gradient underlying neuropathic pain. *Nature* 438:1017-1021.
- Dale N (2008) Dynamic ATP signalling and neural development. *J Physiol* 586:2429-2436.
- Delarasse C, Gonnord P, Galante M, Auger R, Daniel H, Motta I, Kanellopoulos JM (2009) Neural progenitor cell death is induced by extracellular ATP via ligation of P2X₇ receptor. *J Neurochem* 109:846-857.
- Ding S, Sachs F (1999) Single channel properties of P2X₂ purinoceptors. *J Gen Physiol* 113:695-720.
- Doetsch F (2003) The glial identity of neural stem cells. *Nat Neurosci* 6:1127-1134.
- Donnelly-Roberts D, McGaraughty S, Shieh CC, Honore P, Jarvis MF (2008) Painful purinergic receptors. *J Pharmacol Exp Ther* 324:409-415.
- Egan TM, Cox JA, Voigt MM (2004) Molecular structure of P2X receptors. *Curr Top Med Chem* 4:821-829.
- Fountain SJ (2013) Primitive ATP-activated P2X receptors: discovery, function and pharmacology. *Front Cell Neurosci* 7:247.
- Gerevich Z, Borvendég SJ, Schröder W, Franke H, Wirkner K, Nörenberg W, Fürst S, Gillen C, Illes P (2004) Inhibition of N-type voltage-activated calcium channels in rat dorsal root ganglion neurons by P2Y receptors is a possible mechanism of ADP-induced analgesia. *J Neurosci* 24:797-807.
- Gerevich Z, Illes P (2004) P2Y receptors and pain transmission. *Purinergic Signal* 1:3-10.
- Habermacher C, Dunning K, Chataigneau T, Grutter T (2016) Molecular structure and function of P2X receptors. *Neuropharmacology* 104:18-30.
- Hattori M, Gouaux E (2012) Molecular mechanism of ATP binding and ion channel activation in P2X receptors. *Nature* 485:207-212.

- Hogg RC, Chipperfield H, Whyte KA, Stafford MR, Hansen MA, Cool SM, Nurcombe V, Adams DJ (2004) Functional maturation of isolated neural progenitor cells from the adult rat hippocampus. *Eur J Neurosci* 19:2410-2420.
- Illes P, Ribeiro AJ (2004) Molecular physiology of P2 receptors in the central nervous system. *Eur J Pharmacol* 483:5-17.
- Illes P, Messemer N, Rubini P (2013) P2Y receptors in neurogenesis. *WIREs Membr Transp Signal* 1:43-48.
- Jacobson AJ, Jayasekara MPS, Costanzi S (2012) Molecular structure of the P2Y receptors: mutagenesis, modelling and chemical probes. *WIREs Membr Transp Sign* 1:815-827.
- Jacobson KA, Boeynaems JM (2010) P2Y nucleotide receptors: promise of therapeutic applications. *Drug Discov Today* 15:570-578.
- Jacobson KA, Gao ZG, Goblyos A, Ijzerman AP (2011) Allosteric modulation of purine and pyrimidine receptors. *Adv Pharmacol* 61:187-220.
- Jarvis MF, Khakh BS (2009) ATP-gated P2X cation-channels. *Neuropharmacology* 56:208-215.
- Károly R, Mike A, Illes P, Gerevich Z (2008) The unusual state-dependent affinity of P2X3 receptors can be explained by an allosteric two-open-state model. *Mol Pharmacol* 73:224-234.
- Kawate T, Michel JC, Birdsong WT, Gouaux E (2009) Crystal structure of the ATP-gated P2X4 ion channel in the closed state. *Nature* 460:592-598.
- Khakh BS, North RA (2012) Neuromodulation by extracellular ATP and P2X receptors in the CNS. *Neuron* 76:51-69.
- Köles L, Fürst S, Illes P (2007) Purine ionotropic (P2X) receptors. *Curr Pharm Des* 13:2368-2384.
- Köles L, Gerevich Z, Oliveira JF, Zádori ZS, Wirkner K, Illes P (2008) Interaction of P2 purinergic receptors with cellular macromolecules. *Naunyn Schmiedebergs Arch Pharmacol* 377:1-33.
- Kuga N, Sasaki T, Takahara Y, Matsuki N, Ikegaya Y (2011) Large-scale calcium waves traveling through astrocytic networks in vivo. *J Neurosci* 31:2607-2614.
- Lazarowski ER, Shea DA, Boucher RC, Harden TK (2003) Release of cellular UDP-glucose as a potential extracellular signaling molecule. *Mol Pharmacol* 63:1190-1197.
- Lewis C, Neidhart S, Holy C, North RA, Buell G, Surprenant A (1995) Coexpression of P2X2 and P2X3 receptor subunits can account for ATP-gated currents in sensory neurons. *Nature* 377:432-435.
- Lin JH, Takano T, Arcuino G, Wang X, Hu F, Darzynkiewicz Z, Nunes M, Goldman SA, Nedergaard M (2007) Purinergic signaling regulates neural progenitor cell expansion and neurogenesis. *Dev Biol* 302:356-366.
- Lledo PM, Gheusi G (2006) Adult neurogenesis: from basic research to clinical applications. *Bull Acad Natl Med* 190:385-400.
- Mager PP, Weber A, Illes P (2004) Bridging the gap between structural bioinformatics and receptor research: the membrane-embedded, ligand-gated, P2X glycoprotein receptor. *Curr Top Med Chem* 4:1657-1705.
- Marquez-Klaka B, Rettinger J, Nicke A (2009) Inter-subunit disulfide cross-linking in homomeric and heteromeric P2X receptors. *Eur Biophys J* 38:329-338.
- Milligan ED, Watkins LR (2009) Pathological and protective roles of glia in chronic pain. *Nat Rev Neurosci* 10:23-36.
- Mishra SK, Braun N, Shukla V, Fullgrabe M, Schomerus C, Korf HW, Gachet C, Ikehara Y, Sevigny J, Robson SC, Zimmermann H (2006) Extracellular nucleotide signaling in adult neural stem cells: synergism with growth factor-mediated cellular proliferation. *Development* 133:675-684.
- Molliver DC, Wright DE, Leitner ML, Parsadanian AS, Doster K, Wen D, Yan Q, Snider WD (1997) IB4-binding DRG neurons switch from NGF to GDNF dependence in early postnatal life. *Neuron* 19:849-861.
- Morest DK, Silver J (2003) Precursors of neurons, neuroglia, and ependymal cells in the CNS: what are they? Where are they from? How do they get where they are going? *Glia* 43:6-18.

- Nakatsuka T, Gu JG (2001) ATP P2X receptor-mediated enhancement of glutamate release and evoked EPSCs in dorsal horn neurons of the rat spinal cord. *J Neurosci* 21:6522-6531.
- Nakatsuka T, Tsuzuki K, Ling JX, Sonobe H, Gu JG (2003) Distinct roles of P2X receptors in modulating glutamate release at different primary sensory synapses in rat spinal cord. *J Neurophysiol* 89:3243-3252.
- Neary JT, Zimmermann H (2009) Trophic functions of nucleotides in the central nervous system. *Trends Neurosci* 32:189-198.
- Nicke A, Baumert HG, Rettinger J, Eichele A, Lambrecht G, Mutschler E, Schmalzing G (1998) P2X1 and P2X3 receptors form stable trimers: a novel structural motif of ligand-gated ion channels. *EMBO J* 17:3016-3028.
- Nörenberg W, Illes P (2000) Neuronal P2X receptors: localisation and functional properties. *Naunyn Schmiedeberg's Arch Pharmacol* 362:324-339.
- North RA (2002) Molecular physiology of P2X receptors. *Physiol Rev* 82:1013-1067.
- Ormond SJ, Barrera NP, Qureshi OS, Henderson RM, Edwardson JM, Murrell-Lagnado RD (2006) An uncharged region within the N terminus of the P2X6 receptor inhibits its assembly and exit from the endoplasmic reticulum. *Mol Pharmacol* 69:1692-1700.
- Pearson RA, Dale N, Llaudet E, Mobbs P (2005) ATP released via gap junction hemichannels from the pigment epithelium regulates neural retinal progenitor proliferation. *Neuron* 46:731-744.
- Pelegri P (2011) Many ways to dilate the P2X7 receptor pore. *Br J Pharmacol* 163:908-911.
- Platel JC, Bordey A (2016) The multifaceted subventricular zone astrocyte: From a metabolic and pro-neurogenic role to acting as a neural stem cell. *Neuroscience* 323:20-28.
- Rettig J, Neher E (2002) Emerging roles of presynaptic proteins in Ca²⁺-triggered exocytosis. *Science* 298:781-785.
- Roberts JA, Vial C, Digby HR, Agboh KC, Wen H, Atterbury-Thomas A, Evans RJ (2006) Molecular properties of P2X receptors. *Pflugers Arch* 452:486-500.
- Rubini P, Milosevic J, Engelhardt J, Al-Khrasani M, Franke H, Heinrich A, Sperlágh B, Schwarz SC, Schwarz J, Nörenberg W, Illes P (2009) Increase of intracellular Ca²⁺ by adenine and uracil nucleotides in human midbrain-derived neuronal progenitor cells. *Cell Calcium* 45:485-498.
- Saul A, Hausmann R, Kless A, Nicke A (2013) Heteromeric assembly of P2X subunits. *Front Cell Neurosci* 7:250.
- Sawada K, Echigo N, Juge N, Miyaji T, Otsuka M, Omote H, Yamamoto A, Moriyama Y (2008) Identification of a vesicular nucleotide transporter. *Proc Natl Acad Sci U S A* 105:5683-5686.
- Scemes E, Duval N, Meda P (2003) Reduced expression of P2Y1 receptors in connexin43-null mice alters calcium signaling and migration of neural progenitor cells. *J Neurosci* 23:11444-11452.
- Shukla V, Zimmermann H, Wang L, Kettenmann H, Raab S, Hammer K, Seigny J, Robson SC, Braun N (2005) Functional expression of the ecto-ATPase NTPDase2 and of nucleotide receptors by neuronal progenitor cells in the adult murine hippocampus. *J Neurosci Res* 80:600-610.
- Sokolova E, Skorinkin A, Moiseev I, Agrachev A, Nistri A, Giniatullin R (2006) Experimental and modeling studies of desensitization of P2X3 receptors. *Mol Pharmacol* 70:373-382.
- Sperlágh B, Vizi ES, Wirkner K, Illes P (2006) P2X7 receptors in the nervous system. *Prog Neurobiol* 78:327-346.
- Stelmashenko O, Lalo U, Yang Y, Bragg L, North RA, Compan V (2012) Activation of trimeric P2X2 receptors by fewer than three ATP molecules. *Mol Pharmacol* 82:760-766.
- Torres GE, Egan TM, Voigt MM (1999) Hetero-oligomeric assembly of P2X receptor subunits. Specificities exist with regard to possible partners. *J Biol Chem* 274:6653-6659.
- Vial C, Roberts JA, Evans RJ (2004) Molecular properties of ATP-gated P2X receptor ion channels. *Trends Pharmacol Sci* 25:487-493.
- von Kügelgen I (2006) Pharmacological profiles of cloned mammalian P2Y-receptor subtypes. *Pharmacol Ther* 110:415-432.

- von Kügelgen I, Harden TK (2011) Molecular pharmacology, physiology, and structure of the P2Y receptors. *Adv Pharmacol* 61:373-415.
- Wall M, Eason R, Dale N (2010) Biosensor measurement of purine release from cerebellar cultures and slices. *Purinergic Signal* 6:339-348.
- Walsh JA, Price MJ (2014) Cangrelor for treatment of arterial thrombosis. *Expert Opin Pharmacother* 15:565-572.
- Wilkinson WJ, Jiang LH, Surprenant A, North RA (2006) Role of ectodomain lysines in the subunits of the heteromeric P2X2/3 receptor. *Mol Pharmacol* 70:1159-1163.
- Wirkner K, Sperlágh B, Illes P (2007) P2X3 receptor involvement in pain states. *Mol Neurobiol* 36:165-183.
- Young MT (2010) P2X receptors: dawn of the post-structure era. *Trends Biochem Sci* 35:83-90.
- Zemkova H, Yan Z, Liang Z, Jelinkova I, Tomic M, Stojilkovic SS (2007) Role of aromatic and charged ectodomain residues in the P2X4 receptor functions. *J Neurochem* 102:1139-1150.
- Zhang J, Zhang K, Gao ZG, Paoletta S, Zhang D, Han GW, Li T, Ma L, Zhang W, Müller CE, Yang H, Jiang H, Cherezov V, Katritch V, Jacobson KA, Stevens RC, Wu B, Zhao Q (2014) Agonist-bound structure of the human P2Y receptor. *Nature* 509:119-122.
- Zhang K, Zhang J, Gao ZG, Zhang D, Zhu L, Han GW, Moss SM, Paoletta S, Kiselev E, Lu W, Fenalti G, Zhang W, Müller CE, Yang H, Jiang H, Cherezov V, Katritch V, Jacobson KA, Stevens RC, Wu B, Zhao Q (2014) Structure of the human P2Y receptor in complex with an antithrombotic drug. *Nature* 509:115-118.
- Zhang Z, Chen G, Zhou W, Song A, Xu T, Luo Q, Wang W, Gu XS, Duan S (2007) Regulated ATP release from astrocytes through lysosome exocytosis. *Nat Cell Biol* 9:945-953.
- Zimmermann H (2000) Extracellular metabolism of ATP and other nucleotides. *Naunyn Schmiedebergs Arch Pharmacol* 362:299-309.
- Zimmermann H, Braun N (1999) Ecto-nucleotidases--molecular structures, catalytic properties, and functional roles in the nervous system. *Prog Brain Res* 120:371-385.
- Zorec R, Araque A, Carmignoto G, Haydon PG, Verkhratsky A, Parpura V (2012) Astroglial excitability and gliotransmission: an appraisal of Ca²⁺ as a signalling route. *ASN Neuro* 4.

2. Wissenschaftliche Ergebnisse

Meine Habilitation beschäftigt sich mit neuronalen P2R und ihren Funktionen. Die vorgestellten Publikationen können den folgenden Abschnitten zugeordnet werden:

Struktur-Funktions-Zusammenhänge rekombinanter, humaner P2X3 und P2X2/3R in Expressionssystemen

- (1) Agonisten-Bindungsstelle der homomeren P2X3R
- (2) Untereinheiten-Zusammensetzung der heteromeren P2X2/6R
- (3) Untereinheiten-Zusammensetzung der heteromeren P2X2/3R

Vorhandensein und Wirkung von P2X7R an kultivierten adulten neuronalen Vorläuferzellen und Astrozyten

- (4) Nachweis von homomeren P2X7R an NPZ der Maus
- (5) Nachweis der Ko-Lokalisation von P2X4- und P2X7R an NPZ der Maus

(6) Nachweis von P2X7R an Astrozyten der Ratte

Vorhandensein und Wirkung von P2Y1R an embryonalen neuronalen Vorläuferzellen und dedifferenzierten kultivierten striatalen Neuronen

(7) Nachweis der P2Y1R an humanen NPZ

(8) Nachweis der P2Y1R an dedifferenzierten striatalen Neuronen

(9) Modulation der P2Y1R-Funktion in dedifferenzierten striatalen Neuronen durch Dopamin D1- und D2R

Ich fand es dem Verständnis dienlich, die Ergebnisse ohne ausführliche Hinweise auf die einschlägige Literatur zusammenzufassen. Es werden jedoch alle Angaben durch Publikationen gestützt, die im Literaturverzeichnis meiner Arbeiten geführt werden. Darüber hinaus, kann der Leser zahlreiche wesentliche Erkenntnisse in der Einleitung der Habilitation nachprüfen.

2.1. Komplex I. Struktur-Wirkungs-Zusammenhänge rekombinanter, humaner P2X3- und P2X2/3-Rezeptoren in Expressionssystemen

2.1.1. Bodnar M, Wang H, Riedel T, Hintze S, Kato E, Fallah G, Gröger-Arndt H, Giniatullin R, Grohmann M, Hausmann R, Schmalzing G, Illes P, **Rubini P** (2011) *Amino acid residues constituting the agonist binding site of the human P2X3 receptor*. J Biol Chem 286:2739-2749.

Wir erstellten ein Homologie-Modell des P2X3R, das sich auf die publizierte Struktur des trunkierten zfp2X4R stützte. Wie berichtet, befindet sich die Agonisten-Bindungstasche an der Schnittstelle zweier Untereinheiten. Unser Anliegen war es festzustellen, ob die in NBS1-2 und NBS3-4 (s. Abb. 1A der Publikation) integrierten Aminosäuren (AS) für die Auskleidung der Bindungstasche von essenzieller Bedeutung sind, oder ob nur einige dieser AS eine wichtige Rolle in Bindung, Schleusenfunktion („gating“) oder Desensibilisierung spielen. Bereits die Prüfung der Erreichbarkeit der AS-Reste durch den hydrophilen Agonisten anhand des Homologie-Modells besagte, dass einige dieser AS-Reste für die Bindung keine Rolle spielen können, da sie von der extrazellulären Seite nicht erreichbar sind. Wir fragten uns aber: Ist es möglich, dass sie an den beiden restlichen Funktionen beteiligt oder für den Aufbau der Bindungstasche verantwortlich sind?

Um die Fragestellungen beantworten zu können, haben wir alle konservierten AS in den jeweiligen Bindungstaschen auf die neutrale AS Alanin (Ala) mutiert. Einige nicht-konservierte AS haben wir ebenfalls durch Ala ersetzt, um spezifische Teilaspekte klären zu können. Die Rezeptor-Mutanten wurden danach in HEK293-Zellen und/oder *Xenopus laevis* Oozyten exprimiert, um die Wirkung des P2X_{1,3R}-selektiven Agonisten α,β -meATP zu bestimmen. Es wurden Konzentrations-Wirkungskurven erstellt und die EC_{50} -Werte und der maximale Effekt (E_{max}) berechnet. Gemessen wurde die Stromantwort mittels des Patch-Clamp-Verfahrens (HEK293-Zellen) oder der Zwei-Elektroden-Spannungsklemme (Oozyten). Außerdem haben wir den Anstieg der intrazellulären Ca^{2+} -Konzentration ($[Ca^{2+}]_i$) mit Hilfe der Fura-2-Methode bestimmt. Da α,β -meATP die G_q -gekoppelten P2Y_{2,4,6R} nicht aktiviert, kommt es zu keiner Freisetzung des Ca^{2+} aus intrazellulären Speichern. Der Agonist steigert den Einstrom von Ca^{2+} über den Rezeptor-Kanal und erhöht infolgedessen $[Ca^{2+}]_i$ ausschließlich über diesen Weg.

Das Ersetzen aller konservierten Aminosäuren in den NBS durch Ala führte unweigerlich zur Rechtsverschiebung der Konzentrations-Wirkungskurven und/oder der Abnahme des Wirkmaximums im Vergleich zu dem Wildtyp (WT)-Rezeptor. Die größten Änderungen traten beim Austausch der AS Gly (Gly-66), Lys (Lys-63, Lys-176; Lys-284), Asn (Asn-177, Asn-279), Arg (Arg-281, Arg-295) und Thr (Thr-172) auf. Der Austausch zweier benachbarter AS im selben NBS durch Ala führte zu einer additiven Abnahme des E_{max} (z.B. Asn-279/Phe-280), obwohl der Austausch zweier nicht benachbarter AS (Phe-171/Asn-177) keinen vergleichbaren Effekt erzeugte. Darüber hinaus fanden wir, dass eine Hemmung des E_{max} häufig mit der Verminderung der Aktivierungs- und/oder Desensibilisierungs-Zeitkonstanten einherging.

Da einige Ala-Mutationen zu einer kompletten Inhibition der α,β -meATP-Wirkung führten, untersuchten wir, ob die Untereinheiten-Mutanten sich zu trimeren Rezeptoren zusammensetzen und in die Zellmembran als solche eingebaut werden. Diese Experimente wurden am Oozyten-System durchgeführt, nachdem die funktionellen Daten mittels Strommessungen dort reproduziert werden konnten. Verwendet wurden die blau-native Polyacrylamid-Gelelektrophorese („blue native PAGE“), in der [³⁵S]Methionin markierten Form und SDS-PAGE in der Cy5 Zelloberflächen-markierten Form. Es konnte nachgewiesen werden, dass alle Mutanten als trimere Rezeptoren in der Zellmembran exprimiert sind.

Zusammenfassend folgerten wir, dass alle in NBS1-2 und NBS3-4 integrieren AS für die Agonisten-Bindung, Schleusenfunktion und/oder Desensibilisierung des homomeren P2X3R notwendig sind, wenn auch zu unterschiedlichem Ausmaß.

2.1.2. Hausmann R, Bodnar M, Woltersdorf R, Wang H, Fuchs M, Messemer N, Qin Y, Günther J, Riedel T, Grohmann M, Nieber K, Schmalzing G, **Rubini P***, Illes P (2012) *ATP binding site mutagenesis reveals different subunit stoichiometry of functional P2X2/3 and P2X2/6 receptors*. J Biol Chem 287:13930-13943. (*gleichberechtigte Senior-Autorin).

Wir interessierten uns für die Frage, ob die Untereinheiten-Zusammensetzung von P2X2/3- und P2X2/6R identisch oder unterschiedlich ist. Für P2X2/3R wird angenommen, dass die Stöchiometrie $(X2)_1/(X3)_2$ ist, während für P2X2/6R mittels Atomkraftmikroskopie („atomic force microscopy“) eine variable Stöchiometrie (Gemisch von $(X2)_1/(X6)_2$ und $(X2)_2/(X6)_1$) nachgewiesen wurde, mit Überwiegen einer der Varianten, abhängig vom Transfektionsverhältnis der verwendeten cDNA-Plasmide.

Der Ausgangspunkt unserer Experimente war die Erkenntnis, dass Ala-Substitutionen einiger positiv geladener AS in den NBS der P2X3R-Untereinheiten (Lys-63, Lys-176, Arg-281, Lys-299; Publikation 2.1.1.) zu einem (fast) vollständigen Verlust der Wirkung von α,β -meATP führten. Die verwendeten Methoden waren elektrophysiologisch/biochemisch; als Expressionssysteme wurden Säugerzellen (HEK293) und Oozyten eingesetzt. Als Erstes zeigten wir, dass P2X3R-homologe Ala-Mutationen, bei P2X2R ebenfalls Inaktivität herbeiführten. Allerdings musste dafür der unselektive Agonist 2-Methylthio ATP (2-MeSATP) benutzt werden, da P2X2R auf α,β -meATP nicht reagieren. Erwähnenswert ist, dass α,β -meATP nicht nur an P2X3R sondern auch an P2X2/3R eine voll-agonistische Wirkung entfaltet, allerdings mit dem Unterschied, dass P2XR-Ströme schnell, P2X2/3R-Ströme hingegen langsam desensibilisieren. P2X2-, P2X3- und P2X2/3R konnten somit bereits durch die Wahl des Agonisten α,β -meATP voneinander unterschieden werden. Die Unterscheidungsmerkmale waren die folgenden: P2X2R, kein Effekt von α,β -meATP; P2X3R, schnell desensibilisierender α,β -meATP-Effekt; P2X2/3R, langsam desensibilisierender α,β -meATP-Effekt.

Falls die HEK293-Zellen mit P2X2- und P2X3-cDNA in einem Verhältnis von 1:2 transfiziert wurden, hemmten die besagten P2X3-Mutanten die α,β -meATP-Effekte

an den heteromeren P2X2-WT/P2X3-Mut Rezeptor vollständig. Danach ko-transfizierten wir inaktive P2X2R-Untereinheiten mit WT P2X3R-Untereinheiten im o.g. Verhältnis und fanden, dass der gebildete P2X2-Mut/P2X3-WT Rezeptor in seiner Empfindlichkeit gegenüber α,β -meATP nur geringfügig eingeschränkt war. Daraus schlussfolgerten wir, dass dieser Agonist sowohl an der Schnittstelle von X3-X3 als auch von X2-X3 wirken kann und die Besetzung zweier Bindungsstellen für die Agonisten-Wirksamkeit ausreicht.

Bei der P2X2/6-Heteromere war die Beweislage schwieriger. Homomere P2X6R haben ein Trafficking-Defizit; ihre drei Untereinheiten schließen sich zwar intrazellulär zum vollständigen Rezeptor zusammen, werden aber danach nicht in die Zellmembran gefördert und eingebaut. P2X2/6R sind funktionsfähig, unterscheiden sich in ihren Stromantworten auf Agonisten jedoch nur geringfügig vom homomeren P2X2R. Berichtet wurden unterschiedliche pH-Empfindlichkeiten, E_{max} -Werte der jeweiligen Konzentrations-Wirkungskurven und Zeitkonstanten der Aktivierung. All diese Unterschiede konnten nachgewiesen werden, indem die WT-P2X2- und WT-P2X6-cDNA in einem Verhältnis von 1:4 in HEK293-Zellen transfiziert wurden. Die Kombinationen der inaktiven P2X2-Mut und P2X6-Mut Untereinheiten mit ihren komplementären WT-Rezeptoren erbrachten Resultate, die den mit P2X2-Mut und P2X3-Mut Kombinationen mit ihren WT-Gegenstücken gewonnenen Ergebnisse entgegengesetzt waren. Wir folgerten deshalb, dass die P2X2/6R in der $(X2)_2/(X3)_1$ Stöchiometrie vorliegen.

Alle Resultate konnten mithilfe der Fura-2-Technik und der Messung von Ca^{2+} Transienten an HEK293-Zellen bestätigt werden. Bei Untersuchungen zu den P2X2/3-Heteromeren wurde α,β -meATP als Agonist verwendet, bei Messungen an den P2X2/6-Rezeptoren, wegen der bereits diskutierten Problematik, 2-MeSATP. Da jedoch 2-MeSATP im Gegensatz zu α,β -meATP, G_q -gekoppelte P2YR stimulieren kann, haben wir diese Effekte bei den Patch-Clamp Messungen durch die der Pipettenlösung beigegebenen GDP- β -S ausgeschlossen. Bei den Ca^{2+} -Imaging Experimenten wurden HEK293-Zellen mit Rezeptor-cDNA-freiem Transfektionsmedium behandelt („mock transfection“). Der tatsächliche 2-MeSATP-Effekt an P2X2- oder P2X2/6R wurde berechnet, indem die Mock-Effekte abgezogen wurden. Ferner bestätigten biochemische Untersuchungen, dass in *Xenopus laevis* Oocyten die untersuchten Mutanten intrazellulär trimere Rezeptoren bildeten und in die Zellmembran ungehindert einwandern konnten.

Zusammenfassend folgerten wir, dass spezifische Erkennungsstellen der P2X2-Untereinheiten einerseits und der P2X3- bzw. P2X6-Untereinheiten andererseits deren Assoziation in trimere Rezeptoren steuern. Allerdings schloss dieser regulatorische Mechanismus keinesfalls die Möglichkeit der Bildung zweier Stöchiometrien innerhalb einer Untereinheiten-Kombination aus, wurde aber durch das Mengenverhältnis der zur Transfektion verwendeten cDNA bestimmt (z.B. $(X2)_1/(X3)_2 > (X2)_2/(X3)_1$ und $(X2)_2/(X6)_1 > (X2)_1/(X6)_2$).

2.1.3. Kowalski M, Hausmann R, Schmid J, Dopychai A, Stephan G, Tang Y, Schmalzing G, Illes P, **Rubini P** (2016) *Flexible subunit stoichiometry of functional human P2X2/3 heteromeric receptors*. *Neuropharmacology* 99:115-130.

In Fortsetzung der in Publikation 2.1.2. bearbeiteten Problematik fragten wir uns, ob - wie in der zusammenfassenden Bewertung der vorhergehenden Publikation spekuliert - für P2X2/3 tatsächlich zwei Untereinheiten-Kombinationen, nämlich $(X2)_1/(X3)_2$ und $(X2)_2/(X3)_1$, vorliegen. Eine solche Situation wäre hochinteressant, vor allem, falls die beiden Rezeptor-Varianten unterschiedliche Empfindlichkeiten gegenüber allosterischen Modulatoren und/oder pharmakologischen Antagonisten aufweisen würden. Da P2X2/3R in sensorischen Ganglien vorkommen und in der Empfindung und Übertragung schmerzhafter Stimuli von Bedeutung sind (s. Einleitung), hätten diese Erkenntnisse auch eine potentielle physiologisch-/therapeutische Bedeutung.

Die experimentellen Vorgehensweisen waren weitgehend identisch mit denen, die in Publikation 2.1.2. genutzt wurden. Wir verwendeten, um die Untereinheiten-Kombinationen P2X2-Mut/P2X3-WT und P2X2-WT/P2X3-Mut zu gewinnen, die Transfektionsverhältnisse 1:2 und 4:1. Unsere Resultate bestätigten die Eingangshypothese. Das heißt, dass bei 1:2 Transfektion der HEK293-Zellen mit den P2X2- und P2X3R-cDNA, die Untereinheiten-Kombinationen in einem Verhältnis von $(X2)_1/(X3)_2 > (X2)_2/(X3)_1$ gebildet wurden, während bei der 4:1 Transfektion, das umgekehrte Verhältnis $(X2)_2/(X3)_1 > (X2)_1/(X3)_2$ vorherrschte.

Da ein Ansäuern des Badmediums die Agonisten-induzierten Ströme an P2X2R steigert, an P2X3R jedoch hemmt, untersuchten wir die Wirkung der allosterisch modulierenden Protonen auf beide Varianten des P2X2/3R (sowohl 1:2 als auch 4:1 Transfektionen von P2X2- und P2X3R-cDNA). Wir fanden jedoch keinen Unterschied

der Agonisten-induzierten Ströme bei den verwendeten pH-Werten (7,4-6,4-5,4). Der allosterische Modulator Zn^{2+} steigert bei niedrigen Konzentrationen P2X2R-Ströme und hemmt sie bei höheren Konzentrationen, während P2X3R-Ströme durchgehend inhibiert werden. Unterschiede in der Modulation der zwei Varianten von P2X2/3R durch Zn^{2+} konnten jedoch nicht demonstriert werden.

Anders verhielt sich der kompetitive P2X3- und P2X2/3R-Antagonist A-317491 (nicht aber TNP-ATP). Bei steigenden Konzentrationen reduzierte er den Effekt von α,β -meATP, jedoch bei den zwei verwendeten Transfektionsverhältnissen in unterschiedlichem Ausmaß. Diese Unterschiede waren relativ gering (25-30%) aber statistisch hochsignifikant.

Den überzeugendsten Beweis für das Vorhandensein der beiden P2X2/3R-Varianten lieferten biochemische Experimente, in denen GFP-fusionierte P2X2-Untereinheiten mit TrepII-getaggten P2X3-Untereinheiten in *Xenopus laevis*-Oocyten exprimiert wurden. Homotrimere P2X3R und heterotrimere P2X2/3R wurden mit Dodecyl-Maltosid solubilisiert, über ihre StrepII-Tags aufgereinigt und in der nicht-denaturierten Form mithilfe von blau-nativer PAGE analysiert. Die an Plasmamembran-gebundenen P2X2/3R erschienen an zwei klar unterscheidbaren Stellen am Gel und bewiesen somit, dass die $(P2X2-GFP)_2/(P2X3)$ - und $(P2X2-GFP)/(P2X3)_2$ -Proteinkomplexe vergesellschaftet vorkommen.

2.2. Komplex II. *Vorhandensein und Wirkung von P2X7R an kultivierten adulten neuronalen Vorläuferzellen und Astrozyten*

2.2.1. Messemer N, Kunert C, Grohmann M, Sobottka H, Nieber K, Zimmermann H, Franke H, Nörenberg W, Straub I, Schaefer M, Riedel T, Illes P, **Rubini P** (2013) *P2X7 receptors at adult neural progenitor cells of the mouse subventricular zone*. *Neuropharmacology* 73C:122-137.

Wie in der Einleitung geschildert, vermitteln P2X7R vorwiegend Apoptose/Nekrose, einige ihrer Splice-Varianten jedoch auch Proliferation verschiedener Zelltypen. Sie sind in erster Linie an peripheren und zentralen Immunzellen lokalisiert (z.B. Lymphozyten, Monozyten, Makrophagen, Mikroglia). Astrozyten exprimieren ebenfalls P2X7R; dieser Zelltyp übt zahlreiche Funktionen im ZNS aus, u.a. besitzt er eine Immunkompetenz. Da NPZ Radialglia-ähnliche Zellen sind, liegt es auf der Hand zu untersuchen, ob an ihnen P2X7R vorhanden sind und wenn ja, welche Effekte die Aktivierung dieses Rezeptortyps auslösen kann.

Wir kultivierten proliferierende SVZ-NPZ aus dem Gehirn adulter (8-14 Wochen alter Mäuse), nach den in der Literatur beschriebenen Methoden und zeigten, dass sie nach Differenzierungsvorgängen reife Astrozyten, Oligodendrozyten und Neurone generieren können. Die proliferierenden NPZ wurden immunhistochemisch mit dem Stammzellenmarkern Nestin und Musashi-1 immunhistochemisch charakterisiert. Mit der Ganzzellvariante der Patch-Clamp-Technik fand eine Subklassifizierung der NPZ in einen passiven, Astrozyten-ähnlichen Zelltyp und verschiedene auswärtsgleichrichtende Zelltypen statt. Nur ein sehr niedriger Prozentsatz der Zellen feuerte nach depolarisierender Strominjektion abortierte Aktionspotentiale.

Trotz der elektrophysiologischen Inhomogenität (aber homogener Nestin-Immunpositivität) reagierten alle NPZ in einem niedrigen Ca^{2+} -haltigen und Mg^{2+} -freien Badmedium auf Bz-ATP mit prominenten Einwärtsströmen. Nachdem das Haltepotential vom Ruhepotential-ähnlichen Wert von -70 mV in die depolarisierende und hyperpolarisierende Richtungen verschoben wurde, zeigte die Strom-Spannungskurve ein Umkehrpotential in der Nähe von 0 mV. Dieses Verhalten ist typisch für Liganden-aktivierte Kationenkanäle, wie für P2X7R. Falls exzidierte Patches durch Zurückziehen der Ableitpipette hergestellt wurden, kam es zu keinem Verlust des Bz-ATP Effektes. Offenbar waren die P2X7R an den NPZ selbst lokalisiert und nicht an benachbarten Zellen, von denen indirekte Wirkungen hätten ausgehen können.

Weitere Charakteristika, die auf das Vorhandensein eines P2X7R an NPZ hinweisen, waren die folgenden: (1) Bz-ATP war ein potenterer Agonist als ATP selbst; (2) Die selektiven P2X7R-Antagonisten Brilliant Blue G und A-438079 unterdrückten den Bz-ATP-Effekt; (3) Bz-ATP war an NPZ, die aus P2X7R K.O.-Mäusen präpariert wurden, inaktiv; (4) Die Agonisten-Ströme zeigten einen biphasischen Verlauf (früher schneller Anstieg, gefolgt von einem späten, langsamen, in ein Plateau mündenden, weiteren Anstieg), der bereits eine Dilatation des Rezeptor-Kanals bei langdauernder Aktivierung andeutete; (5) Bei langdauernder Agonisten-Exposition fand eine Aufnahme des Fluoreszenz-Farbstoffs Yo-Pro-1 in den Intrazellulärraum statt. Dieser Farbstoff kann unter normalen Bedingungen wegen seines relativ großen Molekül-Durchmessers den Rezeptor-Kanal nicht passieren. Erst nach Erweiterung des Kanals in eine Membranpore wird dies möglich.

Alle Resultate der Patch-Clamp-Messungen konnten mit der Fura-2-Methode bestätigt werden. Da in einem Ca^{2+} -freien Extrazellulärmedium Bz-ATP keine $[\text{Ca}^{2+}]_i$ -Transienten mehr auslöste, betrachteten wir es als erwiesen, dass an WT-NPZ der Agonist nicht in der Lage war, P2YR zu aktivieren. Dies scheint aber auf NPZ von P2X7R K.O.-Mäusen nicht zuzutreffen. Im Gegensatz zu den Strommessungen, war der E_{max} -Wert der Bz-ATP Konzentrations-Wirkungskurve im Vergleich zu der der WT-NPZ reduziert, wurde aber nicht vollständig unterdrückt. Wir glauben, dass bei solchen Mäusen die Funktion von P2X7R im Laufe der Entwicklung von einer nicht identifizierten Gruppe von P2YR übernommen wird.

Wichtige Ergebnisse zu Folgeerscheinungen der P2X7R-Aktivierung an den NPZ lieferten der MTT-Test und die Expression einer aktiven Caspase-Immunreaktivität nach Bz-ATP-Applikation. Der MTT-Test registrierte ein konzentrationsabhängiges Absterben der NPZ (Nekrose), während das Erscheinen der Caspase-Immunreaktivität die Stimulation eines Schlüsselenzyms der apoptotischen Reaktionskaskade signalisierte.

Ein häufiger Einwand bzgl. der Verwendung von NPZ-Zellkulturen zielt auf die unphysiologisch hohen Wachstumsfaktor-Konzentrationen im Nährmedium und die Plastizität des Zelltyps nach Kultivierung ab, die zur Änderung der in vivo-Eigenschaften führen kann. Deshalb haben wir Schnitte aus der SVZ-Zone des Gehirns GFP-Nestin-Transgener Mäuse angefertigt und aus ihnen NPZ Ströme abgeleitet. Die an Zellkulturen gewonnenen Resultate konnten voll bestätigt werden und belegten die Bedeutung der P2X7R an den NPZ.

Im Folgenden schlugen wir vor, dass der P2X7R ein pathophysiologisch bedeutsamer Rezeptor sein könnte, der erst bei zellschädigenden Vorgängen, wie bei metabolischer Einschränkung, exprimiert wird. Nach Status epilepticus könnten, die Zahl der in Überschuss produzierten NPZ der SGZ im Hippocampus, durch die regulatorische Wirkung von P2X7R auf den Normalwert reduziert werden. Proliferierende NPZ wandern in den Hilus hippocampi ein, werden dort als reife Körnerzellen in falsche neuronale Regelkreise integriert und tragen somit zur Chronifizierung der Temporallappen-Epilepsie bei. Diese Hypothese konnte mit einer weiteren Publikation der Arbeitsgruppe um Illes kürzlich bestätigt werden (Rozmer et al., Cerebral Cortex, im Druck).

2.2.2. Messemer N, Kunert R, Illes P, **Rubini P** (2013) *Co-expression of functional P2X4 and P2X7 receptors at adult neural precursor cells of the mouse subventricular zone*. The Open Neuroscience Journal 7:1-4.

In dieser Arbeit gingen wir einer in Publikation 2.2.1. nicht beantworteten Frage nach. Der Ausgangspunkt unserer Überlegungen war, dass P2X4 und P2X7R häufig vergesellschaftet auf derselben Zelle vorkommen und ihre Aktivierung neuartige Funktionen auslöst. Es wird zwar kontrovers diskutiert, ob es sich um zwei getrennte Rezeptoren handelt, die in der Zellmembran miteinander interagieren oder um einen heteromeren Rezeptor, der aus P2X4 und P2X7-Untereinheiten gebildet wird, aber die grundsätzliche Tatsache der Rezeptorinteraktion wird nicht bezweifelt.

Bz-ATP-induzierte Ströme an NPZ wurden nicht nur durch P2X7 (A-438079) sondern auch durch P2X4R-Antagonisten (hohe Konzentrationen von TNP-ATP und 5-BDBD) reduziert. Ivermectin, ein allosterischer Modulator von P2X4R potenzierte die Bz-ATP-Ströme und dieser Effekt konnte durch 5-BDBD aufgehoben werden. Da Bz-ATP P2X4 und P2X7R gleichermaßen stimuliert, sehen wir es als erwiesen an, dass beide Rezeptortypen an NPZ vorhanden sind und bei neuroinflammatorischen Erkrankungen eine Rolle spielen könnten.

2.2.3. **Rubini P**, Pagel G, Soghra M, Marquardt P, Riedel T, Illes P (2014) *Functional P2X7 receptors at cultured hippocampal astrocytes but not neurons*. Naunyn-Schmiedberg's Arch Pharmacol 387:943-954.

Wie es aus der Diskussion von Publikation 2.2.1. entnommen werden kann, nehmen wir an, dass der P2X7R unter Ruhebedingungen nur in sehr geringen Mengen exprimiert ist und erst bei pathophysiologischen Bedingungen, d.h. bei neuronalen Schäden jeglicher Art, hochreguliert wird. Zwar wird berichtet, dass neuronale Axone/Dendriten und synaptosomale Präparate P2X7R exprimieren, aber diese Beobachtungen wurden mehrfach in Frage gestellt.

Gemischte neuronale/astrozytäre Zellkulturen des Hippocampus wurden aus neugeborenen Ratten präpariert. Die Konzentration von $[Ca^{2+}]_i$ in den Zellkörpern oder Zellausläufern der Neurone blieb nach der Applikation von Bz-ATP unverändert, obwohl es gleichzeitig in den Astrozyten angestiegen ist. Das Badmedium enthielt allerdings keine Mg^{2+} -Ionen, die bekanntermaßen die P2X7R-Effekte vermindern. Zu messbaren $[Ca^{2+}]_i$ -Transienten in den Zellausläufern kam es erst, wenn die rasenartig aufliegenden Gliazellen unter den Nervenfasern falsch positive Ergebnisse

lieferten. Im Gegensatz zu den Neuronen reagierten Astrozyten bei Mg^{2+} -Mangel auf Bz-ATP mit einem Anstieg von $[Ca^{2+}]_i$. Dieser Effekt verschwand in Abwesenheit von Ca^{2+} in der Extrazellulärlösung, im Einklang mit der Annahme, dass Ca^{2+} über den P2X7R-Kanal in das Zellinnere einströmte und nicht aus intrazellulären Speichern freigesetzt wurde. Der P2X7R-Antagonist A-438079 hob die Wirkung von Bz-ATP konzentrationsabhängig auf.

Patch-Clamp-Untersuchungen an neuronalen/astrozytären Zellkulturen des Hippocampus führten zu ähnlichen Resultaten. Die geringen Bz-ATP-Ströme der Astrozyten konnten durch ein niedriges Ca^{2+} -haltiges und Mg^{2+} -freies Badmedium potenziert werden. Gleichzeitig löste aber Bz-ATP weder im normalen Badmedium noch in solchem, das niedrige divalenten Kationen-Konzentrationen einhielt, Stromantworten auf Bz-ATP aus. Ähnlich verhielten sich die spontanen exzitatorischen Ströme der hippocampalen Neurone, die auf die spontane quantale Freisetzung von Glutamat zurückzuführen sind. Sie konnten durch Bz-ATP weder in ihrer Amplitude noch in ihrer Frequenz beeinflusst werden. Dies schließt das Vorhandensein von präsynaptischen, Glutamat-Freisetzung steigernden P2X7R aus.

Die vorliegenden Experimente zeigen, dass Astrozyten P2X7R enthalten, Neurone jedoch weder an ihren Zellkörpern, noch an ihren Axonen/Dendriten oder an ihren Axon-Terminalen mit P2X7R ausgestattet sind. Wir denken, dass die NPZ im Laufe ihrer terminalen Differenzierung in Astrozyten die P2X7R behalten, aber nach Ausdifferenzierung in Neurone diese Rezeptoren verlieren.

2.3. Komplex III. *Vorhandensein und Wirkung von P2Y1-Rezeptoren an embryonalen neuralen Vorläuferzellen und dedifferenzierten kultivierten striatalen Neuronen*

2.3.1. **Rubini P**, Milosevic J, Engelhardt J, Al-Khrasani M, Franke h, Heinrich A, Sperlagh B, Schwarz SC, Schwarz J, Nörenberg W, Illes P (2009) *Increase of intracellular Ca^{2+} by adenine and uracil nucleotides in human midbrain-derived neuronal precursor cells.* Cell Calcium 45:485-498.

In diesen Experimenten wurden kultivierte, mesencephale NPZ verwendet, die aus humanen Föten gewonnen wurden. Die NPZ wurden in einem Kulturmedium gehalten, das hohe Konzentrationen von Wachstumsfaktoren enthielt, die die Proliferation förderten und die Differenzierung verhinderten. Ein Teil der Zellen reagierte auf depolarisierende Strominjektionen nur mit elektrotonischen Potentialen,

während der andere Teil abortierte Aktionspotentiale feuerte. P2XR fehlten an den NPZ-Zellmembranen, da im Gegensatz zu AMPA, das einen Subtyp des ionotropen Glutamat-Rezeptor aktiviert, ATP keine Membranströme auslösen konnte. In einem zweiten Ansatz verabreichten wir steigende Konzentrationen von ATP/ADP und UTP/UDP, um $[Ca^{2+}]_i$ -Transienten zu induzieren. Die Wirksamkeit der Agonisten entsprach der Reihenfolge ATP > ADP > UTP > UDP. Im Einklang mit den Strommessungen, die keinen Hinweis auf P2XR lieferten, wurden die $[Ca^{2+}]_i$ -Transienten durch das Weglassen von Ca^{2+} aus dem Badmedium nur geringfügig beeinflusst, während Cyclopiazonsäure (CPA) sie stark hemmte. CPA inhibiert eine Ca^{2+} -ATPase, die das freie, intrazelluläre Ca^{2+} in seine Speicher zurückpumpt und demzufolge depletiert CPA diese Speicher.

Danach haben wir nachgewiesen, dass die Wirkung von ATP durch selektive oder nicht-selektive P2Y1R-antagonistische Substanzen (MRS2179, PPADS) und das ATP-Abbauenzym Apyrase, aufgehoben werden konnte. Der UTP-Effekt wurde in einer ähnlichen Weise beeinflusst; der einzige Unterschied war, dass der gemischte P2Y1,2-Antagonist Suramin nur geringfügig mit ATP interagierte, die Wirkung von UTP jedoch vollständig eliminierte. Bereits in diesem Stadium der Experimente folgerten wir, dass P2Y2R an der Aktivität von UTP beteiligt sein müssten.

Tatsächlich lieferte dazu die direkte Bestimmung der ATP-Freisetzung aus den NPZ, nach Applikation von UTP einen überzeugenden Hinweis. Die Bestimmung von ATP im Extrazellulärmedium erfolgte mithilfe einer Biosensor-Elektrode. Die Reihenfolge der Ereignisse schien deshalb die Folgende zu sein: UTP setzt aus den NPZ über P2Y2R-Aktivierung ATP frei, das wiederum auf dieselben NPZ zurückwirkt und durch die Stimulation ihrer P2Y1R eine Erhöhung der $[Ca^{2+}]_i$ auslöst. Immunhistochemische Färbungen belegten, dass P2Y1- und P2Y2R an den NPZ vergesellschaftet vorkommen.

Die P2Y1R an NPZ könnten sowohl unmittelbare, als auch zeitlich protrahierte Effekte herbeiführen. (1) Kurz nach ihrer Applikation entstehen Oszillationen des $[Ca^{2+}]_i$, die als eine Möglichkeit zur interzellulären Kommunikation von NPZ in ihren Netzwerken betrachtet werden. (2) Wenn über mehrere Tage hindurch ATP dem Kulturmedium beigemischt wurde, kam es zur Abnahme der NPZ-Proliferation und -Differenzierung, wie durch Auszählen der Ki67- bzw. Doublecortin-immunpositiven Zellen belegt wurde. UTP erhöhte die Zahl der Doublecortin- und Tyrosinhydroxylase-immunreaktiven Zellen, als Marker reifer, dopaminergischer Neurone.

Wir folgerten, dass ATP (und UTP) über die Ca^{2+} -Wellenaktivität die Reifung der NPZ erhöht und, dass ATP im Zusammenspiel mit UTP in Proliferations- und Differenzierungsvorgänge eingreift.

2.3.2. **Rubini P**, Pinkwart C, Franke H, Gerevich Z, Nörenberg W, Illes P (2006) *Regulation of intracellular Ca^{2+} by P2Y_1 receptors may depend on the developmental stage of cultured rat striatal neurons*. J Cell Physiol 209:81-93.

Neurobasalmedium (NBM) wird bei der Kultivierung von Neuronen verwendet, um ein Überleben dieser Zellen in weitgehender Abwesenheit von Astrozyten zu gewährleisten (~90% Neurone). Wir stellten uns die Frage, ob die in NBM-haltigem Medium gezüchteten, striatalen Neurone dieselben Eigenschaften aufweisen, wie die in DMEM (Dulbecco's Modified Eagle's Medium)-haltigem Medium gezüchteten. Zu allererst untersuchten wir die beiden Zellkulturen elektrophysiologisch. Wir fanden, dass die NBM-Neurone auf depolarisierende Strompulse hin entweder kein Aktionspotential oder nur ein einziges Aktionspotential feuerten. Die DMEM-Neurone feuerten unter denselben Bedingungen Serien von Aktionspotentialen.

In den Ca^{2+} -Imaging Experimenten nutzten wir, wie bereits im Vorhergehenden, einen $[\text{K}^+]_o$ -Puls, um Neurone von Astrozyten zu unterscheiden. Ein Anstieg der extrazellulären K^+ -Konzentration depolarisiert die neuronale Zellmembran, führt zur Öffnung spannungsabhängiger Ca^{2+} -Kanäle und zum Einstrom von Ca^{2+} in das Zellinnere, entsprechend seinem elektrochemischen Gradienten. Dieses Unterscheidungsmerkmal bestand sowohl in den NBM-, als auch in den DMEM-Kulturen. Im Gegensatz dazu, steigerte ATP das neuronale $[\text{Ca}^{2+}]_i$ ausschließlich in NBM, während in DMEM dieser Effekt entfiel. Astrozyten reagierten unter beiden Kultivierungsbedingungen auf ATP mit $[\text{Ca}^{2+}]_i$ -Transienten. Es lag nun die Annahme nahe, dass in NBM die Neurone Astrozyten-ähnliche Eigenschaften erworben hatten, was möglicherweise die Folgeerscheinung eines Dedifferenzierungs-Vorgangs war. Tatsächlich beobachteten wir eine Ko-Lokalisation der MAP2- (neuronaler Marker) und GFAP- (astrozytärer und Stammzellmarker) Immunreaktivitäten.

Da wir in erster Linie an den ATP-sensitiven, dedifferenzierten Neuronen interessiert waren, wurden alle weiteren Experimente an solchen Zellen, vergleichend mit Astrozyten durchgeführt. Astrozyten und Neurone im NBM-haltigen Kulturmedium reagierten identisch. (1) Sowohl Ca^{2+} -freies Badmedium, als auch eine CPA-Vorbehandlung verminderte die ATP-induzierten $[\text{Ca}^{2+}]_i$ -Transienten, schaltete

sie aber nicht vollständig aus. (2) Selektive (MRS2179) und nicht-selektive (PPADS) P2Y1R-Antagonisten unterdrückten die ATP-Effekte komplett. (3) Der P2Y12R-Antagonist AR-C69931MX beeinflusste die Wirkung von ATP nicht. Da die P2Y1R-Immunreaktivität sowohl an Neuronen als auch an Astrozyten nachweisbar war, obwohl P2Y1R typischerweise eher an Astrozyten und NPZ vorkommen, lieferte dieser Befund einen weiteren Hinweis für die Dedifferenzierung der striatalen Neurone in NBM.

Es blieb noch die Frage zu klären, über welchen Mechanismus die ATP-Effekte auf $[Ca^{2+}]_i$ entstanden sind, obwohl P2XR an den striatalen Neuronen offenbar nicht vorhanden waren und somit nicht als Ca^{2+} -Eintrittswege fungieren konnten. In dieser Hinsicht war es von Interesse, dass CPA unmittelbar nach seiner Applikation $[Ca^{2+}]_i$ -Transienten in den Neuronen hervorrief, deren erste schnell ansteigende Phase auf Entleerung der intrazellulären Speicher beruhte, während die zweite Plateau-Phase auf die Öffnung von „store-operated channels“ (SOC) zurückgeführt werden konnte. Ca^{2+} -freies Badmedium oder der SOC-Blocker SKF 96365 hemmten diese zweite Phase der CPA-Antwort gleichermaßen. Deshalb nahmen wir an, dass ATP/ADP wohl über die P2Y1R-bedingte Bildung von Inositol 1,4,5-Trisphosphat intrazelluläre Ca^{2+} -Speicher entleerte und demzufolge SOC öffnete. Ferner stellten wir die Hypothese auf, dass ATP/ADP über den Anstieg der intrazellulären Ca^{2+} -Konzentration die Proliferation und Migration striataler Progenitorzellen regulieren könnte.

2.3.3. **Rubini P**, Engelhardt J, Wirkner K, Illes P (2008) *Modulation by D1 and D2 dopamine receptors of ATP-induced release of intracellular Ca^{2+} in cultured rat striatal neurons*. *Neurochem Int* 52:113-118.

In diesen Experimenten verwendeten wir ebenfalls NBM, für den Erhalt von an Neuronen angereicherten striatalen Zellkulturen. Solche Kulturen bestehen überwiegend aus GABAergen Projektionsneuronen des Striatum, die entweder mit D1- (striatopallidale Projektionen) oder D2- (striatonigrale Projektionen) Rezeptoren ausgestattet sind. Die Neurone wurden, wie bereits in Publikation 2.3.1. beschrieben, durch einen $[K^+]_o$ -Puls von den Astrozyten unterschieden.

Der gemischte D1,2R-Agonist Dopamin beeinflusste die $[K^+]_o$ -Effekte nicht, steigerte aber die Wirkung von ATP an allen Neuronen. Kompetitive Antagonisten an D1- (SKF 83566) oder D2R (Sulpirid) hatten keinen Eigeneffekt. SKF 83566

demaskierte jedoch einen bis dorthin verdeckten, inhibitorischen Effekt von Dopamin am D2R. Dieser Effekt entfiel, sobald SKF 83566 und Sulpirid ko-appliziert wurden. Deshalb kann angenommen werden, dass D1R an einer Subpopulation von Neuronen den ATP-Effekt potenzieren, während D2R an der anderen Subpopulation eine Hemmwirkung ausüben.

In Kenntnis der Langzeitwirkungen von ATP auf Proliferation/Differenzierung hypothetisierten wir, dass D1/D2R zusätzlich zu ihrer akuten regulatorischen Wirkung auf die neuronale Erregbarkeit, möglicherweise P2YR-vermittelte ATP/ADP-Langzeiteffekte modulieren können.

3. Zusammenfassung und Ausblick

P2-Rezeptoren sind im zentralen und peripheren Nervensystem weit verbreitet und demzufolge in zahlreiche regulatorische Funktionen eingebunden. Wir haben uns den Schmerz-vermittelnden P2X3R und den Apoptose/Nekrose- und Zellproliferation-vermittelnden P2X7- bzw. P2Y1R gewidmet. Während die uns interessierenden P2X3R an sensorischen Nervenfasern und ihren Zellkörpern untergebracht sind, befinden sich die P2X7/P2Y1R an neuralen Stammzellen und Astrozyten. Das Vorhandensein von P2X7R an Neuronen konnten wir nicht bestätigen.

Eine Reihe der hier präsentierten Ergebnisse könnte eine praktische Relevanz besitzen: (1) Die Kenntnis der Aminosäure-Reste, die die Agonisten-Bindungstasche der P2X3R ausbilden bzw. die der Untereinheiten-Zusammensetzung desselben Rezeptors, ist für die Entwicklung von P2X3R-antagonistischen Analgetika von beträchtlicher Bedeutung. In diesem Zusammenhang ist vorteilhaft, dass die P2X3R eine sehr eingeschränkte Verteilung aufweisen und deshalb die Verwendung ihrer Antagonisten nur geringe Nebenwirkungen erwarten lassen. (2) Die von uns gesammelten Erkenntnisse bzgl. der P2X7R an adulten NPZ des Hippocampus deuten darauf hin, dass diese Rezeptoren am nekrotisch/apoptotischen Absterben der nach metabolischen Schäden im Überschuss gebildeten und ektop angesiedelten NPZ beteiligt sind. Ektope NPZ im Hilus hippocampi differenzieren in Körnerzellen, die in pathologische Regelkreise integriert werden können und bei der Manifestation einer Temporallappen-Epilepsie eine entscheidende Rolle spielen. (3) P2Y1R-Agonisten induzieren Proliferation/Differenzierung und Migration von NPZ. Deshalb können ATP/ADP zahlreiche wichtige Funktionen bei der Reparatur von gehirnschädigenden Vorgängen zugeschrieben werden.

4. Erklärungen, Lebenslauf, Danksagung

Erklärung über die eigenständige Anfertigung der Arbeit

Hiermit versichere ich, dass ich die vorliegende Habilitationsschrift „Beteiligung purinerner Rezeptoren am Schmerzgeschehen und an der neuronalen Entwicklung“ selbständig und nur unter Zuhilfenahme der angegebenen Quellen und Hilfsmittel angefertigt habe. Die den Quellen wörtlich und inhaltlich übernommenen Stellen wurden als solche gekennzeichnet. Die von anderen Personen erbrachten Dienstleistungen wurden als solche kenntlich gemacht. Diese Arbeit hat in dieser oder ähnlicher Form noch keiner anderen Prüfungsbehörde vorgelegen.

Leipzig, 23. Juni 2016



Dr. rer. med. Patrizia Rubini

Erklärung über den eigenen Anteil an den einzelnen Arbeiten

Die hier vorgestellten Ca^{2+} -Imaging-Daten wurden teilweise von mir persönlich, teilweise von den von mir betreuten Doktoranden im Rahmen ihrer Doktorarbeiten erstellt. Namentlich möchte ich Christina Pinkwart, Mahmud Al-Khrasani, Johannes Engelhardt, Stephan Hintze, Martin Fuchs, Christine Kunert, Gregor Pagel, Carlo Steppel und Julia Schmid erwähnen (allesamt Studenten der Medizinischen Fakultät). Darüber hinaus betreute ich die elektrophysiologisch und molekularbiologisch ausgerichteten Arbeiten von Gastwissenschaftlern (Haihong Wang, Erzsebet Kato, Soghra Mehri) und Doktoranden der Naturwissenschaftlichen Fakultät (Mandy Bodnar, Nanette Messemer) gemeinsam mit Prof. Dr. Peter Illes.

Kooperationen bestanden mit der Arbeitsgruppe von PD Dr. Heike Franke (Histologie, Immunhistochemie, RT-PCR; unser Institut), und den Arbeitsgruppen von Prof. Dr. Günther Schmalzing (Molekularbiologie, Biochemie; Institut für Pharmakologie und Toxikologie, Technische Universität Aachen) und Prof. Dr. Johannes Schwarz (Gewinnung und Kultivierung menschlicher embryonaler Stammzellen; Neurologische Klinik, Universität Leipzig).

Die ersten Versionen der Publikationen mit meiner Erst- und Seniorautorschaft wurden von mir selbst verfasst, und danach mit Herrn Prof. Dr. Peter Illes abgestimmt. In einem ähnlichen Vorgehen fand die Planung der jeweils durchzuführenden Experimente statt.

Leipzig, 23. Juni 2016



Dr. rer. med. Patrizia Rubini

Lebenslauf

Name: Dr. Patrizia Rubini Illes
 Adresse: Mainzer Straße 5
 04109 Leipzig
 Geburtsdatum, -ort: 28.03.1956, Milano, Italien
 Familienstand: verheiratet, 2 Töchter, 2 Söhne
 Nationalität: deutsche und italienische

Schulbildung und Studium

1974 Abitur am Humanistischen Gymnasium des Ursulinen-Ordens in Mailand
 1974 - 1979 Studium der Biologie an der Universität Mailand, Italien
 1980 Promotion als „Dottore in scienze biologiche / Univ. Mailand“ mit dem Thema „Zentrale Wirkung von Loperamid auf die Darmpassage von Ratten“

Beruflicher Werdegang

1980 - 1981 Stipendiatin der Planck-Gesellschaft am Max-Planck-Institut für Psychiatrie, München
 1981 -1982 wissenschaftliche Angestellte am Institut für Neuropathologie der Universität Freiburg
 1993 - 1994 freiberufliche Mitarbeiterin in der Abteilung für Präklinische Forschung der Fa Gödecke, Freiburg
 1994 - 1995 Habilitationsstipendium des Landes Baden-Württemberg am Institut für Physiologie der Universität Freiburg
 1995 - 2002 Gründung und Betreiben einer Firma für pharmakologisch-toxikologische Beratung
 2000 - 2000 6 Monate Forschungstätigkeit am Department of Pharmacology, University of Colorado Health Sciences Center, Denver, Colorado, U.S.A.
 seit 2002 wissenschaftliche Mitarbeiterin am Rudolf-Boehm-Institut für Pharmakologie und Toxikologie der Universität Leipzig.

Seit 2015 „Adjunct Faculty Member“ des Molecular Medicine and Drug Research Centre der University of Karachi, Pakistan

2016 Promotion als Dr. rer. med. an der Medizinischen Fakultät der Universität Leipzig mit dem Thema „Opioidrezeptortypen; Bindungsstudien und selektive Toleranz

Lehrtätigkeit

seit 2002 Kurse im Fach „Allgemeine Pharmakologie und Toxikologie“ für Studenten der Humanmedizin, Universität Leipzig

seit 2008 Praktika für Studenten der Pharmazie, Universität Leipzig

2012-2014 jährliche Betreuung eines POL-Kurses

2012 Vorlesungen und Kurse an der 2nd IBRO School of Neuroscience, Teheran, Iran

Oktober 2010-13 Vorlesungen für Studenten der Humanmedizin an der Tongji University, Medical School, Shanghai, China

Danksagung

Prof. Dr. Peter Illes, dem Leiter unserer Arbeitsgruppe danke ich dafür, dass er mein Interesse an der Erforschung purinerner Mechanismen erweckt und meine Experimente stets mit hilfreichen Ratschlägen begleitet hat.

Bei Prof. Dr. Michael Schaefer bedanke ich mich auf das Herzlichste für seine Unterstützung bei der Lösung aller administrativer Probleme und seiner Förderung in den Bereichen Forschung und Lehre.

Mein Dank geht an PD Dr. Kerstin Wirkner, PD Dr. Zoltan Gerevich, PD Dr. Heike Franke, PD Ute Krügel und Prof. Dr. Wolfgang Nörenberg für ihre Diskussionsbereitschaft in methodischen und theoretischen Fragestellungen und für ihre freundliche Kooperationsbereitschaft.

Wertvolle Kooperationspartner waren für mich die Gruppe um Prof. Günther Schmalzing und PD Ralf Hausmann in Aachen, die unsere elektrophysiologischen und Ca^{2+} -Messdaten mit biochemischen Untersuchungen ergänzten.

Besonders bedanken möchte ich mich bei den Doktoranden meiner Arbeitsgruppe (Christina Pinkwart, Mahmud Al-Khrasani, Johannes Engelhardt, Stephan Hintze, Martin Fuchs, Christine Kunert und Gregor Pagel) die mich in der tagtäglichen Arbeit unterstützt haben, sowie Helga Sobottka und Katrin Krause, die mit Zellkulturtechniken und Züchtung der Tiere die Grundlagen für ein effizientes Arbeiten geschaffen haben. Bei meiner Tochter Monica bedanke ich mich für linguistische Korrekturen.

Ein großes Dankeschön gilt meinem Mann und unseren Kindern, die akzeptiert haben, dass ich trotz einer Halbtageseinstellung die meiste Zeit des Tages im Labor verbracht habe und dadurch zwangsläufig meine Aufgaben zuhause einschränken musste.

Amino Acid Residues Constituting the Agonist Binding Site of the Human P2X3 Receptor*[§]

Received for publication, July 26, 2010, and in revised form, November 16, 2010. Published, JBC Papers in Press, November 22, 2010, DOI 10.1074/jbc.M110.167437

Mandy Bodnar^{†1}, Haihong Wang^{†1,2}, Thomas Riedel[†], Stefan Hintze[‡], Erzsebet Kato[‡], Ghada Fallah[§], Helke Gröger-Arndt[‡], Rashid Giniatullin[¶], Marcus Grohmann[‡], Ralf Hausmann[§], Günther Schmalzing[§], Peter Illes^{‡3}, and Patrizia Rubini[‡]

From the [†]Rudolf-Boehm Institute of Pharmacology and Toxicology, University of Leipzig, 04107 Leipzig, Germany, the [§]Department of Molecular Pharmacology, University Hospital of Rheinisch Westfaelische Technische Hochschule Aachen University, 52074 Aachen, Germany, and the [¶]Department of Neurobiology, A.I. Virtanen Institute, 70211 Kuopio, Finland

Homomeric P2X3 receptors are present in sensory ganglia and participate in pain perception. Amino acid (AA) residues were replaced in the four supposed nucleotide binding segments (NBSs) of the human (h) P2X3 receptor by alanine, and these mutants were expressed in HEK293 cells and *Xenopus laevis* oocytes. Patch clamp and two-electrode voltage clamp measurements as well as the Ca²⁺ imaging technique were used to compare the concentration-response curves of the selective P2X_{1,3} agonist α,β -methylene ATP obtained at the wild-type P2X3 receptor and its NBS mutants. Within these NBSs, certain Gly (Gly-66), Lys (Lys-63, Lys-176, Lys-284, Lys-299), Asn (Asn-177, Asn-279), Arg (Arg-281, Arg-295), and Thr (Thr-172) residues were of great importance for a full agonist response. However, the replacement of further AAs in the NBSs by Ala also appeared to modify the amplitude of the current and/or [Ca²⁺]_i responses, although sometimes to a minor degree. The agonist potency decrease was additive after the simultaneous replacement of two adjacent AAs by Ala (K65A/G66A, F171A/T172A, N279A/F280A, F280A/R281A) but was not altered after Ala substitution of two non-adjacent AAs within the same NBS (F171A/N177A). SDS-PAGE in the Cy5 cell surface-labeled form demonstrated that the mutants appeared at the cell surface in oocytes. Thus, groups of AAs organized in NBSs rather than individual amino acids appear to be responsible for agonist binding at the hP2X3 receptor. These NBSs are located at the interface of the three subunits forming a functional receptor.

ATP-gated, cation-permeable P2X receptor channels form a family of seven subunits, referred to as P2X1 through P2X7 (1). The subunits consist of two transmembrane domains, a large extracellular loop containing the ATP binding site, as

well as intracellular N- and C-terminal tails. Biochemical evidence indicates that both homomeric and heteromeric receptors occur as stable trimers (2–4).

Mutagenesis studies at homomeric P2X receptors uniformly suggested that the negatively charged phosphate groups of ATP occupy some positively charged amino acids (AAs),⁴ specifically Lys or Arg, in the extracellular loop of the receptor (5–7). Moreover, aromatic Phe residues were assumed to be associated with binding the adenine ring of ATP (8). Molecular models were generated on the basis of these studies, under the assumption that each subunit of the P2X receptor family contains one individual binding site (9, 10). The three-subunit composition of P2X receptors was supported in addition to the already mentioned biochemical evidence (2) by a wealth of further data. (a) Single channel analysis of P2X receptor currents indicated 2–3 sequential binding steps (11, 12). (b) The kinetic behavior of P2X receptor currents was simulated with an allosteric model describing channel opening in the di- or triliganded state (13, 14). (c) Atomic force microscopy provided evidence for three receptor subunits, which moved away from the central pore as the channel opened (15, 16). (d) Fluorescence resonance energy transfer and electron microscopy supplied a rough structure of three interacting subunits (17). (e) The crystal structure of a zebrafish (zf) P2X4 receptor mutant supported the existence of corresponding intersubunit pockets as the binding site for ATP (17, 18).

Because in P2X receptors, instead of a few amino acid residues, four clusters of AAs, termed nucleotide binding domains (NBD1–4 (19); here nucleotide binding segments; NBS1–4), were identified as possible docking places for ATP (see Fig. 1A), we investigated by Ala scanning mutagenesis the functional significance of these NBSs. For this purpose, the human (h) recombinant P2X3 receptor, located at sensory neurons and participating in pain sensation (20, 21), was expressed in HEK293 cells or *Xenopus laevis* oocytes, and the P2X_{1,3} receptor-selective α,β -methylene ATP (α,β -meATP) was used as an agonist (22). In contrast to α,β -meATP, ATP itself would have the drawback of also activating P2Y recep-

* This work was supported by grants from the Deutsche Forschungsgemeinschaft (Grants IL 20/11-3; WI 1674/4-1; and IL20/18-2) and the Volkswagen Foundation (Grant I/82 940).

[§] The on-line version of this article (available at <http://www.jbc.org>) contains supplemental Figs. 1 and 2.

¹ Both authors contributed equally to this work.

² Present address: Dept. of Physiology, Medical School, Tongji University, Shanghai 200092, China.

³ To whom correspondence should be addressed: Rudolf-Boehm-Institute of Pharmacology and Toxicology, University of Leipzig, Haertelstrasse 16-18, D-04107 Leipzig, Germany. Tel.: 49-341-9724614; Fax: 49-341-9724609; E-mail: Peter.Illes@medizin.uni-leipzig.de.

⁴ The abbreviations used are: AA, amino acids; NBS, nucleotide binding segment; h, human; r, rat; zf, zebrafish; ORI, oocyte Ringer's solution; α,β -meATP, α,β -methylene ATP; FR, fluorescence ratio; TNP-ATP, 2'-(3')-O-(2,4,6-trinitrophenyl)adenosine 5'-triphosphate; BzATP, dibenzoyl-ATP.

P2X3 Receptor Agonist Binding Site

tors negatively interacting with the stimulatory effect at P2X3 (23).

P2X1 and P2X3 receptors show, in contrast to all other P2X receptor subtypes, a rapidly desensitizing behavior; this may be due to differences in either the AA composition/length of the N or C terminus (24–27) or the AA composition/length of the second transmembrane domain (27). Moreover, the phosphorylation of consensus protein kinase C sites at the extracellular loop of the P2X3 receptor might also modify the agonist-induced desensitization (28, 29). Eventually, rapid desensitization may also depend on agonist binding to a non-conserved AA at the extracellular loop, which is absent in the slowly desensitizing receptor types. Thus, patch clamp and two-electrode voltage clamp measurements, as well as the Ca^{2+} imaging technique, were used to investigate the role of all conserved and some non-conserved AA residues arranged in NBSs and located at the interface of two subunits for determining the amplitude and time course of the agonist-induced responses.

EXPERIMENTAL PROCEDURES

Culturing of HEK293-hP2X3 Cells—HEK293 cells were kept in Dulbecco's modified Eagle's medium also containing 4.5 mg/ml D-glucose (Invitrogen), 2 mM L-glutamine (Sigma-Aldrich), 10% fetal bovine serum (Invitrogen) at 37 °C and 10% CO_2 in humidified air.

Site-directed Mutagenesis and Transfection Procedures—The human P2X3 receptor (hP2X3) cDNA (GenBank™ accession number NM-002559.2) was subcloned per PstI and EcoRI restriction sites into pIRES2-EGFP vector from Clontech Laboratories for independent expression of P2X3 and EGFP, creating the pIR-P2 plasmid. All P2X3 receptor mutants were generated by introducing replacement mutations into the pIR-P2 construct using the QuikChange site-directed mutagenesis protocol from Stratagene according to the instruction manual. HEK293 cells were plated in plastic dishes (electrophysiology) or onto coverslips (Ca^{2+} imaging) 1 day before transient transfection. 0.5 μg of plasmid DNA per dish was combined with 10 μl of PolyFect reagent from Qiagen and 100 μl of Opti-MEM (Invitrogen). After 10 min of incubation, the lipid-DNA complexes were introduced to the cells. Approximately 18 h after transfection, the medium was replaced with Opti-MEM to remove residual plasmid DNA.

Whole-cell Patch Clamp Recordings—Whole-cell patch clamp recordings were performed 2–3 days after the transient transfection of HEK293 cells, at room temperature (20–22 °C), using an Axopatch 200 B patch clamp amplifier (Molecular Devices). The pipette solution contained (in mM): 140 CsCl, 1 CaCl_2 , 2 MgCl_2 , 10 HEPES, and 11 EGTA, pH adjusted to 7.4 using CsOH. The external physiological solution contained (in mM): 135 NaCl, 4.5 KCl, 2 CaCl_2 , 2 MgCl_2 , 10 HEPES, and 10 glucose, pH adjusted to 7.4 using NaOH. The pipette resistances were 3–6 megaohms. The liquid junction potential (V_{LJ}) between the bath and pipette solution at 21 °C was calculated and was found to be 4.5 mV. Holding potential values given in this study were corrected for V_{LJ} . All recordings were made at a holding potential of –65 mV. Data were filtered at 2 kHz with the inbuilt filter of the amplifier, digi-

tized at 5 kHz, and stored on a laboratory computer using a Digidata 1440 interface and pClamp 10.2 software (Molecular Devices).

Drugs were dissolved in the external solution and locally superfused to single cells (detected by their EGFP fluorescence), using a rapid solution change system (SF-77B Perfusion Fast-Step, Warner Instruments; 10–90% rise time of the junction potential at an open pipette tip was 1–4 ms; but see below). Concentration-response curves were established by applying increasing concentrations of α,β -methylene ATP (α,β -meATP; Sigma-Aldrich) for 2 s. The intervals between applications were 5 min for 0.03–1 μM and 7 min for 3–300 μM . Under these conditions, agonist responses were reproducible at the given concentrations (30).

In experiments investigating the kinetics of P2X3 currents, α,β -meATP (100 μM) was applied for 10 s with 7-min intervals three times in total. The current induced by the second application was used for calculations. The decay phases of the curves were fitted by the following biexponential equation

$$y = A_1 \times e^{-t/\tau_{des1}} + A_2 \times e^{-t/\tau_{des2}} + P \quad (\text{Eq. 1})$$

using the in-built function of the pClamp 10.2 software (Molecular Devices), where A_1 and A_2 are the relative amplitudes of the first and second exponential, τ_{des1} and τ_{des2} are the desensitization time constants, and P is the plateau. The onset time constants ($\tau_{on(10-90\%)}$) were calculated from the individual recordings under the assumption that despite the relatively slow local application, they give a rough approximation of the kinetics of channel opening.

Macroscopic Conductance Kinetics—Macroscopic conductance kinetics were analyzed by a hidden Markov model (see supplemental Fig. 2A, panel a; derived from Ref. 14) that includes binding, gating, and desensitization. Kinetic modeling and fitting were performed by the QuB software (31). To estimate solution exchange times of the rapid superfusion system used, 150 mM KCl was applied to the cell. The time constant of this test pulse (~140 ms) was determined by a single exponential fit and used for modeling the wash in and wash out of α,β -meATP.

High α,β -meATP concentrations induce large and rapidly activating currents, leading to a reduced membrane potential. Hence, for kinetic fits, the whole-cell conductance σ was calculated from the measured current I , the access resistance R_a , the membrane resistance R_m , and the holding potential U_h , using the following equation.

$$\sigma = \frac{(R_a + R_m)^2}{R_a^2 R_m + R_a R_m^2 + \frac{R_m^2 U_h}{I}} \quad (\text{Eq. 2})$$

Ca^{2+} Microfluorometry—HEK293 cells were loaded 2–3 days after transient transfection with the Ca^{2+} -sensitive fluorescent dye Fura-2 acetoxymethyl ester (2.5 μM ; Sigma-Aldrich) at 37 °C for 30 min in culture medium. To remove extracellular traces of the dye, the cells were then washed in physiological solution of the same composition as that used for patch clamp measurements. Cells plated onto coverslips were mounted into a perfusion chamber and placed on the

stage of an inverted microscope (IX-70; Olympus) with epifluorescence optics and a cooled CCD camera (IMAGO; Till Photonics). Throughout the experiments, cells were continuously superfused at 0.8 ml/min by means of a roller pump with external solution. Intracellular Fura-2 was alternately excited at 340 and 380 nm, and the emitted light was measured at a wavelength of 510 nm. The TILL vision software (3.3 Till Photonics) was used for data acquisition, system control, and later, off-line analysis. The fluorescence ratio (FR; 340/380 nm) provides a relative measure of the cytosolic free Ca^{2+} concentration ($[\text{Ca}^{2+}]_i$).

For the determination of concentration-response relationships, α,β -meATP was pressure-injected locally, by means of a computer-controlled DAD12 superfusion system (ALA Scientific Instruments, Inc.). The application time was 5 s, and the intervals between two subsequent agonist applications were kept, independent of the concentration used, at 15 min.

Expression of P2X3 Receptors and Their Mutants in *X. laevis* Oocytes—An oocyte expression plasmid harboring the cDNA for an N-terminally hexahistidine-tagged (His-tagged) hP2X3 subunit was available from a previous study. Replacement mutations were introduced by QuikChange site directed-mutagenesis (Stratagene). All constructs were verified by restriction analysis and nucleotide sequencing. Capped cRNAs were synthesized and injected into collagenase-defolliculated *X. laevis* oocytes using a Nanoliter 2000 injector (World Precision Instruments) as described previously (2, 32). Oocytes were cultured at 19 °C in sterile oocyte Ringer's solution (ORi: 90 mM NaCl, 1 mM KCl, 1 mM CaCl_2 , 1 mM MgCl_2 , and 10 mM Hepes, pH 7.4) supplemented with 50 $\mu\text{g}/\text{ml}$ gentamycin.

Two-electrode Voltage Clamp Electrophysiology—2–3 days after cRNA injection, current responses were evoked by α,β -meATP as indicated, at ambient temperature (21–24 °C), and recorded by conventional two-electrode voltage clamp with a Turbo TEC-05 amplifier (npi Electronics) at a holding potential of –60 mV as described previously (33). Oocytes were continuously perfused by gravity (5–10 ml/min) in a small flow-through chamber with a nominally calcium-free ORi solution (designated Mg-ORi), in which CaCl_2 was replaced by equimolar MgCl_2 to avoid a possible contribution of endogenous Ca^{2+} -dependent Cl^- channels to the α,β -meATP response.

Dilutions of agonists and antagonists in Mg-ORi were prepared daily and applied by bath perfusion. Switching between bath solutions was controlled by a set of magnetic valves, enabling computer-controlled applications of compounds (Cell-Work Lite 5.1 software; npi Electronics). For concentration-response analysis, rapidly desensitizing hP2X3 receptors were first repetitively activated in 1-min intervals by 10-s applications of 100 μM α,β -meATP (which is maximally effective at the wild-type (WT) hP2X3 receptor) until constant current responses were obtained (for further experimental details, see Ref. 33).

Protein Labeling, Purification, and PAGE—cRNA-injected oocytes were metabolically labeled by overnight incubation with L- ^{35}S methionine and, just before protein extraction, additionally surface-labeled with Cy5 NHS ester, an amine-reactive, membrane-impermeant fluorescent dye (34). His-

tagged proteins were purified by nickel-nitrilotriacetic acid agarose (Qiagen) chromatography from digitonin (1%, w/v) extracts of oocytes and analyzed by blue native PAGE as described previously (2, 3). Where indicated, samples were treated before blue native PAGE for 1 h at 37 °C with 0.1% (w/v) SDS or a combination of 0.1% (w/v) SDS and 100 mM DTT, to induce partial dissociation of hP2X3 complexes.

For SDS-urea-PAGE, proteins were denatured by incubation with reducing SDS sample buffer for 15 min at 56 °C and electrophoresed in parallel with ^{14}C -labeled molecular mass markers (Rainbow, Amersham Biosciences) on SDS-urea-PAGE gels (10% acrylamide). SDS-urea-PAGE gels were scanned wet with a fluorescence scanner (Typhoon, GE Healthcare) for visualization of fluorescently labeled plasma membrane-bound proteins and then dried and exposed to a phosphor screen for subsequent PhosphorImager (Storm 820, GE Healthcare) detection of ^{35}S incorporation. The figures were prepared by using ImageQuant TL v2005 (Amersham Biosciences) for contrast adjustments and Adobe Photoshop CS 8.0 for level adjustment and cropping.

Homology Modeling—We modeled, based on the published crystal structure of the zfp2X4 channel in its closed state (18), the extracellular loop and transmembrane areas of the hP2X3 receptor. The software used was Modeler 9, version 7 (35). The alignment was determined by the align2D function, which also takes the secondary structure of the template into consideration. Homology modeling was made with the loop-model function with high optimization settings. Visualization of the results was by VMD (36).

Data Analysis—Concentration-response curves for α,β -meATP were fitted by using a three-parametric Hill plot (SigmaPlot; SPSS). The figures show mean \pm S.E. values of n experiments. One-way analysis of variance followed by Holm-Sidak post hoc test was used for statistical analysis. We compared the various current and $[\text{Ca}^{2+}]_i$ parameters (amplitude and/or time course) of the mutants within NBS1–4 with the WT data. A probability level of 0.05 or less was considered to reflect a statistically significant difference.

RESULTS

Agonist Sensitivity of hP2X3 Receptor Mutants

Patch Clamp Investigations—The underlined, conserved AA residues in NBS1–4 of hP2X3 were sequentially replaced by Ala, one or two at a time (Fig. 1A). In addition, the conserved Ala-283 was substituted by Asp or Arg. We have also chosen non-conserved AA residues in each NBS and replaced them by Ala (Fig. 1A). The functional significance of AAs was checked by using the P2X1,3-selective α,β -meATP as an agonist.

The hP2X3 receptor or its mutants were transiently expressed either in HEK293 cells or in *X. laevis* oocytes. Fig. 1B documents the agonist application protocols in WT HEK293-hP2X3 cells. When recorded by the whole-cell variant of the patch clamp technique, at a holding potential of –65 mV, α,β -meATP had already caused a prominent desensitization of the inward current during its 2-s superfusion period (Fig. 1B, panel a). We kept a 5–7-min interval between the applica-

P2X3 Receptor Agonist Binding Site

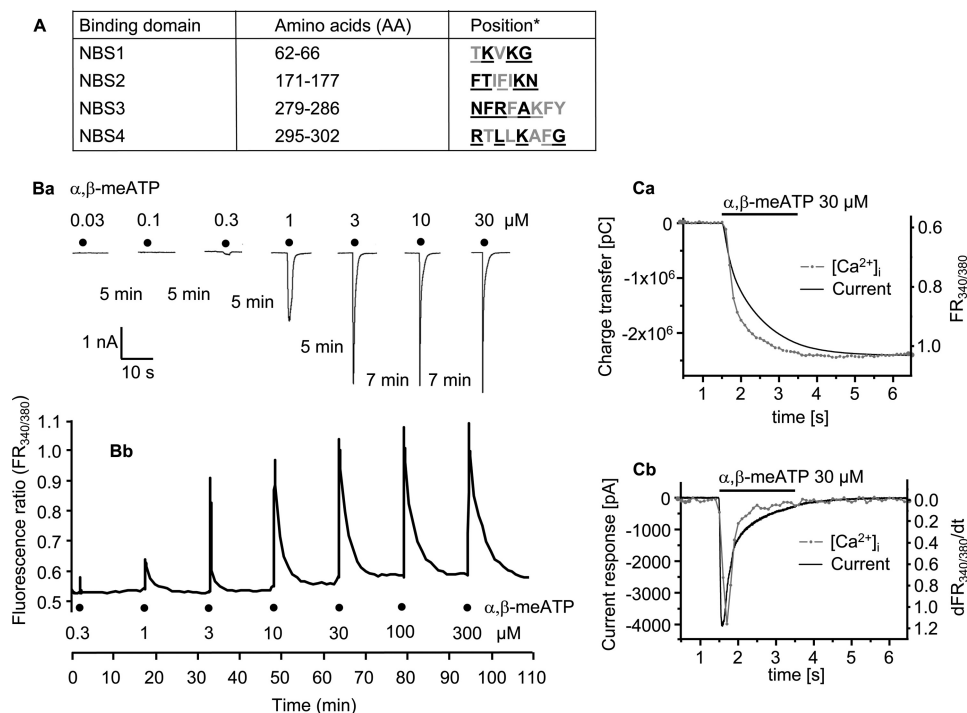


FIGURE 1. Current responses to α,β -meATP of the WT hP2X3 receptor and its NBS mutants in HEK293 cells. *A*, AA residues of the supposed nucleotide binding segments (NBS1–4). **Bold characters**, conserved AAs; **underlined characters**, substitution by Ala. *B*, *panel a*, whole-cell current responses, induced by α,β -meATP (0.03–30 μM), were recorded with the patch clamp technique at a holding potential of -65 mV. Increasing concentrations of the agonist were locally superfused for 2 s with 5- or 7-min intervals as indicated. *Panel b*, increases in the intracellular calcium concentration ($[\text{Ca}^{2+}]_i$) were induced by α,β -meATP (0.3–300 μM). Increasing concentrations of the agonist were locally superfused for 5 s with 15-min intervals. The cells were labeled with the calcium-sensitive fluorescent dye Fura-2, and fluorescence ratio ($\text{FR}_{340/380}$) measurements were made with a dual wavelength spectrometer (alternating excitation at 340 and 380 nm). The changes in FR were used as a measure of $[\text{Ca}^{2+}]_i$. Representative tracings are shown in both *panels a* and *b*. *C*, *panel a*, α,β -meATP (30 μM)-induced charge transfer measured by the patch clamp technique and fluorescence ratio determined by Ca^{2+} imaging as a function of time. The time courses of these responses were similar. Two representative experiments are shown out of a total of three (current response) and four ($[\text{Ca}^{2+}]_i$ transients) similar ones (2-s application time). pC, picocolombs. *Panel b*, the current response to α,β -meATP (30 μM) and the differentiated $\text{FR}_{340/380}/\text{dt}$ also have similar time courses. The recordings from *panel a* were replotted in *panel b*.

tion of successively increasing α,β -meATP concentrations to allow recovery of agonist sensitivity. α,β -meATP caused a concentration-dependent increase of the intracellular $[\text{Ca}^{2+}]_i$ transients in HEK293-hP2X3 cells as well, with a slow decline to the pre-drug level. In these experiments, we superfused α,β -meATP for 5 s and correspondingly prolonged the application intervals from 5–7 to 15 min (Fig. 1*B*, *panel b*). It is noteworthy that extracellular Ca^{2+} appeared to enter the cells via the P2X3 receptor channels only because a Ca^{2+} -free bath medium almost abolished the effect of α,β -meATP (37). Finally, the α,β -meATP-induced inward currents and $[\text{Ca}^{2+}]_i$ transients were strongly depressed by the P2X1–3 antagonist TNP-ATP or the P2X3-selective antagonist A317491 (37).

In the following experiments, we singly or doubly replaced all conserved AA residues within NBS1–4 of the hP2X3 subunit by Ala (Fig. 2); the only exception was the neutral Ala-283 itself, which was substituted by the negatively charged Asp or the positively charged Arg. Then, we transfected both the WT receptor and its NBS mutants into HEK293 cells and compared the current responses measured by the patch clamp technique. The concentration-response curve for α,β -meATP at the WT receptor yielded an EC_{50} of 2.66 ± 0.67 μM , an I_{max} of $4,110 \pm 310$ pA, and a Hill coefficient of 1.47 ± 0.47 ($n = 8$ –12). It is noteworthy that the EC_{50} values correlated well with those reported previously, both by ourselves (30) and by other authors (38).

When concentration-response curves were determined for α,β -meATP at the mutant receptors, it became evident that several AA substitutions interfered with the agonist effect. First of all, replacement of Ala-283 by Asn or Arg caused a decrease in the activity of α,β -meATP. It was not possible to determine EC_{50} or I_{max} values at the A283D and A283R mutants because no clear maximum of the concentration-response curve was reached up to 300 μM . The current amplitudes at this α,β -meATP concentration were 380.7 ± 95.9 pA (A283D; $n = 6$) and $2,996 \pm 1,553$ pA (A283R; $n = 5$), respectively; a statistically significant inhibition was observed only when the I_{max} value at the WT receptor ($4,110 \pm 310$ pA; see above) was compared with effect of α,β -meATP (300 μM) at the A283D mutant. Thus, AAs carrying a negative or positive charge at position 283 perturbed the ability of the receptor channel to open.

In NBS1, the amino acid residues Lys-63 and Gly-66, in NBS2, the residues Thr-172, Lys-176, and Asn-177, in NBS3, the residues Asn-279, Arg-281, and Lys-284, and eventually in NBS4, the residues Lys-299 and Arg-295 were essential for the agonist response. Although of less importance, modifications at Lys-65 (NBS1), Phe-174 (NBS2), Phe-280 and Phe-282 (NBS3), and Gly-302 (NBS4) also caused moderate changes. Replacements of Thr-62 (NBS1), Phe-171 (NBS2), and Leu-297 or F301A (NBS4) by Ala had no effect. There was no obligatory relationship between an AA being con-

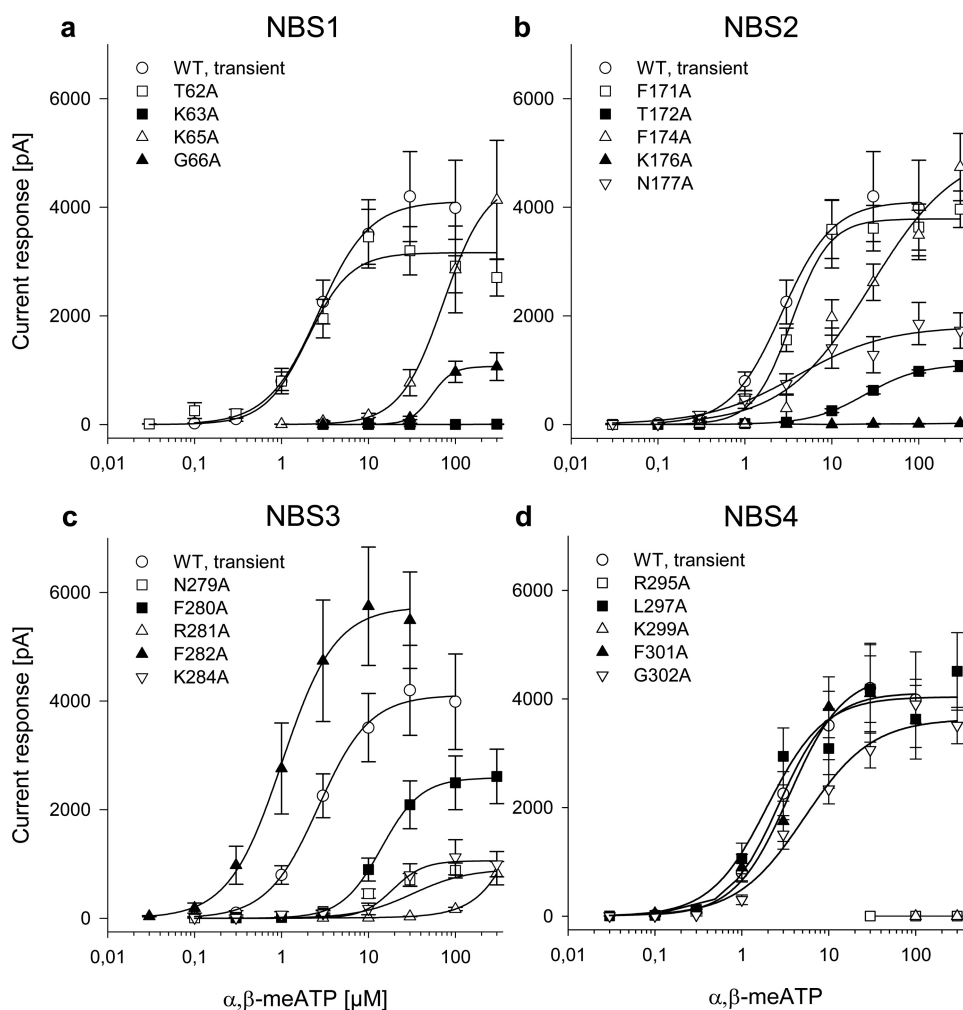


FIGURE 2. **Current responses to α,β -meATP in HEK293 cells transfected with the WT hP2X3 receptor and its mutants.** Whole-cell patch clamp recordings were made as described in the legend for Fig. 1. Concentration-response curves for α,β -meATP were constructed both for the WT hP2X3 receptor and for its point mutants, where the indicated AAs in their nucleotide binding segments were replaced by Ala (in Fig. 1A, see *underlined* one-letter coding of AAs). Ala was sequentially introduced to substitute individual AAs in NBS1 (a), NBS2 (b), NBS3 (c), and NBS4 (d). Each symbol indicates the mean \pm S.E. of 5–13 cells.

served or non-conserved and the magnitude of inhibition. Some conserved (e.g. Lys-63) and non-conserved (e.g. Lys-284) AAs were both of great importance for the agonist effect, whereas other non-conserved (e.g. Thr-62) and conserved (e.g. Phe-171) AAs were of minor significance. It turned out to be especially interesting that although some single mutations of adjacent, conserved AAs in NBS1, -2, and -3 failed to abolish the current response, the respective double mutations (K65A/G66A, F171A/T172A, N279A/F280A, F280A/R281A) caused complete inhibition (supplemental Fig. 1). However, the double mutation of two non-adjacent, conserved AAs (F171A/N177A) within NBS2 did not decrease the α,β -meATP response further when compared with F171A alone.

Ca²⁺ Imaging Studies—The evaluation of the α,β -meATP concentration-response curves for [Ca²⁺]_i transients in HEK293 cells transfected with the WT hP2X3 receptor yielded an EC₅₀ value of $1.86 \pm 0.21 \mu\text{M}$, an $\Delta\text{FR}_{\text{max}}$ of 0.45 ± 0.01 , and a Hill coefficient of 3.16 ± 0.64 ($n = 14$ – 19) (Fig. 3). The agonist effects were modified by mutations of individual AAs within NBS1–4 to Ala. Moreover, the replacement of Ala-283 by Asp or Arg decreased the α,β -meATP-induced

increase of [Ca²⁺]_i. It was not possible to determine EC₅₀ or I_{max} values at the A283D and A283R mutants because no clear maximum of the concentration-response curve was reached up to $300 \mu\text{M}$. The [Ca²⁺]_i transients at this agonist concentration were 0.15 ± 0.01 (A283D; $n = 32$) and 0.35 ± 0.04 (A283R; $n = 35$), respectively; a statistically significant inhibition was observed when the $\Delta\text{FR}_{\text{max}}$ value at the WT receptor (0.45 ± 0.01 ; see above) was compared with the effect of α,β -meATP ($300 \mu\text{M}$) at both mutants. Thus, AAs carrying a negative or positive charge at position 283 perturbed the ability of the receptor to interact with its agonist.

All these changes were basically similar to the situation when current responses were used as a measure of agonist potency. However, in contrast to patch clamp measurements, where T62A, F172A, L297A, and F301A did not considerably modify the α,β -meATP sensitivity, Ca²⁺ imaging also demonstrated small changes with these mutants. It should be kept in mind that because of the possibility to measure [Ca²⁺]_i simultaneously in many cells, the number of experiments was in this case higher than with patch

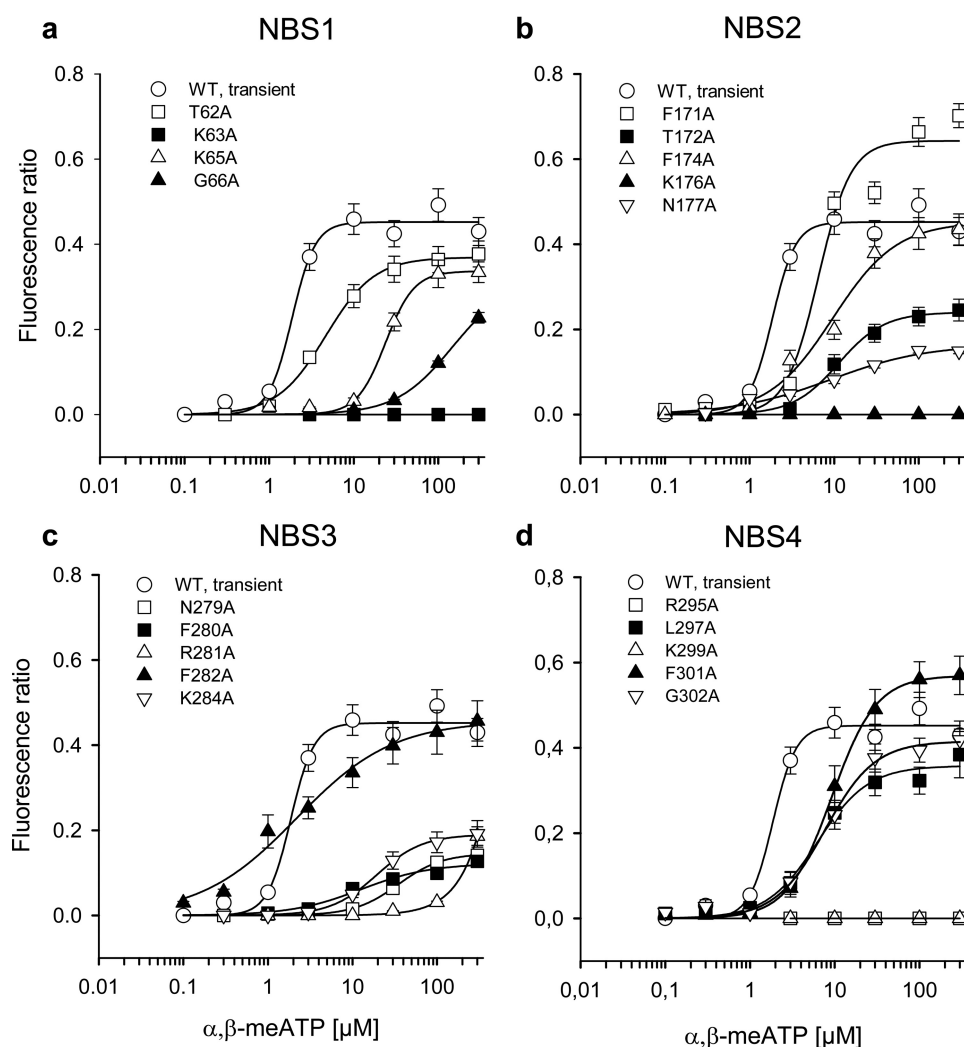


FIGURE 3. **Increases of intracellular calcium by α,β -meATP in HEK293 cells transfected with the WT hP2X3 receptor and its mutants.** FR measurements were made as described in the legend for Fig. 1 and were taken as a measure of $[Ca^{2+}]_i$. Concentration-response curves for α,β -meATP were constructed both for the WT hP2X3 receptor and for its point mutants, where the indicated AAs in their nucleotide binding segments were replaced by Ala (in Fig. 1A, see *underlined* one-letter coding of AAs). Ala was sequentially introduced to substitute individual AAs in NBS1 (a), NBS2 (b), NBS3 (c), and NBS4 (d). Each symbol indicates the mean \pm S.E. of 9–20 cells.

clamp recordings, where each cell had to be patched separately. We assume that the combination of these two methods allows a more reliable observation of subtle changes than the measurement of current responses or $[Ca^{2+}]_i$ transients alone (39, 40).

It is certainly true that electrophysiology directly determines the cationic fluxes through the P2X3 receptor channel, whereas $[Ca^{2+}]_i$ transients are only a consequence of the entry of Ca^{2+} via this receptor channel into the intracellular space. However, the two methods equally well describe the same phenomenon. In representative experiments, we integrated the α,β -meATP (30 μM) currents through the WT P2X3 receptor to obtain the total amount of transferred charge ($n = 3$) and found its time course similar to that of the $[Ca^{2+}]_i$ transients (measured as fluorescence ratio; ΔFR) ($n = 4$; Fig. 1C, panel a). Then, the shape of the current response to α,β -meATP was compared with that of the differentiated $[Ca^{2+}]_i$ response and was found to perfectly correlate (Fig. 1C, panel b) (41); rapid desensitization was a characteristic fea-

ture of the receptor when either method was used for recording.

Comparison of Data Obtained by Patch Clamp Measurements and Ca^{2+} Imaging Studies

Fig. 4 summarizes the data obtained by electrophysiology and Ca^{2+} imaging. The EC_{50} and the maximal effect E_{max} (I_{max} and ΔFR_{max} , respectively) values calculated from the concentration-response curves are shown both for the WT receptor and for its Ala-substituted single or double mutants. As already mentioned above, qualitatively identical results were obtained by the two techniques, although quantitative differences exist. With some of the mutants, no clear maximum of the concentration-response curve (and as a consequence EC_{50} or E_{max} values) could be determined with one or both of these techniques. With these limitations in mind, there was no response to α,β -meATP at the K63A, K176A, R295A, and K299A mutants, in agreement with the suggestion that certain positively charged AAs are associated with

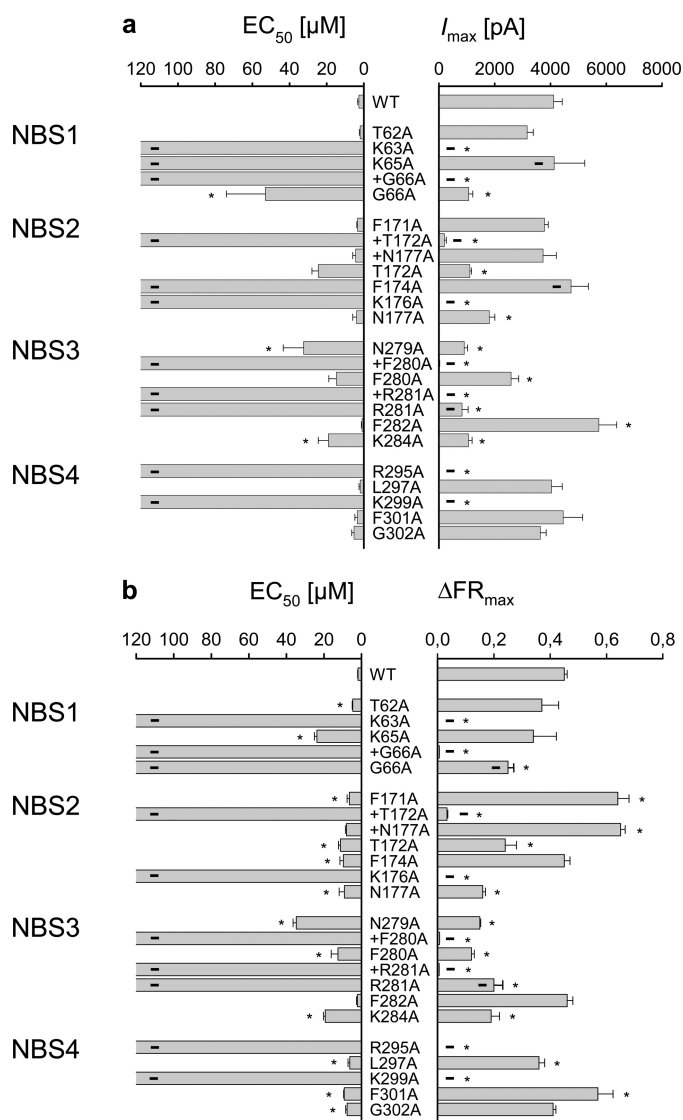


FIGURE 4. Summary of α,β -meATP concentration-response curves for the hP2X3 receptor and its NBS mutants in HEK293 cells. Curves presented in Figs. 2 and 3, and supplemental Fig. 1 were fitted as described under "Experimental Procedures" to obtain the EC_{50} and E_{max} (I_{max} or $\Delta\text{FR}_{\text{max}}$) values. On the left-side graph, the EC_{50} values of the indicated mutants are expressed in μM . On the right-side graph, the E_{max} values of the same mutants are expressed in pA and ΔFR , respectively. Current (a) and FR (b) measurements are indicated for each single and double mutant. Each symbol indicates mean \pm S.E. of 4–13 (a) and 9–20 (b) cells. With several mutants, no clear maximum of the concentration-response curve was reached, and therefore neither the EC_{50} nor the E_{max} values could be reliably determined. In such cases, the EC_{50} values were not indicated, and the E_{max} values were replaced with the effect of the highest agonist concentration tested (300 μM ; designated by a thick line). *, $p < 0.05$; statistically significant difference from the respective value measured with the WT receptor.

the binding of the negatively charged phosphate groups of ATP (5–7). The changes in EC_{50} and E_{max} with the additional mutants, as well as the experiments with mutating Ala-283 to Asp or Arg, confirmed our assumption that all conserved AAs in the NBSs play some role in agonist binding, the stabilization of the secondary protein structure, or the transduction of receptor binding to channel gating. A comparable function of at least some of the non-conserved AAs was also evident.

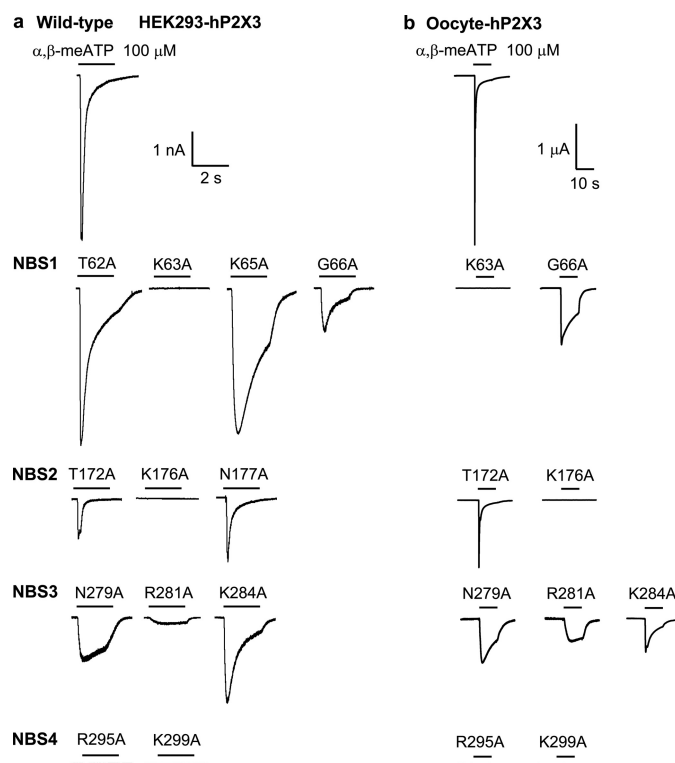


FIGURE 5. Original recordings of α,β -meATP-induced currents at hP2X3 receptors or its NBS mutants. The expression systems of the HEK293 cell (a, left panel; experimental conditions were as described in the legend for Fig. 1) or the *Xenopus laevis* oocyte (b, right panel; holding potential, -60 mV; agonist application was for 10 s every 1 min) were used. a, α,β -meATP (100 μM) effects are shown at those mutants only, where either the amplitude or the time course of the current responses appeared to be modified in comparison with the WT receptor. b, α,β -meATP (100 μM) effects are shown at nine selected mutants only, where the amplitude and/or the time course of current responses appeared to be modified in comparison with the WT receptor. These mutants were tested for assembly and surface expression in the oocyte system in the following experiments (Fig. 6B). Representative recordings for 5–14 experiments are shown.

Activation, Gating, and Desensitization of hP2X3 Receptor Mutants

A further question to be answered was whether some of the mutations altered the shape of the current response by interfering with channel activation or desensitization. Fig. 5a shows original tracings of α,β -meATP (100 μM) responses on mutants, where the current amplitude, its activation time, or the rate of desensitization appeared to change in comparison with the WT receptor. It is noteworthy that a slower rate of desensitization (higher τ_{des1} , τ_{des2} values; see below) may also be caused by a slower gating of the P2X3 receptor channel. In these experiments, α,β -meATP was applied for only 2 s; the rate constants were calculated from similar experiments with 10-s application times (not shown; see "Experimental Procedures"). According to expectations, WT P2X3 exhibited a rapid activation time constant (τ_{on} , 38 ± 4 ms) and an extremely rapid fading of the current amplitude with the two desensitization time constants τ_{des1} (935 ± 128 ms) and τ_{des2} (133 ± 12 ms; $n = 8$ each). The T62A, F171A, and L297A mutants exhibited current amplitudes similar to those of the WT receptor (Figs. 2 and 4); neither their τ_{on} nor their $\tau_{\text{des1}}/\tau_{\text{des2}}$ values differed in a statistically significant manner from the WT controls. The mutation of Lys-65 to Ala did not

P2X3 Receptor Agonist Binding Site

change the current amplitude but prolonged the onset time constant τ_{on} (270 ± 50 ms; $p < 0.05$) and increased both desensitization time constants (τ_{des1} , $4,121 \pm 945$ ms; τ_{des2} , 690 ± 95 ms; $n = 7$; $p < 0.05$). The G66A mutant exhibited smaller current responses than the WT receptor, with a reduction of the rise and decay times (τ_{on} , 310 ± 45 ms; τ_{des1} , $5,477 \pm 1,480$ ms; τ_{des2} , 740 ± 105 ms; $n = 10$; $p < 0.05$). The current responses at the T172A and N177A mutants were also smaller than those at the WT receptor, although the rate of desensitization was unaltered. Eventually, smaller amplitudes were accompanied either by decelerated (N279A, τ_{on} , 487 ± 60 ms; τ_{des1} , $21,830 \pm 7,060$ ms; τ_{des2} , $2,168 \pm 501$ ms; $n = 9$; $p < 0.05$) or by practically non-existent desensitization (R281A), at least during the 2–10-s application times of the present experiments. In the case of K284A, the τ_{on} values increased (151 ± 18 ms; $p < 0.05$), whereas the τ_{des1} ($2,376 \pm 133$ ms) and τ_{des2} values (418 ± 30 ms; $n = 10$ and $p > 0.05$ each) did not alter.

For the WT P2X3 receptor and a number of its mutants, we constructed kinetic fits of the α, β -meATP-induced currents by using a hidden Markov model obtained by simplification of the model of Karoly *et al.* (14). The rate constants characterizing transitions between the unbound, closed-state receptor (C_1), and the receptor binding one- (C_2), two (C_3)-, or three (C_4)-agonist molecules, as well as the two open-state receptors (O_5 , O_6) and the two desensitized receptors (C_7 , C_8) are shown for WT P2X₃ on the [supplemental Fig. 2A, panel a](#). By using the on- and off-rate constants, the shape and amplitude of the α, β -meATP (0.3–300 μM)-induced currents could be computer-modeled; the quality of the fits can be judged by the close parallelism of the *black lines* (original tracings) and the current traces (*orange lines*) calculated with the indicated rate constants for binding (C_1 – C_4), gating (C_3 – O_5 ; C_4 – O_6), and desensitization (C_3 – C_7 and O_5 – C_7 ; C_4 – C_8 and O_6 – C_8). Best fits for the α, β -meATP currents were computed by modifying the rate constants as indicated in the individual panels of [supplemental Fig. 2](#). By comparing these constants with those of the WT receptor, it appears that in the case of K65A (*B*) and F280A (*D*), binding was altered, whereas in the case of F174A (*C*), both binding and gating were altered. Thus, selected mutations within NBS1–3 are suggested to modify agonist binding to a variable degree, although in some cases, gating may also be affected. The quality of the best fit for R281A (*E*) was moderate, indicating on the one hand changes in binding, but on the other hand raising the possibility of additional complicating factors such as the interruption of hydrogen bonds formed between Arg-281 and Glu-156 on the same subunit and/or Asp-76 on the neighboring subunit (see “Homology Modeling of the hP2X3 Receptor” below). Similarly, the modification of the rate constants failed to produce a good fit for agonist currents at Lys-284 (not shown). This may be due to the fact that Lys-284 is situated at the entry of the ion pore region and is not directed toward the binding groove. We simplified the model of Karoly *et al.* (14) by omitting the kinetic constants determining high affinity desensitization and the recovery from desensitization but maintained those involved in the early phase of desensitization. Of course, this simplification means a loss of quality, but the obtained fits

should be sufficient to decide whether binding and/or gating are responsible for the modified amplitudes and time courses of the current responses.

Assembly and Plasma Membrane Trafficking of hP2X3 Receptor Mutants

To check for expression system-specific differences and also to assess their assembly capacitance, we expressed selected mutants (K63A, G66A, T172A, K176A, N279A, R281A, K284A, R295A, and K299A), which responded in HEK cells with rather small or even no current amplitudes to α, β -meATP (100 μM) in *X. laevis* oocytes. The α, β -meATP concentration-response curve of oocyte-expressed WT hP2X3 receptors exhibited EC_{50} and E_{max} values of 3.14 ± 0.75 μM and 3.68 ± 0.41 μA , respectively; the Hill coefficient was 1.28 ± 0.49 ($n = 6$ each). In agreement with the patch clamp data in HEK293 cells, the α, β -meATP (100 μM)-induced current responses were markedly depressed or even abolished on the selected mutants in comparison with WT hP2X3 receptor currents (Fig. 6A). In addition, changes in the speed of activation and desensitization were also comparable in recordings from oocytes and HEK293 cells (compare Fig. 5b with 5a). It should be noted, however, that because of the relatively slow application speed and the short inter-application interval of α, β -meATP (100 μM) (see “Experimental Procedures”), no time constants for activation/desensitization were calculated for oocytes.

The mutations may affect the assembly and cell surface expression of the hP2X3 mutants. To address this issue, we used the nine single mutants with impaired function in the oocyte expression system, which has the strong advantage that the cell integrity needed for reliable cell surface labeling can be easily assessed by visual inspection. Assembly (Fig. 6B, *panel a*) and cell surface expression (Fig. 6B, *panel b*) were investigated by blue native PAGE in the [³⁵S]methionine-labeled form and by SDS-PAGE in the Cy5 cell surface-labeled form, respectively. Like the WT hP2X3 receptor subunit, all P2X3 mutants with impaired function were also capable of assembling to homotrimers (Fig. 6B, *panel b*). All mutants appeared at the cell surface, albeit at different levels (note for example the rather weak surface expression of R295A and K299A). Thus, with these two mutants, the failure of α, β -meATP (100 μM) to induce a current response (Fig. 6A) may be due at least partly to the low degree of plasma membrane expression. However, in the case of all other mutants investigated in the oocyte system, the trafficking to the cell membrane was roughly equal with that of the WT receptor.

Homology Modeling of the hP2X3 Receptor

Eventually, based on the published crystal structure of the zfP2X4 (18), we modeled the hP2X3 receptor. The NBSs shown to be involved in agonist binding were situated at opposite sites of the same subunit (Fig. 7B) and were therefore able to form a binding pocket only at the interface of two adjacent subunits (Fig. 7A, *panels a* and *b*). Of the conserved residues investigated, many were oriented toward the groove of the pocket, indicating that they may bind ATP directly (Lys-63, Lys-65, Lys-176, Asn-279, Arg-281, Arg-295, Lys-

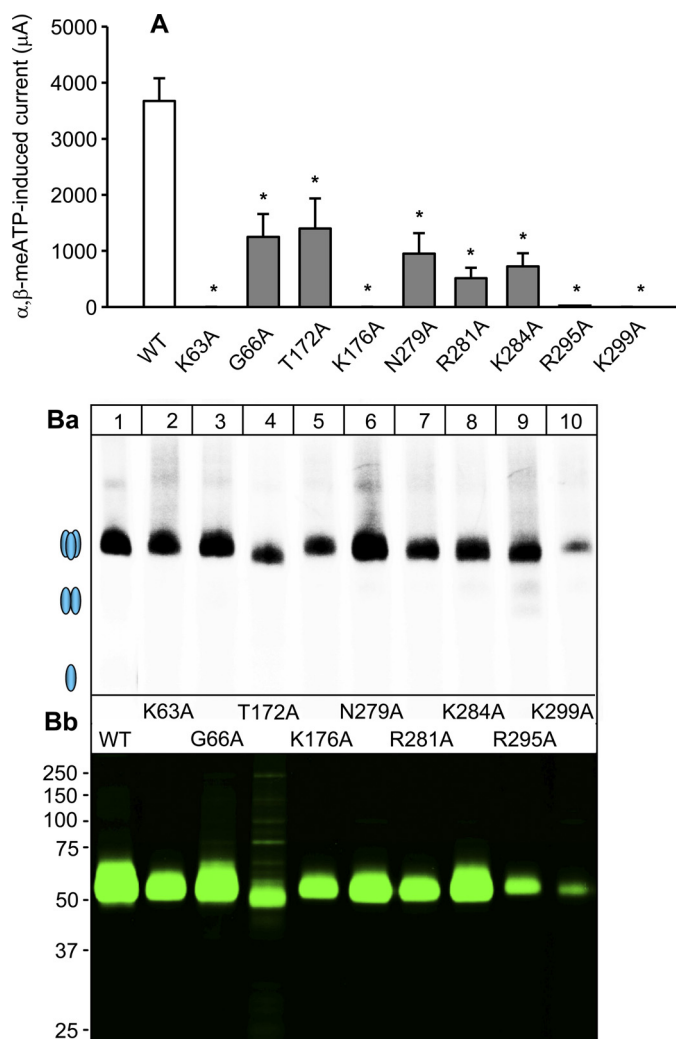


FIGURE 6. Sensitivity to α,β -meATP and assembly and surface expression of hP2X3 mutants in *X. laevis* oocytes. *A*, typical two-electrode voltage clamp current traces recorded from oocytes expressing the hP2X₃ receptor or its selected NBS mutants as indicated. α,β -meATP (100 μ M) caused smaller current amplitudes at all nine mutants tested than at the WT receptor. Mutants K63A, K276A, and K299A were unable to mediate any current response. Each symbol indicates mean \pm S.E. of 5–6 oocytes. *, $p < 0.05$; statistically significant difference from the WT receptor. *B*, [³⁵S]methionine-labeled oocytes were chased for 24 h and surface-labeled with the membrane-impermeant fluorescent Cy5 dye prior to protein purification by non-denaturing nickel-nitrilotriacetic acid chromatography. *B*, *panel a*, oligomeric state of the P2X3 proteins as visualized by blue native PAGE and ³⁵S phosphorimaging. The ovals schematically illustrate the migration positions of the non-denatured trimeric state and dimeric and monomeric states produced by partial or complete denaturation with SDS treatment, respectively. *Panel b*, aliquots of the same samples shown in *panel a* were denatured with reducing SDS-PAGE sample buffer, resolved by SDS-urea-PAGE, and visualized in their Cy5-labeled surface form by Typhoon fluorescence scanning. Each mutant was analyzed at least twice with identical results.

299); our experiments confirm that Ala substitution of these AA residues causes marked changes in the amplitude and/or gating and possibly desensitization kinetics of the current responses. In contrast, some of the conserved AA residues, such as Thr-172, Asn-177, and Phe-280, were oriented away from the groove, although their replacement with Ala caused pronounced changes, suggesting that they may participate in transducing conformational information changes from the binding pocket to the ion channel. Ala-283 is located rela-

tively far from the binding pocket; however, the substitution of Ala by negatively (Asn) or positively (Arg) charged AAs had prominent effects. Ala substitution of the non-conserved AAs Thr-62, Phe-174, Phe-282, and Phe-301 caused only minor changes, irrespective of their orientation toward (Phe-174, Phe-301) or away (Thr-62, Phe-282) from the binding pocket. Replacement of the non-conserved Lys-284 by Ala had a marked effect both on the current amplitude and on its time course. However, structural considerations in conjunction with our poor kinetic fits make the involvement of this AA in agonist binding unlikely (see “Activation, Gating, and Desensitization of hP2X3 Receptor Mutants”).

DISCUSSION

P2X3 receptors are mostly limited to the neuronal pathways involved in the perception and conduction of painful stimuli (20, 21). This highly circumscribed distribution in the peripheral and central nervous system is a prerequisite to develop new drugs for the selective treatment of pain. The peripheral terminals of sensory neurons, situated for example in dorsal root ganglia, possess P2X3 receptors, which react to ATP released by all types of nociceptive stimuli. Antagonists at these receptors have been shown to effectively block both hyperalgesia and allodynia in different models of pathological pain (42).

In view of the great significance of P2X3 receptors for future therapeutic strategies to medicate various pain states, we set out to investigate the AA residues involved in agonist binding, the more so because in contrast to most P2X receptor types, in the case of P2X3, we dispose of some selective agonists and antagonists (22). Our purpose was to characterize the ATP binding site of the P2X3 receptor to alleviate the computer-assisted design of new antagonists for therapeutic purposes. Although mutagenesis studies at P2X1 (6, 8, 43, 44), P2X2 (7, 45), and P2X4 (39, 40) have identified several AA residues of the respective receptors, which are indispensable for agonist binding, similar information for P2X3 receptors is scarce (45) (Table 1). Bioinformatics and receptor modeling suggested the existence of four putative ATP binding sites per each subunit (19, 46). The possibility of there being more than one ATP binding site per monomer cannot be ruled out at the present (17) but is rather unlikely. More importantly, instead of individual amino acids, groups of AAs organized in four nucleotide binding segments were proposed to mediate the nucleotide effects (19).

In the present study, we systematically replaced all conserved AAs in the NBSs of the hP2X3 subunit (plus 1–2 non-conserved AAs in each NBS) and searched for changes in agonist potency by means of electrophysiology and Ca²⁺ imaging in two expression systems (HEK293 cells, *X. laevis* oocytes). In the first place, we confirmed our previous results relating to the critical importance of a few positively charged AAs (K63A, K65A, K176A, R281A, R295A, K299A (37, 45)). Then, the involvement of a range of further AAs in agonist binding, agreeing with a comparable role of these AAs in the hP2X1, rP2X2, and rP2X4, was also documented (Table 1 and references cited therein). However, we report in addition three key findings. 1) Unequivocal, although sometimes minor, changes

P2X3 Receptor Agonist Binding Site

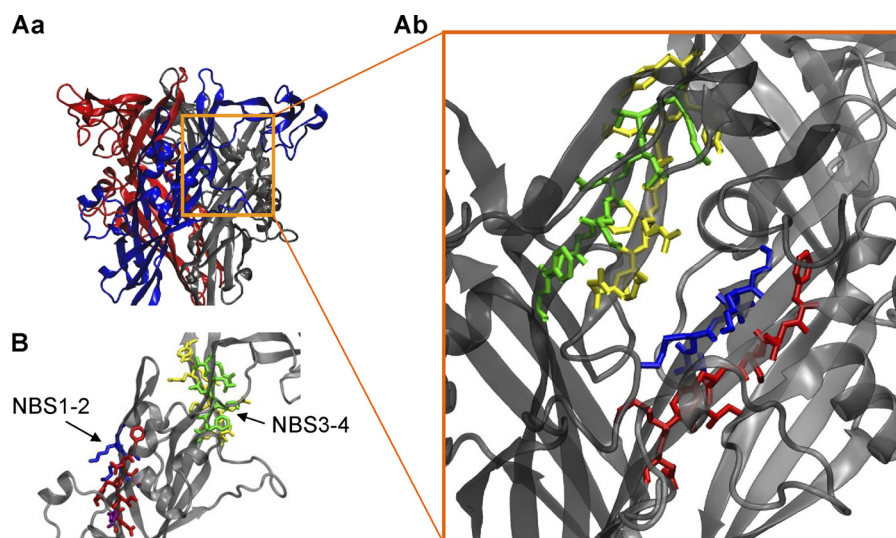


FIGURE 7. **Model of the hP2X3 receptor.** *A, panel a*, extracellular loop of the hP2X3 trimer. The individual subunits are labeled by different colors. *Panel b*, detailed view of the supposed binding site at the interface of two neighboring subunits containing four binding segments (NBSs). Color coding of the amino acid residues is: blue, NBS1; red, NBS2; yellow, NBS3; green, NBS4. *B*, NBS1–2 and NBS3–4 are located at opposite sites of a single subunit.

TABLE 1

Nucleotide binding segments of P2X receptors

Closed circle, major decrease in activity; *open circle*, slight decrease in activity or change only with Ca^{2+} imaging; *h*, human receptor; *r*, rat receptor; *zf*, zebrafish receptor mutant; conserved amino acids are indicated with bold lettering.

P2X receptor-type	NBS1	NBS2	NBS3	NBS4
hP2X1 ¹	67-71 V K L K G	185-191 F T L F I K N	290-297 N F R F A R H F	305-312 R H L F K V F G
rP2X2 ²	68-72 T K V K G	183-189 F T L I K N	288-295 N F R F A K Y Y	304-311 R T L I K A F G
hP2X3 ³	62-66 T K V K G	171-177 F T L F K N	279-286 N F R F A K Y Y	295-302 R T L I K A F G
rP2X4 ⁴	66-70 T K A K G	185-191 F T L L V K N	293-300 N F R F A K Y Y	309-316 R T L T K A Y G
zfP2X4 ⁵	69-73 T K V K G	188-194 F T V L I K N	296-303 N F R F A K Y Y	312-319 R T L I K G Y G

¹ Mutagenesis by alanine or cysteine with ATP or BzATP as agonists (6, 8, 44, 45).

² Mutagenesis by alanine or cysteine with ATP as the agonist (7, 45).

³ Replacement of alanine-283 by aspartate or arginine, or replacement of all residual investigated amino acids by alanine with α,β -meATP as the agonist (present study).

⁴ Mutagenesis by alanine or cysteine with ATP as the agonist (39, 40, 45).

⁵ Prediction based on the crystal structure (18, 45).

occurred in the amplitude of the current and/or $[\text{Ca}^{2+}]_i$ response when further conserved (Phe-171, Leu-297) or non-conserved (Thr-62, Phe-174, Lys-284, Phe-301) AAs were replaced by Ala or Ala itself was substituted by other AAs (A283D, A283R). 2) The agonist potency decrease was additive when two adjacent AAs were replaced simultaneously by Ala (Lys-65/Gly-66, Phe-171/Thr-172, Asn-279/Phe-280, Phe-280/Arg-281) but was not altered after Ala substitution of two non-adjacent AAs of the same NBS (Phe-171/Asn-177). 3) The decrease in current amplitude was accompanied in many cases by a pronounced decrease in the activation and/or desensitization rate of the receptor mutants (K65A, G66A, N279A). With R281A, a depression of the current amplitude was not accompanied by a concomitant change in the speed of activation or desensitization.

Signals that regulate intracellular trafficking of P2X receptors and thereby their membrane expression are usually associated with the N (47) or C terminus of these receptors (48, 49). Disrupting some of the conserved disulfide bridges of the extracellular loop of P2X subunits also markedly depresses their trafficking to the cell surface (50, 51). However, in this case, the normal folding of the protein appears to be altered, and the trafficking defects might be due to a failure to pass the quality check test that takes place in the endoplasmic reticulum rather than due to a trafficking defect *per se*. Thus, it was not astonishing that the present mutations in the NBSs in general did not modify the insertion of the P2X3 receptor mutants into the cell membrane of oocytes. A major change occurred only with R295A and K299A, which were expressed at a lower quantity, partially explaining the abolition of current amplitudes in the voltage clamp recordings. In the case of all other mutants, the decrease of the current response was certainly not the consequence of a disturbed trafficking behavior.

An inventive approach demonstrated by co-expression of wild-type P2X3 and a mutant P2X2, where Lys-69 or -308 was mutated to Ala, that the resulting P2X2/3 receptor functioned normally but not when both Lys residues were mutated to Ala (52). However, co-expression of wild-type P2X2 with a correspondingly mutated P2X3 subunit (K63A or K299A) produced non-functional heteromers. Thus, the failure to rescue function in the P2X2 subunit with both Lys residues mutated, by wild-type P2X3, suggests that residues from two different subunits interact in agonist binding. Similarly, the replacement of two conserved residues, Lys-68 and Phe-291 (Lys-63, Phe-280; P2X3 numbering), by cysteine led to disulfide cross-linking between neighboring P2X1 subunits (53). Because mutation of these residues results in a decreased ATP potency and cysteine cross-linking is prevented in the presence of ATP, an intersubunit ATP binding site was proposed to operate. In agreement with this idea, our P2X3 receptor model, developed on the basis of the crystal structure of the P2X4

receptor (18), suggested in conjunction with the mutagenesis results that NBS1–2 and NBS3–4 as a whole shape the binding pocket for ATP. These findings lend support to our previous hypothesis (19, 46) that instead of a few amino acid residues as generally believed, at least four NBSs are needed for the docking of ATP to the P2X3 receptor. The kinetic modeling of the agonist-induced currents on some of the receptor mutants suggested the involvement of AA residues (Lys-65, Phe-174, Phe-280, Arg-281) in ligand binding, although a gating function could also be attributed to Phe-174. In accordance with these results, the use of the full agonist ATP and the partial agonist BzATP for P2X1 suggested that certain AAs of the extracellular loop have a gating function (8). The homology modeling of the receptor structure documented that a few conserved AA residues, such as Thr-172, Asn-177, and Phe-280, were in the closed state oriented away from the groove, although their replacement with Ala caused marked changes, suggesting that they may participate in transducing conformational information changes from the binding pocket to the ion channel. In addition, the replacement of Gly-66 by Ala markedly depressed both the current and the $[Ca^{2+}]_i$ responses. It is quite possible that the flexible nature of this AA would allow conformational changes to occur, as suggested for Gly-250 in P2X1 receptors (43).

In conclusion, polypeptide clusters, rather than individual AAs, might be responsible for agonist binding, gating, and desensitization of P2X3 receptors.

Acknowledgments—We are grateful to Sara Wiese, Nanette Messermer, and Martin Fuchs for methodological help. We thank Dr. Kerstin Wirkner for useful discussions.

REFERENCES

- Khakh, B. S., and North, R. A. (2006) *Nature* **442**, 527–532
- Nicke, A., Bäumert, H. G., Rettinger, J., Eichele, A., Lambrecht, G., Mutschler, E., and Schmalzing, G. (1998) *EMBO J.* **17**, 3016–3028
- Aschrafi, A., Sadtler, S., Niculescu, C., Rettinger, J., and Schmalzing, G. (2004) *J. Mol. Biol.* **342**, 333–343
- Illes, P., and Alexandre Ribeiro, J. (2004) *Eur. J. Pharmacol.* **483**, 5–17
- Freist, W., Verhey, J. F., Stühmer, W., and Gauss, D. H. (1998) *FEBS Lett.* **434**, 61–65
- Ennion, S., Hagan, S., and Evans, R. J. (2000) *J. Biol. Chem.* **275**, 29361–29367
- Jiang, L. H., Rassendren, F., Surprenant, A., and North, R. A. (2000) *J. Biol. Chem.* **275**, 34190–34196
- Roberts, J. A., and Evans, R. J. (2004) *J. Biol. Chem.* **279**, 9043–9055
- Vial, C., Roberts, J. A., and Evans, R. J. (2004) *Trends Pharmacol. Sci.* **25**, 487–493
- Evans, R. J. (2009) *Eur. Biophys. J.* **38**, 319–327
- Ding, S., and Sachs, F. (1999) *J. Gen. Physiol.* **113**, 695–720
- Riedel, T., Lozinsky, I., Schmalzing, G., and Markwardt, F. (2007) *Biophys. J.* **92**, 2377–2391
- Sokolova, E., Skorinkin, A., Fabbretti, E., Masten, L., Nistri, A., and Giniatullin, R. (2004) *Br. J. Pharmacol.* **141**, 1048–1058
- Karoly, R., Mike, A., Illes, P., and Gerevich, Z. (2008) *Mol. Pharmacol.* **73**, 224–234
- Nakazawa, K., Yamakoshi, Y., Tsuchiya, T., and Ohno, Y. (2005) *Eur. J. Pharmacol.* **518**, 107–110
- Shinozaki, Y., Sumitomo, K., Tsuda, M., Koizumi, S., Inoue, K., and Torimitsu, K. (2009) *PLoS Biol.* **7**, e103
- Young, M. T. (2010) *Trends Biochem. Sci.* **35**, 83–90
- Kawate, T., Michel, J. C., Birdsong, W. T., and Gouaux, E. (2009) *Nature* **460**, 592–598
- Mager, P. P., Weber, A., and Illes, P. (2004) *Curr. Top. Med. Chem.* **4**, 1657–1705
- Chizh, B. A., and Illes, P. (2001) *Pharmacol. Rev.* **53**, 553–568
- Wirkner, K., Sperlagh, B., and Illes, P. (2007) *Mol. Neurobiol.* **36**, 165–183
- Jarvis, M. F., and Khakh, B. S. (2009) *Neuropharmacology* **56**, 208–215
- Gerevich, Z., Zadori, Z., Müller, C., Wirkner, K., Schröder, W., Rubini, P., and Illes, P. (2007) *Br. J. Pharmacol.* **151**, 226–236
- Koshimizu, T., Koshimizu, M., and Stojilkovic, S. S. (1999) *J. Biol. Chem.* **274**, 37651–37767
- He, M. L., Koshimizu, T. A., Tomić, M., and Stojilkovic, S. S. (2002) *Mol. Pharmacol.* **62**, 1187–1197
- Fountain, S. J., and North, R. A. (2006) *J. Biol. Chem.* **281**, 15044–15049
- Zhou, Z., Monsma, L. R., and Hume, R. I. (1998) *Biochem. Biophys. Res. Commun.* **252**, 541–545
- Wirkner, K., Stanchev, D., Köles, L., Klebingat, M., Dihazi, H., Flehmig, G., Vial, C., Evans, R. J., Fürst, S., Mager, P. P., Eschrich, K., and Illes, P. (2005) *J. Neurosci.* **25**, 7734–7742
- Stanchev, D., Flehmig, G., Gerevich, Z., Nörenberg, W., Dihazi, H., Fürst, S., Eschrich, K., Illes, P., and Wirkner, K. (2006) *Neurosci. Lett* **393**, 78–83
- Gerevich, Z., Zadori, Z. S., Köles, L., Kopp, L., Milius, D., Wirkner, K., Gyires, K., and Illes, P. (2007) *J. Biol. Chem.* **282**, 33949–33957
- Milescu, L. S., Akk, G., and Sachs, F. (2005) *Biophys. J.* **88**, 2494–2515
- Schmalzing, G., Gloor, S., Omay, H., Kröner, S., Appelhans, H., and Schwarz, W. (1991) *Biochem. J.* **279**, 329–336
- Hausmann, R., Rettinger, J., Gerevich, Z., Meis, S., Kassack, M. U., Illes, P., Lambrecht, G., and Schmalzing, G. (2006) *Mol. Pharmacol.* **69**, 2058–2067
- Becker, D., Woltersdorf, R., Boldt, W., Schmitz, S., Braam, U., Schmalzing, G., and Markwardt, F. (2008) *J. Biol. Chem.* **283**, 25725–25734
- Fiser, A., and Sali, A. (2003) *Methods Enzymol.* **374**, 461–491
- Humphrey, W., Dalke, A., and Schulten, K. (1996) *J. Mol. Graph.* **14**, 33–38
- Fischer, W., Zadori, Z., Kullnick, Y., Gröger-Arndt, H., Franke, H., Wirkner, K., Illes, P., and Mager, P. P. (2007) *Eur. J. Pharmacol.* **576**, 7–17
- North, R. A., and Surprenant, A. (2000) *Annu. Rev. Pharmacol. Toxicol.* **40**, 563–580
- Yan, Z., Liang, Z., Tomic, M., Obsil, T., and Stojilkovic, S. S. (2005) *Mol. Pharmacol.* **67**, 1078–1088
- Zemkova, H., Yan, Z., Liang, Z., Zelinkova, I., Tomic, M., and Stojilkovic, S. S. (2007) *J. Neurochem.* **102**, 1139–1150
- Egan, T. M., and Khakh, B. S. (2004) *J. Neurosci.* **24**, 3413–3420
- Donnelly-Roberts, D., McGaraughty, S., Shieh, C. C., Honore, P., and Jarvis, M. F. (2008) *J. Pharmacol. Exp. Ther.* **324**, 409–415
- Digby, H. R., Roberts, J. A., Sutcliffe, M. J., and Evans, R. J. (2005) *J. Neurochem.* **95**, 1746–1754
- Roberts, J. A., Digby, H. R., Kara, M., El Ajouz, S., Sutcliffe, M. J., and Evans, R. J. (2008) *J. Biol. Chem.* **283**, 20126–20136
- Browne, L. E., Jiang, L. H., and North, R. A. (2010) *Trends Pharmacol. Sci.* **31**, 229–237
- Mager, P. P., and Illes, P. (2006) *Expert Opin. Drug Discov.* **1**, 202–309
- Ormond, S. J., Barrera, N. P., Qureshi, O. S., Henderson, R. M., Edwardson, J. M., and Murrell-Lagnado, R. D. (2006) *Mol. Pharmacol.* **69**, 1692–1700
- Chaumont, S., Jiang, L. H., Penna, A., North, R. A., and Rassendren, F. (2004) *J. Biol. Chem.* **279**, 29628–29638
- Murrell-Lagnado, R. D., and Qureshi, O. S. (2008) *Mol. Membr. Biol.* **25**, 321–331
- Newbolt, A., Stoop, R., Virginio, C., Surprenant, A., North, R. A., Buell, G., and Rassendren, F. (1998) *J. Biol. Chem.* **273**, 15177–15182
- Ennion, S. J., and Evans, R. J. (2002) *Mol. Pharmacol.* **61**, 303–311
- Wilkinson, W. J., Jiang, L. H., Surprenant, A., and North, R. A. (2006) *Mol. Pharmacol.* **70**, 1159–1163
- Marquez-Klaka, B., Rettinger, J., Bhargava, Y., Eisele, T., and Nicke, A. (2007) *J. Neurosci.* **27**, 1456–1466

ATP Binding Site Mutagenesis Reveals Different Subunit Stoichiometry of Functional P2X2/3 and P2X2/6 Receptors*[§]

Received for publication, January 21, 2012, and in revised form, February 27, 2012. Published, JBC Papers in Press, February 29, 2012, DOI 10.1074/jbc.M112.345207

Ralf Hausmann^{‡1}, Mandy Bodnar^{§1}, Ronja Woltersdorf[‡], Haihong Wang[§], Martin Fuchs[§], Nanette Messemer[§], Ying Qin[§], Janka Günther[‡], Thomas Riedel[§], Marcus Grohmann^{‡§}, Karen Nieber[¶], Günther Schmalzing[‡], Patrizia Rubini^{§2}, and Peter Illes^{§2,3}

From the [‡]Department of Molecular Pharmacology, University Hospital of Rheinisch Westfaelische Technische Hochschule, Aachen University, 52074 Aachen, Germany, the [§]Rudolf Boehm Institute of Pharmacology and Toxicology, University of Leipzig, Haertelstrasse 16-18, 04107 Leipzig, Germany, and the [¶]Department of Pharmacology for Natural Sciences, Institute of Pharmacy, University of Leipzig, 04103 Leipzig, Germany

Background: Heteromeric P2X receptors increase the diversity of rapid ATP signaling.

Results: Non-functional P2X2, P2X3, and P2X6 subunit mutants were used to investigate the composition of heteromeric P2X2/3 and P2X2/6 receptors.

Conclusion: The subunit stoichiometry of P2X2/3 and P2X2/6 is 1:2 and 2:1, respectively.

Significance: Recognition sites between P2X2 and its partners rather than random association may govern the subunit composition of the receptor trimers.

The aim of the present experiments was to clarify the subunit stoichiometry of P2X2/3 and P2X2/6 receptors, where the same subunit (P2X2) forms a receptor with two different partners (P2X3 or P2X6). For this purpose, four non-functional Ala mutants of the P2X2, P2X3, and P2X6 subunits were generated by replacing single, homologous amino acids particularly important for agonist binding. Co-expression of these mutants in HEK293 cells to yield the P2X2 WT/P2X3 mutant or P2X2 mutant/P2X3 WT receptors resulted in a selective blockade of agonist responses in the former combination only. In contrast, of the P2X2 WT/P2X6 mutant and P2X2 mutant/P2X6 WT receptors, only the latter combination failed to respond to agonists. The effects of α,β -methylene-ATP and 2-methylthio-ATP were determined by measuring transmembrane currents by the patch clamp technique and intracellular Ca^{2+} transients by the Ca^{2+} -imaging method. Protein labeling, purification, and PAGE confirmed the assembly and surface trafficking of the investigated WT and WT/mutant combinations in *Xenopus laevis* oocytes. In conclusion, both electrophysiological and biochemical investigations uniformly indicate that one subunit of P2X2 and two subunits of P2X3 form P2X2/3 heteromeric receptors, whereas two subunits of P2X2 and one subunit of P2X6 constitute P2X2/6 receptors. Further, it was shown that already two binding sites of the three possible ones are sufficient to allow these receptors to react with their agonists.

Cys-loop, pentameric (1–3), and tetrameric (4, 5) ligand-gated ion channels usually consist of the heteromeric composi-

tion of structurally divergent subunits. Homomeric assemblies of identical subunits are, however, to a minor extent also possible (e.g. for the 5HT₃ receptor and certain neuronal nicotinic and GABA_A receptor subtypes). More recently, an additional ATP-gated ionotropic receptor family has been discovered by cloning seven distinct P2X receptor subunits from mammalian species (P2X1 to -7) (6–9). Again, P2X subunits appeared to form not only homomeric receptor channels but also heteromeric ones. Original work based on co-immunoprecipitation with epitope-tagged subunits demonstrated that only P2X6 was not able to form homooligomers, and P2X7 was the only exception of constituting heterooligomeric complexes (10). Subsequently, it was found that P2X1/2 (11, 12), P2X1/4 (13), P2X1/5 (14), P2X2/3 (15), P2X2/6 (16), and P2X4/6 (17) receptors combine the original pharmacological and biophysical properties of their parent subunits. The huge diversity of native P2X receptors and their characteristics, often differing from those of the recombinant receptors, have been explained by the existence of heteromeric subunit compositions (18).

Despite these findings relating to recombinant receptors and the evidence that three subunits form both homomeric and heteromeric P2X receptors (6, 19, 20), two further points still need extensive clarification. First, only P2X2/3 (sensory ganglia) (21, 22), P2X1/5 (astrocytes) (23, 24), and probably P2X2/6 (neural stem cells) (25, 26) receptors were shown to occur under native conditions, whereas native P2X1/2, P2X1/4, and P2X4/6 receptors were hitherto not identified. Second, the subunit stoichiometry of functional P2X2/3 receptors appears to be 1:2 (27, 28), but for the residual heteromeric receptors, there are no comparable data available.

In the case of the P2X2/3 receptor, two homologous amino acid (AA)⁴ residues participating in agonist binding were

* This work was supported by Deutsche Forschungsgemeinschaft Grant FOR 748 and the Volkswagen Foundation.

[§] This article contains supplemental Figs. 1 and 2.

¹ Both authors contributed equally to this work.

² Both authors contributed equally to this work.

³ To whom correspondence should be addressed. Tel.: 49-341-9724614; Fax: 49-341-9724609; E-mail: Peter.Illes@medizin.uni-leipzig.de.

⁴ The abbreviations used are: AA, amino acid; NBS, nucleotide binding segment; hP2X2, hP2X3, and hP2X6, human P2X2, P2X3, and P2X6, respectively; 2-MeSATP, 2-methylthio-ATP; α,β -meATP, α,β -methylene-ATP; BN, blue native.

replaced individually with alanine to yield inactive mutants of P2X2 and P2X3 subunits; combination of the mutant P2X3 with wild-type (WT) P2X2 resulted in a non-functional receptor, whereas the opposite combination was fully active (28). Unfortunately, there were no accompanying biochemical data presented to confirm that the functionally silent AA mutants of P2X2 and P2X3 and their compositions with their WT counterparts still exhibited undisturbed trafficking behavior and were expressed at the cell surface.

In P2X receptors, instead of a few AA residues, four clusters of AAs, termed nucleotide binding domains (NBD1 to -4) (29) (here nucleotide binding segments, NBS1 to -4), were identified as possible docking places for ATP. NBS1 and -2 appear to be located at one subunit, whereas NBS3 and -4 are situated at the neighboring subunit (30) in accordance with the recently described crystal structure of the zebrafish P2X4 receptor (31).

The aim of the present experiments was to find out whether two heteromeric receptors (P2X2/3 and P2X2/6), where P2X2 combines with two different partners, have an obligatory subunit stoichiometry of 1:2 or whether the subunit stoichiometry may be variable. For this purpose, we used the ATP structural analogues 2-methylthio-ATP (2-MeSATP) and α,β -methylene-ATP (α,β -meATP) as well as non-functional mutants of P2X2 and P2X3 with a single Ala mutation in NBS1 to -4 each. Moreover, we also used homologous mutants of P2X6 to clarify the subunit stoichiometry of the P2X2/6 receptor. Electrophysiological measurements and Ca^{2+} imaging as well as protein labeling, purification, and PAGE suggested that P2X2/6 receptors consist of two P2X2 subunits and one P2X6 subunit and thereby differ from P2X2/3 receptors.

EXPERIMENTAL PROCEDURES

Culturing of HEK293 Cells—HEK293 cells were kept in Dulbecco's modified Eagle's medium also containing 4.5 mg/ml D-glucose (Invitrogen), 2 mM K-glutamine (Sigma-Aldrich), 10% fetal bovine serum (Invitrogen) at 37 °C and 10% CO_2 in humidified air.

Site-directed Mutagenesis and Transfection Procedures—The human P2X2 (hP2X2_A), hP2X3 (gift of J. N. Wood, University College, London, UK), and hP2X6 (gift of A. Surprenant, University of Manchester, Manchester, UK) cDNAs were subcloned at PstI and EcoRI restriction sites into pIRES2-EGFP (P2X3 and P2X6) or pIRES2-Ds-Red (P2X2) vectors from Clontech for independent expression of the respective P2X subunit and EGFP or Ds-Red, creating the pIR-P2X plasmid. All P2X subunit mutants were generated by introducing replacement mutations into the pIR-P2X construct using the QuikChange site-directed mutagenesis protocol from Stratagene according to the instruction manual. HEK293 cells were plated in plastic dishes (electrophysiology) or onto coverslips (Ca^{2+} imaging) 1 day before transient transfection. 0.5 μg of plasmid DNA (homomeric P2X2, P2X3, and P2X6 receptors; heteromeric P2X2/3 and P2X2/6 receptors, 1:2 ratio) or 0.75 μg of plasmid DNA (P2X2/6 receptors, 1:4 ratio) was combined with 10 μl of PolyFect reagent from Qiagen and 100 μl of Opti-MEM (Invitrogen).

Whole-cell Patch Clamp Recordings—Whole-cell patch clamp recordings were made after transient transfection of

HEK293 cells, at room temperature (20–22 °C), using an Axopatch 200B patch clamp amplifier (Molecular Devices) as described previously (30). Transfected HEK293 cells were searched for by means of a reverse differential interference contrast microscope with epifluorescent optics (Axiovert 100, Zeiss). The pipette solution contained 140 mM CsCl, 1 mM CaCl_2 , 2 mM MgCl_2 , 10 mM HEPES, and 11 mM EGTA, pH adjusted to 7.3 using CsOH. When 2-MeSATP was used as an agonist, GDP- β -S (300 μM) was also included, in order to eliminate the negative interaction between P2Y and P2X receptors in HEK293 cells (31). The external physiological solution contained 135 mM NaCl, 4.5 mM KCl, 2 mM CaCl_2 , 2 mM MgCl_2 , 10 mM HEPES, and 10 mM glucose, pH adjusted to 7.4 using NaOH. The pipette resistances were 3–6 megaohms. Holding potential values were corrected for the calculated liquid junction potential between the bath and pipette solution. All recordings were made at a holding potential of –65 mV. Data were filtered at 2 kHz with the built-in filter of the amplifier, digitized at 5 kHz, and stored on a laboratory computer using a Digidata 1440 interface and pClamp 10.2 software (Molecular Devices).

Drugs were dissolved in the external solution and locally superfused over single cells (detected by their EGFP and/or DS-Red fluorescence), using a rapid solution change system (SF-77B Perfusion Fast Step, Warner Instruments). Concentration-response curves were established by applying increasing concentrations of α,β -meATP or 2-MeSATP (both from Sigma-Aldrich) for 2 s. The intervals between applications were kept at 5 min throughout. Under these conditions, agonist responses were reproducible, with the exception of those to 2-MeSATP at HEK293-P2X3 cells; the marked desensitization at higher concentrations of 2-MeSATP (>3 μM) was in accordance with the reported long period of time required to regain 50% of control peak amplitude when determined with a paired-pulse protocol (32) (see also supplemental Fig. 1Ac, right).

The desensitization time constants (τ_{des1} and τ_{des2}) and the recovery of P2X3 receptors from desensitization were determined as described previously (supplemental Fig. 1Ac, left) (33). For the measurement of the recovery from desensitization, HEK293 cells were stimulated repetitively with α,β -meATP (30 μM ; 2-s pulses) with a progressive increase in the interpulse intervals. We measured the t_{50} value, which is the time needed to regain 50% of maximally recovered currents. Only the τ_{des1} values are indicated, because the rapid phase of desensitization appears to be the more relevant one.

Ca^{2+} Microfluorometry—HEK293 cells were loaded 2–3 days after transient transfection, with the Ca^{2+} -sensitive fluorescent dye Fura-2 acetoxymethyl ester (2.5 μM ; Sigma-Aldrich) at 37 °C for 1 h in culture medium. Cells plated onto coverslips were mounted into the superfusion chamber and placed on the stage of an inverted microscope (IX-70; Olympus) with epifluorescent optics and a cooled CCD camera (IMAGO; Till Photonics). Throughout the experiments, cells were continuously superfused at 0.8 ml/min by means of a roller pump with external solution. Intracellular Fura-2 was alternately excited at 340 and 380 nm, and the emitted light was measured at a wavelength of 510 nm. The Till Vision software (version 3.3, Till Photonics) was used for data acquisition, system control,

Subunit Stoichiometry of P2X Receptors

and, later, off-line analysis. The fluorescence ratio (340/380 nm) provides a relative measure of the cytosolic free Ca^{2+} concentration ($[\text{Ca}^{2+}]_i$).

For the determination of concentration-response relationships, α, β -meATP or 2-MeSATP was pressure-injected locally, by means of a computer-controlled DAD12 superfusion system (ALA Scientific Instruments, Inc.). The application time was 5 s, and the intervals between two subsequent agonist applications were kept, independent of the concentration used, at 15 min. α, β -meATP is a selective P2X1, P2X3, P2X1/2, P2X1/5, and P2X2/3 receptor agonist (34), which does not activate endogenous P2Y receptors of HEK 293 cells (35). In contrast, 2-MeSATP is a non-selective P2X/Y receptor agonist (34, 36), which may cause an increase of $[\text{Ca}^{2+}]_i$ through the activation of G_q protein-coupled P2Y₁ receptors (35). In order to account for this problem, concentration-response curves for 2-MeSATP were constructed at HEK293 cells transfected with P2X2 subunits, P2X6 subunits, or their mutants as well as on mock-transfected cells. $[\text{Ca}^{2+}]_i$ responses caused by 2-MeSATP after mock transfection were subtracted from those obtained after transfection with the respective subunit plasmids (Fig. 3C*b*) and yielded the $[\text{Ca}^{2+}]_i$ transients due to receptor stimulation only.

Expression of P2X2, P2X3, and P2X6 Receptors and Their Mutants in *Xenopus laevis* Oocytes—Oocyte expression plasmids harboring the cDNAs for N-terminally hexahistidine-tagged (His-tagged) hP2X2_A, hP2X3, or hP2X6 subunit have been described previously (12, 30). Replacement mutations or a StrepII affinity tag-encoding sequence 5' of the stop codon were introduced by QuikChange site-directed mutagenesis (Stratagene). Capped cRNAs were synthesized and injected in aliquots of 46 nl into collagenase-defolliculated *X. laevis* oocytes using a Nanoliter 2000 injector (World Precision Instruments) as described previously (37). For expression of the heteromeric P2X2/3 receptor, cRNAs for the P2X2 and P2X3 subunit were co-injected at a 1:2 ratio (w/w). For expression of the heteromeric P2X2/6 receptor, the cRNAs for the P2X2 and P2X6 subunit were co-injected at a 1:4 ratio (w/w). Oocytes were cultured at 19 °C in sterile oocyte Ringer's solution (90 mM NaCl, 1 mM KCl, 1 mM CaCl_2 , 1 mM MgCl_2 , and 10 mM HEPES, pH 7.4) supplemented with 50 $\mu\text{g}/\text{ml}$ gentamycin.

Two-electrode Voltage Clamp Electrophysiology—1–2 days after cRNA injection, current responses were evoked by 2-MeSATP (P2X2 and P2X2/6 receptors) or α, β -meATP (P2X2/3 receptors) as indicated at ambient temperature (21–24 °C), and recorded by conventional two-electrode voltage clamp with a Turbo TEC-05 amplifier (npi Electronics) at a holding potential of –60 mV as described previously (37). For concentration-response analysis, P2X receptor-mediated currents were induced in 60-s intervals by 10-s applications of increasing concentrations of the indicated agonist.

Protein Labeling, Purification, and PAGE—cRNA-injected oocytes were metabolically labeled by overnight incubation with L-[³⁵S]methionine (PerkinElmer Life Sciences) and, just before protein extraction, surface-labeled with the membrane-impermeable fluorescent dye Cy5 NHS ester (GE Healthcare) as described previously (38). Affinity-tagged proteins were purified by non-denaturing Ni^{2+} -NTA chromatography (Qiagen) or Strep-Tactin chromatography (IBA Germany) from

digitonin (1%, w/v) extracts of oocytes as indicated. The P2X receptors were released in the non-denatured state from the Ni^{2+} -NTA-Sepharose or the Strep-Tactin-Sepharose with elution buffer consisting of 1% (w/v) digitonin in 250 mM imidazole/HCl (pH 7.6) or 1% (w/v) digitonin in 0.1 M sodium phosphate buffer, pH 8.0, supplemented with 10 mM biotin, respectively. Native proteins were analyzed by blue native PAGE (BN-PAGE) as described previously (12, 39). Where indicated, samples were treated before BN-PAGE for 1 h at 37 °C with 0.1% (w/v) SDS to induce partial dissociation of P2X receptor complexes. To avoid quenching of the fluorescence by the Coomassie G250 dye, BN-polyacrylamide gels were destained prior to fluorescence imaging by repeated cycles of incubation in 50% (v/v) acetonitrile (Biosolve) supplemented with 25 mM ammonium carbonate as described previously (40). The destained polyacrylamide gel was repeatedly washed in 0.1 M sodium phosphate buffer, pH 8.0, and scanned wet by a Typhoon 9410 scanner (GE Healthcare) for fluorescence detection. For the subsequent visualization of the ³⁵S-labeled proteins, the BN-polyacrylamide gels were dried, exposed to a phosphor screen, and scanned by a PhosphorImager (Storm 820, GE Healthcare).

For reducing SDS-PAGE, proteins were denatured by incubation with SDS sample buffer containing 20 mM DTT for 15 min at 56 °C and electrophoresed in parallel with ¹⁴C-labeled molecular mass markers (Rainbow, Amersham Biosciences) on SDS-polyacrylamide gels (10% acrylamide). SDS-polyacrylamide gels were scanned wet with a fluorescence scanner (Typhoon 9410, GE Healthcare) for visualization of Cy5-labeled plasma membrane-bound proteins, and then we dried the gels for the subsequent detection of ³⁵S incorporation as described above.

The intensity of the fluorescent protein bands was quantified using the ImageQuant TL software version 7.0 (GE Healthcare). Images of polyacrylamide gels were prepared with ImageQuant TL for contrast adjustments. For better visibility of weak and strong protein bands, individual lanes from the same, but differently enhanced, ImageQuant image were cropped and positioned using Adobe Photoshop CS4. Microsoft PowerPoint 2003 was used for labeling. Each experiment was performed at least twice with equivalent results.

Homology Modeling—We modeled, based on the published crystal structure of the zebrafish P2X4 channel in its closed state (31), the extracellular loop and transmembrane areas of the hP2X2, hP2X3, and hP2X6 receptors. The software used was Modeler 9, version 7 (41). The alignment was determined by the align2D function, which also takes the secondary structure of the template into consideration. Homology modeling was made with the loop model function with high optimization settings. Visualization of the results was by VMD (42).

Data Analysis—Concentration-response curves for agonists were fitted by using a three-parametric Hill plot (SigmaPlot; SPSS). The figures show mean \pm S.E. values of *n* experiments. One-way analysis of variance followed by the Holm-Sidak post hoc test was used for multiple comparisons with a control group or multiple pairwise comparisons. The differences between two groups were evaluated by the normality test followed by the Student's *t* test or the rank sum test, as appropriate.

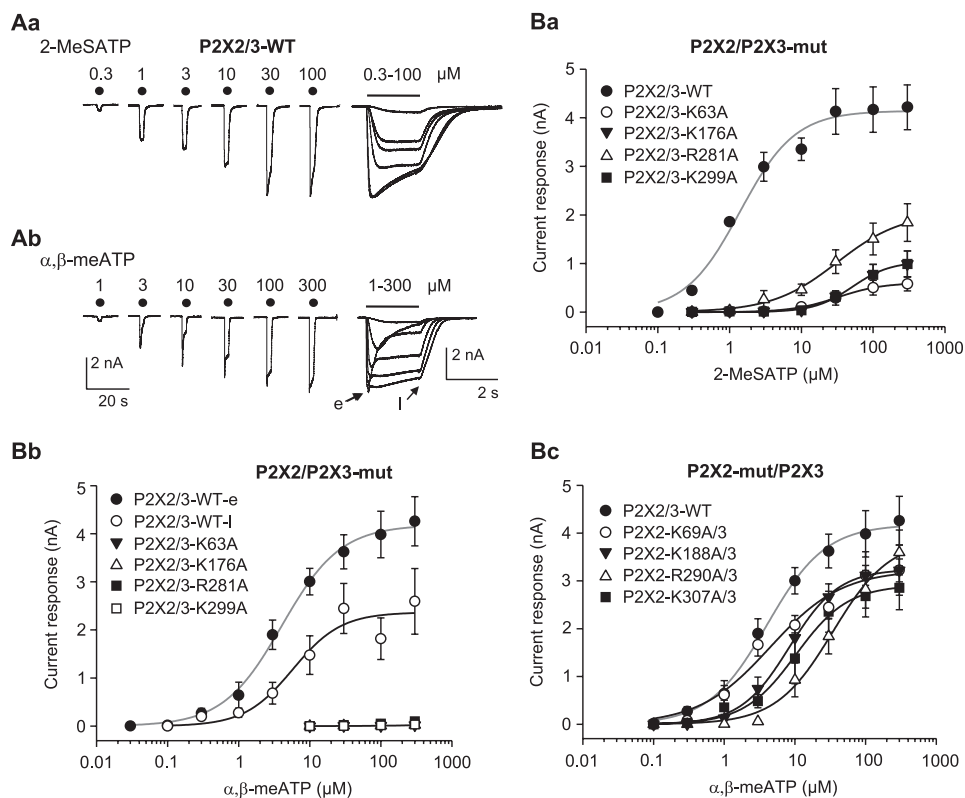


FIGURE 1. Current responses at wild-type (WT) hP2X2/3 receptors and at the combinations of mutant (mut) hP2X2 or hP2X3 subunits with their WT partners expressed in HEK293 cells. *A*, whole-cell currents induced by 2-MeSATP (*Aa*) or $\alpha,\beta\text{-meATP}$ (*Ab*; 0.3–100 μM) were recorded with the patch clamp technique at a holding potential of -65 mV. Increasing concentrations of the two agonists were locally superfused for 2 s with 5-min intervals (as indicated by filled circles or a horizontal bar), and the resulting currents were reproduced at two different time scales (note the divergent calibration bars on the right and left). $\alpha,\beta\text{-meATP}$ caused a rapidly desensitizing early current (*e*), followed by a more constant late current (*l*). *B*, concentration-response relationships constructed for 2-MeSATP (*Ba*) and $\alpha,\beta\text{-meATP}$ (*Bb* and *Bc*) at WT P2X2/3 receptors and their non-functional mutants, whose selected Lys and Arg residues were replaced by Ala. The concentration-response relationships at the WT homomeric or heteromeric receptor are shown in gray. Means \pm S.E. (error bars) of 5–8 experiments are shown. The Hill coefficients for the respective concentration-response curves at WT P2X2/3 receptors were as follows: 1.1 ± 0.2 (2-MeSATP); 1.1 ± 0.1 ($\alpha,\beta\text{-meATP}$, early), 1.3 ± 0.5 ($\alpha,\beta\text{-meATP}$, late). The E_{max} and EC_{50} values for the late $\alpha,\beta\text{-meATP}$ concentration-response curves at WT P2X2/3 receptors were $2,365 \pm 241$ pA and 5.7 ± 2.2 μM . For all further E_{max} and EC_{50} values as well as the exact number of experiments, see Table 1.

ate. A probability level of 0.05 or less was considered to reflect a statistically significant difference.

RESULTS

Patch Clamp Investigations in HEK293 Cells—Alanine-scanning mutagenesis in the four NBSs in hP2X3 showed that the conserved K63A, K176A, R281A, and K299A mutants did not react with $\alpha,\beta\text{-meATP}$ (300 μM) at all or responded with very small current amplitudes only (30). The inactivity of the homologous Ala or Cys mutants in P2X1, P2X2, and P2X4 with ATP as an agonist was demonstrated previously (see Refs. 19, 43, and 44).

Both $\alpha,\beta\text{-meATP}$ and 2-MeSATP (0.3–100 μM each) caused fast inward currents at the holding potential of -65 mV (supplemental Fig. 1, *Aa* and *Ab*). The current responses desensitized already during the 2-s application period with a rapid onset, which was similar both for $\alpha,\beta\text{-meATP}$ and 2-MeSATP (30 μM each) (supplemental Fig. 1*Ac*, left). However, the recovery from desensitization, which probably reflects the dissociation of the agonist from the receptor, was much slower for 2-MeSATP than for $\alpha,\beta\text{-meATP}$ (30 μM each) (supplemental Fig. 1*Ac*, right; $p < 0.05$). In accordance with this observation, the E_{max} value of the concentration-response curve for 2-MeSATP was smaller than that of $\alpha,\beta\text{-meATP}$ (supplemental Fig. 1*B*; $p <$

0.05). At the same time, the EC_{50} values of the two agonists also differed. In addition, we investigated the effect of 2-MeSATP (10–300 μM) at the mutant K176A and found that neither this agonist nor $\alpha,\beta\text{-meATP}$ (10–300 μM) caused any current response. Thus, K176A-hP2X3 was an inactive mutant irrespective of the type of agonist used.

In the following experiments, HEK293 cells transfected with WT or mutant P2X2 plus P2X3 cDNA plasmids, in a ratio of 1:2, were superfused with 2-MeSATP (0.1–300 μM) or $\alpha,\beta\text{-meATP}$ (0.03–300 μM) for 2 s every 5 min (Fig. 1, *A* and *B*). Although the E_{max} values and Hill coefficients of the concentration-response curves were comparable, the EC_{50} values of the two agonists differed from each other (Fig. 1, *A* and *B*, and Table 1; the peaks of the agonist-induced currents were evaluated at this stage). By keeping a 5-min interval between the applications of increasing 2-MeSATP concentrations, there was little desensitization within the 2-s application time (Fig. 1*Aa*). By contrast, with the same application protocol, $\alpha,\beta\text{-meATP}$ caused a rapid peak followed by a quasi-steady-state response (at the end of the 2-s superfusion period; Fig. 1*Ab*). Accordingly, a plot of the early peak response against the logarithmic $\alpha,\beta\text{-meATP}$ concentration resulted in a maximum of the curve (Table 1), which was higher than that obtained by plotting the late, quasi-steady-state current against the loga-

Subunit Stoichiometry of P2X Receptors

TABLE 1

Agonist sensitivities of P2X2, P2X3, P2X6, P2X2/3, and P2X2/6 receptors as well as of the combinations of the respective WT and mutant subunits expressed in HEK293 cells

Concentration-response curves for α,β -meATP or 2-MeSATP were determined by the whole-cell patch clamp method.

Receptor	Agonist	E_{\max}	EC_{50}	n	
		pA	μM		
P2X2 WT	α,β -meATP		>300	6	
P2X3 WT		4,891 \pm 85	2.1 \pm 0.1	7	
P2X3-K176A			>300	6	
P2X2/3 WT		4,182 \pm 93 ^a	4.1 \pm 0.4	8	
P2X2/3-K63A			>300	6	
P2X2/3-K176A			>300	6	
P2X2/3-R281A			>300	6	
P2X2/3-K299A			>300	6	
P2X2-K69A/3		3,231 \pm 240 ^b	4.5 \pm 1.4	6	
P2X2-K188A/3		3,245 \pm 45 ^b	8.4 \pm 0.4	7	
P2X2-R290A/3		3,870 \pm 266	34.3 \pm 6.8 ^b	7	
P2X2-K307A/3		2,911 \pm 101 ^b	10.3 \pm 1.2	7	
P2X3 WT		2-MeSATP	1,811 \pm 131 ^a	0.9 \pm 0.3	7
P2X3-K176A				>300	6
P2X2 WT	6,448 \pm 29 ^a		14.4 \pm 0.2 ^a	10	
P2X2-K69A			>300	6	
P2X2-K188A			>300	6	
P2X2-R290A			>300	6	
P2X2-K307A			>300	7	
P2X2/3 WT	4,140 \pm 139 ^a		1.4 \pm 0.2 ^c	6	
P2X2/3-K63A	607 \pm 10 ^b		31.7 \pm 1.4 ^b	7	
P2X2/3-K176A	1,042 \pm 32 ^b		51.5 \pm 3.5 ^b	8	
P2X2/3-R281A	2,044 \pm 123 ^b		31.6 \pm 5.9 ^b	6	
P2X2/3-K299A	1,042 \pm 32 ^b		51.5 \pm 3.5 ^b	6	
P2X6 WT			>300	7	
P2X2/6 WT	3,202 \pm 145 ^a		30.5 \pm 3.8	10	
P2X2/6-K68A	3,385 \pm 144		26.5 \pm 3.2	6	
P2X2/6-K191A	3,092 \pm 93		24.3 \pm 2.0	8	
P2X2/6-R287A	4,488 \pm 98 ^b		18.2 \pm 1.1 ^b	6	
P2X2/6-K305A	4,946 \pm 131 ^b		14.6 \pm 1.2 ^b	7	
P2X2-K69A/6		>300	6		
P2X2-K188A/6		>300	6		
P2X2-R290A/6		>300	6		
P2X2-K307A/6		>300	6		

^a $p < 0.05$; statistically significant difference from the respective values at the WT P2X3 receptor (P2X3 WT).

^b $p < 0.05$; statistically significant difference from the respective values at the WT receptor.

^c $p < 0.05$; statistically significant difference from the respective EC_{50} value at the P2X3 WT receptor with α,β -meATP as the agonist.

rhythmic α,β -meATP concentration (Fig. 1*Bb*). However, the EC_{50} values of the “early” (Table 1) and “late” curves (Fig. 1*Bb*; $p > 0.05$) were similar. Thus, under our experimental conditions, a mixed P2X3-P2X2/3 initial response with a rapidly desensitizing P2X3 component was followed by a slowly desensitizing P2X2/3 component. It is noteworthy that the P2X2/3 currents could be investigated in isolation, when the receptor mutants were expressed in *X. laevis* oocytes (no early peak current because of strong residual desensitization at a drug-free interval of 1 min; supplemental Fig. 2*Aa*).

Then we demonstrated that although 2-MeSATP and α,β -meATP equally well activated the WT P2X2/3 receptor, 2-MeSATP still slightly stimulated the P2X2/3 heteromeric receptors containing WT P2X2 and mutant P2X3 (K63A, K176A, R281A, and K299A), whereas α,β -meATP had no effect at all at these complexes (Fig. 1, compare *Ba* and *Bb*, and Table 1). By contrast, when WT P2X3 was co-transfected together with the non-functional P2X2 mutants (K69A, K188A, R290A, and K307A) (Fig. 1*Bc*, and Table 1), at positions homologous to those targeted in the P2X3 mutants, the E_{\max} values of α,β -meATP at all heteromeric receptors only slightly decreased, and all EC_{50} values with the exception of P2X2-R290A/P2X3 did not change (Fig. 1*Bc* and Table 1). Thus, heteromeric

P2X2/3 receptors lost their original sensitivity toward agonists (α,β -meATP) or became much less sensitive (2-MeSATP) when the P2X3 subunits carried inactivating mutations but were only slightly affected when the P2X2 subunits carried the homologous mutations. These results can be explained by the assumption that one P2X2 subunit associates with two P2X3 subunits to form a P2X2/3 heteromer.

The following experiments were designed to clarify the subunit stoichiometry of P2X2/6 receptors. First of all, we transfected HEK293 cells with P2X6 subunits only and did not obtain any current response to 2-MeSATP (0.3–300 μM ; Fig. 2*Aa*). Subsequently, transfections were made by P2X2 and P2X6 in combinations of 1:2 and 1:4. The WT P2X2/6 receptors at the 1:2 and 1:4 transfection ratios exhibited decreasing sensitivities to 2-MeSATP; the respective E_{\max} values gradually decreased from the WT P2X2 to P2X2/6 (Fig. 2*Aa*; $p < 0.05$ each).

The slope of the current responses measured during the last 1 s of agonist application (out of the total 2-s duration) also differed between P2X2 and P2X2/6 ($p < 0.05$) (e.g. at 30 μM 2-MeSATP (*inset* to Fig. 2*Ab*; compare also the *right panels* of Fig. 2, *Ca* and *Cb*). At 2-MeSATP concentrations higher than 3 μM , there was an increasingly positive slope for the P2X2 curve up to a concentration of 100 μM , whereas the slope for the P2X2/6 (1:4 transfection ratio) curve was negative in this range of concentrations. The P2X2/6 (1:2 transfection ratio) curve was found to lie between the two other ones.

Gradual acidification of the bath solution from pH 7.4 to 5.4 only slightly increased the amplitudes of the 2-MeSATP (30 μM)-induced P2X2 but not P2X2/6 (1:2 transfection ratio; $p > 0.05$) currents, whereas there was a marked potentiation of the P2X2/6 (1:4 transfection ratio; $p < 0.05$) current amplitudes (Fig. 2, *Ba–Bc*). The sudden increase in amplitude with acidification observed with the transfection ratio 1:4, in contrast to the transfection ratio 1:2, may indicate that an excess of P2X6 over P2X2 is needed to generate a sufficient amount of P2X2/6 in the plasma membrane. Thus, all three experimental approaches prove that co-transfection with P2X2 and P2X6 subunits resulted in a presumably heteromeric receptor with functional properties differing from P2X2 only if the plasmid cDNA ratios amounted to 1:4. Therefore, this transfection procedure was used for all subsequent investigations.

Fig. 2, *Ca* and *Cb*, shows individual concentration response relationships for 2-MeSATP (1–300 μM) at homomeric P2X2 and heteromeric P2X2/6 receptors. As previously mentioned, the Ala replacement of four conserved AA residues in P2X2 at positions homologous to those targeted in P2X3 produced non-functional P2X2 receptors (Fig. 2*D* and Table 1). When WT P2X2 was used together with P2X6 mutants (K68A, K191A, R287A, and K305A) for co-transfecting HEK293 cells, the E_{\max} and EC_{50} values indicated higher activity for the P2X2/P2X6-R287A and -K305A mutants, when compared with the WT P2X2/6 receptor, but not for the P2X2/P2X6-K68A and -K191A mutants (Fig. 2*Ea* and Table 1). In contrast, the non-functional P2X2 mutant components abolished the 2-MeATP effects at the respective P2X2/6 receptors. The results can be explained by the assumption that two P2X2 subunits associate with one P2X6 subunit to form a P2X2/6 heteromer (see also

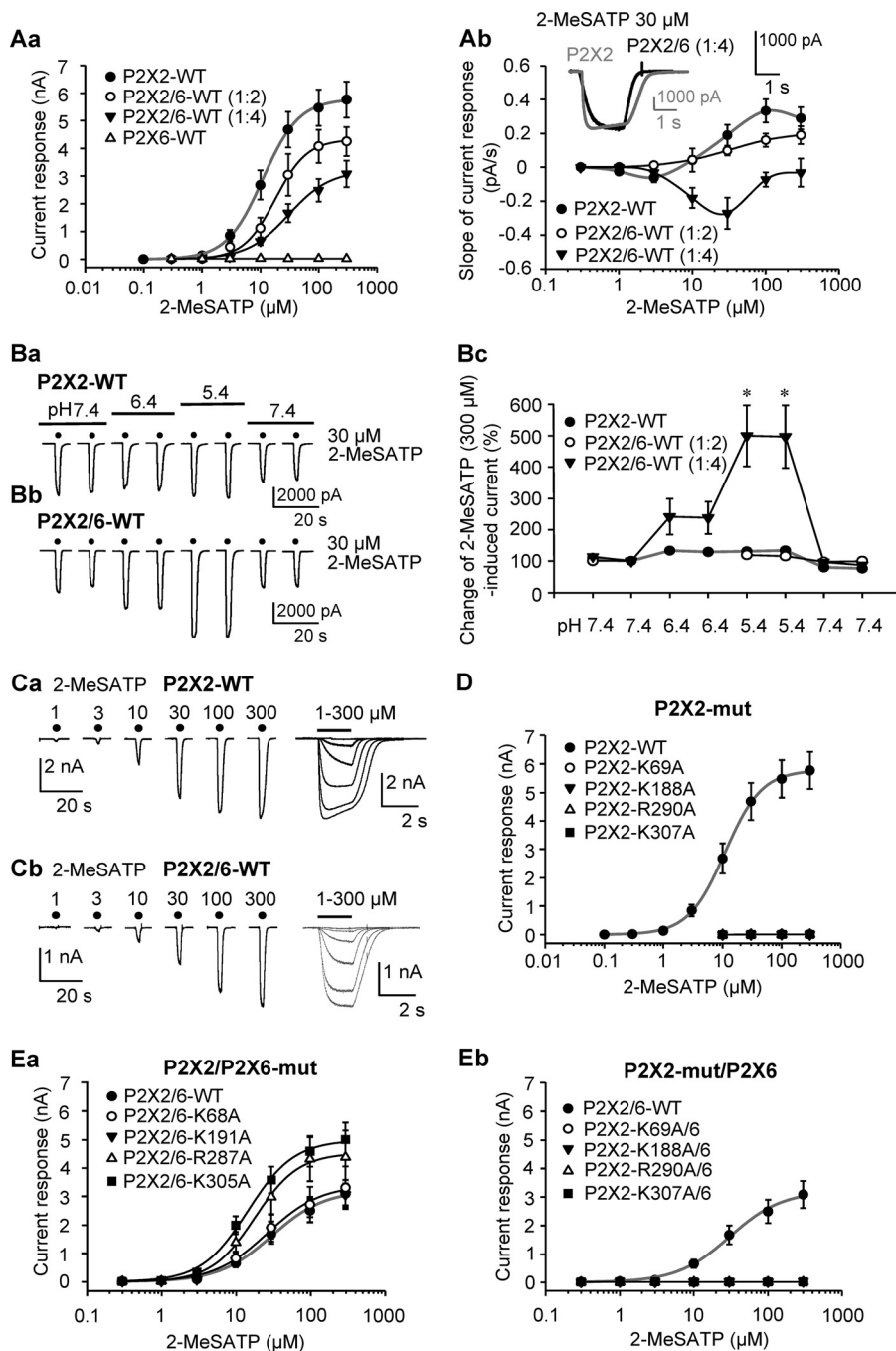


FIGURE 2. Current responses at WT hP2X2, hP2X6, and hP2X2/6 receptors and at the combinations of the respective WT and mutant subunits expressed in HEK293 cells. *A*, whole-cell currents at P2X2 or P2X2/6 (transfection ratios 1:2 or 1:4) receptors induced by 2-MeSATP (0.1–300 μ M) were recorded with the patch clamp technique at a holding potential of -65 mV. Increasing concentrations of the two agonists were locally superfused for 2 s with 5-min intervals (for representative recordings and application protocol, see *C*). Shown are concentration-response relationships for the amplitude of the 2-MeSATP-induced current at WT P2X2 and WT P2X2/6 receptors (see transfection ratios in parentheses). Means \pm S.E. (error bars) of 6–10 experiments both in this panel and in all further experiments are shown. The Hill coefficients for the respective WT receptors with 2-MeSATP as an agonist were as follows: P2X2, 1.8 ± 0.1 ; P2X2/6 (1:4 transfection), 1.2 ± 0.1 . For the E_{max} and EC_{50} values as well as the exact number of experiments, see Table 1. The E_{max} and EC_{50} values as well as the Hill coefficients at the P2X2/6 receptor (1:2 transfection) were as follows: $4,327 \pm 116$ nA, 18.6 ± 1.4 μ M, and 1.6 ± 0.2 (*Aa*). Shown are concentration-dependent changes of the slopes of the current responses from the beginning of the second s of application until its end (2-s applications in total; *Ab*). The inset shows the amplitude and shape of two representative scaled currents in response to 2-MeSATP (30 μ M); the slopes of the current responses measured during the last 1 s of agonist application were 0.19 ± 0.06 pA/s for P2X2 and -0.27 ± 0.09 pA/s for P2X2/6. *B*, dependence of 2-MeSATP (30 μ M)-induced current amplitudes on a gradual decrease of the external pH value from 7.4 to 5.4 for P2X2 and P2X2/6 receptors. Shown are representative recordings (*Ba* and *Bb*) and mean percentage changes with respect to the second current response (5-min intervals between agonist applications) at a normal pH of 7.4 (*Bc*). *, $p < 0.05$; statistically significant difference from the effect of 2-MeSATP at the P2X2 receptor. When the statistical comparison was with the predrug value of 100%, the percentage potentiation was by $33.6 \pm 7\%$ (P2X2; $p < 0.05$), $16.1 \pm 11.4\%$ (P2X2/6; transfection ratio 1:2; $p > 0.05$), and $397.2 \pm 99.6\%$ (P2X2/6; transfection ratio 1:4; $p < 0.05$). *C*, original recordings of current responses induced by increasing concentrations of 2-MeSATP at WT P2X2 (*Ca*) and WT P2X2/6 (*Cb*) receptors (indicated by filled circles or a horizontal bar). *D* and *E*, concentration-response relationships constructed for 2-MeSATP at WT and mutant (*mut*) P2X2 (*D*) or WT and mutant P2X2/6 (*E*) receptors; P2X2/6 contained either WT P2X2 and presumably non-functional mutants of P2X6 (*Ea*) or WT P2X6 and non-functional mutants of P2X2 (subunits) (Fig. 1*D*). The concentration-response relationships at the WT homomeric or heteromeric receptor are gray.

Subunit Stoichiometry of P2X Receptors

the respective oocyte voltage clamp measurements in supplemental Fig. 2, *Da* and *Db*).

Ca²⁺ Imaging in HEK293 Cells—In order to lend more support to our findings, we measured, in addition to the transmembrane current responses, also the [Ca²⁺]_i transients in HEK293 cells bearing P2X2, P2X3, P2X2/3, and P2X2/6 receptors. Whereas α,β -meATP (10–300 μM) caused a rapidly rising and, after its washout, also rapidly declining [Ca²⁺]_i response at homomeric P2X3 receptors (e.g. see Fig. 3*Ab*, *right*), similar concentrations of this agonist induced biphasic responses, slowly recovering to base line at heteromeric P2X2/3 receptors (Fig. 3*Aa*). 2-MeSATP (300 μM) at the P2X2/P2X3-K63A mutant and 2-MeSATP (10 μM) at the WT P2X2/3 receptor evoked [Ca²⁺]_i transients of practically undistinguishable shape (Fig. 3, *Aa* and *Ab*, *left*). It is noteworthy that although α,β -meATP is a selective P2X1, P2X3, P2X1/2, P2X1/5, and P2X2/3 receptor agonist without any activity at the endogenous P2Y receptors of HEK293 cells (see “Experimental Procedures”), its EC₅₀ value for [Ca²⁺]_i transients in HEK293 transfected with WT P2X2/3 receptors was higher than that for transmembrane currents ($p < 0.05$; compare Figs. 1 and 3). The Hill coefficients of the two concentration-response relationships also differed from each other ($p < 0.05$). At the moment, we have no unequivocal explanation for these discrepancies. However, we tentatively suggest that Ca²⁺ influx from the extracellular space may be slightly modified by Ca²⁺-induced Ca²⁺ release from the endoplasmic reticulum and simultaneous sequestration of [Ca²⁺]_i by its intracellular storage sites. In perfect agreement with the patch clamp investigations, Ala substitutions of the relevant AAs in the P2X3 component of the P2X2/3 receptor markedly depressed the α,β -meATP (10–300 μM)-induced current amplitudes (Fig. 3*Ba*). By contrast, replacement of the same AAs by Ala in the P2X2 component of this receptor complex had no major effect (Fig. 3*Bb*).

Because 2-MeSATP is a general P2X/P2Y receptor agonist, the amplitudes of the 2-MeSATP (0.3–300 μM)-induced [Ca²⁺]_i transients in mock-transfected HEK293 cells (mediated by endogenous P2Y receptors) were subtracted from those induced by this agonist in cells transfected with P2X2 or P2X2 plus P2X6 subunits (Fig. 3*Cb*, *left* and *right panels*; see “Experimental Procedures”). Interestingly, this time the [Ca²⁺]_i measurement yielded a lower EC₅₀ value ($p < 0.05$) but identical Hill coefficient ($p > 0.05$) of the 2-MeSATP concentration-response curve as the corresponding values obtained by patch-clamp recording (compare Figs. 1 and 3), a finding that also awaits explanation.

The biphasic [Ca²⁺]_i responses appear to be typical for WT P2X2 receptors (Fig. 3*Cb*, *left*) and heteromeric receptors containing this subunit (for P2X2/6, see Fig. 3*Ca*). Again in agreement with the patch clamp investigations, Ala substitutions of the relevant AAs in the P2X6 component of the P2X2/6 receptor had no major effect on the 2-MeSATP (10–300 μM)-induced [Ca²⁺]_i transients (Fig. 3*Da*), whereas replacement of the homologous AAs in the P2X2 component of this receptor were strongly inhibitory (Fig. 3*Db*).

Two-electrode Voltage Clamp Measurements in *X. laevis* Oocytes—The subunit composition of the above homomeric and heteromeric receptors and their expression at the cell sur-

face were investigated by biochemical methods in the non-mammalian *X. laevis* oocyte expression system. Therefore, it was important to prove that the functional data generated on HEK293 cells and *X. laevis* oocytes are basically identical.

In fact, in oocytes injected with cRNAs for P2X2, P2X3, and P2X6 receptor subunits, we made observations similar to those described for the mammalian cell line HEK293. Non-desensitizing current amplitudes were evoked both by α,β -meATP and 2-MeSATP (1–300 μM each) at P2X2/3 and P2X2/6 receptors, respectively (supplemental Fig. 2, *Aa* and *Ab*). When the P2X2/3 receptor complexes consisted of the P2X2 WT and P2X3 mutant subunits, the α,β -meATP (1–300 μM) current responses were greatly depressed (supplemental Fig. 2*Ca*). By contrast, the expression of the P2X3 WT subunit together with non-functional P2X2 subunits (see Fig. 2*D* and supplemental Fig. 2*B* for HEK293 cells and oocytes, respectively) only slightly displaced the α,β -meATP concentration-response curve of the WT P2X2/3 receptor to the right, indicating a moderate decrease in potency (supplemental Fig. 2*Cb*).

At P2X2/6 receptors, 2-MeSATP up to 300 μM failed to induce a notable current response at P2X2 mutant/P2X6 WT heteromers (supplemental Fig. 2*Db*), whereas the concentration-response curves of 2-MeSATP at P2X2 WT/P2X6 mutant heteromers were only modestly shifted to the left in comparison with those constructed at the WT P2X2/6 receptor (supplemental Fig. 2*Da*).

A shift of the extracellular pH from 7.4 to 5.4 depressed the E_{max} of the 2-MeSATP concentration-response curve from 34.0 ± 1.1 to $25.8 \pm 0.5 \mu\text{A}$ ($n = 6$ each; $p < 0.05$) and the EC₅₀ value from 4.6 ± 0.5 to $3.3 \pm 0.3 \mu\text{M}$ ($p < 0.05$) but did not change its Hill coefficient significantly. Such a decrease of ATP-activated inward currents at rat P2X2/6 receptors by a decrease of the external pH from 7.5 to 5.5 was described previously (16) and appears to be valid for the oocyte expression system but not for HEK293 cells (see Fig. 2*Bc*).

Assembly and Cell Surface Trafficking of P2X2/3 and P2X2/6 Receptors—To assess the impact of the point mutations on the assembly and cell surface expression, BN-PAGE and SDS-PAGE analysis was performed. Like the homomeric wild type and mutant P2X2 receptor (data not shown) and the P2X3 receptor (30), also all of the functionally impaired heteromeric P2X2/3 mutant receptors were capable of assembling to heterotrimers and appearing at the cell surface (Fig. 4*A*, *top*). The significantly larger mass of the P2X2 protomer of 72 kDa as compared with the 55 kDa of the P2X3 protomer is reflected by a clearly detectable retarded migration of the P2X2 protomer and homotrimer in the BN-PAGE (Fig. 4, *A* and *B*, *top*) and the SDS-PAGE (Fig. 4, *A* and *B*, *bottom*) gels, respectively. As expected, the heterotrimeric assemblies of P2X2 WT and P2X3 WT or P2X3 mutant subunits migrated at a lower molecular mass than the homotrimeric P2X2 and significantly above that of the homotrimeric P2X3 receptor, clearly indicating the formation of intermediate sized heteromeric assemblies consisting of P2X2 WT and P2X3 WT or P2X3 mutant subunits (Fig. 4*A*, *top*).

A physically stable interaction between P2X2 WT and P2X3 WT or P2X3 mutant subunits is also apparent from a co-purification assay, in which we co-expressed the His-P2X2-StrepII

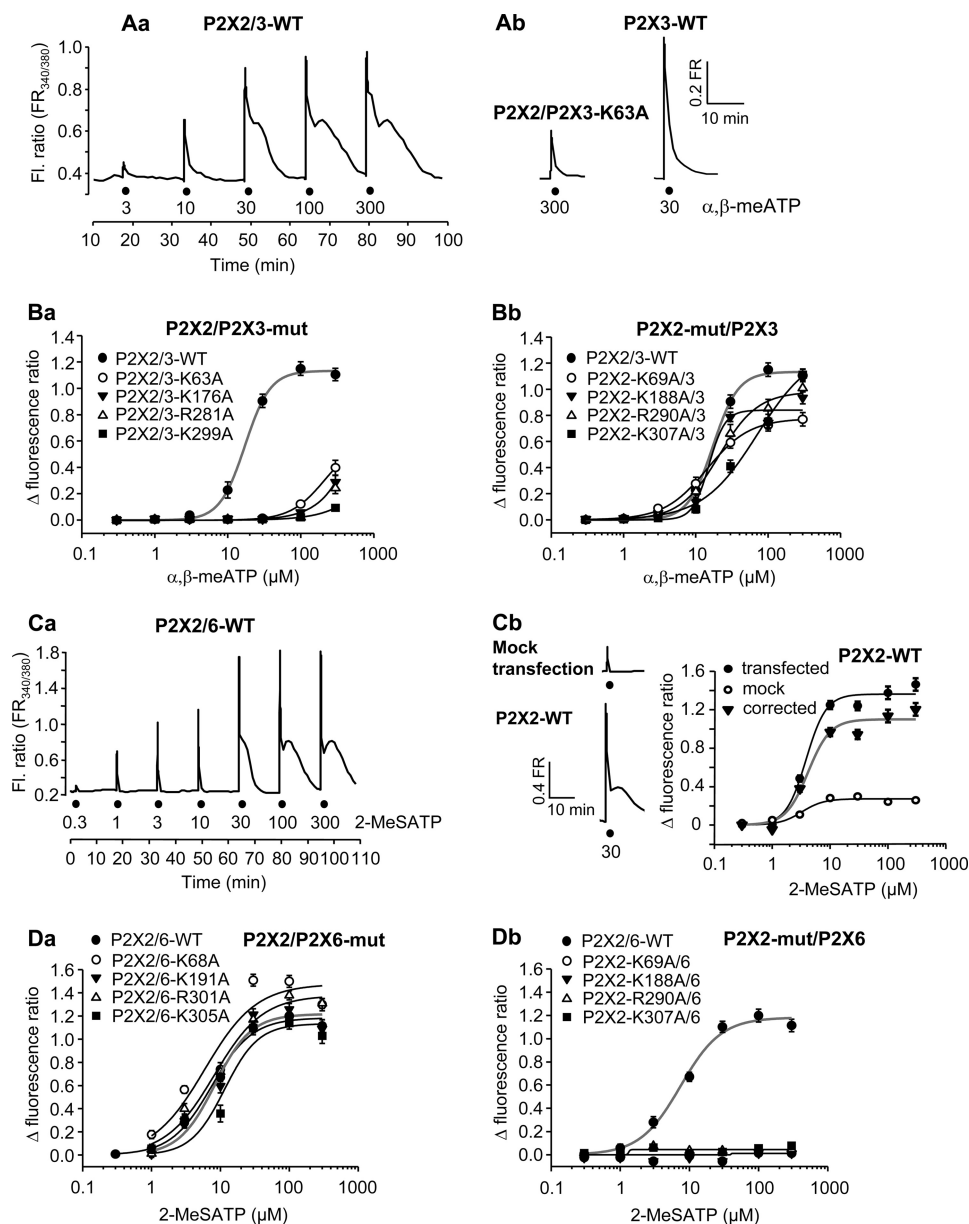


FIGURE 3. Increase of the cytosolic free Ca^{2+} concentration ($[Ca^{2+}]_i$) by Ca^{2+} influx from the extracellular space through wt-hP2X2, hP2X6, and hP2X2/6 receptors and through the combinations of the respective WT and mutant subunits expressed in HEK293 cells. A, Ca^{2+} imaging was carried out on HEK293 cells loaded by the fluorescence dye Fura-2 acetoxymethyl ester. The fluorescent ratio (Fl. Ratio; FR) provides a relative measure of $[Ca^{2+}]_i$. Increasing concentrations of 2-MeSATP (3–300 μM) were locally superfused for 5 s with 15-min intervals (as indicated by filled circles in the original recording shown). The shape and amplitude of the individual 2-MeSATP-induced $[Ca^{2+}]_i$ transients at WT P2X2/3 receptors (Aa) can be compared with the same parameters at the P2X2/P2X3-K63A mutant (Ab; left) and at the WT P2X3 receptor (Ab; right). B, concentration-response relationships constructed for α,β -meATP at P2X2/3 receptors containing either WT P2X2 and non-functional P2X3 subunits (Ba) or WT P2X3 and non-functional P2X2 subunits (Bb). Concentration-response curves at WT P2X2/3 receptors are also shown. C, original recording for a typical experiment with 2-MeSATP (0.3–300 μM) at WT P2X2/6 receptors. The shape and amplitude of the individual 2-MeSATP-induced $[Ca^{2+}]_i$ transients at WT P2X2/6 receptors (Ca) can be compared with the same parameters at the WT P2X2 receptor (Cb, bottom left) and in mock-transfected cells (Cb, top left). The 2-MeSATP-induced $[Ca^{2+}]_i$ transients measured in mock-transfected HEK293 cells were subtracted from the $[Ca^{2+}]_i$ transients measured in cells transfected with WT P2X2 receptors to yield the concentration-response curve of 2-MeSATP non-contaminated by the release of Ca^{2+} from intracellular pools (Cb, right). D, concentration-response relationships constructed for 2-MeSATP at P2X2/6 receptors, which contained either WT P2X2 and presumably non-functional mutants of P2X6 (Da) or WT P2X6 and non-functional mutants of P2X2 (Db). Concentration-response curves at WT P2X2/6 receptors are also shown. The concentration-response relationships at the WT homomeric or heteromeric receptors are gray. Shown are mean \pm S.E. of 19–42 experiments. The E_{max} and EC_{50} values as well as the Hill coefficients of the corrected WT concentration-response curves were as follows: P2X2/3 and α,β -meATP, 1.134 ± 0.021 , $17.2 \pm 0.9 \mu M$, and 2.5 ± 0.2 ; P2X2 and 2-MeSATP, 1.099 ± 0.072 , $4.1 \pm 0.9 \mu M$, and 2.3 ± 1.0 ; P2X2/6 and 2-MeSATP (1:4 transfection), 1.183 ± 0.043 , $7.4 \pm 0.9 \mu M$, and 1.5 ± 0.2 .

(a protein bearing a C-terminal, nine-AA StrepII tag in addition to the N-terminal hexahistidine tag) as a bait together with WT or mutant His-P2X3 as the prey. Purification using metal affinity chromatography or Strep-Tactin chromatography allowed us to verify the expression of the two proteins (Fig. 4A, bottom)

and to screen for the presence of co-purified His-P2X3 protein (Fig. 4A, bottom), respectively. His-P2X2-StrepII and WT or mutant His-P2X3 proteins could both be isolated by Ni^{2+} -NTA chromatography from the cells in which they were co-expressed. Purification by Strep-Tactin chromatography led to

Subunit Stoichiometry of P2X Receptors

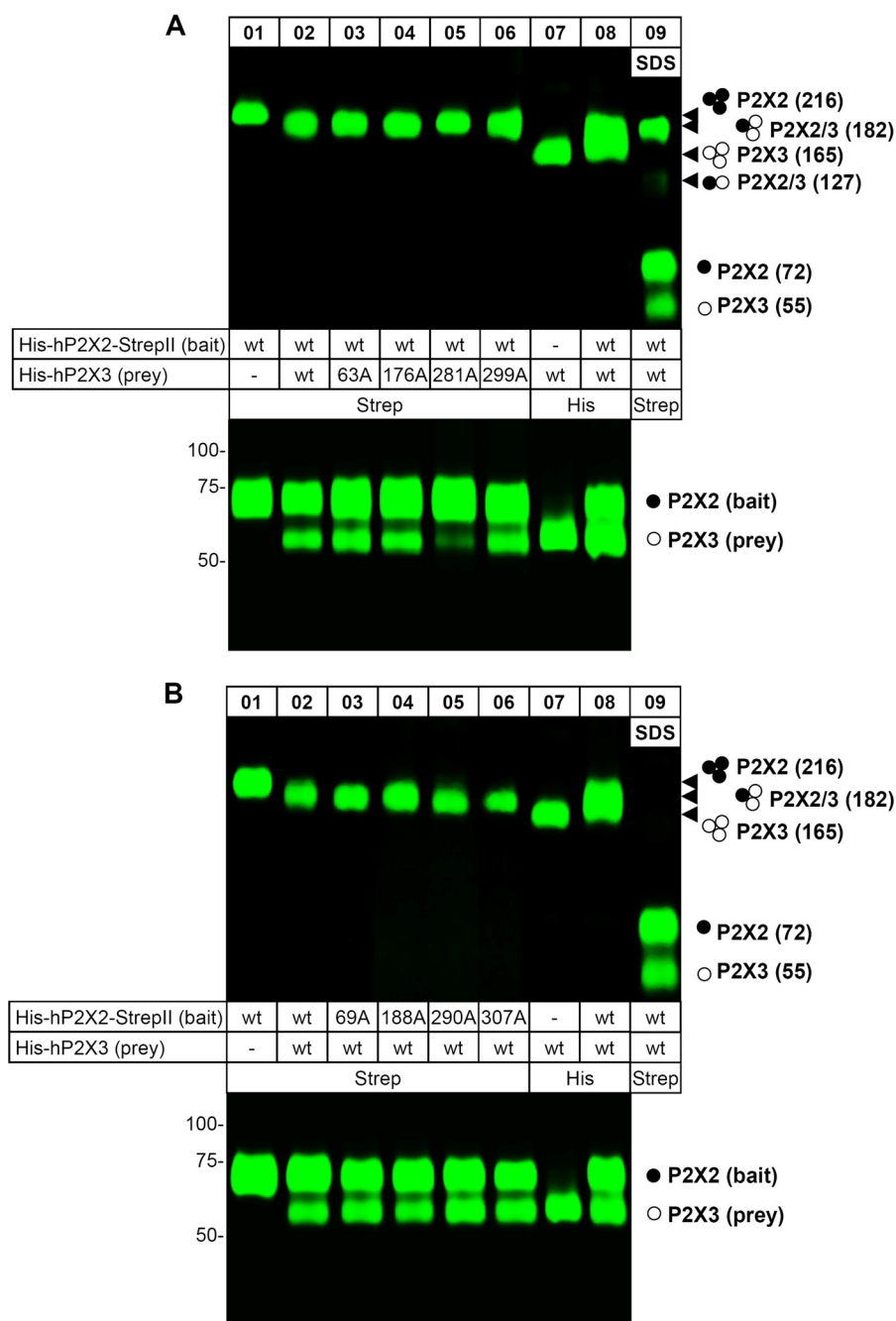


FIGURE 4. The hP2X3 subunit co-assembles and co-purifies with the hP2X2 subunit. The indicated proteins were purified under non-denaturing conditions from *X. laevis* oocytes by Ni^{2+} -NTA chromatography or Strep-Tactin chromatography, as indicated, resolved by BN-PAGE (top) or reducing SDS-PAGE (bottom), and visualized by Typhoon fluorescence scanning. Both the co-assembly of the WT His-hP2X2-StrepII subunit with the His-hP2X3 mutants (A) and the His-hP2X2-StrepII mutants with the WT His-hP2X3 subunit (B) are shown. The rightmost lane designated SDS, shows P2X2/3 protein migration after partial denaturation by a 1-h incubation with 0.1% SDS. The solid and open circles on the right indicate the numbers of hP2X2 and/or hP2X3 subunits, respectively, incorporated in the respective protein band. Migration positions of the corresponding trimeric assemblies are indicated by arrowheads. The numbers given in parenthesis on the right indicate the molecular masses calculated by referring to the SDS-PAGE-derived masses of 72 and 55 kDa for the hP2X2 and the hP2X3 protomer, respectively.

the co-isolation of the non-StrepII-tagged WT or mutant His-P2X3 proteins (Fig. 4A, bottom). When expressed alone, the His-P2X3 was not isolated (data not shown), indicating the absence of nonspecific binding of the His-P2X3 protein to the Strep-Tactin resin and thus confirming the suitability of this method for the analysis of P2X2 and P2X3 protein interaction.

Using the same biochemical techniques, we also found that the co-expression of P2X2 mutant subunits with P2X3 WT

subunits resulted in the formation of heterotrimeric receptors, as judged from the characteristic migration positions in the BN-polyacrylamide gel between those of the P2X2 and P2X3 homomers (Fig. 4B, top). Also, Strep-Tactin affinity purification of co-expressed mutant His-P2X2-StrepII proteins as bait together with WT His-P2X3 as the prey led to the co-isolation of the non-StrepII-tagged WT His-P2X3 proteins (Fig. 4B, bottom).

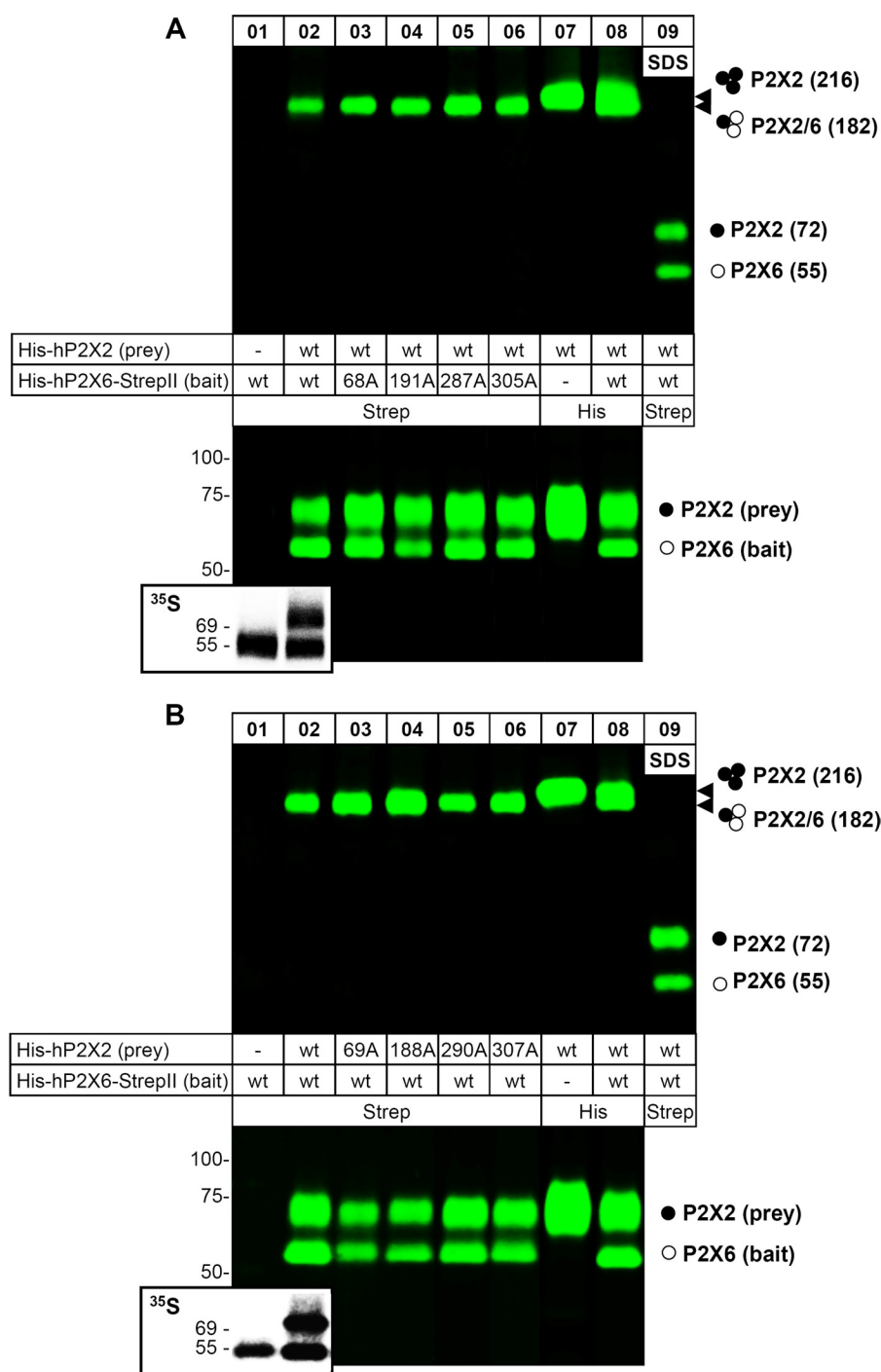


FIGURE 5. The hP2X2 subunit coassembles and co-purifies with the hP2X6 subunit. The indicated proteins were purified under non-denaturing conditions from *X. laevis* oocytes by Ni^{2+} -NTA chromatography or Strep-Tactin chromatography, as indicated, resolved by BN-PAGE (*top*) or reducing SDS-PAGE (*bottom*), and visualized by Typhoon fluorescence scanning. The *inset* of the *bottom* panel shows the total protein forms from corresponding lanes by [^{35}S]methionine incorporation. Both the co-assembly of the WT His-hP2X2 subunit with the His-hP2X6-StrepII mutants (*A*) and the His-hP2X2 mutants with the WT His-hP2X6-StrepII subunit (*B*) are shown. The *rightmost* lane, designated *SDS*, shows P2X2/6 protein migration after partial denaturation by a 1-h incubation with 0.1% SDS. The *solid* and *open circles* on the *right* indicate the numbers of hP2X2 and/or hP2X6 subunits, respectively, incorporated in the respective protein band. Migration positions of the corresponding trimeric assemblies are indicated by *arrowheads*. The *numbers* given in *parenthesis* on the *right* indicate the molecular masses calculated by referring to the SDS-PAGE-derived masses of 72 and 55 kDa for the hP2X2 and the hP2X6 protomer, respectively.

Oocyte-expressed heteromeric P2X2/6 receptors were also analyzed biochemically. Consistent with previous data (12), the singly expressed P2X6 subunit could be detected in the [^{35}S]methionine-labeled total form (Fig. 5, *A* and *B*, *inset* of *bottom*) but was absent at the plasma membrane (Fig. 5, *A* and

B, lane 1). However, upon co-expression of the WT or a mutant His-hP2X6-StrepII subunit with the WT His-hP2X2 subunit, a distinct protein band was observed in the BN-polyacrylamide gel that migrated with a lower mass than that of the homomeric P2X2 receptor (Fig. 5*A*, *top*). The reduced mass of this protein

Subunit Stoichiometry of P2X Receptors

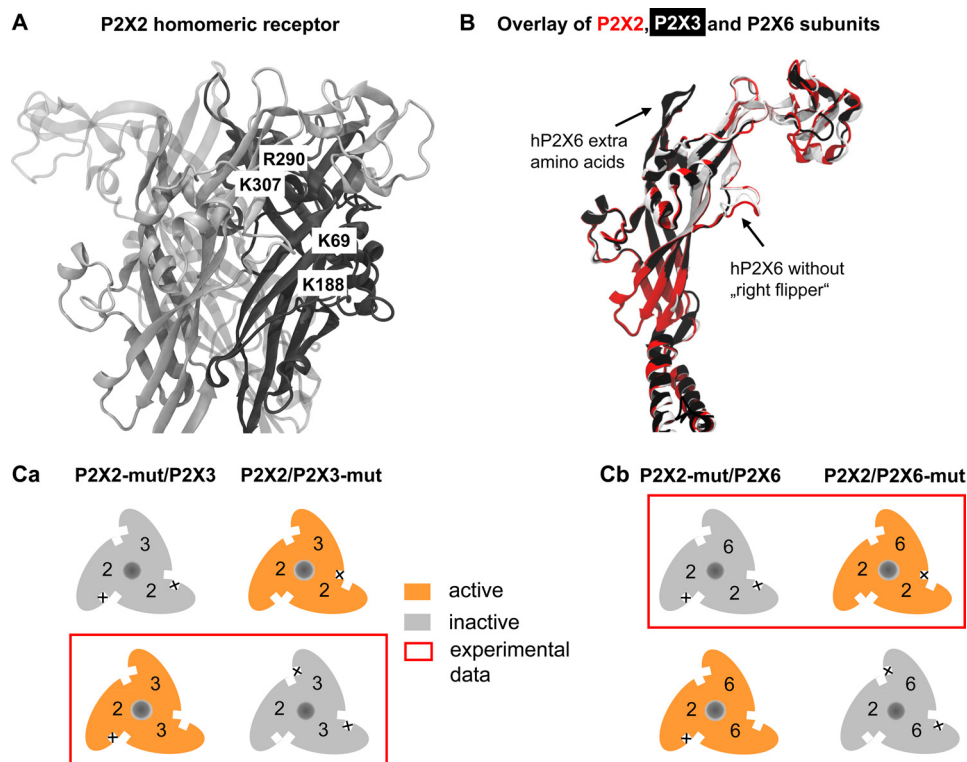


FIGURE 6. Homology model of the P2X2 receptor and of various P2X receptor subunits; schematic representation of the subunit stoichiometry of P2X2/3 and P2X2/6 receptors. A, binding-relevant Lys and Arg residues (Arg²⁹⁰, Lys³⁰⁷, Lys⁶⁹, and Lys¹⁸⁸; P2X2 numbering) of the homomeric hP2X2 receptor. Individual subunits are shown as *black*, *dark gray*, and *light gray* loops. Arg²⁹⁰ and Lys³⁰⁷ are situated at one subunit, and Lys⁶⁹ and Lys¹⁸⁸ are located at the neighboring one. The four AA residues are parts of one of the three agonist binding pouches of the P2X2 receptor. B, overlay of P2X2 (*red*), P2X3 (*light gray*), and P2X6 (*black*) subunits. The *right flipper* of the dolphin-like structure of these subunits is missing in P2X6. C, summary schematic showing the assumed subunit stoichiometry of (P2X2)₁/(P2X3)₂ (Ca) and (P2X2)₂/(P2X6)₁ (Cb). The experimental data obtained by co-expressing WT P2X2, P2X3, and P2X6 subunits and their non-functional mutants with the respective subunit partners supported the above assumption.

band can easily be reconciled with a P2X2/6 heteromer co-assembled of the larger 72-kDa P2X2 subunit and the smaller 55-kDa P2X6 subunit. The presence of the P2X6 subunit in this protein band could be demonstrated by denaturing treatment with 0.1% SDS, which led to the dissociation into two polypeptides, the larger P2X2 and the smaller P2X6 subunit (Fig. 5A, *lane 9, top*). The mass difference of these two polypeptides is also apparent from dissociation of the WT P2X2/6 trimeric protein complex in SDS-PAGE analysis (Fig. 5A, *bottom*).

Strep-Tactin affinity purification of co-expressed WT or mutant His-P2X6-StrepII proteins with WT His-P2X2 as the bait and the prey, respectively, led to the co-isolation of the non-StrepII-tagged WT His-P2X2 protein (Fig. 5A, *bottom*). Co-expression of P2X2 mutant subunits with P2X6 WT subunits resulted also in the formation of heterotrimeric receptors, as evident from the characteristic mobility shift in the BN-polyacrylamide gel toward a lower mass (Fig. 5B, *top*). Also, Strep-Tactin affinity purification of co-expressed WT His-P2X6-StrepII proteins with mutant His-P2X2 as bait and prey, respectively, led to the co-isolation of the non-StrepII-tagged mutant His-P2X2 proteins (Fig. 5B, *bottom*).

Homology Modeling of hP2X2 Receptor and of hP2X2, hP2X3, and hP2X6 Subunits; Schematic Representation of Subunit Stoichiometry of P2X2/3 and P2X2/6 Receptors—Using the published x-ray structure of the zebrafish P2X4 (31) as a template, we homology-modeled the hP2X2 receptor. The individual subunits are shown as *black*, *dark gray*, and *light gray* loops. The

aromatic AA residues replaced by Ala and thereby yielding non-functional mutants are indicated in Fig. 6A; they are located pairwise (Arg²⁹⁰-Lys³⁰⁶ and Lys⁶⁹-Lys¹⁸⁸) at two adjacent subunits and participate in the formation of a binding pocket. The overlay of the P2X2, P2X3, and P2X6 subunits shows that P2X6 does not contain the AAs forming the right flipper of the dolphin shaping all other subunits (Fig. 6B) (19, 31). In addition, P2X6 contains a series of extra AAs between the head and the left flipper.

A summary schematic shows our conclusions. In theory, two subunit stoichiometries are conceivable for the P2X2/P2X3 heterotrimer; 1:2 or 2:1 (Fig. 6C). Because our experiments indicated a loss of function only in the WT P2X2/P2X3 mutant combination (see the *framed assembly* in Fig. 6Ca), the 1:2 stoichiometry is compatible with the present findings. By contrast, for the P2X2/P2X6 heterotrimer, a loss of function was found only in the P2X2 mutant/WT P2X6 combination (see the *framed assembly* in Fig. 6Cb); therefore, in this case the combination 2:1 is compatible with the present findings.

DISCUSSION

The three-subunit composition of homomeric and heteromeric P2X receptors was originally suggested on the basis of biochemical data, including co-immunoprecipitation (6, 7) and BN-PAGE analysis as well as chemical cross-linking of subunits (12, 39). More recently, it was pointed out that co-immunopre-

cipitation may not be able to differentiate between receptor hetero-oligomers and two individual homo-oligomeric receptors closely interacting in the cell membrane (for the supposed P2X4/7 receptor, see Refs. 45 and 46). At the present time, a wealth of data supply compelling evidence for the fact that three subunits form a functional P2X receptor. Our experiments were designed to investigate the subunit composition of two neuronal heteromeric P2X receptors, composed of P2X2 and another partner (P2X3 or P2X6).

α,β -meATP activates recombinant, rapidly desensitizing P2X1 and P2X3 but not slowly desensitizing P2X2 receptors (6, 20, 34). Trinitrophenyl-ATP blocked P2X1, P2X2, and P2X2/3 receptors equally well; by contrast, diinosine pentaphosphate inhibited P2X1 receptors with a much higher affinity than P2X3 receptors (47, 48). Eventually, the selective P2X3 antagonist A-317491 exhibits comparable activities in blocking P2X2 and P2X2/3 receptors (34). Thus, P2X2/3 receptors have a ligand sensitivity resembling that of homomeric P2X3 receptors and non-desensitizing gating characteristics resembling those of homomeric P2X2 receptors (15, 49).

The situation with P2X2/6 receptors appears to be much more complex. Although co-immunoprecipitation identified P2X2 and P2X6 as possible partners for generating hetero-oligomeric complexes (10), and an oocyte expression study meticulously searched for differences between singly injected P2X2 and co-injected P2X2 and P2X6 to yield P2X2/6 (16), most differences were rather modest. It was reported that, in contrast to currents through P2X2 receptors, those through P2X2/6 receptors 1) were of smaller amplitude; 2) were sometimes biphasic and occasionally showed two phases of current decay; and 3) exhibited minor differences in their agonist and antagonist sensitivities. However, a property that unequivocally distinguished the two receptors was their opposite modulation by extracellular pH. Whereas P2X2 currents were increased after acidification of the bath solution (50), P2X2/6 currents were depressed under the same conditions (16).

It is noteworthy that only some (51) and not all groups of scientists were able to detect functional homomeric P2X6 receptors in the cell membrane (52). The reason for this discrepancy might be that P2X6 receptors either do not pass the quality check of the endoplasmic reticulum (53, 54), or if they do so, only in a partially glycosylated and non-functional form (55). Further glycosylation may result in a gain of function for some of the receptors inserted into the plasma membrane. These results perfectly agree with our own findings; homomeric P2X6 receptors failed to express at the plasma membrane of HEK293 cells.

The first part of our study confirmed and extended the observations of North and colleagues (28) by co-expressing WT P2X2 or WT P2X3 with the non-functional mutant counterparts of these subunits. In addition to the P2X3 mutants K63A and K299A situated at neighboring receptor subunits, which may interfere with binding as well as gating of the channel, because their positions are adjacent to the transmembrane segments 1 and 2 forming the channel pore, two additional mutants (K176A and R281A), being less likely to interfere with gating, were also used in the present study. We found by utilizing both HEK293 cells and oocytes as expression systems that a combination of the WT P2X2 with mutated P2X3 subunits

(chosen from non-functional Ala mutants introduced in any of the four NBSs) (29) strongly inhibited or even abolished the current response to α,β -meATP, whereas the opposite combination of WT P2X3 with mutated P2X2 subunits had very little effect. Consistent with data published previously (28) these results clearly demonstrate a $(P2X2)_1/(P2X3)_2$ stoichiometry of heteromeric P2X2/3 channels, as illustrated in Fig 6Ca. As a correlate of the cationic fluxes induced by P2X2/3 receptor activation, $[Ca^{2+}]_i$ transients were also measured and yielded similar data. Further, we asked ourselves whether this observation might be true only when the P2X3-selective α,β -meATP is used (28), which occupies the agonist binding pouches between the P2X3/P2X3 and P2X2/P2X3 subunits but most probably not that one lying at the interface of the P2X2/P2X2 subunit (Fig. 6 Ca). For this purpose we applied also 2-MeSATP, which is an agonist both at homomeric P2X2 and P2X3 receptors and therefore occupies the binding sites of any of the participating receptor subunits. Thereby, it was possible to confirm that the observed phenomenon is agonist-independent.

In the second part of our study, we attempted to strengthen the hypothesis that the P2X6 subunit as a constituent of the P2X2/6 receptor complex is able to modify the original P2X characteristics, despite not being able to form a functional homomeric receptor by itself. In a mammalian cell line, the ratio of the P2X2 and P2X6 protein in P2X2/6 was either 4.1:1 or 1:2.5, depending on the ratio of the P2X2 and P2X6 plasmid cDNAs used for transfection (1:1 and 1:4) (56). However, there were no functional measurements accompanying this biochemical and atomic force microscopy investigation. We varied the plasmid cDNA ratios of the P2X2 and P2X6 subunits in the transfection reagent between 1:2 and 1:4 (the maximum ratio tested by Barrera *et al.*) (56). Indication of the formation of P2X2/6 heteromeric receptors with characteristics clearly different from those of P2X2 homomeric receptors (lower maximum current amplitude, no run-down of the current response during a 2-s application period, marked dependence of the current amplitude on the external pH) was found only at the higher transfection ratio of 1:4. A combination of the WT P2X2 subunit with P2X6 subunits mutated at sites homologous to those proven to yield non-functional P2X2 and P2X3 receptors did not alter the current response to 2-MeSATP, whereas the opposite combination of WT P2X6 with mutant P2X2 subunits resulted in non-functional receptors. Of course it cannot be excluded that at still higher transfection ratios than used by us (1:>4), P2X2/6 receptor channels with the reverse stoichiometry are formed; however, the functionality of these channels still awaits confirmation (56). In the present experiments, only P2X2/6 channels containing a minimum of two unmutated ATP binding sites were functional (Fig. 6Cb), as was the case also with the P2X2/3 heteromer (Fig. 6Ca). Therefore, a $(P2X2)_2/(P2X6)_1$ stoichiometry is the most likely one to occur.

The measurement of $[Ca^{2+}]_i$ transients caused by 2-MeSATP fully confirmed these results. In addition, our two-electrode voltage clamp data generated in *X. laevis* oocytes expressing P2X2/6 were almost identical to those obtained in the HEK293 system; the only difference was the opposite pH sensitivity of the P2X2/6 heteromer.

Subunit Stoichiometry of P2X Receptors

To exclude the possibility that the non-functional phenotype of the alanine replacement mutants within the ATP binding site originates from deficits in trimeric assembly or cell surface trafficking rather than a change in agonist action, biochemical analysis of oocytes expressing the corresponding WT and mutant P2X receptor channels was performed. Our results show that all mutants were capable of proper trimeric assembly and displayed unaltered plasma membrane trafficking. This view is further supported by the Strep-Tactin co-purification assay, which showed that all of the mutants were able to interact physically with the respective reciprocal WT subunit. Because His-P2X6-StrepII subunits reached the plasma membrane only as integral parts of the P2X2/6 heteromer (Fig. 6, A and B, *bottom*), affinity purification via the P2X6-StrepII subunit as bait (and non-Strep-tagged P2X2 as the prey) enabled us to isolate exclusively the P2X2/6 heteromer. Quantification of the relative abundance of the plasma membrane form of P2X2 and P2X6 subunits in SDS-PAGE analysis yielded a 2:1 ratio, thus also suggesting a $(P2X2)_2/(P2X6)_1$ stoichiometry.

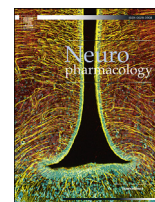
The null hypothesis predicts that at a 1:1 protein expression ratio after transfection with two different subunits, the channel ratios for P2XA and P2XB should be 1:3:3:1 for $(P2XA)_3$, $(P2XA)_2/(P2XB)_1$, $(P2XA)_1/(P2XB)_2$, and $(P2XB)_3$; these ratios change to 1:6:12:8 and to 1:12:48:64, when the protein expression ratios are modified to 1:2 (P2X2-P2X3) and 1:4 (P2X2-P2X6), respectively. Although we did not determine the actual expression of the three receptor proteins, for P2X2/3 the subunit composition generated under the conditions of the present experiments will be by the highest likelihood $(P2X2)_1/(P2X3)_2$. Both the electrophysiological and biochemical measurements supported the existence of this preferential subunit composition in the cell membrane and its ability to respond to P2X agonists; the other possible heteromer was apparently not expressed. However, P2X2 assembled with P2X6 according to a stoichiometry of 2:1, which was not compatible with a random process of association. Nevertheless, the only subunit combination observed in the plasma membrane was $(P2X2)_2/(P2X6)_1$, which was also supported by electrophysiological measurements. Hence, recognition sites between P2X2 and its partners rather than random association may govern the subunit composition of the receptor trimers. In conclusion, P2X2 was a dominant subunit in the P2X2/6 heteromer only, and already two binding sites of the three possible ones were sufficient to allow P2X2/3 and P2X2/6 to react with their agonists (also see Refs. 32, 57, and 58).

Acknowledgments—We are most grateful to Professor Richard A. North for critically reading a previous version of the manuscript. The expert methodological support of Maria Kowalski, Nick Helms, and Gregor Pagel is gratefully acknowledged.

REFERENCES

- Griffon, N., Büttner, C., Nicke, A., Kuhse, J., Schmalzing, G., and Betz, H. (1999) Molecular determinants of glycine receptor subunit assembly. *EMBO J.* **18**, 4711–4721
- Klausberger, T., Sarto, I., Ehya, N., Fuchs, K., Furtmüller, R., Mayer, B., Huck, S., and Sieghart, W. (2001) Alternate use of distinct intersubunit contacts controls GABA_A receptor assembly and stoichiometry. *J. Neurosci.* **21**, 9124–9133
- Zhou, Y., Nelson, M. E., Kuryatov, A., Choi, C., Cooper, J., and Lindstrom, J. (2003) Human $\alpha 4\beta 2$ acetylcholine receptors formed from linked subunits. *J. Neurosci.* **23**, 9004–9015
- Mansour, M., Nagarajan, N., Nehring, R. B., Clements, J. D., and Rosenmund, C. (2001) Heteromeric AMPA receptors assemble with a preferred subunit stoichiometry and spatial arrangement. *Neuron* **32**, 841–853
- Schüler, T., Mesic, I., Madry, C., Bartholomäus, I., and Laube, B. (2008) Formation of NR1/NR2 and NR1/NR3 heterodimers constitutes the initial step in *N*-methyl-D-aspartate receptor assembly. *J. Biol. Chem.* **283**, 37–46
- North, R. A. (2002) Molecular physiology of P2X receptors. *Physiol. Rev.* **82**, 1013–1067
- Egan, T. M., Cox, J. A., and Voigt, M. M. (2004) Molecular structure of P2X receptors. *Curr. Top. Med. Chem.* **4**, 821–829
- Roberts, J. A., Vial, C., Digby, H. R., Agboh, K. C., Wen, H., Atterbury-Thomas, A., and Evans, R. J. (2006) Molecular properties of P2X receptors. *Pflugers Arch.* **452**, 486–500
- Köles, L., Fürst, S., and Illes, P. (2007) Purine ionotropic (P2X) receptors. *Curr. Pharm. Des.* **13**, 2368–2384
- Torres, G. E., Egan, T. M., and Voigt, M. M. (1999) Hetero-oligomeric assembly of P2X receptor subunits. Specificities exist with regard to possible partners. *J. Biol. Chem.* **274**, 6653–6659
- Haines, W. R., Torres, G. E., Voigt, M. M., and Egan, T. M. (1999) Properties of the novel ATP-gated ionotropic receptor composed of the P2X1 and P2X5 isoforms. *Mol. Pharmacol.* **56**, 720–727
- Aschrafi, A., Sadtler, S., Niculescu, C., Rettinger, J., and Schmalzing, G. (2004) Trimeric architecture of homomeric P2X2 and heteromeric P2X1+2 receptor subtypes. *J. Mol. Biol.* **342**, 333–343
- Nicke, A., Kerschensteiner, D., and Soto, F. (2005) Biochemical and functional evidence for heteromeric assembly of P2X1 and P2X4 subunits. *J. Neurochem.* **92**, 925–933
- Torres, G. E., Haines, W. R., Egan, T. M., and Voigt, M. M. (1998) Co-expression of P2X1 and P2X5 receptor subunits reveals a novel ATP-gated ion channel. *Mol. Pharmacol.* **54**, 989–993
- Lewis, C., Neidhart, S., Holy, C., North, R. A., Buell, G., and Surprenant, A. (1995) Coexpression of P2X2 and P2X3 receptor subunits can account for ATP-gated currents in sensory neurons. *Nature* **377**, 432–435
- King, B. F., Townsend-Nicholson, A., Wildman, S. S., Thomas, T., Spyer, K. M., and Burnstock, G. (2000) Coexpression of rat P2X2 and P2X6 subunits in *Xenopus* oocytes. *J. Neurosci.* **20**, 4871–4877
- Lê, K. T., Babinski, K., and Séguéla, P. (1998) Central P2X4 and P2X6 channel subunits coassemble into a novel heteromeric ATP receptor. *J. Neurosci.* **18**, 7152–7159
- Nörenberg, W., and Illes, P. (2000) Neuronal P2X receptors. Localization and functional properties. *Naunyn-Schmiedeberg's Arch. Pharmacol.* **362**, 324–339
- Browne, L. E., Jiang, L. H., and North, R. A. (2010) New structure enlivens interest in P2X receptors. *Trends Pharmacol. Sci.* **31**, 229–237
- Coddou, C., Yan, Z., Obsil, T., Huidobro-Toro, J. P., and Stojilkovic, S. S. (2011) Activation and regulation of purinergic P2X receptor channels. *Pharmacol. Rev.* **63**, 641–683
- Burnstock, G. (2006) Purinergic P2 receptors as targets for novel analgesics. *Pharmacol. Ther.* **110**, 433–454
- Wirkner, K., Sperlagh, B., and Illes, P. (2007) P2X3 receptor involvement in pain states. *Mol. Neurobiol.* **36**, 165–183
- Lalo, U., Pankratov, Y., Wichert, S. P., Rossner, M. J., North, R. A., Kirchhoff, F., and Verkhratsky, A. (2008) P2X1 and P2X5 subunits form the functional P2X receptor in mouse cortical astrocytes. *J. Neurosci.* **28**, 5473–5480
- Palygin, O., Lalo, U., Verkhratsky, A., and Pankratov, Y. (2010) Ionotropic NMDA and P2X1/5 receptors mediate synaptically induced Ca^{2+} signaling in cortical astrocytes. *Cell Calcium* **48**, 225–231
- Majumder, P., Trujillo, C. A., Lopes, C. G., Resende, R. R., Gomes, K. N., Yuahasi, K. K., Britto, L. R., and Ulrich, H. (2007) New insights into purinergic receptor signaling in neuronal differentiation, neuroprotection, and brain disorders. *Purinergic Signal.* **3**, 317–331
- Schwindt, T. T., Trujillo, C. A., Negraes, P. D., Lameu, C., and Ulrich, H. (2011) Directed differentiation of neural progenitors into neurons is ac-

- accompanied by altered expression of P2X purinergic receptors. *J. Mol. Neurosci.* **44**, 141–146
27. Jiang, L. H., Kim, M., Spelta, V., Bo, X., Surprenant, A., and North, R. A. (2003) Subunit arrangement in P2X receptors. *J. Neurosci.* **23**, 8903–8910
 28. Wilkinson, W. J., Jiang, L. H., Surprenant, A., and North, R. A. (2006) Role of ectodomain lysines in the subunits of the heteromeric P2X2/3 receptor. *Mol. Pharmacol.* **70**, 1159–1163
 29. Mager, P. P., Weber, A., and Illes, P. (2004) Bridging the gap between structural bioinformatics and receptor research. The membrane-embedded, ligand-gated, P2X glycoprotein receptor. *Curr. Top. Med. Chem.* **4**, 1657–1705
 30. Bodnar, M., Wang, H., Riedel, T., Hintze, S., Kato, E., Fallah, G., Gröger-Arndt, H., Giniatullin, R., Grohmann, M., Hausmann, R., Schmalzing, G., Illes, P., and Rubini, P. (2011) Amino acid residues constituting the agonist binding site of the human P2X3 receptor. *J. Biol. Chem.* **286**, 2739–2749
 31. Kawate, T., Michel, J. C., Birdsong, W. T., and Gouaux, E. (2009) Crystal structure of the ATP-gated P2X4 ion channel in the closed state. *Nature* **460**, 592–598
 32. Sokolova, E., Skorinkin, A., Moiseev, I., Agrachev, A., Nistri, A., and Giniatullin, R. (2006) Experimental and modeling studies of desensitization of P2X3 receptors. *Mol. Pharmacol.* **70**, 373–382
 33. Gerevich, Z., Zadori, Z., Müller, C., Wirkner, K., Schröder, W., Rubini, P., and Illes, P. (2007) Metabotropic P2Y receptors inhibit P2X3 receptor-channels via G protein-dependent facilitation of their desensitization. *Br. J. Pharmacol.* **151**, 226–236
 34. Jarvis, M. F., and Khakh, B. S. (2009) ATP-gated P2X cation channels. *Neuropharmacology* **56**, 208–215
 35. Fischer, W., Wirkner, K., Weber, M., Eberts, C., Köles, L., Reinhardt, R., Franke, H., Allgaier, C., Gillen, C., and Illes, P. (2003) Characterization of P2X3, P2Y1, and P2Y4 receptors in cultured HEK293-hP2X3 cells and their inhibition by ethanol and trichloroethanol. *J. Neurochem.* **85**, 779–790
 36. von Kügelgen, I., and Harden, T. K. (2011) Molecular pharmacology, physiology, and structure of the P2Y receptors. *Adv. Pharmacol.* **61**, 373–415
 37. Hausmann, R., Rettinger, J., Gerevich, Z., Meis, S., Kassack, M. U., Illes, P., Lambrecht, G., and Schmalzing, G. (2006) The suramin analog 4,4',4''-(carbonylbis(imino-5,1,3-benzenetriylbis (carbonylimino)))tetra-kis-benzenesulfonic acid (NF110) potently blocks P2X3 receptors. Subtype selectivity is determined by location of sulfonic acid groups. *Mol. Pharmacol.* **69**, 2058–2067
 38. Becker, D., Woltersdorf, R., Boldt, W., Schmitz, S., Braam, U., Schmalzing, G., and Markwardt, F. (2008) The P2X7 carboxyl tail is a regulatory module of P2X7 receptor channel activity. *J. Biol. Chem.* **283**, 25725–25734
 39. Nicke, A., Bäumert, H. G., Rettinger, J., Eichele, A., Lambrecht, G., Mutschler, E., and Schmalzing, G. (1998) P2X1 and P2X3 receptors form stable trimers. A novel structural motif of ligand-gated ion channels. *EMBO J.* **17**, 3016–3028
 40. Fallah, G., Romer, T., Detro-Dassen, S., Braam, U., Markwardt, F., and Schmalzing, G. (2011) TMEM16A(a)/anoctamin-1 shares a homodimeric architecture with CLC chloride channels. *Mol. Cell. Proteomics* **10**, M110.004697
 41. Fiser, A., and Sali, A. (2003) Modeller. Generation and refinement of homology-based protein structure models. *Methods Enzymol.* **374**, 461–491
 42. Humphrey, W., Dalke, A., and Schulten, K. (1996) VMD. Visual molecular dynamics. *J. Mol. Graph.* **14**, 33–38
 43. Evans, R. J. (2010) Structural interpretation of P2X receptor mutagenesis studies on drug action. *Br. J. Pharmacol.* **161**, 961–971
 44. Stojilkovic, S. S., Yan, Z., Obsil, T., and Zemkova, H. (2010) Structural insights into the function of P2X4. An ATP-gated cation channel of neuroendocrine cells. *Cell Mol. Neurobiol.* **30**, 1251–1258
 45. Guo, C., Masin, M., Qureshi, O. S., and Murrell-Lagnado, R. D. (2007) Evidence for functional P2X4/P2X7 heteromeric receptors. *Mol. Pharmacol.* **72**, 1447–1456
 46. Nicke, A. (2008) Homotrimeric complexes are the dominant assembly state of native P2X7 subunits. *Biochem. Biophys. Res. Commun.* **377**, 803–808
 47. King, B. F., Liu, M., Pintor, J., Gualix, J., Miras-Portugal, M. T., and Burnstock, G. (1999) Diinosine pentaphosphate (IP5I) is a potent antagonist at recombinant rat P2X1 receptors. *Br. J. Pharmacol.* **128**, 981–988
 48. Khakh, B. S., Burnstock, G., Kennedy, C., King, B. F., North, R. A., Séguéla, P., Voigt, M., and Humphrey, P. P. (2001) International union of pharmacology. XXIV. Current status of the nomenclature and properties of P2X receptors and their subunits. *Pharmacol. Rev.* **53**, 107–118
 49. Chizh, B. A., and Illes, P. (2001) P2X receptors and nociception. *Pharmacol. Rev.* **53**, 553–568
 50. King, B. F., Wildman, S. S., Ziganshina, L. E., Pintor, J., and Burnstock, G. (1997) Effects of extracellular pH on agonism and antagonism at a recombinant P2X2 receptor. *Br. J. Pharmacol.* **121**, 1445–1453
 51. Collo, G., North, R. A., Kawashima, E., Merlo-Pich, E., Neidhart, S., Surprenant, A., and Buell, G. (1996) Cloning of P2X5 and P2X6 receptors and the distribution and properties of an extended family of ATP-gated ion channels. *J. Neurosci.* **16**, 2495–2507
 52. Soto, F., Garcia-Guzman, M., Karschin, C., and Stühmer, W. (1996) Cloning and tissue distribution of a novel P2X receptor from rat brain. *Biochem. Biophys. Res. Commun.* **223**, 456–460
 53. Barrera, N. P., Ormond, S. J., Henderson, R. M., Murrell-Lagnado, R. D., and Edwardson, J. M. (2005) Atomic force microscopy imaging demonstrates that P2X2 receptors are trimers but that P2X6 receptor subunits do not oligomerize. *J. Biol. Chem.* **280**, 10759–10765
 54. Ormond, S. J., Barrera, N. P., Qureshi, O. S., Henderson, R. M., Edwardson, J. M., and Murrell-Lagnado, R. D. (2006) An uncharged region within the N terminus of the P2X6 receptor inhibits its assembly and exit from the endoplasmic reticulum. *Mol. Pharmacol.* **69**, 1692–1700
 55. Jones, C. A., Vial, C., Sellers, L. A., Humphrey, P. P., Evans, R. J., and Chessell, I. P. (2004) Functional regulation of P2X6 receptors by N-linked glycosylation. Identification of a novel α,β -methylene ATP-sensitive phenotype. *Mol. Pharmacol.* **65**, 979–985
 56. Barrera, N. P., Henderson, R. M., Murrell-Lagnado, R. D., and Edwardson, J. M. (2007) The stoichiometry of P2X2/6 receptor heteromers depends on relative subunit expression levels. *Biophys. J.* **93**, 505–512
 57. Ding, S., and Sachs, F. (1999) Single channel properties of P2X2 purinoreceptors. *J. Gen. Physiol.* **113**, 695–720
 58. Karoly, R., Mike, A., Illes, P., and Gerevich, Z. (2008) The unusual state-dependent affinity of P2X3 receptors can be explained by an allosteric two-open state model. *Mol. Pharmacol.* **73**, 224–234



Flexible subunit stoichiometry of functional human P2X2/3 heteromeric receptors



Maria Kowalski ^{a,1}, Ralf Hausmann ^{b,1}, Julia Schmid ^a, Anke Dopychai ^b,
Gabriele Stephan ^a, Yong Tang ^c, Günther Schmalzing ^b, Peter Illes ^a, Patrizia Rubini ^{a,*}

^a Rudolf-Boehm-Institute of Pharmacology and Toxicology, University of Leipzig, 04107 Leipzig, Germany

^b Molecular Pharmacology, RWTH Aachen University, 52074 Aachen, Germany

^c Acupuncture and Tuina School, Chengdu University of Traditional Chinese Medicine, 610075 Chengdu, China

ARTICLE INFO

Article history:

Received 13 February 2015

Received in revised form

1 July 2015

Accepted 9 July 2015

Available online 13 July 2015

Keywords:

Heteromeric P2X receptors

P2X2/3 receptors

Subunit stoichiometry

Mutagenesis

ABSTRACT

The aim of the present work was to clarify whether heterotrimeric P2X2/3 receptors have a fixed subunit stoichiometry consisting of one P2X2 and two P2X3 subunits as previously suggested, or a flexible stoichiometry containing also the inverse subunit composition. For this purpose we transfected HEK293 cells with P2X2 and P2X3 encoding cDNA at the ratios of 1:2 and 4:1, and analysed the biophysical and pharmacological properties of the generated receptors by means of the whole-cell patch-clamp technique. The concentration-response curves for the selective agonist α,β -meATP did not differ from each other under the two transfection ratios. However, co-expression of an inactive P2X2 mutant and the wild type P2X3 subunit and *vice versa* resulted in characteristic distortions of the α,β -meATP concentration-response relationships, depending on which subunit was expressed in excess, suggesting that HEK293 cells express mixtures of (P2X2)₁/(P2X3)₂ and (P2X2)₂/(P2X3)₁ receptors. Whereas the allosteric modulators H⁺ and Zn²⁺ failed to discriminate between the two possible heterotrimeric receptor variants, the α,β -meATP-induced responses were blocked more potently by the competitive antagonist A317491, when the P2X2 subunit was expressed in deficit of the P2X3 subunit. Furthermore, blue-native PAGE analysis of P2X2 and P2X3 subunits co-expressed in *Xenopus laevis* oocytes and HEK293 cells revealed that plasma membrane-bound P2X2/3 receptors appeared in two clearly distinct heterotrimeric complexes: a (P2X2-GFP)₂/(P2X3)₁ complex and a (P2X2-GFP)₁/(P2X3)₂ complex. These data strongly indicate that the stoichiometry of the heteromeric P2X2/3 receptor is not fixed, but determined in a permutational manner by the relative availability of P2X2 and P2X3 subunits.

© 2015 Elsevier Ltd. All rights reserved.

1. Introduction

Extracellular nucleotide receptors belong to the P2X (ligand-gated cationic channels) or P2Y type (G protein-coupled receptors) (Abbracchio and Burnstock, 1994; Ralevic and Burnstock, 1998).

Abbreviations: 2-MeSATP, 2-methylthio ATP; ASIC, acid-sensing ion channel; BN-PAGE, blue native PAGE; DRG, dorsal root ganglion; EC₅₀, half maximal effective concentration; FR, fluorescent ratio; GFP, green fluorescent protein; I_{max}, peak current caused by maximum agonist concentration; LGIC, ligand-gated ion channel; η_H , Hill coefficient; TNP-ATP, trinitrophenyl-ATP; wt, wild type; α,β -meATP, α,β -methylene ATP.

* Corresponding author. Rudolf-Boehm-Institute of Pharmacology and Toxicology, University of Leipzig, Haertelstrasse 16-18, 04107 Leipzig, Germany.

E-mail address: Patrizia.Rubini@medizin.uni-leipzig.de (P. Rubini).

¹ These authors contributed equally to the work.

Seven distinct P2X receptor subunits have been cloned from mammalian species (P2X1-7); they were found to form both homomeric and heteromeric channels. P2X receptors consist of three subunits (Nicke et al., 1998; Aschrafi et al., 2004; Kawate et al., 2009), each of them exhibiting two transmembrane regions, intracellular N- and C-termini and a large extracellular loop (North, 2002; Köles et al., 2007; Hausmann et al., 2015).

Early studies based on co-immunoprecipitation experiments with epitope-tagged subunits demonstrated that only the P2X6 subunit was not able to form homotrimers, and P2X7 was the only exception of constituting heterotrimeric complexes (Torres et al., 1999; Coddou et al., 2011). Because heteromeric P2X receptors mostly combine the pharmacological and biophysical properties of their parent subunits, the functional diversity of native P2X receptor-mediated responses has been explained by the existence of heteromeric assemblies (Nörenberg and Illes, 2000).

However, in spite of a large variability in recombinant P2X subunit combinations in expression systems, convincing evidence for native heteromeric P2X receptors is rather limited (Saul et al., 2013). The existence of P2X_{2/3} receptors has been firmly established in sensory ganglia involved in the transduction of painful stimuli from peripheral tissues to the spinal cord dorsal horn (Lewis et al., 1995; Wirkner et al., 2007). Quantitative real time PCR and pharmacological characterization by whole-cell patch-clamp experiments suggest the presence of P2X_{1/5} receptors in cortical astrocytes (Lalo et al., 2008) and possibly also at sympathetic neuroeffector junctions in submucosal arteries (Surprenant et al., 2000). Although during neuronal differentiation of neural progenitor cells, the expression of both P2X₂ and P2X₆ subunits was up-regulated (Schwindt et al., 2011), there is no clear evidence for the presence of functional heteromeric P2X_{2/6} assemblies in native cells (Saul et al., 2013). In the case of co-expressed P2X₄ and P2X₇ subunits, the current view is that P2X₄ and P2X₇ receptors exist as independent homomeric channels interacting with each other (Nicke, 2008; Boumechache et al., 2009; Antonio et al., 2011) rather than as heterotrimeric P2X_{4/7} channels (Guo et al., 2007; Casas-Pruneda et al., 2009).

For heterotrimeric P2X_{2/3} receptors in HEK293 cells transfected with a lower amount of P2X₂ cDNA than of P2X₃ cDNA (P2X₂:P2X₃ cDNA ratio <0.5) it was concluded that the subunit stoichiometry is (P2X₂)₁/(P2X₃)₂ (Jiang et al., 2003; Wilkinson et al., 2006; Hausmann et al., 2012). Functional analysis of wild type (wt) or mutated heteromeric P2X_{2/6} receptors in HEK293 cells transfected with an excess of P2X₆ encoding cDNA over P2X₂ cDNA (P2X₂:P2X₆ cDNA ratio 0.25) revealed that the functional P2X_{2/6} channels have a (P2X₂)₂/(P2X₆)₁ stoichiometry (Hausmann et al., 2012). However, an atomic force microscopy study suggested that the subunit stoichiometry of the P2X_{2/6} receptor depends on the relative expression level of the two subunits (Barrera et al., 2007). Thus, in this study the ratio of P2X₂ and P2X₆ cDNA during the transfection procedure appeared to determine the relative amount of expression of the simultaneously occurring (P2X₂)₁/(P2X₆)₂ and (P2X₂)₂/(P2X₆)₁.

Based on these findings we decided to investigate whether human (h)P2X_{2/3} receptors have a fixed subunit composition in which hP2X₃ predominates over hP2X₂ or whether the reverse stoichiometry is also feasible. For this purpose we modified the hP2X₂ and hP2X₃ cDNA ratios when transfecting HEK293 cells. The patch-clamp method allowed the functional discrimination of two co-existing heteromeric receptor variants. Furthermore, blue native (BN)-PAGE analysis of hP2X₂ and hP2X₃ subunits co-expressed in *Xenopus laevis* oocytes revealed the simultaneous presence of heterotrimeric (hP2X₂)₁/(hP2X₃)₂ and (hP2X₂)₂/(hP2X₃)₁ protein complexes in their plasma membranes. In conclusion, we suggest that hP2X_{2/3} receptors have a variable rather than a fixed subunit stoichiometry.

2. Methods

2.1. Cell culture, mutagenesis and transfection procedures in HEK293 cells

HEK293 cells were kept in Dulbecco's modified Eagle's medium additionally containing 4.5 mg/ml D-glucose, 10% fetal bovine serum (Biochrom) and 2 mM L-glutamine (Life technologies) at 37 °C and 5% CO₂ in humidified air.

The hP2X₂ (hP2X_{2A}) and the hP2X₃ receptor cDNAs were subcloned into pIRES2-DsRed (hP2X_{2A}) and pIRES2-EGFP (hP2X₃) vectors from Clontech by *Pst*I and *Eco*RI restriction sites (Bodnar et al., 2011). hP2X₂ and hP2X₃ replacement mutants were generated by QuikChange site directed-mutagenesis (Stratagene).

HEK293 cells were plated 6 h before transient transfection in plastic dishes and glass coverslips for electrophysiology and Ca²⁺ microfluorometry, respectively. For transfection 0.5 μg (homomeric hP2X₂ and hP2X₃ receptors, heteromeric hP2X₂/hP2X₃ receptors and heteromeric hP2X₂/hP2X₃-mut receptors) to 0.75 μg (heteromeric hP2X₂-mut/hP2X₃ receptors) of plasmid DNA was combined with 10 μl of PolyFect reagent (Qiagen) and 100 μl of OptiMEM (Life technologies). About 18 h after transfection, the medium was replaced by OptiMEM for removal of residual plasmid DNA, as previously described (Kowalski et al., 2014).

2.2. Whole-cell patch-clamp recordings in HEK293 cells

Whole-cell patch-clamp recordings were performed 2–4 days after transient transfection of HEK293 cells at room temperature (20–22 °C) using an Axopatch 200 B patch clamp amplifier (Molecular Devices). Transfected HEK293 cells were identified by means of an inverted differential interference contrast microscope with epifluorescent optics (Axiovert 100, Zeiss). The pipette solution contained (in mM) CsCl 135, MgCl₂ 2, HEPES 20, EGTA 11, CaCl₂ 1, Mg-ATP 1.5, and Li-GTP 0.3; pH adjusted to 7.4 with CsOH. When 2-methylthio ATP (2-MeSATP) was used as an agonist, Li-GTP was replaced by GDP-β-S (0.3 mM) in order to block G protein-coupled P2Y receptors, which might interfere with P2X receptor mediated responses (Gerevich et al., 2007). The external physiological solution contained (in mM) NaCl 135, KCl 5, MgCl₂ 2, CaCl₂ 2, HEPES 10, and D-glucose 11; pH adjusted to 7.4 with NaOH.

The pipette resistances varied between 3 and 7 MΩ. The liquid junction potential (V_{LJ}) between the bath and pipette solution at 21 °C was calculated and was found to be –4.5 mV. Holding potential values given in this study were corrected for V_{LJ} . All recordings were carried out at a holding potential of –65 mV. Data were filtered at 2 kHz with the inbuilt filter of the amplifier, digitized at 5 kHz, and stored on a computer using a Digidata 1440 interface and pClamp 10.2 software (Molecular Devices).

Drugs were dissolved in the external solution and locally superfused to single cells using a rapid solution exchange system (SF-77B Perfusion Fast-Step, Warner Instruments). Concentration-response curves were constructed by applying increasing concentrations of the P2X_{1,3}-selective agonist α,β-methylene ATP (α,β-meATP) or the non-selective P2X agonist 2-MeSATP (0.3–300 μM each; both from Tocris) for 2 s. In all further experiments, stable concentrations (30 μM) of α,β-meATP or 2-MeSATP were applied repeatedly. The intervals between applications were kept at 2 min (hP2X₂, hP2X_{2/3}) or 5 min (hP2X₃), in order to avoid desensitization. Under these conditions, agonist responses were reproducible (for hP2X₃ receptors see Suppl. Fig. 1C).

In experiments analysing the effects of modulators or antagonists, low pH external solutions as well as increasing concentrations of Zn²⁺, TNP-ATP and A317491 (all from Sigma–Aldrich) were superfused 2–5 min before (depending on the inter-agonist interval) and during α,β-meATP or 2-MeSATP application.

2.3. Ca²⁺ microfluorimetry in HEK293 cells

HEK293 cells were loaded 2–3 days after transient transfection, with the Ca²⁺ sensitive fluorescent dye Fura-2 acetoxymethyl ester (Fura-2/AM; 2.5 μM; Sigma–Aldrich) at 37 °C for 1 h in culture medium. Cells plated onto coverslips were mounted into the superfusion chamber and placed on the stage of an inverted microscope (IX-70; Olympus) with epifluorescence optics and a cooled CCD camera (IMAGO; Till Photonics). Throughout the experiments, cells were continuously superfused at 0.8 ml/min by means of a roller pump with external solution. Intracellular Fura-2 was alternately excited at 340 and 380 nm, and the emitted light

was measured at a wavelength of 510 nm. The Till Vision software (version 3.3, Till Photonics) was used for data acquisition, system control, and later, off-line analysis. The fluorescence ratio (340/380 nm) provides a relative measure of the cytosolic free Ca^{2+} concentration ($[\text{Ca}^{2+}]_i$).

For the determination of the concentration–response relationships, α, β -meATP was pressure-ejected locally, by means of a computer-controlled DAD12 superfusion system (ALA Scientific Instruments). The application time was 5 s and the intervals between two subsequent agonist applications were kept at 10 min, independent of the concentration used.

2.4. Expression of the hP2X2 and hP2X3 subunit in *X. laevis* oocytes

Oocyte expression plasmids harbouring the cDNAs for the His-tagged hP2X2 or hP2X3 subunit have been previously described (Bodnar et al., 2011; Hausmann et al., 2012). A StrepII affinity tag-encoding sequence 5' of the stop codon of the His-hP2X3 construct was introduced by QuikChange site directed-mutagenesis (Stratagene). An EGFP-encoding sequence was PCR-amplified from the pIRES2-EGFP vector (Clontech) and introduced 5' of the stop codon of the His-hP2X2 construct by domain-swapping using the Mega-primer method (Kirsch and Joly, 1998). All cDNA constructs were verified by sequencing (MWG Germany). Capped cRNAs were synthesized and injected in aliquots of 46 nl (0.96–1.05 ng/nl) into collagenase-defolliculated *X. laevis* oocytes using a Nanoliter 2000 injector (World Precision Instruments) as previously described (Hausmann et al., 2014). For expression of the heteromeric hP2X2/3 receptor, the His-hP2X2-GFP and His-hP2X3-StrepII encoding cRNAs were co-injected at 4:1, 1:1 or 1:4 ratios (w/w). Oocytes were cultured at 19 °C in sterile oocyte Ringer's solution (in mM): NaCl 90, KCl 1, CaCl_2 1, MgCl_2 1, and HEPES 10, pH 7.4 supplemented with 50 $\mu\text{g}/\text{ml}$ of gentamycin.

2.5. Biochemical analysis of hP2X2/hP2X3 subunit oligomerisation in *X. laevis* oocytes

cRNA-injected oocytes were metabolically labelled by overnight incubation with L- ^{35}S methionine (Perkin Elmer Life Sciences) and, just before protein extraction, surface-labelled with the membrane-impermeant fluorescent dye Cy5 NHS ester (GE Healthcare Biosciences) as previously described (Becker et al., 2008; Hausmann et al., 2012). Affinity-tagged proteins were purified by non-denaturing Ni^{2+} -NTA chromatography (Qiagen) or Strep-Tactin chromatography (IBA Germany) from n-dodecyl-beta-D-maltoside (DDM, 0.2%, w/v) extracts of the oocytes as indicated. The hP2X receptor proteins were released in the non-denatured state from the Ni^{2+} -NTA sepharose or the Strep-Tactin sepharose with elution buffer consisting of 0.5% (w/v) digitonin in 250 mM imidazole/HCl (pH 7.6) or 0.5% (w/v) digitonin in 0.1 M sodium phosphate buffer, pH 8.0 supplemented with 10 mM biotin, respectively. The proteins were analysed by BN-PAGE or SDS-PAGE in the non-denatured or SDS-denatured state, respectively, as previously described (Fallah et al., 2011; Hausmann et al., 2012). Where indicated, samples were treated before BN-PAGE (4–14 % acrylamide) for 1 h at 37 °C with 0.05 or 0.1% (w/v) SDS, to induce partial dissociation of the hP2X receptor complexes. For non-reducing or reducing SDS-PAGE, proteins were denatured by incubation with SDS sample buffer (0.2% (w/v) SDS) in absence or presence of 20 mM dithiothreitol, respectively, for 15 min at 37 °C and electrophoresed in parallel with the Precision Plus Protein™ All Blue molecular mass marker (Bio-Rad Laboratories) on SDS-Urea-PAGE gels (10% acrylamide, 5.9 M urea). The Cy5-labelled plasma membrane-bound proteins and the GFP-tagged hP2X2 subunits were visualized by a Typhoon 9410 fluorescence scanner (GE Healthcare). Images of PAGE-gels were

prepared with the ImageQuant software for contrast adjustments. Where indicated, individual lanes from PAGE gels were differently enhanced by the ImageQuant software for better visibility of weak and strong protein bands. The image sections were cropped and positioned using Adobe Photoshop CS5. Microsoft PowerPoint 2013 was used for labelling. Each experiment was performed at least two times with equivalent results.

2.6. Biochemical analysis of hP2X2/hP2X3 subunit oligomerisation in HEK293 cells

A Gateway-compatible pcDNA3.1(+)-Zeo vector was generated by cloning the Gateway cassette (Invitrogen) into the EcoRV-opened multiple cloning site. The coding regions of His-hP2X2-GFP and His-hP2X3-StrepII were then singly subcloned from the oocyte vector into the pcDNA3.1(+)-Zeo vector by Gateway cloning. Culture dishes (30 mm) each containing 1×10^6 HEK293 cells were transiently transfected with a total of 3 μg of the desired plasmid(s) using Lipofectamin LTX (Life Technologies) according to the manufacturer's protocol. For expression of the heteromeric hP2X2/3 receptor, the plasmid DNAs for His-hP2X2-GFP and His-hP2X3-StrepII were co-transfected in ratios of 4:1, 1:2 and 1:4 (w/w). The transfection reagent was removed after 6 h. Two days following transfection, the FCS-containing culture medium was removed by washing the cells with phenol red-free HBSS medium containing calcium and magnesium (Invitrogen), followed by surface-labelling of the cells with the lysine-reactive Cy5 NHS ester (50 $\mu\text{g}/\text{ml}$ in HBSS, pH 8.5) (GE Healthcare Life Sciences) for 30 min at 37 °C. The labelled cells were washed with HBSS and solubilized with DDM, 0.2%, w/v in PBS, pH 8.0. The P2X receptors were purified by affinity chromatography and resolved by PAGE as specified above (chapter 2.5) and previously (Fallah et al., 2011; Hausmann et al., 2012; Kowalski et al., 2014).

2.7. Data analysis

The agonist concentration–response curves were fitted using the three parametric Hill equation

$$I = I_{\max} \times [A]^{n_H} / (EC_{50}^{n_H} + [A]^{n_H}),$$

where I is defined as peak current evoked by α, β -meATP or 2-MeSATP concentration $[A]$, I_{\max} is the peak current evoked by a maximal agonist concentration, EC_{50} is the half-maximal effective concentration and n_H is the Hill coefficient (Origin 8.0; OriginLab). The data are presented as the means \pm S.E.M. of n experiments. The effects of lowering the pH as well as adding Zn^{2+} , TNP-ATP or A317491 were calculated as percentage of the current induced by the second agonist application in a series. In addition, the percentage changes were compared within each treatment group. Statistical analysis was performed by a One-Way Analysis of Variance (ANOVA) followed by the Holm-Sidak *post hoc* test. A probability level of $P < 0.05$ was considered to describe a statistically significant difference. Furthermore, the effects of H^+ , Zn^{2+} and the two antagonists TNP-ATP and A317491 were evaluated by the Wilcoxon-Mann-Whitney-Test.

3. Results

3.1. Heteromeric hP2X2/3 receptors containing inactive hP2X2 or hP2X3 mutants; patch-clamp electrophysiology in transfected HEK293 cells

Throughout the present manuscript the $(\text{hP2X2})_1/(\text{hP2X3})_2$ and

(hP2X2)₂/(hP2X3)₁ nomenclature has been used to indicate the stoichiometry of heterotrimeric hP2X2/3 receptors, which differs from the IUPHAR nomenclature of ligand-gated ion channels (Collingridge et al., 2009). We believe that our nomenclature is advantageous to indicate the number of P2X2 or P2X3 subunits included in P2X2/3 heteromeric channels when dealing with subunits harbouring additional mutations or affinity- or fluorescence tags.

In a first series of experiments, we used functionally inactive mutants of hP2X2 (hP2X2-K69A, hP2X2-K307A; Suppl. Fig. 1A) and hP2X3 (hP2X3-K63A, hP2X3-K299A; Suppl. Fig. 1B) receptors, in which lysine residues essential for agonist induced receptor activation were replaced by alanine (Browne et al., 2010; Bodnar et al., 2011). Combinations of wt and mutant hP2X2 and hP2X3 subunits were utilized to reveal whether the 'conventional' (hP2X2)₁/(hP2X3)₂ and the 'non-conventional' (hP2X2)₂/(hP2X3)₁ stoichiometry of the hP2X2/3 receptor are equally possible variants. To increase the frequency of occurrence of hP2X2/3 heteromers containing an excess of hP2X2 subunits (non-conventional, (hP2X2)₂/(hP2X3)₁ receptors), HEK293 cells were transfected with hP2X2 and hP2X3 cDNA at a ratio of 4:1 instead of the usual ratio of 1:2. Heteromeric hP2X2/3 receptors generated by the co-transfection of HEK293 cells by the hP2X2 and hP2X3 cDNA at ratios of 1:2 or 4:1 were herein afterwards referred to as hP2X2/hP2X3-1:2 or hP2X2/hP2X3-4:1 variants, respectively. Concentration-response curves for the P2X2/3 and P2X3 agonist α,β -meATP were constructed for hP2X3, hP2X2/hP2X3-1:2 and -4:1 receptors (Fig. 1A, B, E). However, none of these curves differed from each other in a statistically significant manner (for the EC_{50} , I_{max} values and Hill coefficients see Suppl. Table 1). Further, there were no apparent differences in the very slow desensitization of the two hP2X2/3 receptor variants.

Alanine replacement of the lysine residues in position 63 or 299 of the hP2X3 subunit (hP2X3-K63A, hP2X3-K299A) resulted in the inability of α,β -meATP to stimulate either hP2X2/3 receptor variant up to a concentration of 100 μ M (Fig. 1C, D, F, G). By contrast, analogous mutations of the hP2X2 subunit (hP2X2-K69A, hP2X2-K307A) caused significantly smaller α,β -meATP (100, 300 μ M) induced current amplitudes at the hP2X2/hP2X3-4:1 than at hP2X2/hP2X3-1:2 variant (Fig. 1C, D, F, G). These findings support the notion that the hP2X2/hP2X3-1:2 and hP2X2/hP2X3-4:1 variant exhibit slightly different pharmacological properties and suggest that the (hP2X2)₁/(hP2X3)₂ variant is the predominant heteromeric receptor at the transfection ratio of 1:2, while the (hP2X2)₂/(hP2X3)₁ variant predominates at the transfection ratio of 4:1 (see Discussion and Fig. 9).

3.2. Allosteric modulators of hP2X2 and hP2X2/3 receptors; patch-clamp electrophysiology in transfected HEK293 cells

Next, we analysed, whether acidification of the extracellular medium or Zn^{2+} are able to differentiate between the hP2X2/hP2X3-1:2 and hP2X2/hP2X3-4:1 variants. A gradual decrease of the pH from the normal value of 7.4 to 6.4 and 5.4 correspondingly increased the amplitude of the 2-MeSATP (30 μ M)-induced currents at homomeric hP2X2 receptors (Fig. 2A–C). Homomeric hP2X3 receptor currents were gradually reduced by these changes in pH (Fig. 2B, C). The potentiating effect of an increased proton concentration on the 2-MeSATP induced current amplitudes was equally pronounced at the hP2X2 receptor and the hP2X2/hP2X3-4:1 variant, but significantly less at the hP2X2/hP2X3-1:2 variant (Fig. 2B, C). However, this may be largely due to the 2-MeSATP induced activation of homomeric hP2X2 receptors, which appear in a markedly larger quantity after the transfection of the 4:1 cDNA ratio (hP2X2:hP2X3) as compared to the 1:2 ratio (cf. Fig. 9B). In support of this idea, the currents of the hP2X2/hP2X3-1:2 and

hP2X2/hP2X3-4:1 variants induced by 30 μ M α,β -meATP were similarly facilitated at the pH values of 6.4 and 5.4, irrespective of the transfection ratios (Fig. 2D, E). The P2X3 receptor currents were again depressed by the decrease in pH (Fig. 2D, E).

Extracellular Zn^{2+} (100 μ M) only moderately reduced the current amplitude elicited by 30 μ M 2-MeSATP at hP2X2 receptors (Suppl. Fig. 2A–C); the depression of the currents induced by 30 μ M α,β -meATP was yet less pronounced (Suppl. Fig. 2D, E). In addition, there was no difference between the Zn^{2+} -induced inhibition of the hP2X2/hP2X3-1:2 and the hP2X2/hP2X3-4:1 variant with either agonist (Suppl. Fig. 2B–E). In view of the rather small depression of hP2X2 mediated currents by Zn^{2+} we generated an R225C mutant of the hP2X2 receptor, which exhibited a slightly increased sensitivity to Zn^{2+} in comparison with its wild type counterpart (Fig. 3D, E; note different scaling on the abscissa of D and E).

Concentration-response curves of 2-MeSATP (0.3–300 μ M) demonstrated a lower agonist potency (EC_{50}) and I_{max} values at the hP2X2-R225C receptor as compared to the hP2X2-wt receptor (Fig. 3A–C and Suppl. Table 2). The I_{max} values of the heteromeric hP2X2-R225C/hP2X3 receptor at both transfection ratios (hP2X2-R225C/hP2X3-1:2, hP2X2-R225C/hP2X3-4:1) were between those of the homomeric hP2X2 and hP2X2-R225C receptors. Subsequent experiments showed that 30 or 100 μ M Zn^{2+} reduced the current elicited by 30 μ M 2-MeSATP at the hP2X2-wt receptor less efficiently than at the hP2X2-R225C mutant (Fig. 3D–F). Moreover, the inhibition of the 2-MeSATP-induced current by 30 μ M Zn^{2+} at the hP2X2-R225C receptor, roughly equalled the inhibition caused by a higher concentration of Zn^{2+} (300 μ M) at the hP2X2-wt receptor (cf. Fig. 3D, E). Eventually, there was no significant difference between the effects of Zn^{2+} at the heteromeric hP2X2-R225C/hP2X3 at either transfection ratio (hP2X2-R225C/hP2X3-1:2, hP2X2-R225C/hP2X3-4:1 variant).

3.3. Competitive antagonists of hP2X3 and hP2X2/3 receptors; patch-clamp electrophysiology in transfected HEK293 cells

Because our analysis of the effect of protons or Zn^{2+} on agonist induced current amplitudes of the hP2X2/hP2X3-1:2 and the hP2X2/hP2X3-4:1 variant did not reveal significant differences in dependence on the transfection ratio, we decided to investigate the effects of selective P2X3 and P2X2/3 antagonists. Both TNP-ATP and A317491 in concentrations up to 3 μ M each caused only slight inhibition of 30 μ M 2-MeSATP induced currents at the homomeric hP2X2 receptor (Figs. 4B, C and 5B, C). By contrast, both TNP-ATP and A317491 (0.03–3 μ M each) concentration-dependently inhibited homomeric hP2X3 and heteromeric hP2X2/3 receptor mediated currents independent of whether 2-MeSATP or α,β -meATP (30 μ M each) were used as agonists (Figs. 4 and 5). TNP-ATP appeared to be of higher inhibitory potency at α,β -meATP induced currents than at 2-MeSATP induced currents (compare Fig. 4B, C with Fig. 4D, E). Interestingly, 0.03 μ M TNP-ATP inhibited the α,β -meATP (0.03 μ M) induced currents of the hP2X2/hP2X3-4:1 variant to a somewhat larger degree as compared to the hP2X2/hP2X3-1:2 variant (Fig. 4D, E). Because this rather moderate difference occurred only at a single concentration of α,β -meATP, we considered not to overemphasize its significance.

A317491 (0.03–3 μ M) inhibited 2-MeSATP induced currents of the hP2X2/hP2X3-1:2 and hP2X2/hP2X3-4:1 variants to a similar extent, and both of them to a lower extent than hP2X3 receptor mediated currents (Fig. 5B, C). We assume that - at least in part - the existence of 2-MeSATP sensitive but A317491 insensitive homomeric hP2X2 receptors generated following co-transfection may contribute to the lower potency of A317491 at the heteromeric hP2X2/3 receptors as compared to the homomeric hP2X3 receptor. Moreover, the inhibitory effect of 0.03–0.3 μ M A317491 on the

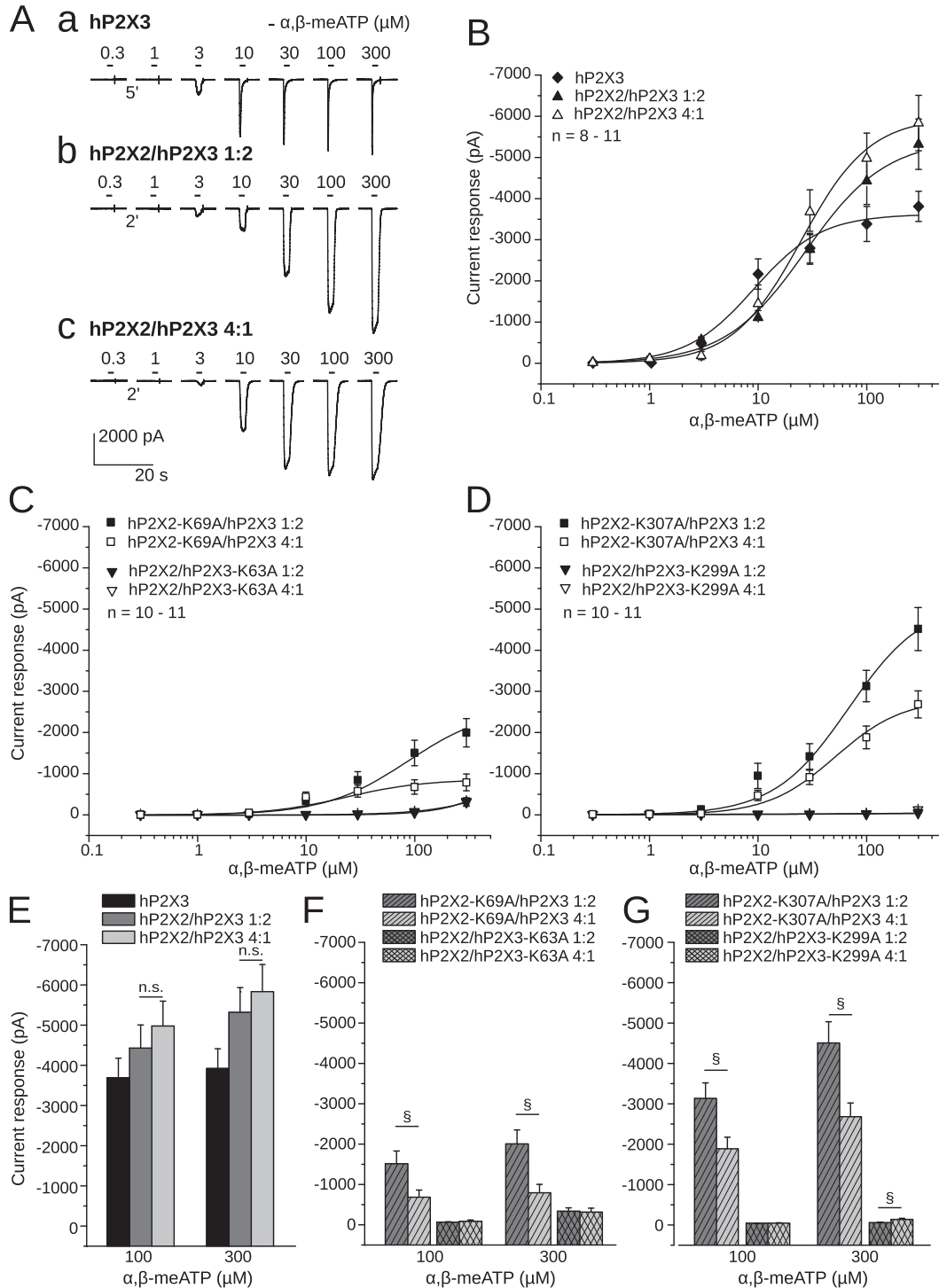


Fig. 1. Current responses at wild-type (wt) hP2X3 and hP2X2/3 receptors as well as the combinations of mutant (mut) hP2X2 or hP2X3 subunits with their wt partners expressed in HEK293 cells. The holding potential was -65 mV. A, Whole-cell currents induced by α,β -methylene ATP (α,β -meATP) at hP2X3 (a; rapid desensitization), and hP2X2/hP2X3 (b, c; slow desensitization) transfected into HEK293 cells, the latter ones with 1:2 and 4:1 ratios, respectively. Increasing concentrations of α,β -meATP (0.3–300 μ M) were locally superfused for 2 s, with 5-min (hP2X3) or 2-min (hP2X2/hP2X3) intervals, as indicated by the horizontal bars. Numbers between the current traces designate the time (in min) which elapsed between agonist applications. B, Concentration-response curves for α,β -meATP at the wt hP2X3 receptor and the wt hP2X2/hP2X3 receptors, the latter ones with the transfection ratios 1:2 and 4:1. C, D, Concentration-response curves for α,β -meATP at the non-functional hP2X2 and hP2X3 mutant subunits and their wt counterparts transfected by 1:2 and 4:1 ratios, as indicated. Selected lysine residues were replaced by alanine, to generate the non-functional mutants. Mutations introduced at the position corresponding to K69 of the hP2X2 subunit (K63 in hP2X3) (C) or at the position corresponding to K307 of the hP2X2 subunit (K299 in hP2X3) (D). E, F, G, Statistical evaluation of the current responses at α,β -meATP concentrations of 100 and 300 μ M. $P > 0.05$; no significant difference (n.s.) between the current amplitudes derived from panel B (E). $P < 0.05$; statistically significant differences between the current amplitudes for 1:2 and 4:1 transfection ratios in panel C and D are marked by a paragraph. (One-Way ANOVA; F, G). Each symbol indicates the mean \pm S.E.M. of 8–11 cells.

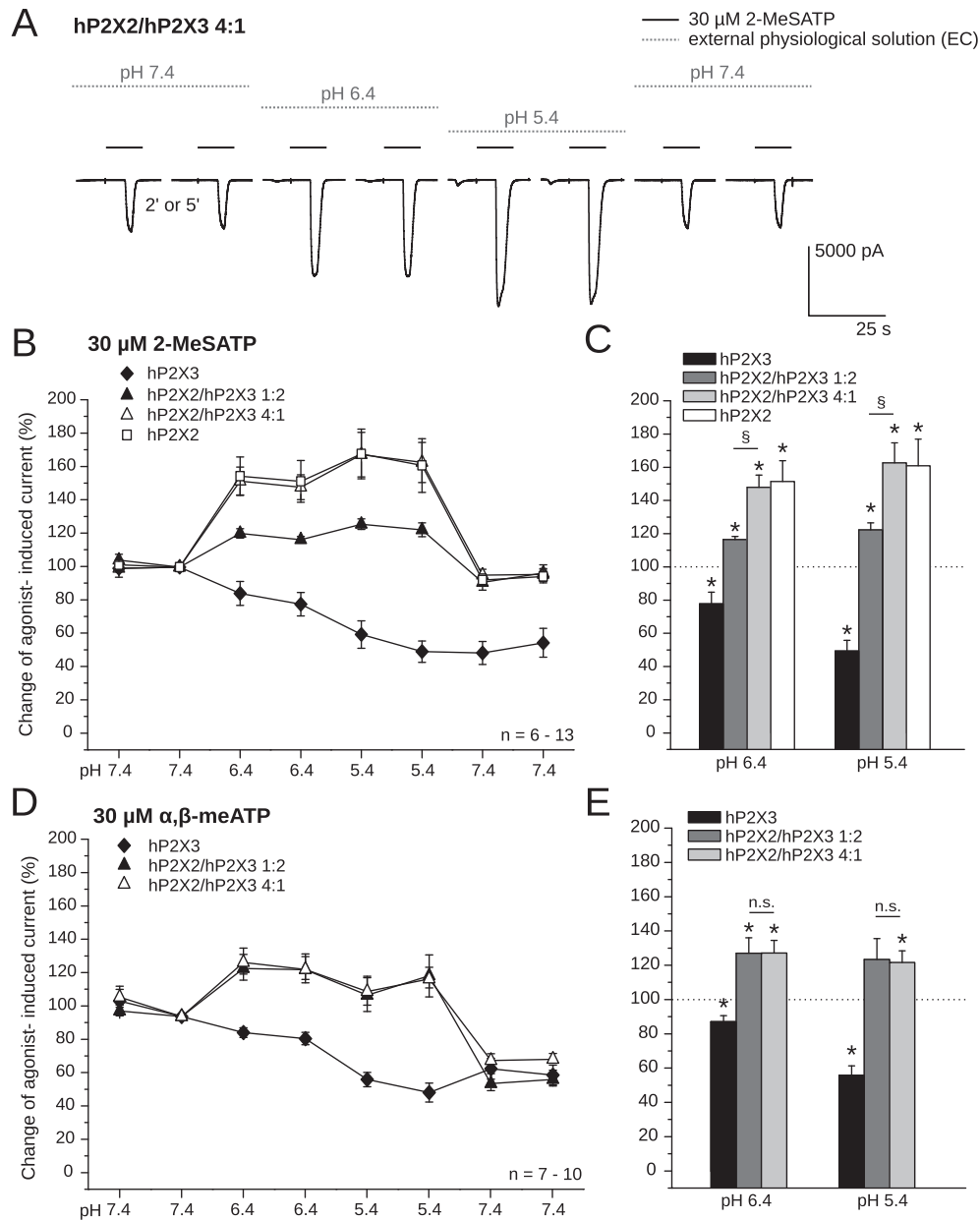


Fig. 2. Dependence of 2-methylthio ATP (2-MeSATP) and α,β -meATP-induced current responses on a stepwise decrease of the external pH value from 7.4 to 6.4 and then to 5.4 for hP2X2 and hP2X3 receptor homomers and hP2X2/hP2X3 receptor heteromers. Both agonists were applied locally for 2 s at a holding potential of -65 mV with 5-min (hP2X3) or 2-min (hP2X2, hP2X2/hP2X3) intervals. A, B, C, Representative tracings of 2-MeSATP ($30 \mu\text{M}$) currents in HEK293 cells transfected with the hP2X2/hP2X3 receptor at a 4:1 ratio (A). Percentage changes of the 2-MeSATP-induced current by pH 6.4 and 5.4 were calculated with respect to the second control current (100%; dashed line in C) in a normal extracellular solution of pH 7.4 (B). Statistical evaluation of the 2-MeSATP-induced current responses at different pH values (C). $P < 0.05$; statistically significant differences between the current amplitudes for 1:2 and 4:1 transfection ratios in panel C marked by paragraph (One-Way ANOVA; B, C). D, E, Percentage changes of the α,β -meATP-induced current by pH 6.4 and 5.4 were calculated with respect to the second control current (100%; dashed line in E) in a normal extracellular solution of pH 7.4 (D). Statistical evaluation of the α,β -meATP-induced current responses at different pH values (E). $P > 0.05$; no significant difference (n.s.) between the current amplitudes derived from panel D (One-Way ANOVA). $P < 0.05$; statistically significant differences from 100% are marked by an asterisk throughout (Wilcoxon-Mann-Whitney-Test; C, E). Each symbol indicates the mean \pm S.E.M. of 6–13 cells.

current induced by $30 \mu\text{M}$ α,β -meATP was significant larger at the hP2X2/hP2X3-1:2 variant than at the hP2X2/hP2X3-4:1 variant (Fig. 5D, E). Taken together, our results show that the A317491 sensitivity of α,β -meATP induced currents of hP2X2/3 heteromers differs between cells transfected with a cDNA ratio of 1:2 and 4:1 (hP2X2/hP2X3-1:2 and hP2X2/hP2X3-4:1 variants), suggesting that the sensitivity to this antagonist depends on the stoichiometry of hP2X2/3 receptors.

3.4. Heteromeric P2X2/3 receptors containing inactive hP2X2 or hP2X3 mutants; Ca^{2+} microfluorimetry in transfected HEK293 cells

In these experiments, we used the selective P2X3 and P2X2/3 agonist α,β -meATP, which opens the respective ligand-gated cationic channels and leads to the influx of Ca^{2+} from the extracellular space, without the accompanying activation of P2Y receptors. Thereby, P2Y receptor-mediated release of Ca^{2+} from its intracellular pools does not interfere with the α,β -meATP-induced $[\text{Ca}^{2+}]_i$ transients.

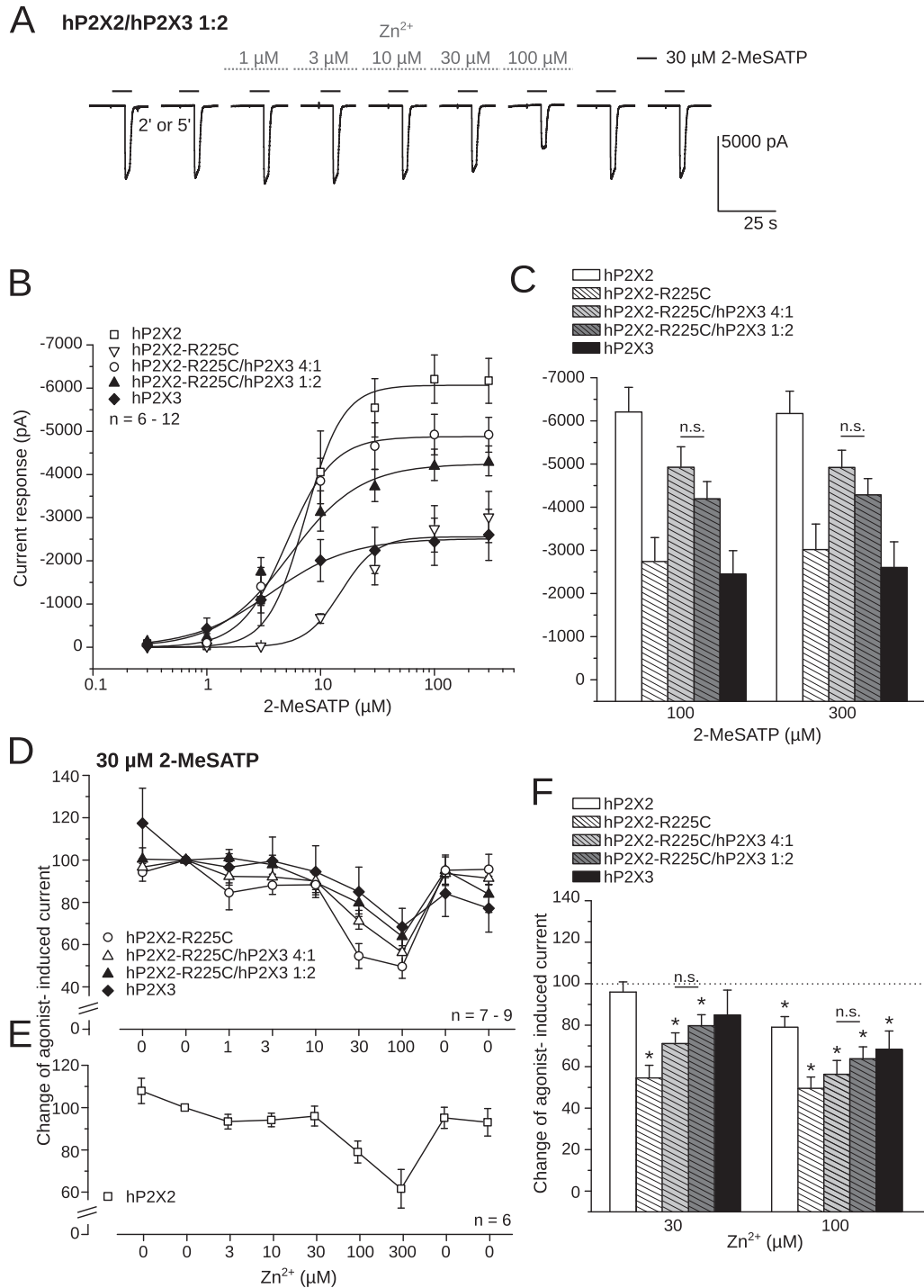


Fig. 3. Effect of Zn²⁺ on 2-MeSATP-induced currents at the homomeric wt hP2X3 receptor, the wt hP2X2 receptor and its mutant, in which Arg-225 was replaced by Cys. In addition, heteromeric hP2X2-R225C/hP2X3 receptors were generated by 1:2 and 4:1 transfection of HEK293 cells with the respective cDNAs. The current responses to 2-MeSATP applied for 2 s with intervals of 5 min (hP2X3) or 2 min (hP2X2, hP2X2-R225C, or its heteromeric combinations with hP2X3) were recorded at a holding potential of -65 mV. A, B, C, Representative tracings documenting the concentration-dependent inhibition of hP2X2/hP2X3 receptors (1:2 transfection ratio) by Zn²⁺ (A). Concentration–response relationships for the current amplitudes evoked by 2-MeSATP (0.3–300 μM) at the indicated homomeric or heteromeric receptors (B). *P* > 0.05; no significant difference (n.s.) between the current amplitudes at 100 and 300 μM agonist concentrations, derived from panel B (Wilcoxon–Mann–Whitney–Test; C). D, E, F, Percentage inhibition by increasing concentrations of Zn²⁺ (1–100 μM) of 2-MeSATP (30 μM) currents through homomeric hP2X2-R225C and homomeric wt hP2X3 receptors as well as their combinations to yield heteromeric receptors (1:2 and 4:1 transfection ratios) (D). Percentage inhibition by increasing concentrations of Zn²⁺ (3–300 μM) of 2-MeSATP (30 μM) currents through the investigated homomeric hP2X2 receptor (E). The second current amplitude before applying Zn²⁺ was set at 100% (dashed line in F). *P* > 0.05; no significant difference (n.s.) between the current amplitudes at 30 and 100 μM Zn²⁺ derived from panel D. *P* < 0.05; statistically significant differences from 100% are marked by an asterisk (F). Each symbol indicates the mean ± S.E.M. of 6–9 cells.

The fluorescence ratio (340/380 nm) of Fura-2 was utilized to obtain a relative measure of [Ca²⁺]_i in transfected HEK293 cells. The application of α,β-meATP (1–300 μM) onto hP2X2/hP2X3-1:2

caused a concentration-dependent increase of [Ca²⁺]_i (Fig. 6A, B). All experiments were started by adding 10 μM α,β-meATP (an effect omitted from further evaluations, because it was found to be non-

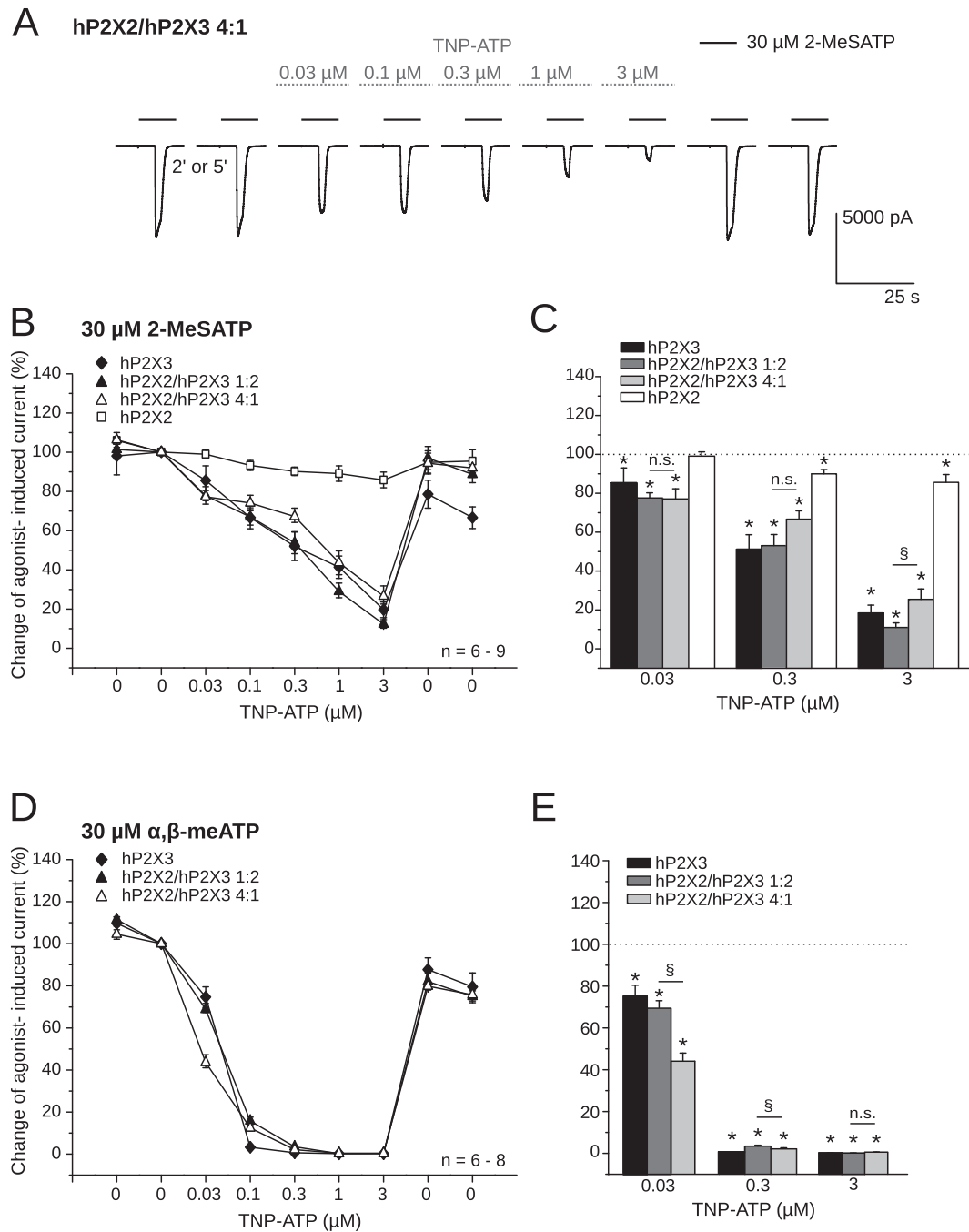


Fig. 4. Effects of TNP-ATP on 2-MeSATP- or α,β -meATP-induced currents at the homomeric wt hP2X2 and wt hP2X3 receptors as well as heteromeric hP2X2/hP2X3 receptors (1:2 and 4:1 transfection). HEK293 cells were used as expression systems. The current responses to 2-MeSATP (30 μ M) applied for 2 s with intervals of 5 min (hP2X3) or 2 min (hP2X2, hP2X2/hP2X3) were recorded at a holding potential of -65 mV. A, B, C, Representative tracings documenting the concentration-dependent inhibition of hP2X2/hP2X3 receptors (4:1 transfection ratios) by TNP-ATP (A). Percentage changes of the 2-MeSATP-induced current by TNP-ATP (0.03–3 μ M) were calculated with respect to the second control current before applying TNP-ATP (100%, dashed line in C) (B). Statistical evaluation of the 2-MeSATP (30 μ M)-induced current responses at different TNP-ATP concentrations (C). $P > 0.05$; no significant difference (n.s.) between the current amplitudes derived from panel B. $P < 0.05$; statistically significant difference between the current amplitudes derived from panel B are marked by a paragraph (One-Way ANOVA). D, E, Percentage changes of the α,β -meATP (30 μ M)-induced current by TNP-ATP (0.03–3 μ M) were calculated with respect to the second control current before applying TNP-ATP (100%; dashed line in E) (D). Statistical evaluation of the α,β -meATP-induced current responses at different TNP-ATP concentrations (E). $P > 0.05$; no significant difference (n.s.) between the current amplitudes derived from panel D. $P < 0.05$; statistically significant difference between the current amplitudes derived from panel D are marked by a paragraph (One-Way ANOVA). $P < 0.05$; statistically significant differences from 100% are marked by an asterisk throughout (Wilcoxon-Mann-Whitney-Test; C, E). Each symbol indicates the mean \pm S.E.M. of 6–9 cells.

reproducible), before constructing concentration–response relationships to this agonist. In contrast to current measurements (but see a tendency for change in Fig. 1B), the I_{max} value of the hP2X2/hP2X3-4:1 curve was larger than those of the hP2X2/hP2X3-1:2 and hP2X3 curves (Fig. 6A, B, E and Suppl. Table 3). All

residual findings obtained by patch-clamp recordings and Ca^{2+} microfluorimetry yielded comparable although not identical results. For instance, in agreement with patch-clamp analysis the inactivating mutants of the hP2X3 subunit (K63A, K299A) co-transfected with the hP2X2-wt subunit encoding cDNA either at

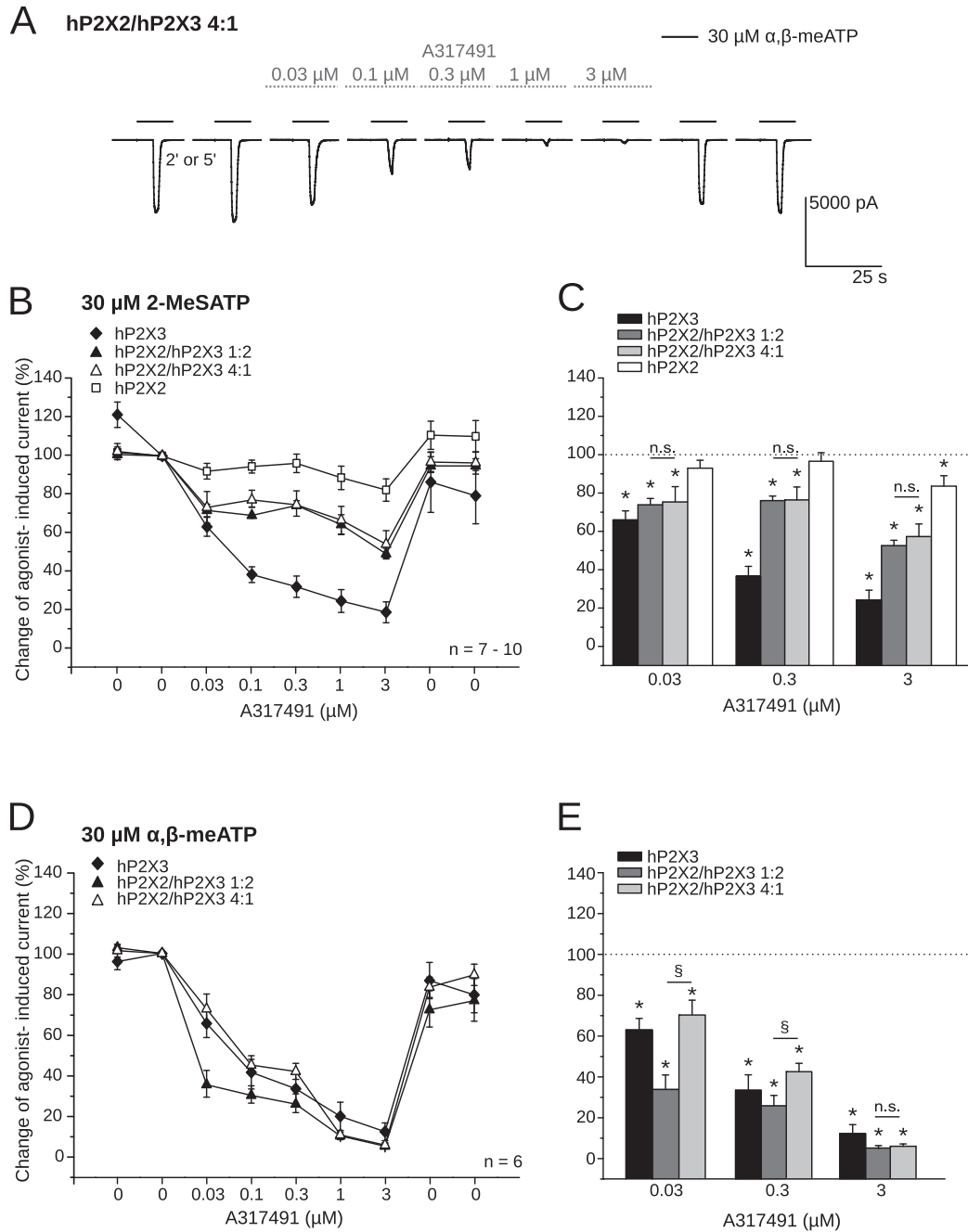


Fig. 5. Effects of A317491 on 2-MeSATP- or α,β -meATP-induced currents at the homomeric wt hP2X2 and wt hP2X3 receptors as well as heteromeric hP2X2/hP2X3 receptors, the latter ones generated by 1:2 and 4:1 transfection. HEK293 cells were used as expression systems. The current responses to 2-MeSATP (30 μ M) applied for 2 s with intervals of 5 min (hP2X3) or 2 min (hP2X2, hP2X2/hP2X3) were recorded at a holding potential of -65 mV. A, B, C, Representative tracings documenting the concentration-dependent inhibition of hP2X2/hP2X3 receptors (4:1 transfection ratios) by A317491 (A). Percentage changes of the 2-MeSATP-induced current by A317491 (0.03–3 μ M) were calculated with respect to the second control current before applying TNP-ATP (100%; dashed line in C) (B). Statistical evaluation of the 2-MeSATP (30 μ M)-induced current responses at different A317491 concentrations (C). $P > 0.05$; no significant difference (n.s.) between the current amplitudes derived from panel B (One-Way ANOVA). D, E, Percentage changes of the α,β -meATP (30 μ M)-induced current by A317491 (0.03–3 μ M) were calculated with respect to the second control current before applying A317491 (100%; dashed line in E) (D). Statistical evaluation of the α,β -meATP-induced current responses at different A317491 concentrations (E). $P > 0.05$; no significant difference (n.s.) between the current amplitudes derived from panel D. $P < 0.05$; statistically significant difference between the current amplitudes derived from panel D are marked by a paragraph (One-Way ANOVA). $P < 0.05$; statistically significant differences from 100% are marked by an asterisk throughout (Wilcoxon-Mann-Whitney-Test; C, E). Each symbol indicates the mean \pm S.E.M. of 6–10 cells.

1:2 or 4:1 ratios virtually abolished the effect of α,β -meATP, but analogous mutations in the hP2X2 subunit (K69A, K307A) co-transfected with the hP2X3-wt subunit encoding cDNA still gave rise to α,β -meATP induced increase of $[Ca^{2+}]_i$ (Fig. 6C, D, F, G). Again, in accordance with electrophysiology, 30–300 μ M α,β -meATP produced smaller $[Ca^{2+}]_i$ transients at the hP2X2-K69A/hP2X3-4:1

variant than at the hP2X2-K69A/hP2X3-1:2 variant. However, in contrast to electrophysiology, 100 and 300 μ M α,β -meATP evoked similar current amplitudes at the hP2X2-K307A/hP2X3-4:1 and hP2X2-K307A/hP2X3-1:2 variant. In this case, it should be taken into consideration that the current amplitudes elicited by 10–300 μ M α,β -meATP were already considerably larger for the

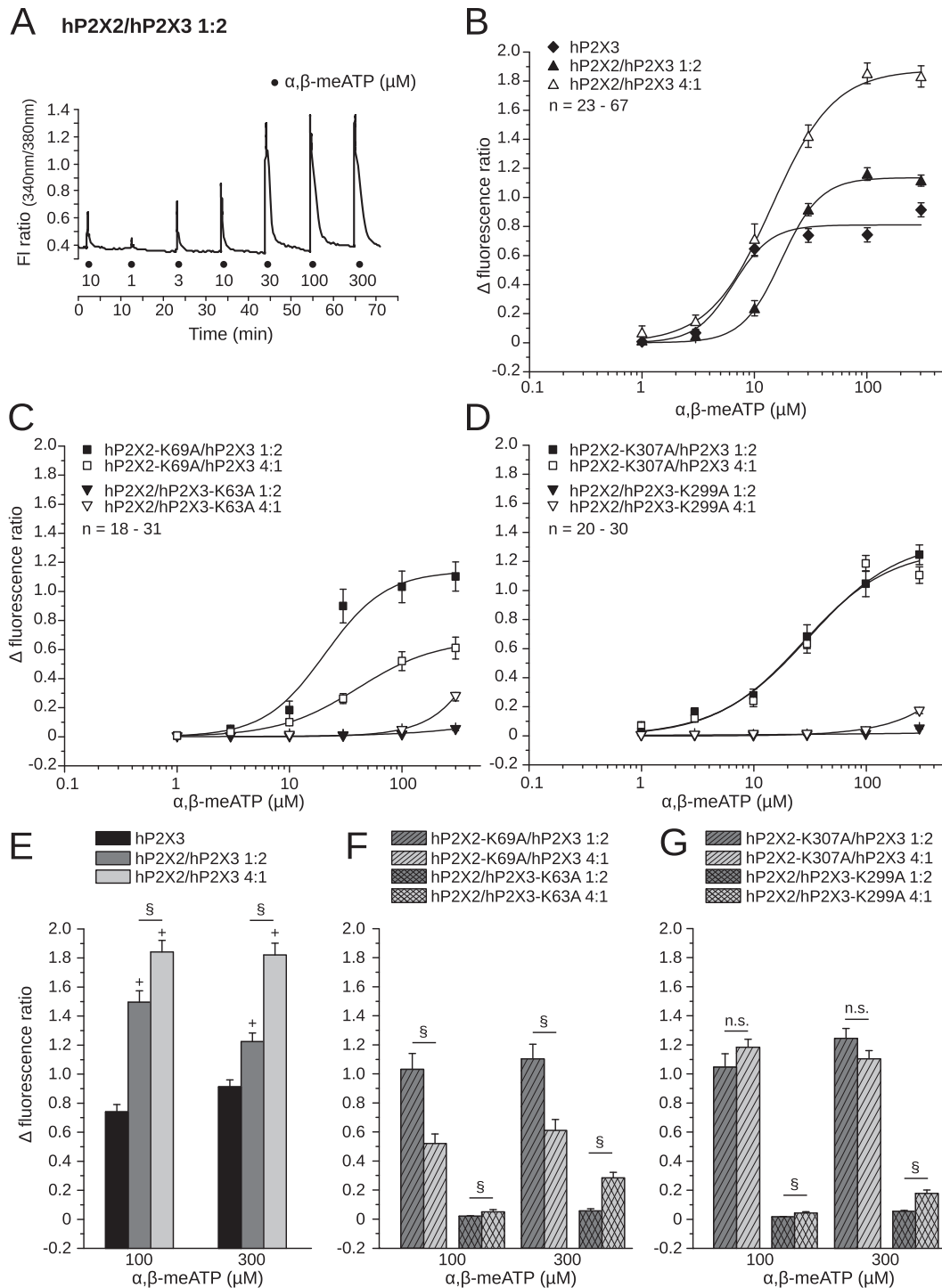


Fig. 6. Increase of the cytosolic free Ca^{2+} concentration ($[\text{Ca}^{2+}]_i$) by Ca^{2+} influx from the extracellular space through wt hP2X3 and hP2X2/hP2X3 receptors as well as the combinations of (mut) hP2X2 or hP2X3 subunits with their wt partners expressed in HEK293 cells. Ca^{2+} imaging was carried out on HEK293 cells loaded by the fluorescence dye Fura-2 acetoxyethyl ester. The fluorescence ratio (FI ratio; FR) provides a relative measure of $[\text{Ca}^{2+}]_i$. A, B, Increasing concentrations of α, β -meATP (1–300 μM) were locally superfused onto the wt hP2X2/hP2X3 receptor (1:2 transfection ratio) for 5 s with 10-min intervals, as indicated by filled circles in the original recording shown (A). $[\text{Ca}^{2+}]_i$ transients induced by α, β -meATP at hP2X3 and hP2X2/hP2X3 receptors transfected into HEK293 cells with 1:2 and 4:1 ratios, respectively (B). C, D, Concentration-response curves for α, β -meATP at wt hP2X2/hP2X3 receptors generated with the transfection ratios 1:2 and 4:1. Selected lysin residues were replaced by alanin, to generate non-functional mutants. Mutations introduced near to TM1 (C) and TM2 (D). E, F, G, Statistical evaluation of the α, β -meATP-induced current responses. $P < 0.05$; significant difference between the current amplitudes from the first column in each group of columns derived from panel B are marked by a cross (One-Way ANOVA; E). $P < 0.05$; statistically significant differences between the current amplitudes derived from C and D are marked by paragraph (One-Way ANOVA; F, G). $P > 0.05$; no significant differences (n.s.) between the current amplitudes derived from panel D.

hP2X2/hP2X3-4:1 than for the hP2X2/hP2X3-1:2 variant (Fig. 6B).

Taken together, the slight differences of the pharmacological properties between the hP2X2/hP2X3-1:2 and the hP2X2/hP2X3-4:1 variant are compatible with the assumption that the

predominant heteromeric receptors at the two transfection ratios 1:2 and 4:1 are $(\text{hP2X2})_1/(\text{hP2X3})_2$ and $(\text{hP2X2})_2/(\text{hP2X3})_1$, respectively.

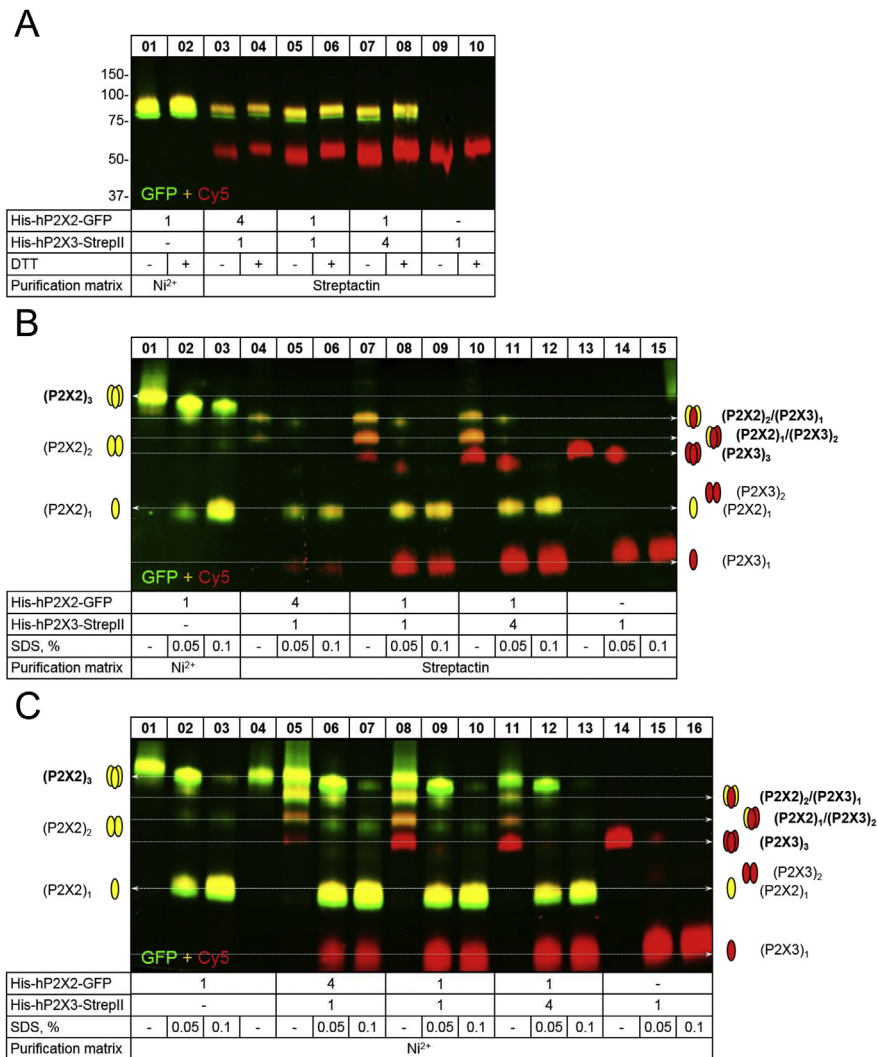


Fig. 7. Plasma membrane expression and heterotrimeric assembly of co-expressed hP2X2 and hP2X3 subunits in *Xenopus laevis* oocytes. *X. laevis* oocytes expressing the indicated proteins were surface labelled with the membrane-impermeant fluorescent Cy5 dye before protein purification. The indicated proteins were purified under non-denaturing conditions from *X. laevis* oocytes by Ni²⁺-NTA chromatography or Strep-Tactin chromatography, as indicated, resolved by SDS-PAGE (A) or BN-PAGE (B, C), and visualized by Typhoon fluorescence scanning. A, Overlay of the Cy5-labelled surface form (red) of the His-hP2X2-GFP and the His-hP2X3-StrepII protomers and the GFP fluorescence (green) of the His-hP2X2-GFP protomer. The positions of molecular mass markers (in kDa) are shown on the left. B, Overlay of GFP and Cy5 fluorescence of the homomeric P2X2 (lanes 1–3) and P2X3 (lanes 13–15) and the heteromeric hP2X2/3 (lanes 4–12) receptors in their native or partial SDS denatured forms isolated by Ni²⁺-NTA (lanes 1–3) or Strep-Tactin (lanes 4–15) chromatography as indicated. hP2X2/3 receptors (lanes 4–12) originate from the co-expression of the His-hP2X2-GFP and His-hP2X3-StrepII subunit in cRNA ratios as indicated. The schematics and the labelling on the left or right margins indicate the numbers of hP2X2 and/or hP2X3 subunits/protomers incorporated in the respective trimeric (bold) or dimeric or monomeric protein band of the hP2X2, hP2X2/3 or hP2X3 receptor complexes, respectively. C, Overlay of Cy5 and GFP fluorescence of the homomeric and heteromeric His-hP2X2-GFP and His-hP2X3-StrepII receptor complexes in their native or partial SDS denatured forms extracted by Ni²⁺-NTA affinity chromatography. The data shown in each subfigure represent samples run on the same SDS-PAGE gel or BN-PAGE gel. (For interpretation of the references to colour in this figure legend, the reader is referred to the web version of this article.)

3.5. Biochemical analysis of heteromeric P2X2/3 receptors in *X. laevis* oocytes and HEK293 cells

To provide further insight into the subunit stoichiometry of the hP2X2/3 heterotrimer, we co-expressed His-hP2X3-StrepII as a bait protein together with His-hP2X2-GFP as the prey. While the N-terminal His-tags allow the simultaneous verification of the expression of both proteins, the additional nine amino acid StrepII tag present exclusively at C-terminal end of the hP2X3 subunit allows for the co-isolation of the co-assembled non-StrepII-tagged His-hP2X2-GFP. We knew from previous experiments that non-StrepII-tagged P2X subunits do not directly bind to the Strep-Tactin resin (Becker et al., 2008), which was also valid for the His-hP2X2-GFP subunit (data not shown). The purpose of the fusion

with GFP was twofold, (i) to increase the mass of the hP2X2 subunit and (ii) to allow for the unequivocal detection of oligomers incorporating the hP2X2 subunit by GFP fluorescence scanning, particularly of bands detected in the BN-PAGE gel. In addition, we selectively labelled the plasma membrane-bound pool of both subunits with the lysine-reactive fluorescence dye Cy5-NHS, which harbours two negative charges that prevent its penetration of the plasma membrane of intact cells to which it was added before receptor purification.

We performed these experiments with both *X. laevis* oocytes and HEK-293 cells. *X. laevis* oocytes offer the unique advantage that the delivery of two distinct cRNAs at an exactly defined molar ratio into every cells can be controlled by microinjection (Terhag et al., 2010). SDS-PAGE combined with fluorescence scanning revealed a

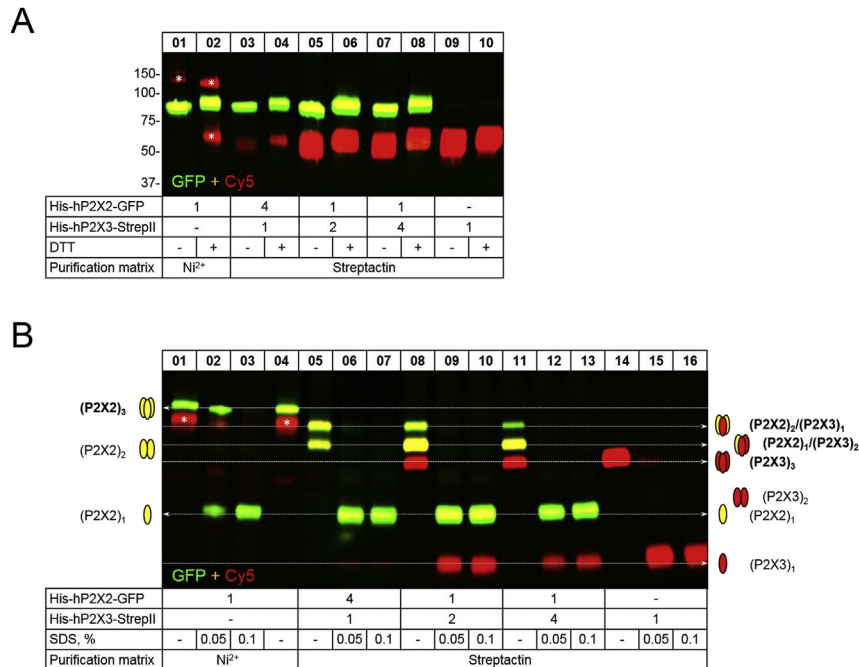


Fig. 8. Plasma membrane expression and heterotrimeric assembly of co-expressed hP2X2 and hP2X3 subunits in HEK293 cells. HEK293 cells expressing the indicated proteins were surface labelled with the membrane-impermeant fluorescent Cy5 dye before protein purification. The indicated proteins were purified under non-denaturing conditions from HEK293 cells by Ni²⁺-NTA chromatography or Strep-Tactin chromatography, as indicated, resolved by SDS-PAGE (A) or BN-PAGE (B), and visualized by Typhoon fluorescence scanning. A, Overlay of the Cy5-labelled surface form (red) of the His-hp2X2-GFP and the His-hp2X3-StrepII promoters and the GFP fluorescence (green) of the His-hp2X2-GFP promoter. The positions of molecular mass markers (in kDa) are shown on the left. The additional bands lacking GFP fluorescence (marked by the asterisks) that appear in Fig. 8A and B following single expression of the His-hp2X2-GFP subunit and native purification by Ni²⁺-NTA affinity chromatography can be attributed to HEK293 cell proteins that non-specifically bind to the Ni²⁺-NTA resin. These bands were visible in variable extent in independent experiments and were also present when the His-hp2X3-StrepII subunit was purified by Ni²⁺-NTA affinity chromatography (data not shown). B, Overlay of GFP and Cy5 fluorescence of the homomeric P2X2 (lanes 1–4) and P2X3 (lanes 14–16) and the heteromeric hP2X2/3 (lanes 5–13) receptors in their native or partial SDS denatured forms isolated by Ni²⁺-NTA (lanes 1–4) or Strep-Tactin (lanes 5–16) chromatography as indicated. hP2X2/3 receptors (lanes 5–13) originate from the co-expression of the His-hp2X2-GFP and His-hp2X3-StrepII subunit in cDNA ratios as indicated. Lanes 5–7 were uniformly enhanced by a factor of 2 compared to all other lanes by the ImageQuant software for better visibility of weak protein bands. The schematics and the labelling on the left or right margins indicate the numbers of hP2X2 and/or hP2X3 subunits/promoters incorporated in the respective trimeric (bold) or dimeric or monomeric protein band of the hP2X2, hP2X2/3 or hP2X3 receptor complexes, respectively. The data shown in each subfigure represent samples run on the same SDS-PAGE gel or BN-PAGE gel. (For interpretation of the references to colour in this figure legend, the reader is referred to the web version of this article.)

molecular mass of the His-hp2X2-GFP subunit of ~85 kDa following native purification by Ni²⁺-NTA affinity chromatography and subsequent denaturation by SDS from *X. laevis* oocytes (Fig. 7A, lanes 1–2) and HEK293 cells (Fig. 8A, lanes 1–2). The yellow colour results from the overlay of GFP fluorescence (green) and Cy5 fluorescence (red), corresponding to the total amount and the plasma membrane-fraction of the His-hp2X2-GFP subunit, respectively. The singly expressed His-hp2X3-StrepII subunit could also be purified in its plasma membrane-bound form from *X. laevis* oocytes and HEK293 cells, as visualized by the red (Cy5) fluorescent ~54 kDa polypeptide in the SDS-PAGE gel (Fig. 7A, lanes 9–10 and Fig. 8A, lanes 9–10). Following co-expression of both subunits in *X. laevis* oocytes or HEK293 cells, the non-StrepII-tagged His-hp2X2-GFP subunit was co-purified in amounts that varied depending on the indicated ratios of the injected cRNAs (Fig. 7A, lanes 3–8) or the transfected plasmid DNAs (Fig. 8A, lanes 3–8), respectively. The yellow overlay confirms that also the plasma membrane-bound form of the His-hp2X2-GFP subunit was co-purified with the plasma membrane-bound form of the His-hp2X3-StrepII subunit.

The same samples as in Figs. 7A and 8A from *X. laevis* oocytes and HEK293 cells, respectively, were also resolved in the non-denatured or partially denatured state by BN-PAGE (Figs. 7B and 8B). The singly expressed His-hp2X2-GFP and His-hp2X3-StrepII receptors (purified by Ni²⁺-NTA resin and Strep-Tactin resin, respectively) migrated each as a single band (Fig. 7B, lanes 1 and 13

and Fig. 8B, lanes 1, 4 and 14). The His-hp2X2-GFP receptor complex is significantly larger than the His-hp2X3-StrepII receptor consistent with the larger size of the genuine hP2X2 subunit and its fusion with the 27 kDa GFP moiety. The homotrimeric state of both receptors was verified by partial denaturing of the native receptor complexes with low concentrations of SDS, which resulted in the appearance of (weakly visible) homodimers and prominent monomers (Fig. 7B, lanes 2–3 and 14–15 and Fig. 8B, lanes 2–3 and 15–16). These findings are all consistent with extensive previously published data (Nicke et al., 1998; Aschrafi et al., 2004; Bodnar et al., 2011; Hausmann et al., 2012).

BN-PAGE analysis of non-denatured samples that include the His-hp2X3-StrepII bait and the co-assembled His-hp2X2-GFP from *X. laevis* oocytes or HEK293 cells resulted in a pattern of two to three bands representing oligomers of distinct masses (Fig. 7B, lanes 4, 7 and 10 and Fig. 8B, lanes 5, 8 and 11). By referring to the singly expressed His-hp2X2-GFP and His-hp2X3-StrepII receptors as mass markers (Fig. 7B, lanes 1 and 13, respectively or Fig. 8B, lanes 4 and 14, respectively), the fastest migrating band could be clearly assigned to be the His-hp2X3-StrepII homotrimer (visible in lanes 7 and 10 or 8 and 11, but not in lane 4 or 5 of Fig. 7B or Fig. 8B, respectively). As expected, the homotrimeric His-hp2X2-GFP could not be isolated because it lacked the StrepII tag for direct binding to the Strep-Tactin resin. The two other non-denatured protein bands must incorporate (i) the His-hp2X2-GFP subunit as evidenced by the presence of the GFP fluorescence and (ii) the His-hp2X3-StrepII

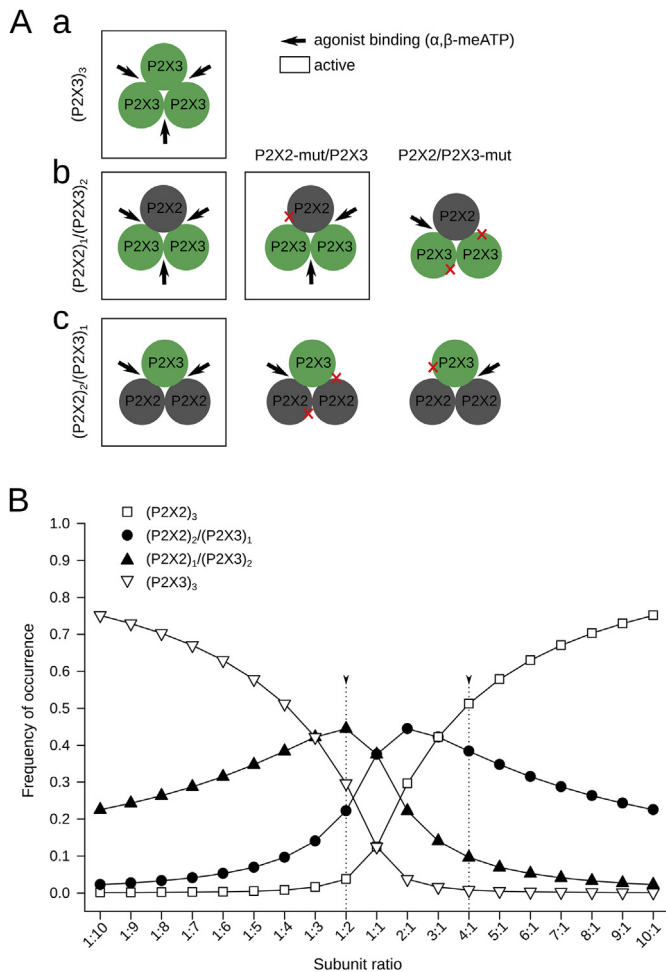


Fig. 9. A, Summary schematic showing the assumed subunit stoichiometry of the homotrimeric P2X3, as well as the heterotrimeric (P2X2)₁/(P2X3)₂ and (P2X2)₂/(P2X3)₁ receptors. The experimental data obtained by co-expressing wt P2X2 and P2X3 subunits as well as their non-functional mutants (note the red crosses) with the respective subunit partners supported assumption that the two subunit variants occur simultaneously. The agonist binding sites are indicated with arrows; at least two binding sites are needed for receptor activation. B, Theoretical calculation for the ratio of P2X2 and P2X3 subunits in trimeric receptors [(P2X2)₃, (P2X2)₁/(P2X3)₂, (P2X2)₂/(P2X3)₁ and (P2X3)₃] following transfection with ratios from 1:10 to 10:1. (For interpretation of the references to colour in this figure legend, the reader is referred to the web version of this article.)

bait subunit needed for the co-isolation of the co-assembled His-hP2X2-GFP prey subunit. The only plausible explanation for the detection of two distinct heterotrimers is that the intermediate bands reflect two distinct stoichiometries of the hP2X2/3 heterotrimer: (hP2X2)₂/(hP2X3)₁ and (hP2X2)₁/(hP2X3)₂.

From the relative abundance of the heterotrimeric (hP2X2)₂/(hP2X3)₁ and (hP2X2)₁/(hP2X3)₂ bands and the homotrimeric hP2X3 band within each experimental subgroup, it can be deduced that the stoichiometry changes depending on the cRNA or cDNA ratio delivered to *X. laevis* oocytes or HEK293 cells, respectively. An excess of hP2X2 over hP2X3 strongly favoured the formation of hP2X2/3 heterotrimers of obviously both stoichiometries, (hP2X2)₂/(hP2X3)₁ and (hP2X2)₁/(hP2X3)₂, each reflected by one of the two non-denatured protein bands in Fig. 7B (lane 4) and Fig. 8B (lane 5). Increasing the expression of the P2X3 subunit relative to the hP2X2 subunit resulted in the increased formation of the (hP2X2)₁/(hP2X3)₂ heterotrimer (relative to the (hP2X2)₂/(hP2X3)₁ heterotrimer) and in the hP2X3 homotrimers (Fig. 7B,

lanes 7 and 10 and Fig. 8B, lanes 8 and 11). His-hP2X2-GFP incorporating heterotrimers of both stoichiometries, (hP2X2)₂/(hP2X3)₁ and (hP2X2)₁/(hP2X3)₂, are present (Fig. 7B, lanes 4, 7 and 10 and Fig. 8B, lanes 5, 8 and 11) in variable amounts at all cRNA or cDNA ratios used. The data strongly indicate that the stoichiometry of the heteromeric hP2X2/3 receptor expressed in *X. laevis* oocytes or HEK293 cells is not fixed, but determined by the relative availability of hP2X2 and hP2X3 subunits.

Based on the SDS-PAGE-derived masses of 85 kDa and 54 kDa of the His-hP2X2-GFP and His-hP2X3-StrepII protomers (Fig. 7A), the masses of the (hP2X2)₂/(hP2X3)₁ and (hP2X2)₁/(hP2X3)₂ heterotrimers can be calculated to be 224 kDa and 193 kDa, respectively. To compare this prediction with our experimental data, we used homotrimeric His-hP2X2-GFP and His-hP2X3-StrepII receptors as well-defined mass markers to assess the masses of the hP2X2/3 heterotrimers from the BN-PAGE (Fig. 7B). In excellent agreement with the calculated predictions, we determined masses of 222 kDa (predicted 224 kDa) and 189 kDa (predicted 193 kDa) for the (hP2X2)₂/(hP2X3)₁ and (hP2X2)₁/(hP2X3)₂ heterotrimers.

Consistent with the above results, direct purification via the His-tag present at the N-terminal tail of both subunits by Ni²⁺-NTA chromatography from *X. laevis* oocytes demonstrated the simultaneous presence of all four possible trimeric protein complexes: the two homotrimeric His-hP2X2-GFP and His-hP2X3-StrepII receptors and the two heterotrimeric (hP2X2)₂/(hP2X3)₁ and (hP2X2)₁/(hP2X3)₂ receptors (Fig. 7C, lanes 5, 8 and 11). Increasing the expression of the P2X2 subunit relative to the hP2X3 subunit results in the preferred formation of homotrimeric His-hP2X2-GFP receptors and heterotrimeric (hP2X2)₂/(hP2X3)₁ receptors and vice versa.

4. Discussion

The homomeric P2X3 and heteromeric P2X2/3 receptor subtypes are located at C-fibre nerve terminals in peripheral tissues and are activated by ATP released by noxious stimulation (Burnstock, 2006, 2013). In consequence, the blockade of these receptors by pharmacological antagonists (Jarvis, 2003), their down regulation by antisense oligonucleotides (Dorn et al., 2001) or short interfering (si)RNAs (Hemmings-Mieszczak et al., 2003) or their genetic deletion (Cockayne et al., 2005) has been shown to inhibit acute pain or chronic inflammatory and neuropathic pain. Sensory neurons, such as those of the dorsal root ganglia (DRG), contain the cell bodies of the nociceptive C fibre terminals, which display a variety of current responses to activation by α,β -meATP (Petruska et al., 2000; Pankratov et al., 2001). Basically three types of responses were observed in DRGs, classified as fast (P2X3), slow (P2X2/3) and mixed ones (P2X3 and P2X2/3); nodose ganglia were described to exhibit only slow α,β -meATP-induced currents (P2X2/3; Virginio et al., 1998a). We hypothesized that the functional diversity may be further increased by the co-expression of (P2X2)₁/(P2X3)₂ and (P2X2)₂/(P2X3)₁ heteromeric receptors that possess slightly different pharmacological properties.

We used functionally inactive mutants of the hP2X2 subunit (hP2X2-K69A, hP2X2-K307A) and the hP2X3 subunit (hP2X3-K63A, hP2X3-K299A), in which lysine residues essential for receptor activation were replaced by alanine (Jiang et al., 2000; Fischer et al., 2007). Previous work indicated that P2X2/3 receptors containing such alanine substitutions in the P2X3 subunit were inactive, whereas P2X2/3 receptors containing similar alanine substitutions in the P2X2 subunit continued to respond to agonists (Wilkinson et al., 2006; Hausmann et al., 2012). On the basis of these findings it was concluded that the subunit stoichiometry of the heteromeric receptor is (P2X2)₁/(P2X3)₂, when HEK293 cells were transfected with a lower amount of P2X2 encoding cDNA than

of P2X3 encoding cDNA (P2X2:P2X3 cDNA ratio ≤ 0.5) (Wilkinson et al., 2006; Hausmann et al., 2012). From electrophysiological analysis and mathematical modelling of the activation and deactivation kinetics of the P2X3 receptors it was derived that occupation of already a minimum of two of the available three binding sites is sufficient to open the P2X3 receptor-channel (Karoly et al., 2008; Riedel et al., 2012). A similar conclusion was reached for P2X2/3 and P2X2/6 heteromeric receptors by ATP-binding site mutagenesis and functional analysis (Hausmann et al., 2012) and the P2X2 receptor by using concatenated P2X2 receptors (Stelmashenko et al., 2012).

Provided the conventional subunit stoichiometry of (hP2X2)₁/(hP2X3)₂, the hP2X2-K69A/hP2X3 and hP2X2-K307A/hP2X3 receptors should remain sensitive to α,β -meATP, because two functional ATP-binding sites are present, while hP2X2/hP2X3-K63A and hP2X2/hP2X3-K299A might become inactive because only one functional binding site remains (Fig. 9Ab). By contrast, provided the reverse (non-conventional) subunit stoichiometry of (hP2X2)₂/(hP2X3)₁, alanine replacements in either the hP2X2 or hP2X3 subunit should result in heteromeric receptors that cannot be activated by α,β -meATP, because only one functional α,β -meATP-binding site remains in both cases (Fig. 9Ac). To drive the expression of heteromeric hP2X2/3 receptors to a larger relative amount of the putative (non-conventional) (hP2X2)₂/(hP2X3)₁ stoichiometry, HEK293 cells were transfected with a higher amount of hP2X2 cDNA than of hP2X3 cDNA (P2X2:P2X3 cDNA ratio 4:1) instead of the 'usual' ratio of 1:2. The null hypothesis predicts that at variable cDNA ratios the frequency of occurrence of trimeric hP2X2/3 receptors fluctuates between 0 and <0.8 (Fig. 9B). Hence, at the two transfection ratios of 1:2 and 4:1, (hP2X2)₁/(hP2X3)₂ and (hP2X2)₂/(hP2X3)₁ are the predominant heterotrimeric forms, respectively. Homomeric hP2X2 receptors do not interfere with measurements, if the selective P2X3 and P2X2/3 agonist α,β -meATP is used. In spite of the presence of considerable amounts of strongly desensitizing homomeric hP2X3 receptors, currents through these receptor channels do not appreciably contribute to the amplitude of the non-desensitizing hP2X2/3 responses (cf. Fig. 1Aa with b, c). It should be noted, however, that the quantity of a receptor cDNA does not necessarily correlate in a linear manner with the expression of the appropriate receptor protein.

The recording of α,β -meATP currents and [Ca²⁺]_i transients unanimously showed that transfection with hP2X2-mut and hP2X3-wt encoding cDNAs at a 4:1 ratio caused significantly smaller responses than transfection with the same mutant and wt subunit encoding cDNAs at a ratio of 1:2. Moreover, the combination of hP2X2-wt and hP2X3-mut encoding cDNAs at both ratios of 1:2 and 4:1 virtually abolished all responses to α,β -meATP. Therefore, we conclude that HEK293 cells express both (hP2X2)₁/(hP2X3)₂ and (hP2X2)₂/(hP2X3)₁ in their plasma membrane with a frequency of occurrence depending on the relative amount of cDNA ratio encoding for the individual subunits used for transfection (cf. Fig. 9B).

To estimate the pharmacological differences between the two stoichiometries of the hP2X2/3 heterotrimeric receptor, it was important to find out, whether (hP2X2)₁/(hP2X3)₂ and (hP2X2)₂/(hP2X3)₁ heterotrimeric receptors react identically or differentially to allosteric modulators or competitive antagonists. Extracellular acidification increased the ATP-induced current of the rat (r)P2X2 receptor expressed in HEK293 cells; at the same time acidification depressed rP2X3 and rP2X2/3 mediated currents (Stoop et al., 1997; Clyne et al., 2002). It has been reported that human P2X2 receptors are inhibited by Zn²⁺ over the range of 2–100 μ M, whereas rat P2X2 receptors are strongly potentiated and then inhibited by Zn²⁺ in concentrations higher than 100 μ M (Punthambaker et al., 2012). It was found, however, that mutating R225 to cysteine was

sufficient to confer Zn²⁺ potentiation onto the hP2X2b receptor (Tittle and Hume, 2008). Interestingly, in the present study, the corresponding hP2X2 (hP2X2a) receptor mutation increased the Zn²⁺-induced inhibition of the 2-MeSATP current rather than turning the hP2X2 receptor more sensitive to Zn²⁺ potentiation. More importantly neither H⁺ nor Zn²⁺ appeared to differentially modulate the 2-MeSATP or α,β -meATP responses at (hP2X2)₁/(hP2X3)₂ and (hP2X2)₂/(hP2X3)₁.

Finally, we investigated whether competitive antagonists of the homomeric P2X3 and heteromeric P2X2/3 receptors exhibit differences in the ability to inhibit current response mediated by the (hP2X2)₁/(hP2X3)₂ or the (hP2X2)₂/(hP2X3)₁ variant. We used the P2X3 and P2X2/3 antagonists TNP-ATP (Virginio et al., 1998b; Neelands et al., 2003) and A317491 (Jarvis et al., 2002; McGaraughty and Jarvis, 2005) for this purpose. Interestingly, only A317491 was more potent at the (hP2X2)₁/(hP2X3)₂ variant than at the (hP2X2)₂/(hP2X3)₁ variant. The fact that both heterotrimeric receptors cannot be easily discriminated by a pharmacological approach may be attributed to the fact that, according to our biochemical results, both heterotrimers, (P2X2)₂/(P2X3)₁ and (P2X2)₁/(P2X3)₂, are expressed at the plasma membrane following co-expression of P2X2 and P2X3 subunits in variable (for instance 4:1 or 1:2) ratios. Both forms share identical heteromeric ATP binding pockets at the heteromeric subunit interfaces and differ only in the single homomeric interface, which is either P2X2/P2X2 or P2X3/P2X3. Accordingly, the pharmacological differences between the two heterotrimeric receptors may escape detection by the use of agonists, although in the case of antagonists accessory binding sites may alleviate differentiation.

Following co-expression of His-hP2X2-GFP and His-hP2X3-StrepII subunits in *X. laevis* oocytes or HEK293 cells, BN-PAGE analysis revealed two distinct trimeric bands that both incorporated hP2X2 as well as hP2X3 subunits. The detection of these two distinct heterotrimers can only be explained by the existence of two distinct stoichiometries of the hP2X2/3 heterotrimer: (hP2X2)₂/(hP2X3)₁ and (hP2X2)₁/(hP2X3)₂. Moreover, the relative availability of hP2X2 and hP2X3 subunits determined the individual fraction of homotrimeric hP2X2 and hP2X3 and heterotrimeric (hP2X2)₂/(hP2X3)₁ and (hP2X2)₁/(hP2X3)₂ receptors.

In the Cys-loop or glutamate receptor families of ligand-gated ion channels (LGICs), both fixed as well as variable stoichiometries of heteromeric channels exist and variable subunit arrangements can account for different subunit interfaces formed between the four subunits (Barrera and Edwardson, 2008; Herguedas et al., 2013). By contrast, in heterotrimeric LGICs composed of two non-identical subunits the subunit stoichiometry definitely determines the arrangement of subunits and thus the formed subunit interfaces harbouring for instance the ligand binding site in case of P2X receptors. The subunit composition of a heteromer of acid-sensing ion channels (ASICs), another class of trimeric ion channels was also elucidated recently (Bartoi et al., 2014). By electrophysiology and a sophisticated single-molecule photobleaching technique it was shown that ASIC1a and ASIC2a subunits assemble randomly into ASIC1a/ASIC2a heterotrimers, indicating that ASIC1a/ASIC2a heterotrimers have no preferred composition.

In eukaryotic pentameric LGICs (pLGICs) such as the $\alpha 7$ nAChR (Castillo et al., 2009), the $\rho 1$ GABA_A receptor (Wong et al., 2014) and the $\alpha 1$ or $\alpha 1\beta$ GlyRs (Kuhse et al., 1993; Griffon et al., 1999) intersubunit interactions of the N-terminal domains were shown to be critical for assembly. Also, in heteromeric kainate receptors, high-affinity interaction domains of the KA2 and GluR6 subunits control subunit assembly (Kumar et al., 2011). The resolution of the zebrafish P2X4 receptor X-ray structure has shown the extracellular contact interfaces of adjacent subunits (Kawate et al., 2009), which has together with mutagenesis studies (Hausmann et al., 2015) shed

light on the intersubunit interaction domains that control subunit assembly of P2X receptors.

These findings suggest that also in P2X receptors specific domains inherent to individual subunits govern the assembly of P2X subunits and thus the stoichiometry of the functional oligomers. In a structural point of view, the same two subunit–subunit interfaces between the non-identical P2X2 and P2X3 subunits (one P2X2/P2X3 and one P2X3/P2X2 interface) are present in heterotrimeric (P2X2)₂/(P2X3)₁ or (P2X2)₁/(P2X3)₂ receptors. Consequently, the single interface between the two identical subunits, the P2X2/P2X2 or the P2X3/P2X3 interface constitutes the difference in subunit–subunit contacts between the two stoichiometries of heterotrimeric P2X2/3 receptors. Thus, the assembly of either heterotrimeric P2X2/3 receptor stoichiometry should be structurally feasible in terms of compatible subunit–subunit interactions.

Taken together, we demonstrate that the stoichiometry of the heterotrimeric hP2X2/3 receptor is not fixed, but determined by the relative availability of P2X2 and P2X3 subunits. Accordingly, the regulation of the P2X2 and P2X3 expression contributes to the fine-tuning and thus plasticity of ATP signal transduction.

Author contributions

Conceived and designed the experiments: MK RH YT GSch PI PR. Performed the experiments: MK JS AD GS. Analysed the data: MK JS AD GS RH. Contributed reagents/materials/analysis tools: RH YT GSch PI PR. Wrote the manuscript: MK RH GSch PI PR.

Acknowledgements

This work was supported by the Deutsche Forschungsgemeinschaft (IL 20/21-1; HA 6095/1-1; Schm 536/8-2) and the Sino-German Centre for the Support of Science (GZ 919). We are grateful to Dr. Thomas Riedel for many helpful discussions and for constructing Fig. 9B.

Appendix A. Supplementary data

Supplementary data related to this article can be found at <http://dx.doi.org/10.1016/j.neuropharm.2015.07.008>.

References

- Abbraccio, M.P., Burnstock, G., 1994. Purinoceptors: are there families of P2X and P2Y purinoceptors? *Pharmacol. Ther.* 64, 445–475.
- Antonio, L.S., Stewart, A.P., Xu, X.J., Varanda, W.A., Murrell-Lagnado, R.D., Edwardson, J.M., 2011. P2X4 receptors interact with both P2X2 and P2X7 receptors in the form of homotrimers. *Br. J. Pharmacol.* 163, 1069–1077.
- Aschrafi, A., Sadtler, S., Niculescu, C., Rettinger, J., Schmalzing, G., 2004. Trimeric architecture of homomeric P2X2 and heteromeric P2X1+2 receptor subtypes. *J. Mol. Biol.* 342, 333–343.
- Barrera, N.P., Henderson, R.M., Murrell-Lagnado, R.D., Edwardson, J.M., 2007. The stoichiometry of P2X2/6 receptor heteromers depends on relative subunit expression levels. *Biophys. J.* 93, 505–512.
- Barrera, N.P., Edwardson, J.M., 2008. The subunit arrangement and assembly of ionotropic receptors. *Trends Neurosci.* 31, 569–576.
- Bartoi, T., Augustinowski, K., Polleichtner, G., Grunder, S., Ulbrich, M.H., 2014. Acid-sensing ion channel (ASIC) 1a/2a heteromers have a flexible 2:1/1:2 stoichiometry. *Proc. Natl. Acad. Sci. U. S. A.* 111, 8281–8286.
- Becker, D., Woltersdorf, R., Boldt, W., Schmitz, S., Braam, U., Schmalzing, G., Markwardt, F., 2008. The P2X7 carboxyl tail is a regulatory module of P2X7 receptor channel activity. *J. Biol. Chem.* 283, 25725–25734.
- Bodnar, M., Wang, H., Riedel, T., Hintze, S., Kato, E., Fallah, G., Gröger-Arndt, H., Giniatullin, R., Grohmann, M., Hausmann, R., Schmalzing, G., Illes, P., Rubini, P., 2011. Amino acid residues constituting the agonist binding site of the human P2X3 receptor. *J. Biol. Chem.* 286, 2739–2749.
- Browne, L.E., Jiang, L.H., North, R.A., 2010. New structure enlivens interest in P2X receptors. *Trends Pharmacol. Sci.* 31, 229–237.
- Boumechache, M., Masin, M., Edwardson, J.M., Górecki, D.C., Murrell-Lagnado, R., 2009. Analysis of assembly and trafficking of native P2X4 and P2X7 receptor complexes in rodent immune cells. *J. Biol. Chem.* 284, 13446–13454.
- Burnstock, G., 2006. Purinergic P2 receptors as targets for novel analgesics. *Pharmacol. Ther.* 110, 433–454.
- Burnstock, G., 2013. Purinergic mechanisms and pain—an update. *Eur. J. Pharmacol.* 716, 24–40.
- Casas-Pruneda, G., Reyes, J.P., Perez-Flores, G., Perez-Cornejo, P., Arreola, J., 2009. Functional interactions between P2X4 and P2X7 receptors from mouse salivary epithelia. *J. Physiol.* 587, 2887–2901.
- Castillo, M., Mulet, J., Aldea, M., Gerber, S., Sala, S., Sala, F., Criado, M., 2009. Role of the N-terminal alpha-helix in biogenesis of $\alpha 7$ nicotinic receptors. *J. Neurochem.* 108, 1399–1409.
- Clyne, J.D., LaPointe, L.D., Hume, R.I., 2002. The role of histidine residues in modulation of the rat P2X2 purinoceptor by zinc and pH. *J. Physiol.* 539, 347–359.
- Cockayne, D.A., Dunn, P.M., Zhong, Y., Rong, W., Hamilton, S.G., Knight, G.E., Ruan, H.Z., Ma, B., Yip, P., Nunn, P., McMahon, S.B., Burnstock, G., Ford, A.P., 2005. P2X2 knockout mice and P2X2/P2X3 double knockout mice reveal a role for the P2X2 receptor subunit in mediating multiple sensory effects of ATP. *J. Physiol.* 567, 621–639.
- Coddou, C., Yan, Z., Obsil, T., Huidobro-Toro, J.P., Stojilkovic, S.S., 2011. Activation and regulation of purinergic P2X receptor channels. *Pharmacol. Rev.* 63, 641–683.
- Collingridge, G.L., Olsen, R.W., Peters, J., Spedding, M., 2009. A nomenclature for ligand-gated ion channels. *Neuropharmacology* 56, 2–5.
- Dorn, G., Abdel'Al, S., Natt, F.J., Weiler, J., Hall, J., Meigel, I., Mosbacher, J., Wishart, W., 2001. Specific inhibition of the rat ligand-gated ion channel P2X3 function via methoxyethoxy-modified phosphorothioated antisense oligonucleotides. *Antisense Nucleic Acid Drug Dev.* 11, 165–174.
- Fallah, G., Romer, T., Detro-Dassen, S., Braam, U., Markwardt, F., Schmalzing, G., 2011. TMEM16A₃/anoctamin-1 shares a homodimeric architecture with CLC chloride channels. *Mol. Cell. Proteomics* 10, M110.
- Fischer, W., Zádori, Z., Kullnick, Y., Gröger-Arndt, H., Franke, H., Wirkner, K., Illes, P., Mager, P.P., 2007. Conserved lysin and arginin residues in the extracellular loop of P2X3 receptors are involved in agonist binding. *Eur. J. Pharmacol.* 576, 7–17.
- Gerevich, Z., Zádori, Z.S., Köles, L., Kopp, L., Milius, D., Wirkner, K., Gyires, K., Illes, P., 2007. Dual effect of acid pH on purinergic P2X3 receptors depends on the histidine 206 residue. *J. Biol. Chem.* 282, 33949–33957.
- Griffon, N., Buttner, C., Nicke, A., Kuhse, J., Schmalzing, G., Betz, H., 1999. Molecular determinants of glycine receptor subunit assembly. *EMBO J.* 18, 4711–4721.
- Guo, C., Masin, M., Qureshi, O.S., Murrell-Lagnado, R.D., 2007. Evidence for functional P2X4/P2X7 heteromeric receptors. *Mol. Pharmacol.* 72, 1447–1456.
- Hausmann, R., Bodnar, M., Woltersdorf, R., Wang, H., Fuchs, M., Messermer, N., Qin, Y., Günther, J., Riedel, T., Grohmann, M., Nieber, K., Schmalzing, G., Rubini, P., Illes, P., 2012. ATP binding site mutagenesis reveals different subunit stoichiometry of functional P2X2/3 and P2X2/6 receptors. *J. Biol. Chem.* 287, 13930–13943.
- Hausmann, R., Bahrenberg, G., Kuhlmann, D., Schumacher, M., Braam, U., Bieler, D., Schlusche, I., Schmalzing, G., 2014. A hydrophobic residue in position 15 of the rP2X3 receptor slows desensitization and reveals properties beneficial for pharmacological analysis and high-throughput screening. *Neuropharmacology* 79, 603–615.
- Hausmann, R., Kless, A., Schmalzing, G., 2015. Key sites for P2X receptor function and multimerization: overview of mutagenesis studies on a structural basis. *Curr. Med. Chem.* 22, 799–818.
- Hemmings-Mieszczak, M., Dorn, G., Natt, F.J., Hall, J., Wishart, W.L., 2003. Independent combinatorial effect of antisense oligonucleotides and RNAi-mediated specific inhibition of the recombinant rat P2X3 receptor. *Nucleic Acids Res.* 31, 2117–2126.
- Herguedas, B., Krieger, J., Greger, I.H., 2013. Receptor heteromeric assembly—how it works and why it matters: the case of ionotropic glutamate receptors. *Prog. Mol. Biol. Transl. Sci.* 117, 361–386.
- Jarvis, M.F., Burgard, E.C., McGaraughty, S., Honore, P., Lynch, K., Brennan, T.J., Subieta, A., et al., 2002. A-317491, a novel potent and selective non-nucleotide antagonist of P2X3 and P2X2/3 receptors, reduces chronic inflammatory and neuropathic pain in the rat. *Proc. Natl. Acad. Sci. U. S. A.* 99, 17179–17184.
- Jarvis, M.F., 2003. Contributions of P2X3 homomeric and heteromeric channels to acute and chronic pain. *Expert. Opin. Ther. Targets* 7, 513–522.
- Jiang, L.H., Rassendren, F., Surprenant, A., North, R.A., 2000. Identification of amino acid residues contributing to the ATP-binding site of a purinergic P2X receptor. *J. Biol. Chem.* 275, 34190–34196.
- Jiang, L.H., Kim, M., Spelta, V., Bo, X., Surprenant, A., North, R.A., 2003. Subunit arrangement in P2X receptors. *J. Neurosci.* 23, 8903–8910.
- Karoly, R., Mike, A., Illes, P., Gerevich, Z., 2008. The unusual state-dependent affinity of P2X3 receptors can be explained by an allosteric two-open-state model. *Mol. Pharmacol.* 73, 224–234.
- Kawate, T., Michel, J.C., Birdsong, W.T., Gouaux, E., 2009. Crystal structure of the ATP-gated P2X4 ion channel in the closed state. *Nature* 460, 592–598.
- Kirsch, R.D., Joly, E., 1998. An improved PCR-mutagenesis strategy for two-site mutagenesis or sequence swapping between related genes. *Nucleic Acids Res.* 26, 1848–1850.
- Köles, L., Fürst, S., Illes, P., 2007. Purine ionotropic (P2X) receptors. *Curr. Pharm. Des.* 13, 2368–2384.
- Kowalski, M., Hausmann, R., Dopychai, A., Grohmann, M., Franke, H., Nieber, K., Schmalzing, G., Illes, P., Riedel, T., 2014. Conformational flexibility of the agonist binding jaw of the human P2X3 receptor is a prerequisite for channel opening. *Br. J. Pharmacol.* 171, 5093–5112.
- Kuhse, J., Laube, B., Magalei, D., Betz, H., 1993. Assembly of the inhibitory glycine receptor: identification of amino acid sequence motifs governing subunit

- stoichiometry. *Neuron* 11, 1049–1056.
- Kumar, J., Schuck, P., Mayer, M.L., 2011. Structure and assembly mechanism for heteromeric kainate receptors. *Neuron* 71, 319–331.
- Lalo, U., Pankratov, Y., Wichert, S.P., Rossner, M.J., North, R.A., Kirchhoff, F., Verkhratsky, A., 2008. P2X1 and P2X5 subunits form the functional P2X receptor in mouse cortical astrocytes. *J. Neurosci.* 28, 5473–5480.
- Lewis, C., Neidhart, S., Holy, C., North, R.A., Buell, G., Surprenant, A., 1995. Coexpression of P2X2 and P2X3 receptor subunits can account for ATP-gated currents in sensory neurons. *Nature* 377, 432–435.
- McGaraughty, S., Jarvis, M.F., 2005. Antinociceptive properties of a non-nucleotide P2X3/P2X2/3 receptor antagonist. *Drug News Perspect.* 18, 501–507.
- Neelands, T.R., Burgard, E.C., Uchic, M.E., McDonald, H.A., Niforatos, W., Faltynek, C.R., Lynch, K.J., Jarvis, M.F., 2003. 2', 3'-O-(2,4,6-trinitrophenyl)-ATP and A-317491 are competitive antagonists at a slowly desensitizing chimeric human P2X3 receptor. *Br. J. Pharmacol.* 140, 202–210.
- Nicke, A., Baumert, H.G., Rettinger, J., Eichele, A., Lambrecht, G., Mutschler, E., Schmalzing, G., 1998. P2X1 and P2X3 receptors form stable trimers: a novel structural motif of ligand-gated ion channels. *EMBO J.* 17, 3016–3028.
- Nicke, A., 2008. Homotrimeric complexes are the dominant assembly state of native P2X7 subunits. *Biochem. Biophys. Res. Commun.* 377, 803–808.
- Nörenberg, W., Illes, P., 2000. Neuronal P2X receptors: localisation and functional properties. *Naunyn Schmiedeb. Arch. Pharmacol.* 362, 324–339.
- North, R.A., 2002. Molecular physiology of P2X receptors. *Physiol. Rev.* 82, 1013–1067.
- Pankratov, Y., Lalo, U.V., Dashkin, A.N., Krishtal, A., 2001. Heterogeneity of the functional expression of P2X3 and P2X2/3 receptors in the primary nociceptive neurons of rat. *Neurochem. Res.* 26, 993–1000.
- Petruska, J.C., Cooper, B.Y., Johnson, R.D., Gu, J.G., 2000. Distribution patterns of different P2X receptor phenotypes in acutely dissociated dorsal root ganglion neurons of adult rats. *Exp. Brain Res.* 134, 126–132.
- Punthambaker, S., Blum, J.A., Hume, R.L., 2012. High potency zinc modulation of human P2X2 receptors and low potency zinc modulation of rat P2X2 receptors share a common molecular mechanism. *J. Biol. Chem.* 287, 22099–22111.
- Ralevic, V., Burnstock, G., 1998. Receptors for purines and pyrimidines. *Pharmacol. Rev.* 50, 413–492.
- Riedel, T., Wiese, S., Leichsenring, A., Illes, P., 2012. Effects of nucleotide analogs at the P2X3 receptor and its mutants identify the agonist binding pouch. *Mol. Pharmacol.* 82, 80–89.
- Saul, A., Hausmann, R., Kless, A., Nicke, A., 2013. Heteromeric assembly of P2X subunits. *Front. Cell. Neurosci.* 7, 250.
- Schwindt, T.T., Trujillo, C.A., Negraes, P.D., Lameu, C., Ulrich, H., 2011. Directed differentiation of neural progenitors into neurons is accompanied by altered expression of P2X purinergic receptors. *J. Mol. Neurosci.* 44, 141–146.
- Stelmashenko, O., Lalo, U., Yang, Y., Bragg, L., North, R.A., Compan, V., 2012. Activation of trimeric P2X2 receptors by fewer than three ATP molecules. *Mol. Pharmacol.* 82, 760–766.
- Stoop, R., Surprenant, A., North, R.A., 1997. Different sensitivities to pH of ATP-induced currents at four cloned P2X receptors. *J. Neurophysiol.* 78, 1837–1840.
- Surprenant, A., Schneider, D.A., Wilson, H.L., Galligan, J.J., North, R.A., 2000. Functional properties of heteromeric P2X1/5 receptors expressed in HEK cells and excitatory junction potentials in guinea-pig submucosal arterioles. *J. Auton. Nerv. Syst.* 81, 249–263.
- Terhag, J., Cavara, N.A., Hollmann, M., 2010. Cave Canalem: how endogenous ion channels may interfere with heterologous expression in *Xenopus* oocytes. *Methods* 51, 66–74.
- Tittle, R.K., Hume, R.L., 2008. Opposite effects of zinc on human and rat P2X2 receptors. *J. Neurosci.* 28, 11131–11140.
- Torres, G.E., Egan, T.M., Voigt, M.M., 1999. Hetero-oligomeric assembly of P2X receptor subunits. Specificities exist with regard to possible partners. *J. Biol. Chem.* 274, 6653–6659.
- Virginio, C., North, R.A., Surprenant, A., 1998a. Calcium permeability and block at homomeric and heteromeric P2X2 and P2X3 receptors, and P2X receptors in rat nodose neurones. *J. Physiol.* 510, 27–35.
- Virginio, C., Robertson, G., Surprenant, A., North, R.A., 1998b. Trinitrophenyl-substituted nucleotides are potent antagonists selective for P2X1, P2X3, and heteromeric P2X2/3 receptors. *Mol. Pharmacol.* 53, 969–973.
- Wilkinson, W.J., Jiang, L.H., Surprenant, A., North, R.A., 2006. Role of ectodomain lysines in the subunits of the heteromeric P2X2/3 receptor. *Mol. Pharmacol.* 70, 1159–1163.
- Wirkner, K., Sperlagh, B., Illes, P., 2007. P2X3 receptor involvement in pain states. *Mol. Neurobiol.* 36, 165–183.
- Wong, L.W., Tae, H.S., Cromer, B.A., 2014. Role of the rho1 GABAC receptor N-terminus in assembly, trafficking and function. *ACS Chem. Neurosci.* 5, 1266–1277.



Contents lists available at SciVerse ScienceDirect

Neuropharmacology

journal homepage: www.elsevier.com/locate/neuropharm

P2X7 receptors at adult neural progenitor cells of the mouse subventricular zone



Nanette Messemer^a, Christin Kunert^a, Marcus Grohmann^a, Helga Sobottka^a, Karen Nieber^b, Herbert Zimmermann^c, Heike Franke^a, Wolfgang Nörenberg^a, Isabelle Straub^a, Michael Schaefer^a, Thomas Riedel^a, Peter Illes^{a,*}, Patrizia Rubini^{a,**}

^aRudolf Boehm Institute of Pharmacology and Toxicology, University of Leipzig, Haertelstrasse 16-18, 04107 Leipzig, Germany

^bDepartment of Pharmacology for Natural Sciences, Institute of Pharmacy, University of Leipzig, 04103 Leipzig, Germany

^cInstitute of Cell Biology and Neuroscience, Goethe University, 60438 Frankfurt am Main, Germany

ARTICLE INFO

Article history:

Received 1 October 2012

Received in revised form

1 May 2013

Accepted 4 May 2013

Keywords:

Adult neural progenitor cells

Brain subventricular zone

P2X7 receptors

Extracellular ATP

ABSTRACT

Neurogenesis requires the balance between the proliferation of newly formed progenitor cells and subsequent death of surplus cells. RT-PCR and immunocytochemistry demonstrated the presence of P2X7 receptor mRNA and immunoreactivity in cultured neural progenitor cells (NPCs) prepared from the adult mouse subventricular zone (SVZ). Whole-cell patch-clamp recordings showed a marked potentiation of the inward current responses both to ATP and the prototypic P2X7 receptor agonist dibenzoyl-ATP (Bz-ATP) at low Ca^{2+} and zero Mg^{2+} concentrations in the bath medium. The Bz-ATP-induced currents reversed their polarity near 0 mV; in NPCs prepared from P2X7^{-/-} mice, Bz-ATP failed to elicit membrane currents. The general P2X/P2Y receptor antagonist PPADS and the P2X7 selective antagonists Brilliant Blue G and A-438079 strongly depressed the effect of Bz-ATP. Long-lasting application of Bz-ATP induced an initial current, which slowly increased to a steady-state response. In combination with the determination of YO-PRO uptake, these experiments suggest the dilation of a receptor-channel and/or the recruitment of a dye-uptake pathway. Ca^{2+} -imaging by means of Fura-2 revealed that in a Mg^{2+} -deficient bath medium Bz-ATP causes $[Ca^{2+}]_i$ transients fully depending on the presence of external Ca^{2+} . The MTT test indicated a concentration-dependent decrease in cell viability by Bz-ATP treatment. Correspondingly, Bz-ATP led to an increase in active caspase 3 immunoreactivity, indicating a P2X7-controlled apoptosis. In acute SVZ brain slices of transgenic Tg(nestin/EGFP) mice, patch-clamp recordings identified P2X7 receptors at NPCs with pharmacological properties identical to those of their cultured counterparts. We suggest that the apoptotic/necrotic P2X7 receptors at NPCs may be of particular relevance during pathological conditions which lead to increased ATP release and thus could counterbalance the ensuing excessive cell proliferation.

© 2013 Elsevier Ltd. All rights reserved.

Abbreviations: α,β -meATP, α,β -methylene ATP; 5-BDBD, 5-(3-bromophenyl)-1,3-dihydro-2H-benzofuro[3,2-e]-1,4-diazepin-2-one; BBG, Brilliant Blue G; Bz-ATP, 2'-(3')-O-(4-benzoylbenzoyl)adenosine-5'-triphosphate; $[Ca^{2+}]_i$, intracellular Ca^{2+} concentration; CNS, central nervous system; E_{max} , maximal effect; EC_{50} , concentration of agonist producing 50% of E_{max} ; EGF, epidermal growth factor; FGF-2, fibroblast growth factor-2; GAPDH, glyceraldehyde 3-phosphate dehydrogenase; GFAP, glial fibrillary acidic protein; 2-methylthio ATP, 2-MeSATP; MTT, 3-(4,5-dimethylthiazol-2-yl)-2,5-diphenyltetrazoliumbromid; Msi1, musashi1; NPC, neural progenitor cell; PPADS, pyridoxal phosphate-6-azophenyl-2',4'-disulfonic acid; SVZ, subventricular zone; TNP-ATP, 2',3'-O-(2,4,6-trinitrophenyl) adenosine 5'-triphosphate; wt, wild-type; X^2 concentration, divalent cation concentration.

* Corresponding author. Tel.: +49 341 9724614; fax: +49 341 9724609.

** Corresponding author. Tel.: +49 341 9724634; fax: +49 341 9724609.

E-mail addresses: Peter.Illes@medizin.uni-leipzig.de (P. Illes), Patrizia.Rubini@medizin.uni-leipzig.de (P. Rubini).

1. Introduction

Besides acting as metabolic intermediates, ATP, ADP or uracil nucleoside tri- and diphosphates (UTP, UDP, UDP-glucose and UDP-galactose) are now recognized to act as key extracellular signalling molecules in various organ systems including the central nervous system (CNS) (Abbracchio and Burnstock, 1994). The cellular effects of these compounds are mediated by seven P2X receptors (P2X1-7 subtypes, which are ligand-gated cation channels; Khakh and North, 2006) and eight G-protein-coupled P2Y receptors (P2Y_{1,2,4,6,11,12,13,14} receptors; Abbracchio et al., 2006).

Neuroepithelial stem cells in the embryonic nervous system generate most of the neurons and glia in the developing brain (Doetsch, 2003). In addition neurogenesis continues in the adult

mammalian brain in specific neurogenic niches, the subgranular zone of the hippocampal dentate gyrus and the subventricular zone (SVZ) of the lateral ventricle, contributing mature neurons to the dentate gyrus and olfactory bulb, respectively (Götz and Huttner, 2005; Zhao et al., 2008).

Extracellular nucleotides can influence the proliferation and fate decision of neural progenitor cells (NPCs) both during embryonic development and in the adult brain (Mishra et al., 2006; Rubini et al., 2009). Previous work has demonstrated that P2Y₁ receptors are present at NPCs of the SVZ *in vitro* and *in situ* (Mishra et al., 2006; Grimm et al., 2009; Suyama et al., 2012), causing rapid [Ca²⁺]_i transients and augmenting growth factor-mediated proliferation.

Neurogenesis requires the balance between the proliferation of newly formed progenitor cells and subsequent death of surplus cells. This is of particular relevance in pathological conditions such as traumatic injury, hypoxia/ischemia, and epilepsy that cause excessive proliferation of NPCs (Suh et al., 2009). The functional properties of the P2X₇ receptor make it a candidate for counter regulation of excessive neuro- and/or gliogenesis. This receptor mediates various cell damaging effects of ATP, such as actin reorganization/membrane blebbing, interleukin-1 processing/release, channel dilation with or without the involvement of pannexin-1, and caspase activation with subsequent apoptosis (Sperlágh et al., 2006). P2X₇ receptors are activated by high concentrations of ATP which are released from dying or metabolically stressed cells (Burnstock et al., 2011).

Although P2X₇ receptors were shown to induce apoptosis/necrosis in embryonic NPCs (Delarasse et al., 2009, 2011) and P2X₇ mRNA was present in undifferentiated neural cell-lines (Yuahasi et al., 2012) convincing electrophysiological evidence for the membrane location of such ligand-gated cationic channels in neural or non-neural stem cells is missing. We therefore searched for functional P2X₇ receptors at both undifferentiated cultured mouse NPCs prepared from the adult SVZ and at NPCs in the SVZ of acute brain slices. We show that in low divalent cation-containing extracellular medium, which favours the generation of epileptiform spontaneous neuronal discharges in hippocampal brain slices (Heinemann et al., 1992), P2X₇ receptors become unmasked at NPCs previously exhibiting only a low sensitivity to ATP and its structural analogue dibenzoyl-ATP (Bz-ATP). The activation of these apoptotic/necrotic P2X₇ receptors may thus limit excessive neuro- and gliogenesis induced by seizure disorders or other types of neuronal damage.

2. Methods

2.1. Experimental animals

Unless otherwise stated, experiments were performed with primary cultures of adult NPCs obtained from C57Bl/6N wild type (wt) mice. In addition, P2X₇^{-/-} (Charles River; Solle et al., 2001), P2Y₁^{-/-} (gift of Dr. Beverly H. Koller, Chapel Hill, NC, USA) (Fabre et al., 1999), and transgenic mice [Tg(nestin/EGFP)] overexpressing enhanced green fluorescent protein (EGFP) under the control of the rat nestin promoter (gift of Dr. Helmut Kettenmann, Berlin, Germany) were used. For the experiments with P2Y₁^{-/-}, the corresponding wt background mouse was of the 129Sv strain (Harlan).

2.2. Preparation and culture of neural progenitor cells (NPCs)

Primary cultures of adult NPCs from the SVZ were prepared from 8 to 14 weeks old mice (Grimm et al., 2009). After 7 days of culturing as neurospheres cells were dispersed and seeded onto coated culture dishes (patch-clamp, RT-PCR) or coated glass coverslips (Ca²⁺ imaging, immunocytochemistry, YO-PRO-1 uptake) with proliferation medium containing 20 ng/ml epidermal growth factor (EGF) and 10 ng/ml fibroblast growth factor-2 (FGF-2). A combination of poly-L-ornithin (PLO; 0.5 mg/ml) and fibronectin (5 µg/ml) was used to coat culture dishes or coverslips (both Sigma-Aldrich). For testing the possible dependence of P2X₇ receptor function on the type of coating, laminin (20 µg/ml) or collagen (100 µg/ml) were used

alternatively (both Sigma-Aldrich). In some of the experiments, adherent NPCs were cultured in the presence of growth factors for only 1 day and thereafter the growth factors were omitted for further 3 days.

Multipotency of NPCs was tested via replacing growth factors with 2% foetal calf serum (FCS; Biochrom) in the proliferation medium. After 1–4 days of adherent cultivation in proliferation medium, it was changed to this FCS containing medium, and cells were additionally grown for 6 days at 37 °C and in 5% CO₂.

2.3. RT-PCR and immunocytochemistry

mRNA was isolated from 1 day old adherent NPCs using TRIzol reagent as described in the manual (Invitrogen). cDNA was synthesized using SuperScript[®] II Reverse Transcriptase and oligo (dT) primer (Invitrogen). A PCR with 35 cycles was performed using GoTaq Flexi DNA polymerase (Promega) and specific primers for P2X₁–7 and glyceraldehyde 3-phosphate dehydrogenase (GAPDH). The forward and reverse primer sequences were the following; P2X₁, CCAGGACTCCGAAGCCTTGC, AGAACTGTGGCACTCCAAGATG; P2X₂, ATCGGGGTGGGCTCCTTCTCG, TCCCAATGCTGTGCAAGAGTGTGTC; P2X₃, TCTTGCACGAGAAGGCTACCAA, GATCTCACA GGTCGACGGACA; P2X₄, GAGAATGACGCTGGTGTGCCAA, CCCTGTAGTACTGGCAAA CCTGA; P2X₅, GAGTCTGTGGTCCACCAAGATCA, CTGGGCCACCAAGCAAAGATCTCA; P2X₆, TGTTACCGAGAGAACCAAGATG, GCTTTGGCAAGCTTTACTTCAGCA; P2X₇, TTGCTTTGGTGGAGCGATAAGCTGT, GCCAGTCTCGAATTCCTTTGCTCT; and GAPDH, CAAGGTCATCCATGACAACCTTG, GGGCCATCCACAGTCTTCTG.

Immunocytochemical staining of NPCs was performed by procedures similar to those previously described for astrocytes (Fischer et al., 2009).

Antibodies were used as follows: rabbit anti-P2X₇ receptor (1:600, polyclonal; Alomone), rabbit anti-musashi1 (Msi1, 1:200, monoclonal; Abcam), mouse anti-nesstin (1:100, monoclonal), mouse anti-CNPase (1:250, monoclonal) (both Chemicon), mouse anti-βIII Tubulin (1:1000, monoclonal; Promega), rabbit anti-active caspase 3 (1:50; MBL International) and mouse anti-GFAP (1:1000, monoclonal; Sigma-Aldrich). The appropriate Cy3- and Cy2-conjugated secondary antibodies were obtained from Jackson ImmunoResearch. Nuclei were stained with Hoechst 33342 (Molecular Probes).

Because of the reported problems with the selectivity of P2X₇ receptor antibodies especially for immunohistochemistry in the CNS (Sim et al., 2004; Brass et al., 2012), we purchased two antibodies from different commercial sources. They were tested by Western-blotting for the recombinant human P2X₇ receptor transfected in HEK293 cells (not shown). With the antibody of Abcam (ab77413; directed against an epitope at the extracellular loop of P2X₇) a specific band at about 75 kDa was observed, but in addition several (at least four) further, non-specific bands appeared, which were also observed in non-transfected HEK293 cells. By contrast, the antibody of Alomone (APR-004; directed against an epitope at the intracellular C terminus of P2X₇) exhibited only a single specific band at about 70 kDa in transfected HEK293 cells. Therefore, we used the Alomone antibody in all immunocytochemistry experiments.

Stained cells were examined with a confocal laser scanning microscope (see Fischer et al., 2009). For quantitative evaluation of undifferentiated NPCs, a series of 10 images from 3 independent experiments across the axis of the coverslip were taken with a 40× objective. These pictures were evaluated with ImageJ software; the percentage of Msi1- or nestin-positive cells was calculated in relation to the total number of cell nuclei stained with Hoechst. For documentation of the expression of active caspase 3-immunoreactivity, NPCs from wt and P2X₇^{-/-} mice were seeded onto PLO/fibronectin-coated coverslips in Petri dishes and incubated for 2 h at 37 °C in a Bz-ATP (300 µM)-containing or Bz-ATP-free culture medium.

2.4. Whole-cell patch clamp recordings and drug application protocols; cultured NPCs

Whole-cell current-clamp and voltage-clamp recordings were made at room temperature (20–24 °C) on 1–4 days old adherent NPCs, using an Axopatch 200B patch clamp amplifier (Molecular Devices). The pipette solution contained (in mM): K-gluconate 140, NaCl 10, CaCl₂ 0.2, MgCl₂ 2.3, HEPES 10, EGTA 10, Mg-ATP 4, Li-GTP 0.3 (pH 7.2, with KOH). In a few experiments, EGTA was replaced by BAPTA (5 mM) and K-gluconate was increased correspondingly. Two different bath solutions were used, one of them contained normal and the other one low divalent cation (low X²⁺) concentrations. For seal formation and some initial experiments, we used a normal artificial cerebrospinal fluid (aCSF; in mM): NaCl 140, KCl 2.5, CaCl₂ 1, MgCl₂ 1.2, HEPES 25, glucose 10.5 (pH 7.3, with NaOH). For low X²⁺ solution MgCl₂ was omitted, and the concentration of CaCl₂ was decreased to 0.1 mM. Pipettes had resistances of 3–8 MΩ. A relatively high holding potential of –80 mV was selected (by taking into account a calculated liquid junction potential of –14 mV), because adult NPCs were reported to have astrocytic characteristics (Yasuda et al., 2008).

The resting membrane potential (U_m) was measured within 30 s after establishing whole-cell access. Membrane capacitance (C_m) and resistance (R_m) as well as the access resistance (R_a) were monitored and recorded before and during individual experiments. Cells with R_a values higher than 25 MΩ were discarded. The current- and voltage-step protocols are described in chapter 3.2. pClamp 10.2 software (Molecular Devices) was used to store the recorded data for offline analysis/filtering and to trigger the fast drug application system.

Agonists, antagonists, and allosteric modulators were applied locally by means of a computer-controlled solenoid valve-driven pressurized superfusion system (DAD-12, ALA Scientific Instruments). Agonists were applied usually for 5 s every 1–2 min, in a low X^{2+} solution. Agonist effects were determined before, during and after superfusion with a low X^{2+} solution alone, or during and after superfusion with a low X^{2+} solution containing antagonists or allosteric modulators. Membrane currents were measured as peak responses and transformed in most cases to current densities in order to take into account changes in cell size which directly relate to the cell capacitance (C_m).

Concentration–response curves were fitted by the three-parametric Hill equation. The following parameters were derived from the equation of the curve: E_{max} , the maximal effect; n , the Hill coefficient; and EC_{50} , the concentration of agonist producing 50% of E_{max} . The software package SigmaPlot 11.0 was used for these calculations. In case of the antagonist/allosteric modulator studies, current densities were normalized to the 3rd application of the agonist after starting the experiment (300 μ M Bz-ATP, low X^{2+} , 2-min intervals between applications). Then, concentrations of antagonists/allosteric modulators were applied for 6 min each, and the change in the agonist effect was expressed in comparison with the time-matched normalized controls recorded in the absence of antagonists/allosteric modulators. Thus, i.e. the 3rd application of Bz-ATP in the presence of antagonist/allosteric modulator was compared with the 3rd application of Bz-ATP in the absence of these drugs (control). A basically similar procedure was adapted to calculate changes in the Bz-ATP-induced $[Ca^{2+}]_i$ transients (see below).

2.5. Intracellular calcium measurements

The cytosolic free Ca^{2+} concentration ($[Ca^{2+}]_i$) was measured with the Fura-2 method as described previously (Rubini et al., 2009). Experiments were performed at room temperature in an oxygenated bath solution with the following composition (in mM): NaCl 135, KCl 4.5, $CaCl_2$ 2, $MgCl_2$ 1, HEPES 10, glucose 10; pH 7.4 with NaOH. An inverted microscope equipped for epifluorescence and a Peltier-cooled charge-coupled device camera (IMAGO; Till Photonics) were used. Intracellular Fura-2 was alternately excited at 340 nm and at 380 nm and the emitted light was measured at 510 nm. The fluorescence ratio (FR; 340/380 nm) was taken as a relative measure of $[Ca^{2+}]_i$. 5–6 coverslips were recorded for each experiment; the $[Ca^{2+}]_i$ increases were analysed by setting the regions of interest (ROIs) at the entire NPC. Selected areas without cells were chosen for background subtraction.

Agonists, antagonists, and allosteric modulators were applied locally by means of a computer-controlled superfusion system (DAD-12, ALA Scientific Instruments). Bz-ATP was applied for 10 s every 10 min, in a Mg^{2+} -free bath solution. Agonist effects were determined before, during and after superfusion with antagonists, allosteric modulators, or a Ca^{2+} -free bath medium. A Ca^{2+} -free medium was prepared by omitting $CaCl_2$ from the normal bath solution and adding EGTA (1 mM) to chelate the residual Ca^{2+} . Concentration–response curves were fitted by the three-parametric Hill equation, as described for electrophysiology. Antagonists/allosteric modulators and a Ca^{2+} -free bath medium were present 8–10 min before and during agonist application. The Bz-ATP (300 μ M)-induced $[Ca^{2+}]_i$ transients were normalized to the effect of the 2nd agonist application after starting the experiment. The effects of antagonists/allosteric modulators on the agonist-induced increase of $[Ca^{2+}]_i$ were expressed in comparison with the time-matched normalized controls measured in the absence of drugs.

2.6. YO-PRO-1 uptake

YO-PRO-1 uptake was measured as described by Nöberg et al. (2011). In short, adult adherent NPCs were kept in low X^{2+} aCSF, and pictures were taken at 2 s-intervals. After 60 s, YO-PRO-1 (Invitrogen, Darmstadt) was added at a final concentration of 2 μ M. After 420 s, Bz-ATP (300 μ M; Sigma-Aldrich) or low X^{2+} aCSF (as control) was added. The experiment was stopped after 1080 s with the addition of the detergent Triton X-100 (0.5% w/v), which destroyed the cell membrane and immediately increased YO-PRO-1 fluorescence in the cells. For quantitative analysis, ROIs were defined at selected areas with and without cells, the latter ones for background subtraction. The slope of the YO-PRO-1 fluorescence increase was determined for every cell (between 500 and 1000 s after beginning the experiment).

2.7. MTT viability test

To test the possible cytotoxicity of P2X7 activation in NPCs, enzymatic conversion of 3-(4,5-dimethylthiazol-2-yl)-2,5-diphenyltetrazoliumbromid (MTT) was used. NPCs from wt and P2X7^{-/-} mice were seeded onto a 96-well plate coated with POL/fibronectin and allowed to grow for 24 h. The next day, varying concentrations of BzATP diluted in cell culture medium were added, and cells were incubated for 4 h at 37 °C. For colorimetric detection, the medium was exchanged to a phenol red-free medium (100 μ l per well), containing 1.2 mM MTT, and cells were placed in the incubator for 3 h. Arizing formazan complexes were solubilized with DMSO; absorbance was measured at 560 nm and 670 nm with the transmission spectrometer head of a plate reader device (Polarstar Omega, BMG Labtech). A solvent control was set as 100% and measurements in the presence of the indicated

substances were normalized to this value. Triplicate measurements were made in each experiment.

2.8. Preparation of brain slices containing the SVZ; whole-cell patch clamp recordings from nestin-fluorescent cells of transgenic mice

Corticostriatal slices (thickness, ~250 μ m) including the SVZ were prepared from Tg(nestin/EGFP) mice (Wang et al., 2003). Whole-cell patch-clamp recordings from NPCs situated below the ependymal cell layer were made using fluorescence microscopy (for astroglial cells of Tg(GFAP/EGFP) mice see Oliveira et al., 2011). Brain slices were superfused with oxygenated aCSF consisting of (in mM): NaCl 126, KCl 2.5, $CaCl_2$ 2.4, $MgCl_2$ 1.3, NaH_2PO_4 1.2, $NaHCO_3$ 25, and glucose 11; pH 7.4. To create low divalent cation (low X^{2+}) conditions, $MgCl_2$ was omitted from the medium and the $CaCl_2$ concentration was decreased to 0.5 mM. Patch pipettes were filled with intracellular solution of the following composition (in mM): K-gluconic acid 140, NaCl 10, $MgCl_2$ 1, HEPES 10, EGTA 11, Mg-ATP 1.5, Li-GTP 0.3, and Lucifer Yellow 0.2; pH 7.2 adjusted with KOH. Pipette resistances were in the range of 5–7 M Ω . Drugs were applied by means of a DAD-12 system.

2.9. Materials

All agonists and antagonists were from Sigma-Aldrich except of A-438079, 5-BDBD and TNP-ATP which were from Tocris.

2.10. Statistics

Means \pm S.E.M. are given throughout. SigmaPlot (version 11.0) was used for all statistical evaluations. Pairwise comparisons were made by the Student's *t* test or the Mann–Whitney rank sum test, as appropriate. Multiple comparisons were performed by one-way analysis of variance (ANOVA) followed by the Holm–Sidak *post hoc* test, or the Kruskal–Wallis ANOVA on Ranks followed by the Dunn's *post hoc* test. In all cases, a probability level of 0.05 or less was considered to be statistically significant.

3. Results

3.1. mRNA and immunoreactivity for P2X7 receptors at cultured NPCs

In a first series of experiments, we performed RT-PCR measurements to determine mRNAs for all known P2X receptor-subtypes in cultures of adult NPCs prepared from the mouse SVZ (Fig. 1A). RT-PCR indicated the presence of all seven P2X receptor mRNAs including that for P2X7 (323 base pairs). Determinations were made at day one after preparing adherent cultures (1 DIV).

Immunocytochemistry proved co-staining of adult SVZ-derived NPCs for the stem/progenitor cell markers musashi1 and nestin (Fig. 1Ba–c) as well as staining for P2X7 receptors (Fig. 1Bd). The immunoreactivity for the P2X7 antibody was strongly decreased by preincubating NPCs with the respective peptide antigen (Fig. 1Be), and was absent in NPCs of P2X7^{-/-} mice (Fig. 1f). The overwhelming majority of the NPCs were nestin- (98.9 \pm 0.3%, n = 3, 1581 cells in total) and musashi1-positive (99.5 \pm 0.2%, n = 3, 1598 cells in total), indicating that they consist of an almost homogeneous population of neural stem/progenitor cells. Because of the slight, residual staining of the wt preparations by the P2X7 antibody used, after preincubation with the peptide antigen, we did not evaluate quantitatively the co-expression of nestin/musashi1- and P2X7-immunoreactivities (see also Methods Section).

When NPCs were kept instead of the proliferation medium in a differentiation medium (no growth factors, but FCS added), they turned into neurons, oligodendrocytes and astrocytes, as characterized by the respective immunocytochemical markers, β III tubulin, CNPase and GFAP (Fig. 1C; Kriegstein and Alvarez-Buylla, 2009). Co-staining with Hoechst proved the allocation of these markers to individual cells bodies and processes. GFAP is expressed by NPCs, astrocytes, and radial glia – an embryonic progenitor of neurons, astrocytes and oligodendrocytes, and the putative origin of the neurogenic zones.

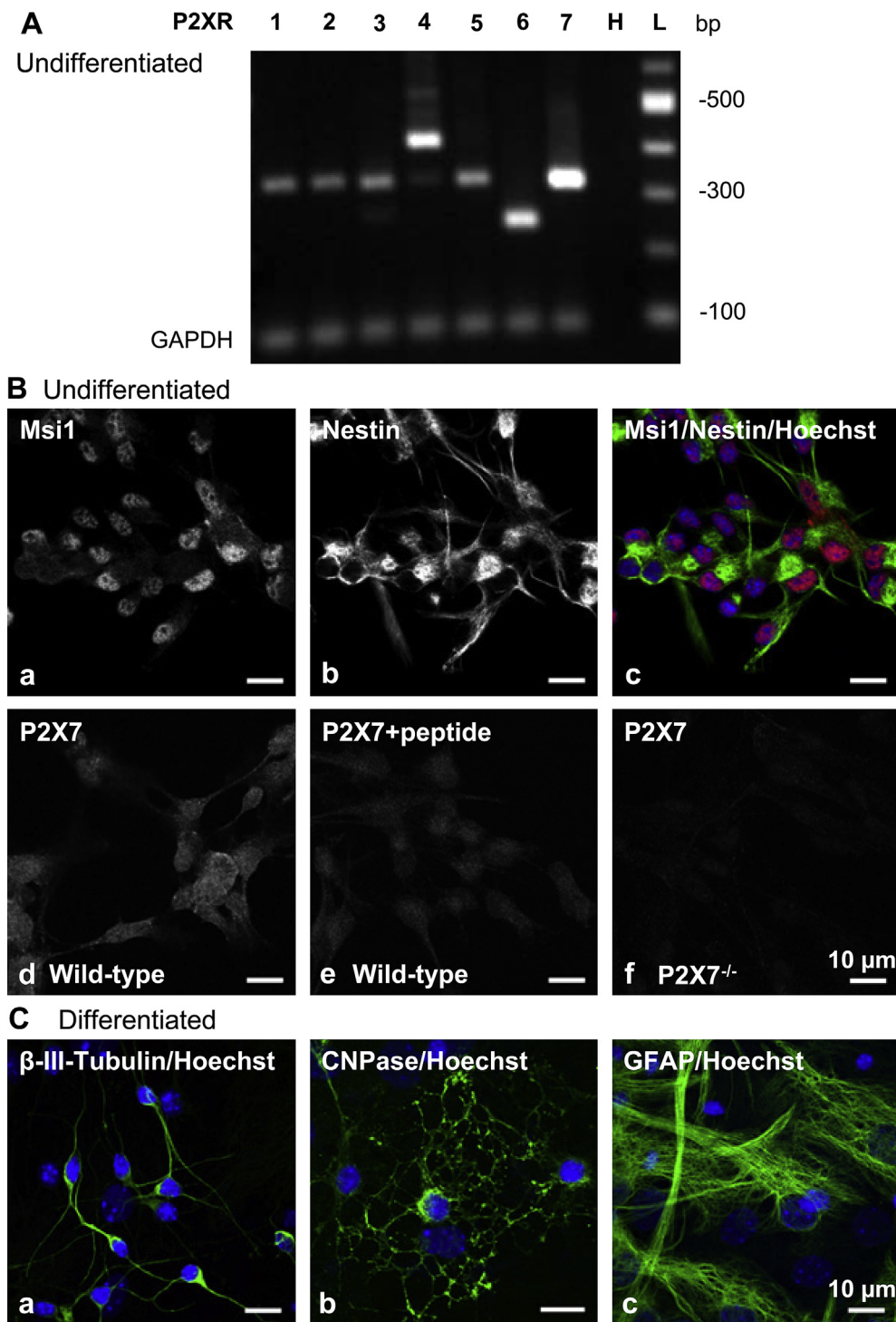


Fig. 1. Determination of the mRNA and immunoreactivity for P2X receptors in undifferentiated neural progenitor cells (NPCs) prepared from the subventricular zone of the adult mouse. (A) RT-PCR indicates the presence of all seven P2X receptor mRNAs including that for P2X7 (323 base pairs; see the base pair ladder L). Glyceraldehyde 3-phosphate dehydrogenase (GAPDH) was used as a housekeeping gene control (90 base pairs). The P2X receptors are designated by numbering at the upper part of the gel (lane H, H₂O control). (B) Immunocytochemistry proves co-staining of undifferentiated NPCs with the stem cell markers musashi1 (Msi1) and nestin; a–c), as well as staining of NPCs with a P2X7 receptor antibody (d). Pre-incubation of the P2X7 antibody with a specific blocking peptide results in a slight, non-selective staining; in NPCs of P2X7^{-/-} mice P2X7-immunopositivity is lacking. (C) Immunopositivity of differentiated NPCs for the markers of neurons (a, βIII tubulin), oligodendrocytes (b, CNPase), and astrocytes (c, glial fibrillary acidic protein; GFAP). Hoechst 33342 (Hoechst) was used to label the cell nuclei (Bc, Ca–c); scale bars for all panels, 10 μm. Ba/Bb and Bd/Be are presented in black-and-white for better visibility.

3.2. Electrophysiological characterization of cultured NPCs

In this and all further series of experiments throughout the paper, cultured undifferentiated NPCs were utilized and for the matter of simplicity referred to as “cultured NPCs”. Whole-cell

patch clamp recordings allowed the classification of NPCs into four types. Type 1 cells ($n = 130$) constituted the largest population out of the investigated total number of NPCs ($n = 277$) (Fig. 2A). They reacted to the injection of depolarizing current above a certain threshold with wide-amplitude, rudimentary action potentials,

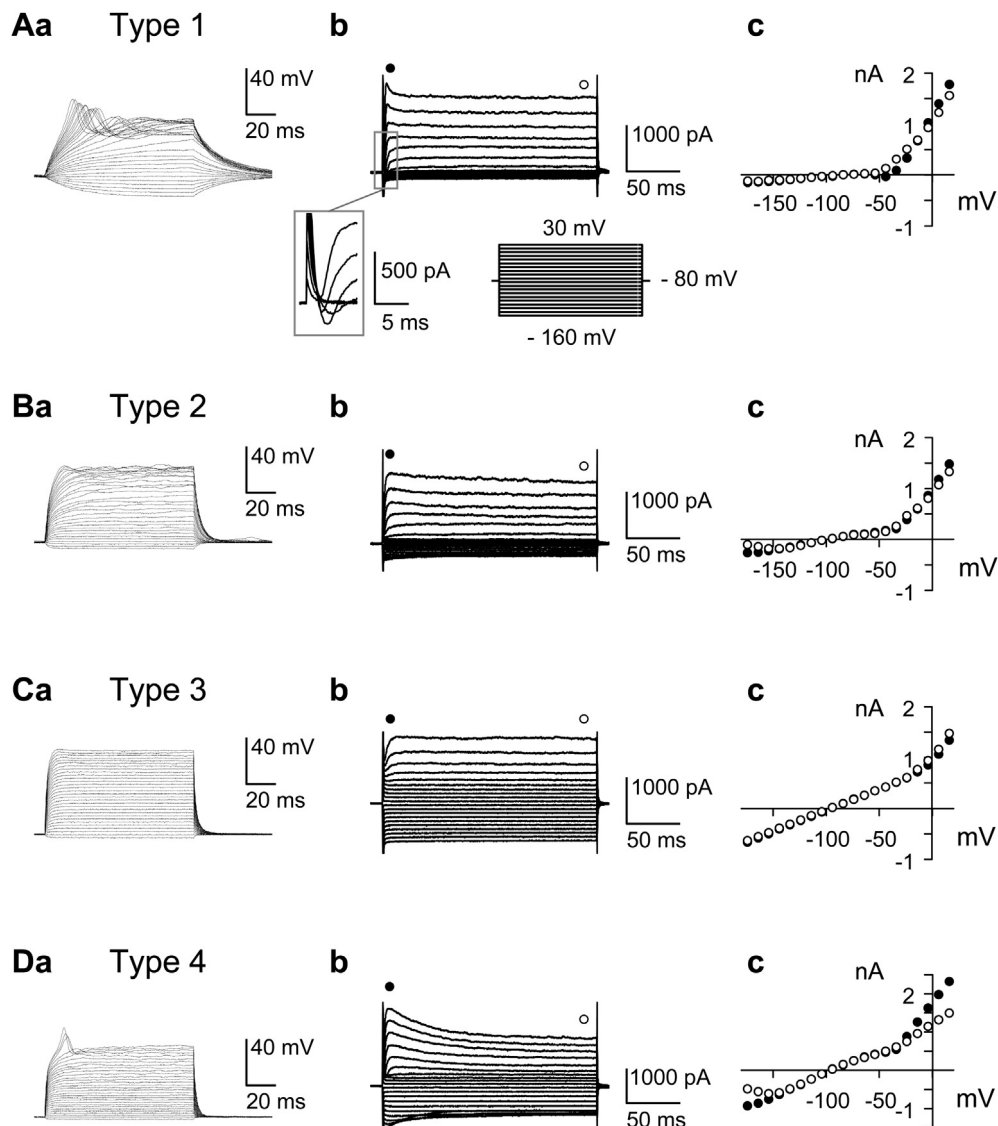


Fig. 2. Classification of cultured undifferentiated NPCs on the basis of their voltage–current characteristics. The resting membrane potential of 277 cells varied between -65 and -105 mV. Experiments with 4 representative cells are shown (A–D). (a) Current–step protocols, starting with the injection of -20 pA hyperpolarizing current and continuing with currents steps (2 – 80 pA increments; depending on the membrane resistance; 100 -ms duration), were applied every 1 s to cause a peak depolarization of up to -20 mV. (b) Voltage–step protocols evoking current responses by a series of 200 -ms duration voltage steps in the range of -160 to $+30$ mV, in 10 mV increments, and at 1 s intervals were delivered (see right inset in Ab). (c) Voltage–current relationships plotted from the original tracings shown in a. ●, early current measured at its peak after the capacitive artefact; ○, late current measured at the end of the current response. For further details see the chapter “Electrophysiological characterization of cultured NPCs”.

with correspondingly slow up- and down-strokes. The voltage–current curves were strongly outwardly rectifying and depolarizing voltage-steps caused rapidly inactivating inward currents. These cells had a lower membrane potential (-83.6 ± 1.3 mV) and a higher membrane resistance (488.0 ± 36.9 M Ω) than the residual types; it is suggested that they belong to a cell class intermediary between radial glia and neuroblasts. Type 2 cells ($n = 59$) were still outwardly rectifying but did not deliver action potentials on depolarizing current injection; their outward and inward current responses to voltage steps moderately inactivated (Fig. 2B). The membrane potential and membrane resistance of these cells were -91.0 ± 1.5 mV and 267.0 ± 48.7 M Ω , respectively. Type 3 NPCs, resembling classic radial glia ($n = 67$), did not fire action potentials in response to the injection of even large depolarizing currents and exhibited a symmetrical voltage–current pattern with an almost linear I/V curve (Fig. 2C). They had a high membrane potential

(-95.9 ± 0.9 mV) and low membrane resistance (76.3 ± 19.2 M Ω) suggesting electrical coupling with neighbouring NPCs. Type 4 cells ($n = 21$) exhibited complex behaviour (Fig. 2D). They generated a rudimentary spike, when depolarized and showed inactivation of both outward and inward current responses to voltage steps. Their membrane potential (-93.6 ± 2.1 mV) was similar to that of the Type 3 NPCs and their membrane resistance (160.4 ± 51.0 M Ω) was found to be intermediary between those of the Type 2 and 4 cells.

The I/V curves of Type 2–4 cells intersected the voltage axis at around -100 mV, indicating the involvement of potassium currents (reversal potential for potassium, -104 mV with the present extra- and intracellular medium). However, this was less clear for Type 1 cells, because of the strong outward rectification. Therefore, we used a tail current protocol (not shown), by clamping these cells for 50 ms from the holding potential to $+60$ mV, and then performing voltage steps from -120 to $+20$ mV in 10 mV

increments for 50 ms, with an interval of 0.2 s. We found that current reversal was in fact near the potassium equilibrium potential (-90.9 ± 0.6 mV, $n = 39$).

Our classification of cultured NPCs into 4 types is based on current- and voltage-step protocols and extends a previous classification based only on current-injection (Liu et al., 1999). Whereas Liu et al. (1999) discriminated spiking and non-spiking NPCs with outwardly rectifying properties, and an additional subgroup of “passive” NPCs, we found that NPCs with a quasi linear I/V curve may also generate rudimentary spikes.

3.3. P2X7 receptor-mediated current responses in cultured NPCs

We then locally applied by means of a fast superfusion system identical concentrations of ATP (1 mM; Fig. 3Aa) or Bz-ATP (300 μ M; Fig. 3Ba), both in the presence of a normal Ca^{2+} - (1 mM) and Mg^{2+} - (1.2 mM) containing aCSF and aCSF containing no Mg^{2+} and a low concentration of Ca^{2+} (0.1 mM) (low X^{2+} aCSF). Agonist application was for 5 s every min. As compared to normal aCSF, the ATP- (Fig. 3Ab) and Bz-ATP- (Fig. 3Bb) induced responses greatly increased in low X^{2+} aCSF. In this series and in all further experiments we never detected cells which were insensitive to ATP/Bz-ATP in low X^{2+} medium. Because of the potentiation of the nucleotide effects in low X^{2+} aCSF, all further electrophysiological measurements were carried out under these conditions, except when explicitly stated.

We found that the lack of the growth factors EGF and FGF-2 from the beginning of the 2nd until the end of the 4th day after plating the neurospheres in order to yield adherent cultures, led to a decrease of the Bz-ATP-induced currents, especially 3 days after their withdrawal (Fig. 3Ca, b). The omission of growth factors from the medium is known to initiate differentiation of NPCs. The lower activity of Bz-ATP could be prevented by re-applying EGF/FGF-2 to the culture medium daily (Fig. 3Ca, b). The properties of undifferentiated NPCs did not depend on the coating of the culture dishes; the current responses to Bz-ATP (300 μ M) were the same irrespective of whether PLO/fibronectin, laminin or collagen was used for coating (Fig. 3D).

Increasing concentrations of Bz-ATP (3–1000 μ M) were superfused (5 s application, 2-min intervals) onto NPCs in order to construct a concentration-response curve (Fig. 2Ea, b). After determining the EC_{50} and E_{max} values as well as the Hill coefficients (see Legend to Fig. 2), we slowly withdrew the patch pipette to detach the cell from the surrounding tissue. However, this procedure did not change the effect of Bz-ATP. Thus, Bz-ATP acted directly at the specific NPC from which we recorded current responses, rather than by releasing a signalling molecule from neighbouring cells which in turn activated this NPC. Importantly, the Bz-ATP concentration of 300 μ M used throughout the experiments was submaximal and therefore suitable to measure both potentiation and inhibition of P2X7 receptor currents. Current amplitudes in Fig. 3Eb were expressed in pA rather than pA/pF for better comparability of the whole-cell currents and the currents at detached patches, where C_m is rather meaningless.

Although the concentration-response curve constructed for Bz-ATP did not show a clear maximum at 1000 μ M (Fig. 3Eb), we did not investigate the effects of higher concentrations of this agonist. We wanted to avoid a possible cell-damage of the NPCs, which – albeit at a longer time-scale – could be demonstrated by the MTT cell viability method (see Fig. 9A), and probably would impede the reliable determination of Bz-ATP currents. Otherwise all parameters characterizing the BzATP concentration-response curve correspond reasonably well to those obtained in a low X^{2+} extracellular medium at native P2X7 receptors of rat astrocytes (Nörenberg et al., 2010; Oliveira et al., 2011). Thus, we decided to

use 1000 μ M Bz-ATP as the highest agonist concentration both for the patch-clamp recordings and the measurements of $[\text{Ca}^{2+}]_i$ transients throughout this study.

Since the Bz-ATP- (300 μ M) induced current measured at holding potentials between -80 and $+60$ mV reversed polarity near 0 mV (-9.8 ± 4.6 mV; $n = 8$; $P > 0.05$; Mann–Whitney test) (Fig. 4Aa, b) (corresponding to the reversal potential of non-selective cationic currents), a pre-requisite for the involvement of P2X receptors was fulfilled. Neither ATP (300–3000 μ M; $n = 5–10$) nor Bz-ATP (100–1000 μ M; $n = 5–10$) caused any current response in cells from P2X7 $^{-/-}$ mice, whereas these agonists were fully active in the wt C57BL/6 animals (Fig. 4Ba–c), another strong argument in favour of the presence of a functional P2X7 receptor in wt animals. The concentration-response curves for ATP (30–10,000 μ M) and Bz-ATP (3–1000 μ M) revealed a higher efficiency of Bz-ATP as compared to ATP. The failure, however, to reach a maximum effect with Bz-ATP concentrations up to 1000 μ M prevented the calculation of the usual parameters characterizing concentration-response curves (but see Fig. 3Eb). Nonetheless, the ATP currents were considerably smaller at 100–1000 μ M than the corresponding Bz-ATP currents (Fig. 4Bc).

We hypothesized that P2Y₁ receptors (increasing $[\text{Ca}^{2+}]_i$ by release from intracellular stores) and P2X7 receptors (increasing $[\text{Ca}^{2+}]_i$ by allowing its entry from the extracellular space) may interact with each other. However, the effects of the non-selective P2 receptor agonist ATP (1 mM) and the more selective P2X7 agonist Bz-ATP (300 μ M), remained both unaltered on NPCs prepared from either P2Y₁ $^{-/-}$ or the wt backgrounds (Fig. 4Ca, b).

In the following experiments, pharmacological tools were employed to further identify the P2 receptor subtype involved. The repetitive application of Bz-ATP (300 μ M) with the usual protocol (5 s application, 2 min intervals) caused stable currents from the 3rd response onwards (Fig. 5Aa, b). Low concentrations of the selective P2X7 antagonist Brilliant Blue G (BBG; 0.1–1 μ M) tended to potentiate the effect of Bz-ATP (still below the level of statistical significance; Fig. 5Bc), whereas high concentrations of BBG (3–10 μ M) were inhibitory (Fig. 5Ba–c). These effects became more pronounced when the highly selective P2X7 antagonist A-438079 (0.01–10 μ M) was applied instead of BBG. The triphasic action of A-438079 (and possibly BBG) may be due to an interplay between allosteric modulation and competitive antagonism (Fig. 5C). According to our expectations the non-selective P2X/Y antagonist PPADS (30 μ M) depressed the Bz-ATP (300 μ M) responses; TNP-ATP at 10 μ M, but not at 3 μ M was inhibitory (Fig. 5D). 5-BDBD (3, 30 μ M) and ivermectin (3 μ M) failed to interfere with Bz-ATP. At high concentrations TNP-ATP is an antagonist for P2X4 and to a lower extent also for P2X7 receptors; 5-BDBD is supposed to be a highly selective blocker and ivermectin a positive allosteric modulator of P2X4 receptors (Jarvis and Khakh, 2009). Two negative allosteric modulators of P2X7 receptors, Zn^{2+} (100, 300 μ M) and protons (acidification to pH 6.4) (Jarvis and Khakh, 2009) interacted with Bz-ATP in the expected inhibitory manner. We thus conclude that NPCs are endowed with P2X7 but not P2X4 receptors. Neither the P2X_{1,3} agonist α, β -methylene ATP (3, 10 μ M) nor 2-methylthio ATP (3, 30 μ M), which prefers P2X over P2Y receptors, but still activates e.g. P2Y₁ receptors with considerable potency, caused an inward current in a normal or low X^{2+} extracellular medium (Supplementary Fig. 1).

Thereafter, we investigated whether nucleotides are the only agonists to influence the holding current of the undifferentiated NPCs (Supplementary Fig. 1). The ionotropic glutamate receptor agonists AMPA (100 μ M) and NMDA (100 μ M) were also without effect. The GABA_A receptor agonist muscimol (30 μ M) caused small current responses (-4.2 ± 1.1 pA/pF; $n = 12$; $P < 0.05$ from zero;

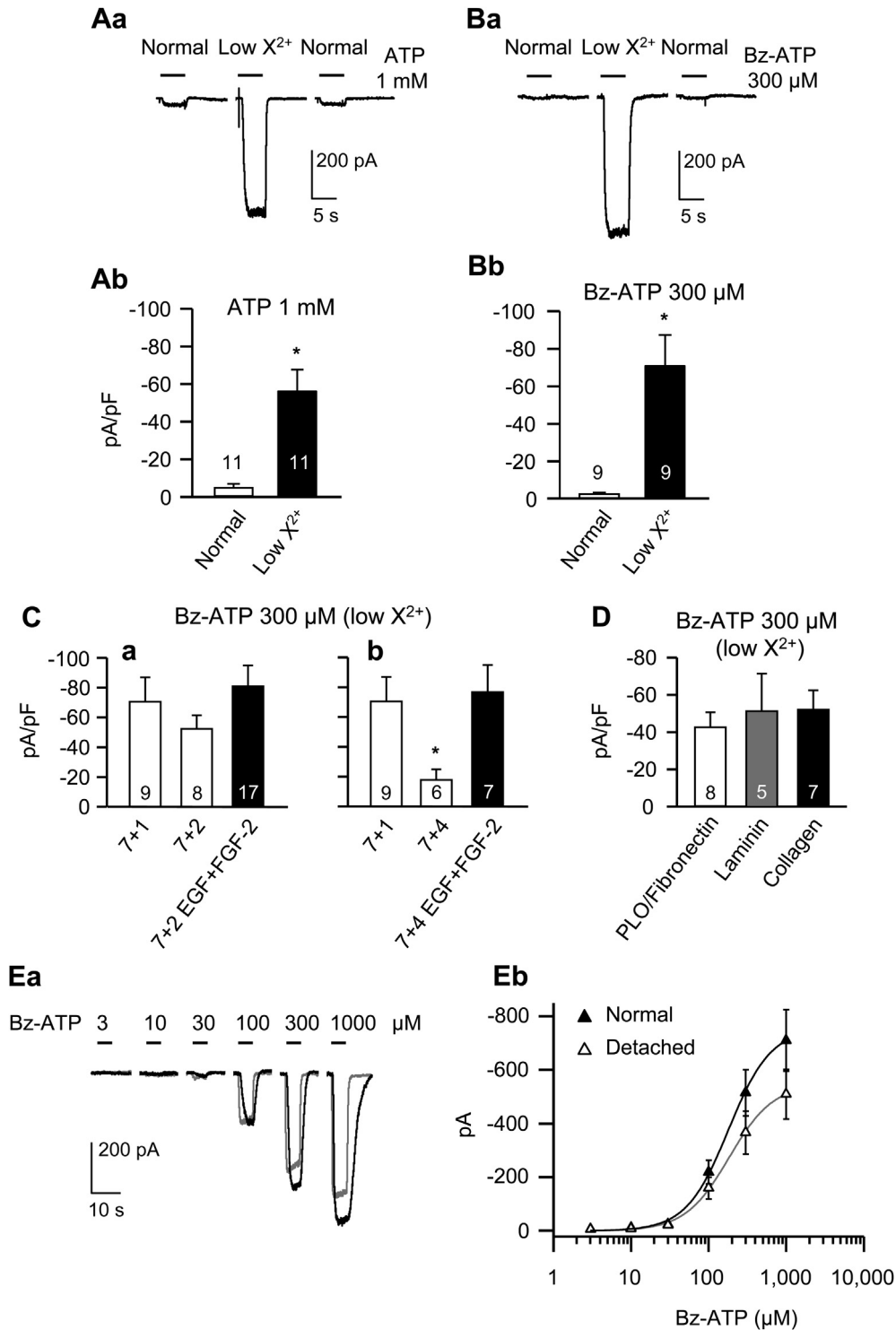


Fig. 3. ATP- and Bz-ATP-induced currents of undifferentiated NPCs; dependence on the composition of the extracellular medium, the coating of the dishes and the existence of a surrounding cell population. The holding potential in the whole-cell mode of the patch-clamp recordings was -80 mV. Individual concentrations of the two agonists were applied every 1 min for 5 s. (A) Effect of ATP (1 mM) in a normal and low divalent cation- (low X²⁺) containing extracellular medium. Representative tracing of 1 cell (a) and mean \pm S.E.M. current of 11 cells (b). (B) Effect of Bz-ATP (300 μ M) under similar conditions; representative tracing of 1 cell (a) and mean \pm S.E.M. current of 9 cells (b). * $P < 0.05$; in both Ab and Bb, statistically significant difference from the group "normal" (Mann–Witney test) (C) Effect of Bz-ATP (300 μ M) on NPCs 1 (a) and 3 (b) days after withdrawing growth factors, as well as after their re-application every day. The growth factors EGF and FGF-2 were routinely present in the medium during the culturing of neurospheres for 7 days. Then, the neurospheres were plated to yield NPCs, which were cultured for another day in the continued presence of growth factors ("7 + 1"). In the experiments shown, the growth factors were thereafter omitted for 1 or 3 days ("7 + 2" or "7 + 4"). Depression of the Bz-ATP currents under these conditions could be prevented by the daily re-application of EGF + FGF-2. * $P < 0.05$; statistically significant difference from the group "7 + 1" (measurements in the presence of growth factors; Dunn's test). (D) Effect of Bz-ATP (300 μ M) on NPCs cultured on dishes coated with poly-L-ornithin (PLO)/fibronectin, laminin, or collagen. There was no statistically significant difference between the individual groups ($P > 0.05$; one way ANOVA). (E) Concentration–response relationships for Bz-ATP at adhering (black) and detached NPCs (grey). Original tracings (a), and mean current responses of 5 cells before and after detachment (b). The number of cells tested is indicated in all columns. * $P < 0.05$; significantly different from the preceding column. The EC_{50} and E_{max} values as well as the Hill coefficients of the Bz-ATP concentration–response curves for the attached (181.8 ± 52.0 μ M; -754.3 ± 101.0 pA; 1.60 ± 0.53 , respectively; $n = 5$) and detached cells (EC_{50} , 185.1 ± 68.0 μ M; E_{max} , -546.2 ± 93.0 pA; Hill coefficient, 1.53 ± 0.62 ; $n = 5$; $P > 0.05$; Student's t -test) did not differ from each other.

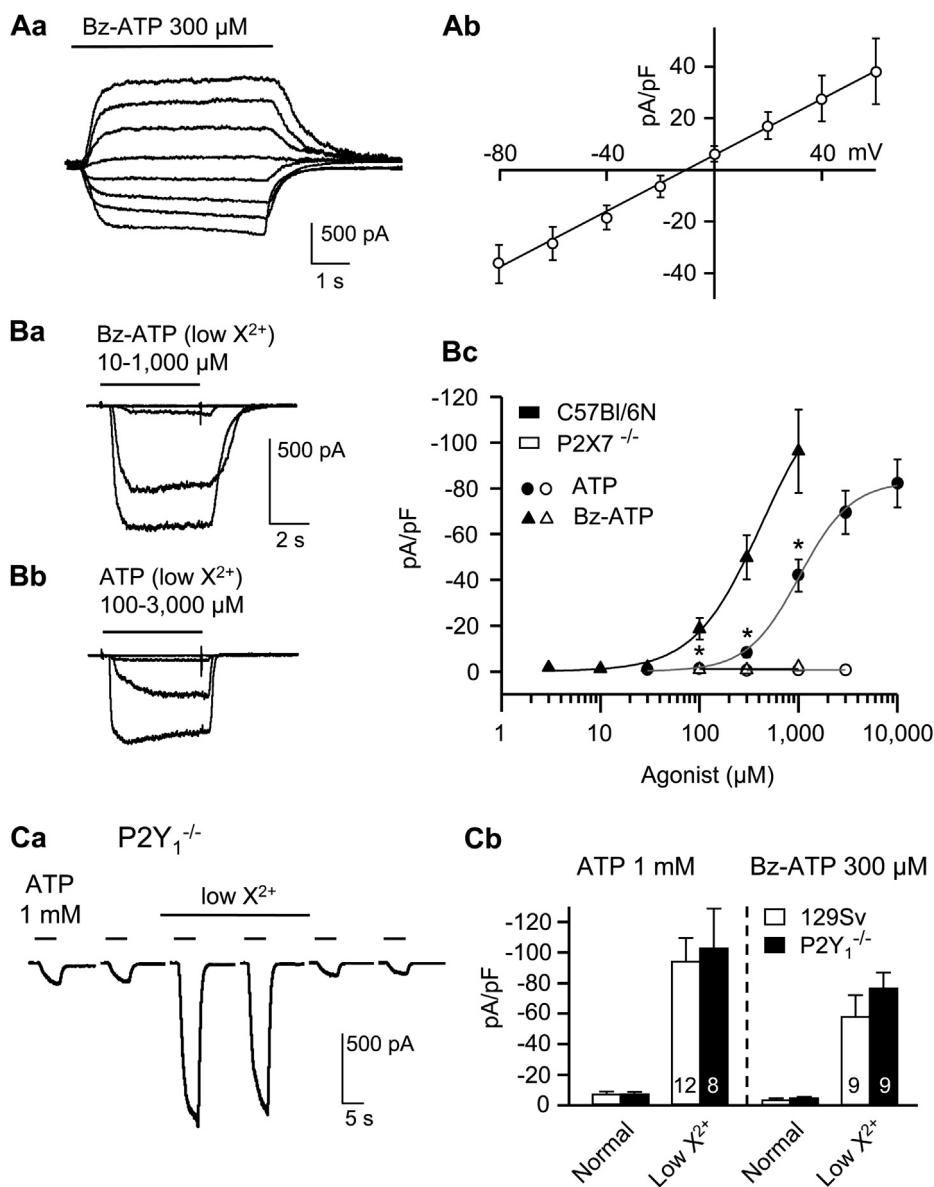


Fig. 4. Mediation of ATP- and Bz-ATP-induced currents in undifferentiated NPCs by P2X7 receptors. Individual concentrations of the two agonists were applied every 2 min for 5 s. (A) Current responses to consecutive applications of Bz-ATP (300 μ M), at 8 different holding potentials changed between -80 and $+60$ mV in 20 mV increments. Original tracings for 1 cell (a) and mean \pm S.E.M. of the peak current amplitudes for 8 cells (b). (B) Concentration–response relationships for Bz-ATP and ATP at NPCs prepared from wild-type (wt; C57Bl/6N) and P2X7 $^{-/-}$ mice. Representative recordings of the application of increasing concentrations of Bz-ATP (a) and ATP (b) at a holding potential of -80 mV. Amplitudes of current responses plotted against the logarithmic concentrations of Bz-ATP ($n = 12$) and ATP ($n = 10$) in wt mice; inefficiency of the two agonists in P2X7 $^{-/-}$ mice ($n = 5–10$ each)(c). * $P < 0.05$; statistically significant difference from the effect of Bz-ATP at the same concentration (Mann–Whitney test). (C) ATP- (1 mM) and Bz-ATP (300 μ M)-induced currents at NPCs prepared from wt and P2Y $_1^{-/-}$ mice. Original tracing for ATP in a P2Y $_1^{-/-}$ NPC (a), and mean \pm S.E.M. current responses for ATP and Bz-ATP in wt (129Sv) as well as P2Y $_1^{-/-}$ NPCs, both in normal and low X^{2+} extracellular solution (b). The number of cells tested is indicated in the columns. There was no statistically significant difference between knockout and wildtype animals in either normal or low X^{2+} groups for both ATP and Bz-ATP. (Student's t -test).

Mann–Whitney test). In a low X^{2+} extracellular medium, in which we observed a large response to Bz-ATP (300 μ M; -55.8 ± 6.8 pA/pF; $n = 27$), only NMDA (100 μ M; -2.8 ± 0.5 pA/pF; $n = 12$; $P < 0.05$; Mann–Whitney test) became active (see also Supplementary Fig. 1). It is possible that the appearance of a small NMDA effect is due to the unblocking of these receptor-channels in a Mg^{2+} -free superfusion medium. We do not know why the effect of muscimol has been abolished under the low X^{2+} conditions. The failure or very low activity of the ionotropic glutamate or GABA $_A$ receptor agonists to induce current responses in NPCs further emphasizes the significance of ATP as an extracellular signalling molecule in this cell type.

P2X7 receptors in macrophages or lymphocytes were reported to dilate during long-lasting application of high ATP or Bz-ATP concentrations (Ferrari et al., 2006). This effect is, however, by no way a general phenomenon and not valid for all native P2X7 receptors (Nörenberg et al., 2010). In fact, when the superfusion-time of Bz-ATP (300 μ M) onto NPCs was consecutively increased from 2 s to 120 s, up to 10 s an early peak amplitude followed by a slowly developing steady-state amplitude was observed (Fig. 6A). Then, both the early peak and the maximum steady state response consecutively decreased resulting in smaller and rather constant current amplitudes. Repetitive applications of Bz-ATP (300 μ M) for 30 s or longer time-periods resulted in a decrease in the

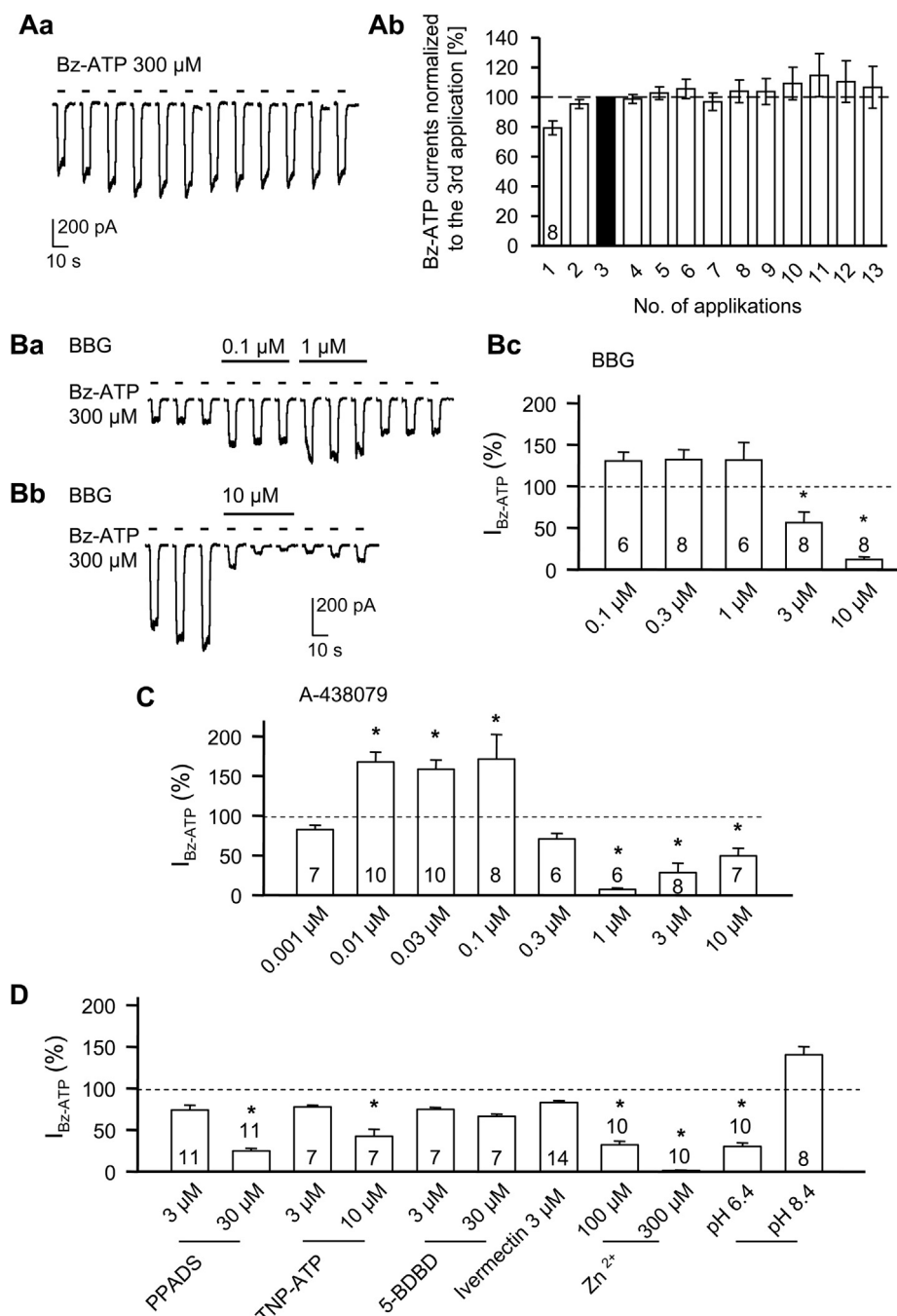


Fig. 5. Interaction between Bz-ATP and various antagonists/allosteric modulators of P2X receptors on undifferentiated NPCs at a holding potential of -80 mV. (A) Constancy of Bz-ATP ($300 \mu\text{M}$)-induced current responses; individual concentrations were applied every 2-min for 5 s. Original tracings of 1 cell (a) and means \pm S.E.M. of the percentage changes with respect to the 3rd application in 8 cells (b). There was no statistically significant difference between the currents throughout (Kruskal-Wallis ANOVA on Ranks). (B) Inhibition of the Bz-ATP ($300 \mu\text{M}$) current ($I_{\text{Bz-ATP}}$) by Brilliant Blue G (BBG; 0.1 – $10 \mu\text{M}$). Original tracings demonstrating the effect of BBG on the Bz-ATP-induced responses and their reversibility on washout (a, b; two different cells). Mean \pm S.E.M. of the percentage inhibitory effect of BBG calculated in comparison with the time-matched controls (c). (C) Experiments similar to those shown in Bc were also carried out with A-438079 (0.001 – $10 \mu\text{M}$). (D) Interaction between Bz-ATP ($300 \mu\text{M}$) and various antagonists/allosteric modulators of P2X receptors. These compounds were applied for 6 min at each concentration (see also in B and C). The drug effects were expressed as percentage changes in comparison with the time-matched controls. The number of cells tested is indicated in the columns. * $P < 0.05$; significantly different from time-matched controls in Bc, C and D (Holm–Sidak test).

amplitude of the current response (not shown, but see Fig. 6A). We therefore applied Bz-ATP ($300 \mu\text{M}$) in further experiments only a single time to each NPC for 120 s. In 7 out of 9 cells with the usual pipette solution containing EGTA (10mM) the current was larger at the end of a Bz-ATP pulse than at its beginning (Fig. 6Ba, b). In the residual 2 cells, there was no change in amplitude during 120-s of Bz-ATP application (Fig. 6Bc, d). When EGTA was substituted in the pipette solution for the more rapid Ca^{2+}

chelating agent BAPTA (5mM), in 10 out of 12 cells both the current shape and its increase from the early to the late amplitude was similar to that measured with intracellular EGTA (10mM ; Fig. 6Ca, b). In the residual 2 cells the current responses were again stable (Fig. 6Cc, d). We conclude that the P2X7 receptor channels dilated during the long-lasting application of Bz-ATP in most NPCs, and that this effect was basically independent of the intracellular Ca^{2+} concentration.

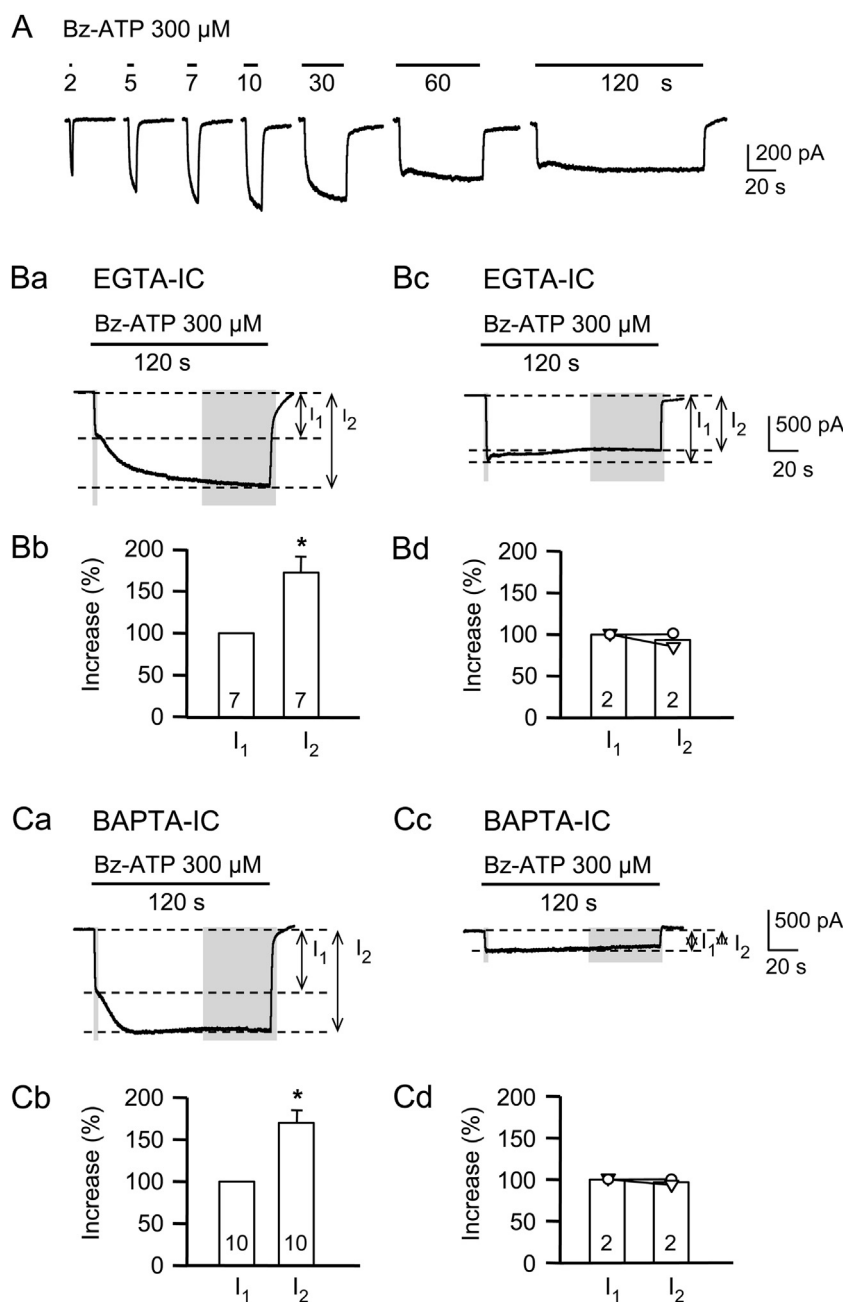


Fig. 6. Time-dependent changes in the amplitude of Bz-ATP currents of undifferentiated NPCs. The holding potential in the whole-cell mode of the patch-clamp recordings was -80 mV. (A) Increase of the application-time of Bz-ATP ($300 \mu\text{M}$) from 2 to 120 s; original tracings (one typical cell out of four similar ones). (B) Bz-ATP ($300 \mu\text{M}$)-induced initial (I_1) and steady-state currents (I_2) recorded by a patch-clamp pipette filled with intracellular (IC) solution containing EGTA (10 mM). The agonist was applied only once to each cell for 120 s. Two types of cells were identified. One of them responded with an I_1 which was smaller than its I_2 (a, original tracing; b, mean \pm S.E.M. 7 cells). The other one responded with nearly identical I_1 and I_2 (c, original tracing; d, mean percentage increase from I_1 to I_2 in 2 cells). (C) Experiments similar to those demonstrated in B, but with a patch-clamp pipette filled with intracellular solution containing BAPTA (5 mM) instead of EGTA (10 mM) (a–d). The number of experiments is indicated in the columns throughout. * $P < 0.05$; significantly different from the group “ I_1 ” (Mann–Whitney test).

3.4. P2X7 receptor-mediated increase of the intracellular Ca^{2+} concentration in cultured NPCs

The effect of Bz-ATP on the undifferentiated NPCs was also determined using Ca^{2+} -imaging. Opening of P2X7 receptor-channels allows the entry of Ca^{2+} from the extracellular space and thereby increases the intracellular Ca^{2+} concentration ($[\text{Ca}^{2+}]_i$), which is detected by the fluorescent indicator fura-2. As a first approach, we established conditions to minimize the stimulation of P2Y receptors by ATP and especially Bz-ATP. Bz-ATP ($300 \mu\text{M}$)

caused large $[\text{Ca}^{2+}]_i$ transients in a Mg^{2+} -free bath medium, that entirely depended on the presence of external Ca^{2+} , and therefore were due to P2X7 receptor-activation (Fig. 7). In a normal Ca^{2+} -containing and Mg^{2+} -free aCSF, the application of Bz-ATP ($300 \mu\text{M}$) with the usual protocol (10-s duration, 10-min intervals) and in the absence of any further drugs, caused slightly decreasing $[\text{Ca}^{2+}]_i$ transients from the 2nd response onwards (at 10-min, 100%; at 20-min, $93.2 \pm 0.6\%$; at 30-min, $86.6 \pm 0.8\%$; $n = 144$; $P < 0.05$ each; Dunn's test). This spontaneous decrease was corrected by comparing drug effects with their time-matching controls (see

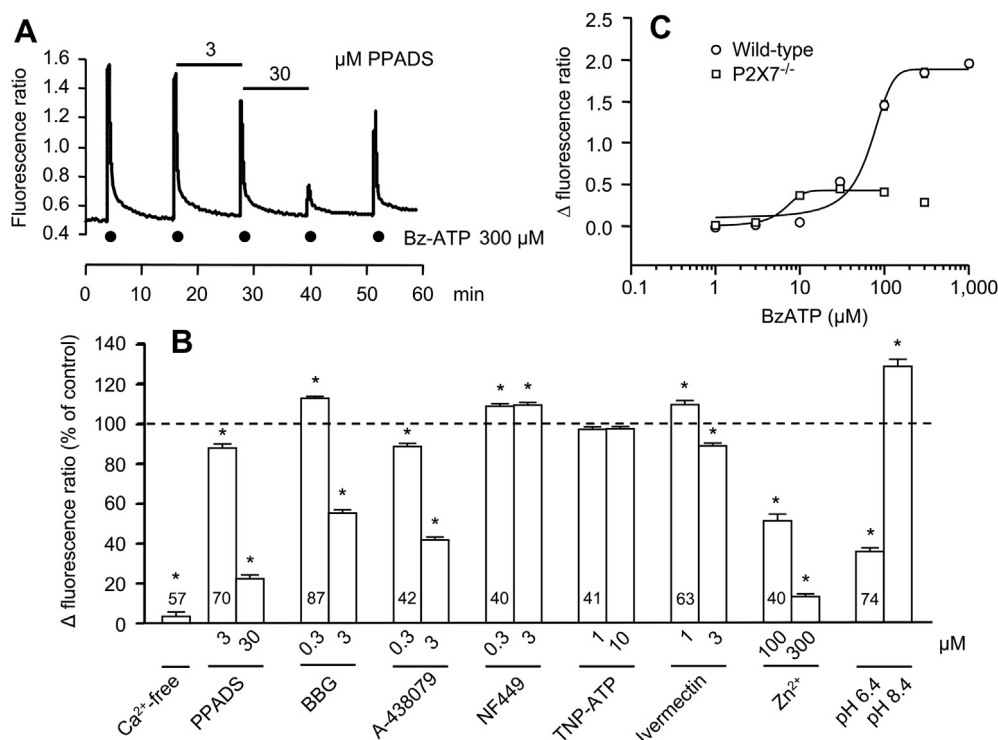


Fig. 7. Bz-ATP-induced increases of intracellular Ca²⁺ in undifferentiated NPCs. The fluorescence ratio (340/380 nm) measured after pre-incubation of NPCs with Fura-2 provides a relative measure of the cytosolic free Ca²⁺ concentration ([Ca²⁺]_i). Bz-ATP (300 μM) was applied for 10 s every 10 min in a Mg²⁺-free bath solution. (A) PPADS at 3 and 30 μM concentration-dependently depressed the Bz-ATP effect (original tracing). (B) Antagonists/allosteric modulators were applied in increasing concentrations according to the protocol shown in A (10-min superfusion). The drug effects were normalized to the 2nd application of the agonist after starting the experiment and were expressed thereafter as percentage changes of the time-matched normalized controls. The number of cells tested is indicated in the columns. *P < 0.05; significantly different from time-matched controls (Holm–Sidak test). (C) Concentration–response relationship for Bz-ATP on NPCs prepared from wild-type (wt) and P2X7^{-/-} mice and the respective plots of [Ca²⁺]_i transients against the logarithmic agonist concentrations. The EC₅₀, E_{max}, and Hill coefficients of the concentration–response curves were for the wt mouse 53.3 ± 2.2 μM, 1.95 ± 0.03 FR and 1.73 ± 0.09 (n = 59), and for the P2X7^{-/-} mice 5.5 ± 0.5 μM, 0.44 ± 0.01 FR, and 3.11 ± 0.48 (n = 60). The difference between the respective values is statistically significant (P < 0.05; Student's t-test).

Methods); no correction was applied for Bz-ATP concentration–response curves. The P2X/P2Y antagonist PPADS (3, 30 μM) concentration-dependently depressed the effect of Bz-ATP (Fig. 7A, B). The selective P2X7 receptor antagonists A-438079 (0.3, 3 μM) and BBG (3 μM) were also inhibitory (Fig. 7B). In agreement with the patch-clamp data, BBG at a lower concentrations (in this case 0.3 μM) slightly facilitated the Bz-ATP-induced [Ca²⁺]_i transients. Pharmacological blockers of P2X1 (NF449; 0.3, 3 μM), and P2X1,3,4 (TNP-ATP; 1, 10 μM) as well as the allosteric modulator of P2X4 (ivermectin; 1, 3 μM) exerted statistically significant but minor effects. Zn²⁺ and protons (pH 6.4) depressed the [Ca²⁺]_i responses to Bz-ATP; alkalization to pH 8.4 inverted the low pH-induced inhibition.

Increasing concentrations of Bz-ATP (3–1000 μM) were applied to construct a concentration–response relationship for NPCs of both wt and P2X7^{-/-} mice (Fig. 7C). The effect of Bz-ATP was considerably reduced but not entirely abolished in the knockout animals; the E_{max} value decreased to about 23% of its original size after the genetic deletion of P2X7 receptors (see Legend to Fig. 7C). In addition, the threshold concentration of Bz-ATP was lower in P2X7^{-/-} than in wt mice; Bz-ATP at 10 μM had already a maximum effect in the former but no effect in the latter strain. This was paralleled by a lower EC₅₀ value in the P2X7^{-/-} animals than in their wt counterparts. We suppose that in the knockout mice another P2X or P2Y receptor partially replaced the previous function of P2X7. However, further experiments classifying this receptor-type were considered not to be essential for the main message of the present study.

3.5. P2X7 receptor-mediated dye-uptake in cultured NPCs

The uptake of the fluorescent dye YO-PRO-1, which normally does not permeate the plasma membrane but passes through open P2X7 receptor-channels (Virginio et al., 1999), was used as a measure of channel-dilation during the long-lasting application of Bz-ATP (300 μM; Fig. 8). The YO-PRO-1 uptake was increased by Bz-ATP (300 μM) in NPCs prepared from wt mice (Fig. 8C). It did not change, however, when the same concentration of Bz-ATP was applied onto NPCs from P2X7^{-/-} animals. All data are expressed as arbitrary units (see Methods).

3.6. P2X7 receptor-mediated necrosis/apoptosis in cultured NPCs

As revealed by the MTT assay, Bz-ATP (30–1000 μM) induced a concentration-dependent decrease in NPC viability when cells were prepared from wt but not from P2X7^{-/-} mice (Fig. 9A). Bz-ATP was added to the cell culture medium and cell viability was determined 4 h after drug application.

Immunoreactivity for active caspase 3 (aCasp-3), a key enzyme for apoptosis, was also determined on NPCs (Fig. 9B). The qualitative evaluation of the images obtained indicates that Bz-ATP increased the aCasp-3 immunoreactivity at nestin-immunopositive cells in wt but not in P2X7^{-/-} NPCs, as compared to solvent-treated controls. We decided not to perform quantitative measurements in view of the repeatedly reported apoptotic activity of P2X7 receptors in various cell types including astrocytes (Illes et al., 2012; Franke et al., 2012) and even embryonic NPCs (Delarasse et al., 2009, 2011).

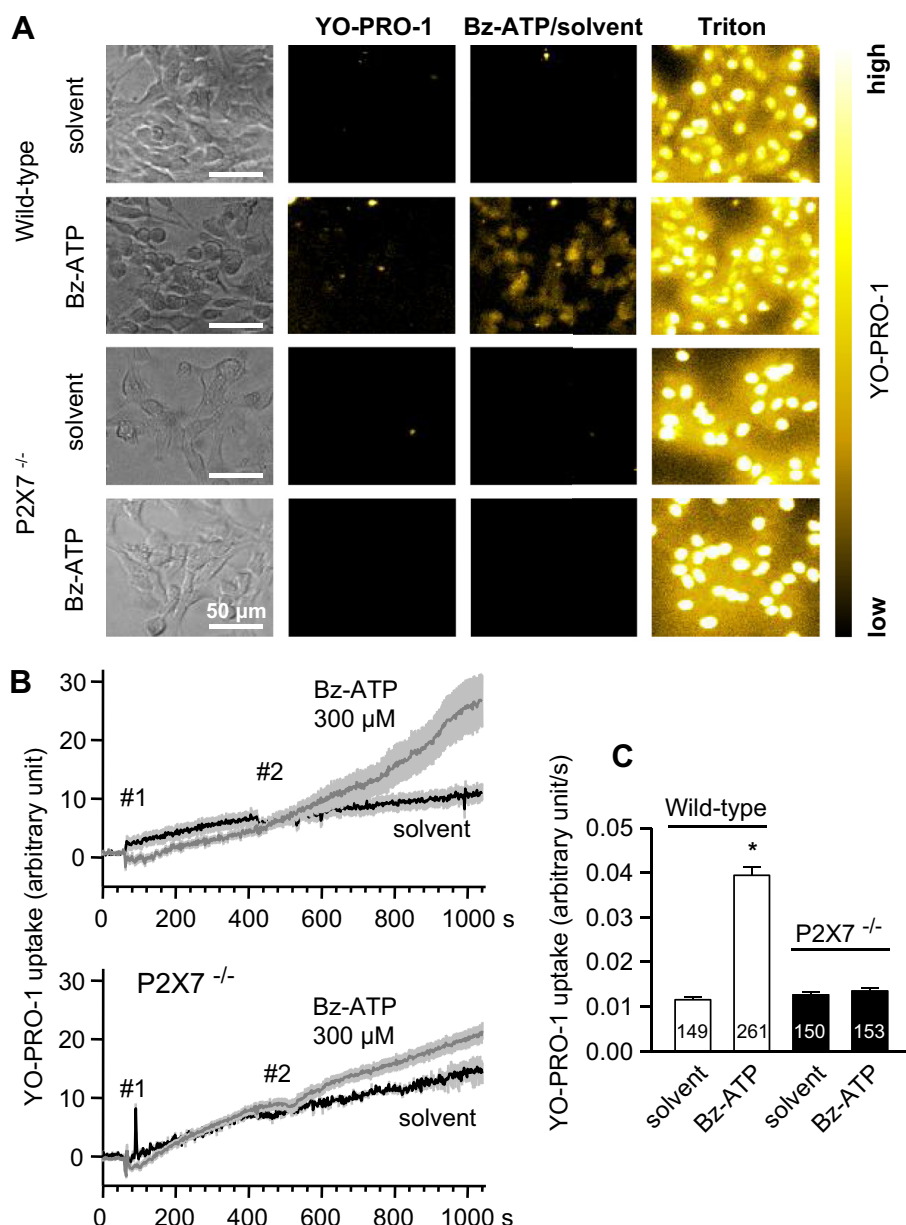


Fig. 8. Increase of YO-PRO-1 fluorescence in undifferentiated NPCs of wild-type (wt) mice but not of their P2X7 receptor-deficient (P2X7^{-/-}) counterparts in a low X²⁺ medium. (A) Representative pictures at different time points from movies recording YO-PRO-1 uptake in NPCs of wt and P2X7^{-/-} mice. The first column shows phase contrast photomicrographs of adherent NPCs before starting the experiment. The second column shows fluorescence photomicrographs of the NPCs of the first column after the addition of YO-PRO-1 (2 μM) at time point 200 s. The photomicrographs of the third column show the YO-PRO-1 fluorescence intensity after addition of Bz-ATP (300 μM) or low X²⁺ aCSF (solvent; time point, 960 s). The last columns show YO-PRO-1 fluorescence intensity at a time point of 1100 s, after the addition of the detergent Triton X-100. (B) Representative tracings (mean ± S.E.M, in arbitrary units) showing YO-PRO-1 uptake over time in 30 cells for each experimental condition. After 60 s, YO-PRO-1 (2 μM) was added (#1). After 420 s Bz-ATP (300 μM) in low X²⁺ aCSF, or low X²⁺ aCSF alone (solvent) was added (#2). (C) Summary of YO-PRO-1 uptake experiments showing the slope (arbitrary unit/s) of YO-PRO-1 fluorescence increase in NPCs of wt and P2X7^{-/-} mice after addition of Bz-ATP or the solvent. Mean ± S.E.M.; slope measured between 500 and 1000 s; number of cells indicated at the bottom of the bars from 5 to 9 independent experiments; *P < 0.05; statistically significant difference between solvent and Bz-ATP-stimulated cells in wt mice (Dunn's test). Note that A and B show arbitrary units, whereas C shows their change per second.

3.7. P2X7 receptor-mediated current responses in NPCs of subventricular zone brain slices

Based on their green fluorescence, NPCs in brain slices of Tg(nestin/EGFP) mice were localized below the layer of ependymal cells (Fig. 10Aa, b). NPCs did not fire action potentials in response to depolarizing current injection and exhibited an outwardly rectifying voltage–current pattern (Fig. 10Ba, b). Thereby, they conformed to the type-2 NPCs described in the SVZ (Wang et al., 2003) and the subgranular zone of the dentate gyrus (Filippov et al., 2003; defined as glia-like progenitors (Lacar et al., 2010).

At a holding potential of –80 mV BzATP (300 μM) caused a small inward current response only, which however strongly increased when normal aCSF was changed to a low X²⁺ medium containing no Mg²⁺ and only 0.5 mM Ca²⁺ instead of the original 2.4 mM Ca²⁺ (Fig. 10Bc, d). In spite of the gradual potentiation of the BzATP current, a steady-state might be reached after 5 min (see Fig. 10Ca, b). In this second series of experiments, brain slices were superfused with zero Mg²⁺/0.5 mM Ca²⁺ aCSF for 5 min, before BzATP was applied for the first time. The BzATP current remained stable with two subsequent agonist applications, indicating maximum potentiation. Two-min superfusion with the inhibitor A438079

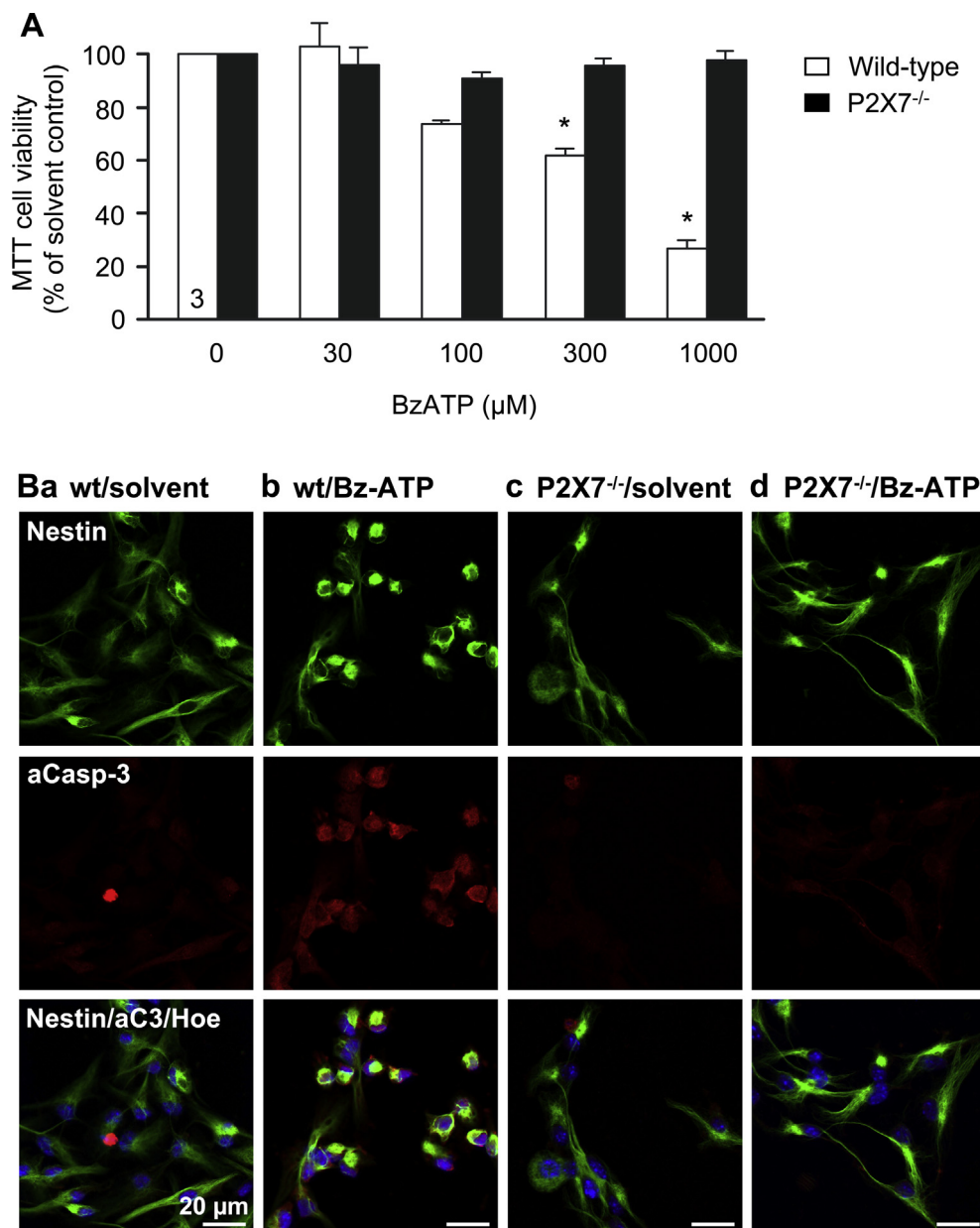


Fig. 9. Necrotic/apoptotic effects of Bz-ATP in NPCs in undifferentiated NPCs of wild-type (wt) mice but not of their P2X7 receptor-deficient (P2X7^{-/-}) counterparts in a normal X²⁺ culture medium. (A) After 2-h of incubation, Bz-ATP (30–1000 μM) concentration-dependently decreases the MTT cell viability of the wt preparations, in comparison with the respective solvent controls. Solvent controls were set as 100% and measurements in the presence of the indicated concentrations of Bz-ATP were normalized to this value. Mean ± S.E.M of 3 independent experiments. **P* < 0.05; statistically significant difference both from wt solvent controls and from effects of the respective Bz-ATP concentrations at NPCs of P2X7^{-/-} mice (Holm–Sidak test). (B) After 2-h of incubation, Bz-ATP (300 μM) increases the active caspase 3 (aCasp-3) immunoreactivity in nestin-immunopositive wt NPCs (Ba, b). There was no comparable effect in the P2X7^{-/-} mice (Bc, d). Hoechst 33342 (Hoechst) was used to label the cell nuclei in the lowest panels of each row; scale bars for all panels were 20 μm, as indicated.

(10 μM) depressed the response to BzATP (Fig. 10Cb). This effect was fully reversible on washout.

4. Discussion

Here we demonstrate that multipotent NPCs cultured from adult mouse brain as well as NPCs expressing green fluorescent protein under the control of the nestin promoter in the SVZ of acute striatal slices express functional P2X7 receptors. The activity of this apoptotic/necrotic receptor may counteract the excessive proliferation of NPCs under pathological conditions.

Out of the identified signals regulating the proliferation, differentiation and migration of NPCs, purine and pyrimidine nucleotides

are of particular significance (Zimmermann, 2011). ATP is released from mouse NPCs, and feeds back to regulate cell proliferation, before its degradation to inactive metabolites is initiated by ATP hydrolysing enzymes sharply localized to the neurogenic zones of the brain (Braun et al., 2003; Lin et al., 2007; Suyama et al., 2012).

Isolated primary neurospheres of the adult mouse SVZ possess mRNA for all P2Y receptor-types with the exception of P2Y₄ (Mishra et al., 2006; Grimm et al., 2009). Intermediate neural embryonic progenitors originating from the SVZ were shown to express functional P2Y₁ receptors (Mishra et al., 2006) and P2Y₁ receptor-immunoreactivity (Liu et al., 2008). Both P2Y₁ and P2Y₂ receptors were found to be involved in regulating proliferation and migration of adult NPCs (Zimmermann, 2011).

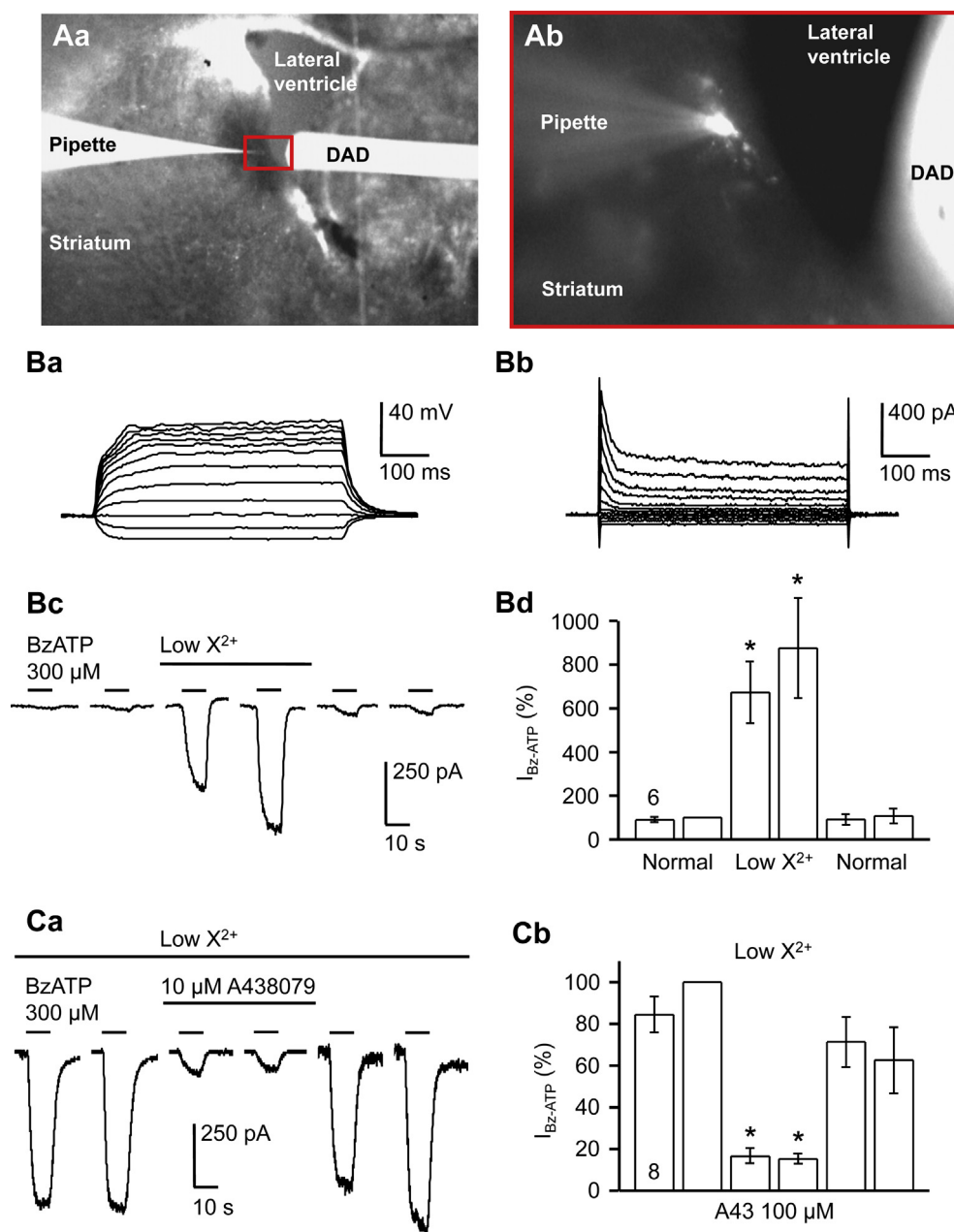


Fig. 10. Bz-ATP-induced currents of NPCs located in brain slices of the subventricular zone prepared from Tg(nestin/EGFP) mice; dependence on the composition of the extracellular medium and mediation by P2X7 receptors. The membrane potential of all NPCs varied between -47 and -78 mV (14 cells). The holding potential in the whole-cell mode of the patch-clamp amplifier was -80 mV. (A) Localization and shape of the patched NPCs. Light/fluorescence microscopic image ($4\times$ magnification) (a) and fluorescence microscopic image ($40\times$ magnification of the boxed part of a) (b). DAD, DAD-12 local application pipette. (B) Injection of hyper- and depolarizing current pulses at the resting membrane potential of -52 mV caused passive, electrotonic responses (the current pulses were changed by 20 pA increments between -40 and -180 pA and were applied for 500 ms) (a). Delivery of voltage steps changed by 10 mV increments between -90 and 10 mV from a holding potential of -50 mV (b). The voltage–current relationships were outwardly rectifying. Low divalent concentration-containing medium (low X^{2+}) strongly increased the effect of Bz-ATP (300 μ M); representative tracing of 1 cell (c) and mean \pm S.E.M. current of 7 cells normalized to the 2nd current amplitude (d). (C) A438079 (10 μ M) depressed the effect of BzATP (300 μ M). Representative tracing of 1 cell (a) and mean \pm S.E.M. current of 8 cells normalized to the 2nd current amplitude (b). Bz-ATP was applied every 2 min for 10 s. Horizontal lines indicate the superfusion times of pharmacological ligands and a low X^{2+} medium. $*P < 0.05$; significantly different from 100% (Dunn's test).

In contrast to the abundant information on P2Y receptors at NPCs, similar data are scarce for P2X receptors. Patch-clamp measurements at mouse ependymal cells localized along the lateral cerebral ventricle demonstrate the presence of Bz-ATP sensitive P2X7 receptors mediating ATP/Bz-ATP-induced inward currents. These results were supported by immunohistochemical experiments and measurements of Bz-ATP-induced $[Ca^{2+}]_i$ transients (Genzen et al., 2009). Because ependymal cells cover the ventricle wall and are in immediate contact with neural progenitors of the

SVZ, it was suggested that P2X7 receptors may play a role in NPC reaction to injury and inflammation.

Experiments using undifferentiated NPCs from the rat hippocampus are in agreement with but do not prove the existence of functional P2X7 receptors at this cell type; Bz-ATP caused an inward current which was abolished by the non-selective P2 antagonist PPADS (Hogg et al., 2004). Moreover, high concentrations of ATP induced current responses with a reversal potential around 0 mV in NPCs in dentate gyrus slices of mice whose NPCs expressed

nestin promoter-driven green fluorescent protein (Shukla et al., 2005). This effect was apparently due to P2X receptor-stimulation but the receptor subtype involved was not characterized.

Our experiments identified for the first time P2X7 receptors at adult SVZ NPCs, both *in vitro* and in acute slices. These receptors became strongly functional only in low X^{2+} external medium. Originally it was assumed that ATP acts at P2X7 receptors as ATP^{4-} and therefore the chelation with divalent cations would decrease the concentration of the active agonist form in the cellular micro-environment (Jiang, 2009). More recently, it has been shown that Ca^{2+} affects the receptor function by acting as an allosteric modulator (Yan et al., 2011) rather than by altering the permeability dynamics of the ion channel (Khakh et al., 1999a).

In addition to the potentiation of the ATP/Bz-ATP-induced current responses, a whole range of data strongly suggests that P2X7 receptors were involved in the effects observed in this study. (1) Bz-ATP was more potent than ATP itself (Sperlágh et al., 2006; Anderson and Nedergaard, 2006). (2) The general P2X/P2Y antagonist PPADS as well as the selective P2X7 receptor antagonists BBG and A-438079 counteracted the effects of Bz-ATP. (3) The prominent blockade of the Bz-ATP response by Zn^{2+} and H^+ further identifies the receptor as belonging to the P2X7 type (Stoop et al., 1997). (4) Long-lasting application of Bz-ATP caused an early peak current amplitude followed by a larger, late steady-state amplitude. We suggest that this is due to the time-dependent dilation of the P2X7 receptor-channel observed in whole-cell recording conditions (Virginio et al., 1999; Yan et al., 2010). Although fluorescent dyes, after receptor-activation by Bz-ATP, were reported to permeate through pannexin-1 channels instead of the receptor-channels itself (Pelegrin and Surprenant, 2006), our results demonstrating an increased YO-PRO-1 uptake into NPCs, equally concord with the involvement of P2X7 receptors. (5) The MTT viability test and the analysis of active caspase 3 immunoreactivity indicated that Bz-ATP at adult neural NPCs causes necrosis/apoptosis in agreement with similar findings raised in embryonic NPCs (Delarasse et al., 2009, 2011).

The Bz-ATP-induced current reversed near 0 mV and was thereby certainly due to the opening of P2X receptor-channels. This effect persisted in detached NPCs excluding the possibility that a P2X receptor-mediated release of an unidentified signalling molecule from neighbouring cells was the primary cause of NPC activation. We were especially interested to find out, whether P2X4 receptors co-exist with P2X7 receptors (Antonio et al., 2011); this is, however, most unlikely, in view of the lack of the effect of ivermectin (Khakh et al., 1999b) and 5-BDBD on the Bz-ATP-induced current responses.

Four further observations still require explanation. (1) Already 3-days culturing of in an EGF/FGF-2-free medium decreased the Bz-ATP-induced current amplitudes; this effect was fully reversible upon reapplication of the growth factors. We assume that the density of P2X7 receptors decreased as a first sign of cellular differentiation. (2) The P2X7 receptor-mediated currents did not change when the coating of culture dishes was changed from fibronectin to laminin or collagen. Hence, cell matrix molecules such as integrins, which bind to fibronectin *via* their RGD (Arg-Gly-Asp) motifs, do not seem to alter P2X7 receptor-density (for P2X4 see Tsuda et al., 2008). (3) P2Y₁ receptors present at mouse NPCs and increasing $[Ca^{2+}]_i$ (Mishra et al., 2006; Zimmermann, 2011) failed to interact with P2X7 receptors. By contrast, a negative interaction between P2Y₁ and P2X₃ receptors was previously demonstrated in rat dorsal root ganglion neurons (Gerevich et al., 2007). (4) Repetitive application of the same Bz-ATP concentration resulted in stable current amplitudes. This finding disagrees with the reported increase of Bz-ATP- and ATP-currents at recombinant rat P2X7 receptors transfected in HEK293 cells, and was ascribed to the stimulation of a C-terminal calmodulin binding site of the receptor (Roger et al., 2008). However, in native cell-types

such as cortical or hippocampal astrocytes, no comparable facilitation was observed either in a normal or a low X^{2+} external medium (Oliveira et al., 2011; Leichsenring et al., 2013).

The measurement of $[Ca^{2+}]_i$ transients in NPCs basically supported the electrophysiological data. In Mg^{2+} -free extracellular solution, Bz-ATP increased $[Ca^{2+}]_i$ solely by opening P2X receptor-channels, which allowed the entry of Ca^{2+} from the extracellular space. All agonists and allosteric modulators acted in the expected manner. In addition, the Bz-ATP-induced $[Ca^{2+}]_i$ transients were markedly decreased, although not abolished in NPCs of P2X7^{-/-} mice. We assume that in the knockout mice another P2X or P2Y receptor partially replaced the previous function of P2X7. However, characterization of this type of receptor was outside of the scope of the present study.

Culturing NPCs may change their characteristics making it difficult to draw firm conclusions regarding their *in situ* properties. We therefore recorded membrane currents from NPCs in SVZ brain slice preparations obtained from Tg(nestin/EGFP) mice. Importantly, the current–voltage characteristics of these cells corresponded to that of a subgroup of cultured NPCs; moreover, all of the cells recorded were endowed with functional P2X7 receptors.

Prolonged seizures were reported to increase the expression of P2X7 receptors in the hippocampus and the injection of P2X7 receptor antagonists suppressed seizures (Engel et al., 2012a, b; Klafit et al., 2012). In the present study, conditions known to increase the susceptibility for neuronal discharges/seizures, such as a low concentration of divalent cations in the extracellular medium (Heinemann et al., 1992), or its alkalisation (Schuchmann et al., 2006), largely increased the sensitivity of P2X7 receptors to ATP. It has been found that excessive neuro- and/or gliogenesis is induced by CNS damage due to traumatic brain injury (Yu et al., 2008), hypoxia/ischemia (Kunze et al., 2006), and epileptic seizures (Hüttmann et al., 2003). We hypothesize that the apoptotic/necrotic P2X7 receptors may counterregulate progenitor cell survival under these pathological conditions.

Acknowledgements

This work was supported by a grant of the Deutsche Forschungsgemeinschaft to P.I. and W.N. (IL 20/19–1). We thank Prof. Helmut Kettenmann, Berlin for the generous supply of transgenic Tg(nestin/EGFP) mice and Christoph Hempel for expert methodological support.

Appendix A. Supplementary data

Supplementary data related to this article can be found at <http://dx.doi.org/10.1016/j.neuropharm.2013.05.017>.

References

- Abbracchio, M.P., Burnstock, G., 1994. Purinoceptors: are there families of P2X and P2Y purinoceptors? *Pharmacol. Ther.* 64, 445–475.
- Abbracchio, M.P., Burnstock, G., Boeynaems, J.M., Barnard, E.A., Boyer, J.L., Kennedy, C., Knight, G.E., Fumagalli, M., Gachet, C., Jacobson, K.A., Weisman, G.A., 2006. International Union of Pharmacology LVIII: update on the P2Y G protein-coupled nucleotide receptors: from molecular mechanisms and pathophysiology to therapy. *Pharmacol. Rev.* 58, 281–341.
- Anderson, C.M., Nedergaard, M., 2006. Emerging challenges of assigning P2X7 receptor function and immunoreactivity in neurons. *Trends Neurosci.* 29, 257–262.
- Antonio, L.S., Stewart, A.P., Xu, X.J., Varanda, W.A., Murrell-Lagnado, R.D., Edwardson, J.M., 2011. P2X4 receptors interact with both P2X2 and P2X7 receptors in the form of homotrimers. *Br. J. Pharmacol.* 163, 1069–1077.
- Brass, D., Grably, M.R., Bronstein-Sitton, N., Gohar, O., Meir, A., 2012. Using antibodies against P2Y and P2X receptors in purinergic signaling research. *Purinergic Signal* 8 (Suppl. 1), 61–79.
- Braun, N., Seigny, J., Mishra, S.K., Robson, S.C., Barth, S.W., Gerstberger, R., Hammer, K., Zimmermann, H., 2003. Expression of the ecto-ATPase NTPDase2

- in the germinal zones of the developing and adult rat brain. *Eur. J. Neurosci.* 17, 1355–1364.
- Burnstock, G., Krügel, U., Abbraccio, M.P., Illes, P., 2011. Purinergic signalling: from normal behaviour to pathological brain function. *Prog. Neurobiol.* 95, 229–274.
- Delarasse, C., Gonnord, P., Galante, M., Auger, R., Daniel, H., Motta, I., Kanellopoulos, J.M., 2009. Neural progenitor cell death is induced by extracellular ATP via ligation of P2X7 receptor. *J. Neurochem.* 109, 846–857.
- Delarasse, C., Auger, R., Gonnord, P., Fontaine, B., Kanellopoulos, J.M., 2011. The purinergic receptor P2X7 triggers alpha-secretase-dependent processing of the amyloid precursor protein. *J. Biol. Chem.* 286, 2596–2606.
- Doetsch, F., 2003. The glial identity of neural stem cells. *Nat. Neurosci.* 6, 1127–1134.
- Engel, T., Gomez-Villafuertes, R., Tanaka, K., Mesuret, G., Sanz-Rodriguez, A., Garcia-Huerta, P., Miras-Portugal, M.T., Henshall, D.C., Diaz-Hernandez, M., 2012a. Seizure suppression and neuroprotection by targeting the purinergic P2X7 receptor during status epilepticus in mice. *FASEB J.* 26, 1616–1628.
- Engel, T., Jimenez-Pacheco, A., Miras-Portugal, M.T., Diaz-Hernandez, M., Henshall, D.C., 2012b. P2X7 receptor in epilepsy: role in pathophysiology and potential targeting for seizure control. *Int. J. Physiol. Pathophysiol. Pharmacol.* 4, 174–187.
- Fabre, J.E., Nguyen, M., Latour, A., Keifer, J.A., Audoly, L.P., Coffman, T.M., Koller, B.H., 1999. Decreased platelet aggregation, increased bleeding time and resistance to thromboembolism in P2Y₁-deficient mice. *Nat. Med.* 5, 1199–1202.
- Ferrari, D., Pizzirani, C., Adinolfi, E., Lemoli, R.M., Curti, A., Idzko, M., Panther, E., Di Virgilio, F., 2006. The P2X7 receptor: a key player in IL-1 processing and release. *J. Immunol.* 176, 3877–3883.
- Filippov, V., Kronenberg, G., Pivneva, T., Reuter, K., Steiner, B., Wang, L.P., Yamaguchi, M., Kettenmann, H., Kempermann, G., 2003. Subpopulation of nestin-expressing progenitor cells in the adult murine hippocampus shows electrophysiological and morphological characteristics of astrocytes. *Mol. Cell Neurosci.* 23, 373–382.
- Fischer, W., Appelt, K., Grohmann, M., Franke, H., Nörenberg, W., Illes, P., 2009. Increase of intracellular Ca²⁺ by P2X and P2Y receptor-subtypes in cultured cortical astroglia of the rat. *Neuroscience* 160, 767–783.
- Franke, H., Verkhatsky, A., Burnstock, G., Illes, P., 2012. Pathophysiology of astroglial purinergic signalling. *Purinergic Signal* 8, 629–657.
- Genzen, J.R., Platel, J.C., Rubio, M.E., Bordey, A., 2009. Ependymal cells along the lateral ventricle express functional P2X7 receptors. *Purinergic Signal* 5, 299–307.
- Gerevich, Z., Zádori, Z., Müller, C., Wirkner, K., Schröder, W., Rubini, P., Illes, P., 2007. Metabotropic P2Y receptors inhibit P2X3 receptor-channels via G protein-dependent facilitation of their desensitization. *Br. J. Pharmacol.* 151, 226–236.
- Götz, M., Huttner, W.B., 2005. The cell biology of neurogenesis. *Nat. Rev. Mol. Cell Biol.* 6, 777–788.
- Grimm, I., Messemer, N., Stanke, M., Gachet, C., Zimmermann, H., 2009. Coordinate pathways for nucleotide and EGF signaling in cultured adult neural progenitor cells. *J. Cell Sci.* 122, 2524–2533.
- Heinemann, U., Albrecht, D., Kohr, G., Rausche, G., Stabel, J., Wisskirchen, T., 1992. Low-Ca²⁺-induced epileptiform activity in rat hippocampal slices. *Epilepsy Res. Suppl.* 8, 147–155.
- Hogg, R.C., Chipperfield, H., Whyte, K.A., Stafford, M.R., Hansen, M.A., Cool, S.M., Nurcombe, V., Adams, D.J., 2004. Functional maturation of isolated neural progenitor cells from the adult rat hippocampus. *Eur. J. Neurosci.* 19, 2410–2420.
- Hüttmann, K., Sadgrove, M., Wallraff, A., Hinterkeuser, S., Kirchhoff, F., Steinhäuser, C., Gray, W.P., 2003. Seizures preferentially stimulate proliferation of radial glia-like astrocytes in the adult dentate gyrus: functional and immunocytochemical analysis. *Eur. J. Neurosci.* 18, 2769–2778.
- Illes, P., Verkhatsky, A., Burnstock, G., Franke, H., 2012. P2X receptors and their roles in astroglia in the central and peripheral nervous system. *Neuroscientist* 18, 422–438.
- Jarvis, M.F., Khakh, B.S., 2009. ATP-gated P2X cation-channels. *Neuropharmacology* 56, 208–215.
- Jiang, L.H., 2009. Inhibition of P2X7 receptors by divalent cations: old action and new insight. *Eur. Biophys. J.* 38, 339–346.
- Khakh, B.S., North, R.A., 2006. P2X receptors as cell-surface ATP sensors in health and disease. *Nature* 442, 527–532.
- Khakh, B.S., Bao, X.R., Labarca, C., Lester, H.A., 1999a. Neuronal P2X transmitter-gated cation channels change their ion selectivity in seconds. *Nat. Neurosci.* 2, 322–330.
- Khakh, B.S., Proctor, W.R., Dunwiddie, T.V., Labarca, C., Lester, H.A., 1999b. Allosteric control of gating and kinetics at P2X4 receptor channels. *J. Neurosci.* 19, 7289–7299.
- Klaft, Z.J., Schulz, S.B., Maslarova, A., Gabriel, S., Heinemann, U., Gerevich, Z., 2012. Extracellular ATP differentially affects epileptiform activity via purinergic P2X7 and adenosine A1 receptors in naive and chronic epileptic rats. *Epilepsia* 53, 1978–1986.
- Kriegstein, A., Alvarez-Buylla, A., 2009. The glial nature of embryonic and adult neural stem cells. *Annu. Rev. Neurosci.* 32, 149–184.
- Kunze, A., Grass, S., Witte, O.W., Yamaguchi, M., Kempermann, G., Redecker, C., 2006. Proliferative response of distinct hippocampal progenitor cell populations after cortical infarcts in the adult brain. *Neurobiol. Dis.* 21, 324–332.
- Lacar, B., Young, S.Z., Platel, J.C., Bordey, A., 2010. Imaging and recording subventricular zone progenitor cells in live tissue of postnatal mice. *Front Neurosci.* 4.
- Leichsenring, A., Riedel, T., Qin, Y., Rubini, P., Illes, P., 2013. Anoxic depolarization of hippocampal astrocytes: possible modulation by P2X7 receptors. *Neurochem. Int.* 62, 15–22.
- Lin, J.H., Takano, T., Arcuino, G., Wang, X., Hu, F., Darzynkiewicz, Z., Nunes, M., Goldman, S.A., Nedergaard, M., 2007. Purinergic signaling regulates neural progenitor cell expansion and neurogenesis. *Dev. Biol.* 302, 356–366.
- Liu, R.H., Morassutti, D.J., Whittemore, S.R., Sosnowski, J.S., Magnuson, D.S., 1999. Electrophysiological properties of mitogen-expanded adult rat spinal cord and subventricular zone neural precursor cells. *Exp. Neurol.* 158, 143–154.
- Liu, X., Hashimoto-Torii, K., Torii, M., Haydar, T.F., Rakic, P., 2008. The role of ATP signaling in the migration of intermediate neuronal progenitors to the neocortical subventricular zone. *Proc. Natl. Acad. Sci. U. S. A.* 105, 11802–11807.
- Mishra, S.K., Braun, N., Shukla, V., Fullgrabe, M., Schomerus, C., Korf, H.W., Gachet, C., Ikehara, Y., Sevigny, J., Robson, S.C., Zimmermann, H., 2006. Extracellular nucleotide signaling in adult neural stem cells: synergism with growth factor-mediated cellular proliferation. *Development* 133, 675–684.
- Nörenberg, W., Schunk, J., Fischer, W., Sobottka, H., Riedel, T., Oliveira, J.F., Franke, H., Illes, P., 2010. Electrophysiological classification of P2X7 receptors in rat cultured neocortical astroglia. *Br. J. Pharmacol.* 160, 1941–1952.
- Nörenberg, W., Hempel, C., Urban, N., Sobottka, H., Illes, P., Schaefer, M., 2011. Clemastine potentiates the human P2X7 receptor by sensitizing it to lower ATP concentrations. *J. Biol. Chem.* 286, 11067–11081.
- Oliveira, J.F., Riedel, T., Leichsenring, A., Heine, C., Franke, H., Krügel, U., Nörenberg, W., Illes, P., 2011. Rodent cortical astroglia express in situ functional P2X7 receptors sensing pathologically high ATP concentrations. *Cereb. Cortex* 21, 806–820.
- Pelegrin, P., Surprenant, A., 2006. Pannexin-1 mediates large pore formation and interleukin-1 β release by the ATP-gated P2X7 receptor. *EMBO J.* 25, 5071–5082.
- Roger, S., Pelegrin, P., Surprenant, A., 2008. Facilitation of P2X7 receptor currents and membrane blebbing via constitutive and dynamic calmodulin binding. *J. Neurosci.* 28, 6393–6401.
- Rubini, P., Milosevic, J., Engelhardt, J., Al-Khrasani, M., Franke, H., Heinrich, A., Sperlåg, B., Schwarz, S.C., Schwarz, J., Nörenberg, W., Illes, P., 2009. Increase of intracellular Ca²⁺ by adenine and uracil nucleotides in human midbrain-derived neuronal progenitor cells. *Cell Calcium* 45, 485–498.
- Schuchmann, S., Schmitz, D., Rivera, C., Vanhatalo, S., Salmen, B., Mackie, K., Sipila, S.T., Voipio, J., Kaila, K., 2006. Experimental febrile seizures are precipitated by a hyperthermia-induced respiratory alkalosis. *Nat. Med.* 12, 817–823.
- Shukla, V., Zimmermann, H., Wang, L., Kettenmann, H., Raab, S., Hammer, K., Sevigny, J., Robson, S.C., Braun, N., 2005. Functional expression of the ecto-ATPase NTPDase2 and of nucleotide receptors by neuronal progenitor cells in the adult murine hippocampus. *J. Neurosci.* 25, 600–610.
- Sim, J.A., Young, M.T., Sung, H.Y., North, R.A., Surprenant, A., 2004. Reanalysis of P2X7 receptor expression in rodent brain. *J. Neurosci.* 24, 6307–6314.
- Solle, M., Labasi, J., Perregaux, D.G., Stam, E., Petrushova, N., Koller, B.H., Griffiths, R.J., Gabel, C.A., 2001. Altered cytokine production in mice lacking P2X7 receptors. *J. Biol. Chem.* 276, 125–132.
- Sperlåg, B., Vizi, E.S., Wirkner, K., Illes, P., 2006. P2X7 receptors in the nervous system. *Prog. Neurobiol.* 78, 327–346.
- Stoop, R., Surprenant, A., North, R.A., 1997. Different sensitivities to pH of ATP-induced currents at four cloned P2X receptors. *J. Neurophysiol.* 78, 1837–1840.
- Suh, H., Deng, W., Gage, F.H., 2009. Signaling in adult neurogenesis. *Annu. Rev. Cell Dev. Biol.* 25, 253–275.
- Suyama, S., Sunabori, T., Kanki, H., Sawamoto, K., Gachet, C., Koizumi, S., Okano, H., 2012. Purinergic signaling promotes proliferation of adult mouse subventricular zone cells. *J. Neurosci.* 32, 9238–9247.
- Tsuda, M., Toyomitsu, E., Komatsu, T., Masuda, T., Kunifusa, E., Nasu-Tada, K., Koizumi, S., Yamamoto, K., Ando, J., Inoue, K., 2008. Fibronectin/integrin system is involved in P2X4 receptor upregulation in the spinal cord and neuropathic pain after nerve injury. *Glia* 56, 579–585.
- Virginio, C., MacKenzie, A., North, R.A., Surprenant, A., 1999. Kinetics of cell lysis, dye uptake and permeability changes in cells expressing the rat P2X7 receptor. *J. Physiol.* 519 (2), 335–346.
- Wang, D.D., Krueger, D.D., Bordey, A., 2003. Biophysical properties and ionic signature of neuronal progenitors of the postnatal subventricular zone in situ. *J. Neurophysiol.* 90, 2291–2302.
- Yan, Z., Khadra, A., Li, S., Tomic, M., Sherman, A., Stojilkovic, S.S., 2010. Experimental characterization and mathematical modeling of P2X7 receptor channel gating. *J. Neurosci.* 30, 14213–14224.
- Yan, Z., Khadra, A., Sherman, A., Stojilkovic, S.S., 2011. Calcium-dependent block of P2X7 receptor channel function is allosteric. *J. Gen. Physiol.* 138, 437–452.
- Yasuda, T., Bartlett, P.F., Adams, D.J., 2008. K_{IR} and K_V channels regulate electrical properties and proliferation of adult neural precursor cells. *Mol. Cell Neurosci.* 37, 284–297.
- Yu, T.S., Zhang, G., Liebl, D.J., Kerner, S.G., 2008. Traumatic brain injury-induced hippocampal neurogenesis requires activation of early nestin-expressing progenitors. *J. Neurosci.* 28, 12901–12912.
- Yuhasi, K.K., Demasi, M.A., Tamajusuku, A.S., Lenz, G., Sogayar, M.C., Fornazari, M., Lameu, C., Nascimento, I.C., Glaser, T., Schwandt, T.T., Negraes, P.D., Ulrich, H., 2012. Regulation of neurogenesis and gliogenesis of retinoic acid-induced P19 embryonal carcinoma cells by P2X2 and P2X7 receptors studied by RNA interference. *Int. J. Dev. Neurosci.* 30, 91–97.
- Zhao, C., Deng, W., Gage, F.H., 2008. Mechanisms and functional implications of adult neurogenesis. *Cell* 132, 645–660.
- Zimmermann, H., 2011. Purinergic signaling in neural development. *Semin. Cell Dev. Biol.* 22, 194–204.

Co-Expression of Functional P2X4 and P2X7 Receptors at Adult Neural Progenitor Cells of the Mouse Subventricular Zone

Nanette Messemer, Christin Kunert, Peter Illes* and Patrizia Rubini

Rudolf Boehm Institute of Pharmacology and Toxicology, University of Leipzig, 04107 Leipzig, Germany

Abstract: Co-localization of P2X4 and P2X7 subunits has been demonstrated in a number of tissues. It appears that these subunits form functionally interacting homomeric P2X4 and P2X7 receptors rather than heteromeric P2X4/7 receptors. We have recently reported that adult neural progenitor cells (NPCs) of the mouse subventricular zone (SVZ) possess P2X7 receptors. Cultured proliferating NPCs responded to higher concentrations of the prototypic P2X7 agonist dibenzoyl-ATP (Bz-ATP) with inward current, strongly inhibited by the selective P2X7 antagonist A438079, and moderately depressed by the P2X1-3,4 antagonist TNP-ATP, or the selective P2X4 antagonist 5-BDBD. Now we show in addition that ivermectin, a selective allosteric modulator of P2X4 receptors, uniformly potentiated the effect of lower Bz-ATP concentrations; this potentiation was abolished by 5-BDBD. In conclusion, astrocyte-like cultured SVZ NPCs are endowed with P2X4 and P2X7 receptors shaping the characteristics of these cells with respect to ATP-dependent signalling.

Keywords: Neural progenitor cell, P2X4 receptor, P2X7 receptor, membrane current, ligand-gated cation channel.

INTRODUCTION

Neuroepithelial stem cells in the embryonic nervous system generate most of the neurons and glia in the developing brain [1]. In addition, neurogenesis continues in the adult mammalian brain in specific neurogenic niches, the subgranular zone of the hippocampal dentate gyrus and the subventricular zone (SVZ) of the lateral ventricle, contributing mature neurons to the dentate gyrus and olfactory bulb, respectively [2,3].

Extracellular nucleotides can influence the proliferation and fate decision of neural progenitor cells (NPCs) both during embryonic development and in the adult brain [4,5]. The cellular effects of nucleotides are mediated by seven P2X receptors (P2X1-7 subtypes, which are ligand-gated cation channels; [6]) and eight G-protein-coupled P2Y receptors (P2Y_{1,2,4,6,11,12,13,14} receptors; [7]). Previous work has demonstrated that P2Y₁ receptors are present at NPCs of the SVZ *in vitro* and *in situ* [4,8,9], causing rapid [Ca²⁺]_i transients and augmenting growth factor-mediated proliferation. Subsequently, P2X7 receptors of SVZ NPCs have been shown to cause apoptosis/necrosis [10] and thereby most likely decrease the neuro- and/or gliogenesis induced by excessive proliferation of NPCs during pathological conditions such as traumatic injury, hypoxia/ischemia, and epilepsy [11].

In the present work, we searched in SVZ NPCs for P2X4 receptors often accompanying P2X7 receptor-expression in various tissues [12] to find out if the two receptor-types interact with each other to shape ATP-dependent intracellular signalling.

Primary cultures of adult NPCs from the SVZ were prepared according to Grimm *et al.* [8] from 8-14-weeks old C57Bl/6N mice. After 7 days of culturing as neurospheres, cells were dispersed and seeded onto coated culture dishes with proliferation medium containing 20 ng/ml epidermal growth factor and 10 ng/ml fibroblast growth factor-2.

Whole-cell voltage-clamp recordings were made at room temperature (20-24°C) on 1-4-days old adherent NPCs, using an Axopatch 200B patch clamp amplifier (Molecular Devices). The pipette solution contained (in mM): K-gluconate 140, NaCl 10, CaCl₂ 0.2, MgCl₂ 2.3, HEPES 10, EGTA 10, Mg-ATP 4, Li-GTP 0.3 (pH 7.2, with KOH). For seal formation and some initial experiments, we used a normal artificial cerebrospinal fluid (aCSF; in mM): NaCl 140, KCl 2.5, CaCl₂ 1, MgCl₂ 1.2, HEPES 25, glucose 10.5 (pH 7.3, with NaOH). For low X²⁺ solution MgCl₂ was omitted, and the concentration of CaCl₂ was decreased to 0.1 mM. Pipettes had resistances of 3-8 MΩ. A holding potential of -80 mV was selected.

Agonists, antagonists, and allosteric modulators were applied locally by means of a computer-controlled solenoid valve-driven pressurized superfusion system (DAD-12, ALA Scientific Instruments). Bz-ATP and ivermectin were from Sigma-Aldrich, while A-438079, 5-BDBD and TNP-ATP were from Tocris.

In a first series of experiments, we applied Bz-ATP (300 μM) onto NPCs for 5 s every 2 min in a low X²⁺ external solution. Previously we have shown that a low X²⁺ medium markedly increased the effect of Bz-ATP when compared with measurements in a normal Ca²⁺/Mg²⁺-containing medium, and repetitive application of Bz-ATP with the above time-schedule resulted in stable responses [10]. Thus, the divalent cations Ca²⁺ and Mg²⁺ depressed the Bz-ATP-induced current responses in agreement with their reported influence on native and recombinant P2X7 receptors [13].

*Address correspondence to this author at the Rudolf Boehm Institute of Pharmacology and Toxicology, University of Leipzig, Haertelstrasse 16-18, 04107 Leipzig, Germany; Tel: (+49)341-9724614; Fax: (+49)341-9724609; E-mail: Peter.Illes@medizin.uni-leipzig.de

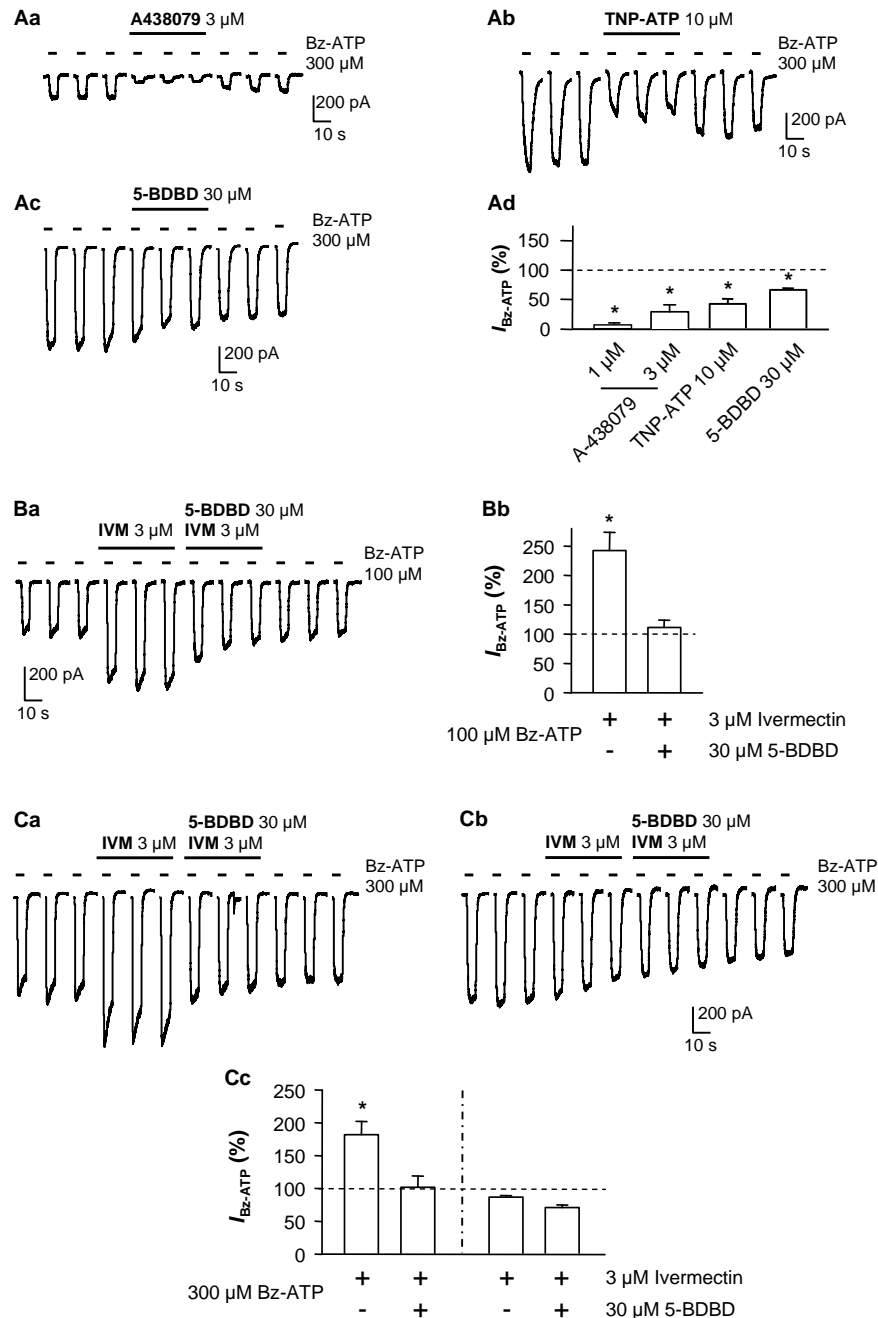


Fig. (1). Functional P2X7 and P2X4 receptors in undifferentiated, cultured neural progenitor cells (NPCs) prepared from the subventricular zone of the adult mouse brain. The holding potential in the whole-cell mode of the patch-clamp recording was -80 mV. Stable concentrations of Bz-ATP (300 or 100 μ M) were applied every 2 min for 5 s. All antagonists or allosteric modulators were superfused for 6 min in total. **(A)** Inhibition by A-438079 (3 μ M), TNP-ATP (10 μ M) and 5-BDBD (30 μ M) of the Bz-ATP (300 μ M)-induced currents. Representative tracings (**a-c**) were recorded in this and all other panels of this Fig. from separate cells. Mean \pm S.E.M. of 6-8 cells from 2 culture dishes each (**d**). In these and all following experiments the change by the antagonist/modulator of the 3rd Bz-ATP current response was compared with the time matched current response in the absence of antagonists/modulators. * $P < 0.05$; statistically significant difference from 100 % (ANOVA, Holm-Sidak test). **(B)** Increase by ivermectin (3 μ M) of the Bz-ATP (100 μ M) currents and its antagonism by 5-BDBD (30 μ M). Representative tracings (**a**). Mean \pm S.E.M. of 8 cells from 2 culture dishes (**b**). * $P < 0.05$; statistically significant difference from 100 % (ANOVA, Holm-Sidak test). **(C)** Potentiation of Bz-ATP (300 μ M) currents by ivermectin (3 μ M) and its antagonism by 5-BDBD (30 μ M) in a subpopulation of NPCs (**a**); no effect of ivermectin and 5-BDBD in another subpopulation (**b**). Representative tracings (**a**, **b**). Mean \pm S.E.M. of 12 (left side) and 15 (right side) cells from 3 culture dishes each (**c**). Ivermectin-sensitive and -insensitive cells were found in either culture dish. * $P < 0.05$; statistically significant difference from 100 % (ANOVA, Holm-Sidak test).

We also showed that under low X^{2+} conditions the effect of Bz-ATP (0.3-1000 μ M) was concentration-dependent and 300 μ M Bz-ATP was a submaximal concentration of this agonist at all cells investigated. Both P2X7 (A-438079) and P2X4 (TNP-ATP; 5-BDBD) receptor antagonists decreased the effect of Bz-ATP (Fig. 1Aa-d), in a manner which only slowly reversed on washout. The inspection of recordings from separate cells demonstrated that the amplitude of the Bz-ATP (300 μ M)-induced currents exhibited a considerable scatter (compare Figs. 1Aa, b and c). Therefore, in all experiments the change by the antagonist/modulator of the 3rd Bz-ATP current response was compared with the time matched current response in the absence of antagonists/modulators [10]. It is noteworthy that whereas A-438079 and 5-BDBD are highly selective for P2X7 and P2X4 receptors, respectively, TNP-ATP is a P2X_{1,3} receptor antagonist, which however at higher concentrations blocks also P2X4 receptors [14].

At a relatively low Bz-ATP concentration of 100 μ M, ivermectin (3 μ M), a selective allosteric modulator of rodent P2X4 receptors [15] potentiated the nucleotide effect in all investigated NPCs (Fig. 1Ba, b). The selective P2X4 receptor antagonist 5-BDBD (30 μ M; [16]) abolished the effect of ivermectin. By contrast, at a higher Bz-ATP concentration of 300 μ M, ivermectin acted only in a subpopulation of NPCs; 5-BDBD again reversed the potentiation by ivermectin (Fig. 1Ca, c). In the residual subpopulation of NPCs, neither ivermectin nor 5-BDBD modified the Bz-ATP current amplitudes in a statistically significant manner (Fig. 1Cc), although there was some decrease of the Bz-ATP responses by ivermectin in the individual experiment shown in (Fig. 1Cb).

The agonistic effect of Bz-ATP in a low X^{2+} external medium and its antagonism by A-438079 bears out the existence of P2X7 receptors at mouse SVZ NPCs. Recently published data (stronger agonistic effect of Bz-ATP than of ATP itself; inhibitory interaction between Bz-ATP and the selective P2X7 antagonists Brilliant Blue G and A-438079; dilation of the P2X7 receptor-channel during long-lasting application of Bz-ATP; no effect of Bz-ATP in NPCs of P2X7^{-/-} mice) are also compatible with the presence of such a receptor at NPCs [10]. Our novel findings relate to the co-expression of P2X7 and P2X4 receptors; at a relatively low Bz-ATP concentration all NPCs expressed functional P2X4 receptors sensitive to ivermectin and 5-BDBD in opposite ways.

The overlapping expression of P2X4 and P2X7 receptors has been documented in multiple tissues and nonexcitatory cell types, including epithelial cells from the salivary gland, exocrine pancreas, airways, macrophages and microglial cells [12]. Although the reason for this co-expression has not been completely clarified, it is suggested that these receptors play a role in inflammatory regulation [17]. The recent literature is divided about the suggestion whether P2X4 and P2X7 receptors exist as independent homomeric channels interacting with each other or whether they constitute heteromeric P2X_{4/7} channels. There are a number of arguments for each assumptions, especially since Guo *et al.* [18] published data on the co-immunoprecipitation of P2X4 with P2X7. In addition, it was found that heterologous expression of P2X4 and P2X7 separately did not reproduce all the features of the

ATP activated current recorded in HEK293 cells or salivary epithelial cells unless both receptors were co-expressed [18,19]. It was also shown that ivermectin, which potentiates homomeric P2X4 receptor-channels by binding between transmembrane helices near the extracellular side [20] potentiated the effect of ATP at low concentrations but not at high concentrations [19]. This finding is in good agreement with our results documented in (Fig. 1B, C).

Arguments for the opposite view are still more convincing. It has been shown by co-immunoprecipitation that all P2X subunits are able to form heterooligomeric complexes with the exception of P2X7 [21]. Moreover homotrimeric complexes were found to be the dominant assembly state of P2X7 receptors by using subtype-specific antibodies in combination with BN-PAGE to directly visualize P2X receptor complexes from membrane extracts of native tissues [22]. Lipopolysaccharide (LPS)-induced activation differentially regulated microglial P2X4 and P2X7 receptor membrane expression [23]. Eventually, it was concluded based on atomic-force microscopy investigations that these individual homomeric P2X4 and P2X7 receptors closely interact in the plasma membrane [24].

In conclusion, we found that in addition to the previously described P2X7 receptors also P2X4 receptors occur in proliferating mouse NPCs. It is suggested that the failure of Bz-ATP to activate P2X4 receptors in NPCs of P2X7^{-/-} mice is due to the strong functional interdependence of P2X4 and P2X7 receptors. These two receptor types act as sensors of ATP and most likely participate in the reactions of NPCs to inflammatory conditions in the CNS.

CONFLICT OF INTEREST

The author(s) confirm that this article content has no conflicts of interest.

ACKNOWLEDGEMENT

This work was supported by a grant of the Deutsche Forschungsgemeinschaft (IL 20/19-1). We are grateful to Prof. Herbert Zimmermann for many helpful discussions.

REFERENCES

- Doetsch F. The glial identity of neural stem cells. *Nat Neurosci* 2003; 6(11):1127-34.
- Götz M, Huttner WB. The cell biology of neurogenesis. *Nat Rev Mol Cell Biol* 2005; 6(10):777-88.
- Zhao C, Deng W, Gage FH. Mechanisms and functional implications of adult neurogenesis. *Cell* 2008; 132(4):645-60.
- Mishra SK, Braun N, Shukla V, *et al.* Extracellular nucleotide signaling in adult neural stem cells: synergism with growth factor-mediated cellular proliferation. *Development* 2006; 133(4):675-84.
- Rubini P, Pinkwart C, Franke H, Gerevich Z, Nörenberg W, Illes P. Regulation of intracellular Ca^{2+} by P2Y₁ receptors may depend on the developmental stage of cultured rat striatal neurons. *J Cell Physiol* 2006; 209(1):81-93.
- Khakh BS, North RA. P2X receptors as cell-surface ATP sensors in health and disease. *Nature* 2006; 442(7102): 527-32.
- Abbracchio MP, Burnstock G, Boeynaems JM, *et al.* International Union of Pharmacology LVIII: update on the P2Y G protein-coupled nucleotide receptors: from molecular mechanisms and pathophysiology to therapy. *Pharmacol Rev* 2006; 58(3):281-341.
- Grimm I, Messemer N, Stanke M, Gachet C, Zimmermann H. Coordinate pathways for nucleotide and EGF signaling in cultured adult neural progenitor cells. *J Cell Sci* 2009; 122(Pt 14): 2524-33.

- [9] Suyama S, Sunabori T, Kanki H, *et al.* Purinergic signaling promotes proliferation of adult mouse subventricular zone cells. *J Neurosci* 2012; 32(27):9238-47.
- [10] Messemer N, Kunert C, Grohmann M, *et al.* P2X7 receptors at adult neural progenitor cells of the mouse subventricular zone. *Neuropharmacology* 2013; 73C:122-37.
- [11] Suh H, Deng W, Gage FH. Signaling in adult neurogenesis. *Annu Rev Cell Dev Biol* 2009; 25:253-75.
- [12] Dubyak GR. Go it alone no more - P2X7 joins the society of heteromeric ATP-gated receptor channels. *Mol Pharmacol* 2007; 72(6):1402-5.
- [13] Sperlágh B, Vizi ES, Wirkner K, Illes P. P2X7 receptors in the nervous system. *Prog Neurobiol* 2006; 78(6):327-46.
- [14] Jarvis MF, Khakh BS. ATP-gated P2X cation-channels. *Neuropharmacology* 2009; 56(1): 208-15.
- [15] Khakh BS, Proctor WR, Dunwiddie TV, Labarca C, Lester HA. Allosteric control of gating and kinetics at P2X4 receptor channels. *J Neurosci* 1999; 19(17):7289-99.
- [16] Chen K, Zhang J, Zhang W, Zhang J, Yang J, Li K, He Y. ATP-P2X4 signaling mediates NLRP3 inflammasome activation: a novel pathway of diabetic nephropathy. *Int J Biochem Cell Biol* 2013; 45(5): 932-43.
- [17] Burnstock G. Purinergic P2 receptors as targets for novel analgesics. *Pharmacol Ther* 2006; 110(3): 433-54.
- [18] Guo C, Masin M, Qureshi OS, Murrell-Lagnado RD. Evidence for functional P2X4/P2X7 heteromeric receptors. *Mol Pharmacol* 2007; 72(6):1447-56.
- [19] Casas-Pruneda G, Reyes JP, Perez-Flores G, Perez-Cornejo P, Arreola J. Functional interactions between P2X4 and P2X7 receptors from mouse salivary epithelia. *J Physiol* 2009; 587(Pt 12):2887-901.
- [20] Silberberg SD, Li M, Swartz KJ. Ivermectin interaction with transmembrane helices reveals widespread rearrangements during opening of P2X receptor channels. *Neuron* 2007; 54(2): 263-74.
- [21] Torres GE, Egan TM, Voigt MM. Hetero-oligomeric assembly of P2X receptor subunits. Specificities exist with regard to possible partners. *J Biol Chem* 1999; 274(10): 6653-59.
- [22] Nicke A. Homotrimeric complexes are the dominant assembly state of native P2X7 subunits. *Biochem Biophys Res Commun* 2008; 377(3):803-8.
- [23] Raouf R, Chabot-Dore AJ, Ase AR, Blais D, Seguela P. Differential regulation of microglial P2X4 and P2X7 ATP receptors following LPS-induced activation. *Neuropharmacology* 2007; 53(4):496-504.
- [24] Antonio LS, Stewart AP, Xu XJ, Varanda WA, Murrell-Lagnado RD, Edwardson JM. P2X4 receptors interact with both P2X2 and P2X7 receptors in the form of homotrimers. *Br J Pharmacol* 2011; 163(5):1069-77.

Received: April 22, 2013

Revised: July 05, 2013

Accepted: July 21, 2013

© Messemer *et al.*; Licensee *Bentham Open*.

This is an open access article licensed under the terms of the Creative Commons Attribution Non-Commercial License (<http://creativecommons.org/licenses/by-nc/3.0/>) which permits unrestricted, non-commercial use, distribution and reproduction in any medium, provided the work is properly cited.

Functional P2X7 receptors at cultured hippocampal astrocytes but not neurons

Patrizia Rubini · Gregor Pagel · Soghra Mehri ·
Peter Marquardt · Thomas Riedel · Peter Illes

Received: 21 February 2014 / Accepted: 5 June 2014
© Springer-Verlag Berlin Heidelberg 2014

Abstract P2X7 receptors have been suggested to be located both on neurons and astrocytes of the central and peripheral nervous systems. In the present Ca^{2+} -imaging and patch-clamp study, we reinvestigated these findings on mixed neuronal–astrocytic cell cultures prepared from embryonic or newborn rat hippocampi. We found in a Mg^{2+} -free bath medium that the prototypic P2X7 receptor agonist dibenzoyl-adenosine triphosphate (Bz-ATP) increased the intracellular Ca^{2+} concentration ($[\text{Ca}^{2+}]_i$) both in the neuronal cell bodies and in their axo-dendritic processes only to a very minor extent. However, Bz-ATP produced marked $[\text{Ca}^{2+}]_i$ transients in the neuronal processes, when they grew above a glial carpet, which was uniformly sensitive to Bz-ATP. These glial signals might be misinterpreted as neuronal responses because of the poor focal discrimination by a fluorescent microscope. Most astrocytes had a polygonal shape without clearly circumscribable boundaries, but a subgroup of them had neuron-like appearance. The cellular processes of this astrocytic subgroup, just as their cell somata and their polygonal counterparts, appeared to possess a high density of functional P2X7 receptors. In contrast to astrocytes, in a low Ca^{2+} /no Mg^{2+} -containing bath medium, hippocampal neurons failed to respond to Bz-ATP with membrane currents. In addition, neither the amplitude nor the frequency of spontaneous excitatory postsynaptic currents, representing the quantal release of glutamate, was modified by Bz-ATP. We conclude that cultured hippocampal neurons, in contrast to astrocytes, possess P2X7 receptors, if at all, only at a low density.

Keywords Astrocytes · Neurons · Hippocampus · P2X7 receptors · Ca^{2+} imaging · Patch-clamp recording

Introduction

The P2X7 subclass of ionotropic P2X receptors has unique characteristics in that a single brief application of agonists induces non-selective cationic currents, whereas repeated or prolonged application opens a membrane pore, which renders the membrane permeable to high molecular weight molecules and ions up to the size of 900 Da (Surprenant et al. 1996; Sperlágh et al. 2006). In addition, cytoskeletal rearrangement (membrane blebbing) and the release of inflammatory cytokines occur, possibly leading to necrosis/apoptosis or in some cases cell proliferation (Di Virgilio et al. 2009; Burnstock et al. 2011). There is little doubt that in the brain and spinal cord, microglial and astroglial cells are endowed with functional P2X7 receptors (Abbracchio and Ceruti 2006; Verkhatsky et al. 2009), although there is possibly a regional and species dependent variability (Jabs et al. 2007; Bianco et al. 2009). A lively and ongoing dispute, however, exists on the question whether these receptors are present also on neurons (Sperlágh et al. 2006; Anderson and Nedergaard 2006).

P2X7 receptors appeared to mediate the stimulation of the exocytotic machinery in nerve terminals to release [^3H] gamma-aminobutyric acid (GABA) from rat hippocampal slices (Sperlágh et al. 2002). In agreement with this idea, dibenzoyl-adenosine triphosphate (Bz-ATP) was a more potent agonist than ATP itself, Brilliant Blue G, a selective P2X7 receptor antagonist abolished the ATP effect, and so did the use of P2X7 $^{-/-}$ mice (Papp et al. 2004). Bz-ATP and ATP also elicited high-frequency firing of spinal cord neurons (Deuchars et al. 2001; Wang et al. 2004) and depolarised myenteric and submucous neurons (Hu et al. 2001). Rather extensive evidence was supplied for the presence of P2X7

P. Rubini (✉) · G. Pagel · S. Mehri · P. Marquardt · T. Riedel ·
P. Illes (✉)
Rudolf-Boehm-Institute of Pharmacology and Toxicology,
University of Leipzig, Haertelstrasse 16-18, 04107 Leipzig,
Germany
e-mail: Patrizia.Rubini@medizin.uni-leipzig.de
e-mail: illp@medizin.uni-leipzig.de

receptors on nerve terminals of cultured cerebellar granule neurons (Sanchez-Nogueiro et al. 2005; Miras-Portugal et al. 2003), midbrain GABAergic neurons (Marin-Garcia et al. 2008) and hippocampal neurons (Diaz-Hernandez et al. 2008) of rodents. Immunohistochemically identified P2X7 receptors were suggested to raise $[Ca^{2+}]_i$ in pinched off synaptic terminals (synaptosomes; Miras-Portugal et al. 2003; Marin-Garcia et al. 2008), and the distal domains of hippocampal axons (Diaz-Hernandez et al. 2008) in a manner which was blocked by selective P2X7 antagonists and/or short hairpin (sh)RNA.

However, the alternative view, that instead of direct neuronal effects, ATP/Bz-ATP may indirectly stimulate neurons by the astrocytic release of signalling molecule, is also feasible (see Sperlágh et al. 2006; Illes et al. 2012). Based on these considerations, we determined in mixed neuronal–glial hippocampal cultures of rats the Bz-ATP-induced increase of $[Ca^{2+}]_i$ in cell bodies, as well as in proximal and distal cellular processes of neurons and astrocytes. We found that Bz-ATP uniformly increased the astrocytic $[Ca^{2+}]_i$, but only slightly raised it at the neuronal somata or their axo-dendritic extensions. Moreover, neither the holding current, nor the frequency or amplitude of spontaneous postsynaptic currents (sPSCs) was altered by Bz-ATP.

Materials and methods

Preparation of mixed hippocampal neuronal–astrocytic cell cultures

Cell cultures were prepared from Wistar rat fetuses at gestational day 18 or from newborn rats at postnatal day 1. In short, hippocampi were dissected, minced and pooled in ice-cold (4 °C) Hank's balanced salt solution (HBSS; Invitrogen). Tissue samples were then dissociated in 1.5 ml of 0.05 % trypsin (Invitrogen) in HBSS for 20–30 min at 37 °C. Enzymatic digestion was stopped by trypsin inhibitor (0.7 mg/ml; Sigma-Aldrich) added to a 1:1 mixture of Dulbecco's modified Eagle medium (DMEM; Gibco) containing also 36 mM D(+)-glucose, 15 mM HEPES (pH 7.4 with NaOH) plus 50 µg/ml gentamicin, on the one hand, and neurobasal medium (NBM; Gibco) mixed with B27 supplements (Gibco) also containing 0.5 mM L-glutamine, on the other. After gentle trituration through a fire polished Pasteur pipette and centrifugation (80×g for 5 min; repeated three times in total, separated by washout periods), the remaining cell pellet was taken up and re-suspended in the culture medium of the above composition. The final cell suspension was then seeded into poly-L-lysine-coated 35-mm-diameter polystyrol culture dishes (electrophysiology) or onto glass coverslips (Ca^{2+} imaging) at a plating density of $4 \times 10^3/cm^2$. Cultures were maintained in 2 ml of the culture medium at 37 °C in a humidified

atmosphere of 5 % CO_2 in air. To prevent excessive proliferation of glial cells, 3.3 µM of cytosine-β-D-arabino-furanoside was added for 3–4 days (newborn rats) or for 1 day (embryonic rats) starting with day 3 in vitro (3 DIV). Then the medium was replaced by the original cytosine-β-D-arabino-side-free culturing medium. Cells were used for Ca^{2+} imaging (10–12 DIV) or patch-clamp recording (7–9 DIV).

Intracellular calcium measurements

$[Ca^{2+}]_i$ was measured with the Fura-2 method as described previously (Rubini et al. 2006, 2009). Experiments were performed at room temperature (20–24 °C) in an oxygenated, nominally Ca^{2+} -free bath solution with the following compositions (in mM): NaCl 135, KCl 4.5, $MgCl_2$ 1, HEPES 10 and glucose 10 (pH 7.4 with NaOH). In a high potassium-containing medium, the concentration of KCl was increased to 50 mM, and the concentration of NaCl was decreased accordingly. An inverted microscope equipped for epifluorescence and a Peltier-cooled charge-coupled device camera (IMAGO; Till Photonics) were used. Intracellular Fura-2 was alternately excited at 340 and at 380 nm, and the emitted light was measured at 510 nm. The fluorescence ratio (FR, 340/380 nm) was taken as a relative measure of $[Ca^{2+}]_i$. For each experiment, five to six coverslips were recorded; the $[Ca^{2+}]_i$ increases were analysed by setting the regions of interest (ROIs) at cell bodies and at different parts of the cellular processes. Selected areas without cells were chosen for background subtraction.

A high potassium-containing medium, as well as Bz-ATP and its antagonists, were applied locally by means of a computer-controlled superfusion system (DAD-12, ALA Scientific Instruments). At the beginning of each experiment, 50 mM K^+ was superfused for 5 s in order to discriminate neurons from glial cells (see the 'Results' section). Bz-ATP was applied for 5 s every 10–12 min, six times (S_1 – S_6), in a Mg^{2+} -free bath solution. Agonist effects were determined before (S_1 and S_2) and during superfusion with antagonists (S_3 and S_4) or a Ca^{2+} -free bath medium (S_3) and after their washout (S_5 – S_6 or S_4). A nominally Ca^{2+} -free medium was prepared by omitting $CaCl_2$ from the normal bath solution. Antagonists were present 8 min before agonist application and were washed out together with the agonist. The Ca^{2+} -free bath medium was added 4 min before the application of the agonist and was washed out 2 min later. The Bz-ATP-induced $[Ca^{2+}]_i$ responses at S_2 were set to 100 % (control); the modulation by antagonists or a Ca^{2+} -free bath medium was calculated at S_3 and/or S_4 and was expressed as percent change of the Bz-ATP-induced $[Ca^{2+}]_i$ transients. In some of the experiments, the cultures were incubated in fluorocitrate (100 µM) for 1 h before starting the application of Bz-ATP (300 µM).

Whole-cell patch-clamp recordings and drug application protocols: cultured neural progenitor cells

Whole-cell current-clamp and voltage-clamp recordings were made at room temperature, using an Axopatch 200B patch-clamp amplifier (Molecular Devices). The pipette solution contained (in mM): K-gluconate 140, NaCl 10, CaCl₂ 0.2, MgCl₂ 2.3, HEPES 10, EGTA 10, Mg-ATP 4 and Li-GTP 0.3 (pH 7.2 with KOH). Two different bath solutions were used, one of them contained normal concentrations and the other one low divalent cation (low X²⁺) concentrations. For seal formation and some initial experiments, we used a normal artificial cerebrospinal fluid (aCSF, in mM): NaCl 140, KCl 2.5, CaCl₂ 1, MgCl₂ 1.2, HEPES 25, glucose 10.5 (pH 7.3 with NaOH). For low X²⁺ solution, MgCl₂ was omitted, and the concentration of CaCl₂ was decreased to 0.1 mM. Pipettes had resistances of 3–8 MΩ.

The resting membrane potential (U_m) of neurons (−52 to −66 mV) and astrocytes (−61 to −84 mV) was measured within 30 s after establishing whole-cell access. The holding potential for neurons and astrocytes was −70 and −80 mV, respectively. The membrane and holding potential values were corrected by the liquid junction potential (V_L ; Oliveira et al. 2011; Leichsenring et al. 2013). Compensation of capacitance (C_m) was achieved with the inbuilt circuitry of the amplifier. Access resistance (R_a) was compensated by 40–70 % and did not change appreciably from the beginning to the end of the experiments, indicating stable recording conditions. Cells with R_a values higher than 30 MΩ were discarded. Current and voltage-step protocols were used to differentiate neurons from astrocytes (Oliveira et al. 2011; Leichsenring et al. 2013), since a subgroup of astrocytes were neuron-like in their visual appearance. pClamp 10.2 software (Molecular Devices) was used to store the recorded data for offline analysis/filtering and to trigger the fast drug application system.

Bz-ATP (300 μM) was applied locally by means of a computer-controlled solenoid valve-driven pressurised superfusion system (DAD-12, ALA Scientific Instruments). The agonist was applied for 5 s every 5 min to investigate changes in the holding current. Agonist effects were determined before (S_1 and S_2), during (S_3 and S_4) and after (S_5 – S_6) superfusion with a low X²⁺ solution. The Bz-ATP-induced current responses at S_2 were set to 100 % (control); the modulation by a low X²⁺ medium was calculated at S_3 and/or S_4 and was expressed as percent change of the control current amplitude, both in neurons and astrocytes.

Alternatively, Bz-ATP (300 μM) was superfused in a low X²⁺ medium to measure its effect on the frequency and amplitude of spontaneous postsynaptic currents of hippocampal neurons. A combination of CNQX (10 μM) and AP-5 (50 μM) abolished these currents, confirming that they are due to the spontaneous quantal release of glutamate and may

be termed spontaneous excitatory postsynaptic currents (sEPSCs). sEPSCs were recorded and evaluated before, during and after the application of Bz-ATP, for 5 min each. Effects of higher concentrations of Bz-ATP (>100 μM) should remain stable or even increase during long-time application without an apparent desensitisation (Khadra et al. 2013).

Materials

All agonists and antagonists were from Sigma-Aldrich, except Bz-ATP and A438079, which were from Tocris.

Statistics

Means ± S.E.M. are given throughout. SigmaPlot (version 11.0) was used for all statistical evaluations. Pairwise comparisons were made by the Student's *t* test, if the normality test was passed, or by the Mann–Whitney rank sum test, if the normality test failed. Multiple comparisons were performed by one-way analysis of variance (ANOVA) followed by the Holm–Sidak post hoc test, if ANOVA indicated a statistically significant difference between the samples. In all cases, a probability level of 0.05 or less was considered to be statistically significant.

Results

Absence of P2X7 receptors at cultured hippocampal neurons, but not astrocytes: a Ca²⁺-imaging study

Most astrocytes formed a confluent layer of flat cells, which were devoid of clearly circumscribable borders and appendages (for cortical cell cultures, see Nörenberg et al. 2010). Neurons and a subgroup of astrocytes grew on the surface of the astrocytic carpet or apart of it; they had clear cell boundaries and numerous cellular processes. Light microscopic (Figs. 1Aa, 2Aa) and fluorescent microscopic (Figs. 1Ab, 2Ab) pictures demonstrate the impossibility to differentiate these cells from each other by visual inspection of either their shape or their size (diameter ~10 μm in both cases). The fluorescence microscopic picture shows, in addition, how the regions of interest (ROIs) were chosen to map K⁺ and Bz-ATP effects over neurons and astrocytes. In neurons, a pulse of K⁺ (50 mM) increased [Ca²⁺]_i via opening of voltage-sensitive Ca²⁺ channels (VSCCs), through which this cation was able to enter the intracellular space (Rubini et al. 2006, 2008). Astrocytes, in contrast to neurons, do not possess VSCCs, and therefore, no [Ca²⁺]_i transients were observed after their superfusion with 50 mM K⁺ (compare Fig. 1Ba–f with Fig. 2Ba–d). Bz-ATP is a prototypic P2X7 receptor agonist, which has the advantage over ATP that it stimulates

this receptor subtype with an about five times higher potency. However, Bz-ATP has considerable residual activities at the P2X1 and P2X3 receptor subtypes (Bianchi et al. 1999; Jarvis and Khakh 2009).

Figure 1 shows a representative recording of $[Ca^{2+}]_i$ transients in the cell body of a newborn hippocampal neuron and various segments of its axo-dendritic extension. Whereas K^+ uniformly increased $[Ca^{2+}]_i$ in all parts of the neuron, the preferential P2X7 receptor agonist Bz-ATP (300 μ M) had only a minor effect, except when signals from the underlying astrocytes interfered with measurements, probably because of poor focal discrimination by the fluorescent microscope (compare Fig. 1Bb, c, f with d, e). In addition, the amplitude of the K^+ -induced responses became smaller with increasing distance from the cell body, indicating a lower density of VSCCs (compare Fig. 1Ba with f).

Similar measurements were made also from a subgroup of newborn hippocampal astrocytes which resembled neurons in their shape (Fig. 2). In this case, K^+ failed to elevate $[Ca^{2+}]_i$ in either part of the astrocytes or had only a slight effect, because of the absence or very low density of VSCCs. In contrast, Bz-ATP was active both in the soma and in all segments of its axo-dendritic processes (Fig. 2Ba–d). However, in the cellular processes, the amplitude of the Bz-ATP-induced responses did not change with the distance of the site of measurement from the cell body.

Results obtained by experiments with embryonic and newborn mixed neuronal–astrocytic cell cultures are summarised in Fig. 3A. They indicate that the neuronal somata and their axo-dendritic extensions responded to Bz-ATP (300 μ M) with significant $[Ca^{2+}]_i$ transients only when an underlying glial carpet was present. Moreover, responses of the neuronal somata to Bz-ATP (300 μ M; S_2 – S_4) were, after a preceding high K^+ (50 mM; S_1) stimulation, very stable over time. The application of the P2X7 receptor agonist for 5 s every 12 min caused fluorescence ratios as a measure of $[Ca^{2+}]_i$ transients at S_2 0.013 ± 0.03 , S_3 0.015 ± 0.004 and S_4 0.013 ± 0.003 ($n=12$ each; $P>0.05$). Unfortunately, the amplitude of the Bz-ATP-induced $[Ca^{2+}]_i$ transients considerably varied between the different culture dishes even when measurements were from a large number of cells. Therefore, we determined the Bz-ATP effect on glial cells and the axo-dendritic processes of neurons laying upon an astroglial layer in newborn hippocampal cell cultures both after pretreatment with fluorocitrate (100 μ M for 1 h) and without pretreatment with this selective metabolic poison of astrocytes. We noted that the $[Ca^{2+}]_i$ transients were by 73.9 % ($n=30, 31$) and 85.1 % ($n=20, 54$) larger in glial cells than in the neuronal processes under control conditions and after fluorocitrate pretreatment, respectively; in consequence, fluorocitrate did not interfere with the Bz-ATP-induced increase of $[Ca^{2+}]_i$ in the axo-dendritic extensions.

In the following experiments, we concentrated ourselves on newborn hippocampal glia, by pooling data obtained on

flat/polygonal cells and on those with more typical, astrocyte-like morphology. This was possible, because the investigated pharmacological characteristics of the two classes of astrocytes did not differ from each other in any respect. As a first approach, we confirmed that, in a Mg^{2+} -free bath medium, the stimulation of P2Y receptors by Bz-ATP (releasing Ca^{2+} from its intracellular pools) was practically without effect. Bz-ATP (300 μ M) caused large $[Ca^{2+}]_i$ transients that entirely depended on the presence of external Ca^{2+} and therefore were due only to P2X receptor activation (Fig. 3Ba).

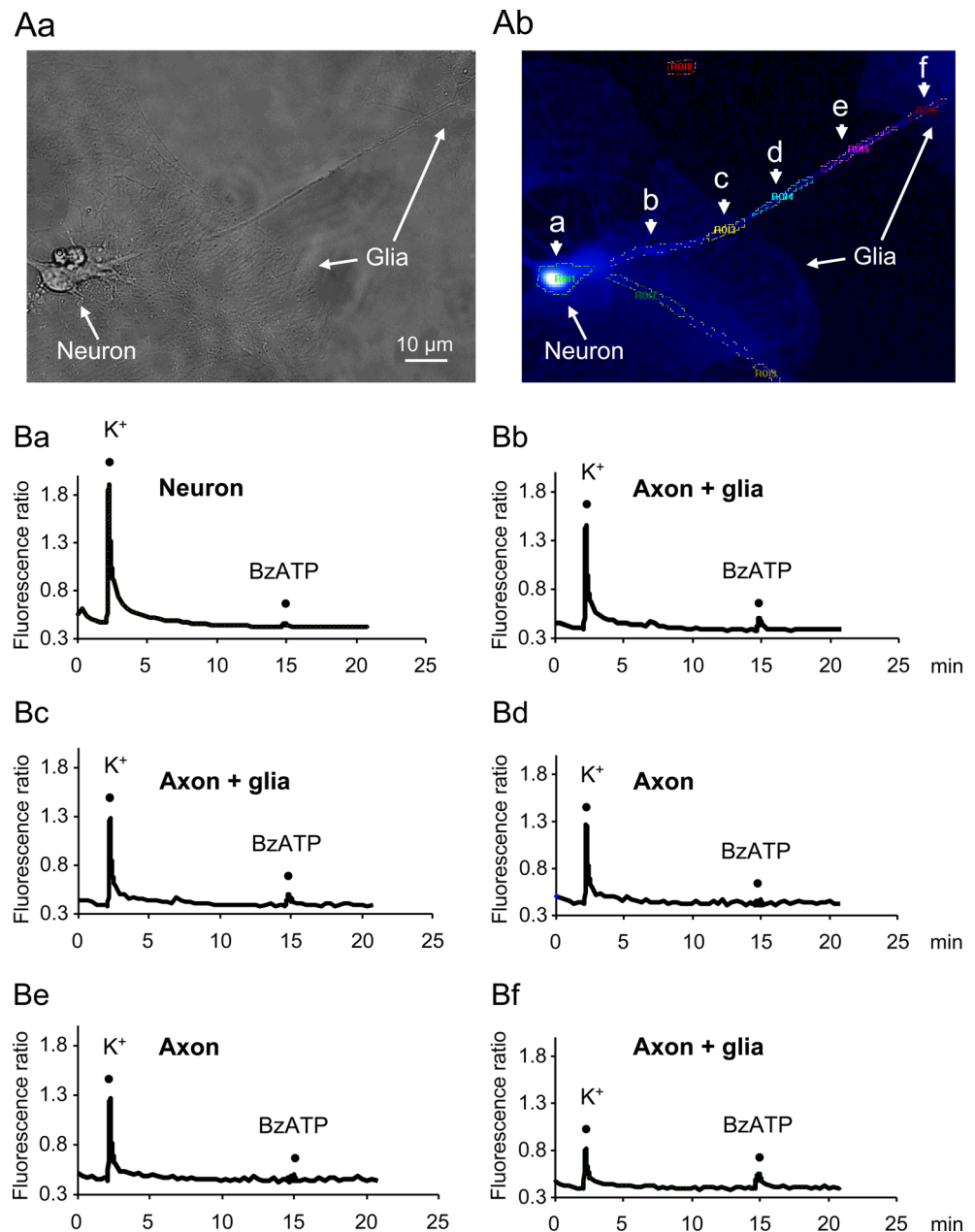
In a normal Ca^{2+} -containing and Mg^{2+} -free medium, the application of Bz-ATP (300 μ M), with the usual protocol (5-s duration, 12-min intervals) and in the absence of any further drug, caused stable $[Ca^{2+}]_i$ responses (at S_2 100 %, at S_3 96.6 ± 2.5 %, at S_4 87.1 ± 3.7 %; $n=23$ and $P>0.05$ each; Fig. 3Bb). Although there was a tendency of the responses to Bz-ATP to decrease, this change did not reach the level of statistical significance and was not used to correct further experimental data. The possible slight overestimation of the inhibitory potency of P2X receptor antagonists might be a consequence of this procedure.

In order to characterise the P2X receptors involved in mediating Bz-ATP (300 μ M)-induced $[Ca^{2+}]_i$ transients, the inhibitory effect of the highly selective P2X7 receptor antagonist A438079 (10 μ M) was investigated (Fig. 3Bc; Jarvis and Khakh 2009). A438079 depressed the effect of Bz-ATP, but failed to abolish it. The residual agonistic activity of Bz-ATP was, however, completely inhibited by the non-selective P2X/P2Y receptor antagonist PPADS (30 μ M), when added to an A438079-containing superfusion medium. The percentage inhibition by a Ca^{2+} -free medium (to 4.0 ± 0.5 %; $n=31$; $P<0.05$), by increasing concentrations of A438079 (at 10 μ M, 47.1 ± 4.6 %; $n=18$; $P<0.05$) and by A438079 plus PPADS (6.6 ± 5.0 %; $n=19$; $P<0.05$) is summarised in Fig. 3Bd. Since the antagonist IC_{50} value of A438079 in Ca^{2+} imaging studies at recombinant rat and human P2X7 receptors is ~ 0.06 μ M (Donnelly-Roberts and Jarvis 2007), a 10 μ M concentration of the antagonist is certainly supramaximal. Hence, it was concluded that only about one half of the Bz-ATP-induced $[Ca^{2+}]_i$ transients was due to the stimulation of P2X7 receptors, while the residual half may depend on the stimulation of other, unidentified P2X receptor types.

Absence of P2X7 receptors at cultured hippocampal neurons, but not astrocytes: a whole-cell patch-clamp study

The Ca^{2+} -imaging experiments demonstrated that astrocytic cell bodies in the rat hippocampus possess Bz-ATP-sensitive P2X7 receptors blocked by A438079. It was concluded, based on indirect evidence, that the Bz-ATP-induced $[Ca^{2+}]_i$ increase relies on the influx of this cation from the extracellular space. In order to directly confirm this assumption, we investigated by means of the whole-cell patch-clamp method,

Fig. 1 Bz-ATP-induced increases of $[Ca^{2+}]_i$ in newborn rat hippocampal cell cultures, loaded with the fluorescent indicator Fura-2. The fluorescence ratio (340/380 nm) provides a relative measure of the cytosolic free Ca^{2+} concentration. Hippocampal neurons were identified by locally superfused high K^+ (for 5 s), which opens voltage-sensitive Ca^{2+} channels and thereby leads to the influx of Ca^{2+} . Then Bz-ATP (for 5 s again) was applied by the same superfusion system. **A** Light microscopic (**a**, with a few ring-like structures in the background due to the use of an oil immersion objective) and fluorescence microscopic (**b**) pictures of the cell body of a neuron and its two cellular processes, taken before starting the experiment. Six areas of interest were defined to measure $[Ca^{2+}]_i$ both in the cell body and in the individual segments of an axo-dendritic extension. **B** $[Ca^{2+}]_i$ responses to high K^+ (50 mM) and Bz-ATP (300 μ M) in the neuron displayed in (A). Bz-ATP had no effect in the cell body (a 'neuron') and in the axo-dendritic extension (d, e 'axon'), except when signals from the underlying glial carpet interfered with measurements (b, c, f 'axon + glia'). This is one representative experiment out of a total of 12

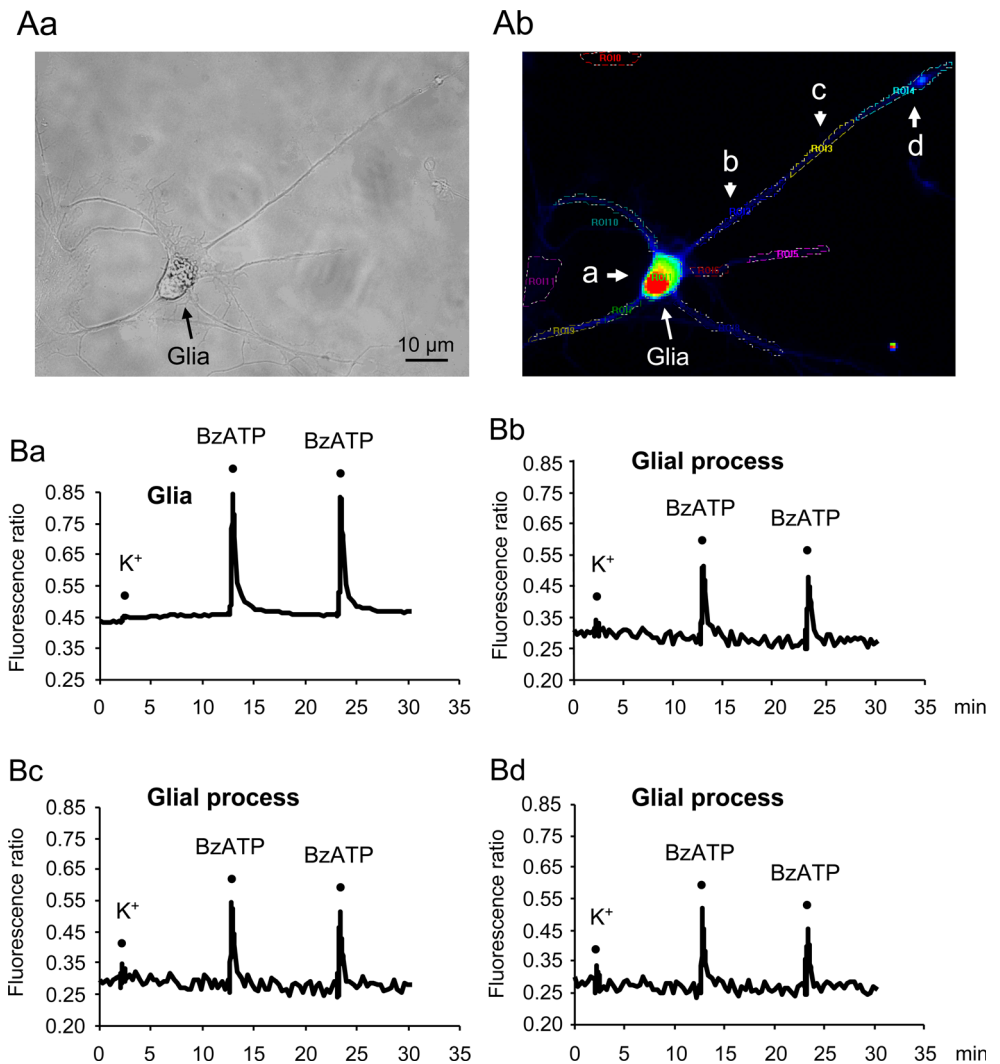


whether Bz-ATP (300 μ M) is able to cause an inward current in newborn astrocytes (Fig. 4A). In fact, in a normal bath medium, Bz-ATP induced a current response which was markedly increased in a low X^{2+} external solution (Fig. 4Aa). This effect was roughly comparable in newborn (275.2 ± 65.6 %; $n=8$; $P<0.05$) and embryonic (387.3 ± 76.1 %; $n=6$; $P<0.05$) astrocytes (Fig. 4Ab–d; consider the large scatter around the mean). The inverse relationship of the divalent cation concentration in the external medium and the ATP/Bz-ATP-induced responses is a typical characteristic of P2X7 receptor involvement (Sperlágh et al. 2006). The inward current is carried by Na^+ and Ca^{2+} ions, the latter of which

being responsible for the $[Ca^{2+}]_i$ increase (Sperlágh et al. 2006; Skaper et al. 2010). The (partial) sensitivity of the astroglial Bz-ATP current to blockade by selective P2X7 receptor antagonists in a low X^{2+} medium has been documented repeatedly (Nörenberg et al. 2010; Oliveira et al. 2011; Messermer et al. 2013) and was, therefore, not studied in the present experiments.

Then Bz-ATP (300 μ M) was applied onto newborn hippocampal neurons to find out whether a change in the holding current occurs. In these experiments, the neurons chosen for impalement were always positioned on a glial cell layer. Under these conditions, there was no current response either

Fig. 2 Bz-ATP-induced increases of $[Ca^{2+}]_i$ in newborn rat hippocampal cell cultures, loaded with the fluorescent indicator Fura-2. Hippocampal astrocytes were identified by locally superfused K^+ (for 5 s), which opens voltage-sensitive Ca^{2+} channels only in neurons and thereby has no effect in astrocytes, where these channels are missing. Then Bz-ATP (for 5 s again) was applied by the same superfusion system. **A** Light microscopic (**a** with a few ring-like structures in the background due to the use of an oil immersion objective) and fluorescence microscopic (**b**) pictures of the cell body of an astrocyte and its five cellular processes, taken before starting the experiment. Four areas of interest were defined to measure $[Ca^{2+}]_i$ both in the cell body and in the individual segments of an astrocytic process. **B** No $[Ca^{2+}]_i$ response to high K^+ (50 mM) and prominent $[Ca^{2+}]_i$ responses to Bz-ATP (300 μ M) in the astrocyte displayed in (A). Bz-ATP was effective both in the cell body (**a** 'glia') and in all segments of the astrocytic process (**b**–**d**). This is one representative experiment in a hippocampal astrocyte, belonging to a subgroup of 14 cells, which resembled neurons in their shape



in a normal or a low X^{2+} superfusion medium (Fig. 4Ba, b), excluding the existence of P2X receptors (e.g. P2X7) at the plasma membrane.

Eventually, spontaneous postsynaptic currents were recorded from newborn hippocampal neurons in a low X^{2+} external solution (Fig. 5). Superfusion with a combination of AMPA and NMDA receptor antagonists (10 μ M CNQX and 50 μ M AP5, respectively) abolished these current responses, demonstrating that they are due to the exocytotic release of glutamate from neuronal terminals interconnecting cultured hippocampal neurons (Fig. 5A). The blockade by the used antagonists of ionotropic glutamate receptors developed rapidly upon application and vanished with a comparable speed after wash-out. Thus, under the conditions of this study and at a holding potential of -70 mV, glutamatergic spontaneous excitatory postsynaptic currents (sEPSCs) were recorded from the patched hippocampal neurons. Bz-ATP without any doubt did not modify either the amplitude or the frequency of the sEPSCs (Fig. 5Ba–c, Ca, b), indicating a failure of presynaptic

or postsynaptic P2X receptors (e.g. P2X7) to interfere with synaptic transmission.

Discussion

The present experiments unequivocally demonstrated that functional P2X7 receptors operate in cultured hippocampal astrocytes irrespective of whether they were prepared from embryonic or newborn rats. These findings are in agreement with previously published data. In fact, quantitative real-time polymerase chain reaction (RT-PCR), Western blotting and immunohistochemistry of primary cultures of astrocytes obtained from the rat cerebral cortex documented the presence of P2X7 receptors (Fischer et al. 2009; Fumagalli et al. 2003; Illes et al. 2012). More importantly, in acutely isolated Müller glial cells of the retina, single-cell RT-PCR identified the message for P2X7 in humans (Pannicke et al. 2000). Further,

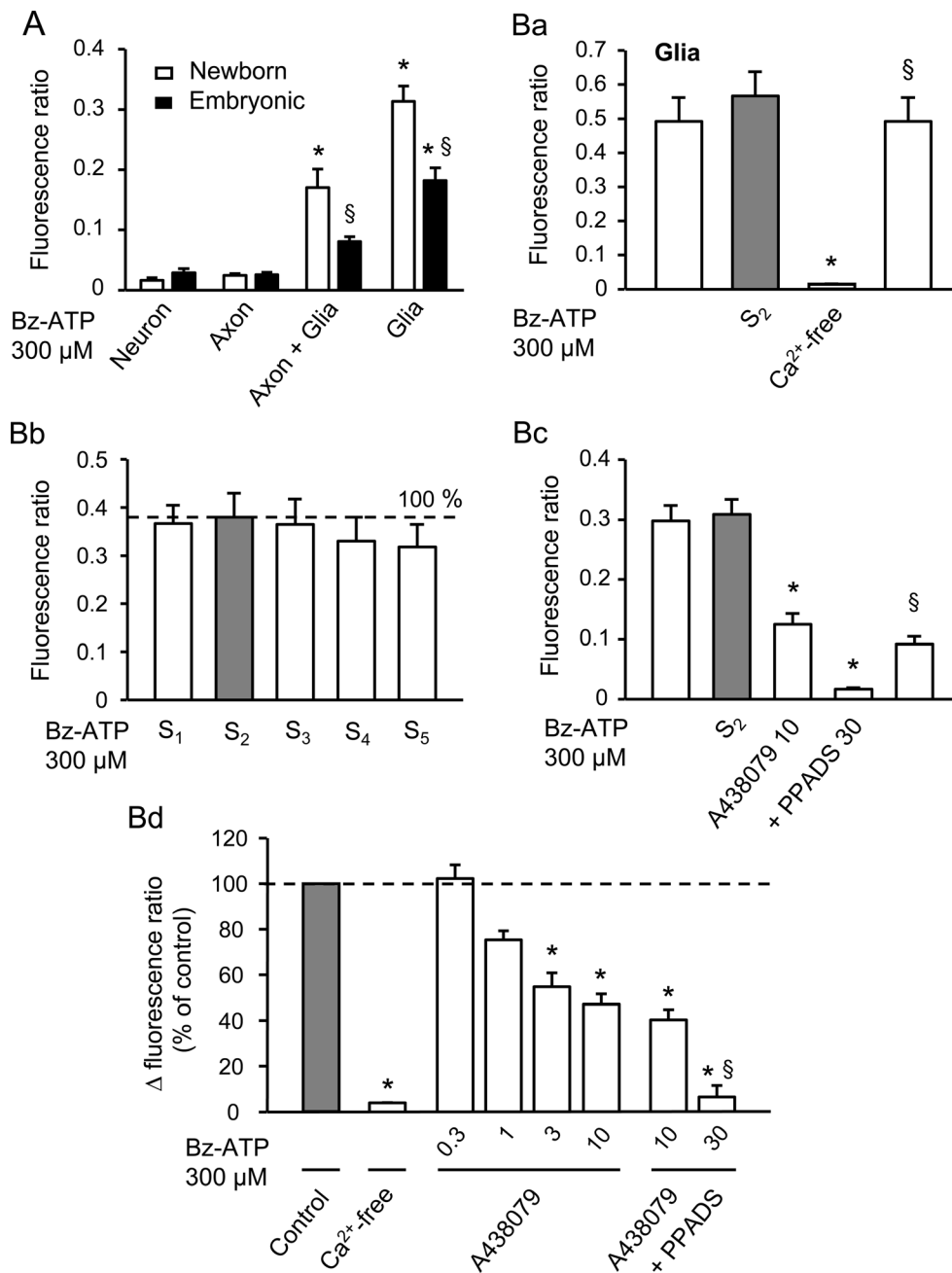


Fig. 3 Bz-ATP-induced $[Ca^{2+}]_i$ transients in rat hippocampal neurons and astrocytes kept in culture and loaded with the fluorescent indicator Fura-2. Neurons and astrocytes were discriminated by locally superfused high K^+ (for 5 s; see Figs. 1, 2). Then Bz-ATP (for 5 s) was applied by a local superfusion system either in the absence or the presence of a Ca^{2+} -free or A438079-containing bath medium, with added PPADS, when indicated. Mean \pm S.E.M of n experiments are shown in this and all subsequent panels. **A** Large Bz-ATP (300 μ M)-induced increases of $[Ca^{2+}]_i$ in axo-dendritic processes with underlying glial cell bodies ('axon + glia') and glial cell bodies ('glia'), but not in neuronal somata ('neuron') and in neuronal axo-dendritic processes ('axon'). Newborn (*empty squares*; $n=12-52$) and embryonic (*filled squares*; $n=33-88$) cell cultures were used. * $P<0.05$; statistically significant difference for newborn (from the first empty column) and embryonic (from the first filled column) neuronal-astrocytic cultures. § $P<0.05$; statistically significant

difference within a pair of empty and filled columns. **B** Results obtained with newborn hippocampal cell cultures by investigating astrocytic cells. **a** Inhibition of Bz-ATP (300 μ M)-induced $[Ca^{2+}]_i$ transients in a nominally Ca^{2+} -free medium ($n=31$). **b** Reproducibility of Bz-ATP (300 μ M)-induced $[Ca^{2+}]_i$ transients during four repetitive applications with 12-min intervals (S_2-S_5). There was no statistically significant difference from S_2 ($P>0.05$). **c** Inhibition of Bz-ATP (300 μ M)-induced $[Ca^{2+}]_i$ transients by A438079 (10 μ M) alone or in combination with PPADS (30 μ M) ($n=19$). **d** Summary picture of the percentage inhibition of Bz-ATP (300 μ M)-induced $[Ca^{2+}]_i$ transients taken from the previous experiments and also from additional ones made in increasing concentrations of A438079 (0.3–10 μ M; $n=18-20$). * $P<0.05$; statistically significant difference from S_2 in all panels. § $P<0.05$; statistically significant difference from the preceding column in all panels. All application protocols are described in the 'Methods' section

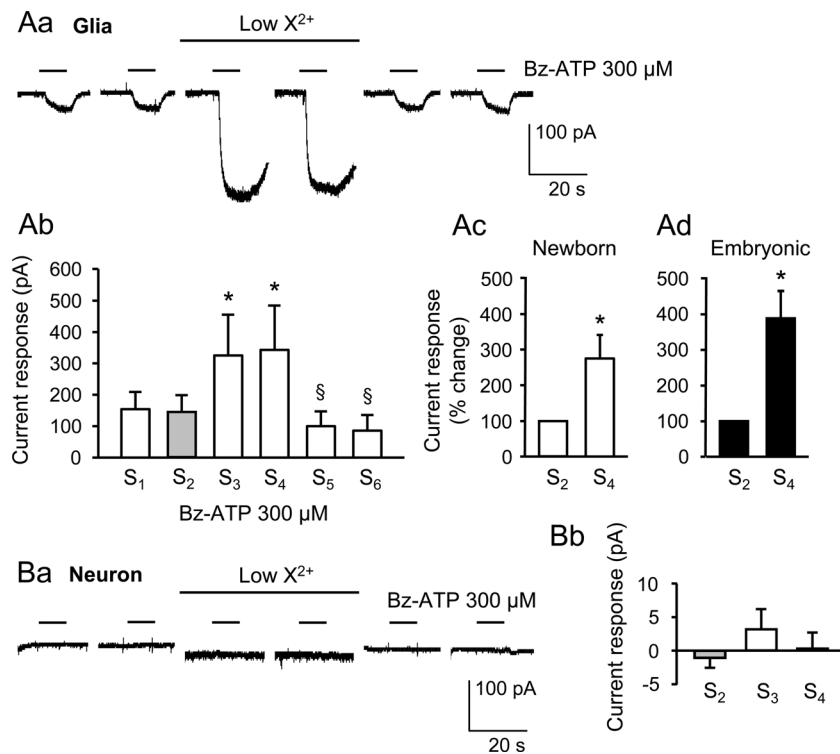


Fig. 4 Bz-ATP-induced currents of rat hippocampal neurons and astrocytes kept in culture. The whole-cell configuration of the patch-clamp method was used for recording. The holding potential for neurons and astrocytes was -70 and -80 mV, respectively. Bz-ATP was applied locally by a fast superfusion system for 5 s every 5 min six times in total (S_1 – S_6). **A** Potentiation of Bz-ATP ($300 \mu\text{M}$)-induced currents in a low Ca^{2+} /no Mg^{2+} (low X^{2+})-containing bath medium in astrocytes. **a** A representative experiment on a newborn glial cell. **b** Mean \pm S.E.M. of eight experiments similar to those shown in (a). Percentage increase of the Bz-ATP effect at S_4 with respect to that measured at S_2 both in

newborn (**c**) and embryonic (**d**) astrocytes ($n=8$, each). $*P<0.05$; statistically significant difference from S_2 . $^{\S}P<0.05$; statistically significant difference from S_4 . **B** Failure of Bz-ATP to act at cultured newborn neurons either in a normal or a low X^{2+} bath medium. **a** A representative experiment demonstrates that a low X^{2+} medium slightly increased the holding current by itself, but still did not alter the Bz-ATP-induced current response. **b** Mean \pm S.E.M. of eight experiments similar to those shown in (a). There was no statistically significant difference ($P>0.05$) at S_3 or S_4 in comparison with the current measured at S_2

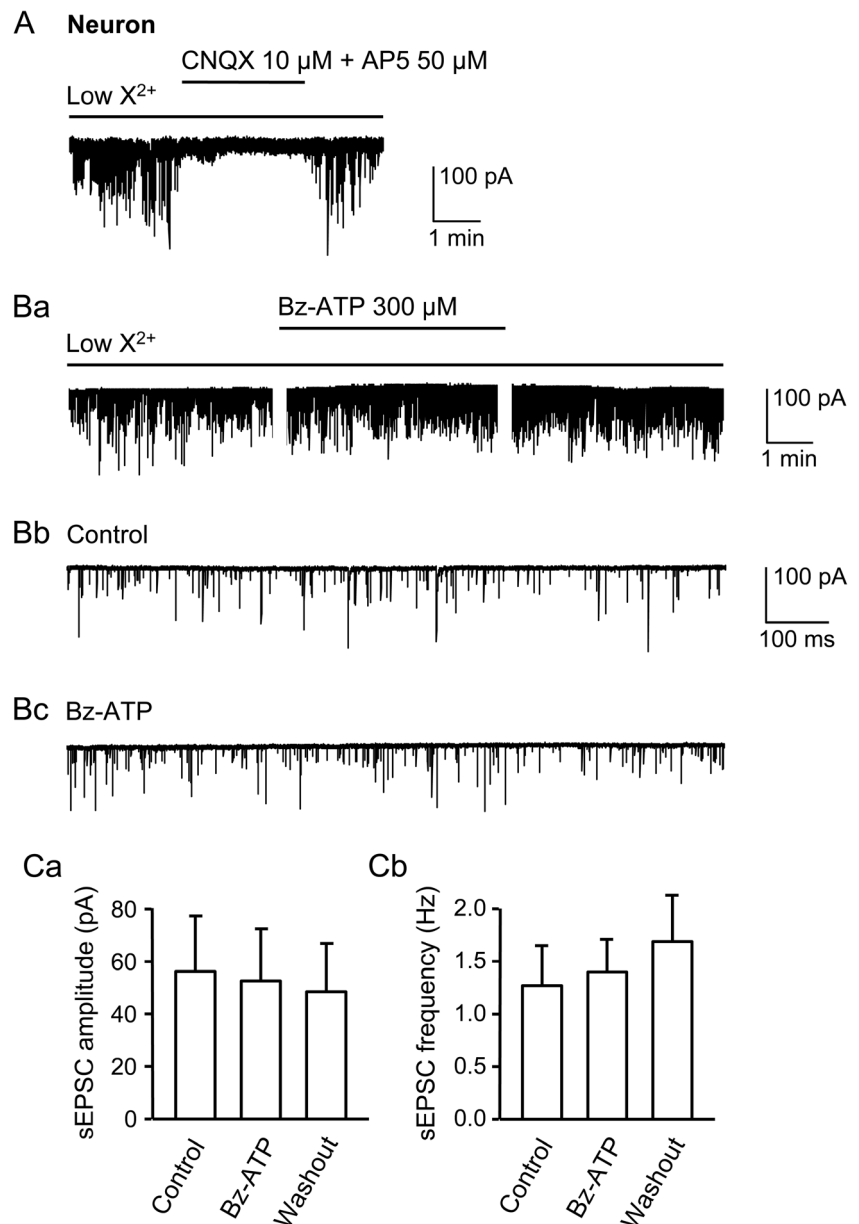
staining with specific antibodies revealed astroglial expression of P2X7 receptors in the juvenile rat hippocampus (Kukley et al. 2001). It is especially interesting that both mechanical and ischemic injury led to the appearance of previously absent P2X7 receptor-immunoreactivity in accumbal and cortical astrocytes of rats (Franke et al. 2001, 2004; Bai and Li 2013).

Patch-clamp studies also confirmed the presence of functional P2X7 receptors in acutely isolated human Müller cells (Pannicke et al. 2000), cultured rodent cortical astrocytes (Duan et al. 2003; Nörenberg et al. 2010) and in astrocytes patch-clamped in acute cortical brain slices of rats and mice (Oliveira et al. 2011). In these cells, the application of ATP and Bz-ATP caused inward currents which were potentiated in a low X^{2+} medium, were blocked by selective antagonists and were absent in $\text{P2X7}^{-/-}$ mice. Based on the considerable Ca^{2+} permeability of P2X receptors, $[\text{Ca}^{2+}]_i$ recordings were repeatedly used to investigate the existence of these receptors in astroglia. In fact, such experiments with cultured cerebrocortical (Fumagalli et al. 2003) and cerebellar astrocytes (Carrasquero et al. 2009) supplied evidence for the presence of P2X7 receptors. Eventually, the activation of

signalling cascades of P2X7 receptors and the long-term trophic or apoptotic/necrotic consequences of their operation have also been demonstrated after the application of exogenous nucleotides or promoting their endogenous release under in vitro/in vivo conditions (Neary and Zimmermann 2009; Burnstock and Verkhatsky 2010).

It is noteworthy that in the hippocampal CA1 region of transgenic mice with human glial fibrillary acidic protein promoter controlled expression of enhanced green fluorescent protein [Tg(hGFAP/EGFP)], a previous study failed to identify P2X7 receptors at astroglial cells (Jabs et al. 2007). In support of these findings, P2X7 receptor activation induced pore formation and p38 mitogen-activated protein kinase (MAPK) phosphorylation in cultured cortical but not hippocampal astrocytes (Bianco et al. 2009). However, when astroglia was identified in brain slices of the prefrontal cortex of Wistar rats and Tg(hGFAP/EGFP) mice, it responded to Bz-ATP/ATP with current responses (Oliveira et al. 2011). Moreover, stratum oriens astrocytes in the immediate neighbourhood of CA1 neurons in the rat hippocampus were also sensitive to Bz-ATP, albeit especially in a low X^{2+}

Fig. 5 Spontaneous postsynaptic excitatory currents (sEPSCs) recorded from cultured newborn hippocampal neurons prepared from rat brains. The whole-cell configuration of the patch-clamp method was used in these experiments. The holding potential was set at -70 mV. The bath medium contained a low Ca^{2+} concentration and no added Mg^{2+} (low X^{2+}). CNQX ($10 \mu\text{M}$) and AP5 ($50 \mu\text{M}$) were applied locally by means of a fast superfusion system. Bz-ATP ($300 \mu\text{M}$) was applied by the same system for 5 min after a preceding 5 min recording period and was washed out subsequently for again 5 min. **A** Blockade of sEPSC amplitudes by a combination of CNQX and AP5. One representative experiment out of four similar ones. **B a–c** A representative experiment demonstrates the missing effect of Bz-ATP ($300 \mu\text{M}$) on the sEPSCs. **C** Mean \pm S.E.M. of seven experiments similar to those shown in (A); Bz-ATP did not alter either the amplitude (a) or the frequency (b) of sEPSCs. There was no statistically significant difference ($P > 0.05$) between the current responses measured before, during and after the application of Bz-ATP



external medium (Fellin et al. 2006; Oliveira et al. 2011; Leichsenring et al. 2013).

In contrast to the situation in astrocytes, in cultured hippocampal neurons, we were not able to document an unequivocal effect of the prototypic P2X7 receptor agonist Bz-ATP either by means of $[\text{Ca}^{2+}]_i$ measurement or by patch-clamp recording of membrane currents. Numerous studies support the view that axons and especially axonal terminals of cultured or acutely dissociated neurons possess P2X7 receptors (see 'Introduction' section). However, there are a number of relevant points which require further clarification. First, P2X7 antibodies were reported to selectively label the respective receptors at peripheral immunocytes, but not P2X7 receptors located at brain neurons (Sim et al. 2004). A main argument of

these authors was the immunostaining for P2X7 receptors in neuronal structures of the brain in P2X7 $^{-/-}$ mice. This argument was later invalidated by showing that several splice variants of P2X7 receptors occur, which may evade inactivation in the knockout animals (Cheewatrakoolpong et al. 2005; Nicke et al. 2009). Second, ATP was suggested to increase $[\text{Ca}^{2+}]_i$ in synaptophysin-immunopositive synaptosomes prepared from rat midbrain (Miras-Portugal et al. 2003; Marin-Garcia et al. 2008). Staining of synaptosomes by P2X7 antibodies could be also demonstrated. It has been, however, reported by others that astrocytes contain the whole machinery of synaptic proteins, including synaptophysin, and store and exocytotically release ATP/glutamate; this process has been termed gliotransmission (Halassa et al. 2007; Zorec et al.

2012). Thus, the synaptosomal preparations investigated might originate both from neurons and glial cells. Third, it was reported that the axo-dendritic processes of cultured mesencephalic neurons (Marin-Garcia et al. 2008) and cerebellar granule cells (Sanchez-Nogueiro et al. 2005; Leon et al. 2006) react to ATP/Bz-ATP with prominent $[Ca^{2+}]_i$ transients in rodent preparations. These responses could be blocked by P2X7 receptor antagonists or negative allosteric modulators such as Zn^{2+} ; they also became more prominent, the farther the axo-dendritic segment was located from the cell body. Similar data were reported also for cultured embryonic hippocampal neurons (Diaz-Hernandez et al. 2008). However, we were not able to confirm these data in our present study.

Neurons and astroglial cells have been reported to interact with each other in a bidirectional way by means of a multitude of signalling molecules/transmitters (Bezzi and Volterra 2001; Lalo et al. 2011; Illes et al. 2012). The stimulation of astrocytic P2X7 receptors releases glutamate (Duan et al. 2003), GABA (Wang et al. 2002), ATP (Suadicani et al. 2009), endocannabinoids (Witting et al. 2004) and interleukin-1 β (Abbracchio and Ceruti 2006). Thus, Bz-ATP-induced neuronal $[Ca^{2+}]_i$ transients may arise indirectly via a reaction chain initiated by the activation of astroglial P2X7 receptors, followed by the release of a glio-neuronal signalling molecule through its effect at specific receptors of the cell somata/processes of neurons and the subsequent entry of Ca^{2+} into the intracellular space. Under the conditions of the present experiments, we found that Bz-ATP caused an elevation of $[Ca^{2+}]_i$ in the neuronal axo-dendritic extensions only, if they were in close physical contact with the underlying astroglial carpet. Experiments with the selective astrocytic metabolic poison fluorocitrate (Clarke 1991) suggested that the release of a glio-neuronal signalling molecule was not involved in this process. In our opinion, it is more likely that the limited focal resolution of our fluorescence microscope results in its inability to differentiate between $[Ca^{2+}]_i$ transients in the axo-dendritic processes and the underlying glial cells.

The axonal Ca^{2+} entry could have various consequences. First, it may regulate the frequency of action potentials travelling along the axon (Callewaert et al. 1996). Second, it may stimulate axonal elongations during neurite outgrowth (Ramakers et al. 2001). Third, it may imitate the $[Ca^{2+}]_i$ transients causing exocytotic transmitter release in the terminal axons (Jackson et al. 2001). Hence, the limited efficiency of Bz-ATP to increase $[Ca^{2+}]_i$ of the axo-dendritic processes in conjunction with our electrophysiological data, which did not document a modification of the holding current of neurons or the frequency/amplitude of their sEPSCs by Bz-ATP, supports the notion that P2X7 receptors are present only at a very low density at hippocampal neurons or even not at all. Of course, it is still possible that, because of the known plasticity of astrocytes and, to a minor extent, also of

neurons in cell culture preparations, the in vitro and in vivo situations differ from each other.

In conclusion, the present experiments by no way exclude the possibility that, in other areas of the central/peripheral nervous system or in other types of neurons than the present ones, P2X7 receptors exist. For example, we reported ourselves that in cultured embryonic cortical neurons, Bz-ATP increased the frequency but not the amplitude of GABAergic sIPSCs and, at the same time, facilitated the release of previously incorporated $[^3H]GABA$ (Wirkner et al. 2005). However, even in this special case, just as the other ones, there is room for justifiable doubt in allocating these receptors directly to neuronal structures; their astrocytic localisation and the modulation of neighbouring neurons by an astroglial signalling molecule is a pertinent possibility.

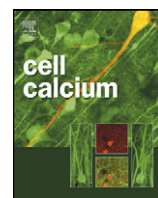
Acknowledgments This work was supported by a grant of the Deutsche Forschungsgemeinschaft (IL 20/19-1). We thank to Mrs. Katalin Rozmer for methodological help. A scholarship of the Mashad University of Medical Sciences, Mashad, Iran to Dr. Soghra Mehri is gratefully acknowledged.

References

- Abbracchio MP, Ceruti S (2006) Roles of P2 receptors in glial cells: focus on astrocytes. *Purinergic Signal* 2:595–604
- Anderson CM, Nedergaard M (2006) Emerging challenges of assigning P2X7 receptor function and immunoreactivity in neurons. *Trends Neurosci* 29:257–262
- Bai HY, Li AP (2013) P2X7 receptors in cerebral ischemia. *Neurosci Bull* 29:390–398
- Bezzi P, Volterra A (2001) A neuron-glia signalling network in the active brain. *Curr Opin Neurobiol* 11:387–394
- Bianchi BR, Lynch KJ, Touma E, Niforatos W, Burgard EC, Alexander KM, Park HS, Yu H, Metzger R, Kowaluk E, Jarvis MF, van Biesen T (1999) Pharmacological characterization of recombinant human and rat P2X receptor subtypes. *Eur J Pharmacol* 376:127–138
- Bianco F, Colombo A, Saglietti L, Lecca D, Abbracchio MP, Matteoli M, Verderio C (2009) Different properties of P2X7 receptor in hippocampal and cortical astrocytes. *Purinergic Signal* 5:233–240
- Burnstock G, Verkhratsky A (2010) Long-term (trophic) purinergic signalling: purinoceptors control cell proliferation, differentiation and death. *Cell Death Dis* 1:e9
- Burnstock G, Krügel U, Abbracchio MP, Illes P (2011) Purinergic signalling: from normal behaviour to pathological brain function. *Prog Neurobiol* 95:229–274
- Callewaert G, Eilers J, Konnerth A (1996) Axonal calcium entry during fast 'sodium' action potentials in rat cerebellar Purkinje neurones. *J Physiol* 495:641–647
- Carrasquero LM, Delicado EG, Bustillo D, Gutierrez-Martin Y, Artalejo AR, Miras-Portugal MT (2009) P2X7 and P2Y₁₃ purinergic receptors mediate intracellular calcium responses to BzATP in rat cerebellar astrocytes. *J Neurochem* 110:879–889
- Cheewatrakoolpong B, Gilchrist H, Anthes JC, Greenfeder S (2005) Identification and characterization of splice variants of the human P2X7 ATP channel. *Biochem Biophys Res Commun* 332:17–27
- Clarke DD (1991) Fluoroacetate and fluorocitrate: mechanism of action. *Neurochem Res* 16:1055–1058
- Deuchars SA, Atkinson L, Brooke RE, Musa H, Milligan CJ, Batten TF, Buckley NJ, Parson SH, Deuchars J (2001) Neuronal P2X7

- receptors are targeted to presynaptic terminals in the central and peripheral nervous systems. *J Neurosci* 21:7143–7152
- Di Virgilio F, Ceruti S, Bramanti P, Abbracchio MP (2009) Purinergic signalling in inflammation of the central nervous system. *Trends Neurosci* 32:79–87
- Diaz-Hernandez M, del Puerto A, Diaz-Hernandez JI, Diez-Zaera M, Lucas JJ, Garrido JJ, Miras-Portugal MT (2008) Inhibition of the ATP-gated P2X7 receptor promotes axonal growth and branching in cultured hippocampal neurons. *J Cell Sci* 121:3717–3728
- Donnelly-Roberts DL, Jarvis MF (2007) Discovery of P2X7 receptor-selective antagonists offers new insights into P2X7 receptor function and indicates a role in chronic pain states. *Br J Pharmacol* 151:571–579
- Duan S, Anderson CM, Keung EC, Chen Y, Chen Y, Swanson RA (2003) P2X7 receptor-mediated release of excitatory amino acids from astrocytes. *J Neurosci* 23:1320–1328
- Fellin T, Pozzan T, Carmignoto G (2006) Purinergic receptors mediate two distinct glutamate release pathways in hippocampal astrocytes. *J Biol Chem* 281:4274–4284
- Fischer W, Appelt K, Grohmann M, Franke H, Nörenberg W, Illes P (2009) Increase of intracellular Ca^{2+} by P2X and P2Y receptor-subtypes in cultured cortical astroglia of the rat. *Neuroscience* 160:767–783
- Franke H, Grosche J, Schädlich H, Krügel U, Allgaier C, Illes P (2001) P2X receptor expression on astrocytes in the nucleus accumbens of rats. *Neuroscience* 108:421–429
- Franke H, Günther A, Grosche J, Schmidt R, Rossner S, Reinhardt R, Faber-Zuschratler H, Schneider D, Illes P (2004) P2X7 receptor expression after ischemia in the cerebral cortex of rats. *J Neuropathol Exp Neurol* 63:686–699
- Fumagalli M, Brambilla R, D'Ambrosi N, Volonte C, Matteoli M, Verderio C, Abbracchio MP (2003) Nucleotide-mediated calcium signaling in rat cortical astrocytes: role of P2X and P2Y receptors. *Glia* 43:218–230
- Halassa MM, Fellin T, Haydon PG (2007) The tripartite synapse: roles for gliotransmission in health and disease. *Trends Mol Med* 13:54–63
- Hu HZ, Gao N, Lin Z, Gao C, Liu S, Ren J, Xia Y, Wood JD (2001) P2X7 receptors in the enteric nervous system of guinea-pig small intestine. *J Comp Neurol* 440:299–310
- Illes P, Verkhatsky A, Burnstock G, Franke H (2012) P2X receptors and their roles in astroglia in the central and peripheral nervous system. *Neuroscientist* 18:422–438
- Jabs R, Matthias K, Grote A, Grauer M, Seifert G, Steinhäuser C (2007) Lack of P2X receptor mediated currents in astrocytes and GluR type glial cells of the hippocampal CA1 region. *Glia* 55:1648–1655
- Jackson VM, Trout SJ, Brain KL, Cunnane TC (2001) Characterization of action potential-evoked calcium transients in mouse postganglionic sympathetic axon bundles. *J Physiol* 537:3–16
- Jarvis MF, Khakh BS (2009) ATP-gated P2X cation-channels. *Neuropharmacology* 56:208–215
- Khadra A, Tomic M, Yan Z, Zemkova H, Sherman A, Stojilkovic SS (2013) Dual gating mechanism and function of P2X7 receptor channels. *Biophys J* 104:2612–2621
- Kukley M, Barden JA, Steinhäuser C, Jabs R (2001) Distribution of P2X receptors on astrocytes in juvenile rat hippocampus. *Glia* 36:11–21
- Lalo U, Verkhatsky A, Pankratov Y (2011) Ionotropic ATP receptors in neuronal–glial communication. *Semin Cell Dev Biol* 22:220–228
- Leichsenring A, Riedel T, Qin Y, Rubini P, Illes P (2013) Anoxic depolarization of hippocampal astrocytes: possible modulation by P2X7 receptors. *Neurochem Int* 62:15–22
- Leon D, Hervas C, Miras-Portugal MT (2006) P2Y₁ and P2X7 receptors induce calcium/calmodulin-dependent protein kinase II phosphorylation in cerebellar granule neurons. *Eur J Neurosci* 23:2999–3013
- Marin-Garcia P, Sanchez-Nogueiro J, Gomez-Villafuertes R, Leon D, Miras-Portugal MT (2008) Synaptic terminals from mice midbrain exhibit functional P2X7 receptor. *Neuroscience* 151:361–373
- Messemer N, Kunert C, Grohmann M, Sobottka H, Nieber K, Zimmermann H, Franke H, Nörenberg W, Straub I, Schaefer M, Riedel T, Illes P, Rubini P (2013) P2X7 receptors at adult neural progenitor cells of the mouse subventricular zone. *Neuropharmacology* 73:122–137
- Miras-Portugal MT, Diaz-Hernandez M, Giraldez L, Hervas C, Gomez-Villafuertes R, Sen RP, Gualix J, Pintor J (2003) P2X7 receptors in rat brain: presence in synaptic terminals and granule cells. *Neurochem Res* 28:1597–1605
- Neary JT, Zimmermann H (2009) Trophic functions of nucleotides in the central nervous system. *Trends Neurosci* 32:189–198
- Nicke A, Kuan YH, Masin M, Rettinger J, Marquez-Klaka B, Bender O, Gorecki DC, Murrell-Lagnado RD, Soto F (2009) A functional P2X7 splice variant with an alternative transmembrane domain 1 escapes gene inactivation in P2X7 knock-out mice. *J Biol Chem* 284:25813–25822
- Nörenberg W, Schunk J, Fischer W, Sobottka H, Riedel T, Oliveira JF, Franke H, Illes P (2010) Electrophysiological classification of P2X7 receptors in rat cultured neocortical astroglia. *Br J Pharmacol* 160:1941–1952
- Oliveira JF, Riedel T, Leichsenring A, Heine C, Franke H, Krügel U, Nörenberg W, Illes P (2011) Rodent cortical astroglia express in situ functional P2X7 receptors sensing pathologically high ATP concentrations. *Cereb Cortex* 21:806–820
- Pannicke T, Fischer W, Biedermann B, Schädlich H, Grosche J, Faude F, Wiedemann P, Allgaier C, Illes P, Burnstock G, Reichenbach A (2000) P2X7 receptors in Muller glial cells from the human retina. *J Neurosci* 20:5965–5972
- Papp L, Vizi ES, Sperlagh B (2004) Lack of ATP-evoked GABA and glutamate release in the hippocampus of P2X7 receptor^{-/-} mice. *Neuroreport* 15:2387–2391
- Ramakers GJ, Avci B, van Hulten P, van Ooyen A, van Pelt J, Pool CW, Lequin MB (2001) The role of calcium signaling in early axonal and dendritic morphogenesis of rat cerebral cortex neurons under non-stimulated growth conditions. *Brain Res Dev Brain Res* 126:163–172
- Rubini P, Pinkwart C, Franke H, Gerevich Z, Nörenberg W, Illes P (2006) Regulation of intracellular Ca^{2+} by P2Y₁ receptors may depend on the developmental stage of cultured rat striatal neurons. *J Cell Physiol* 209:81–93
- Rubini P, Engelhardt J, Wirkner K, Illes P (2008) Modulation by D1 and D2 dopamine receptors of ATP-induced release of intracellular Ca^{2+} in cultured rat striatal neurons. *Neurochem Int* 52:113–118
- Rubini P, Milosevic J, Engelhardt J, Al-Khrasani M, Franke H, Heinrich A, Sperlagh B, Schwarz SC, Schwarz J, Nörenberg W, Illes P (2009) Increase of intracellular Ca^{2+} by adenine and uracil nucleotides in human midbrain-derived neuronal progenitor cells. *Cell Calcium* 45:485–498
- Sanchez-Nogueiro J, Marin-Garcia P, Miras-Portugal MT (2005) Characterization of a functional P2X7-like receptor in cerebellar granule neurons from P2X7 knockout mice. *FEBS Lett* 579:3783–3788
- Sim JA, Young MT, Sung HY, North RA, Surprenant A (2004) Reanalysis of P2X7 receptor expression in rodent brain. *J Neurosci* 24:6307–6314
- Skaper SD, Debetto P, Giusti P (2010) The P2X7 purinergic receptor: from physiology to neurological disorders. *FASEB J* 24:337–345
- Sperlagh B, Köfalvi A, Deuchars J, Atkinson L, Milligan CJ, Buckley NJ, Vizi ES (2002) Involvement of P2X7 receptors in the regulation of neurotransmitter release in the rat hippocampus. *J Neurochem* 81:1196–1211
- Sperlagh B, Vizi ES, Wirkner K, Illes P (2006) P2X7 receptors in the nervous system. *Prog Neurobiol* 78:327–346
- Suadicani SO, Iglesias R, Spray DC, Scemes E (2009) Point mutation in the mouse P2X7 receptor affects intercellular calcium waves in astrocytes. *ASN Neuro* 1(1)
- Surprenant A, Rassendren F, Kawashima E, North RA, Buell G (1996) The cytolytic P2Z receptor for extracellular ATP identified as a P2X receptor (P2X7). *Science* 272:735–738

- Verkhatsky A, Krishtal OA, Burnstock G (2009) Purinoceptors on neuroglia. *Mol Neurobiol* 39:190–208
- Wang CM, Chang YY, Kuo JS, Sun SH (2002) Activation of P2X7 receptors induced [³H]GABA release from the RBA-2 type-2 astrocyte cell line through a Cl⁻/HCO₃⁻-dependent mechanism. *Glia* 37: 8–18
- Wang X, Arcuino G, Takano T, Lin J, Peng WG, Wan P, Li P, Xu Q, Liu QS, Goldman SA, Nedergaard M (2004) P2X7 receptor inhibition improves recovery after spinal cord injury. *Nat Med* 10:821–827
- Wirkner K, Köfalvi A, Fischer W, Günther A, Franke H, Gröger-Armdt H, Nörenberg W, Madarász E, Vizi ES, Schneider D, Sperlágh B, Illes P (2005) Supersensitivity of P2X receptors in cerebrocortical cell cultures after in vitro ischemia. *J Neurochem* 95:1421–1437
- Witting A, Walter L, Wacker J, Möller T, Stella N (2004) P2X7 receptors control 2-arachidonoylglycerol production by microglial cells. *Proc Natl Acad Sci U S A* 101:3214–3219
- Zorec R, Araque A, Carmignoto G, Haydon PG, Verkhratsky A, Parpura V (2012) Astroglial excitability and gliotransmission: an appraisal of Ca²⁺ as a signalling route. *ASN Neuro* 4(2)



Increase of intracellular Ca^{2+} by adenine and uracil nucleotides in human midbrain-derived neuronal progenitor cells

Patrizia Rubini^a, Javorina Milosevic^b, Johannes Engelhardt^a, Mahmoud Al-Khrasani^a, Heike Franke^a, Attila Heinrich^c, Beata Sperlagh^c, Sigrid C. Schwarz^d, Johannes Schwarz^d, Wolfgang Nörenberg^a, Peter Illes^{a,*}

^a Rudolf-Boehm-Institute for Pharmacology und Toxicology, Haertelstrasse 16–18, University of Leipzig, D-04107 Leipzig, Germany

^b Translational Centre for Regenerative Medicine, D-04103 Leipzig, Germany

^c Laboratory of Molecular Pharmacology, Institute of Experimental Medicine, Hungarian Academy of Sciences, H-1450 Budapest, Hungary

^d Department of Neurology, University of Leipzig, D-04103 Leipzig, Germany

ARTICLE INFO

Article history:

Received 11 January 2009

Received in revised form 21 February 2009

Accepted 16 March 2009

Available online 21 April 2009

Keywords:

Human neuronal progenitor cells

Midbrain dopaminergic neurons

Adenine nucleotides

Uracil nucleotides

P2X receptors

P2Y receptors

ABSTRACT

Nucleotides play an important role in brain development and may exert their action *via* ligand-gated cationic channels or G protein-coupled receptors. Patch-clamp measurements indicated that in contrast to AMPA, ATP did not induce membrane currents in human midbrain derived neuronal progenitor cells (hmNPCs). Various nucleotide agonists concentration-dependently increased $[\text{Ca}^{2+}]_i$ as measured by the Fura-2 method, with the rank order of potency $\text{ATP} > \text{ADP} > \text{UTP} > \text{UDP}$. A Ca^{2+} -free external medium moderately decreased, whereas a depletion of the intracellular Ca^{2+} storage sites by cyclopiazonic acid markedly depressed the $[\text{Ca}^{2+}]_i$ transients induced by either ATP or UTP. Further, the P2Y₁ receptor antagonistic PPADS and MRS 2179, as well as the nucleotide catalyzing enzyme apyrase, almost abolished the effects of these two nucleotides. However, the P2Y_{1,2,12} antagonistic suramin only slightly blocked the action of ATP, but strongly inhibited that of UTP. In agreement with this finding, UTP evoked the release of ATP from hmNPCs in a suramin-, but not PPADS-sensitive manner. Immunocytochemistry indicated the co-localization of P2Y_{1,2,4}-immunoreactivities (IR) with nestin-IR at these cells. In conclusion, UTP may induce the release of ATP from hmNPCs *via* P2Y₂ receptor-activation and thereby causes $[\text{Ca}^{2+}]_i$ transients by stimulating a P2Y₁-like receptor.

© 2009 Elsevier Ltd. All rights reserved.

1. Introduction

In vitro expanded brain progenitors might overcome the limited availability of dopaminergic neurons in transplantation for Parkinson's disease. It has been shown, that embryonic mesencephalic stem cells can efficiently differentiate into dopaminergic neurons, survive intrastriatal transplantation and induce functional recovery in hemiparkinsonian rats [1,2]. In view of the possible therapeutic significance of these results, it was important to adapt the conditions of expansion and differentiation to human midbrain-derived neuronal progenitor cells (hmNPCs) [3–5]. Such conditions for expansion include the choice of adequate growth factors, e.g. epidermal growth factor (EGF), fibroblast growth factors (FGF-2, FGF-8) and/or glial derived neurotrophic factor (GDNF) as well as low atmospheric oxygen in serum-free medium. Whereas tissue derived from embryonic stem cells bears a considerable risk to give rise to malignancies following transplantation, hmNPCs fail

to induce such complications. Besides their therapeutic potential, both tissue culture systems provide novel insights into the development of human dopaminergic neurons *in vitro*.

Neurons, neuroglia (astrocytes and oligodendrocytes), and ependymal cells are three distinct categories of neuronal cells in the central nervous system (CNS [6]). As the cerebral ventriculi enlarge and their walls thicken, the primitive neuroepithelial cells elongate, maintaining a radial orientation until they migrate. Inevitably, during development, transitional forms between neuronal progenitors and the neurons, neuroglia and ependymal cells will also occur. NPCs prepared from rodent embryonic central nervous tissue were noted to generate oligodendrocytes, neurons and astrocytes in an approximate ratio of 1:5:25, respectively, when allowed to differentiate spontaneously after removal of growth factors or mitogens [7]. The yield of dopaminergic neurons from hmNPCs could be, however, considerably increased by replacing the expansion medium with mitogen-free, differentiation medium containing fetal calf serum, forskolin and interleukin-1 β [3–5]. These cells were allowed to differentiate for at least 2 weeks.

Adenosine 5' triphosphate (ATP) is a (co)transmitter and extracellular signalling molecule in the CNS [8]. Various

* Corresponding author. Tel.: +49 341 9724614; fax: +49 341 9724609.

E-mail address: Peter.Illes@medizin.uni-leipzig.de (P. Illes).

neurotransmitters including the adenine nucleotide ATP and its degradation product adenosine, are considered to be early signals for CNS development, regulating the proliferation, growth, migration, differentiation and survival of NPCs [9,10]. ATP was shown to activate both G protein-coupled receptors (P2Y) and ligand-gated cationic receptor-channels (P2X) [11]. By contrast, ADP and the uracil nucleotides UTP/UDP stimulated P2Y receptors only.

Low concentrations of UTP enhance dopaminergic differentiation of hmNPCs most probably via P2Y₄ receptor-activation, an effect not shared by the related agonist ATP [4]. Since elevation of the intracellular Ca²⁺ concentration ([Ca²⁺]_i) may be critically involved in differentiation and proliferation of stem cells [12,13], we investigated by which receptor-type ATP and UTP induce [Ca²⁺]_i transients in hmNPCs. We found that UTP may evoke the release of ATP by activating P2Y₂ receptors; this ATP, just like its exogenously applied counterpart, appears to increase [Ca²⁺]_i by in turn activating P2Y₁ receptors, and may thereby produce Ca²⁺ oscillations. Such oscillations may promote glial maturation of hmNPCs. Neither P2Y₄ nor any of the P2X receptor-types are involved in this effect. In contrast, the long-term proliferative and neurogenic effects of UTP may be due to P2Y₄ receptor-stimulation and appear to utilize transduction mechanisms different from increases in [Ca²⁺]_i [4].

2. Materials and methods

2.1. Preparation of human midbrain-derived NPCs (hmNPCs)

Human fetal midbrain tissue was used to generate hmNPC cultures as previously described [4,14]. Samples were harvested and supplied by Advanced Bioscience Resources Inc. (Alameda, CA, USA) according to National Institutes of Health and local Institutional Review Board (IRB) guidelines. Only if there was no evidence of fetal pathology and informed consent had been obtained, were parts of the brain transferred to our laboratory. Expression of key dopaminergic genes such as tyrosine hydroxylase (TH), Nurr1, and dopamine transporter (DAT) were confirmed by rt-PCR and immunoblotting [4].

Tissue from 14 to 18-week-old fetuses were dissociated into single-cell suspension by incubating in 0.1 mg/ml papain/DNase solution (100 µg/ml; Roche, Mannheim, Germany) for 30 min at 37 °C, followed by washing with phosphate-buffered saline (PBS), incubated in antipain (50 µg/ml; Roche) for 30 min at 37 °C, and finally homogenization by gentle trituration using fire-polished Pasteur pipettes. Propagation of hmNPCs was performed in a monolayer by plating on to polyornithine-fibronectin-precoated culture dishes at a density of 30,000 cells/cm². For expansion of hmNPCs, defined media (Dulbecco's modified Eagles's medium/F12) without any xenogenic material (e.g. serum supplements, serum, etc.) were used, but with addition of EGF and FGF2 (20 ng/ml each; both from PromoCell, Heidelberg, Germany). Cells were expanded for prolonged periods (>10 passages) in reduced atmospheric oxygen (3%) [15,16]. Then, cells were seeded onto poly-L-lysine coated polystyrol dishes (electrophysiology, ATP release measurements) or glass coverslips (Ca²⁺ imaging) at a density of 50,000 cells/cm² and cultured at 37 °C in a humidified atmosphere containing 5% CO₂ in air. All experiments were performed 2–3 weeks after the last passage.

2.2. Electrophysiological procedures

Whole-cell current-clamp- and voltage-clamp recordings were made, at room temperature (20–24 °C), consecutively in the same sets of cells by means of an EPC-9 amplifier controlled via Pulse software (v.8.80; both HEKA, Lambrecht, Germany). The bath solution contained (in mM): NaCl 162, KCl 2.4, CaCl₂ 1.3, MgCl₂ 1, HEPES 10 and glucose 11 (~310 mOsm/l; pH 7.3 with NaOH). Patch

pipettes had a resistance of ~5 MΩ, when filled with an intracellular solution of the following composition (mM): potassium gluconate 144, CaCl₂ 1, MgCl₂ 3, HEPES 10, EGTA 11, Mg-ATP 4, Li-GTP 0.3 (~300 mOsm/l; pH 7.2 with KOH). Holding potentials were set and membrane potential values were corrected taking into account a calculated liquid junction potential of 15 mV.

The membrane potential (V_m) of hmNPCs was measured in the fast current-clamp mode of the EPC-9 within the first 3 min after achieving whole-cell access. Voltage responses, evoked by 800 ms de- and hyperpolarizing current-pulses from the zero current level, that were increased in strength by 10–50 pA increments, one current-pulse every 10 s, were then sampled at 20 kHz and filtered at 6.7 kHz.

The presence of voltage-dependent channels in hmNPCs was investigated, after the amplifier had been adjusted to a holding potential of –70 mV in the voltage-clamp mode. Current responses, evoked by series of 100 ms voltage-steps, that were applied at 10 mV increments (from –100 mV to +50 mV), one voltage-step every 10 s, were digitized at 20 kHz and filtered at 4 kHz. Tetrodotoxin (TTX; 0.3 µM) (Sigma–Aldrich, Taufkirchen, Germany) was added after constructing the first family of membrane currents and was left in the medium for a further 5 min, before evoking the second set of membrane currents.

The ligand-gated ion channel profile of hmNPCs was, particularly with respect to the possible presence of functional P2X receptor channels, eventually characterized by means of a pressurized superfusion system (DAD-12; Adams and List, NY, USA; equilibrium exchange times 100–200 ms; see e.g. [17]; holding potential –70 mV). Currents in response to the P2 receptor agonists adenosine-5'-triphosphate (ATP, 300 µM) and uridine-5'-triphosphate (UTP, 300 µM) (both from Sigma–Aldrich), as well as the GABA_A receptor agonist muscimol (30 µM), the non-NMDA receptor agonist (S)-α-amino-3-hydroxy-5-methylisoxazole-4-propionic acid (AMPA, 100 µM) (all from Tocris-Biotrend, Cologne, Germany) and drug-free bath solution, were sampled at 3 kHz and filtered at 1 kHz. Challenges with the individual agonists were 2 s in duration and separated by 2 min superfusion periods with drug-free saline. The order of agonist application was varied between individual experiments.

Voltage – as well as current amplitudes (indicated as current densities: current divided by membrane capacitance, pA/pF) were analyzed with respect to the zero current – and holding current level, respectively, using PulseFit and PulseTools software (v8.80, HEKA). The input resistance (R_i) of the cells was determined by hyperpolarizing current injections causing voltage shifts <20 mV. Outward currents (I_o), which were presumably K⁺ currents, were measured at a fixed time point (90 ms after the start of the 100 ms voltage-steps). Na⁺ currents (I_{Na}) and currents evoked by agonists (e.g. I_{AMPA} , AMPA-induced currents) were measured as peak responses.

Membrane capacitance (C_m) and series resistance (R_s) were monitored repeatedly during the voltage-clamp part of the experiments by the inbuilt compensation routine of the EPC-9 amplifier. R_s was partially compensated (50–60%) and did not change significantly during experiments. The uncompensated values of R_s were 16.7 ± 1.7 MΩ and 17.1 ± 1.6 MΩ ($P > 0.05$; $n = 23$) at the start and the end of the trials, respectively, thus indicating stable recording conditions.

Stock solutions (10–100 mM) of drugs were prepared with distilled water. Aliquots were stored at –20 °C. Further dilutions were made daily with the appropriate bath solution.

2.3. Intracellular calcium measurements

Cultures were loaded for 50–60 min at 37 °C in the dark with the cell permeant acetoxymethylester of the fluorescent Ca²⁺ indicator

Fura-2 (2.5 μM ; Sigma–Aldrich) (see [17]). To remove excess extracellular Fura-2, glass coverslips were washed several times with a bath solution of the following composition (in mM): NaCl 135, KCl 4.5, CaCl_2 2, MgCl_2 1, HEPES 10, glucose 10; pH 7.4 with NaOH) and were allowed to rest for 30 min at room temperature protected from light. Thereafter, Ca^{2+} imaging experiments were performed at room temperature in bath solution using an inverted microscope (IX-70; Olympus, Hamburg, Germany) equipped for epifluorescence and a Peltier-cooled charge-coupled device camera (IMAGO; Till Photonics, Martinsried, Germany). Intracellular Fura-2 was alternately excited at 340 nm and at 380 nm, and the emitted light was measured at a wavelength of 510 nm. The TILL vision software (3.3; Till Photonics) was used for data acquisition, system control, and later, off-line analysis. The fluorescence ratio (340/380 nm) provides a relative measure of the cytosolic free Ca^{2+} concentration ($[\text{Ca}^{2+}]_i$).

The experimental protocol routinely started with the application of bath medium *via* the flush valve of a pressure-operated, computer-controlled rapid drug application device (DAD-12, Adams and List). Concentration–response curves for ATP, UTP, adenosine 5' diphosphate (ADP), and uridine 5' diphosphate (UDP) (all from Sigma–Aldrich) were determined by superfusing increasing concentrations of the agonists for 10 s every 10 min. Then, a high K^+ bath medium containing (in mM): NaCl 89.5, KCl 50, CaCl_2 2, MgCl_2 1, HEPES 10, glucose 10; pH 7.4 with NaOH), was applied for 3 s. When necessary, more than one cell was used to measure the effects of all agonist concentrations. In separate experiments, ATP – (30 μM ; every 10–20 min), ADP – (30 μM ; every 20 min), or UTP – (300 μM ; every 20 min) containing medium was superfused at regular time intervals, for 10 s each (T_1 – T_3). A Ca^{2+} -free medium was prepared by omitting CaCl_2 from the normal bath solution and adding EGTA (1 mM) to chelate the residual Ca^{2+} . The superfusion of this medium started 10 min before T_2 and was present during the subsequent application of ATP or UTP at T_2 . The effect of the Ca^{2+} -free medium was tested for 20 min on the ATP-induced $[\text{Ca}^{2+}]_i$ transients, in order to find out, whether a maximum inhibition develops already after 10 min of superfusion. Since this was not the case, we only investigated the effect of this 10-min superfusion of a Ca^{2+} -free medium on the UTP-induced $[\text{Ca}^{2+}]_i$ transients. A long-lasting contact with a Ca^{2+} -free external medium may on the one hand interfere with the entry of Ca^{2+} from the extracellular space induced e.g. by P2X receptor-activation, and on the other hand also lead to a gradual depletion of the intracellular Ca^{2+} pools, thereby, diminishing the efficiency of e.g. P2Y receptor-activation.

Cyclopiazonic acid (CPA; 30 μM), suramin (100 μM), and apyrase (4 U/ml; all from Sigma–Aldrich) was superfused 15 min before and during the application of ATP or UTP at T_2 . Pyridoxal-5'-phosphate-6-azophenyl-2',4'-disulfonic acid (PPADS), 2'-deoxy- N^6 -methyladenosine 3',5'-bisphosphate (MRS 2179; 30 μM ; both from Tocris–Biotrend, Cologne, Germany), and N^6 -(2-methylthioethyl)-2-(3,3,3-trifluoropropylthio)- β , γ -dichloromethylene-ATP (AR-C69931MX; 3 μM ; The Medicines Company, Waltham, MA, USA) were applied 10 min before and during the second application of ATP or UTP at T_2 . The effects at T_2 were expressed in all cases as a percentage change compared with the responses at T_1 .

Concentration–response curves for ATP were fitted using the following logistic function:

$$E = E_{\min} + \frac{E_{\max} - E_{\min}}{1 + (\text{EC}_{50} + A)^n}$$

where E is the steady-state effect produced by the agonist at the concentration A , E_{\max} and E_{\min} are the maximal and minimal effects, respectively, n the Hill coefficient, and EC_{50} is the concentration of agonist producing 50% of E_{\max} . The software package SigmaPlot 10.0

(Erkrath, Germany) was used for the calculation of the above mean parameters as well as of their S.E.M. values.

2.4. ATP release measurements

ATP release from hmNPC cultures was measured using the microelectrode biosensor technique. The principles and operation of this method have been described previously [18]. ATP sensitive biosensors used in this study were obtained from Sarissa Biomedical (Coventry, UK). The ATP sensor comprised two enzymes, glycerol kinase and glycerol-3-phosphate oxidase, entrapped within a matrix around a fine platinum wire of 50 μm in diameter and 0.5 mm length. To give a measure of net ATP concentrations, the signal from a Null sensor (lacking enzymes, but otherwise identical) was used to measure background signals, which were then subtracted from the signals generated by the ATP biosensor. Cell cultures seeded in monolayer on poly-L-lysine coated 6-cm diameter polystyrol dishes (50,000 cells/cm²) were used in these experiments. ATP and Null biosensors were each gently placed into the medium over the hmNPCs such that the sensing part of the sensor was not contacted with cells. The culture then was superfused at a rate of 5 ml/min with the bath solution of the following composition (in mM): NaCl 140, KCl 5, CaCl_2 2, MgCl_2 2, HEPES 10, glucose 11 and glycerol 2 (pH 7.3 with NaOH, 36–37 °C). After reaching a steady-state baseline, UTP (6–60 μM) was superfused for 5 min. Then, in most experiments, after a washout period of 45 min, UTP was re-administered in the presence of a P2 receptor antagonist (suramin, PPADS). The antagonists were applied for 20 min before and during UTP (30 μM) administration and 20 min thereafter. It is noteworthy that the effect of UTP on ATP release was constant with this time-interval.

Before insertion and after removal, the sensors were calibrated with known concentrations of ATP (0.2–50 μM) and UTP (6–60 μM), both in the absence and presence of suramin (100 μM) and PPADS (30 μM). Thus, to take into account that biosensor sensitivity varies during different experiments, we used the calibration of the sensor to ATP to normalize the signal. Signals from the biosensor were acquired at 10 kHz using the pCLAMP 9 software package (Molecular Devices, CA, USA) and displayed on a laboratory computer. For calculation, the values corresponding to the peak increase in response to the agonist were taken into account. Concentration–response curves were constructed as described in Section 2.3.

2.5. Immunocytochemistry

The immunostaining procedures were similar to those described previously [19]. hmNPCs were fixed with 4% paraformaldehyde in phosphate buffered saline (PBS) for 10 min at room temperature (RT), washed in PBS, and counterstained with the DNA-binding dye 4,6-diamino-2-phenylindole (DAPI; 2 $\mu\text{g}/\text{ml}$ in PBS) for 15 min at RT. After washing twice with Tris buffered saline (TBS, 0.05 M; pH 7.6) and blocking with 5% foetal calf serum (FCS) in TBS, the cells were incubated in an antibody mixture of rabbit anti-P2Y₁ (1:1000; MBL International Corporation, Woburn, MA, USA), rabbit anti-P2Y₂ (1:1000; Neuromics, Edina, MN, USA) or rabbit anti-P2Y₄ (1:1000; Alomone Laboratories, Jerusalem, Israel) and mouse anti-*nestin* (1:400; Pharmingen, San Diego, CA, USA) with 0.2% Triton X-100 in 5% FCS in TBS for 24 h at 4 °C. As secondary antibodies Cy3-conjugated donkey anti-rabbit IgG (1:1000) and Cy2-conjugated donkey anti-mouse IgG (1:400; Jackson ImmunoResearch, West Grove, PA, USA each) were used. After intensive washing, the preparations were covered with Immu-Mount (Thermo Scientific, Pittsburgh, PA, USA).

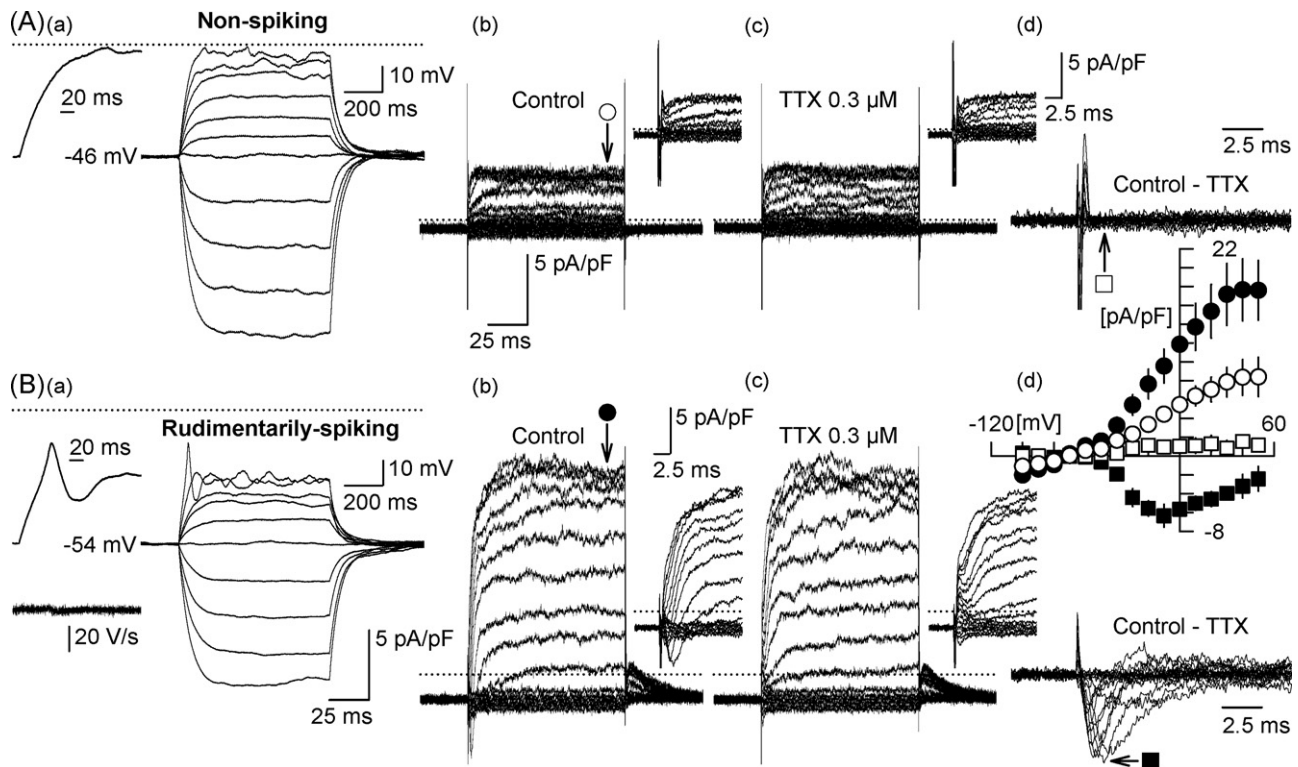


Fig. 1. Electrophysiological characterization of human midbrain-derived neuronal precursor cells (hmNPCs). A a, B a, Families of superimposed membrane potential responses evoked by hyperpolarizing- and depolarizing current pulses in a representative non-spiking hmNPC (A a) and a representative rudimentarily spiking hmNPC (B a). Current pulses, 800 ms in duration, that were increased in strength by 10–50 pA increments, were imposed every 10 s on the resting membrane potential. The voltage traces shown in A a were in response to depolarizing currents up to +60 pA (10 pA increments) and hyperpolarizing currents up to –80 pA (20 pA increments). Those in B a were evoked by depolarizing currents up to +150 pA (25 pA increments) and hyperpolarizing currents up to –200 pA (50 pA increments). The upper insets in A a and B a illustrate, on a faster time scale, the initial phase of the voltage-response evoked by the strongest depolarizing current-command. Please note that only the cell in B a was able to produce a spike-like event. This response was, however, abortive showing no peak in the first derivative (lower inset in B a). Dotted lines in A a and B a represent the zero voltage level. A b–A d and B b–B d, Families of superimposed membrane currents (upper panels; insets represent the initial part of the current traces on faster time scale), evoked first in the absence (A b, B b) and then in the presence of tetrodotoxin (TTX, 0.3 μ M; A c, B c), by series of hyperpolarizing- and depolarizing voltage-steps, in the same non-spiking hmNPC and rudimentarily spiking hmNPC, from which the current-clamp recordings in A a and B a were derived. Voltage-steps, from –100 mV to +50 mV, 100 ms in duration, were imposed every 10 s on the holding potential of –70 mV. Hyperpolarizing voltage-commands did not elicit active membrane current responses, neither in the non-spiking hmNPC (A b, A c) and, a transient inward current followed by I_o in the rudimentarily spiking cell (B b). The transient inward current was blocked by TTX and, hence, a Na^+ current (I_{Na} ; B c). A d and B d, illustrate the TTX-sensitive current components, obtained by subtraction of the current traces evoked in the presence of TTX from those evoked in its absence (Control–TTX). The inset in B d gives the current-voltage relations for I_o (\circ , \bullet) and I_{Na} (\square , \blacksquare) in non-spiking-hmNPCs (open symbols; $n = 12$) and rudimentarily spiking hmNPCs (filled symbols; $n = 11$), measured at the time points indicated by arrows in A b, B b and A d, B d, respectively. Dotted lines in A b, B b and A c, B c represent the zero current level.

The distribution pattern of the cell proliferation marker Ki67 in hmNPCs was determined by immunofluorescence double staining for Ki67 and the stem cell marker nestin. Staining for doublecortin (DCX) was used to identify newborn neurons and to track neurogenesis *in vitro*. Expanded hmNPCs were treated as described above and were then incubated with anti-nestin primary antibody (PharMingen), anti-Ki67 primary antibody (Novocastra Laboratories, Newcastle upon Tyne, UK) and anti-doublecortin primary antibody (Santa Cruz Biotechnology, Santa Cruz, CA) for 2 h at RT in blocking buffer. The cells were rinsed 3 times for 10 min in blocking buffer prior to incubation with secondary antibodies. Fluorescently labelled secondary antibodies (Alexa Fluor 488 or Alexa Fluor 594 conjugates) were purchased from Invitrogen (Invitrogen, Carlsbad, CA).

Coverslips were mounted onto glass slides and examined by a confocal laser scanning microscope (LSM 510, Zeiss, Jena, Germany) at an excitation wavelength of 543 and 594 nm (helium/neon1, red Cy3 (543)- or Alexa 594-immunofluorescence), 488 nm (argon, yellow-green Cy2- or Alexa 488-immunofluorescence), and 351–362 nm (argon UV-laser, blue fluorescence of DAPI). Control experiments were carried out without primary antibodies or by pre-adsorption of the antibody with the peptides used for its generation.

For quantitative evaluation of the effects of ATP and UTP on neurogenesis and proliferation, an equal number of hmNPCs (30,000 cells/cm²) were seeded in 4-chamber slides and further expanded in reduced oxygen (3% O₂) [4]. Cells were treated about 24 h after plating with ATP (100 μ M), UTP (100 μ M) or MRS 2179 (30 μ M) alone. Alternatively, MRS 2179 (30 μ M) was applied and 30 min later ATP or UTP (100 μ M each) were co-applied with the antagonist. After 5 days of expansion, the cells were fixed and immunostained for the neurogenesis marker DCX or the proliferation marker Ki67 (together with nestin and DAPI). The DCX-immunoreactive as well as the Ki67/nestin/DAPI-immunoreactive cells were counted in randomly selected fields by means of the image-analysis software AxioVision 4 (Zeiss, Jena, Germany).

2.6. Statistics

Mean \pm SEM of n trials are shown, n being the number of single cells. Differences between means were tested for significance by the Mann-Whitney Rank Sum Test for single comparisons and by the Kruskal–Wallis One Way Analysis of Variance on Ranks followed by a modified t test (Bonferroni–Dunn) for multiple comparisons. $P < 0.05$ was the accepted level of significance.

3. Results

3.1. Electrophysiology: passive membrane properties and voltage-dependent currents in hmNPCs

The hmNPCs selected for recording had a morphological appearance different from mature neurons. They could, nevertheless, readily be identified as rather small cells with ovoid or round somata that had already developed one or two neurite-like processes (Fig. 3A a; upper white arrow). It was not attempted to record from larger, phase contrast-dark, flat cells devoid of such neurite-like appendages that formed a glia-like sheet at the bottom of the culture dishes (Fig. 3A a; lower white arrow).

Two different groups of hmNPCs could be discriminated under current-clamp conditions (Fig. 1A a, B a). Cells of the first group (12 out of 23; 52.2%) had a membrane potential of -41.4 ± 2.5 mV, a rather high input resistance of 1.42 ± 0.18 G Ω and an outwardly rectifying response pattern to step-current injection. They were, however, not at all able to generate action potentials and were, hence, termed non-spiking hmNPCs (Fig. 1A a).

Cells of the second group (11 out of 23; 47.8%), by contrast, had a significantly more hyperpolarized V_m (-58.1 ± 1.8 mV), as well as an approximately threefold lower R_i (0.47 ± 0.06 G Ω , $P < 0.05$). They responded to depolarizing current injection also with outward-rectification but produced, additionally, a single, rather broad, non-overshooting spike followed by an after-hyperpolarization (Fig. 1B a). No repetitive firing could, however, be induced with supra-threshold current-steps, in some cases even when the current strength was increased up to 500 pA (data not shown). Analysis of the first derivatives, then, revealed that the spikes were abortive (Fig. 1B a). In consequence, spike-thresholds could not be defined reliably, a fact that prohibited the proper measurement of common spike parameters as e.g. amplitudes or duration. Cells of the second group were, hence, termed rudimentarily spiking hmNPCs.

Since, half-maximal voltage-dependent inactivation of neuronal, TTX-sensitive Na^+ channels commonly occurs in the voltage range between -50 and -60 mV, a significant proportion of Na^+ channels in the rudimentarily spiking hmNPCs, due to their relatively depolarized V_m , might have been trapped in an inactivated state under current clamp conditions. Therefore, we have tried to elicit action potentials in these cells, when the membrane potential was shifted to more negative values (-70 to -80 mV) by constant current injection. Unfortunately, cells either rapidly perished or showed a continuous depolarizing shift in V_m that prohibited this approach. Anyhow, the voltage-dependent Na^+ channel inactivation, was most likely not a decisive factor accounting for the rudimentary spike pattern in a proportion of the hmNPCs. Rat midbrain dopaminergic neurons e.g., were able to fire fully developed, repetitive spikes from a V_m between -50 and -60 mV (e.g. [20]), a potential range where the underlying channel population should also be half-maximally inactivated. Moreover, the maximum Na^+ peak current in the rudimentarily spiking hNPCs, evoked by voltage-steps from a holding potential of -70 mV (where one would expect that over 80% of the Na^+ channel population should be available for activation), was only -87 ± 16 pA. By using an R_i of 0.47 G Ω and according to Ohm's law, this current could have evoked a 41 mV depolarization at best, and, hence, again a non-overshooting spike.

There were no obvious morphological differences between the two classes of hmNPCs, neither with respect to the number of neurite-like processes nor to the cell size. Thus, the surface area was roughly $1300 \mu\text{m}^2$ for non-spiking- and rudimentarily spiking hmNPCs, as estimated (assumed specific membrane capacitance $10 \text{ fF}/\mu\text{m}^2$) from their C_m values, which were 13.2 ± 1.4 pF ($n = 12$) and 13.7 ± 2.2 pF ($n = 11$, $P > 0.05$), respectively. A progressively more hyperpolarized membrane potential, together with a concomitant

reduction in input resistance, amongst others due to an increase in membrane channel density, however, are established hallmarks of neuronal maturation [21,22]. In fact, we noticed a good correlation when R_i was plotted as a function of V_m (Fig. 1A a; $r = 0.89$, $n = 23$). Hence, it seems as if not only some degree of development from the non-spiking- to the rudimentarily spiking phenotype had occurred spontaneously, even in the absence of known differentiating stimuli, but also, that the respective changes in the ion channel profile had preceded morphological maturation (see also [23]).

Depolarizing voltage-steps, applied under voltage-clamp conditions (holding potential -70 mV), evoked a slowly activating outward current (I_o) in all non-spiking hmNPCs (Fig. 1A b–A d; $n = 12$) and, a transient inward current followed by I_o , in all rudimentarily spiking hmNPCs (Fig. 1B b–B c; $n = 11$). I_o activated at around -40 mV and saturated between $+30$ and $+50$ mV (Fig. 1B d). Maximum I_o amplitudes (measured at $+50$ mV) were significantly smaller in non-spiking hmNPCs (8.8 ± 2.1 pA/pF), when compared to those in rudimentarily spiking hmNPCs (17.7 ± 3.3 pA/pF, $n = 12$ and 11 , $P < 0.05$). The current was not characterized pharmacologically, but resembled, with respect to its slow onset and its voltage dependence, delayed-rectifying K^+ currents described in neuronal progenitors from humans [24] and rodents [25]. Regardless of that, the presence of I_o , in combination with the observed lack of inward-rectifier currents in response to hyperpolarizing voltage-steps (up to -100 mV; e.g. Fig. 1A b, B b), may provide the most reasonable explanation for the exclusively outwardly rectifying response pattern seen under current-clamp conditions in both groups of neuronal progenitor cells (Fig. 1A a, B a).

The transient inward currents, found only in the rudimentarily spiking cell population, were blocked by TTX ($0.3 \mu\text{M}$; Fig. 1B c), and, hence, were Na^+ currents (I_{Na}). The TTX-sensitive current activated around -50 mV, peaked at -10 mV (-6.3 ± 1.2 pA/pF, $n = 11$) and, then, declined towards zero upon stronger depolarizations (Fig. 1B d). Even though the reversal potential of I_{Na} could not be determined (zero Na^+ -containing pipette solution), this current was, beyond any reasonable doubt, responsible for the aborted action potentials seen in the rudimentarily spiking hmNPCs.

3.2. Electrophysiology: ligand-gated channels in hmNPCs

After the electrophysiological characterization of proliferating hmNPCs had been accomplished, currents induced by pressure application of the P2 receptor agonists ATP ($300 \mu\text{M}$) and UTP ($300 \mu\text{M}$), the ionotropic glutamate receptor agonist AMPA ($100 \mu\text{M}$) and the GABA_A receptor agonist muscimol ($30 \mu\text{M}$) were measured in the same set of cells (holding potential -70 mV). Bath solution with no added receptor agonists was used as a control. It should be mentioned that the reported half-maximally effective concentrations of ATP were between ~ 0.5 and $\sim 300 \mu\text{M}$ at all known homomeric- or heteromeric P2X receptor channels [26]. Hence, the ATP concentration ($300 \mu\text{M}$) used in the present study appeared to be appropriate for the detection of P2X receptor-mediated currents.

Responses of a representative non-spiking hmNPC (same cell as in Fig. 1A) and a representative rudimentarily spiking hmNPC (same cell as in Fig. 1B) are shown in Fig. 2A and B, respectively. The statistical evaluation of a greater number of cells is given in Fig. 2C. Pressure application of ATP, UTP and muscimol failed to evoke current responses in non-spiking- (Fig. 2A, C) or rudimentarily spiking cells (Fig. 2B, C). In contrast to that, significant inward currents were evoked by AMPA in both types of hmNPCs (Fig. 2A–C). However, it was obvious that the non-NMDA receptor-mediated responses were approximately threefold smaller in non-spiking hmNPCs (-2.1 ± 0.2 pA/pF, $n = 12$) than in rudimentarily spiking hmNPCs (-6.0 ± 1.1 pA/pF, $P < 0.05$; Fig. 2C). Thus, these cells possessed

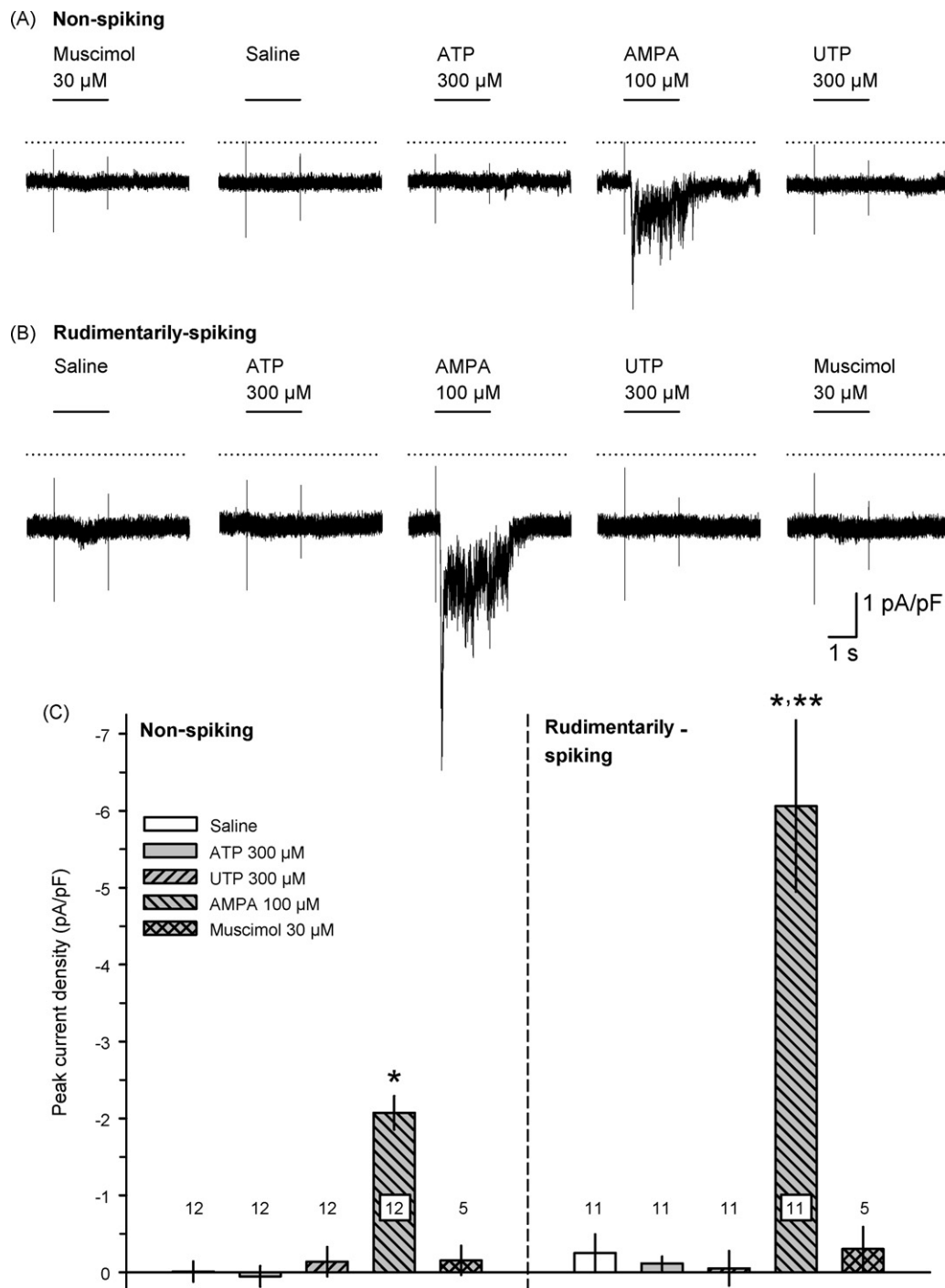


Fig. 2. Agonist-induced transmembrane currents in non-spiking (A, C) and rudimentarily spiking hmNPCs (B, C). A, B, Transmembrane currents in response to pressure application of bath solution (saline), the P2 receptor agonists ATP (300 μ M) and UTP (300 μ M), the ionotropic glutamate receptor agonist AMPA (100 μ M) and the GABA_A receptor agonist muscimol (30 μ M), obtained in the same non-spiking hmNPC (A) and rudimentarily spiking hmNPC (B) shown also in Fig. 1A and B, respectively. Agonist were subsequently applied for 2 s each in random order. Single challenges with the agonist were separated by 2 min superfusion periods with drug-free saline. The holding potential was -70 mV. The dotted lines indicate the zero current levels and the horizontal bars above the current traces indicate the times of agonist application. C, Statistical evaluation of the data derived from similar experiments as illustrated in A and B in non-spiking hmNPCs (left) and rudimentarily spiking hmNPCs (right). The numbers above or within the bars indicate the number of cells challenged by the individual agonists. * $P < 0.05$, significant differences from the effects of saline alone and *** $P < 0.001$, significant differences between the effects of agonist in non-spiking hmNPCs and rudimentarily spiking hmNPCs, respectively.

ionotropic glutamate receptors of the AMPA-type, but no GABA_A or P2X receptors. Shortcomings in the experimental techniques used were most likely not responsible for the failure to detect functional P2X receptors in the neuronal progenitors, because, by means of very similar methods, the presence of P2X receptor currents could be readily demonstrated e.g. in dorsal root ganglion cells [27].

3.3. Ca²⁺ imaging: characterization of P2 receptors at hmNPCs

The morphological characteristics of hmNPCs selected for Ca²⁺ imaging (Fig. 3A) were identical to those from which membrane currents were recorded with the patch-clamp technique. Immunocytochemical co-labelling with the stem cell marker nestin and the proliferation marker Ki67 demonstrated that hmNPCs were

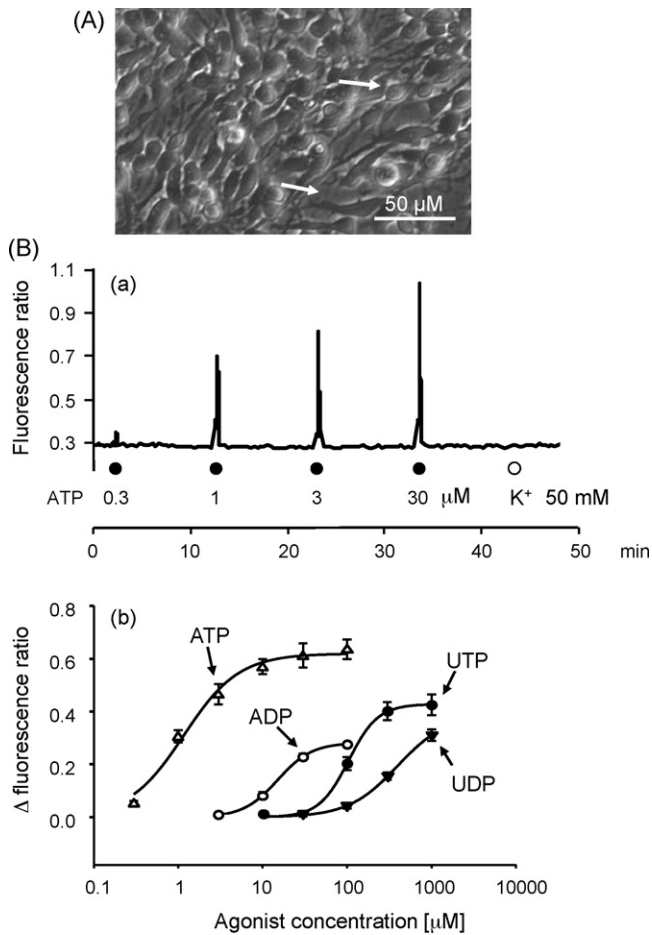


Fig. 3. Concentration-dependent increase of the cytosolic free Ca^{2+} concentration ($[\text{Ca}^{2+}]_i$) of hmNPCs by adenine and uracil nucleotides. The fluorescence ratio (340/380 nm) of cells loaded by the Ca^{2+} -sensitive dye fura-2 provided a relative measure of $[\text{Ca}^{2+}]_i$. Concentration–response curves for ATP, ADP, UTP and UDP were determined by superfusing increasing concentrations of the agonists for 10 s every 10 min. (A) Morphological characteristics of hmNPCs. Representative phase-contrast photomicrograph of hmNPCs kept in adherent cultures growing on polyornithine-fibronectin pre-coated dishes. Upper arrow, typical mesencephalic neuronal progenitor cell; lower arrow, gli-like cell. Scale bar: 50 μm . (B a) Tracings showing $[\text{Ca}^{2+}]_i$ transients of a hmNPC in response to increasing concentrations of ATP. A high K^+ (50 mM)-containing medium had no effect in this cell, excluding the presence of voltage-sensitive Ca^{2+} channels in the plasma membrane. (B b) Concentration–response relationships for ATP (Δ), ADP (\circ), UTP (\bullet) and UDP (\blacktriangledown) established in experiments similar to those shown in (B a). The agonist rank order of potency was $\text{ATP} > \text{ADP} > \text{UTP} > \text{UDP}$.

proliferating (Fig. 9A b) in the present expansion medium containing growth factors (EGF and FGF-2) and B-27 supplement (see Section 2). In addition, a low percentage of cells exhibited immunopositivity for DCX, a marker of newborn, migrating neurons (Fig. 9A a). Further dopaminergic differentiation of hmNPCs would need replacement of the expansion medium by mitogen-free medium containing fetal calf serum, forskolin and interleukin-1 β [4]. In fact, only 13.4% out of the total investigated 253 hmNPCs reacted to 50 mM K^+ with an increase of $[\text{Ca}^{2+}]_i$ (0.1 ± 0.01 ; $n = 34$). Fig. 3B a shows a more typical cell, which did not respond to the high K^+ medium with a $[\text{Ca}^{2+}]_i$ transient. It is noteworthy that neurons, but not glial cells possess a high density of voltage-sensitive Ca^{2+} channels in their cell membrane [28] and therefore depolarization by an elevation of the external K^+ concentration is expected to trigger the entry of Ca^{2+} into the intracellular space of this cell-type only. Thus, some, but not all hmNPCs appeared already to acquire neuronal properties, in agreement with the assumption that in a subpopulation of the electrophysiologi-

cally characterized rudimentarily spiking cells the aborted action potentials may lead to the opening of voltage-gated Ca^{2+} channels.

The fluorescence ratios (340/380 nm) were used to provide a relative measure of $[\text{Ca}^{2+}]_i$ in hmNPCs. We constructed concentration–response curves for ATP, ADP, UTP, and UDP (Fig. 3B). The concentration response curves for ATP ($E_{\text{max}} = 0.62 \pm 0.02$, Hill coefficient = 1.33 ± 0.22 , $\text{EC}_{50} = 1.2 \pm 0.2 \mu\text{M}$), ADP ($E_{\text{max}} = 0.28 \pm 0.01$, Hill coefficient = 2.14 ± 0.08 , $\text{EC}_{50} = 15.1 \pm 0.3 \mu\text{M}$), and UTP ($E_{\text{max}} = 0.43 \pm 0.02$, Hill coefficient = 2.50 ± 0.71 , $\text{EC}_{50} = 103.9 \pm 6.5 \mu\text{M}$) were fitted by the logistic equation presented in Section 2 ($n = 45$ –61 cells in all experiments). It was not possible to calculate EC_{50} values for UDP, because we did not reach a maximum of the curve even at a concentration of 1000 μM . Even so it was clear that the rank order of agonist potencies was $\text{ATP} > \text{ADP} > \text{UTP} > \text{UDP}$. It is noteworthy that the maximum response to ADP was considerably lower than that to ATP; hence, ADP may be a partial agonist under our experimental conditions. Another possibility is that ADP simultaneously activates two different P2Y receptor-types, one of them stimulatory, coupled to G_q , and releasing $[\text{Ca}^{2+}]_i$ (P2Y $_1$; see below), and the other one inhibitory, e.g. coupled to G_i , and counteracting the effect of P2Y $_1$ receptor-occupation. However, this latter receptor does not appear to be either P2Y $_{12}$ or P2Y $_{13}$, since AR-C69931MX, which antagonizes both receptor-types, moderately inhibited rather than facilitated the effect of the P2Y $_1$ agonistic ATP (strong blockade by MRS 2179; see below). Thus, the existence of a hitherto unknown ATP/ADP-sensitive inhibitory receptor still remains a remote possibility.

P2X receptors are ligand-gated cationic channels whose activation leads to the entry of Ca^{2+} from the extracellular space into the cell interior [29]. In contrast, P2Y receptors are coupled to G proteins; stimulation of the $G_{q/11}$ -linked P2Y $_{1,2,4,6}$ receptors causes the release of Ca^{2+} from intracellular pools [30]. As a prerequisite for a feasible protocol, the $[\text{Ca}^{2+}]_i$ transients in response to consecutive ATP (30 μM ; $3.6 \pm 0.01\%$, $n = 50$), ADP (30 μM ; $5.9 \pm 0.01\%$, $n = 44$) and UTP (300 μM ; $13.0 \pm 0.02\%$, $n = 34$) applications only slightly decreased from T_1 to T_2 ($P < 0.05$ in all cases; Fig. 5B a, b). However, when compared with this change, during superfusion with a Ca^{2+} -free medium, the effect of ATP exhibited a more marked decline after 10 min at T_2 ($26.5 \pm 0.01\%$) and still continued to decrease after a further 10 min at T_3 ($37.0 \pm 0.01\%$, $n = 87$ each, $P < 0.05$) (Figs. 4A a and 5B a). The omission of Ca^{2+} from the superfusion medium resulted in a similar inhibition of the UTP-induced $[\text{Ca}^{2+}]_i$ transients (T_2 ; $22.5 \pm 0.01\%$, $n = 32$, $P < 0.05$) (Figs. 4B a and 5B b). Thus, extracellular Ca^{2+} may be a partial source of the $[\text{Ca}^{2+}]_i$ responses. Nevertheless, the residual increase of $[\text{Ca}^{2+}]_i$ by ATP and UTP appears to be due to the release of Ca^{2+} from intracellular storage sites; cyclopiazonic acid (CPA; 30 μM) known to deplete such sites depressed with a much higher efficiency the effects of both ATP ($77.6 \pm 0.01\%$, $n = 74$, $P < 0.05$) and UTP (93.0 ± 0.02 , $n = 26$, $P < 0.05$) than superfusion with a Ca^{2+} -free bath solution (Figs. 4A b, B b and 5B a, B b). The protracted, transient increase of $[\text{Ca}^{2+}]_i$ by CPA alone may be the consequence of an interference with Ca^{2+} sequestration into the endoplasmic reticulum by the blockade of Ca^{2+} -ATPase and the subsequent activation of store-operated Ca^{2+} channels (SOCs). A similar long-lasting increase in $[\text{Ca}^{2+}]_i$ which did not return to baseline in spite of superfusing CPA for 15 min, was described previously for striatal neurons and astrocytes cultured in neurobasal medium, and was shown to be due to the opening of SOCs (see Fig. 5 of [17]).

Experiments with a Ca^{2+} -free medium and CPA in conjunction with the rank order of agonist potencies of the nucleotides tested suggested the presence of ATP/ADP- and probably also UTP/UDP-sensitive P2Y receptors. The $G_{q/11}$ -coupled P2Y $_1$ receptor reacts to the agonists ATP/ADP, whereas P2Y $_{2,4,6}$ receptors sharing their transduction pathways with P2Y $_1$, are sensitive to ATP/UTP or UDP

[30]. In the present study, ATP was more active than ADP, which in turn was equal or even surmounted the activities of UTP and UDP. In addition, the mixed P2X/P2Y receptor antagonist PPADS, having some preference for P2Y₁ over the residual P2Y receptor-types [31], abolished the effect of ATP (30 μM) (97.8 ± 0.01%, *n* = 52, *P* < 0.05; Fig. 5B a). More importantly, the highly selective P2Y₁ receptor antagonist MRS 2179 (30 μM) caused a pronounced inhibition of the effect of ATP from *T*₁ to *T*₂, by 89.5 ± 0.01% (*n* = 142, *P* < 0.05) (Fig. 5A, B a). In contrast, the P2Y_{12,13} selective antagonist AR-C69931MX (3 μM) only slightly depressed the ATP-induced increase of [Ca²⁺]_i (7.2 ± 0.01, *n* = 62, *P* < 0.05) (Fig. 5B a). Finally, MRS 2179 almost abolished the ADP effect.

PPADS markedly inhibited the responses to UTP, a finding which would be compatible with P2Y_{4,6} receptor involvement (Fig. 5B b). However, the abolishment of the effect of UTP by MRS 2179 strongly indicated that UTP, probably by releasing ATP from hmNPCs (for rat neuronal progenitor cells on the one hand, as well as astrocytes and Schwann cells on the other, see [32–34], respectively), activated P2Y₁-like receptors (Fig. 5B b). This assumption was

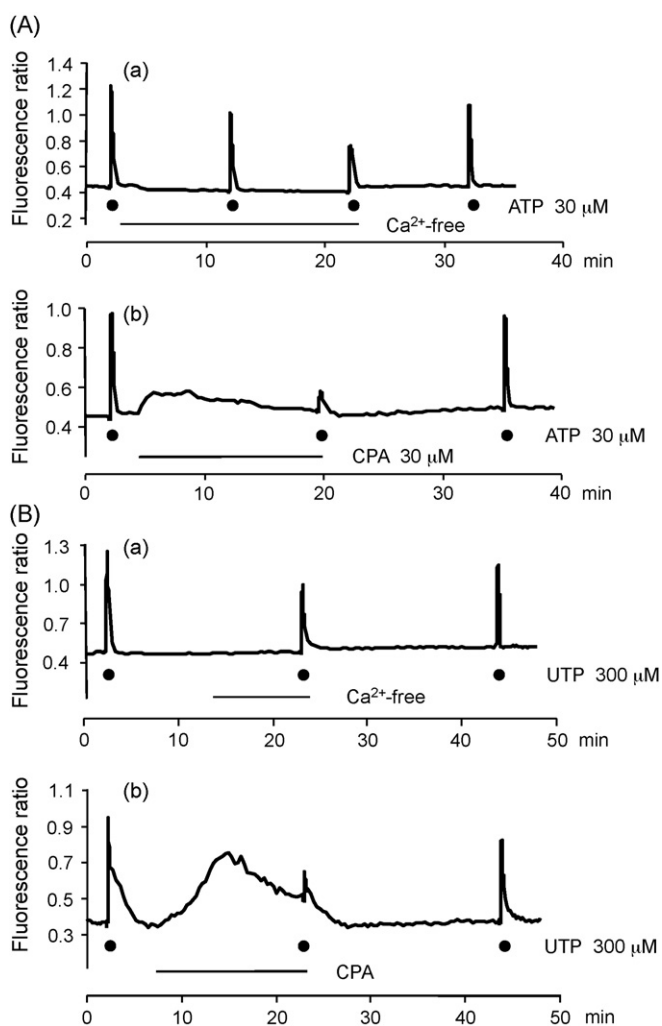


Fig. 4. ATP- and UTP-induced increases of intracellular Ca²⁺ in hmNPCs. Tracings showing [Ca²⁺]_i transients of these cells in response to near maximal concentrations of ATP (30 μM; A) and UTP (300 μM; B), respectively. Depression of the effect ATP in a Ca²⁺-deficient medium (A a) and in the presence of cyclopiazonic acid (CPA, 30 μM; A b). Representative cells out of a total number of 87 (A a) and 74 (A b), respectively. Depression of the effect UTP in a Ca²⁺-deficient medium (B a) and in the presence of CPA (30 μM; B b). Representative cells out of a total number of 32 (B a) and 26 (B b), respectively. Horizontal bars indicate superfusion with a Ca²⁺-free or CPA-containing medium. After returning to a normal superfusion medium, there was a partial recovery of the [Ca²⁺]_i transients caused by ATP or UTP.

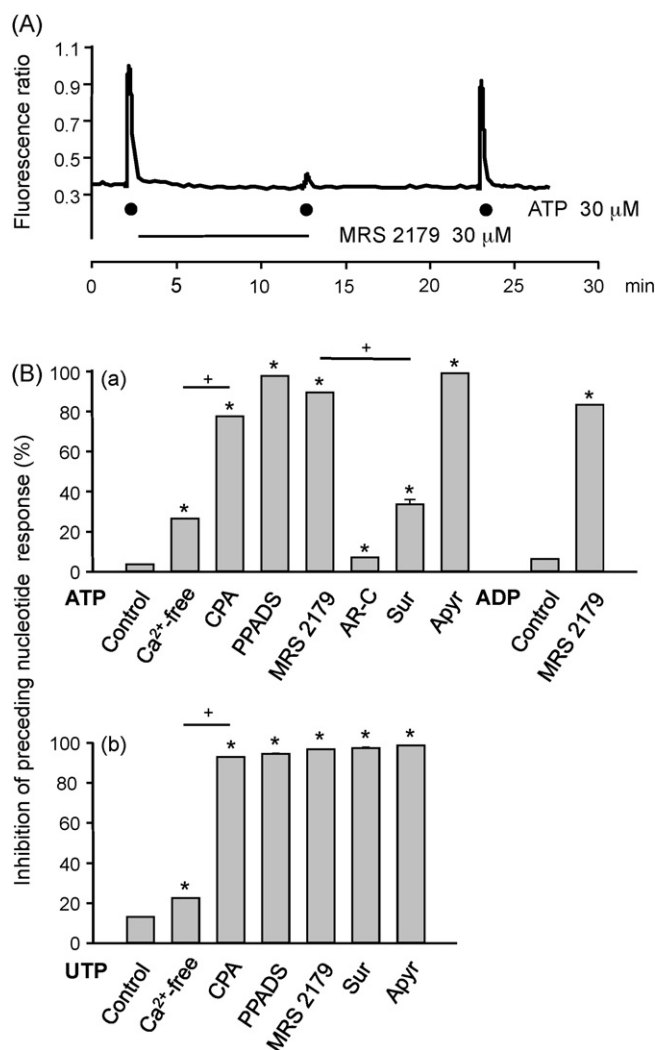


Fig. 5. ATP-, ADP- and UTP-induced increases of intracellular Ca²⁺ in hmNPCs and their modulation by a low extra- or intracellular Ca²⁺ concentration, as well as by P2 receptor antagonists and a nucleotide catalyzing enzyme. (A) Representative tracing showing [Ca²⁺]_i transients evoked by ATP (30 μM). Abolition of the effect of ATP by MRS 2179 (30 μM). Horizontal bars indicate superfusion with a medium containing the P2 receptor antagonist. Typical cell out of a total number of 142. (B) Inhibition of nucleotide-induced [Ca²⁺]_i transients. Submaximal concentrations of ATP, ADP (30 μM each; B a) and UTP (300 μM; B b) were applied for the first time (*T*₁; control) in a normal medium and for the second time (*T*₂) in a Ca²⁺-free medium or in one containing CPA (30 μM), PPADS (30 μM), MRS 2179 (30 μM), AR-C69931MX (3 μM), suramin (100 μM), or apyrase (4 U/ml). For the time-schedule of these experiments see (A) and Section 2. The nucleotide effects at *T*₂ were expressed as a percentage change compared with the response at *T*₁. All drugs and manipulations caused comparable changes irrespective of whether ATP, ADP or UTP were used as agonists. Mean ± S.E.M. of 26–142 experiments. The absence of vertical bars is due to the fact that the S.E.M. values were smaller than the thickness of the column lines. Asterisks indicate statistically significant difference (*P* < 0.05) from the respective control values (first column in each group); lines with plus signs indicate statistically significant differences between two columns).

supported by subsequent experiments demonstrating the release of ATP by UTP into the biophase (see Section 3.5). In perfect agreement with this suggestion, the P2X/P2Y receptor antagonist suramin (100 μM), which, however, prefers P2Y_{1,2,12} over the residual P2Y receptor-types, eliminated the effect of UTP (97.5 ± 0.31%, *n* = 27, *P* < 0.05; Fig. 5B b), but only slightly depressed the effect of ATP (33.6 ± 2.45%, *n* = 62, *P* < 0.05; Fig. 5B a) on [Ca²⁺]_i. Moreover, the nucleotide catalyzing enzyme apyrase (4 U/ml) abolished both the ATP- (99.1 ± 0.09%, *n* = 48) and UTP-induced (98.8 ± 0.09%, *P* < 0.05 each) [Ca²⁺]_i transients (Fig. 5B a, B b), also supporting P2

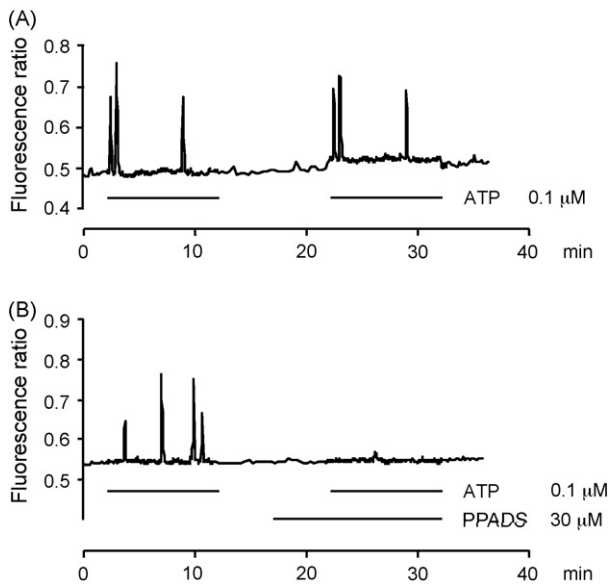


Fig. 6. PPADS prevents the appearance of oscillations of intracellular Ca^{2+} induced by ATP. Tracings showing repetitive $[Ca^{2+}]_i$ transients of these cells in response to 10-min superfusion with a concentration of ATP ($0.1 \mu\text{M}$), three times lower than that ($0.3 \mu\text{M}$) causing a small increase of $[Ca^{2+}]_i$ within a 10-s application period (see Fig. 3B b). (A) Reproducible Ca^{2+} oscillations after a 10-min interval between two applications of ATP ($0.1 \mu\text{M}$) for 10 min. (B) Blockade by PPADS ($30 \mu\text{M}$) of the second oscillatory response to ATP ($0.1 \mu\text{M}$). Between the two applications of ATP with or without PPADS, the series of images were taken at 20 s intervals instead of the usual 2 s intervals. Representative cells out of a total number of 29 (A) and 22 (B).

receptor-activation and excluding a role of the active metabolite adenosine.

3.4. Ca^{2+} imaging: P2 receptor-induced Ca^{2+} oscillation in hmNPCs

Elevations in $[Ca^{2+}]_i$ immediately after agonist superfusion were determined by applying increasing concentrations of ATP (0.3 – $100 \mu\text{M}$) for 10 s each (Fig. 3B b). ATP at $0.3 \mu\text{M}$ induced a small Δ fluorescence ratio of 0.05 ± 0.01 ($n = 48$) under these conditions. A still lower concentration of $0.1 \mu\text{M}$ for 10 min caused irregular Ca^{2+} oscillations of a somewhat larger mean amplitude (0.11 ± 0.01 ; $n = 57$ oscillations in 26 cells). The mean number of oscillatory waves during this 10-min period were 2.19 ± 0.03 per cell. The effect of ATP was reproducible after washout for 10–15 min and was completely blocked by PPADS ($30 \mu\text{M}$; Fig. 6A, B). Fig. 6 shows cells with a higher amplitude and number of oscillations than usually observed. The $[Ca^{2+}]_i$ waves propagated from one cell to several neighbouring ones, because the shapes and frequencies of the waves were similar in 5–7 cells in each culture dish.

3.5. ATP biosensors: demonstration of ATP releasing P2Y receptors at hmNPCs

In the absence of drugs, biosensors placed into the medium over hmNPCs failed to detect any significant changes in the extracellular concentration of ATP. When the cell cultures were superfused with the P2 receptor agonist UTP ($30 \mu\text{M}$) for 5 min, an increase in the extracellular level of ATP was detected (Fig. 7A) ($0.99 \pm 0.04 \mu\text{M}$; $n = 12$), which was concentration-dependent (6 – $60 \mu\text{M}$; Fig. 7B) and reversible upon washout. Because at concentrations of UTP higher than $30 \mu\text{M}$, the response was on a log scale outside of the linear range, a maximal response could not be obtained. As a consequence, an EC_{50} value could not be calculated either. The repetitive application of UTP ($30 \mu\text{M}$) with an interval of 45 min caused stable

responses (change from the first to the second response, $2.0 \pm 0.6\%$ increase; $n = 3$; $P > 0.05$). The UTP-induced ATP release was also examined in the presence of two antagonists acting on P2 receptors (Fig. 7C). The effect of UTP ($30 \mu\text{M}$) was almost completely inhibited by suramin ($100 \mu\text{M}$) ($0.14 \pm 0.05 \mu\text{M}$; $n = 5$; $P < 0.05$) (Fig. 7A, C). On the other hand, PPADS ($30 \mu\text{M}$; $1.00 \pm 0.08 \mu\text{M}$; $n = 5$; $P > 0.05$), did not alter the UTP-stimulated ATP release (Fig. 7C). When superfused alone, none of these antagonists changed the basal efflux of ATP. An important difference in the antagonistic profiles of suramin and PPADS is that only the former compound blocks P2Y₂ receptors [31]. Hence, it can be assumed that UTP stimulates via P2Y₂ receptor-activation the release of ATP from hmNPCs.

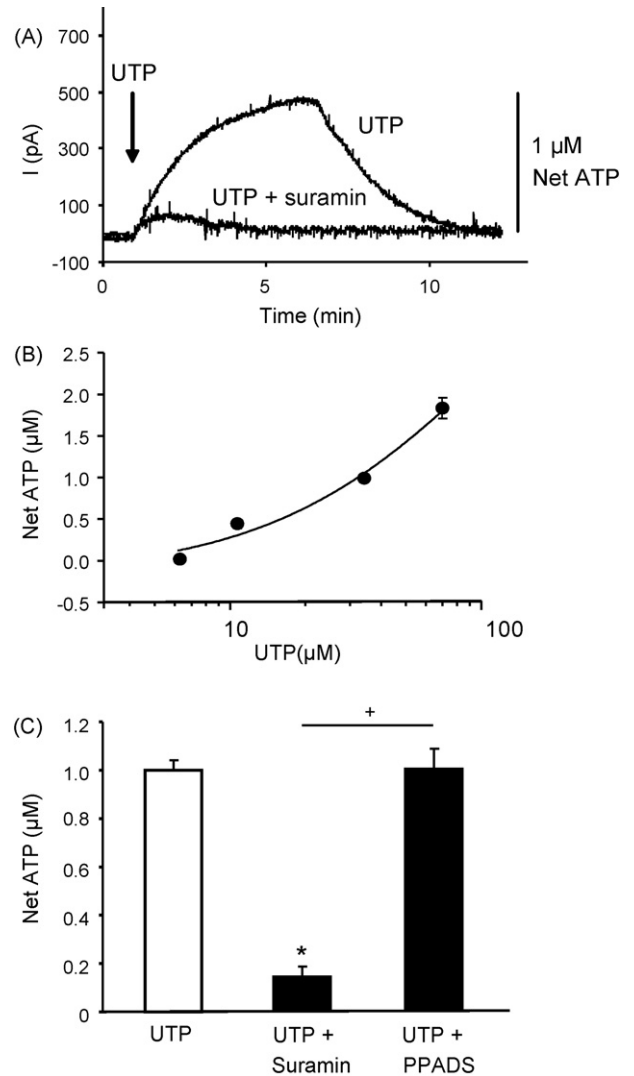


Fig. 7. UTP-induced increase of ATP release from hmNPCs. The current recorded by the biosensor electrode is provided as a measure of net ATP concentration above the cells. Increasing concentrations of UTP (6 – $60 \mu\text{M}$) were applied to separate cells for 5 min each to construct concentration–response curves. UTP ($30 \mu\text{M}$) was applied twice every 45 min for 5 min each; the first application was in the absence, while the second one in the presence of suramin ($100 \mu\text{M}$) or PPADS ($30 \mu\text{M}$). (A) Tracings showing the net release of ATP from a cell by UTP ($30 \mu\text{M}$) alone and from another cell by the same concentration of UTP in the presence of suramin. UTP was applied as indicated by the arrow. (B) Concentration–response curve for the effect of UTP on ATP release ($n = 4$ – 12 cells for each point). (C) Effect of P2 receptor antagonists on UTP ($30 \mu\text{M}$)-induced ATP release. Suramin ($100 \mu\text{M}$) but not PPADS ($30 \mu\text{M}$) attenuated the release by UTP ($30 \mu\text{M}$) of ATP ($n = 5$ – 12 cells for each column). Asterisks indicate statistically significant difference ($P < 0.05$) from the response caused by UTP alone; the line with a plus sign indicates statistically significant differences between the two columns.

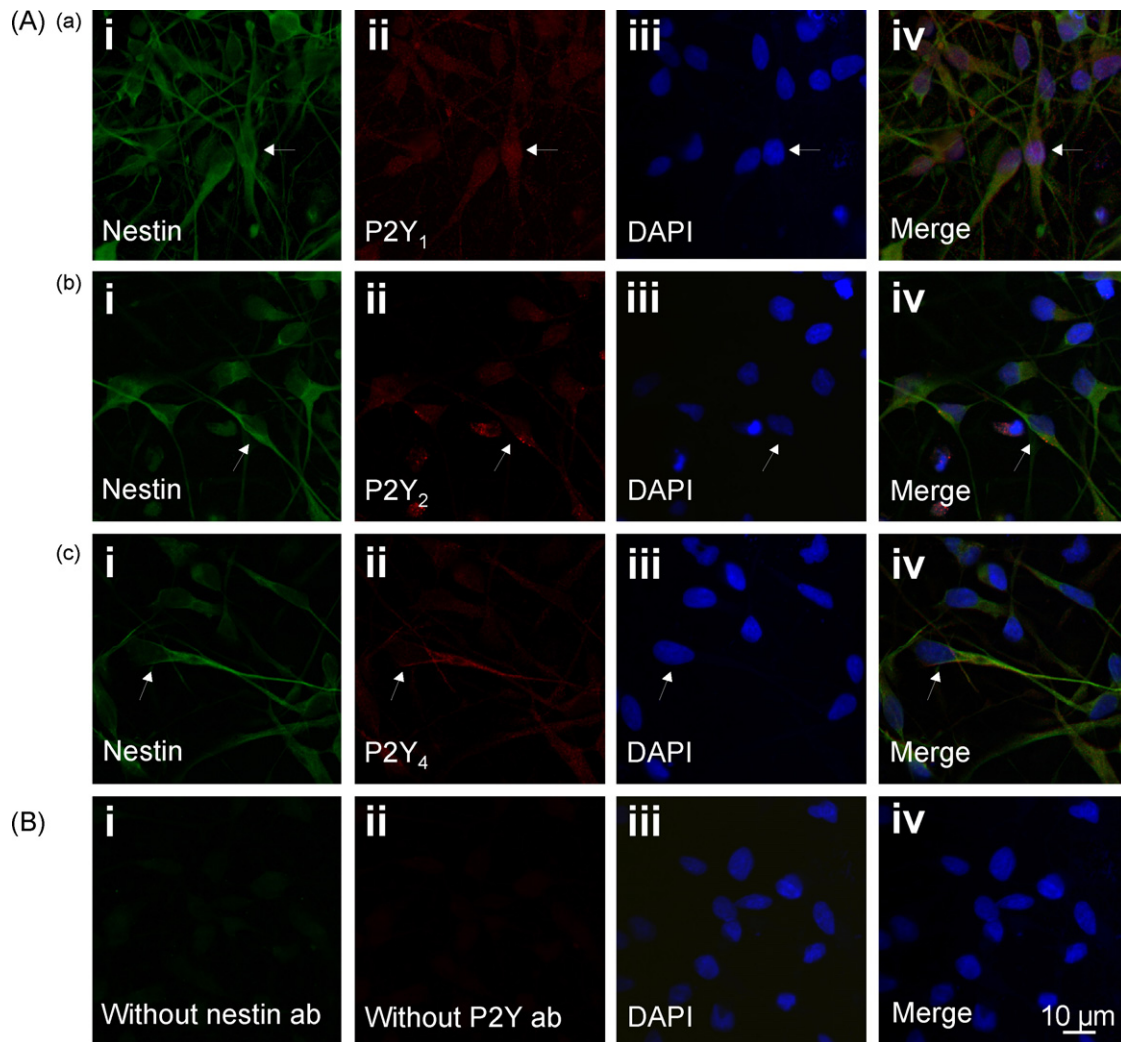


Fig. 8. Presence of P2Y receptor-immunoreactivities (IR) at hmNPCs. (A, B) Confocal images of immunofluorescence labelling to characterize the localization of P2Y₁ (A a ii), P2Y₂ (A b ii), and P2Y₄ (A c ii) receptors (red fluorescence) on nestin-positive cells (A a–c i; yellow-green fluorescence). (A a–c, i–iv) Examples of co-localization (arrows) of nestin with the P2Y receptor-immunopositive cells are indicated. DAPI (blue immunofluorescence) was used to characterize the cell nucleus. Examples of labelling without primary antibodies for nestin (B i) and the P2Y receptors (B ii). No unspecific labelling was observed. The co-localization of nestin with each P2Y receptor-IR and DAPI is also documented (iv; merge). Scale bar: 10 μm.

3.6. Immunocytochemistry: presence of P2Y receptor-types at hmNPCs and effects of P2Y receptor agonists on proliferation and neurogenesis of these cells

In view of the functional receptor-profile of the various pharmacological ligands investigated it was important to search by immunocytochemistry for the presence of P2Y₁, P2Y₂ and P2Y₄ receptors in hmNPCs. In fact, immunopositivity for all three receptors was observed in these cells (Fig. 8). As a stem cell marker we used nestin, which labelled practically every hmNPC, as indicated by co-localization with the DNA-staining dye DAPI, a marker of cell nuclei (Fig. 8A a–c, iv). P2Y₁ receptor-IR diffusely labelled cell bodies and processes in most nestin-positive cells. P2Y₂ receptor-IR exhibited a pronounced punctuate distribution both at the cell somata and their processes; the staining was especially pronounced at some of the cells studied. P2Y₄ receptor-IR was expressed only at a few cells and was mostly limited to their processes.

ATP (100 μM) reduced the number of newborn neurons (DCX-IR cells) to 6.5 ± 0.6 cells/field in comparison with 9.3 ± 0.5 cells counted in untreated samples ($P < 0.05$; $n = 4$; both in these and all following experiments) (Fig. 9A a, B a). Treatment with MRS 2179 (30 μM) alone did not alter the number of cells/field (10.3 ± 0.8 ;

$P > 0.05$), although ATP in the presence of MRS 2179 markedly increased the number of DCX-IR cells (17.8 ± 1.8 ; $P < 0.05$), when compared with both the MRS- and ATP-treated groups. By contrast, UTP (100 μM) increased to a similar extent both alone (19.0 ± 0.7 cells/field) and in the presence of MRS 2179 (19.8 ± 1.3 ; $P < 0.05$ each vs. untreated) the number of DCX-IR neurons. Consistent with our previous findings [4], ATP alone exhibited an anti-proliferative effect, reducing the number of Ki67-IR cells to 135.7 ± 20.6 ($P < 0.05$) vs. the control 219.2 ± 26.5 cells/field obtained in untreated controls (Fig. 9A b, B b). Whereas MRS 2179 alone again did not alter the number of cells/field (239.5 ± 20.6 ; $P > 0.05$), it clearly antagonized the effect of ATP (252.3 ± 13.4 ; $P < 0.05$). Eventually, UTP was inactive both alone (275.0 ± 11.1 cells/field) and in combination with MRS 2179 (290.8 ± 13.6 cells/field; $P > 0.05$ each vs. untreated).

In conclusion, ATP inhibited both neurogenesis and cell proliferation by P2Y₁ receptor-activation. By contrast, UTP did not alter proliferation, but promoted neurogenesis most likely *via* P2Y₄ receptor-stimulation. The ATP-induced facilitation of neurogenesis was uncovered only after the blockade of P2Y₁ receptors. We did not investigate which P2Y receptor-type is involved in this latter effect, although it is certainly not P2Y₄, because of the insensitivity of the human P2Y₄ receptor to ATP.

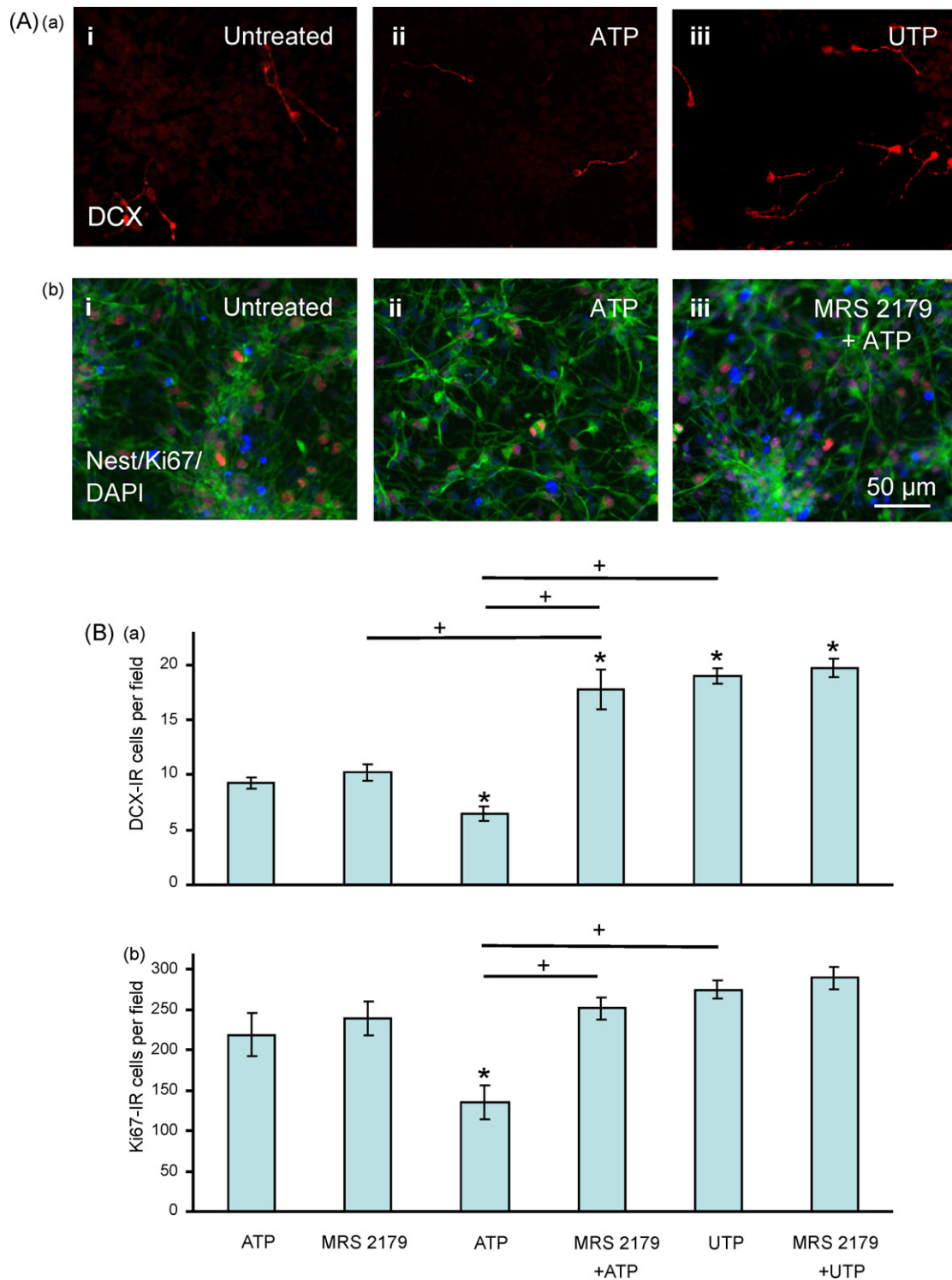


Fig. 9. Differential effect of P2Y receptor agonists on proliferation and neurogenic differentiation of human neuronal progenitor cells. hmNPCs were seeded into 4-well chamber slides (30,000 cells/well) and expanded for 5 days as described in Section 2. (A a, B a) To determine neurogenesis *in vitro*, the P2 receptor agonists ATP (100 μ M), UTP (100 μ M) and the selective P2Y₁ receptor antagonist MRS 2179 (30 μ M) given alone or 30 min prior to ATP or UTP treatment were supplied 24 h after cell plating. Doublecortin (DCX)-immunopositive cells (Aa; red) were counted. (A b, B b). In parallel to these experiments, to determine the proliferation rate, Ki67-immunopositive cells (A b; red) were subjected to the same treatment and then stained and counted. Note that virtually all DAPI stained cells (total cell number) (A b; blue) also stained for nestin (Ab; yellow-green). Ki67- or DCX-immunopositive cells were counted in 4 randomly selected fields of nucleotide-treated or untreated samples. An average number *per* field for DCX-immunoreactivity (B a) or Ki67-immunoreactivity (B b) was determined and shown for each treatment group. Asterisks indicate statistically significant difference ($P < 0.05$) from untreated cells; lines with plus signs indicate statistically significant differences between two columns.

4. Discussion

Patch-clamp experiments indicated that proliferating hmNPCs can be classified on the basis of their passive membrane properties

and voltage-dependent currents into the non-spiking and rudimentarily spiking groups. Only hmNPCs belonging to the second group responded with TTX-sensitive I_{Na} to depolarizing voltage steps. Thus, the density of voltage-sensitive Na^+ channels in the

cell membrane was apparently not sufficient to allow the firing of full action potentials in either case. Similar primitive action potential equivalents have been described e.g. in immature cortical [35] and striatal neurons [17], as well as neuronal progenitors from the subventricular zone of rats [36] and mice [22,25].

It should be noted, however, that I_{Na} was generally rather small in rudimentarily spiking cells. Human neuronal progenitors from fetal brain tissue, fully differentiated to become neurons that were able to produce overshooting spikes, had maximum Na^+ currents more than threefold greater (-20 pA/pF) than our hmNPCs and, in addition, their maximum K^+ currents (40 pA/pF) were greater as well [37]. From this, it may be inferred in addition that hmNPCs not reacting to a high K^+ medium with $[Ca^{2+}]_i$ transients mostly belong to the non-spiking group of cells. In good agreement with this suggestion it has been reported that neuronal progenitors from humans generally have a limited electrical competence [24]. Moreover, our data indicate that the electrophysiological properties of the hmNPCs described here, in many aspects closely resemble those of neuronal progenitors from mice [22,25], rats [35,38] and humans [24,37].

The failure of ATP to cause inward currents in hmNPCs indicates the absence of P2X receptor-channels in progenitors isolated from the fetal human mesencephalon. Divergent data were reported for neuronal stem cells, found in the adult rat [39] or mouse [40] hippocampus, in that ATP or its P2X₇ receptor-preferring analogue dibenzoyl-ATP evoked inward current responses which were antagonized by the non-selective P2X/Y receptor preferential antagonist PPADS. Differences in the species, the age of the individuals and the brain area selected may offer plausible explanations for the respective presence or absence of P2X receptor-channels.

hmNPCs possessed AMPA-sensitive ionotropic glutamate receptors, which had, similar to voltage-activated channels, a lower density in the non-spiking cell population. By contrast, GABA_A receptors were missing in both groups of hmNPCs. In fact, no GABA_A receptor-mediated responses could be obtained in neuronal progenitors from human fetal brain tissue [37]. Moreover, even in rat midbrain-derived neuronal progenitors, AMPA-sensitive cells (67%) outnumbered those responding to GABA_A receptor stimulation (42% [41]). Hence, the earliest point of time when GABA_A receptors become expressed in neuronal progenitor cells may depend on the brain region and/or species studied.

Although all investigated hmNPCs reacted to nucleotide agonists with an increase of the intracellular Ca^{2+} concentration, high K^+ -induced $[Ca^{2+}]_i$ transients were observed in a minority of these cells only. The reason for this phenomenon may be the relatively low density or even absence of voltage-sensitive Ca^{2+} channels in the cell membrane of most undifferentiated neuronal progenitors [37,39]. Since the depletion of intracellular Ca^{2+} by cyclopiazonic acid eliminated a major part of the ATP/UTP effect, we concluded that both nucleotides primarily mobilize Ca^{2+} from the endoplasmic reticulum. This may be due to P2Y receptor occupation by ATP/UTP and the subsequent $G_{q/11}$ -mediated activation of phospholipase C, which generates increased levels of inositol 1,4,5-trisphosphate (IP_3) being a stimulus for Ca^{2+} release.

It still remains to be explained why a Ca^{2+} deficient medium moderately inhibited the nucleotide effects, although electrophysiological experiments excluded the existence of P2X receptor-channels as Ca^{2+} entry pathways. The most likely possibility is that the depletion of the Ca^{2+} storage sites by P2Y₁ receptor-activation signals to the cell membrane and thereby opens SOCs supposed to refill the depleted stores. These channels are found in many non-excitable cell types, where SOCs are the main mechanism of regulated Ca^{2+} entry [42]. However, SOCs are also present in some neurons and glial cells from the central nervous system [43]. G protein-coupled receptors were described to mediate the activation of SOCs that belong to the transient receptor

potential (TRP) family [44], and with respect to P2Y receptors, such mechanisms have already been demonstrated for members of the canonical TRP subfamily [45]. The involvement of SOCs in mediating the P2Y₁ receptor-induced Ca^{2+} influx into immature, cultured striatal neurons has recently been reported by our group [17]. In these neurons, CPA caused an early $[Ca^{2+}]_i$ transient, followed by a late one. The late $[Ca^{2+}]_i$ response was selectively inhibited by a Ca^{2+} -deficient superfusion medium or by SKF 96365, a blocker of SOCs [46], identifying it as being due to capacitive Ca^{2+} current triggered by the depletion of intracellular Ca^{2+} stores. It is noteworthy that in further analogy, both in cultured striatal neurons [17] and in hmNPCs (present study) the ATP/ADP-induced $[Ca^{2+}]_i$ transients partly depended on the presence of external Ca^{2+} , although P2X receptors were missing in the cell membrane.

After having established that both purine and pyrimidine nucleotides cause an increase of $[Ca^{2+}]_i$ by a mechanism relying primarily on the release of intracellular Ca^{2+} from its storage sites, we attempted to identify the P2 receptor-type(s) involved. Microarray RT-PCR measurements indicated the presence of P2Y₁ and P2Y₄ receptor-mRNA in hmNPCs [4]. Our immunocytochemical experiments confirmed the existence of the respective receptor-proteins and in addition proved the expression of P2Y₂ receptors (for P2 receptor-profiles of variable types of neuronal progenitors from humans and rats see [32,47–49]). In our experiments, the rank order of agonist potencies with respect to $[Ca^{2+}]_i$ transients was ATP > ADP > UTP > UDP and thereby did not fully conform to any of the classic P2Y receptor-types [50]. At the ATP/ADP-sensitive group of P2Y receptors (P2Y_{1,12,13}), ADP is expected to be more effective than ATP; the reverse potency order was found in the present study. However, the blockade of the ATP/ADP effect by PPADS and especially MRS 2179 suggests that this receptor is P2Y₁-like.

The higher potency of UTP, when compared with that of UDP suggested the participation of either a P2Y₂ (responsive also to ATP) or a P2Y₄ (responsive only to UTP) receptor. The blockade of the UTP effect by both PPADS and MRS 2179, however, confined again the possible sites of action to the P2Y₁-like receptor. Since UTP does not directly activate P2Y₁ receptors, it appeared likely that UTP evokes the release of ATP from hmNPCs, which in turn acts as the immediate agonist (see also [32–34]). In fact, our experiments with the microelectrode biosensor technique demonstrated a concentration-dependent increase of the extracellular ATP concentration by applying UTP onto hmNPCs. Suramin, with affinities for P2Y_{1,2,12} almost completely abolished the effect of UTP, whereas PPADS which prefers P2Y₁ over the other members of the P2Y receptor-family did not alter the UTP-induced ATP release. In agreement with this finding, suramin was a much weaker antagonist of ATP on $[Ca^{2+}]_i$ transients than PPADS, whereas both antagonists inhibited the effect of UTP to a similar extent. The possible mechanism of the UTP-induced release of ATP may be exocytotic as reported previously for astrocytes and Schwann cells [33,34].

Concentrations of ATP below those able to cause an immediate $[Ca^{2+}]_i$ transient, triggered low frequency Ca^{2+} oscillations in hmNPCs. Thus, ATP by itself, and UTP via the release of endogenous ATP may coordinate the activity of hmNPCs in a manner similar to that described for astrocytic networks [51]. However, Ca^{2+} oscillations in neuronal stem cells occurred predominantly during early stages of differentiation and positively correlated with neurite outgrowth and the onset of the acquisition of the neurotransmitter phenotype [52]. In radial glial cells, giving also rise to neuronal progenitors, ATP-initiated calcium wave propagation was found to modulate proliferation both in the developing retina [53] and neocortex [48].

Nucleotide signaling is involved in nervous system development, including progenitor cell proliferation, migration, and differentiation [54]. P2Y₁ receptors were found in human (NT2 cell line [47]), mice (striatal neuronal progenitor cells [55]) and rat neuronal progenitor cells (radial glia [48]), where they were

essential for proliferation and migration [48,55]. These receptors may be targets both for endogenously released and exogenously applied nucleotides [56]. The nucleotide signaling may be terminated by nucleoside triphosphate diphosphohydrolase 2 (NPTDase2) and tissue non-specific alkaline phosphatase located at the progenitor cells themselves [57]. ATP may stimulate proliferation/differentiation on the one hand via the specific transduction pathways of P2Y_{1,2} receptors [protein kinase C, IP₃, Ca²⁺, phosphoinositide 3 (PI3)-kinase] [58], but also by an interaction with the signaling pathways of the growth factor receptors TrkA (tyrosin receptor kinase A, extracellular receptor kinase (ERK) 1/2, Akt) [49,59].

In the present study, both adenine and uracil nucleotides increased [Ca²⁺]_i in hmNPCs expanded under *in vitro* conditions. Although two developmental stages of the cells could be discriminated by electrophysiological methods (non-spiking and rudimentarily spiking) and Ca²⁺ imaging techniques (responsive and non-responsive to high extracellular K⁺ stimulation), none of these cells reached full maturity. Irrespective of the absence or low density of voltage-sensitive Na⁺ and Ca²⁺ channels, all cells possessed P2Y₁-like receptors, but none of the P2X receptor-subtypes.

In adult neuronal progenitor cells of rodents, both ATP and UTP produced [Ca²⁺]_i transients, although ATP was the more potent agonist [32,49]. In addition, P2Y₂ and especially P2Y₁ receptor-activation led to proliferation as indicated by an increase in cell number and an enhanced incorporation of 5-bromo-2'-deoxyuridine (BrdU) into cells [32,49]. Human neuronal progenitor cells exhibited complex reactions to ATP and UTP [4]. Whereas ATP inhibited proliferation at all concentrations tested, UTP increased it at low (<10 μM), but did not alter it at high concentrations (>10 μM); the number of living cells, the overall protein content and the expression of the proliferation marker 'proliferating cell nuclear antigen' (PCNA) were determined in these series of experiments. All these results were confirmed in the present study by using 100 μM ATP, which decreased the number of Ki67-IR cells indicating a reduced proliferative activity. The effect of ATP was due to the activation of P2Y₁ receptors, because MRS 2179 was strongly antagonistic. Further, 100 μM UTP did not alter the number of Ki67-IR cells. In agreement with data generated both at rodent [32] and human [4] progenitors, 100 μM ATP inhibited, whereas the same concentration of UTP increased the number of DCX-IR cells, which were considered to be migrating neurons. Both ATP and UTP uniformly raised the intracellular Ca²⁺ concentration of hmNPCs by direct and indirect effects at P2Y₁ receptors, respectively, most probably to initiate propagating Ca²⁺ waves as a physiological consequence. However, since ATP and UTP exhibited divergent regulatory activities on proliferation and neuronal differentiation, we conclude that the long-term effects of UTP are due to P2Y₄ rather than P2Y₂ (or indirectly P2Y₁) receptor-stimulation. Thus, P2Y₄ receptors may initiate ERK1/2 phosphorylation and thereby modulate proliferation and dopaminergic differentiation of hmNPCs [4]. By contrast, ATP and UTP may foster via the induction of P2Y₁ receptor-mediated Ca²⁺ waves the maturation of glial rather than neuronal cells in hmNPCs.

Acknowledgements

We thank Mrs. H. Sobottka and Mrs. Lia Barabás for expert technical assistance. This work was supported by the Deutsche Forschungsgemeinschaft (IL 20/16-1).

References

- [1] L. Studer, V. Tabar, R.D. McKay, Transplantation of expanded mesencephalic precursors leads to recovery in parkinsonian rats, *Nat. Neurosci.* 1 (1998) 290–295.
- [2] J.H. Kim, J.M. Auerbach, J.A. Rodríguez-Gómez, I. Velasco, D. Gavin, N. Lumelsky, S.H. Lee, J. Nguyen, R. Sánchez-Pernaute, K. Bankiewicz, R. McKay, Dopamine neurons derived from embryonic stem cells function in an animal model of Parkinson's disease, *Nature* 418 (2002) 50–56.
- [3] A. Storch, M. Sabolek, J. Milosevic, S.C. Schwarz, J. Schwarz, Midbrain-derived neural stem cells: from basic science to therapeutic approaches, *Cell Tissue Res.* 318 (2004) 15–22.
- [4] J. Milosevic, A. Brandt, U. Roemuss, A. Arnold, F. Wegner, S.C. Schwarz, A. Storch, H. Zimmermann, J. Schwarz, Uracil nucleotides stimulate human neural precursor cell proliferation and dopaminergic differentiation: involvement of MEK/ERK signalling, *J. Neurochem.* 99 (2006) 913–923.
- [5] J. Schwarz, S.C. Schwarz, A. Storch, Developmental perspectives on human midbrain-derived neural stem cells, *Neurodegener. Dis.* 3 (2006) 45–49.
- [6] D.K. Morest, J. Silver, Precursors of neurons, neuroglia, and ependymal cells in the CNS: what are they? Where are they from? How do they get where they are going? *Glia* 43 (2003) 6–18.
- [7] A. Gritti, B. Rosati, M. Lecchi, A.L. Vescovi, E. Wanke, Excitable properties in astrocytes derived from human embryonic CNS stem cells, *Eur. J. Neurosci.* 12 (2000) 3549–3559.
- [8] G. Burnstock, Physiology and pathophysiology of purinergic neurotransmission, *Physiol. Rev.* 87 (2007) 659–797.
- [9] L. Nguyen, J.M. Rigo, V. Rocher, S. Belachew, B. Malgrange, B. Rogister, P. Leprieux, G. Moonen, Neurotransmitters as early signals for central nervous system development, *Cell Tissue Res.* 305 (2001) 187–202.
- [10] R.A. Martins, R.A. Pearson, Control of cell proliferation by neurotransmitters in the developing vertebrate retina, *Brain Res.* 1192 (2008) 37–60.
- [11] M.P. Abbracchio, G. Burnstock, Purinoceptors: are there families of P2X and P2Y purinoceptors? *Pharmacol. Ther.* 64 (1994) 445–475.
- [12] S. Kawano, K. Otsu, A. Kuruma, S. Shoji, E. Yanagida, Y. Muto, F. Yoshikawa, Y. Hirayama, K. Mikoshiba, T. Furuichi, ATP autocrine/paracrine signaling induces calcium oscillations and NFAT activation in human mesenchymal stem cells, *Cell Calcium* 39 (2006) 313–324.
- [13] J.S. Heo, H.J. Han, ATP stimulates mouse embryonic stem cell proliferation via protein kinase C, phosphatidylinositol 3-kinase/Akt, and mitogen-activated protein kinase signaling pathways, *Stem Cells* 24 (2006) 2637–2648.
- [14] F. Wegner, R. Kraft, K. Busse, W. Härtig, G. Schaarschmidt, S.C. Schwarz, J. Schwarz, W. Hevers, Functional and molecular analysis of GABA receptors in human midbrain-derived neural progenitor cells, *J. Neurochem.* 107 (2008) 1056–1069.
- [15] A. Storch, G. Paul, M. Csete, B.O. Boehm, P.M. Carvey, A. Kupsch, J. Schwarz, Long-term proliferation and dopaminergic differentiation of human mesencephalic neural precursor cells, *Exp. Neurol.* 170 (2001) 317–325.
- [16] J. Milosevic, S.C. Schwarz, K. Krohn, M. Poppe, A. Storch, J. Schwarz, Low atmospheric oxygen avoids maturation, senescence and cell death of murine mesencephalic neural precursors, *J. Neurochem.* 92 (2005) 718–729.
- [17] P. Rubini, C. Pinkwart, H. Franke, Z. Gerevich, W. Nörenberg, P. Illes, Regulation of intracellular Ca²⁺ by P2Y₁ receptors may depend on the developmental stage of cultured rat striatal neurons, *J. Cell. Physiol.* 209 (2006) 81–93.
- [18] E. Llaudet, N.P. Botting, J.A. Crayston, N. Dale, A three-enzyme microelectrode sensor for detecting purine release from central nervous system, *Biosens. Bioelectron.* 18 (2003) 43–52.
- [19] H. Franke, U. Krügel, J. Grosche, C. Heine, W. Härtig, C. Allgaier, P. Illes, P2Y receptor expression on astrocytes in the nucleus accumbens of rats, *Neuroscience* 127 (2004) 431–441.
- [20] C.D. Richards, T. Shiroyama, S.T. Kitai, Electrophysiological and immunocytochemical characterization of GABA and dopamine neurons in the substantia nigra of the rat, *Neuroscience* 80 (1997) 545–557.
- [21] R.H. Liu, D.J. Morassutti, S.R. Whittemore, J.S. Sosnowski, D.S.K. Magnuson, Electrophysiological properties of mitogen-expanded adult rat spinal cord and subventricular zone neural precursor cells, *Exp. Neurol.* 158 (1999) 143–154.
- [22] A. Carleton, L.T. Petreanu, R. Lansford, A. Alvarez-Buylla, P.M. Lledo, Becoming a new neuron in the adult olfactory bulb, *Nat. Neurosci.* 6 (2003) 507–518.
- [23] D.H. Feldman, J.S. Thinschmidt, A.L. Peel, R.L. Papke, P.J. Reier, Differentiation of ionic currents in CNS progenitor cells: dependence upon substrate attachment and epidermal growth factor, *Exp. Neurol.* 140 (1996) 206–217.
- [24] D.R. Piper, T. Mujtaba, M.S. Rao, M.T. Lucero, Immunocytochemical and physiological characterization of a population of cultured human neural precursors, *J. Neurophysiol.* 84 (2000) 534–548.
- [25] D.D. Wang, D.D. Krueger, A. Bordey, Biophysical properties and ionic signature of neuronal progenitors of the postnatal subventricular zone in situ, *J. Neurophysiol.* 90 (2003) 2291–2302.
- [26] J.R. Gever, D.A. Cockayne, M.P. Dillon, G. Burnstock, A.P.D.W. Ford, Pharmacology of P2X channels, *Pflügers Arch.* 452 (2006) 513–537.
- [27] Z. Gerevich, S.J. Borvendeg, W. Schröder, H. Franke, K. Wirkner, W. Nörenberg, S. Fürst, C. Gillen, P. Illes, Inhibition of N-type voltage-activated calcium channels in rat dorsal root ganglion neurons by P2Y receptors is a possible mechanism of ADP-induced analgesia, *J. Neurosci.* 24 (2004) 797–807.
- [28] A. Verkhratsky, C. Steinhäuser, Ion channels in glial cells, *Brain Res. Brain Res. Rev.* 32 (2000) 380–412.
- [29] V. Ralevic, G. Burnstock, Receptors for purines and pyrimidines, *Pharmacol. Rev.* 50 (1998) 413–492.
- [30] P. Illes, A.J. Ribeiro, Molecular physiology of P2 receptors in the central nervous system, *Eur. J. Pharmacol.* 483 (2004) 5–17.

- [31] I. von Kügelgen, Pharmacological profiles of cloned mammalian P2Y-receptor subtypes, *Pharmacol. Ther.* 110 (2006) 415–432.
- [32] J.H. Lin, T. Takano, G. Arcuino, X. Wang, F. Hu, Z. Darzynkiewicz, M. Nunes, S.A. Goldman, M. Nedergaard, Purinergic signaling regulates neural progenitor cell expansion and neurogenesis, *Dev. Biol.* 302 (2007) 356–366.
- [33] A. Abdipranoto, G.J. Liu, E.L. Werry, M.R. Bennett, Mechanisms of secretion of ATP from cortical astrocytes triggered by uridine triphosphate, *Neuroreport* 14 (2003) 2177–2181.
- [34] G.J. Liu, E.L. Werry, M.R. Bennett, Secretion of ATP from Schwann cells in response to uridine triphosphate, *Eur. J. Neurosci.* 21 (2005) 151–160.
- [35] H.J. Luhmann, R.A. Reiprich, I. Hanganu, W. Kilb, Cellular physiology of the neonatal rat cerebral cortex: intrinsic membrane properties, sodium and calcium currents, *J. Neurosci. Res.* 62 (2000) 574–584.
- [36] O. Arias-Carrión, S. Hernández-López, O. Ibañez-Sandoval, J. Bargas, A. Hernández-Cruz, R. Drucker-Colín, Neuronal precursors within the adult rat subventricular zone differentiate into dopaminergic neurons after substantia nigra lesion and chromaffin cell transplant, *J. Neurosci. Res.* 84 (2006) 1425–1437.
- [37] D.R. Piper, T. Mujtaba, H. Keyoung, N.S. Roy, S.A. Goldman, M.S. Rao, M.T. Lucero, Identification and characterization of neuronal precursors and their progeny from human fetal tissue, *J. Neurosci. Res.* 66 (2001) 356–368.
- [38] O. Belluzzi, M. Benedusi, J. Ackman, J.J. LoTurco, Electrophysiological differentiation of new neurons in the olfactory bulb, *J. Neurosci.* 23 (2003) 10411–10418.
- [39] R.C. Hogg, H. Chipperfield, K.A. Whyte, M.R. Stafford, M.A. Hansen, S.M. Cool, V. Nurcombe, D.J. Adams, Functional maturation of isolated neural progenitor cells from the adult rat hippocampus, *Eur. J. Neurosci.* 19 (2004) 2410–2420.
- [40] V. Shukla, H. Zimmermann, L. Wang, H. Kettenmann, S. Raab, K. Hammer, J. Sévigny, S.C. Robson, N. Braun, Functional expression of the ecto-ATPase NTPDase2 and of nucleotide receptors by neuronal progenitor cells in the adult murine hippocampus, *J. Neurosci. Res.* 80 (2005) 600–610.
- [41] F. Schlesinger, J. Meywirth, K. Krampfl, J. Grosskreutz, S. Petri, C. Mauth, L. Just, A. Bader, J. Bufler, Ligand-gated channels in early mesencephalic neuronal precursors: immunocytochemical and electrophysiological analysis, *Eur. J. Neurosci.* 19 (2004) 2371–2376.
- [42] A.B. Parekh, J.W. Putney, Store-operated calcium channels, *Physiol. Rev.* 85 (2005) 757–810.
- [43] N.J. Emptage, C.A. Reid, A. Fine, Calcium stores in hippocampal synaptic boutons mediate short-term plasticity, store-operated Ca^{2+} entry, and spontaneous transmitter release, *Neuron* 29 (2001) 197–208.
- [44] M.M. Moran, H. Xu, D.E. Clapham, TRP ion channels in the nervous system, *Curr. Opin. Neurobiol.* 14 (2004) 362–369.
- [45] M. Schaefer, T.D. Plant, A.G. Obukhov, T. Hofmann, T. Gudermann, G. Schultz, Receptor-mediated regulation of the nonselective cation channels TRPC4 and TRPC5, *J. Biol. Chem.* 275 (2000) 17517–17526.
- [46] C.R. Jan, C.M. Ho, S.N. Wu, C.J. Tseng, Multiple effects of 1- β -[3-(4-methoxyphenyl)propoxy]-4-methoxyphenethyl]-1H-imidazole hydrochloride (SKF 96365) on Ca^{2+} signaling in MDCK cells: depletion of thapsigargin-sensitive Ca^{2+} store followed by capacitative Ca^{2+} entry, activation of a direct Ca^{2+} entry, and inhibition of thapsigargin-induced capacitative Ca^{2+} entry, *Naunyn-Schmiedeberg's Arch. Pharmacol.* 359 (1999) 92–101.
- [47] D.J. Moore, J.K. Chambers, P.R. Murdock, P.C. Emson, Human Ntera-2/D1 neuronal progenitor cells endogenously express a functional P2Y₁ receptor, *Neuropharmacology* 43 (2002) 966–978.
- [48] T.A. Weissman, P.A. Riquelme, L. Ivic, A.C. Flint, A.R. Kriegstein, Calcium waves propagate through radial glial cells and modulate proliferation in the developing neocortex, *Neuron* 43 (2004) 647–661.
- [49] S.K. Mishra, N. Braun, V. Shukla, M. Füllgrabe, C. Schomerus, H.W. Korf, C. Gachet, Y. Ikehara, J. Sévigny, S.C. Robson, H. Zimmermann, Extracellular nucleotide signaling in adult neural stem cells: synergism with growth factor-mediated cellular proliferation, *Development* 133 (2006) 675–684.
- [50] M.P. Abbracchio, G. Burnstock, J.M. Boeynaems, E.A. Barnard, J.L. Boyer, C. Kennedy, G.E. Knight, M. Fumagalli, C. Gachet, K.A. Jacobson, G.A. Weisman, International Union of Pharmacology LVIII: update on the P2Y G protein-coupled nucleotide receptors: from molecular mechanisms and pathophysiology to therapy, *Pharmacol. Rev.* 58 (2006) 281–341.
- [51] R.A. North, A. Verkhratsky, Purinergic transmission in the central nervous system, *Pflügers Arch.* 452 (2006) 479–485.
- [52] F. Ciccolini, T.J. Collins, J. Sudhoelter, P. Lipp, M.J. Berridge, M.D. Bootman, Local and global spontaneous calcium events regulate neurite outgrowth and onset of GABAergic phenotype during neural precursor differentiation, *J. Neurosci.* 23 (2003) 103–111.
- [53] O. Uckeremann, J. Grosche, A. Reichenbach, A. Bringmann, ATP-evoked calcium responses of radial glial (Müller) cells in the postnatal rabbit retina, *J. Neurosci. Res.* 70 (2002) 209–218.
- [54] H. Zimmermann, Nucleotide signaling in nervous system development, *Pflügers Arch.* 452 (2006) 573–588.
- [55] E. Scemes, N. Duval, P. Meda, Reduced expression of P2Y₁ receptors in connexin43-null mice alters calcium signaling and migration of neural progenitor cells, *J. Neurosci.* 23 (2003) 11444–11452.
- [56] R.A. Pearson, N. Dale, E. Llaudat, P. Mobbs, ATP released via gap junction hemichannels from the pigment epithelium regulates neural retinal progenitor proliferation, *Neuron* 46 (2005) 731–744.
- [57] N. Braun, J. Sévigny, S.K. Mishra, S.C. Robson, S.W. Barth, R. Gerstberger, K. Hammer, H. Zimmermann, Expression of the ecto-ATPase NTPDase2 in the germinal zones of the developing and adult rat brain, *Eur. J. Neurosci.* 17 (2003) 1355–1364.
- [58] H. Franke, P. Illes, Involvement of P2 receptors in the growth and survival of neurons in the CNS, *Pharmacol. Ther.* 109 (2006) 297–324.
- [59] D.B. Arthur, K. Akassoglou, P.A. Insel, P2Y₂ receptor activates nerve growth factor/TrkA signaling to enhance neuronal differentiation, *Proc. Natl. Acad. Sci. U.S.A.* (2005) 19138–19143.

Regulation of Intracellular Ca^{2+} by P2Y_1 Receptors May Depend on the Developmental Stage of Cultured Rat Striatal Neurons

PATRIZIA RUBINI, CHRISTINA PINKWART, HEIKE FRANKE, ZOLTAN GEREVICH,
WOLFGANG NÖRENBERG, AND PETER ILLES*

*Rudolf-Boehm-Institut für Pharmakologie und Toxikologie,
Universität Leipzig, Leipzig, Germany*

Mixed striatal cell cultures containing neurons and glial cells were grown either in neurobasal medium (NBM) or Dulbecco's modified Eagle's medium (DMEM). Whole-cell patch-clamp recordings indicated that, if at all, only a single, low amplitude spike was evoked shortly after starting the injection of a depolarizing current pulse into NBM neurons. In contrast, DMEM neurons fired series of high amplitude action potentials, without apparent spike frequency adaptation. The possible reason for the observed action potential failure in NBM neurons was a low density of Na^+ channels per unit of membrane surface area. However, both in NBM and DMEM neurons, ATP did not induce inward current responses via P2X receptor-channels, although GABA_A and N -methyl-D-aspartate (NMDA) receptor-channels could be activated by muscimol and NMDA, respectively. Ca^{2+} imaging experiments by means of the Fura-2 method were utilized to measure intracellular Ca^{2+} ($[\text{Ca}^{2+}]_i$) in neurons and glial cells. NBM, but not DMEM neurons responded to ATP with $[\text{Ca}^{2+}]_i$ transients; glial cells grown in either culture medium were equally sensitive to ATP. ATP caused an increase of $[\text{Ca}^{2+}]_i$ by a mechanism only partly dependent on external Ca^{2+} ; the residual ATP effect was blocked by cyclopiazonic acid (CPA) and was therefore due to the release of Ca^{2+} from its intracellular pools. The receptor involved was characterized by P2 receptor antagonists (PPADS, MRS 2179, AR-C69931MX) and was found to belong to the P2Y_1 subtype. CPA caused an early $[\text{Ca}^{2+}]_i$ response due to release from intracellular storage sites, followed by a late $[\text{Ca}^{2+}]_i$ response due to the influx of this cation from the extracellular space, probably triggered by the opening of store-operated channels (SOCs) in the plasma membrane. It is concluded that in partial analogy with the effect of CPA, ATP releases $[\text{Ca}^{2+}]_i$ via the G_q /phospholipase C/inositoltrisphosphate (IP_3) pathway, thereby opening SOCs. It is hypothesized that this effect of ATP may have an important role for the proliferation and migration of striatal neuronal progenitors. *J. Cell. Physiol.* 209: 81–93, 2006. © 2006 Wiley-Liss, Inc.

Cortical information impinging on the striatum is processed and transmitted to the basal ganglia output nuclei (globus pallidus and subthalamic nucleus; Smith et al., 1998). Glutamatergic and dopaminergic inputs from the cortex and substantia nigra, respectively, control the activity of the medium spiny striatal output neurons. Huntington's disease is an autosomal, dominantly inherited disorder characterized by chorea, involuntary movements, dystonia, intellectual impairments, and emotional disturbances (Reddy et al., 1999). Selective cell loss during this disease occurs in various areas of the brain, particularly in the caudate and putamen of the striatum and the cerebral cortex. The replacement of degenerated striatal medium spiny output neurons by neural stem cells provides a highly migratory, multi potential and sustainable population of transplant material (Roberts et al., 2006; Visnyei et al., 2006). Hence, improved knowledge on the properties of immature striatal neurons as well as their reactions to growth factors is of great theoretical and practical significance.

In the brain, ATP is known to be both a neurotransmitter of its own right and a co-transmitter of various classic transmitters including noradrenaline and probably also dopamine (Edwards et al., 1992; Poelchen et al., 2001). Nucleotide receptors of the ionotropic P2X and metabotropic P2Y types mediate rapid and slow synaptic responses, respectively (Illes and Riebeiro, 2004). In addition, P2Y receptors appear to be involved in nucleotide signaling in nervous system development (Zimmermann, 2006). This includes progenitor cell proliferation, cell migration, neuronal and glial cellular interaction/differentiation and synaptic network formation.

In spite of the detection of various P2X and P2Y receptor mRNAs and proteins in the rat striatum (Nörenberg and Illes, 2000; Khakh, 2001; Illes and Riebeiro, 2004), functional data on the effects of ATP are rare. Cultured striatal neurons react to ATP with an outward potassium current mediated by a G protein-coupled and pertussis toxin-insensitive P2Y receptor (Ikeuchi and Nishizaki, 1995). Further, the stimulation of a pertussis toxin-sensitive P2Y receptor led to the release of dopamine both in the ventral (Krügel et al., 1999) and dorsal striatum (nucleus accumbens; Zhang et al., 1995). Data relating to the signal transduction mechanisms of P2Y receptors in striatal neurons cultured under conditions favoring or disfavoring neuronal differentiation are completely missing.

The aim of the present study was threefold. First, we tried to clarify whether P2 receptor-stimulation in

Wolfgang Nörenberg and Peter Illes equally contributed to the work.

Contract grant sponsor: Bundesministerium für Forschung und Technologie (BMBF; Bonn, Germany); Contract grant number: 01GZ0309; Contract grant sponsor: European Community (Brussels, Belgium); Contract grant number: HPMD-CT-2001-00067.

*Correspondence to: Peter Illes, Rudolf-Boehm-Institut für Pharmakologie und Toxikologie, Universität Leipzig, Haertelstrasse 16-18, D-04107 Leipzig, Germany.
E-mail: illp@medizin.uni-leipzig.de

Received 6 May 2006; Accepted 9 May 2006

DOI: 10.1002/jcp.20705

cultured striatal neurons and glial cells results in an increase of intracellular Ca^{2+} ($[\text{Ca}^{2+}]_i$). Second, we investigated whether these cells grown under various conditions (neurobasal medium, NBM; Dulbecco's modified Eagle's medium, DMEM) react in a different manner to ATP. Third, we searched for the P2 receptor-type involved, by electrophysiological, Ca^{2+} imaging and immunocytochemical methods. Our findings indicate that the embryonic NBM neurons, but not the more mature DMEM neurons are endowed with $[\text{Ca}^{2+}]_i$ releasing P2Y₁ receptors. The depletion of the intracellular Ca^{2+} pools might open store-operated Ca^{2+} channels (SOCs) in the plasma membrane; extracellular Ca^{2+} enters via these SOCs, rather than via P2X receptor-channels. In contrast to neurons, astrocytes do not alter their properties irrespective of cultivation in DMEM or NBM.

MATERIALS AND METHODS

Preparation of striatal cell cultures

Striatal tissue was dissected from 1-day-old Wistar rats (own breed) killed by decapitation, and collected in Hank's balanced salt solution (HBSS). The tissue was treated with 0.25% trypsin (1:1 in HBSS) for 20 min at 37°C. Then, 100 μl of DNase I (10 $\mu\text{g}/\text{ml}$) was applied, followed by mechanical trituration through a Pasteur pipette in fetal calf serum-supplemented (20%) Dulbecco's modified Eagle's medium (DMEM) containing also 15 mM HEPES, 50 $\mu\text{g}/\text{ml}$ gentamycin, and 30 mM D-glucose. Subsequent to centrifugation, the pellet was resuspended in DMEM of the above composition and was seeded into poly-L-lysine-coated polystyrol dishes (electrophysiology) or glass coverslips (Ca^{2+} imaging) at a density of 3×10^4 cells per dish/coverslip, and cultured at 37°C in a humidified atmosphere containing 6.8% CO_2 in air. For some of the dishes, after 4 days of cultivation, the medium was replaced by Neurobasal™ medium (NBM) supplemented with B27 (v/v 50/1), 2.5 mM L-glutamine and 50 $\mu\text{g}/\text{ml}$ gentamycin.

Electrophysiological procedures

Whole-cell recordings from rat neostriatal neurons were performed in 13–15-day-old cultures (14–15 DIV) grown either in DMEM only, or in DMEM followed by NBM. To investigate the basic electrophysiological properties as well as putative P2 receptor endowments, current-clamp and voltage-clamp experiments were made consecutively in the same sets of cells by means of an EPC-9 amplifier (HEKA, Lambrecht, Germany) at room temperature (20–24°C). The standard external bath solution contained (mM): 162, NaCl; 2.4, KCl; 1.3, CaCl_2 ; 1, MgCl_2 ; 10, HEPES; and 11, glucose (~ 300 mOsm/l; pH 7.3 with NaOH). The standard pipette solution contained (mM): 144, potassium gluconate; 1, CaCl_2 ; 3, MgCl_2 ; 10, HEPES; 11, EGTA; 4, Mg-ATP; 0.3, Li-GTP (~ 300 mOsm/l; pH 7.2 with KOH). Patch pipettes had a resistance of 3–5 M Ω , when filled with this intracellular solution. Holding potentials were set and membrane potential values were corrected taking into account a liquid junction potential of 15 mV.

Action potentials of rat cultured neostriatal neurons were recorded in the fast current-clamp mode of the EPC-9. The resting membrane potential was measured just after passing to the whole-cell configuration. Membrane potential recordings were then sampled at 20 kHz and filtered at 6.7 kHz. The input resistance of the cells was determined by hyperpolarizing current pulses inducing voltage shifts <15 mV. Action potentials were evoked by 500 msec duration depolarizing current pulses, one current pulse every 10 sec that were increased in strength by 10 pA increments. The spike threshold was measured as the voltage difference between the resting potential and the onset of the fast upstroke of the first action potential elicited in response to this series of stepwise increasing depolarizing current pulses. The spike latency was the time from the initiation of the depolarizing current pulse to the spike onset. The action potential amplitude and action potential duration were measured from the onset of the

fast spike upstroke to the peak and at half amplitude, respectively. The after-hyperpolarization (AHP) was measured as the difference between the spike onset and the voltage minimum following the action potential peak. The time to peak of the AHP was the time difference between the spike onset and this voltage minimum (Fig. 1 Ba, Bb).

The presence of functional P2X receptor channels in rat cultured neostriatal neurons was then investigated under voltage-clamp at a holding potential of -80 mV. After the amplifier had been switched to the voltage-clamp mode, cells were allowed to equilibrate first for a 5 min period in a slightly modified, that is, nominally Mg^{2+} -free bath solution, also containing the NMDA receptor co-agonist glycine (10 μM) and the Na^+ channel blocker tetrodotoxin (TTX, 0.3 μM). Transmembrane currents in response to the GABA_A receptor agonist muscimol (30 μM), the NMDA receptor agonist *N*-methyl-D-aspartate (NMDA, 100 μM), the P2X receptor agonist adenosine-5'-triphosphate (ATP, 30–300 μM) and drug-free bath solution were sampled at 3 kHz and filtered at 1 kHz. To this end, agonists were consecutively pressure applied to the same neurons by means of the application cannula of a fast-flow superfusion system (Adams and List, DAD-12, NY) placed in immediate vicinity (20–30 μm) to the cell under investigation. Challenges with the individual agonists (or drug-free bath solution) were 2 sec in duration and separated by 2 min superfusion periods with drug-free bath solution. The order of agonist application was varied between individual experiments. The time to equilibrium exchange (measured as rise time from 20% to 80% of the peak response to distilled water applied at the end of experiments to the open tips of patch pipettes) was 164 ± 13 msec ($n = 11$) and, hence well within the times of agonist application (2 sec). For statistical evaluation, peak current amplitudes were measured and divided by membrane capacitance (peak current densities, pA/pF; PulseFit software, HEKA).

Cell capacitance and series resistance (R_s) were monitored repeatedly during the voltage-clamp part of the experiments by the inbuilt compensation routine of the EPC-9 amplifier. R_s was partially compensated (70%–80%) and did not change significantly during experiments. Its (uncompensated) values were 15.7 ± 0.8 M Ω and 16.2 ± 1.0 M Ω ($P > 0.05$; $n = 94$) at the start and the end of the trials, respectively, thus indicating stable recording conditions.

In some independent experiments, the basic properties of Na^+ currents in rat cultured neostriatal neurons were characterized in addition. In these experiments, the bath solution contained (mM): NaCl, 140; CaCl_2 1; MgCl_2 1; CdCl_2 0.5; HEPES 10; glucose 11 (~ 300 mOsm/l with sucrose; pH 7.3 with NaOH). Patch pipettes had a resistance <2.5 M Ω , when filled with the intracellular solution (in mM): CsF, 120; NaCl, 10; CaCl_2 , 1; MgCl_2 , 1; HEPES, 10; EGTA, 11; TEA-Cl, 5; Mg-ATP, 4; Li-GTP, 0.3; ~ 300 mOsm/l; pH 7.2 with CsOH). Holding potentials were set taking into account a liquid junction potential of 8 mV. R_s was 6.6 ± 0.9 and 6.4 ± 0.7 M Ω ($n = 16$) at the beginning and the end of the recording period. R_s was compensated between 70% and 90%. Thus, the voltage error at the somatic membrane could have been around 3 mV in the worst case considering that maximum Na^+ current amplitudes in the cells included in this study did not exceed 1.5 nA. The neurons had developed dendrite-like processes at the times of current recordings (see Fig. 1Aa, Ab) and, hence, additional space-clamp related problems might have complicated the analysis of sodium currents. Therefore, relatively small cells (3.8 ± 0.5 pF; $n = 16$) having only short processes were selected for recording. Since, the Na^+ current reversal potential (see Fig. 2Ab) was always within a few mV of the prediction based on the Nernst equation, the membrane voltage appeared to be quite adequately controlled under these conditions. Na^+ current signals were filtered at 10 kHz and sampled at 50 kHz. Linear leak and residual capacitance currents were digitally subtracted from raw current traces using a P/4 protocol.

Na^+ currents were evoked by series of 5 msec depolarizing voltage-steps from a holding potential of -80 mV. For the construction of peak current density/voltage curves and voltage-dependent activation curves, increasing voltage steps

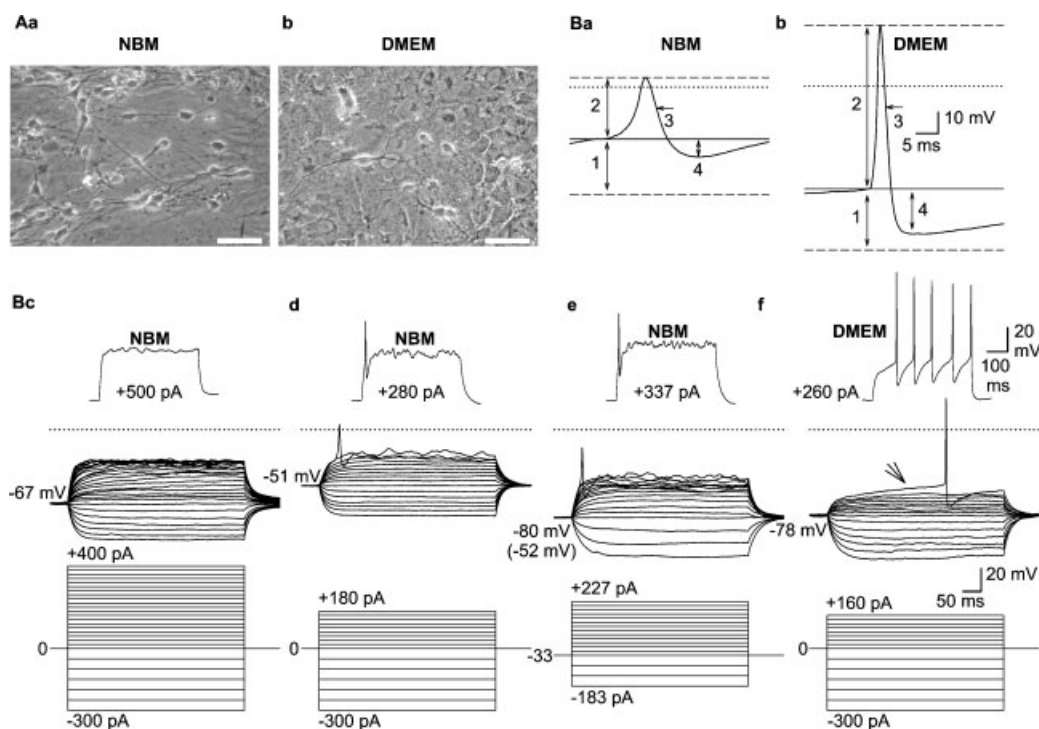


Fig. 1. Morphological (A) and electrophysiological characterization (B) of rat striatal neurons cultured in either neurobasal medium (NBM; Aa, Ba, c, d, e) or Dulbecco's modified Eagle's medium (DMEM; Ab, Bb, f). Aa, Bb: Typical microphotographs mugged under phase contrast optics at magnification 20 \times showing examples of NBM- (Aa) and DMEM-grown striatal neurons (Ab) sitting on top of a background glial cell layer. Scale bars 50 μ m. Ba, Bb: Enlarged action potential waveforms evoked by just threshold depolarizing current pulses in a NBM cell (Ba) and a DMEM cell (Bb) also shown in Bd and f. The upper- and lower dashed lines indicate the action potential peak and the resting membrane potential, respectively, the dotted line is the zero voltage level and the continuous line tags the onset of the spike upstroke. Arrows numbered 1–4 illustrate where the action potential parameters had been measured. Spike threshold (1) and spike amplitude (2) were measured as the voltage differences between the action potential onset and the resting membrane potential and between the action potential onset and the action potential peak, respectively. The spike duration (3) was assessed at half amplitude. The amplitude of the after-hyperpolarization (4) was the voltage

difference between the spike onset and the voltage minimum following the action potential peak. The time to the peak of the after-hyperpolarization was measured as the time difference between the spike onset and this voltage minimum. Bc, d, e, f: Families of membrane potential responses (upper parts) evoked by hyperpolarizing and depolarizing current pulses (lower parts) in three different NBM cells (Bc–e) and a representative DMEM cell (Bf). Current pulses, 500 msec in duration, were imposed every 10 sec either on the resting membrane potential (as indicated on the left side of the membrane potential traces in Bc, d, and f), or when the membrane potential was shifted in the hyperpolarizing direction by constant current injection (as indicated on the left side of the membrane potential traces in Be). The insets in Bd–f illustrate responses to 100 pA supra-threshold depolarizing currents. Please note that the NBM cells in d and e did not fire repetitively, whereas the NBM cell in Bc failed to fire at all. Dotted lines in Bc–f represent the zero voltage level. The arrow in e indicates the slow depolarizing ramp preceding typically the first action potential in DMEM neurons.

(–75 to 70 mV, 5 mV increments) were applied with 5 sec intervals. To assess voltage-dependent Na⁺ channel inactivation, Na⁺ currents were activated by test-pulses (5 msec in duration) to –10 mV after varying pre-pulse potentials (from –95 to –20 mV, 200 msec in duration).

Na⁺ conductance at a given test-pulse (activation) or pre-pulse potential (inactivation) was calculated according to

$$G(V) = I_{\max}/(V - V_{\text{Na}})$$

where I_{\max} is the peak current amplitude, V the test-pulse or pre-pulse potential, and V_{Na} the Na⁺ current reversal potential. The voltage-dependence of activation and inactivation was then determined by fitting to a Boltzmann equation of the form

$$G(V) = G_{\max}/(1 + \exp((V_{50} - V)/k_m))$$

where G_{\max} is the maximum Na⁺ conductance, V_{50} is the voltage where $G(V)$ is half of G_{\max} , and k_m is the slope factor giving the change in membrane potential per e-fold change in conductance.

The fast recovery of Na⁺ channels from voltage-dependent inactivation was eventually assessed by a double-pulse protocol consisting of a conditioning 5 msec pre-pulse from –80 to –10 mV followed by varying recovery periods (1–1,000 msec) at –80 mV and then by a subsequent 5 msec test-pulse to –10 mV. By dividing currents in response to test-pulses (I_2) by

currents in response to the respective pre-pulses (I_1), the fraction of Na⁺ channels available after a given recovery period (t) was obtained. The fast (τ_1) and slow (τ_2) time constants for the fast recovery process were then extracted by the double exponential function:

$$I_2/I_1 = A_0 + A_1(1 - \exp(-t/\tau_1)) + A_2(1 - \exp(-t/\tau_2))$$

where A_0 is the starting amplitude of the function and A_1 and A_2 indicate the relative amplitude contribution of the fast and slow recovery time constant, respectively.

Intracellular calcium measurements

Thirteen to 15 days old cultures (13–15 DIV) grown either in DMEM only, or in DMEM followed by NBM were loaded for 50–60 min at 37°C in the dark with the cell permeant acetoxymethyl ester of the fluorescent Ca²⁺ indicator Fura-2 (2.5 μ M). To remove excess extracellular Fura-2, glass coverslips were washed several times with an artificial cerebrospinal solution (ACSF) of the following composition (in mM): NaCl 135, KCl 4.5, CaCl₂ 2, MgCl₂ 1, HEPES 10, glucose 10; pH adjusted to 7.4 with NaOH) and were allowed to rest for 30 min at room temperature protected from light. Thereafter, Ca²⁺ imaging experiments were performed at room temperature in ACSF using an inverted microscope (IX-70; Olympus, Hamburg, Germany) equipped for epifluorescence and a Peltier-cooled charge-coupled device camera (IMAGO; Till Photonics, Martinsried, Germany). Intracellular Fura-2 was alternately

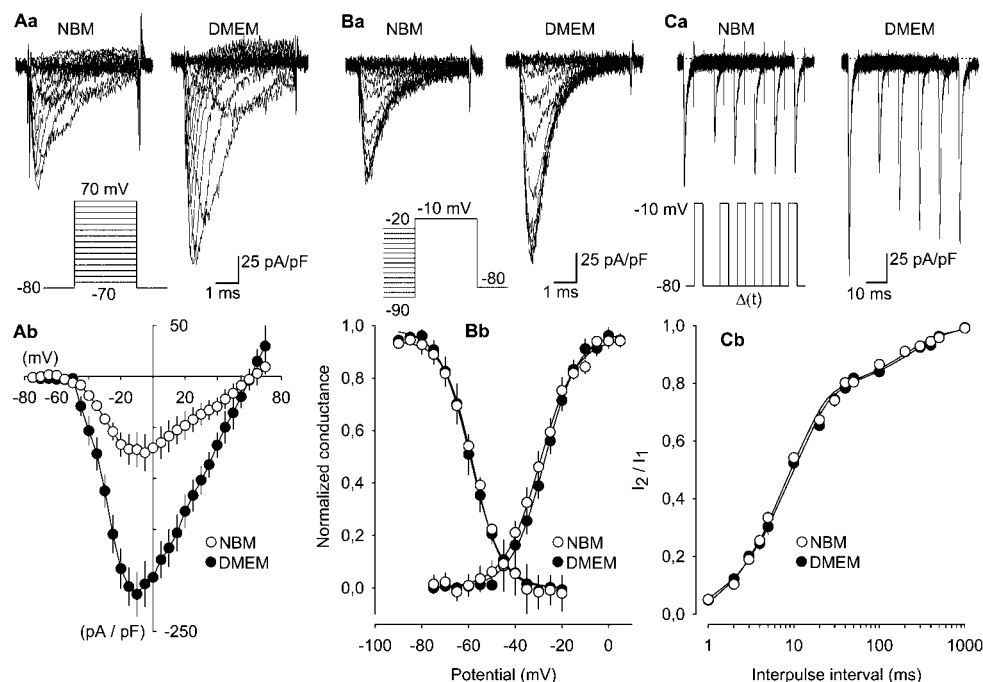


Fig. 2. Comparison between the properties of voltage-dependent Na^+ currents in striatal neurons cultured either in NBM or DMEM ($n = 8$ each). **Aa**: Currents evoked by a series of depolarizing voltage steps (inset), 5 msec in duration, from -70 to 70 mV from a holding potential of -80 mV in a NBM neuron (left) and a DMEM neuron (right). **Ab**: Peak current density/voltage curves derived from similar experiments as shown in Aa in NBM cells (\circ) and DMEM cells (\bullet), respectively. **Ba**: Na^+ currents evoked by a 5 msec test-pulse to -10 mV from increasingly more depolarized pre-pulse potentials (inset) in a NBM- (left) and a DMEM neuron (right). The pre-pulse was 200 msec, in duration and the holding potential was -80 mV. **Bb**: Activation and inactivation curves of the Na^+ current in NBM- (\circ) and DMEM cells (\bullet). The average values of normalized conductance were plotted either against the test-pulse potential, according to the stimulus protocol illustrated in **Aa** (activation), or the pre-pulse potential as

illustrated in **Ba** (inactivation) and fitted with a Boltzmann function (solid lines, see Methods). **Ca**: Fast recovery from inactivation of Na^+ currents in NBM neurons (left) and DMEM neurons (right). Fast recovery from inactivation was investigated using a double pulse protocol (inset) consisting of a conditioning 5 msec pre-pulse from -80 to -10 mV followed by varying recovery periods ($\Delta(t) = 1-1,000$ msec) at -80 mV and then by a subsequent 5 msec test-pulse to -10 mV. For clarity, only the current responses for $\Delta(t) = 10, 20, 30, 40,$ and 50 msec are shown. **Cb**: The fraction of Na^+ current (test-pulse amplitude/pre-pulse amplitude $= I_2/I_1$) available after the various recovery periods in NBM neurons (\circ) and DMEM neurons (\bullet) were plotted versus the duration of the interpulse interval and fitted with a biexponential function (solid lines, see Methods). Dotted lines in **Aa**, **Ba** and **Ca** represent the zero current level.

excited at 340 nm and at 380 nm, and the emitted light was measured at a wavelength of 510 nm. The TILL visION software (3.3; Till Photonics) was used for data acquisition, system control, and later, off-line analysis. The fluorescence ratio (340/380 nm) provides a relative measure of the cytosolic free Ca^{2+} concentration ($[\text{Ca}^{2+}]_i$; Grynkiewicz et al., 1985).

The experimental protocol routinely started with the application of ACSF via the flush valve of a pressure-operated, computer-controlled rapid drug application device (DAD-12, Adams and List) followed by a 3-sec application of a high- K^+ ACSF solution containing (in mM): NaCl 89.5, KCl 50, CaCl_2 2, MgCl_2 1, HEPES 10, glucose 10; pH adjusted to 7.4 with NaOH. Neurons and glial cells were identified both by their morphology and by the presence and absence of $[\text{Ca}^{2+}]_i$ transients, respectively, in response to the superfusion of a high- K^+ containing medium.

Concentration-response curves of ATP were determined by applying increasing concentrations of ATP (0.1–100 μM) for 10 sec every 10 min. Usually 2 lower and 2 higher ATP concentrations were applied to a single cell. In the following experiments either a high (50 mM)- K^+ containing medium or an ATP (30 μM)-containing medium was superfused for 3 and 10 sec, respectively, every 10 min for three-times in total (T_1 – T_3). A Ca^{2+} -free medium was prepared by omitting CaCl_2 from the medium and adding EGTA (1 mM) to chelate the residual Ca^{2+} . The superfusion of this medium started 4 min before the second application of K^+ and 8 min before the second application of ATP (at T_2 each), respectively, for 10 min in total. Cyclopiazonic acid (CPA; 30 μM) was superfused 15 min before and during the second application of ATP at T_2 . MRS 2179 (30 μM) and AR-C69931MX (3 μM) were superfused 10 min before and during the second application of ATP at T_2 . Finally, CPA (30 μM) was superfused twice for 6 min each spaced apart

by 20 min. In some experiments the second application of CPA occurred in the presence of a Ca^{2+} -free, or SKF 96365 (50 μM)-containing medium both being superfused 4 min before and during the application of CPA. The effects at T_2 were expressed in all cases as a percentage change compared with the responses at T_1 .

Concentration-response curves for ATP were fitted using the following logistic function:

$$E = E_{\min} + (E_{\max} - E_{\min}) [1 + (EC_{50} + A)^n]^{-1}$$

where E is the steady-state effect produced by the agonist at the concentration A , E_{\max} and E_{\min} are the maximal and minimal effects, respectively, n the Hill coefficient, and EC_{50} the concentration of agonist producing 50% of E_{\max} .

The inhibition of the CPA (30 μM)-induced increase in $[\text{Ca}^{2+}]_i$ by a Ca^{2+} -free medium or SKF 96365 (50 μM) was calculated by the data under the curve (DUC) method (TopFit, version 2.0; Heinzel et al., 1993). The second response to CPA obtained in the presence of a Ca^{2+} -free medium or SKF 96365 was compared with the first response to CPA obtained in a drug-free normal medium and was expressed as percentage change.

Immunofluorescence and confocal microscopy

The cultures were washed twice for 1 min in PBS and fixed in ice-cold methanol. For permeabilization and blocking, the cells were pretreated with 0.5% Triton X-100 and 5% fetal calf serum (FCS) in Tris-buffered saline (TBS, 0.05 M, pH 7.6) for 40 min. Then, the cultures were incubated as previously described for striatal slices (Franke et al., 2003) with an antibody mixture containing the rabbit P2Y₁ receptor antibody (1:400), together with the mouse MAP2 (1:1,000), mouse GFAP

(1:1,000) or mouse nestin (1:500) antibodies, or alternatively with an antibody mixture containing the mouse nestin antibody (1:500) together with the rabbit MAP2 (1:300) or rabbit GFAP (1:500) antibodies. Afterwards, the cultures were incubated with the secondary antibodies Cy2-conjugated goat anti-mouse IgG (1:400) and Cy3-conjugated goat anti-rabbit IgG (1:1,000) in 5% FCS in TBS for 2 h. After intensive washing, all stained cultures were dehydrated in a series of graded ethanol, processed through *n*-butylacetate and covered with entellan (Merck, Darmstadt, Germany). Control experiments were carried out without the primary antibodies or by pre-adsorption of the antibody with the immunizing peptides.

The immunofluorescence was investigated by a confocal laser scanning microscope (LSM 510, Zeiss, Oberkochen, Germany) at an excitation wavelength of 543 nm (helium/neon1, red Cy3-immunofluorescence), and 488 nm (argon, yellow-green Cy2-immunofluorescence).

Materials

The following drugs and chemicals were used: anti-P2Y₁ receptor-subtype (epitope: peptide (C)RALI YKDLN NSPLR RKS, corresponding to residues 242–258 of rat or human P2Y₁; Alomone Labs, Jerusalem, Israel); mouse anti-nestin, rabbit anti-microtubuline associated protein-2, mouse anti-microtubuline associated protein-2 (MAP2, Chemicon, Temecula, CA); rabbit anti-GFAP (rabbit anti-cow GFAP, DakoCytomation, Glostrup, Denmark); secondary carbocyanine Cy2- and Cy3-conjugated IgGs (Jackson ImmunoResearch, West Grove, PA, USA); Dulbecco's modified Eagle's medium (DMEM), Hank's balanced salt solution (HBSS), neurobasal medium (NBM), gentamycin, trypsin (Life Technologies, Karlsruhe, Germany); DNase I (Roche Diagnostics, Mannheim, Germany); fetal calf serum (Seromed, Berlin, Germany); mouse anti-GFAP, adenosine 5'-triphosphate disodium salt (ATP), adenosine 5'-diphosphate sodium salt (ADP), cyclopiazonic acid, fura-2 acetoxymethyl ester (Fura-2/AM), glycine, L-glutamine, muscimol, *N*-methyl-D-aspartate (NMDA), poly-L-lysine, pyridoxal-5'-phosphate-6-azophenyl-2',4'-disulfonic acid (PPADS), tetrodotoxin (Sigma-Aldrich, Taufkirchen, Germany); N⁶-(2-methylthioethyl)-2-(3,3,3-trifluoropropylthio)-β,γ-dichloromethylene-ATP (AR-C69931MX; The Medicines Company, Waltham, MA); 1-[β-(3-(4-methoxyphenyl)propoxy)-4-methoxyphenethyl]-1H-imidazole hydrochloride (SKF 96365; Calbiochem-Merck, Schwalbach, Germany); 2'-deoxy-N⁶-methyladenosine 3',5'-bisphosphate tetraammonium (MRS 2179; Tocris-Biotrend, Cologne, Germany).

Stock solutions (10–100 mM) of drugs were prepared with distilled water or dimethylsulfoxide. Aliquots were stored at –20°C. Further dilutions were made daily with the appropriate bath solution.

Statistics

Mean ± SEM of *n* trials are shown, *n* being the number of single cells. Differences between means were tested for significance by the Normality test followed by the Student's *t*-test for single comparisons and by the Kruskal–Wallis ANOVA followed by a modified *t*-test (Bonferroni–Dunn or Holm–Sidak) for multiple comparisons. *P* < 0.05 was the accepted level of significance.

RESULTS

Cell selection

The cells used for the electrophysiological and Ca²⁺ imaging experiments were selected based on morphological criteria. Irrespective of whether grown in NBM or DMEM, neuronal cells in our striatal cultures could be easily identified. They were characterized by phase contrast-bright cell bodies and had developed long network-forming dendrite-like processes after 13–15 days in vitro (Figs. 1Aa,Ab; 5a). Glial cells, which appeared to be more prevalent in DMEM-cultures, in contrast, formed a confluent background layer of flat, phase contrast-dark cells with polygonal somata devoid of dendritic appendages (Figs. 1Aa,Ab; 5a).

Electrophysiology: characterization of cultured rat neostriatal neurons

Neither NBM- nor DMEM cells fired spontaneous action potentials during the period of membrane potential recording (usually 10–15 min). However, there were other significant differences when comparing the basic membrane properties between neurons cultured either in NBM or DMEM. NBM cells were smaller than DMEM cells as judged from their approximately one third lower membrane capacitance and their resting membrane potential was about 20 mV more depolarized (Table 1, left hand columns). Still more astonishing, NBM cells either failed to fire action potentials in response to depolarizing current injection (15 of 45 cells; Fig. 1Bc) or fired only one rather wide, low amplitude spike shortly after the onset of membrane depolarization (30 of 45 cells; Fig. 1Ba,Bd,Be, Table 1). No repetitive firing could be induced with supra-threshold current injections (Fig. 1Bd,Be), in some cases even when current strength up to 1 nA were applied. The rudimentary action potentials in NBM cells were followed by slow, low amplitude after-hyperpolarization (AHPs; Fig. 1Ba,Bd, Table 1). Hence, inadequate after-spike repolarization due to a lack of sufficient K⁺ conductance may have hindered repetitive firing in this type of neurons. Since, moreover, up to 80% of Na⁺ channels may rest in the inactivated state at the NBM cell resting potential of about –50 mV (Table 1, Fig. 2Bb), voltage-dependent Na⁺ channel inactivation was a possible reason for the observed inability to fire full-sized action potentials. This was, however not the case, because when the membrane potential was shifted to –80 mV by constant hyperpolarizing current injection, 6 NBM neurons still failed to fire properly (Fig. 1Be).

In contrast, all neurons grown in DMEM (*n* = 49) fired short, high amplitude action potentials with a marked overshoot, that were followed by fast and pronounced AHPs (Fig. 1Bb,Bf, Table 1). At threshold, a slowly developing ramp-like depolarization and long latency to spike discharge were evident (Fig. 1Bf, Table 1 right hand columns). It should be mentioned that this delayed transition to discharge, due to the slow inactivation of an A-type K⁺ current (I_{As}; Gabel and Nisenbaum, 1998), is commonly taken as a hallmark that distinguishes medium spiny neurons from other neurons in the dorsal (Kawaguchi, 1992; Kawaguchi, 1993), as well as ventral striatum (Belleau and Warren, 2000). Supra-threshold

TABLE 1. Comparison between the electrical properties of rat cultured neostriatal neurons grown in neurobasal medium (NBM) or Dulbecco's modified H Eagle's medium (DMEM)

	Cultured striatal neurons	
	NBM (<i>n</i> = 30–45) ^a	DMEM (<i>n</i> = 49)
Capacitance (pF)	5.9 ± 0.3	9.1 ± 0.8*
Resting potential (mV)	–52.8 ± 1.3	–70.1 ± 1.7*
Input resistance (MΩ)	799 ± 82	662 ± 67
Spike threshold (mV)	26.3 ± 1.9	30.5 ± 1.4
Spike latency (msec)	23.9 ± 6.9	192.3 ± 22.7*
Spike amplitude (mV)	28.8 ± 5.1	69.2 ± 2.4*
Spike duration (msec)	13.2 ± 2.2	2.2 ± 0.1*
AHP (mV)	–8.9 ± 1.6	–23.1 ± 1.3*
Time to peak of AHP (msec)	32.7 ± 5.6	20.0 ± 1.1*

Cell capacitance was measured by the inbuilt routine of the EPC-9 amplifier in the voltage-clamp mode. All other parameters were measured under current-clamp conditions (see Materials and Methods).

^aSpike and AHP parameters from cells firing rudimentary action potentials.

**P* < 0.05; statistically significant difference from rat neostriatal cells cultured in NBM. AHP, after-hyperpolarization.

stimuli induced repetitive firing without apparent spike frequency adaptation in these cells (Fig. 1Bf).

Next, we investigated possible reasons for the observed action potential failure in the NBM cells. Under voltage-clamp conditions, depolarizing voltage steps from a holding potential of -80 mV evoked fast inactivating inward currents in all NBM- and DMEM neurons (Fig. 2, $n=8$ each), that were blocked ($97.8 \pm 0.8\%$ inhibition; $n=16$) by TTX ($0.3 \mu\text{M}$), and, hence, were Na^+ currents. Na^+ currents activated around -50 mV, peaked between -10 and -5 mV and had a reversal potential (-63 ± 1 mV, $n=16$) close to the Na^+ equilibrium potential (-67 mV; Fig. 2Aa,Ab,Bb). However, Na^+ currents were considerably smaller in NBM cells than DMEM cells (Fig. 2Aa,Ab). Thus, peak current densities measured at, for example, -10 mV were -74.8 ± 17.9 and -213.5 ± 21.4 pA/pF ($P < 0.05$) in the NBM- and DMEM neurons, respectively. Hence, an approximately three-fold smaller population of Na^+ -channels available per unit of membrane surface area in the former cells was most probably responsible for their inability to fire fully developed spikes. This is all the more likely, because all other Na^+ channel parameters measured did not differ significantly between the two cell types. Sodium conductance was half-activated (V_{50}) at -28.8 ± 1.9 and -27.6 ± 1.5 mV with slope factors (k_m) of 7.2 ± 0.6 and 7.1 ± 0.4 mV per e-fold change in conductance in NBM- and DMEM cells, respectively (Fig. 2Aa,Bb). V_{50} and k_m values for voltage-dependent inactivation were -58.3 ± 1.1 and 6.0 ± 0.5 mV in NBM neurons and -59.9 ± 2.1 and 5.9 ± 0.5 mV in neurons grown in DMEM (Fig. 2Ba,Bb). The fast recovery from voltage-dependent inactivation, eventually, was best

fitted by the sum of two exponential functions with two time constants τ_1 and τ_2 (Fig. 2Ca,Cb; NBM: $\tau_1 = 7.8 \pm 1.1$ msec, $\tau_2 = 192.8 \pm 34.7$ msec; DMEM: $\tau_1 = 8.5 \pm 1.0$ msec, $\tau_2 = 196.9 \pm 23.7$ msec). The fast time constant contributed with $79.5 \pm 4.8\%$ and $74.9 \pm 4.8\%$ to the recovery process in NBM- and DMEM cells, respectively. Remarkably, these parameters were all very similar to those obtained in a variety of other neurons, including, for example, acutely isolated hippocampal neurons (Remy et al., 2004) or acutely dissociated cholinergic striatal interneurons (Maurice et al., 2004).

Electrophysiology: P2X receptors

After the electrophysiological characterization of neurons under current-clamp conditions had been accomplished, currents induced by pressure application of the P2X receptor agonist ATP (30 – $300 \mu\text{M}$), the ionotropic glutamate receptor agonist NMDA ($100 \mu\text{M}$), the GABA_A receptor agonist muscimol ($30 \mu\text{M}$) and bath solution with no added receptor agonists were measured under voltage-clamp at the holding potential of -80 mV in a proportion of the same set of cells. It should be mentioned that reported half-maximal effective concentrations (EC_{50}) of ATP were 1 – $100 \mu\text{M}$ at recombinant P2X_{1–7} receptors (Khakh et al., 2001). Hence, the ATP concentration range used in the present study appeared to be appropriate for the detection of P2X receptor-mediated currents.

Responses of a representative NBM cell and a representative DMEM cell are shown in Figure 3a,b, respectively. The statistical evaluation of a greater number of NBM- and DMEM cells is given in Figure 3c. Pressure application of bath solution without added

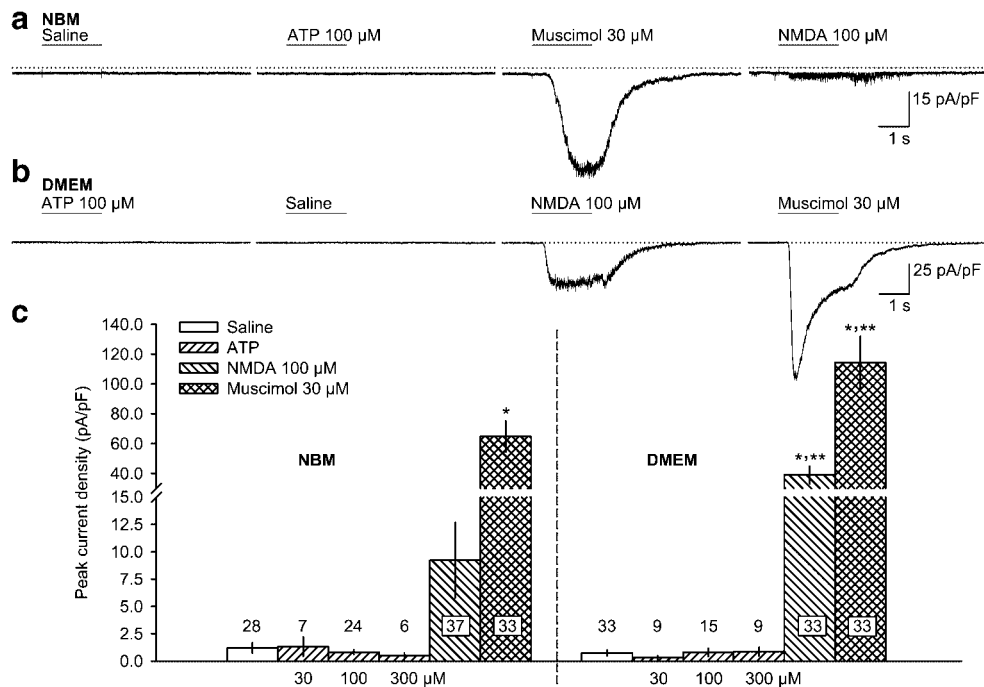


Fig. 3. Agonist-induced transmembrane currents in rat striatal neurons cultured in either NBM (a, c) or DMEM (b, c). a, b: Transmembrane currents in response to pressure application of bath solution (saline), the P2X receptor agonist ATP ($100 \mu\text{M}$), the GABA_A receptor agonist muscimol ($30 \mu\text{M}$) and the ionotropic glutamate receptor agonist NMDA ($100 \mu\text{M}$) in the same NBM- (a) and DMEM neurons (b) from which current clamp-recordings are shown in Figure 1Bd and f, respectively. Agonists were subsequently applied for 2 sec each. Single challenges with the agonist were separated by 2 min superfusion periods with drug-free bath solution. The holding

potential was -80 mV. The dotted lines indicate the zero current levels and the horizontal bars above the current traces indicate the times of agonist application. c: Statistical evaluation of the data derived from similar experiments (ATP was also used at concentrations of 30 and $300 \mu\text{M}$) as illustrated in NBM neurons (left) and DMEM neurons (right). The numbers above or within the bars indicate the number of cells challenged by the individual agonists. * $P < 0.05$, significant differences from the effects of bath solution alone (saline) and ** $P < 0.05$, significant differences between the effects of agonist in NBM neurons and DMEM neurons, respectively.

receptor agonists evoked only small current responses in neurons cultured in NBM (Fig. 3a,c) or DMEM (Fig. 3b,c). ATP, at all concentrations used (30–300 μM), also elicited only tiny currents in NBM- (Fig. 3a,c) and DMEM cells (Fig. 3b,c), which were, however, not significantly different from the currents evoked by bath solution alone (Fig. 3c). In contrast to that, the GABA_A receptor agonist muscimol (30 μM) evoked marked inward currents in both types of neurons (Fig. 3a–c). However, it was obvious that the GABA_A receptor-mediated responses were approximately two-fold smaller in the former cells (Fig. 3c). NMDA (100 μM), eventually, also elicited inward currents in neurons cultured in DMEM (Fig. 3b,c). In NBM cells, on the other hand, current responses to NMDA were only small and did, in the end, not differ significantly from the effects of bath solution alone (Fig. 3a,c).

The failure to detect P2X receptors in these experiments was most likely not caused by shortcomings in the experimental techniques used. That is because we had in previous work no problems to demonstrate, by means of very similar methods, the existence of P2X receptor-mediated currents in cultured neurons (e.g., dorsal root ganglion cells; Gerevich et al., 2004), as well as neurons contained in brain slices (e.g., locus coeruleus neurons; Scheibler et al., 2004). Taken together, these data clearly indicate that functional soma-dendritic P2X receptors were absent from rat cultured neostriatal neurons, irrespective of whether they were cultured in NBM or DMEM (for rat brain slices see Scheibler et al., 2004).

Ca^{2+} imaging: characterization of cultured rat striatal neurons and glial cells

The fluorescence ratios (340/380 nm) were used to provide a relative measure of the cytosolic free Ca^{2+} concentration in striatal neurons and glial cells (Fig. 4a). Both types of cells were chosen in approximately equal number from each culture dish for measurements. When concentration-response curves for ATP (0.1–100 μM) were determined at neurons ($E_{\text{max}} = 0.50 \pm 0.01$; Hill coefficient = 1.03 ± 0.08 ; $\text{EC}_{50} = 1.4 \pm 0.1 \mu\text{M}$; degrees of freedom = 5) and glial cells ($E_{\text{max}} = 0.42 \pm 0.04$; Hill coefficient = 1.57 ± 0.46 ; $\text{EC}_{50} = 3.6 \pm 0.8 \mu\text{M}$; degrees of freedom = 5) grown in NBM, similar curves were obtained (Fig. 4c). The $[\text{Ca}^{2+}]_i$ transients of a striatal neuron in response to increasing concentrations of ATP are shown in Figure 4b. The Hill coefficients of near unity indicated the binding of one molecule of ATP to its receptor both for neurons and glial cells.

In the following experiments, a high K^+ (50 mM)-medium was used to discriminate neurons from glial cells. Since neurons, but not glial cells possess a high density of voltage-sensitive Ca^{2+} channels in their cell membrane (Verkhatsky and Steinhäuser, 2000), depolarization by an elevation of the external K^+ concentration is expected to trigger the entry of Ca^{2+} into the intracellular space of this cell-type only. In fact, neurons cultivated in NBM, reacted with a clear increase of $[\text{Ca}^{2+}]_i$ to a high K^+ (50 mM) stimulus (e.g., Fig. 5Aa; 0.46 ± 0.05 , $n = 58$), whereas glial cells cultivated under the same conditions failed to respond to 50 mM K^+ (e.g., Fig. 5Ba; 0.03 ± 0.01 , $n = 44$). At the same time ATP (30 μM) caused both in neurons (e.g., Fig. 5Aa; 0.63 ± 0.05 , $n = 58$) and glial cells (Fig. 5Ba; 0.58 ± 0.04 , $n = 44$) a comparable increase of $[\text{Ca}^{2+}]_i$. Moreover, neurons (0.36 ± 0.05 , $n = 16$) and glial cells (0.04 ± 0.01 , $n = 16$) cultured in DMEM instead of NBM, could also be differentiated by the presence and absence of K^+

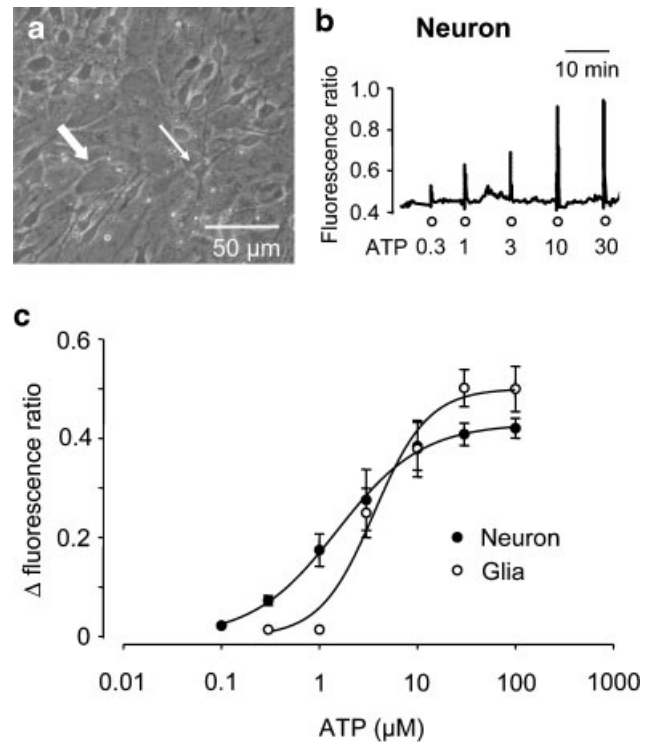


Fig. 4. ATP-induced increases of intracellular Ca^{2+} in rat striatal neurons and glial cells grown in NBM. Tissue cultures were loaded with the fluorescent indicator Fura-2. The then determined fluorescence ratio (340/380 nm) provides a relative measure of the cytosolic free Ca^{2+} concentration. ATP was applied for 10 sec each time. **a**: Microphotograph of a cell culture under phase contrast optics. Thick arrow, typical glial cell; thin arrow, typical neuron. **b**: Original tracing showing $[\text{Ca}^{2+}]_i$ transients of a neurons in response to increasing concentrations of ATP. **c**: Concentration-response relationship for ATP (0.1–100 μM) established in experiments similar to those shown in **b**. ATP was slightly more potent in neurons than in glial cells; both cell-types were selected for measurements in the same culture dish. Mean \pm SEM of 17–50 cells.

(50 mM)-induced $[\text{Ca}^{2+}]_i$ transients, respectively. Under these conditions, however, ATP (30 μM) acted only in glial cells (0.45 ± 0.05 , $n = 16$), but not in neurons (0.05 ± 0.01 , $n = 16$). Hence, DMEM appeared to promote the appearance of a more mature and ATP-insensitive neuronal phenotype capable of firing full action potentials.

In agreement with our assumption, the neuronal $[\text{Ca}^{2+}]_i$ transients induced by K^+ (50 mM) application was absolutely dependent on external Ca^{2+} . Superfusion with high K^+ caused reproducible $[\text{Ca}^{2+}]_i$ transients on repetitive application ($3.5 \pm 3.7\%$ decrease from T_1 to T_2 ; $n = 12$; $P > 0.05$). In contrast, a Ca^{2+} -free solution applied 4 min before and during T_2 almost abolished the high K^+ -evoked increase of intracellular Ca^{2+} ($98.2 \pm 0.6\%$ decrease from T_1 to T_2 ; $n = 8$; $P < 0.05$).

Ca^{2+} imaging: P2Y receptors

P2X receptors are ligand-gated cationic channels whose activation leads to the entry of Ca^{2+} from the extracellular space into the cell interior (Ralevic and Burnstock, 1998). In contrast, P2Y receptors are coupled to G proteins; stimulation of the $\text{G}_{q/11}$ -linked $\text{P2Y}_{1,2,4,6}$ receptors causes the release of Ca^{2+} from intracellular pools (Illes and Riebeiro, 2004). Since the previous patch-clamp measurements excluded the participation of P2X receptors at striatal neurons, we searched for

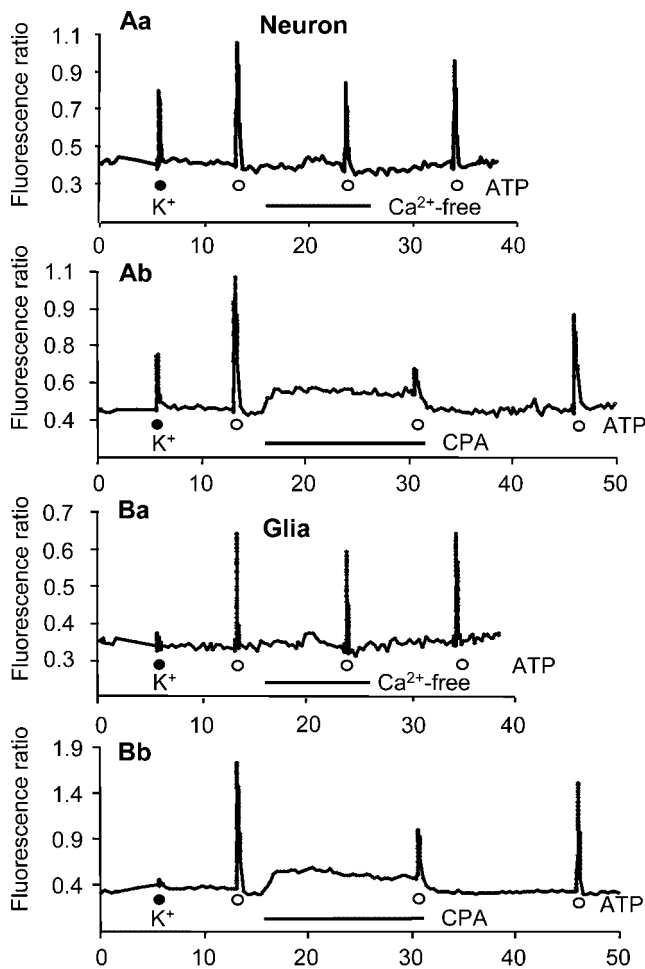


Fig. 5. ATP-induced increases of intracellular Ca^{2+} in rat striatal neurons and glial cells grown in NBM. Original tracings showing $[\text{Ca}^{2+}]_i$ transients of these cells in response to a submaximal concentration of ATP ($30 \mu\text{M}$). Only neurons, but not glial cells reacted with an increase of $[\text{Ca}^{2+}]_i$ to the application of a high K^+ (50 mM)-medium for 3 sec. **A:** Striatal neurons. Depression of the effect of ATP in a Ca^{2+} -deficient medium (**a**) and in the presence of cyclopiazonic acid (CPA; $10 \mu\text{M}$; **b**). Representative cells out of a total number of 58 (**a**) and 23 (**b**), respectively. **B:** Striatal glial cells. Depression of the effect of ATP in a Ca^{2+} -deficient medium (**a**) and in the presence of CPA ($10 \mu\text{M}$; **b**). Representative cells out of a total number of 23 (**a**) and 31 (**b**), respectively. Horizontal bars indicate superfusion with a Ca^{2+} -free or CPA-containing medium. After returning to a normal superfusion medium, there was a partial recovery of the $[\text{Ca}^{2+}]_i$ increases caused by ATP.

P2Y receptors by Ca^{2+} imaging techniques. We investigated in NBM neurons at first, whether in a Ca^{2+} -free medium the ability of ATP ($30 \mu\text{M}$) to increase $[\text{Ca}^{2+}]_i$ is inhibited (Figs. 5Aa,Ba; 7A,B). As a prerequisite for a feasible protocol, the $[\text{Ca}^{2+}]_i$ transients in response to consecutive ATP applications in the absence of any drug or experimental manipulation were considerably stable, that is, they did not change from the first to the second superfusion with ATP (Fig. 7A,B). However, under Ca^{2+} -free conditions, the effect of ATP ($30 \mu\text{M}$) was both in neurons and glial cells decreased, suggesting extracellular Ca^{2+} as a partial source of the ATP-induced $[\text{Ca}^{2+}]_i$ transients. However, the residual increase of $[\text{Ca}^{2+}]_i$ by ATP appears to be due to the release of Ca^{2+} from intracellular storage sites, especially since cyclopiazonic acid (CPA; $30 \mu\text{M}$) known to deplete such sites also markedly inhibited the response to ATP both in neurons and glial cells (Figs. 5Ab,Bb; 8A,B). Whereas a

Ca^{2+} -free medium did not considerably alter the basal level of $[\text{Ca}^{2+}]_i$, CPA elicited a slowly developing and long-lasting increase due to the blockade of Ca^{2+} uptake into the endoplasmic reticulum and the subsequent protracted depletion of Ca^{2+} stores (Plenge-Tellechea et al., 1997). The change of the ATP effect by both a Ca^{2+} -free medium and CPA was partially reversible on washout (Fig. 5).

The following experiments were designed to identify the P2Y receptor-type involved in the release of intracellular Ca^{2+} . The $\text{G}_{q/11}$ -coupled P2Y₁ receptor reacts to the agonists ATP/ADP, whereas P2Y_{2,4,6} receptors sharing their transduction pathways with P2Y₁, are sensitive to ATP/UTP or UDP (Illes and Riebeiro, 2004). In the present study, ADP ($10 \mu\text{M}$) had at T₁ an unequivocal agonistic action both in NBM neurons (0.35 ± 0.07 , $n = 46$) and glial cells (0.32 ± 0.03 , $n = 45$). In addition, the selective P2Y₁ receptor antagonist MRS 2179 ($30 \mu\text{M}$) markedly depressed the effect of ADP in neurons and glial cells from T₁ to T₂, by $91.43 \pm 1.3\%$ ($n = 46$; $P < 0.05$) and $94.3 \pm 0.9\%$ ($n = 45$; $P < 0.05$), respectively (Fig. 6c). MRS 2179 ($30 \mu\text{M}$) also decreased the ATP ($30 \mu\text{M}$)-induced $[\text{Ca}^{2+}]_i$ transients (Figs. 6a; 8A,B). Moreover, the mixed P2X/P2Y receptor antagonist PPADS, having some preference for the P2Y₁ receptor-type, almost abolished the effect of ATP at $30 \mu\text{M}$, whereas the P2Y_{12,13} receptor selective antagonist AR-C69931MX ($3 \mu\text{M}$) only slightly depressed it (Figs. 6b; 8A,B).

Ca^{2+} imaging: entry pathway for Ca^{2+} from the extracellular space

There was no apparent explanation for the question, why a Ca^{2+} -free extracellular medium considerably decreased the ATP-induced $[\text{Ca}^{2+}]_i$ transients both in neurons and glial cells, and CPA only partially inhibited these transients, although patch-clamp measurements failed to prove the existence of Ca^{2+} permeable P2X receptors at the plasma membrane. In order to prove or disprove the hypothesis that the depletion of intracellular Ca^{2+} pools by ATP may initiate the opening of store-operated Ca^{2+} channels (SOCs) allowing the entry of Ca^{2+} , we applied CPA, known to deplete the Ca^{2+} storage sites. CPA ($30 \mu\text{M}$) caused slightly rising $[\text{Ca}^{2+}]_i$ transients, when determined by the data under the curve (DUC) method (to $112.1 \pm 4.4\%$ of T₁ at T₂, $n = 8$; $P < 0.05$). However, the omission of Ca^{2+} from the superfusion medium markedly decreased the effect of CPA ($30 \mu\text{M}$) (to $41.0 \pm 5.8\%$ of T₁ at T₂, $n = 19$; $P < 0.05$). The representative tracings shown in Figure 8a and b document that CPA caused an early upraise of $[\text{Ca}^{2+}]_i$ followed by a late protracted phase, the former probably due to the release of intracellular Ca^{2+} and the latter to the influx of Ca^{2+} via SOC. This hypothesis is corroborated by the fact that the percentage decrease of the response to CPA observed in a Ca^{2+} -free medium (see the above DUC data) is caused by a marked shortening of the duration rather than the amplitude of this response (Fig. 8a,b). In addition, a reapplication of the Ca^{2+} -containing normal superfusion medium after terminating the application of CPA, resulted in a large $[\text{Ca}^{2+}]_i$ transient. The reason for this may be a decrease of the entry of Ca^{2+} followed by its overshooting recovery in the absence and presence of external Ca^{2+} , respectively. If the $[\text{Ca}^{2+}]_i$ response to CPA were shortened because of a massive depletion of $[\text{Ca}^{2+}]_i$ rather than a blockade of SOC, a much slower recovery due to the protracted replenishment of intracellular Ca^{2+} stores would be expected to occur. In further

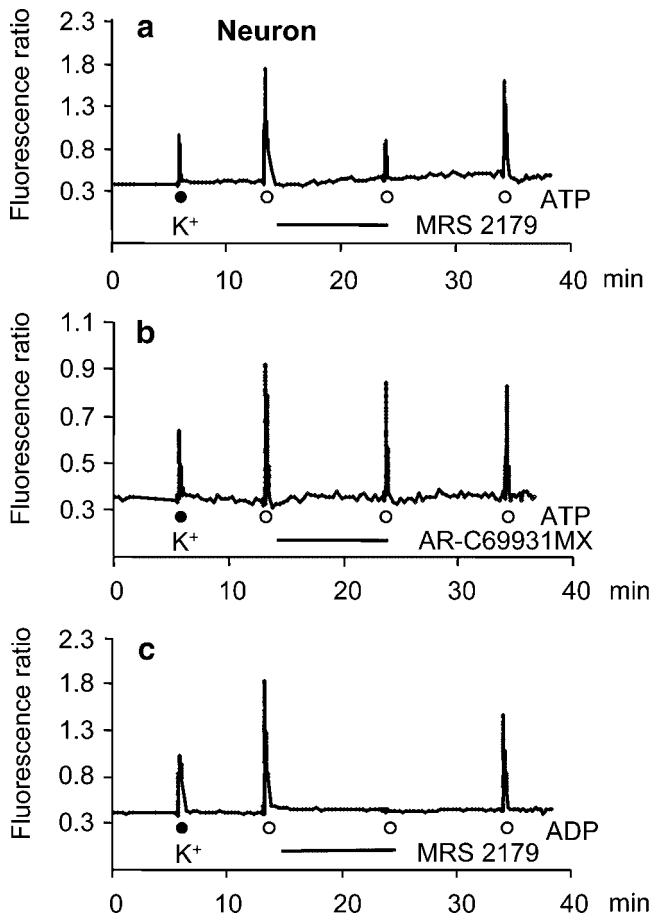


Fig. 6. ATP- and ADP-induced increases of intracellular Ca^{2+} in rat striatal neurons grown in NBM. Original tracings showing $[Ca^{2+}]_i$ transients of neurons in response to a submaximal concentration of ATP (30 μ M) or ADP (10 μ M). Only neurons, but not glial cells reacted with an increase of $[Ca^{2+}]_i$ to a high K^+ (50 mM)-medium. **a**: Marked depression of the effect of ATP in the presence of MRS 2179 (30 μ M). **b**: Slight depression of the effect of ATP in the presence of AR-C69931MX (3 μ M). **c**: Marked depression of the effect of ADP in the presence of MRS 2179 (30 μ M). Horizontal bars indicate superfusion with a medium containing P2 receptor antagonists. Representative cells out of a total number of 53 (**a**), 24 (**b**) and 46 (**c**). After returning to the normal superfusion medium, there was a partial recovery of the $[Ca^{2+}]_i$ increases caused by ATP.

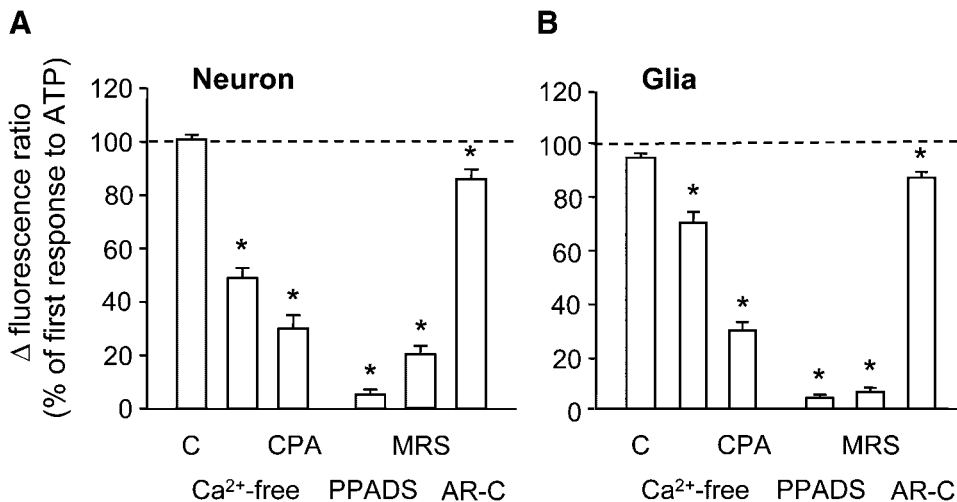


Fig. 7. Inhibition of ATP-induced increases of intracellular Ca^{2+} in striatal neurons and glial cells grown in NBM. Mean \pm SEM of 12–59 cells from experiments similar to those shown in Figures 5 and 6. Hence, ATP (30 μ M) was applied for the first time (T_1 ; control, C) in a normal medium and for the second time (T_2) in a Ca^{2+} -free medium or

support of the assumption that SOCs are involved in the late effect of CPA, SKF96365 (50 μ M) a blocker of this channel type (Jan et al., 1999), imitated the action of a Ca^{2+} -free medium (Fig. 8c; to $76.7 \pm 4.9\%$ of T_1 at T_2 by the DUC method, $n = 14$, $P < 0.05$).

Finally, we asked ourselves, whether the failure of ATP to increase $[Ca^{2+}]_i$ in DMEM neurons was due to the lack of P2Y₁ receptors or the lack of an intracellular Ca^{2+} pool comparable to that present in NBM neurons. For this purpose, CPA (30 μ M) was superfused onto DMEM cells, which were identified by their $[Ca^{2+}]_i$ response to high K^+ (50 mM) as neurons; CPA was found to cause a reproducible increase of intracellular Ca^{2+} under these conditions ($n = 11$; not shown). Hence, only NBM-, in contrast to DMEM neurons, may be endowed with functional P2Y₁ receptors.

It is concluded that striatal neurons and glial cells cultivated in NBM possess P2Y₁ receptors, which lead to the release of intracellular Ca^{2+} probably followed by the activation of SOCs in the plasma membrane of these cell-types. Functional P2X receptors are absent both at neurons and glial cells.

Immunocytochemistry: localization of P2Y receptors

Double immunofluorescence labeling in combination with confocal laser scanning microscopy indicated the co-localization of immunoreactivity (IR) for the P2Y₁ receptor subtype both with the neuronal marker MAP2 and the glial marker GFAP (Fig. 9A,B). The co-localization of nestin-IR (a marker of neuronal progenitor cells; Scemes et al., 2003), with P2Y₁ receptor-IR on cells of both neuronal (thin arrow) and glial morphology (thick arrow) is documented in Figure 9Ca–c. Although many cells exhibited either nestin- or MAP2-IR (Fig. 9D), a co-localization of the two markers was only rarely observed (not shown). However, a large number of cells was double-labeled for nestin- and GFAP-IR (Fig. 9E).

DISCUSSION

Our neuronally enriched striatal cell cultures are expected to consist of the derivatives of the major neostriatal neuronal population, the GABAergic medium-spiny projection neurons (Kawaguchi et al., 1995). It is

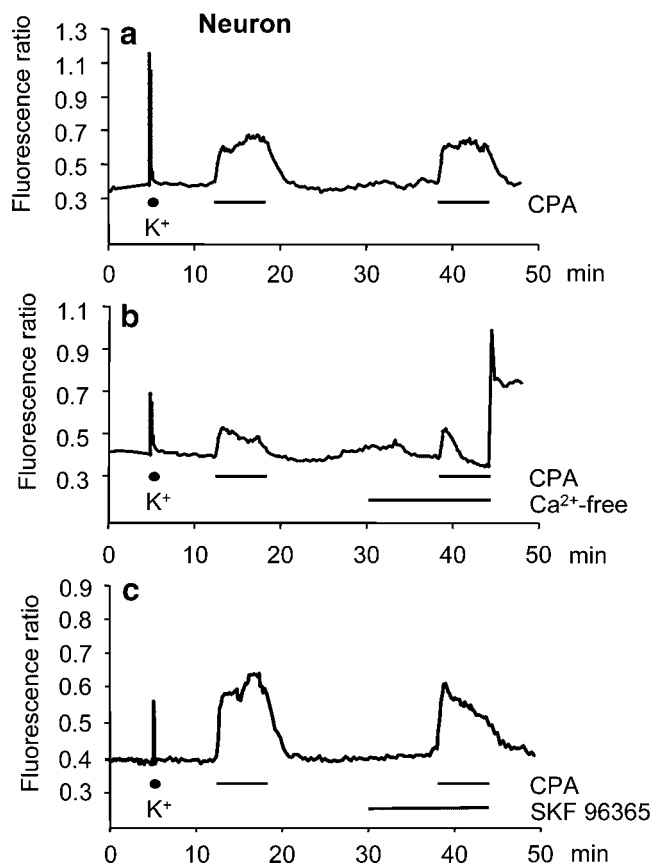


Fig. 8. Cyclopiazonic acid (CPA)-induced increases of intracellular Ca^{2+} in rat striatal neurons grown in NBM. Original tracings showing $[\text{Ca}^{2+}]_i$ transients of neurons in response to CPA ($10 \mu\text{M}$). Only neurons, but not glial cells reacted with an increase of $[\text{Ca}^{2+}]_i$ to a high K^+ (50 mM)-medium. CPA ($10 \mu\text{M}$) was applied twice (T_1 , T_2) for the period indicated by the horizontal bars. **a:** Reproducible $[\text{Ca}^{2+}]_i$ transients in response to CPA. **b:** Decrease of the duration, but not the amplitude of the CPA-induced $[\text{Ca}^{2+}]_i$ transients in a Ca^{2+} -free medium. The reapplication of a normal Ca^{2+} -containing medium evoked a large increase of $[\text{Ca}^{2+}]_i$, suggesting replenishment of the Ca^{2+} pools by a marked influx of Ca^{2+} , probably via store-operated channels (SOCs) of the plasma membrane. **c:** SKF 96365 ($50 \mu\text{M}$) imitated the effect of a Ca^{2+} -free medium. Representative cells out of a total number of 8 (**a**), 19 (**b**) and 14 (**c**).

well known that these neurons undergo profound changes from birth until the end of the third to fourth postnatal week, including the development of densely packed dendritic spines, as well as changes in electrophysiological properties (Misgeld et al., 1986; Tepper et al., 1998; Belleau and Warren, 2000). A progressive decrease in input resistance and a progressively more hyperpolarized membrane potential was paralleled by the concomitant expression of inwardly-rectifying K^+ channels, which were not present in medium spiny neurons in the striatum of neonatal rats (Tepper et al., 1998; Belleau and Warren, 2000).

NBM cells, when compared to DMEM cells, displayed a much lower density of voltage-dependent Na^+ -channels, a feature most probably responsible for their inability to generate either action potentials at all, or repetitive spiking with short and overshooting action potentials. It has previously been described that action potential height and duration reached adult levels in medium spiny neurons from rat striatum at the earliest with the second to third week of postnatal development (Tepper et al., 1998; Belleau and Warren, 2000). NBM cells,

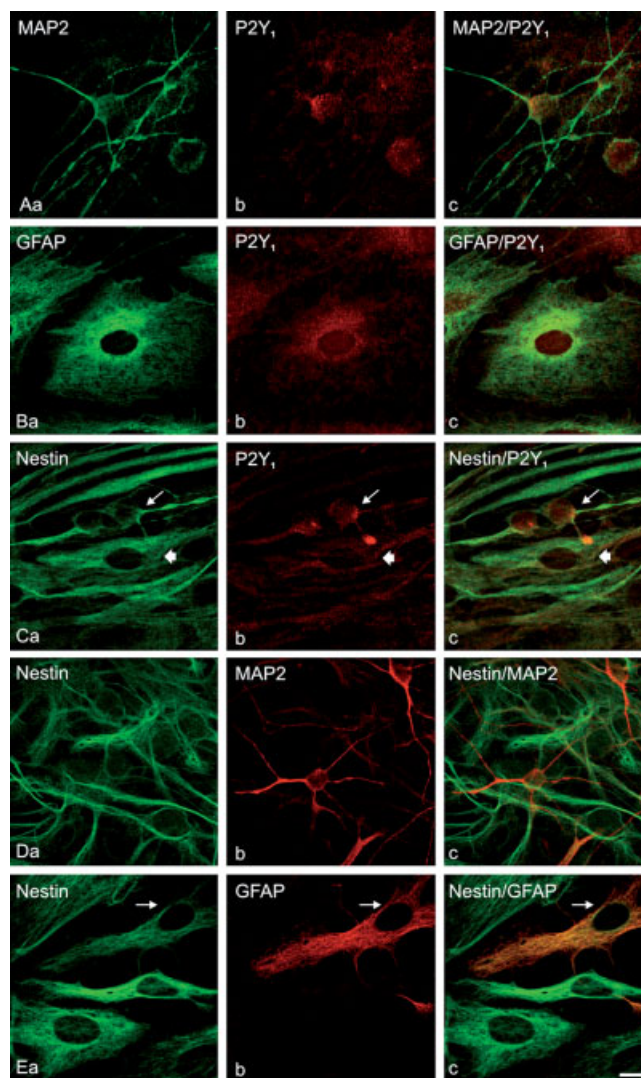


Fig. 9. Confocal images of double-immunofluorescence labeling of neurons (MAP2-positive) and glial cells (GFAP-positive) in striatal cultures of the rat with nestin- and P2Y₁ receptor-immunoreactivity (IR). **A, B:** The P2Y₁ receptor subtype is co-localized with MAP2 (**A**) and GFAP (**B**). **C:** Double-labelling for nestin- and P2Y₁ receptor-IR indicate co-localization on neuron-like structures (thin arrow) and glial cells (thick arrow). **D:** Examples of nestin- and MAP2-positive cells, without co-localization on the same cell. **E:** Expression of GFAP on nestin-immunopositive cells. Example of a clear co-expression is indicated by the thin arrow, whereas examples of nestin-labeling without GFAP-IR were also found. (Scale bar: **A–E** = $10 \mu\text{m}$).

when compared to DMEM cells, also displayed much lower densities of ligand-gated ion channels, GABA_A receptors and particularly NMDA receptors, and, it is well known that NMDA receptor activity in striatal medium spiny neurons reaches adult levels not until the end of the second week of postnatal life (Hurst et al., 2001). Taken together, our data may, hence, suggest that DMEM- and especially NBM-grown neurons represent a more or less juvenile type of striatal neurons, most probably precursors of the adult medium spiny cell-type.

Whereas P2X receptor-mediated ion fluxes in neurons and astrocytes occur within milliseconds, the P2Y receptor-mediated release of $[\text{Ca}^{2+}]_i$ requires a few seconds to fully develop (Illes et al., 2000). In addition to these short-term effects, partly as a consequence of

the stimulation of Ca^{2+} -dependent enzymatic activities, P2Y receptors may stimulate mitogen-activated protein kinases (MAPK), tyrosine kinase, and serine-threonine kinase AKT (von Kügelgen and Wetter, 2000). Classic members of the MAPK family, like extracellular signal-regulated kinases (ERKs), are implicated in cell growth, as well as differentiation, whereas stress-activated protein kinases (SAPKs) and p38 appear to play a role in regulating the cell death machinery; phosphoinositide 3-kinase (PI3K)/AKT pathways are associated with cell proliferation and differentiation (Neary et al., 1996; Franke and Illes, 2006). In fact, P2 (mainly P2Y) receptors have been shown to exert trophic effects on neurons, leading to the induction of neurite outgrowth alone or in interaction with receptors for other growth factors (nerve growth factor, epidermal growth factor; Huang and Kao, 1996; Heine et al., 2006). Similarly, extracellular ATP can act in combination with growth factors to stimulate astrocyte proliferation and contribute to the process of reactive gliosis, a hypertrophic/hyperplastic reaction that is frequently seen in brain trauma, stroke/ischemia and various neurodegenerative disorders (Franke and Illes, 2006).

An interesting long-term effect of ATP relates to the proliferation of neuronal (Ryu et al., 2003) and glial (Agresti et al., 2005) progenitor cells in the CNS. Apparently, functional P2 receptors and the ATP hydrolyzing enzyme NTPDase 2 are co-expressed at neuronal progenitor cells in the murine hippocampus (Braun et al., 2003; Shukla et al., 2005). Further, the migration pattern, but not cell differentiation of neuronal progenitor cells during early CNS development was regulated by P2Y₁ receptors (Scemes et al., 2003). The first step initiating these effects was believed to be an increase of $[\text{Ca}^{2+}]_i$.

Our conclusion derived from the electrophysiological part of this study that striatal neurons grown in NBM exhibit an immature, probably embryonic phenotype, was corroborated by the finding that only NBM- but not DMEM neurons exhibited $[\text{Ca}^{2+}]_i$ transients in response to ATP. It has been reported that certain P2Y receptor-types are transiently expressed in developmental structures that do not have a correlate in the adult animal (Cheung et al., 2003). However, striatal glial cells reacted with $[\text{Ca}^{2+}]_i$ transients to ATP, irrespective of whether they were cultivated in NBM or DMEM. It is noteworthy that radial glia and various precursor cells of parenchymal glia are regarded as neuronal progenitor cells, which share numerous morphological and functional properties with astrocytes (Goldman, 2003; Kempermann et al., 2004). Further, in neurons and glial cells, the concentration-response curves for ATP with respect to its ability to increase intracellular Ca^{2+} , were similar. Hence, all further experiments were made on neurons grown in NBM, in comparison with the respective glial population.

After having established that ATP causes an increase of $[\text{Ca}^{2+}]_i$ in NBM neurons, we attempted to identify the P2 receptor-type(s) involved. Since both a Ca^{2+} -free external medium and the depletion of intracellular Ca^{2+} stores by CPA decreased, but did not abolish the ATP-induced increase of $[\text{Ca}^{2+}]_i$, we concluded that the entry of Ca^{2+} from the extracellular space and its release from intracellular pools equally contribute to the ATP effect. P2Y receptor occupation and the subsequent $G_{q/11}$ -mediated activation of phospholipase C generate increased levels of inositol 1,4,5-trisphosphate (IP_3), which releases Ca^{2+} from the endoplasmic reticulum. The subtype of P2Y receptor involved was characterized

by its sensitivity to ATP and ADP, as well as by its occupation by the antagonistic PPADS (P2X/P2Y) and MRS 2179 (P2Y₁), but not AR-C699931MX (P2Y_{12,13}), bringing out the participation of the P2Y₁ subtype (von Kügelgen, 2006).

As far as the influx of Ca^{2+} into the cells is concerned, the idea of P2X receptor-channels as Ca^{2+} entry pathways had, at least in neurons, to be abandoned, based on the failure of electrophysiological experiments to document an inward current in response to ATP. The most likely possibility is that the depletion of the Ca^{2+} storage sites by P2Y₁ receptor activation signals to the cell membrane and thereby opens store-operated Ca^{2+} channels thought to refill the depleted stores. These channels are found in many non-excitabile cell types where SOCs are the major mechanism of regulated Ca^{2+} entry (Parekh and Putney, 2005). However, SOCs are also present in some neurons and glial cells from the peripheral and central nervous system (Rzagalinski et al., 1999; Emptage et al., 2001; Bouron et al., 2005). G protein-coupled receptors were described to mediate the activation of SOCs that belong to the transient receptor potential (TRP) family (e.g., Moran et al., 2004), and, with respect to P2Y receptors, such mechanisms have already been demonstrated, for example, for members of the canonical TRP (TRPC) subfamily (TRPC4, TRPC5, TRPC1/TRPC5 heteromers; Schaefer et al., 2000; Strübing et al., 2001). It is noteworthy that an increase of $[\text{Ca}^{2+}]_i$ by IP_3 secretion following phospholipase C activation may lead, because of Ca^{2+} store depletion, to SOC opening, however, alternative mechanisms of Ca^{2+} entry from the extracellular space may also be operational, such as the activation of non-selective cationic channels (Zhu et al., 1998) or second messenger-operated channels (Parekh and Putney, 2005).

Eventually the question arises which purpose this P2Y₁ receptor-mediated Ca^{2+} signaling in the immature NBM cells may serve. One may speculate that P2Y₁ receptors are probably essential for some important functional properties of neuronal progenitor cells in the rat striatum. In fact, P2Y₁ receptors were found in human (NT2 cell line; Moore et al., 2002), mice (striatal neuronal progenitor cells from E14 mice; Scemes et al., 2003) and rat neuronal progenitor cells (radial glia from E14–E18 cortex; Weissman et al., 2004), where they were essential for proliferation and migration (Scemes et al., 2003; Weissman et al., 2004). In the present study, immunocytochemical staining indicated the existence of P2Y₁ receptors both at neurons (stained for MAP2; Izant et al., 1980) and glial cells (stained for GFAP). A co-staining for P2Y₁ receptors and nestin as a marker of neuronal progenitor cells could be preferentially demonstrated at cells with glial morphology. Hence, NBM cells identified morphologically as neuron-like (small cell body and branching processes) usually did not stain for nestin, and thereby probably represent a developmental stage between that of progenitor cells and mature neurons.

In the culture systems investigated, P2Y receptor-activation by the outflow of endogenous nucleotides is unlikely, because the investigated cells were continuously superfused with extracellular medium flushing away the released ATP. However, under in vivo conditions, striatal ATP may be released from both neuronal and non-neuronal cells. The first mechanism of action is the exocytotic secretion of ATP, for example, as a co-transmitter of noradrenaline (Poelchen et al., 2001) and GABA (Jo and Schlichter, 1999). In addition,

stimulation of astrocytes by pharmacological means as well as by mechanical or osmotic stimulation may release ATP by four alternative mechanisms. Firstly, by an exocytotic vesicular release (Coco et al., 2003); secondly, by ATP-binding cassette (ABC) proteins such as the multidrug resistance-associated protein (Ballerini et al., 2002); thirdly, by connexin hemichannels providing the substrate for gap junction formation (Cotrina et al., 2000); and finally, by osmolytic transporters linked to anion channels (Darby et al., 2003). In view of the similarities between astrocytes and neuronal stem cells, ATP may be secreted by any of the above mechanisms to act at the progenitor cells themselves.

ACKNOWLEDGMENTS

Helpful discussions with Dr. W. Fischer concerning store-operated Ca^{2+} channels and expert technical assistance of Mrs. H. Sobottka in preparing cell cultures as well as that of Mrs. M. Hentschke in supporting immunocytochemistry are acknowledged. We thank to Dr. J. Teichert (Department of Clinical Pharmacology, University of Leipzig, Germany) for help with the TopFit software and Dr. J. Prats (The Medicines Company, Waltham, MA, USA) for the gift of AR-C69931MX. Dr. Z. Gerevich was a recipient of a Marie-Curie Developmental Fellowship sponsored by the European Community.

LITERATURE CITED

- Agresti C, Meomartini ME, Amadio S, Ambrosini E, Serafini B, Franchini L, Volonte C, Aloisi F, Visentin S. 2005. Metabotropic P2 receptor activation regulates oligodendrocyte progenitor migration and development. *Glia* 50(2): 132–144.
- Ballerini P, Di Iorio P, Ciccarelli R, Nargi E, D'Alimonte I, Traversa U, Rathbone MP, Caciagli F. 2002. Glial cells express multiple ATP binding cassette proteins which are involved in ATP release. *Neuroreport* 13(14):1789–1792.
- Belleau ML, Warren RA. 2000. Postnatal development of electrophysiological properties of nucleus accumbens neurons. *J Neurophysiol* 84(5):2204–2216.
- Bouron A, Altafaj X, Boisseau S, De Waard M. 2005. A store-operated Ca^{2+} influx activated in response to the depletion of thapsigargin-sensitive Ca^{2+} stores is developmentally regulated in embryonic cortical neurons from mice. *Dev Brain Res* 159(1):64–71.
- Braun N, Sevigny J, Mishra SK, Robson SC, Brath SW, Gerstberger R, Hammer K, Zimmermann H. 2003. Expression of the ecto-ATPase NTPDase2 in the germinal zones of the developing and adult rat brain. *Eur J Neurosci* 17(7):1355–1364.
- Cheung KK, Rytten M, Burnstock G. 2003. Abundant and dynamic expression of G protein-coupled P2Y receptors in mammalian development. *Dev Dynam* 228(2): 254–266.
- Coco S, Calegari F, Pravettoni E, Pozzi D, Taverna E, Rosa P, Matteoli M, Verderio C. 2003. Storage and release of ATP from astrocytes in culture. *J Biol Chem* 278(2):1354–1362.
- Cotrina ML, Lin JHC, Lopez-Garcia JC, Naus CCG, Nedergaard M. 2000. ATP-mediated glia signalling. *J Neurosci* 20(8):2835–2844.
- Darby M, Kuzmiski JB, Panenka W, Feighan D, MacVicar BA. 2003. ATP released from astrocytes during swelling activates chloride channels. *J Neurophysiol* 89(4):1870–1877.
- Edwards FA, Gibb AJ, Colquhoun D. 1992. ATP receptor-mediated synaptic currents in the CNS. *Nature* 359(6391):144–147.
- Emptage NJ, Reid CA, Fine A. 2001. Calcium stores in hippocampal synaptic boutons mediate short-term plasticity, store-operated Ca^{2+} entry, and spontaneous transmitter release. *Neuron* 29(1):197–208.
- Franke H, Illes P. 2006. Involvement of P2 receptors in the growth and survival of neurons in the CNS. *Pharmacol Ther* 109(3):297–324.
- Franke H, Kittner H, Grosche J, Illes P. 2003. Enhanced P2Y₁ receptor expression in the brain after sensitisation with d-amphetamine. *Psychopharmacology* 167(2):187–194.
- Gabel LA, Nisenbaum ES. 1998. Biophysical characterization and functional consequences of a slowly inactivating potassium current in neostriatal neurons. *J Neurophysiol* 79(4):1989–2002.
- Gerevich Z, Borvendeg SJ, Schröder W, Franke H, Wirkner K, Nörenberg W, Fürst S, Gillen C, Illes P. 2004. Inhibition of N-type voltage-activated calcium channels in rat dorsal root ganglion neurons by P2Y receptors is a possible mechanism of ADP-induced analgesia. *J Neurosci* 24(4):797–807.
- Goldman S. 2003. Glia as neural progenitor cells. *Trends Neurosci* 26(11):590–596.
- Grynkiwicz G, Poenie M, Tsien RY. 1985. A new generation of Ca^{2+} indicators with greatly improved fluorescence properties. *J Biol Chem* 260(6):3440–3450.
- Heine C, Heimrich B, Vogt J, Wegner A, Illes P, Franke H. 2006. P2 receptor stimulation influences axonal outgrowth in the developing hippocampus *in vitro*. *Neuroscience* 138:303–311.
- Heinzel G, Wolozak R, Thoman P. 1993. Pharmacokinetic and pharmacodynamic data analysis systems for the PC. Stuttgart: Gustav Fischer.
- Huang CM, Kao LS. 1996. Nerve growth factor, epidermal growth factor and insulin differentially potentiate ATP-induced $[Ca^{2+}]_i$ rise and dopamine secretion in PC12 cells. *J Neurochem* 66(1):124–130.
- Hurst RS, Cepeda C, Shumate LW, Levine MS. 2001. Delayed postnatal development of NMDA receptor function in medium-sized neurons of the rat striatum. *Dev Neurosci* 23(2):122–134.
- Ikeuchi Y, Nishizaki T. 1995. ATP-evoked potassium currents in rat striatal neurons are mediated by a P₂ purinergic receptor. *Neurosci Lett* 190(3):89–92.
- Illes P, Riebeiro AJ. 2004. Molecular physiology of P2 receptors in the central nervous system. *Eur J Pharmacol* 483(1):5–17.
- Illes P, Klotz KN, Lohse MJ. 2000. Signaling by extracellular nucleotides and nucleosides. *Naunyn-Schmiedeberg's Arch Pharmacol* 362(4–5):295–298.
- Izant JG, McIntosh JR. 1980. Microtubule-associated proteins: A monoclonal antibody to MAP2 binds to differentiated neurons. *Proc Natl Acad Sci USA* 77(8):4741–4745.
- Jan CR, Ho CM, Tseng CJ. 1999. Multiple effects of 1- β -[3-(4-methoxyphenyl)-propoxy]-4-methoxyphenethyl]-1H-imidazole hydrochloride (SKF 96365) on Ca^{2+} signalling in MDCK cells: Depletion of thapsigargin-sensitive Ca^{2+} store followed by capacitative Ca^{2+} entry, activation of a direct Ca^{2+} entry, and inhibition of thapsigargin-induced capacitative Ca^{2+} entry. *Naunyn-Schmiedeberg's Arch Pharmacol* 359(2):92–101.
- Jo YW, Schlichter R. 1999. Synaptic corelease of ATP and GABA in cultured spinal neurons. *Nat Neurosci* 2(3):241–245.
- Kawaguchi Y. 1992. Large aspiny cells in the matrix of the rat neostriatum *in vitro*: Physiological identification, relation to the compartments and excitatory postsynaptic currents. *J Neurophysiol* 67(6):1669–1682.
- Kawaguchi Y. 1993. Physiological, morphological, and histochemical characterization of three classes of interneurons in rat neostriatum. *J Neurosci* 13(11):4908–4923.
- Kawaguchi Y, Wilson CJ, Augood SJ, Emson PC. 1995. Striatal interneurons: Chemical, physiological and morphological characterization. *Trends Neurosci* 18(12):527–535.
- Kempermann G, Wiskott L, Gage FH. 2004. Functional significance of adult neurogenesis. *Curr Opin Neurobiol* 14(2):186–191.
- Khakh BS. 2001. Molecular physiology of P2X receptors and ATP signalling at synapses. *Nat Rev Neurosci* 2(3):165–174.
- Khakh BS, Burnstock G, Kennedy C, King BF, North RA, Séguéla P, Voigt M, Humphrey PPA. 2001. International Union of Pharmacology. XXIV. Current status of the nomenclature and properties of P2X receptors and their subunits. *Pharmacol Rev* 53(1):107–118.
- Krügel U, Kittner H, Illes P. 1999. Adenosine 5'-triphosphate-induced dopamine release in the rat nucleus accumbens *in vivo*. *Neurosci Lett* 265(1):49–52.
- Maurice N, Mercer J, Chan CS, Hernandez-Lopez S, Held J, Tkatch T, Surmeier DJ. 2004. D₂ dopamine receptor-mediated modulation of voltage-dependent Na⁺ channels reduces autonomous activity in striatal cholinergic interneurons. *J Neurosci* 24(46):10289–10301.
- Misgeld U, Dotti HU, Frotscher M. 1986. Late development of intrinsic excitation in the rat neostriatum: an *in vitro* study. *Brain Res* 392:59–67.
- Moore DJ, Chambers JK, Murdock PR, Emson PC. 2002. Human Ntera-2/D1 neuronal progenitor cells endogenously express a functional P2Y₁ receptor. *Neuropharmacology* 43(6):966–978.
- Moran MM, Xu H, Clapham DE. 2004. TRP ion channels in the nervous system. *Curr Opin Neurobiol* 14(3):362–369.
- Neary JT, Rathbone MP, Cattabeni F, Abbracchio MP, Burnstock G. 1996. Trophic actions of extracellular nucleotides and nucleosides on glial and neuronal cells. *Trends Neurosci* 19(1):13–18.
- Nörenberg W, Illes P. 2000. Neuronal P2X receptors: Localisation and functional properties. *Naunyn-Schmiedeberg's Arch Pharmacol* 362(4–5):324–339.
- Parekh AB, Putney JW. 2005. Store-operated calcium channels. *Physiol Rev* 85(2):757–810.
- Plenge-Tellechea F, Soler F, Fernandez-Belda F. 1997. On the inhibition mechanism of sarcoplasmic or endoplasmic reticulum Ca^{2+} -ATPases by cyclopiazonic acid. *J Biol Chem* 272(5):2794–2800.
- Poelchen W, Sieler D, Wirkner K, Illes P. 2001. Co-transmitter function of ATP in central catecholaminergic neurons of the rat. *Neuroscience* 102(3):593–602.
- Ralevic V, Burnstock G. 1998. Receptors for purines and pyrimidines. *Pharmacol Rev* 50(3):413–492.
- Reddy PH, Williams M, Tagle DA. 1999. Recent advances in understanding the pathogenesis of Huntington's disease. *Trends Neurosci* 22(6):248–255.
- Remy C, Remy S, Beck H, Swandulla D, Hans M. 2004. Modulation of voltage-dependent sodium channels by the δ -agonist SNC80 in acutely isolated rat hippocampal neurons. *Neuropharmacology* 47(7):1102–1112.
- Roberts TJ, Price SCR, Williams SCR, Modo M. 2006. Preservation of striatal tissue and behavioral function after neural stem cell transplantation in a rat model of Huntington's disease. *Neuroscience* 139(4):1187–1199.
- Ryu JK, Choi HB, Hatori K, Heisel RL, Pelech SL, McLarnon JG, Kim SU. 2003. Adenosine triphosphate induces proliferation of human neural stem cells: Role of calcium and p70 ribosomal protein S6 kinase. *J Neurosci Res* 72(3):352–362.
- Rzagalinski BA, Willoughby KA, Hoffman SW, Falck JR, Ellis EF. 1999. Calcium influx factor, further evidence it is 5,6-epoxyeicosatrienoic acid. *J Biol Chem* 274(1):175–182.
- Scemes E, Duval N, Meda P. 2003. Reduced expression of P2Y₁ receptors in connexin43-null mice alters calcium signaling and migration of neural progenitor cells. *J Neurosci* 23(36):11444–11452.
- Schaefer M, Plant TD, Obukhov AG, Hofmann T, Gudermann T, Schultz G. 2000. Receptor-mediated regulation of the nonselective cation channels TRPC4 and TRPC5. *J Biol Chem* 275(23):17517–17526.
- Scheibler P, Pesic M, Franke H, Reinhardt R, Wirkner K, Illes P, Nörenberg W. 2004. P2X₂ and P2Y₁ immunofluorescence in rat neostriatal medium-spiny projection neurons and cholinergic interneurons is not linked to respective purinergic receptor function. *Br J Pharmacol* 143(1):119–131.
- Shukla V, Zimmermann H, Wang L, Kettenmann H, Raab S, Hammer K, Sevigny J, Robson SC, Braun N. 2005. Functional expression of the ecto-ATPase NTPDase2 and of nucleotide receptors by neuronal progenitor cells in the adult murine hippocampus. *J Neurosci Res* 80(5):600–610.
- Smith Y, Bevan MD, Shink E, Bolam JP. 1998. Microcircuitry of the direct and indirect pathways of the basal ganglia. *Neuroscience* 86(2):353–387.

- Strübing C, Krapivinsky G, Krapivinsky L, Clapham DE. 2001. TRPC1 and TRPC5 form a novel cation channel in mammalian brain. *Neuron* 29(3):645–655.
- Tepper JM, Sharpe NA, Koós TZ, Trent F. 1998. Postnatal development of the rat neostriatum: Electrophysiological, light- and electron-microscopic studies. *Dev Neurosci* 20(2–3):125–145.
- Verkhatsky A, Steinhäuser C. 2000. Ion channels in glial cells. *Brain Res Rev* 32(2–3):380–412.
- Visnyei K, Tatsukawa KJ, Erickson RI, Simonian S, Oknaian ST, Kornblum HI. 2006. Neural progenitor implantation restores metabolic deficits in the brain following striatal quinolinic acid lesion. *Exp Neurol* 197(2) 465–474.
- von Kügelgen I. 2006. Pharmacological profiles of cloned mammalian P2Y-receptor subtypes. *Pharmacol Ther* 110:415–432.
- von Kügelgen I, Wetter A. 2000. Molecular pharmacology of P2Y-receptors. *Naunyn-Schmiedeberg's Arch Pharmacol* 362(4–5):310–323.
- Weissman TA, Riquelme PA, Ivic L, Flint AC, Kriegstein AR. 2004. Calcium waves propagate through radial glial cells and modulate proliferation in the developing neocortex. *Neuron* 43(5):647–661.
- Zhang YX, Yamashita H, Ohshita T, Sawamoto N, Nakamura S. 1995. ATP increases extracellular dopamine level through stimulation of P2Y purinoceptors in the rat striatum. *Brain Res* 691(1–2):205–212.
- Zhu X, Jiang M, Birnbaumer L. 1998. Receptor-activated Ca^{2+} influx via human Trp3 stably expressed in human embryonic kidney (HEK)293 cells. *J Biol Chem* 273(1):133–142.
- Zimmermann H. 2006. Nucleotide signaling in the nervous system development. *Pflugers Arch* (in press).

Modulation by D1 and D2 dopamine receptors of ATP-induced release of intracellular Ca^{2+} in cultured rat striatal neurons

Patrizia Rubini, Johannes Engelhardt, Kerstin Wirkner, Peter Illes*

Rudolf-Boehm-Institut für Pharmakologie und Toxikologie, Universität Leipzig, D-04109 Leipzig, Germany

Received 23 February 2007; received in revised form 16 June 2007; accepted 18 June 2007

Available online 27 June 2007

This paper is dedicated to my teacher and long-time friend Professor E.S. Vizi on the occasion of his 70th birthday.

Abstract

The aim of the present study was to investigate, whether dopamine D1 and/or D2 receptors are able to interfere with the ATP-induced increase of the intracellular Ca^{2+} concentration ($[\text{Ca}^{2+}]_i$) in cultured striatal neurons identified by their morphological characteristics and their $[\text{Ca}^{2+}]_i$ transients in response to a high- K^+ superfusion medium. ATP appeared to release Ca^{2+} mostly from an intracellular pool, since its effect was markedly depressed in the presence of cyclopiazonic acid, which is known to deplete such storage sites [Rubini, P., Pinkwart, C., Franke, H., Gerevich, Z., Nörenberg, W., Illes, P., 2006. Regulation of intracellular Ca^{2+} by P2Y_1 receptors may depend on the developmental stage of cultured rat striatal neurons. *J. Cell. Physiol.* 209, 81–93]. The mixed D1/D2 receptor agonist dopamine increased the ATP-induced $[\text{Ca}^{2+}]_i$ transients in a subpopulation of neurons. At the same time, dopamine did not alter the responses to K^+ in these cells. The selective D1 (SKF 83566) and D2 (sulpiride) receptor antagonists failed to modify the effect of ATP, but unmasked in the previously unresponsive neurons an inhibitory and facilitatory effect of dopamine, respectively. A combination of the two antagonists resulted in a failure of dopamine to modulate the $[\text{Ca}^{2+}]_i$ responses in any cell investigated. In conclusion, D1 and D2 receptors may modulate in an opposite manner the signalling pathways of P2Y_1 receptors in striatal neurons and thereby alter their development/growth or their cellular excitability and/or the release of GABA from their terminals.

© 2007 Elsevier Ltd. All rights reserved.

Keywords: Dopamine; Striatal neuron; D1 receptor; D2 receptor; P2 receptor

1. Introduction

P2 receptors of the P2X (ligand-gated cationic channels) and P2Y types (G protein-coupled receptors) mediate the cellular effects of ATP (Abbracchio and Burnstock, 1994; Fredholm et al., 1994). In contrast, the degradation product of ATP, adenosine, acts at four subtypes of P1 receptors, belonging to the A_1 , $\text{A}_{2\text{A}}$, $\text{A}_{2\text{B}}$ and A_3 types, all of them coupled to G proteins (Fredholm et al., 1994). Both P2 and P1 receptors occur in the central nervous system as demonstrated at the mRNA, protein and functional levels (Nörenberg and Illes, 2000; Illes and Ribeiro, 2004; Fredholm et al., 2005).

The principal neuronal cell population of the striatum consists of GABAergic medium spiny projection neurons, which receive glutamatergic input from the cerebral cortex and thalamus and, in addition, dopaminergic input from the substantia nigra pars compacta (Angulo and McEwen, 1994; Di Chiara et al., 1994). Medium spiny neurons contribute to two distinct efferent pathways ending in the internal segment of the globus pallidus/substantia nigra pars reticulata and in the external segment of the globus pallidus, respectively. Striatonigral neurons contain GABA and substance P, while striatopallidal neurons contain GABA and enkephalin (Smith and Bolam, 1990). The large aspiny neurons of the striatum are interneurons and utilize acetylcholine as a transmitter (Kawaguchi et al., 1995).

Whereas A_1 receptor mRNA and immunoreactivities (IR) are rather uniformly distributed over the striatum, the $\text{A}_{2\text{A}}$ receptor mRNA and IR closely matches that of the dopamine D2 receptors, being expressed in striatopallidal medium spiny

* Corresponding author at: Rudolf Boehm Institute of Pharmacology, Haertelstrasse 16-18, 04109 Leipzig, Germany. Tel.: +49 341 9724600; fax: +49 341 9724609.

E-mail address: Peter.Illes@medizin.uni-leipzig.de (P. Illes).

neurons that also express enkephalin (Schiffmann et al., 1991; Ongini and Fredholm, 1996). The dimerization of A_{2A} - D_2 receptors appears to be the morphological basis for a mutual antagonistic interaction and the consequent therapeutic efficacy of A_{2A} receptor antagonists in Parkinson's disease (Fuxe et al., 2005; Schwarzschild et al., 2006). Although both the message and the protein for P2X (Kidd et al., 1995; Kanjhan et al., 1999) and P2Y receptors (Moore et al., 2000, 2001) are present in the striatum, the cellular distribution of these receptors is rather obscure, certainly involving both neurons and glial cells.

Although in striatal slices of adult rats functional P2X and P2Y receptors could not be identified (Scheibler et al., 2004), it has recently been shown that in striatal cell cultures ATP increases the intracellular Ca^{2+} concentration ($[Ca^{2+}]_i$) via the stimulation of P2Y₁ receptors (Rubini et al., 2006). This early response was due to the release of Ca^{2+} from its intracellular storage sites followed by a late influx of Ca^{2+} from the extracellular space, probably triggered by the opening of store-operated channels in the plasma membrane. The aim of the present study was to investigate whether D1 and/or D2 receptors are able to interfere with the ATP-induced $[Ca^{2+}]_i$ increase of striatal neurons.

2. Experimental procedures

2.1. Preparation of striatal cell cultures

Striatal tissue was dissected from 1-day old Wistar rats (own breed) killed by decapitation, and collected in Hank's balanced salt solution (HBSS). The tissue was treated with 0.25% trypsin (1:1 in HBSS) for 20 min at 37 °C. Then, 100 μ l of DNase I (10 μ g/ml) was applied, followed by mechanical trituration through a Pasteur pipette in fetal calf serum-supplemented (20%) Dulbecco's modified Eagle's medium (DMEM) containing also 15 mM HEPES, 50 μ g/ml gentamycine, and 30 mM D-glucose. Subsequent to centrifugation, the pellet was resuspended in DMEM of the above composition and was seeded onto glass coverslips in polystyrol dishes at a density of 3×10^4 cells per coverslip, and cultured at 37 °C in a humidified atmosphere containing 6.8% CO₂ in air. After 4 days of cultivation in DMEM, the medium was replaced by Neurobasal™ medium (NBM) supplemented with B27 (v/v, 50/1), 2.5 mM L-glutamine and 50 μ g/ml gentamycine.

2.2. Intracellular calcium measurements

13–15 day-old cultures (13–15 DIV) grown in DMEM followed by NBM were loaded for 50–60 min at 37 °C in the dark with the cell permeant acetoxymethyl-ester of the fluorescent Ca^{2+} indicator Fura-2 (2.5 μ M). To remove excess extracellular Fura-2, glass coverslips were washed several times with an artificial cerebrospinal solution (ACSF) of the following composition (in mM): NaCl 135, KCl 4.5, CaCl₂ 2, MgCl₂ 1, HEPES 10, glucose 10; pH adjusted to 7.4 with NaOH, and were allowed to rest for 30 min at room temperature protected from light. Thereafter, Ca^{2+} imaging experiments were performed at room temperature in ACSF using an inverted microscope (IX-70; Olympus, Hamburg, Germany) equipped for epifluorescence and a Peltier-cooled charge-coupled device camera (IMAGO; Till Photonics, Martinsried, Germany). Intracellular Fura-2 was alternately excited at 340 and at 380 nm, and the emitted light was measured at a wavelength of 510 nm. The TILL vision software (3.3.; Till Photonics) was used for data acquisition, system control, and later, off-line analysis. The fluorescence ratio (340 nm/380 nm) provides a relative measure of the cytosolic free Ca^{2+} concentration (Grynkiewicz et al., 1985).

The experimental protocol routinely started with the application of ACSF via the flush valve of a pressure-operated, computer-controlled rapid drug application device (DAD-12, Adams and List) followed by a 3-s application of a high-K⁺

ACSF solution containing (in mM): NaCl 89.5, KCl 50, CaCl₂ 2, MgCl₂ 1, HEPES 10, glucose 10; pH adjusted to 7.4 with NaOH. Neurons were differentiated from glial cells by their morphology and by the presence and absence of $[Ca^{2+}]_i$ transients, respectively, in response to the superfusion of a high-K⁺ containing medium. Then, ATP (30 μ M)- and K⁺ (50 mM)-containing media were superfused for 10 and 3 s, respectively; these alternating applications of ATP and K⁺ were spaced apart by 10 min intervals. In another series of experiments, ATP (30 μ M) was superfused for 10 s every 15 min, for three to four times in total. Dopamine was applied 3 min before and during the application of K⁺ or ATP either in the absence or in the presence of the dopamine receptor antagonists, which were superfused as indicated by horizontal bars in Figs. 2 and 3. Drug effects on ATP-induced $[Ca^{2+}]_i$ transients were evaluated by comparing the response to ATP in the presence of dopamine, SKF 83566 and/or sulpiride with the response to ATP immediately before the superfusion of the dopaminergic ligands and were expressed as percentage changes.

The ratio of the K⁺ (K⁺/ATP)- and ATP-induced $[Ca^{2+}]_i$ transients were plotted in a scatter diagram (Fig. 1). The line represents a second-order exponential decay fit to the data according to the equation $y = a \times e^{-bx}$. The analysis was performed with SigmaPlot 2004 Version 9.01 (Systat Software, Inc., Erkrath, Germany).

2.3. Materials

The following drugs and chemicals were used: Dulbecco's modified Eagle's medium (DMEM), Hank's balanced salt solution (HBSS), Neurobasal medium (NBM), gentamycine, trypsin (Life Technologies, Karlsruhe, Germany); DNase I (Roche Diagnostics, Mannheim, Germany); fetal calf serum (Seromed, Berlin, Germany); adenosine 5'-triphosphate disodium salt (ATP), dopamine hydrochloride, fura-2 acetoxymethyl ester (Fura-2/AM) (Sigma-Aldrich, Taufkirchen, Germany); 8-bromo-2,3,4,5-tetrahydro-3-methyl-5-phenyl-1H-3-benzazepin-7-ol hydrobromide (SKF 83566), (RS)-(-)-sulpiride (Tocris, Bristol, UK).

Stock solutions (10–100 mM) of drugs were prepared with distilled water or dimethylsulfoxide. Aliquots were stored at –20 °C. Further dilutions were made daily with the appropriate bath solution.

2.4. Statistics

Means \pm S.E.M. of *n* trials are shown, *n* being the number of single cells. Differences between means were tested for significance by one-way ANOVA followed by the Student–Newman–Keuls method. $P < 0.05$ was the accepted level of significance.

3. Results

The neurons used for the experiments were selected based on morphological criteria. They were characterized by phase contrast-bright cell bodies and had developed long network forming dendrite-like processes after 13–15 days *in vitro*. Glial cells in contrast, formed a confluent background layer of flat, contrast-dark cells with polygonal somata devoid of dendritic appendages. In addition, only those cells with a neuron-like shape were included into the further evaluations, which responded to a depolarizing K⁺ pulse (50 mM, 3 s) with a clear $[Ca^{2+}]_i$ transient. This transient was apparently due to the entry of Ca^{2+} from the extracellular space via voltage-sensitive calcium channels (VSCCs), since it was abolished in the presence of a Ca^{2+} -free external medium (Rubini et al., 2006).

A submaximal ATP concentration (30 μ M; 10 s) was selected for all subsequent experiments (Fig. 1; Rubini et al., 2006). ATP appeared to release Ca^{2+} mostly from an intracellular pool, since its effect was markedly depressed in the presence of cyclopiazonic acid, which is known to deplete such storage sites. When the Δ fluorescence ratio was used as a

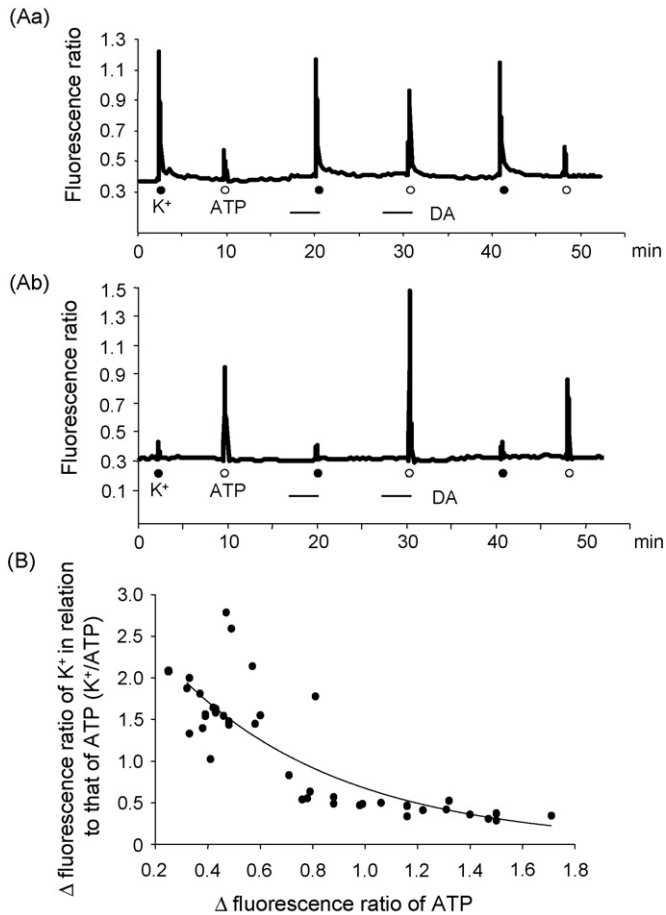


Fig. 1. ATP-induced increases of intracellular Ca^{2+} in rat cultured striatal neurons. Only neurons but not glial cells reacted with an increase of $[\text{Ca}^{2+}]_i$ to the application of a high- K^+ (50 mM) medium for 3 s. (A) Original tracings showing $[\text{Ca}^{2+}]_i$ transients of these cells in response to a submaximal concentration of ATP (30 μM), applied for 10 s. Superfusion with the mixed D1/D2 agonist dopamine (DA; 100 μM) for 3 min, potentiated the ATP-induced $[\text{Ca}^{2+}]_i$ transients in a subset of neurons (41 out of 141). At the same time, dopamine failed to alter the action of a high- K^+ containing medium. Dopamine had comparable effects in neurons with large or small responses to K^+ or ATP (Aa and Ab). (B) The ratio of the K^+ - and ATP-induced $[\text{Ca}^{2+}]_i$ transients is negatively correlated with the increase of $[\text{Ca}^{2+}]_i$ evoked by ATP. Hence, immature neurons possessing a low density of voltage-sensitive calcium channels (VSCCs) reacted to ATP with larger $[\text{Ca}^{2+}]_i$ responses than more mature neurons possessing a high density of VSCCs. Data from 41 cells are plotted in a scatter diagram. The line represents a second-order exponential decay fit to the data according to the equation $y = a \times e^{-bx}$. The Pearson coefficient is $R = 0.82$.

measure of $[\text{Ca}^{2+}]_i$, a negative correlation (Pearson coefficient $R = 0.82$; scatter diagram from 41 cells) could be established between the amplitude of the ATP response and the amplitude of the K^+ response (K^+/ATP ; Fig. 1B). A large $[\text{Ca}^{2+}]_i$ transient induced by K^+ was always accompanied by a small $[\text{Ca}^{2+}]_i$ transient induced by ATP and *vice versa* (Fig. 1Aa and Ab). The reason for this inverse relationship may be due to the fact that immature neurons possessing a low density of VSCCs reacted to ATP with larger $[\text{Ca}^{2+}]_i$ responses than more mature neurons possessing a high density of VSCCs.

In the following experiments, the endogenous agonist dopamine (100 μM) with affinities for both D1 and D2 receptors, increased the ATP-induced $[\text{Ca}^{2+}]_i$ transients in 41

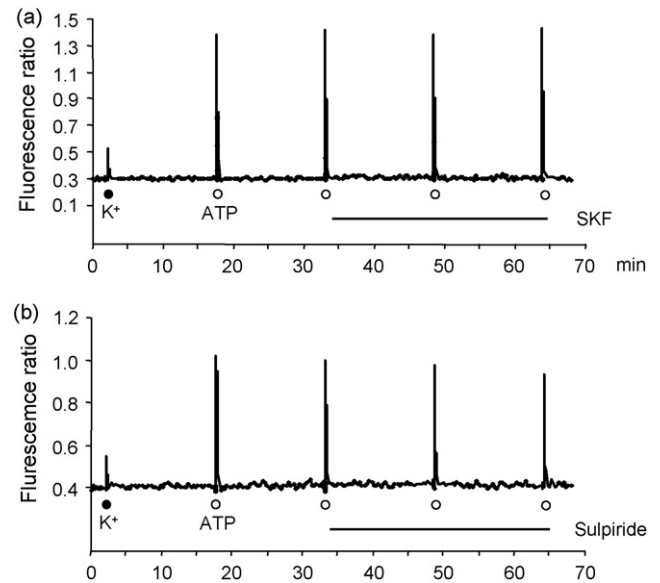


Fig. 2. ATP-induced increases of intracellular Ca^{2+} in rat striatal neurons. Original tracings showing $[\text{Ca}^{2+}]_i$ transients in response to a submaximal concentration of ATP (30 μM). (a) Superfusion with the D1 receptor antagonist SKF 83566 (0.1 μM) did not alter the $[\text{Ca}^{2+}]_i$ responses to ATP (36 out of 36 cells). (b) Superfusion with the D2 receptor antagonist sulpiride (1 μM) did not alter the $[\text{Ca}^{2+}]_i$ responses to ATP (42 out of 42 cells). Horizontal lines indicate the presence of SKF 83566 or sulpiride in the superfusion medium.

out of 141 cells only (Figs. 1Aa and Ab and 4). At the same time, dopamine did not alter the action of K^+ in any of the cells responding to dopamine. In order to differentiate between the D1 and D2 receptor-induced modulation of the ATP effects, selective antagonists of these receptors were used. SKF 83566 (D1; Ohlstein and Berkowitz, 1985) at a concentration of 0.1 μM , which was well below that blocking also D2 receptors, failed to influence the ATP-induced $[\text{Ca}^{2+}]_i$ transients (Figs. 2a and 4). Similarly, sulpiride (D2; Seeman and Van Tol, 1994), at a concentration of 1 μM , which is not expected to considerably block D1 receptors, did not alter the ATP-induced $[\text{Ca}^{2+}]_i$ transients (Figs. 2b and 4).

By abolishing the D1 receptor-mediated component of dopamine (100 μM) by SKF 83566 (0.1 μM), an inhibitory effect arising *via* D2 receptor-activation was unmasked on the ATP-induced $[\text{Ca}^{2+}]_i$ transients in 95 out of 190 cells (Figs. 3a and 4). In contrast, by abolishing the D2 receptor-mediated component of dopamine (100 μM) by sulpiride (1 μM), the number of cells exhibiting a D1 receptor-mediated facilitatory effect was increased to 34 out of 87 cells (39% instead of 29% of the cell population; Figs. 3a and 4). Eventually, a combination of SKF 83566 and sulpiride resulted in a failure of dopamine to modulate the $[\text{Ca}^{2+}]_i$ responses to ATP in all cells investigated (Figs. 3c and 4).

4. Discussion

The main finding of the present study is that D1 and D2 receptor-activation regulates ATP-induced $[\text{Ca}^{2+}]_i$ transients in cultured striatal neurons in an opposite manner. It appears that at the cultured neurons, there is a preponderance of D1

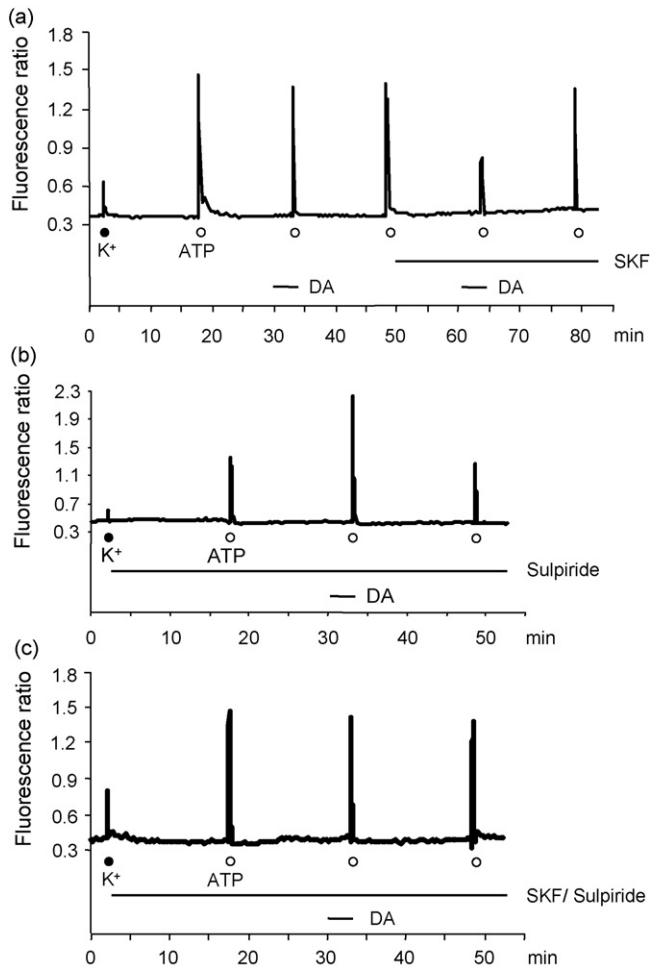


Fig. 3. ATP-induced increases of intracellular Ca^{2+} in rat striatal neurons. Original tracings showing $[\text{Ca}^{2+}]_i$ transients in response to a submaximal concentration of ATP ($30 \mu\text{M}$). (a) Superfusion with the D1 receptor antagonist SKF 83566 ($0.1 \mu\text{M}$) unmasks an inhibitory effect of dopamine ($100 \mu\text{M}$) on the $[\text{Ca}^{2+}]_i$ responses to ATP (95 out of 190 cells). (b) Superfusion with the D2 receptor antagonist sulpiride ($1 \mu\text{M}$) did not alter the $[\text{Ca}^{2+}]_i$ responses to ATP but increased the number of responsive cells (34 out of 87 cells). (c) Superfusion with SKF 83566 ($0.1 \mu\text{M}$) and sulpiride ($1 \mu\text{M}$) in combination abolished the effect of dopamine ($100 \mu\text{M}$) in all cells investigated (95 out of 95 cells). Horizontal lines indicate the presence of SKF 83566, sulpiride and dopamine in the superfusion medium.

receptors, since in the absence of a blocker of D1 (SKF 83566) or D2 (sulpiride) receptors, about 30% of the cells responded to dopamine with an increase of the ATP-induced $[\text{Ca}^{2+}]_i$ transients. However, this effect was abolished in the presence of SKF 83566, unmasking a previously missing D2 receptor-mediated inhibition. Conversely, in the presence of sulpiride, the percentage of cells responding to dopamine with a D1 receptor-mediated facilitation increased. Hence, immature rat striatal neurons may be endowed both with D1 and D2 receptors, probably in contrast to mature neurons of adult rats, where the striatopallidal and striatonigral medium spiny neuronal populations are believed to possess only D2 and D1 receptors, respectively (Schwarzschild et al., 2006). It is, however, noteworthy that there is alternative evidence for the co-localization of D1 and D2 receptors on the majority of adult neostriatal efferent neurons (Surmeier et al., 1993).

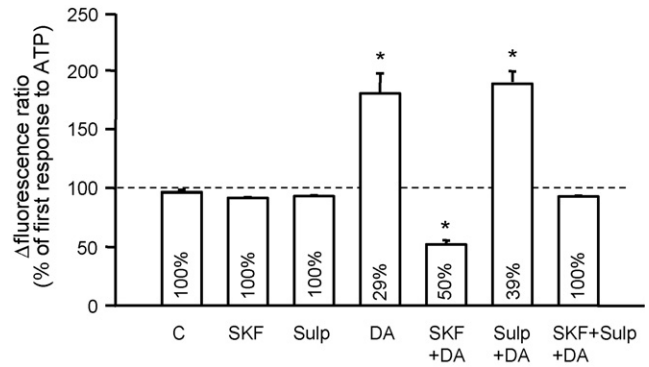


Fig. 4. Modulation of ATP-induced increases of intracellular Ca^{2+} in rat striatal neurons. Mean \pm S.E.M. of 36–95 cells from experiments similar to those shown in Figs. 1–3. Hence, ATP ($30 \mu\text{M}$) was applied for the first time in a normal medium, and for the second time in the presence of a normal medium (control, C), or a medium containing SKF 83566 ($0.1 \mu\text{M}$), or sulpiride ($1 \mu\text{M}$), or the combination of both antagonists. The effect of dopamine ($100 \mu\text{M}$) is shown in a normal medium, or in the presence of SKF 83566, sulpiride, or SKF 83566 plus sulpiride. The second ATP-induced $[\text{Ca}^{2+}]_i$ transient is depicted as a percentage of the first ATP-induced $[\text{Ca}^{2+}]_i$ transient in all cases. Asterisks (*) indicate statistically significant changes ($P < 0.05$) from the respective columns in the absence of dopamine.

In cultured striatal neurons, ATP has been shown to release $[\text{Ca}^{2+}]_i$ via the G_q /phospholipase C/inositoltrisphosphate (IP_3) pathway, thereby opening store-operated Ca^{2+} channels (Rubini et al., 2006). It may be hypothesized that the D1 receptor-mediated facilitation and the D2 receptor-mediated depression may be due to the stimulation and inhibition of adenylate cyclase activity, respectively (Seeman and Van Tol, 1994; Missale et al., 1998). In this case, D1 receptor-activation may lead to a cAMP and protein kinase A-dependent phosphorylation of the store-operated, Ca^{2+} -selective channels in the plasma membrane with an accompanying rise in $[\text{Ca}^{2+}]_i$ (Aromataris et al., 2006). Another possibility is that protein kinase A potentiates the phospholipase C-mediated and IP_3 -dependent release of intracellular Ca^{2+} by positively modulating the signalling pathway of P2Y_1 receptors (Ryning et al., 1998). In contrast, a negative interaction between the D2 and P2Y_1 receptor-regulated signalling mechanisms may be due to a decreased adenylate cyclase and protein kinase A activity.

Microdialysis experiments demonstrated that locally applied ATP releases dopamine in the striatum via P2Y_1 receptor-activation (Zhang et al., 1995, 1996; Krügel et al., 1999, 2001). Non-selective P2Y receptor antagonists such as PPADS, when given alone, depressed the release of dopamine. Therefore, it was suggested that there is a tonic control of dopaminergic activity by endogenous ATP and, in consequence, ATP may be a co-transmitter of dopamine in the terminals of neurons originating in the substantia nigra or ventral tegmentum and impinging on the medium spiny neurons of the ventral or dorsal striatum (Kittner et al., 1999, 2000). Hence, ATP may modulate the release of both dopamine and glutamate in the striatum (for presynaptic nucleotide/nucleoside receptors see the seminal paper of Vizi and Knoll, 1976) and, in consequence, determine the activity of the striatal output neurons which are thought to function as an interface between the limbic cortex and the extrapyramidal motor system (Krügel et al., 2004). Further

arguments for a co-transmitter role of ATP in the striatum are the depolarization-dependent release of ATP from cultured neostriatal neurons (Zhang et al., 1988), and the presence of ATP-hydrolyzing enzymes in synaptic plasma membrane fractions of striatal neurons (Richardson and Brown, 1987; James and Richardson, 1993; Nedeljkovic et al., 2003).

However, ATP may additionally be released both by excitable and non-excitabile cells due to stress, hypoxia/ischemia or mechanical stimulation (Abbraccio et al., 2006). The release of ATP from these cells may be *via* vesicular exocytosis (Coco et al., 2003), ATP-binding cassette (ABC) proteins (Ballerini et al., 2002), connexin hemichannels (Cotrina et al., 2000), osmolytic transporters linked to anion channels (Darby et al., 2003), and retrogradely operating nucleotide transporters (Sperlagh et al., 2003). Endogenous ATP may act in the striatum either at synaptic receptors stimulated by locally released, vesicular ATP or at non-synaptic receptors stimulated by ATP diffusing over a certain distance and released mostly by a range of non-exocytotic mechanisms (Vizi, 1984, 2000). In the rat striatum, the microdialysis technique demonstrated a two-fold increase in ATP levels after focal cerebral ischemia *in vivo* (Melani et al., 2005). Activation of presynaptic P2X receptors at glutamatergic nerve terminals during ischemia potentiated the frequency of miniature excitatory postsynaptic currents (mEPSCs) being a measure of the basal release of glutamate (Zhang et al., 2006). These facilitatory presynaptic receptors may belong to the P2X₇ subtype, because IR for the glutamate transporter VGLUT1 and P2X₇ receptors were co-localized in the rat striatum (Atkinson et al., 2004). High local concentrations of ATP may, then, induce a P2X receptor-mediated, excitotoxic cellular damage (Ryu et al., 2002; Franke and Illes, 2006; Franke et al., 2006). It is interesting to note that neurons, astrocytes and microglia exhibited an up-regulation of the previously observed low P2X₇ receptor-IR in the striatum after stab wound injury or middle cerebral artery occlusion (Franke et al., 2004, 2006; Melani et al., 2006).

It has recently been suggested that striatal neurons cultured in neurobasal medium most probably represent precursors of the adult medium-spiny cell-type (Rubini et al., 2006). They exhibit a low density of voltage-sensitive Na⁺ channels, as well as of NMDA and GABA_A receptor-channels, but a high density of G protein-coupled P2Y₁ receptors. Earlier findings indicate that P2Y receptors are able to exert trophic effects on neurons, leading to the induction of neurite outgrowth alone or in interaction with receptors for other growth factors (nerve growth factor, epidermal growth factor; Huang and Kao, 1996; Heine et al., 2006). An interesting long-term effect of ATP relates to the proliferation of neuronal (Ryu et al., 2003) and glial (Agresti et al., 2005) progenitor cells in the CNS. Apparently, functional P2 receptors and the ATP-hydrolyzing enzyme NTPDase 2 are co-expressed at neuronal progenitor cells in the murine hippocampus (Braun et al., 2003; Shukla et al., 2005). Further, the migration pattern, but not the cell differentiation of neuronal progenitor cells during early CNS development was regulated by P2Y₁ receptors (Scemes et al., 2003). The first step initiating these effects was believed to be an increase of [Ca²⁺]_i.

It may be hypothesized in view of the described effects of D1 and D2 receptors on the ATP-induced [Ca²⁺]_i increase that these receptors indirectly, *via* the modulation of the P2Y₁ receptor signalling pathways, may alter the development/growth of medium spiny neurons or their cellular excitability and/or the release of GABA from their terminals.

Acknowledgements

We are grateful to Dr. W. Nörenberg for many helpful discussions and to the Deutsche Forschungsgemeinschaft (IL 20/12-1) for financial support.

References

- Abbraccio, M.P., Burnstock, G., 1994. Purinoceptors: are there families of P2X and P2Y purinoceptors? *Pharmacol. Ther.* 64, 445–475.
- Abbraccio, M.P., Burnstock, G., Boeynaems, J.M., Barnard, E.A., Boyer, J.L., Kennedy, C., Knight, G.E., Fumagalli, M., Gachet, C., Jacobson, K.A., Weisman, G.A., 2006. International Union of Pharmacology LVIII: update on the P2Y G protein-coupled nucleotide receptors: from molecular mechanisms and pathophysiology to therapy. *Pharmacol. Rev.* 58, 281–341.
- Agresti, C., Meomartini, M.E., Amadio, S., Ambrosini, E., Serafini, B., Franchini, L., Volonte, C., Aloisi, F., Visentin, S., 2005. Metabotropic P2 receptor activation regulates oligodendrocyte progenitor migration and development. *Glia* 50, 132–144.
- Angulo, J.A., McEwen, B.S., 1994. Molecular aspects of neuropeptide regulation and function in the corpus striatum and nucleus accumbens. *Brain Res. Rev.* 19, 1–28.
- Aromataris, E.C., Roberts, M.L., Barritt, G.J., Rychkov, G.Y., 2006. Glucagon activates Ca²⁺ and Cl⁻ channels in rat hepatocytes. *J. Physiol.* 573, 611–625.
- Atkinson, J., Batten, T.F.C., Moores, T.S., Varoqui, H., Erickson, J.D., Deuchars, J., 2004. Differential co-localisation of the P2X₇ receptor subunit with vesicular glutamate transporters VGLUT1 and VGLUT2 in rat CNS. *Neuroscience* 123, 761–768.
- Ballerini, P., Di Iorio, P., Ciccarelli, R., Nargi, E., D'Alimonte, I., Traversa, U., Rathbone, M.P., Caciagli, F., 2002. Glial cells express multiple ATP binding cassette proteins which are involved in ATP release. *Neuroreport* 13, 1789–1792.
- Braun, N., Sevigny, J., Mishra, S.K., Robson, S.C., Brath, S.W., Gerstberger, R., Hammer, K., Zimmermann, H., 2003. Expression of the ecto-ATPase NTPDase2 in the germinal zones of the developing and adult rat brain. *Eur. J. Neurosci.* 17, 1355–1364.
- Coco, S., Calegari, F., Pravettoni, E., Pozzi, D., Tavern, E., Rosa, P., Matteoli, M., Verderio, C., 2003. Storage and release of ATP from astrocytes in culture. *J. Biol. Chem.* 278, 1354–1362.
- Cotrina, M.L., Lin, J.H., Lopez-Garcia, J.C., Naus, C.C., Nedergaard, M., 2000. ATP-mediated glia signaling. *J. Neurosci.* 20, 2835–2844.
- Darby, M., Kuzmiski, J.B., Panenka, W., Feighan, D., MacVicar, B.A., 2003. ATP released from astrocytes during swelling activates chloride channels. *J. Neurophysiol.* 89, 1870–1877.
- Di Chiara, G., Morelli, M., Consolo, S., 1994. Modulatory functions of neurotransmitters in the striatum: Ach/dopamine/NMDA interactions. *Trends Neurosci.* 17, 228–233.
- Franke, H., Illes, P., 2006. Involvement of P2 receptors in the growth and survival of neurons in the CNS. *Pharmacol. Ther.* 109, 297–324.
- Franke, H., Krügel, U., Grosche, J., Heine, C., Härtig, W., Allgaier, C., Illes, P., 2004. P2Y receptor expression on astrocytes in the nucleus accumbens of rats. *Neuroscience* 127, 421–441.
- Franke, H., Krügel, U., Illes, P., 2006. P2 receptors and neuronal injury. *Eur. J. Physiol.* 452, 622–644.
- Fredholm, B.B., Abbraccio, M.P., Burnstock, G., Daly, J.W., Harden, T.K., Jacobson, K.A., Leff, P., Williams, M., 1994. Nomenclature and classification of purinoceptors. *Pharmacol. Rev.* 46, 143–156.

- Fredholm, B.B., Chen, J.F., Masino, S.A., Vaugeois, J.M., 2005. Actions of adenosine at its receptors in the CNS: insights from knockouts and drugs. *Ann. Rev. Pharmacol. Toxicol.* 45, 385–412.
- Fuxe, K., Ferre, S., Canals, M., Torvinen, M., Terasmam, A., Marcellino, D., Goldberg, S.R., Staines, W., Jacobsen, K.X., Lluis, C., Woods, A.S., Agnati, L.F., Franco, R., 2005. Adenosine A_{2A} and dopamine D₂ heteromeric receptor complexes and their function. *J. Mol. Neurosci.* 26, 209–220.
- Grynkiewicz, G., Poenie, M., Tsien, R.Y., 1985. A new generation of Ca²⁺ indicators with greatly improved fluorescence properties. *J. Biol. Chem.* 260, 3440–3450.
- Heine, C., Heimrich, B., Vogt, J., Wegner, A., Illes, P., Franke, H., 2006. P2 receptor stimulation influences axonal outgrowth in the developing hippocampus in vitro. *Neuroscience* 138, 303–311.
- Huang, C.M., Kao, L.S., 1996. Nerve growth factor, epidermal growth factor, and insulin differentially potentiate ATP-induced [Ca²⁺]_i rise and dopamine secretion in PC12 cells. *J. Neurochem.* 66, 124–130.
- Illes, P., Ribeiro, J.A., 2004. Molecular physiology of P2 receptors in the central nervous system. *Eur. J. Pharmacol.* 483, 5–17.
- James, S., Richardson, P.J., 1993. Production of adenosine from extracellular ATP at the striatal cholinergic synapse. *J. Neurochem.* 60, 219–227.
- Kanjhan, R., Housley, G.D., Burton, L.D., Christie, D.L., Kippenberger, A., Thorne, P.R., Luo, L., Ryan, A.F., 1999. Distribution of the P2X₂ receptor subunit of the ATP-gated ion channels in the rat central nervous system. *J. Comp. Neurol.* 407, 11–32.
- Kawaguchi, Y., Wilson, C.J., Augood, S.J., Emson, P.C., 1995. Striatal interneurons: chemical, physiological and morphological characterization. *Trends Neurosci.* 18, 527–535.
- Kidd, E.J., Grahames, C.B.A., Simon, J., Michel, A.D., Barnard, E.A., Humphrey, P.P.A., 1995. Localization of P2X purinoceptor transcripts in the rat nervous system. *Mol. Pharmacol.* 48, 569–573.
- Kittner, H., Krügel, U., El-Ashmawy, I.M., Illes, P., 2000. Suppression of feeding-evoked dopamine release in the rat nucleus accumbens by the blockade of P2 purinoceptors. *Eur. J. Pharmacol.* 406, R13–R14.
- Kittner, H., Krügel, U., Poelchen, W., Reinhardt, R., von Kügelgen, I., Illes, P., 1999. P2 receptor-mediated activation of noradrenergic and dopaminergic neurons in the rat brain. *Prog. Brain Res.* 120, 223–225.
- Krügel, U., Kittner, H., Franke, H., Illes, P., 2001. Stimulation of P2 receptors in the ventral tegmental area enhances dopaminergic mechanisms in vivo. *Neuropharmacology* 40, 1084–1093.
- Krügel, U., Kittner, H., Illes, P., 1999. Adenosine 5'-triphosphate-induced dopamine release in the rat nucleus accumbens in vivo. *Neurosci. Lett.* 265, 49–52.
- Krügel, U., Spies, O., Regenthal, R., Illes, P., Kittner, H., 2004. P2 receptors are involved in the mediation of motivation-related behavior. *Purin. Sign.* 1, 21–29.
- Melani, A., Amadio, S., Gianfriddo, M., Vannucchi, M.G., Volonte, C., Bernardi, G., Pedata, F., Sancesario, G., 2006. P2X₇ receptor modulation on microglial cells and reduction of brain infarct caused by middle cerebral artery occlusion in rat. *J. Cereb. Blood Flow Met.* 26, 974–982.
- Melani, A., Turchi, D., Vannucchi, M.G., Cipriani, S., Gianfriddo, M., Pedata, F., 2005. ATP extracellular concentrations are increased in the rat striatum during in vivo ischemia. *Neurochem. Int.* 47, 442–448.
- Missale, C., Nash, S.R., Robinson, S.W., Jaber, M., Caron, M.G., 1998. Dopamine receptors from structure to function. *Physiol. Rev.* 78, 189–225.
- Moore, D., Chambers, J., Valdvogel, H., Faull, R., Emson, P., 2000. Regional and cellular distribution of the P2Y₁ purinergic receptor in the human brain: striking neuronal localisation. *J. Comp. Neurol.* 421, 374–384.
- Moore, D.J., Chambers, J.K., Wahlin, J.P., Tan, K.B., Moore, G.B., Jenkins, O., Emson, P.C., Murdock, P.R., 2001. Expression pattern of human P2Y receptor subtypes: a quantitative reverse transcription-polymerase chain reaction study. *Biochim. Biophys. Acta* 1521, 107–119.
- Nedeljkovic, N., Banjac, A., Horvat, A., Stojilkovic, M., Nikezic, G., 2003. Ecto-ATPase and ecto-ATP-diphosphohydrolase are co-localized in rat hippocampal and caudate nucleus synaptic plasma membranes. *Physiol. Res.* 797–804.
- Nörenberg, W., Illes, P., 2000. Neuronal P2X receptors: localisation and functional properties. *Naunyn-Schmiedeberg Arch. Pharmacol.* 362, 324–339.
- Ohlstein, E.H., Berkowitz, B.A., 1985. SCH 23390 and SK&F 83566 are antagonists at vascular dopamine and serotonin receptors. *Eur. J. Pharmacol.* 108, 205–208.
- Ongini, E., Fredholm, B.B., 1996. Pharmacology of adenosine A_{2A} receptors. *Trends Pharmacol. Sci.* 17, 364–372.
- Richardson, P.J., Brown, S.J., 1987. ATP release from affinity-purified rat cholinergic nerve terminals. *J. Neurochem.* 48, 622–630.
- Rubini, P., Pinkwart, C., Franke, H., Gerevich, Z., Nörenberg, W., Illes, P., 2006. Regulation of intracellular Ca²⁺ by P2Y₁ receptors may depend on the developmental stage of cultured rat striatal neurons. *J. Cell. Physiol.* 209, 81–93.
- Rynningen, A., Olav Jensen, B., Holmsen, H., 1998. Elevation of cyclic AMP decreases phosphoinositide turnover and inhibits thrombin-induced secretion in human platelets. *Biochim. Biophys. Acta* 1394, 235–248.
- Ryu, J.K., Choi, H.B., Hatori, K., Heisel, R.L., Pelech, S.L., McLarnon, J.G., Kim, S.U., 2003. Adenosine triphosphate induces proliferation of human neural stem cells: role of calcium and p70 ribosomal protein S6 kinase. *J. Neurosci. Res.* 72, 352–362.
- Ryu, J.K., Kim, J., Choi, S.H., Oh, Y.J., Lee, Y.B., Kim, S.U., Jin, B.K., 2002. ATP-induced in vivo neurotoxicity in the rat striatum via P2 receptors. *Neuroreport* 13, 1611–1615.
- Scemes, E., Duval, N., Meda, P., 2003. Reduced expression of P2Y₁ receptors in connexin43-null mice alters calcium signalling and migration of neural progenitor cells. *J. Neurosci.* 23, 11444–11452.
- Scheibler, P., Pesic, M., Franke, H., Reinhardt, R., Wirkner, K., Illes, P., Nörenberg, W., 2004. P2X₂ and P2Y₁ immunofluorescence in rat neostriatal medium-spiny neurones and cholinergic interneurons is not linked to respective purinergic receptor function. *Br. J. Pharmacol.* 143, 119–131.
- Schiffmann, S.N., Jacobs, O., Vanderhaeghen, J.-J., 1991. Striatal restricted adenosine A₂ receptor (RCD8) is expressed by enkephalin but not by substance P neurons: an in situ hybridization histochemistry study. *J. Neurochem.* 57, 1062–1067.
- Schwarzschild, M.A., Agnati, L., Fuxe, K., Chen, J.-F., Morelli, M., 2006. Targeting adenosine A_{2A} receptors in Parkinson's disease. *Trends Neurosci.* 29, 647–654.
- Seeman, P., Van Tol, H.H., 1994. Dopamine receptor pharmacology. *Trends Pharmacol. Sci.* 15, 264–270.
- Shukla, V., Zimmermann, H., Wang, L., Kettenmann, H., Raab, S., Hammer, K., Sevigny, J., Robson, S.C., Braun, N., 2005. Functional expression of the ecto-ATPase NTPDase2 and of nucleotide receptors by neuronal progenitor cells in the adult murine hippocampus. *J. Neurosci. Res.* 80, 600–610.
- Smith, A.D., Bolam, J.P., 1990. The neural network of the basal ganglia as revealed by the study of synaptic connections of identified neurones. *Trends Neurosci.* 13, 259–265.
- Sperligh, B., Szabo, G., Erdelyi, F., Baranyi, M., Vizi, E.S., 2003. Homo- and heteroexchange of adenine nucleotides and nucleosides in rat hippocampal slices by the nucleoside transport system. *Br. J. Pharmacol.* 139, 623–633.
- Surmeier, D.J., Reiner, A., Levine, M.S., Ariano, M.A., 1993. Are neostriatal dopamine receptors co-localized? *Trends Neurosci.* 16, 299–305.
- Vizi, E.S., 2000. Role of high-affinity receptors and membrane transporters in nonsynaptic communication and drug action in the central nervous system. *Pharmacol. Rev.* 52, 63–89.
- Vizi, E.S., Knoll, J., 1976. The inhibitory effect of adenosine and related nucleotides on the release of acetylcholine. *Neuroscience* 1, 391–398.
- Vizi, E.S., 1984. Non-Synaptic Interactions Between Neurons: Modulation of Neurochemical Transmission. John Wiley & Sons, Chichester.
- Zhang, J., Kordecki, E., Jackman, J., Ehrlich, Y.H., 1988. ATP secretion and extracellular protein phosphorylation by CNS neurons in primary culture. *Brain Res. Bull.* 21, 459–464.
- Zhang, Y., Deng, P., Li, Y., Xu, Z.C., 2006. Enhancement of excitatory synaptic transmission in spiny neurons after transient forebrain ischemia. *J. Neurophysiol.* 95, 1537–1544.
- Zhang, Y.-X., Yamashita, H., Ohshita, T., Sawamoto, N., Nakamura, S., 1995. ATP increase extracellular dopamine level through stimulation of P2Y purinoceptors in the rat striatum. *Brain Res.* 691, 205–212.
- Zhang, Y.-X., Yamashita, H., Ohshita, T., Sawamoto, N., Nakamura, S., 1996. ATP induces release of newly synthesized dopamine in the rat striatum. *Neurochem. Int.* 28, 395–400.